Investigation of the actions of Resveratrol on atherosclerosis development using *in vitro* and *in vivo* model systems

Alaa G. Alahmadi MRes, BSc (Hons)

A dissertation presented for the degree of Doctor of Philosophy (Biosciences)

March 2023

Cardiff School of Biosciences
The Sir Martin Evans Building
Cardiff University
Museum Avenue
Cardiff
CF10 3AX

Table of Contents

Table of Figures

Table of Tables

Abstract

Background: Atherosclerosis continues to be a major contributor to cardiovascular disease (CVD), which is one of the leading causes of morbidity and mortality globally. The current pharmacological strategies targeting hyperlipidaemia, such as statins, have shown limited effectiveness in combating cardiovascular risk and have other issues. Considering the limitations associated with statins and other pharmacotherapies, alternative avenues need to be sought. Nutraceuticals, such as resveratrol (RSV), have been highlighted as potential candidates for atherosclerosis prevention and treatment due to its demonstrated ability to modify several atherogenic risk factors and its excellent safety profile. Unfortunately, its effects on the full range of atherosclerotic processes along with the underlying molecular mechanisms are not fully understood. Therefore, the main aims of this study were to investigate the effects of RSV on key cellular processes associated with atherosclerosis development *in vitro* and to elucidate its effects on atherosclerosis progression in a mouse model system.

Methods: Various *in vitro* assays were carried out using different cell lines and primary cell cultures to investigate the effect of RSV treatment on a range of key cellular processes associated with atherosclerosis development. Furthermore, to investigate the effect of RSV on atherosclerotic plaque progression *in vivo*, 8-week-old male low-density lipoprotein receptor-deficient ($LDLR^{-}/^{-}$) mice were fed either a high-fat diet (HFD) or HFD-supplemented with RSV for 12 weeks. This was followed by a comprehensive analysis of risk factors associated with disease initiation and progression, such as plasma lipid profile and staining of resident cells (e.g. macrophages, T-cells and smooth muscle cells (SMCs)) in the plaque.

Results: RSV attenuated several key atherosclerosis-associated processes *in vitro*, such as monocyte migration towards monocyte chemoattractant protein-1(MCP-1), reactive oxygen species (ROS) production in all investigated cell types, and foam cell formation. Furthermore, RSV reduced human aortic smooth muscle cells (HASMCs) invasion and enhanced their proliferation, and exhibited anti-inflammatory actions. Regarding *in vivo* progression study, mice that received RSV-supplemented HFD for 12 weeks showed an improvement in plasma lipid profile, attenuation of plaque inflammation and enhancement markers of plaque stability. Furthermore, additional investigation on liver samples showed that RSV has the ability to reduce steatosis.

Conclusion: The findings from this study provide valuable insights into the anti-atherogenic actions of RSV and implicate it as a potential nutraceutical candidate that could be used globally as a part of ongoing atherosclerotic CVD prevention and management strategies due to the lack of undesirable side effects and the comparatively low cost compared to standard pharmacological medications. The potential of RSV should be investigated however in large clinical trials.

Acknowledgements

First and foremost, I would like to praise Allah the Almighty, the Most, for His granted countless blessing, knowledge, and opportunities given to me during my study, so that I have been finally able to accomplish the thesis satisfactorily.

The work carried out in this thesis would not have been possible without the help, support and guidance of numerous people either directly or indirectly as well as the financial support from Saudi Arabian Cultural Bureau and Jeddah University that gave me the opportunity to pursue my PhD study.

Apart from my efforts, the success and completion of this thesis would not be possible without the constant optimism and encouragement, practical guidelines, support, invaluable advice and constructive feedback throughout this long walk with all its “ups and downs”, from my supervisor, Professor Dipak Ramji. I have been really blessed to work with a supervisor who cared so much about my work, and who responded to my questions and concerns so promptly. I owe him my appreciation and am forever grateful to him for teaching me how well robust scientific research should be conducted and for everything I have learnt and achieved under his guidance. I hope that our fruitful cooperation in the scientific field will continue.

I am also very glad and sincerely grateful for having met and worked with Dr Timothy Hughes who provided me with scientific guidance and support for the *in vivo* experiments whenever I needed them. I would also like to express my deepest thanks to Dr Irina Guschina who also provided valuable guidance.

I would like to extend my thanks to Dr Neil Rodrigues and his team, who were incredibly helpful in the flow cytometry experiments. Special thanks and deep appreciation to Dr Sarab Taha for her invaluable guidance and feedback in the flow cytometry experiments. This part of the work would not have gone well without the support I have received from her.

I am immensely thankful to Drs Yee Chan and Alaa Ismail who provided much-appreciated assistance. I also thank my fellow lab colleagues, both past and present, all of whom contributed to making this project such an enjoyable experience.

I deeply appreciate and thank all my dearest friends, particularly Dr Haneen Alsehli, Dr Alaa Ismail, Dr Sarab Taha, Nouf Alshehri and Hind Alqahtani for their friendship, unlimited support and love, and for being a second family to me. Thank you, girls, for always managing to put the smile back on my face and making this journey such a wonderful and unforgettable experience.

Last but not least, I wish to express my love and my gratitude to my family for their unwavering love, constant support, prayer and encouragement throughout my study, without their love, this work would not have been possible.

Without mentioning my brother Hazem Alahmadi and my soulmate Reem Alotibi, this acknowledgement would not be complete. Throughout my journey here in the UK, they have been my backbone and strength to keep me pushing on and to never give up. Thank you both for always being there for me, for your unconditional love, encouragement and support. Words are countless to convey my thanks and love to both of you.

Publications during PhD

1. Published 4 methods-based chapters as part of a book series: Methods in Molecular Biology (volume 2419, pages 873) (https://link.springer.com/book/10.1007/978-1-0716-1924-7):

   A. **Alaa Alahmadi** and Dipak P. Ramji. (2022). Monitoring modified lipoprotein uptake and macropinocytosis associated with macrophage foam cell formation. Atherosclerosis. Springer, pp. 247-255.

   B. Dipak P. Ramji, Yee-Hung Chan, **Alaa Alahmadi**, Reem Alotibi and Nouf Alshehri. (2022). Survey of approaches for investigation of atherosclerosis *in vivo*. Atherosclerosis. Springer, pp. 57-72.

   C. Yee-Hung Chan, **Alaa Alahmadi**, Reem Alotibi and Dipak P. Ramji. (2022). Evaluation of plaque burden and lipid content in atherosclerotic plaques. *Atherosclerosis*. Springer, pp. 481-496.

   D. Yee-Hung Chan, **Alaa Alahmadi**, Reem Alotibi and Dipak P. Ramji. (2022). Monitoring cellularity and expression of key markers in atherosclerotic plaques. *Atherosclerosis*. Springer, pp. 497-506.

2. Published 2 papers as a co-author:

   A. Victoria O'Morain, Yee-Hung Chan, Jessica O. Williams, Reem Alotibi, **Alaa Alahmadi**, Neil P. Rodrigues, Sue F. Plummer, Timothy R. Hughes, Daryn R. Michael and Dipak P. Ramji. (2021). The Lab4P consortium of probiotics attenuates atherosclerosis in LDL receptor deficient mice fed a high fat diet and causes plaque stabilization by inhibiting inflammation and several pro-atherogenic processes. *Molecular Nutrition & Food Research*. 65(17), e2100214.

   B. Wijdan Al-Ahmadi, Thomas S. Webberley, Alex Joseph, Ffion Harris, Yee-Hung Chan, Reem Alotibi, Jessica O. Williams, **Alaa Alahmadi**, Thomas Decker, Timothy R. Hughes and Dipak P. Ramji (2021). Pro-atherogenic actions of signal transducer and activator of transcription 1 serine 727 phosphorylation in LDL receptor-deficient mice via modulation of plaque inflammation. *The FASEB Journal*. 35(10), e21892.

List of Abbreviations

4CL	4-coumarate:CoA ligase
ABCA1	ATP-binding cassette transporter A1
ACAT	Acyl coenzyme A: cholesterol acyltransferase
ACL	Adenosine triphosphate-citrate lyase
acLDL	Acetylated LDL
agLDL	Aggregated LDL
AKT1	AKT serine/threonine kinase 1
AMPK	AMP-activated protein kinase
ANOVA	One-way analysis of variance
ANSA	8- anilino-4-naphthosulphonic acid
AOPPs	Advanced oxidation protein products
APC	Allophycocyanin
ApoA-1	Apolipoprotein A-1
ApoB	Apolipoprotein B
ApoE	Apolipoprotein E
Arg-1	Arginase 1
BASs	Bile acid sequestrants
BHF	British Heart Foundation
BP	Biological processes
BrdU	5-Bromo-2'-deoxyuridine
BSA	Bovine serum albumin
C4H	Cinnamate-4-hydroxylase
CANTOS	Canakinumab anti-inflammatory thrombosis outcomes study
CBS	Central Biotechnology Services
CC	Cellular components
CCL2	C-C motif chemokine ligand 2
CCR2	C-C chemokine receptor type 2
CD36	Cluster of differentiation antigen 36
cDNA	Complementary DNA
CE	Cholesterol ester
CETP	Cholesterol ester transfer protein
cIMT	Intima media thickness
CIRT	Cardiovascular inflammation reduction trial
CLP	Common lymphoid progenitor
CMP	Common myeloid progenitor
COX-2	Cyclooxygenase 2
CPT-1a	Carnitine palmitoyltransferase 1A
CRP	C-reactive protein
CSF	Cerebrospinal fluid
CSFs	Colony-stimulating factors

CV	Crystal violet
CVDs	Cardiovascular diseases
Cy7	Cyanine7
DAMPs	Damage-associated molecular patterns
DAPI	4’, 6’-diamidino-2-phenylindole
DCFDA	Dichlorofluorescin diacetate
DEGs	Differentially expressed genes
DGE	Differential gene expression
dH_2O	Distilled water
DHR	Dihydroresveratrol
DiI	1,1'-dioctadecyl-3,3,3',3'-tetramethylindocarbocyanine perchlorate
DiI-oxLDL	DiI-oxidized LDL
DKK1	Dickkopf-1
DMEM	Dulbecco’s Modified Eagle Medium
DMSO	Dimethyl sulphoxide
ECM	Extracellular matrix
ECs	Endothelial cells
ECSCRI	European Cancer Stem Cell Research Institute
EDRF	Endothelium-dependent relaxing factor
EDTA	Ethylenediaminetetraacetic acid
ELISA	Enzyme-linked immunosorbent assay
eNOS	Endothelial nitric oxide synthase
ET-1	Endothelin
EtBr	Ethidium bromide
FATP	Fatty acid transport protein
FC	Free cholesterol
FDR	False discovery rate
FFA	Free fatty acids
FGF	Fibroblast growth factor
FH	Familial hypercholesterolaemia
FITC	Fluorescein isothiocyanate
FMD	Flow-mediated dilation
FPKM	Fragments Per Kilobase of transcript sequence per Millions base pairs sequenced
FSC	Forward scatter
GAPDH	Glyceraldehyde-3-phosphate dehydrogenase
GM- CSF	Granulocyte-macrophage colony stimulating factor
GMP	Granulocyte-macrophage progenitor
GO	Gene ontology
GPx	Glutathione peroxidase
GR	Glutathione reductase
GST	Glutathione S-transferases
H&E	Hematoxylin and eosin
H_2O_2	Hydrogen peroxide

HAECs	Human aortic endothelial cells
HASMCs	Human aortic smooth muscle cells
HBSS	Hanks' balanced salt solution
HCAEC	Human coronary artery endothelial cells
HCASMCs	Human coronary artery smooth muscle cells
HDL	High-density lipoprotein
HF	Heart failure
hFABP	Heart-specific fatty acid binding protein
HFD	High-fat diet
HI-FBS	Heat-inactivated foetal bovine serum
HMDMs	Human monocyte-derived macrophages
HMG-CoA	3-hydroxy-3-methyl–glutaryl-coenzyme A
HMOX1	Heme oxygenase 1
HPCs	Hematopoietic progenitor cells
HPF	High power fields
HSCs	Haematopoietic stem cells
HSL	Hormone-sensitive lipase
HSPCs	Haematopoietic stem and progenitor cells
HUVEC	Human umbilical vein endothelial cells
ICAM	Intercellular adhesion molecule
IDO	Indoleamine 2,3-dioxygenase
IF	Immunofluorescence
IFNs	Interferons
IL	Interleukin
ILK	Integrin-linked kinase
iNOS	Inducible nitric oxide synthase
IR	Insulin resistance
JAK2	Janus kinase 2
JAMs	Junctional adhesion molecules
KLF	Kruppel-like factor
LCA	Left carotid artery
LCAT	Lecithin cholesterol acyltransferase
LDH	Lactate dehydrogenase
LDL-C	Low-density lipoprotein-cholesterol
LDLR	Low-density lipoprotein receptor
LFA-1	Lymphocyte function-associated antigen-1
LKB 1	Liver kinase B1
LOX	Lipoxygenases
LOX-1	Lectin-like oxLDL receptor
LPL	Lipoprotein lipase
LPS	Lipopolysaccharide
LRP1	LDL receptor-related protein 1
LT-HSCs	Long-term HSCs

LXRs	Liver X receptors
LY	Lucifer yellow
M-CSF	Macrophage colony-stimulating factor
Mac-1	Macrophage antigen-1
MACE	Major adverse cardiovascular events
Mb	Myoglobin
MCP-1	Monocyte chemoattractant protein-1
MDA	Malondialdehyde
MDSC	Myeloid-derived suppressor cells
MEP	Megakaryocyte-erythroid progenitor
MF	Molecular functions
MHRs	Malignantly hypertensive rats
MI	Myocardial infarction
mitoOS	Mitochondrial oxidative stress
mitoROS	Mitochondrial ROS
mmLDL	Minimally modified LDL
MMLV	Moloney murine leukaemia virus
MMP	Matrix metalloproteinases
MNCs	Mononuclear cells
MPO	Myeloperoxidase
MPP	Multipotent progenitors
mPTP	Mitochondrial permeability transition pore
mRNA	Messenger ribonucleic acid
mtDNA	Mitochondrial DNA
NA	Nicotinic acid
Na_2HPO_4	Sodium phosphate
NAD^+	Nicotinamide adenine diphosphate
NADPH	Nicotinamide adenine dinucleotide phosphate
NAFLD	Non-alcoholic fatty liver disease
NAMPT	Nicotinamide phosphoribosyltransferase
NASH	Non-alcoholic steatohepatitis
NCEH	Neutral cholesteryl ester hydrolases
NEK7	NIMA-related kinase 7
NETs	Neutrophil extracellular traps
NF-κB	Nuclear factor kappa-light-chain-enhancer of activated B cells
NGS	Next generation sequencing
NKs	Natural killers
NLRP3	Nucleotide-binding oligomerisation domain leucine-rich repeat and pyrin domain containing protein 3
NMN	Nicotinamide mononucleotide
NMNAT2	Nicotinamide mononucleotide adenylyltransferase 2
NO	Nitric oxide
NPC1L1P	Nieman Pick C1-like 1 protein

NQO1	NAD(P)H:quinone oxidoreductase 1
NR	Nicotinamide riboside
OA	Oleic acid
OCT	Optimum cutting temperature
OPN	Osteopontin
ORO	Oil Red O
oxLDL	Oxidised LDL
OXPHOS	Oxidative phosphorylation
oxPL	Oxidised phospholipids
PA	Palmitic acid
PAB	Prooxidative balance
PAL	Phenylalanine ammonia lyase
PARP1	Poly ADP-ribose polymerases
PBMCs	Peripheral blood mononuclear cells
PBS	Phosphate-buffered saline
PCA	Principal component analysis
PCSK9	Proprotein convertase subtilisin/kexin type 9
PCWE	Polygonum cuspidatum water extract
PDE	Phosphodiesterase
PDGF	Platelet-derived growth factor
PDGFRβ	PDGF receptor beta
PE	Phycoerythrin
PECAM-1	Platelet endothelial cell adhesion molecule-1
PerCP	Peridinin-chlorophyll- protein
PFA	Paraformaldehyde
PGC-1α	Peroxisome proliferator-activated receptor gamma coactivator 1-alpha
PI3K	Phosphoinositide 3-kinase
PMA	Phorbol 12-myristate 13-acetate
PPAR	Peroxisome proliferator-activated receptor
PRRs	Pattern recognition receptors
PSGL-1	P-selectin glycoprotein ligand-1
PUFAs	Polyunsaturated fatty acids
QC	Quality control
qPCR	Quantitative polymerase chain reaction
RAEC	Rat aortic endothelial cells
RBCs	Red blood cells
RCT	Reverse cholesterol transport
RIN	RNA integrity number
RNAseq	RNAsequencing
ROS	Reactive oxygen species
RPMI	Rosewell Park Memorial Institute
RSV	Resveratrol
RT	Room temperature

SEM	Standard error of the mean
SHRs	Spontaneously hypertensive rats
SIRT1	Sirtuin 1
SLAM	Signaling lymphocytic activation molecule
SM-MHC	Smooth muscle-myosin heavy chain
SMCs	Smooth muscle cells
SOD	Superoxide dismutases
SR-B1	Scavenger receptor class B type 1
SRs	Scavenger receptors
SSC	Side scatter
ST-HSCs	Short-term HSCs
STAT3	Signal transducer and activator of transcription 3
STS	Stilbene synthase
T2DM	Type 2 diabetes mellitus
TAL	Tyrosine ammonia lyase
TBARSs	Thiobarbituric acid reactive substances
TBE	Tris-borate-EDTA
TBHP	Tert-butyl hydrogen peroxide
TCA	Tricarboxylic acid
TG	Triacylglycerol
TGF	Transforming growth factor
Th	T helper cell
TIMP	Tissue inhibitor of matrix metalloproteinase
TLC	Thin layer chromatography
TLRs	Toll-like receptors
TNF-α	Tumour necrosis factor-α
TPL	Total polar lipids
Tregs	Regulatory T cells
TSGs	Tumour suppressor genes
TxA2	Thromboxane A2
Txnrd1	Thioredoxin reductase
VCAM	Vascular cell adhesion molecule
VEGF	Vascular endothelial growth factor
VLA-4	Very late antigen-4
VLDL	Very low-density lipoprotein
VSMCs	Vascular smooth muscle cells
WHO	World Health Organisation
αSMA	Alpha-smooth muscle actin

CHAPTER 1

General Introduction

1.1 Cardiovascular disease- an overview

Cardiovascular diseases (CVDs) are an umbrella term that describes a group of disorders that affect the heart and circulatory systems that persists as a leading cause of global morbidity and mortality (Chan and Ramji 2022). According to the last report from The World Health Organization (WHO), they were responsible for approximately 17.9 million deaths in 2019, which represent around 32% of all global deaths (WHO, 2021). In the UK alone, there are around 7.6 million people living with CVDs (around 4 million males and 3.6 million females). This number is nearly twice as many individuals when cancer and Alzheimer's disease are combined. The high prevalence of CVD costs the UK economy an estimated £19 billion each year (British Heart Foundation 2022). According to this report in 2022, CVDs were responsible for around a quarter of all deaths in the UK, which is more than 160,000 deaths each year (one death every three minutes) (British Heart Foundation 2022). Unfortunately, this number is expected to increase to affect 43.9% of the US adult population by 2030, thereby representing a significant burden for the public healthcare system (Moss et al. 2018). The prevalence of CVDs is expected to rise due to an increase in risk factors such as diabetes and obesity, which may be related to adaptation of a 'westernised' lifestyle.

1.2 Atherosclerosis aetiology

Atherosclerosis is the major underlying cause of CVDs, including ischaemic heart disease and stroke, the leading cause of worldwide morbidity and mortality (Rajamani and Fisher 2017). The understanding of the molecular basis of atherosclerosis has improved over the years and has changed from a lipid deposition disorder to an inflammatory disease, characterised by the accumulation of lipids and infiltration of immunocytes, such as macrophages and T cells, together with the formation of fibrous cap in the arterial walls leading to an atheromatous plaque (Hansson and Hermansson 2011; Mehu et al. 2022). As a result of atheromatous plaque formation and subsequent growth, the arteries become hardened, narrow, and lose their elasticity. Consequently, this causes a reduction or complete blockage of blood flow and oxygen supply to vital organs such as heart muscles, thereby causing thrombosis (Hansson and Hermansson 2011).

A knowledge of the risk factors that are associated with CVDs can help to delay or prevent the incidence of the disease. There are several risk factors for CVDs, some of which can be controlled such as high plasma levels of cholesterol and atherogenic lipoproteins, smoking, high blood pressure, being overweight, diabetes and a sedentary lifestyle. On the other hand, unmodifiable factors, such as family history, old age and gender, can also contribute to atherosclerosis. Research is continuing to find more potential risk factors for atherosclerosis and several emerging risk factors include sleep apnoea, stress and high plasma levels of C-reactive protein (CRP) (Table 1.1) (Rafieian-Kopaei et al. 2014).

1.3 Pathophysiology of Atherosclerosis

Atherosclerosis is a chronic, low-grade inflammatory disease that affects mainly medium and large arteries (Shah 2019), and appears primarily at low-shear stress sites and disturbed laminar blood flow associated with arterial branches or curvatures (Groh et al. 2018). Atherosclerosis pathophysiology is a complex process involving the accumulation of lipids and fibrous elements, inflammatory responses, proliferation of vascular smooth muscle cells (VSMCs), various cell signalling molecules (e.g., cytokines) and genetic mutations in some cases (Wang and Butany 2017). All of these factors and many others orchestrate the initiation, development and progression of the disease. Generally, as illustrated in Figure 1.1, the growth of the atherosclerotic plaque involves different stages resulting in progressive blocking of the lumen, causing arterial blood flow to be interrupted (Gui et al. 2022). In advanced lesions and thrombosis stage, the fibrous covering diminishes, and the necrotic core expands resulting in plaque rupture and hence thrombosis. The clinical manifestation of acute thrombosis depends on the anatomical location of the thrombus within the vascular bed, such as coronary syndromes (including myocardial infarction (MI) or angina pectoris) if the thrombus affects the circulatory system, or gangrene if it affects the peripheral arteries (Libby et al. 2019; Gui et al. 2022).

Table 1.1 Examples of risk factors and how they contribute to atherosclerosis and CVD

Category	Risk factor	Contributions to CVD	References
Modifiable risks factors	Cigarette smoking	• Increases heart rate and blood pressure. • Reduces coronary blood flow. • Stimulates thrombosis. • Reduces the amount of oxygen delivered to red blood cells and other body parts. • Enhances levels of TNF-α. • Stimulates ROS production. • Increases hepatic secretion of IL-6 and CRP that subsequently induces endothelial cell dysfunction.	(Van Gaal et al. 2006; Benowitz and Burbank 2016)
	Obesity	• Associated with dyslipidemia, insulin resistance, and elevated levels of CRP. • Induces inflammation by increasing the production of several cytokines and inflammatory markers. • Induces endothelial dysfunction that leads to increased LDL oxidation. • Induces the levels of adhesion molecule expression by endothelial cells.	(Van Gaal et al. 2006; Akil and Ahmad 2011; Powell-Wiley et al. 2021)
	Hypertension	• Places extra pressure that can damage arteries that then reduces blood flow and causes increased accumulation of LDL in the arterial intima. • Enhances circulating levels of inflammation markers. • Stimulates plaque formation.	(Cachofeiro et al. 2009; Friedman and Hao 2015; Al-Mashhadi et al. 2021)
	Diabetes	• Alters glucose metabolism leading to increased production of ROS and subsequent endothelial dysfunction. • Patients with type 2 diabetes have increased free fatty acids and reduced plasma HDL levels.	(Rask-Madsen and King 2013)

Non-Modifiable risks factors	Age	• Several CVDs risk factors increase with age. • Ageing is associated with increased ROS that results in inflammation and progression to chronic disease such as CVDs.	(Dhingra and Vasan 2012; Rodgers et al. 2019)
	Gender	• Males are more prone to CVDs at an earlier age than females. • Post-menopausal women have a greater risk for CVDs than aged-matched men. • Menopausal females have a decline in estrogen hormone that leads to increased risk of high LDL-C levels, blood pressure, body weight and glucose homeostasis.	(Rodgers et al. 2019)
	Family history	• The risk of developing heart disease is increased if close blood relatives (e.g., parent or sibling) have been diagnosed with the disease under the age of 55 for males or age of 65 for females.	(Allport et al. 2016)
	Mutations	• FH resulting from mutation in the LDLR gene that is involved in the liver uptake of LDL. This leads to increase in LDL-C levels and increase risk of CVDs. • Tangier disease caused by mutation in the gene encoding ABCA1, which results in a significant deficiency in the levels of HDL-C and ApoA-1.	(Negi et al. 2013; Averna et al. 2017)

Abbreviations: TNF-α, tumour necrosis factor-α; ROS, reactive oxygen species; IL-6, interleukin-6; LDL-C, low-density lipoprotein-cholesterol; HDL, high-density lipoprotein; CVDs, cardiovascular diseases; LDLR, low-density lipoprotein receptor; FH, familial hypercholesterolemia; ABCA1, ATP-binding cassette transporter A1; ApoA-1, apolipoprotein A-1.

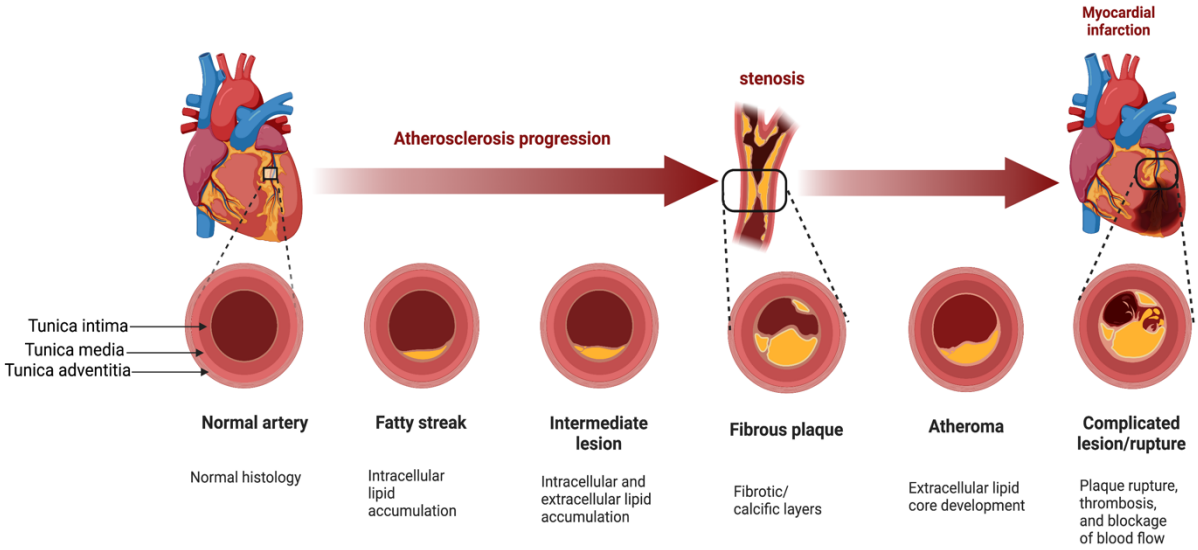

Figure 1.1 Progression of atherosclerotic plaques

The arterial wall of a normal artery is made up of three major layers: the tunica intima (consisting of a layer of ECs lining the lumen of the vessel, as well as a subendothelial layer made up of internal elastic membrane, the tunica media (consisting mostly of SMCs and elastic fibres stacked in roughly spiral layers), and the outer layer called tunica adventitia (consisting of collagen and elastic fibres). The progression of atherosclerotic plaque can be divided into 3 stages, (1) fatty-streak stage, (2) stable fibroatheromatous plaque stage, and (3) advanced lesions and thrombosis. The plaque rupture results in acute thrombosis which is commonly causes heart attack or stroke. **Abbreviations:** ECs, endothelial cells; SMCs, smooth muscle cells. Image adapted from BioRender template and created with BioRender.com.

1.3.1 Lesion initiation: Endothelial cell dysfunction

Endothelial cell (EC) dysfunction is implicated in the earliest step in atherosclerosis development (Björkegren and Lusis 2022). ECs form an active monolayer of cells that are tightly connected by tight junctions forming a semipermeable layer between the bloodstream and the vessel wall. For decades, the ECs were postulated to be nothing more than a cellular barrier. However, extensive studies have revealed the endothelium's complex role. Normal and healthy endothelium maintains vascular tone by releasing numerous dilator and constrictor molecules. Nitric oxide (NO; also identified as 'endothelium-dependent relaxing factor' (EDRF)), which is one of the primary vasodilatory molecules, is produced in ECs from its precursor L-arginine via the action of endothelial nitric oxide synthase (eNOS), requiring tetrahydrobiopterin (BH4) and nicotinamide adenine dinucleotide phosphate (NADPH) as cofactors (Xu et al. 2021).

The binding of the caveolin-1 protein to calmodulin inhibits eNOS activity; however, calcium binding to calmodulin triggers caveolin-1 displacement, leading to eNOS activation and, ultimately, NO generation (Davignon and Ganz 2004). Then, NO diffuses into the surrounding vascular smooth muscle cells (VSMCs), eliciting cGMP-dependent vasodilation via guanylate cyclase activation (Xu et al. 2021). The ECs also produce several vasoconstrictor molecules such as endothelin (ET-1), angiotensin-II, thromboxane A2 (TxA2) and thrombin. These molecules with NO facilitate ECs functions in the regulation of vasomotor homeostasis, by suppression of leukocyte adhesion/infiltration, and VSMCs proliferation, as well as preservation of the non-thrombogenic activities (Davignon and Ganz 2004; Xu et al. 2021). In addition to NO, ECs synthesise hydrogen sulfide (H_2S) from L-cysteine that well-known to mediate vasoprotective effect via inhibiting platelet aggregation and VSMCs proliferation as well as inducing VSMCs relaxation (Altaany et al. 2014; Citi et al. 2021).

ECs are continuously exposed to shear stress generated by the blood flow. The fluid shear stress generates a biomechanical force that is sensed by mechanosensors/mechanosensitive complex on the surface of ECs that is then transduced into biochemical signals, regulating vascular tone and homeostasis (Xu et al. 2021). Under normal physiological conditions (i.e., balance between vasodilator and vasoconstrictor mediators), ECs do not recruit circulating leukocytes from the bloodstream. However, atherogenesis-inducing risk factors associated with CVDs, including elevated plasma low density lipoprotein (LDL), hypertension, oxidative stress and inflammation, all generally act in concert to initiate ECs activation (dysfunction) by inhibiting the production of NO and disturbing the balance between various mediators, resulting in the recruitment of leukocytes (Ramji and Davies 2015; Wang and Butany 2017; Libby 2021). Furthermore, endothelial injury can be induced by other key factors such as exposure to bacterial or viral infection, reactive oxygen species (ROS), hypoxia, smoking, oxidised cholesterol, hyperglycaemia and hemodynamic alterations. These factors trigger a series of biochemical and molecular reactions, including increased ECs permeability, leukocyte adhesion, platelet aggregation and propagation of the inflammatory response (Xu et al. 2021). The increase in endothelium permeability that occurs with endothelial dysfunction facilitates the infiltration of circulating LDL and immune cells into the subendothelial space (intima). In addition to passive diffusion, recent evidence from a study in mice (male $ApoE^{-/-}SR\text{-}B1^{fl/fl}$) revealed that scavenger receptor class B type 1 (SR-B1) in

endothelial cells mediates LDL delivery into intima via transcytosis (Huang et al. 2019). The apolipoprotein B100 (ApoB) within LDL particles then encourages its aggregation and retention within the intima, boosting further endothelial dysfunction (McLaren et al. 2011). In response to their activation, ECs produce various pro-inflammatory mediators such as cytokines (e.g., interleukin-8 (IL-8), tumour necrosis factor-α (TNF-α) and macrophage colony stimulating factor (M-CSF)) and chemokines (e.g., monocyte chemoattractant protein-1 (MCP-1). Along with cytokines and chemokines, ECs express adhesion molecules, including vascular cell adhesion molecule (VCAM)-1 and junctional adhesion molecules (JAMs), which bind monocytes and T cells, and intercellular adhesion molecule (ICAM)-1, which binds other leukocytes. Initially, before migration into the intima layer, the recruited monocytes roll and adhere to adhesion molecules on the surface of activated ECs, such as E-selectins and P-selectins, that mediate monocytes rolling and adhesion through binding to P-selectin glycoprotein ligand-1 (PSGL-1) and other glycosylated ligands expressed on the surface of monocytes, to facilitate their tethering and rolling. This binding enables expressed VCAM-1 and ICAM-1 to initiate interaction with integrins expressed on monocytes, such as very late antigen-4 (VLA-4) and lymphocyte function-associated antigen-1 (LFA-1) respectively (McLaren et al. 2011). Monocyte recruitment is a highly orchestrated process in which MCP-1, also known as C-C motif chemokine ligand 2 (CCL2), plays a crucial role in directing the circulating monocytes and T-lymphocytes towards the inflammation site. MCP-1 is produced by several cell types, including monocytes/macrophages, ECs and VSMCs, and mediates its actions via binding to its receptor, C-C chemokine receptor type 2 (CCR2)(McLaren et al. 2011; Schnoor et al. 2015). Following adhesion and slow rolling, monocytes spread and crawl perpendicular towards the chemoattractant in a process called locomotion, in which monocytes try to find the nearest and suitable junction for transmigration (Gerhardt and Ley 2015; Schnoor et al. 2015). This intraluminal crawling mechanism is strongly dependent on ICAM-1 and macrophage antigen-1 (Mac-1), as well as ICAM-2, as blocking of these molecules leads to disrupted crawling and therefore disabled migration through EC junctions (Schnoor et al. 2015). Collectively, all of these modifications facilitate the adhesion, recruitment and infiltration of circulating leukocytes (e.g., monocytes, T cells, neutrophils and B cells) into the intima layer (Koenen and Weber 2010; McLaren et al. 2011; Weber and Noels 2011; Moore et al. 2013; Schmitt et al. 2014; Zernecke and Weber 2014). Taken together, dyslipidaemia and inflammation are interlinked since the retention and accumulation of LDL within the

arterial wall initiate and maintain chronic inflammation. A summary of triggers of endothelial dysfunction and its consequences are illustrated in Figure 1.2.

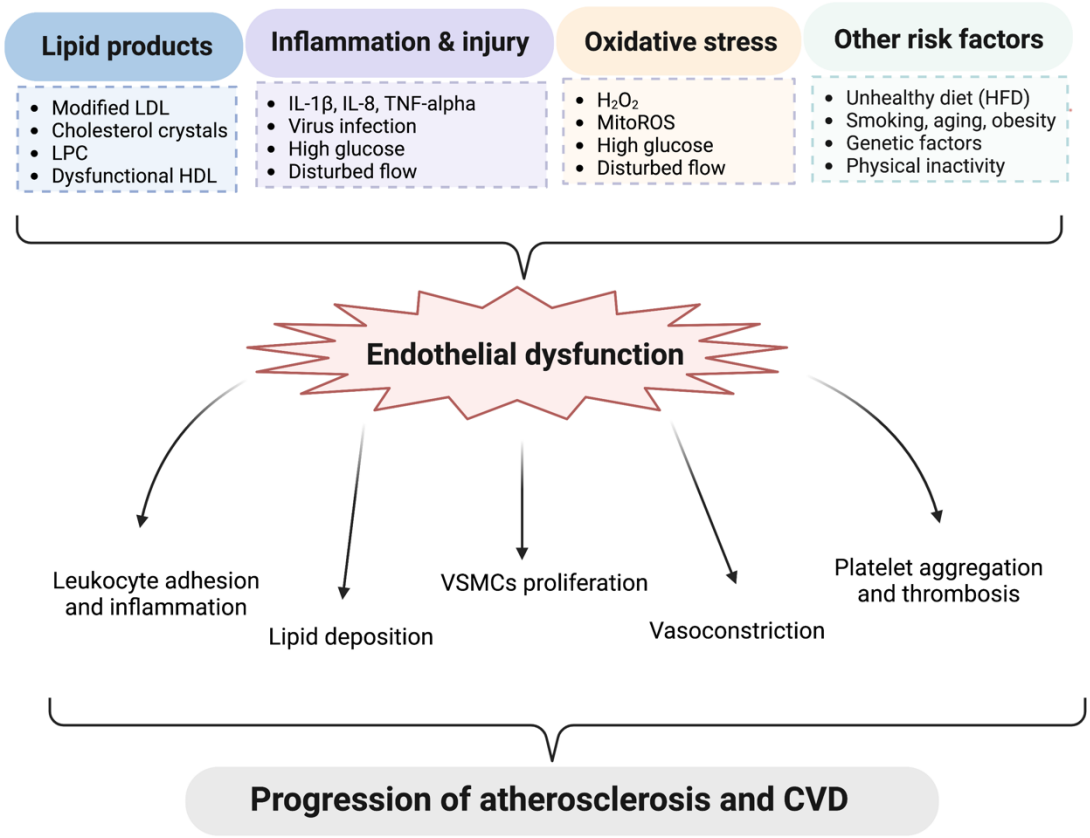

Figure 1.2 Triggers of endothelial dysfunction and its consequences

Different factors can trigger endothelial dysfunction: 1) lipid products (via modified LDL, cholesterol crystals, LPC and dysfunctional HDL); 2) inflammation and injury factors (via proinflammatory cytokines such as TNF-α, IL-1β and IL-8, and LPS or high glucose); 3) oxidative stress, including H_2O_2, mitochondrial ROS, high glucose and disturbed flow; 4) other risk factors associated with endothelial dysfunction, including unhealthy diet, smoking, ageing, obesity, genetic factors and physical inactivity. Endothelial dysfunction then promotes the initiation of atherosclerosis and CVD. **Abbreviations:** LDL, low-density lipoprotein; LPC, lysophosphatidylcholine; HDL, high-density lipoprotein; TNF-α, tumour necrosis factor alpha; IL-1β, interleukin 1 beta; IL-8, interleukin 8; LPS, lipopolysaccharide; H_2O_2; hydrogen peroxide; ROS, reactive oxygen species; HFD, high fat diet; CVD, cardiovascular diseases. Image created with BioRender.com.

1.3.2 Inflammation: a critical driver of all stages of atherosclerosis

Beyond dyslipidaemia, a large body of experimental and clinical data demonstrate the fundamental role of chronic vascular inflammation in atherogenesis (Libby and Hansson 2019; Libby 2021). Inflammation does not supplant or diminish lipid risk; rather, it provides a number of pathways that links lipids and other risk factors to atherosclerosis. For instance, remnant lipoprotein concentration is found to highly correlate with CRP, a biomarker of low-grade inflammation (Hansen et al. 2019). The mechanisms underlying the causation of inflammation in atherosclerosis remains incompletely elucidated; however, it is well-known that deposited mediators within the vessel generate chronic low-grade inflammation which then contributes to the pathogenesis of the disease. Both the innate and adaptive immune responses are regulated by cytokines, a group of diverse proteins that can be divided into several classes: interleukins (ILs), tumour necrosis factors (TNFs), interferons (IFNs), transforming growth factors (TGFs), colony-stimulating factors (CSFs) and other chemokines (Fatkhullina et al. 2016). The role of cytokines has been extensively studied and can be broadly classified into two classes according to their actions in an immune response as either pro- or anti-inflammatory. However, this distinction is not always possible since some cytokines have both pro- and anti-inflammatory actions that are context-dependent such as granulocyte-macrophage colony stimulating factor (GM-CSF) and M-CSF (Ramji and Davies 2015). The balance between pro- and anti-inflammatory cytokines is vital in maintaining cardiovascular health and homeostasis. In atherosclerosis, this balance is disturbed in favour of pro-inflammatory cytokines that are involved in all stages ranging from the initiation of the disease to plaque rupture. Table 1.2 summarises the action of key pro- and anti-inflammatory cytokines implicated in atherosclerosis development.

As shown in Table 1.2, all cell types within an atherosclerotic plaque are capable of producing and releasing cytokines and responding to their actions, resulting in widespread inflammation through a range of mechanisms. For example, macrophages, VSMCs, natural killer cells (NKs) and lymphocytes are all capable of releasing TNF-α, IL-1 and IL-6, which are pro-inflammatory/atherogenic cytokines.

Table 1.2 Role of cytokines in the pathogenesis of atherosclerosis

Cytokine	Producer	Target cells	Role in atherosclerosis
Pro-inflammatory/atherogenic			
IFN-γ	Monocytes/macrophages, T_{h1}, NK and $CD8^+$ T cells	Macrophages, $CD8^+$T cells, NK cells, B cells, SMCs	• Activates target cells • Promotes SR-A expression and mediates foam cell formation • Promotes foam cell apoptosis • Induces M1 macrophage polarisation
TNF-α	T_{h1} cells and myeloid cells	T_{h1} cells, ECs and macrophages	• Upregulates the expression of ICAM-1, VCAM-1 and MCP-1 • Promotes ROS production and endothelial dysfunction
IL-1α/IL-1β	Myeloid cells and macrophages	T_{h1} cells, T_{h17} cells, ECs, and macrophages	• Induces M1 macrophage polarisation • Regulates the activation of ECs and macrophages as well as differentiation of T_{h17} cells • Stimulates the release of MMPs
IL-4	T_{h2} cells, B cells and ECs	T cells, B cells and ECs	• Induces inflammation in ECs via upregulation of various pro-inflammatory mediators, including cytokines, chemokines and adhesion molecules
IL-6	Macrophages and ECs	T_{h1} cells and macrophages	• Propagates the downstream inflammatory response of IL-1 and other cytokines • Promotes fatty streak formation
IL-12	Macrophages, dendritic cells	T_{h1} cells and myeloid cells	• Regulates T_{h1} cells differentiation at the early stage • Induces IFN-γ production with IL-18
IL-18	Macrophages (produced by NLRP3 inflammasome along with IL-1β)	T_{h1} cells	• Upregulates the production of IFN-γ
IL-22	T_{h17}/T_{h22} cells	SMCs	• Stimulates SMC migration from the tunica media to the intima
MCP-1	Macrophages, ECs, neutrophils and fibroblasts	Monocytes/. macrophages	• Induces monocytes mobilisation from the bone marrow • Mediates monocyte and neutrophil recruitment during atherogenesis
Anti-inflammatory/anti-atherogenic			
IL-5	T_{h2} cells and mast cells	B cells	• Stimulates anti-oxLDL antibodies (IgM) production by B cells
IL-10	T_{regs} and M2 macrophages	T_{h1} cells, B cells and macrophages	• Suppresses the activation of T_{h1} cells and macrophages • Regulates TNF-α production and endothelial ICAM-1 expression • Contributes to the survival of B cells and antibody production

IL-33	Macrophages, ECs, dendritic cells and fibroblasts	T_{h2} cells, B cells and macrophages	• Upregulates the production of T_{h2} cytokines • Suppresses IFN-γ production • Attenuates foam cell formation • Reduces the expression of ICAM-1 and MCP-1
IL-35	T_{regs} and B cells	T_{regs} cells, T_{h2} cells, monocytes, ECs and SMCs	• Regulates the expression of anti-inflammatory molecules • Induces T_{regs} • Suppresses VCAM-1 expression
TGF-β	T_{regs} and M2 macrophages	T_{regs}, T_{h1} cells and T_{h2} cells	• Inhibits proliferation, activation and differentiation of T_{h1} and T_{h2} cells • Stimulates T_{regs} differentiation

Data in this table are described in (Tedgui and Mallat 2006; Ait-Oufella et al. 2011; Ramji and Davies 2015; Fatkhullina et al. 2016). **Abbreviations:** IL, interleukin; TNF, tumour necrosis factor; IFN, interferon; ICAM-1, intercellular adhesion molecule-1; VCAM-1; vascular cell adhesion molecule-1; MCP, monocyte chemotactic/chemoattractant protein; TGF, transforming growth factor; EC, endothelial cells; NK, natural killer; Th, helper T; Treg; regulatory T cell; SR, scavenger receptor; ox-LDL, oxidised low-density lipoprotein; ROS, reactive oxygen species; CRP, C-reactive protein; NLRP3; nucleotide-binding oligomerisation domain leucine-rich repeat and pyrin domain containing protein 3.

TNF-α and IL-1 signalling is mainly mediated by the nuclear factor kappa-light-chain-enhancer of activated B cells (NF-κB) pathway that regulates an array of genes involved in inflammatory responses, and affects most of the cells in atherogenesis by promoting the expression of other cytokines and adhesion molecules expression along with encouraging interactions between circulating leucocytes and dysfunctional ECs as well as the migration and mitogenesis of VSMCs and ECs (Tousoulis et al. 2016). Furthermore, IFN-γ and TNF-α are found to promote ECs hyperpermeability by inducing the reorganisation of the actin and tubulin cytoskeletons in ECs, thereby broadening gaps the between adjacent cells (Ramji and Davies 2015).

The activated ECs are capable of secreting various pro-inflammatory cytokines, including MCP-1, IL-1 and IL-8 which in turn induce the expression of adhesion molecules, such as ICAM-1 and VCAM-1, and thereby facilitate the recruitment of circulating immune cells and their binding to the endothelium (Li and Glass 2002). In addition to ICAM-1 and VCAM-1, platelet EC adhesion molecule-1 (PECAM-1) is highly expressed on platelets and ECs, especially at cell

junctions, and plays an additional role in facilitating the transmigration of monocytes across the endothelium and into the intima layer where they differentiate into macrophages by GM-CSF and M-CSF (Winneberger et al. 2021; Chan and Ramji 2022). A simplified illustration of monocyte recruitment is shown in Figure 1.3.

1.3.3 Heterogeneity of macrophages and VSMCs in atherosclerosis

Over the last decade, the heterogeneity of macrophages in atherosclerotic plaques has been discovered. Due to their heterogeneity and plasticity, macrophages can undergo metabolic reprogramming as a result of being exposed to various local signals and stimuli within the atherosclerotic microenvironment (Chan and Ramji 2022). Macrophages can be polarised into several phenotypes with two common being the pro-inflammatory (M1) phenotype (classically activated) or the anti-inflammatory (M2) phenotype (alternatively activated)(Orekhov et al. 2019). However, additional plaque-specific macrophage phenotypes have been recently identified (Figure 1.4). Each phenotype has distinct properties, surface markers, secreted cytokines and functions and can be generated by different extracellular signals. (Kong et al. 2022).

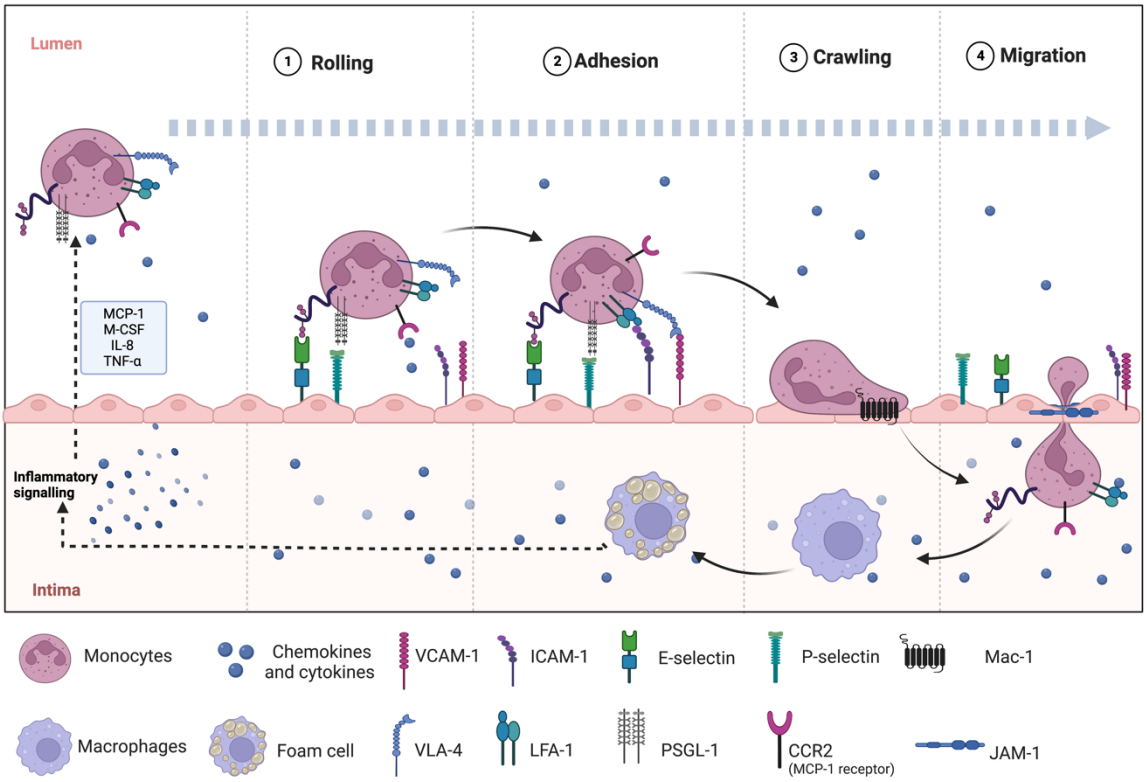

Figure 1.3 A schematic view of monocyte recruitment during atherosclerosis

CVDs risk factors along with the retention and aggregation of LDL in the intima induce endothelial dysfunction, resulting in increased ECs permeability as well as the release of various cytokines and chemokines including MCP-1, M-CSF, IL-8 and TNF-α along with the expression of a number of cell adhesion molecules, including ICAM-1 and VCAM-1. All of these factors contribute to facilitating the recruitment and migration of circulating leukocytes (e.g., monocytes and T cells). Circulating monocytes are attracted towards the inflammation sites (arterial wall) with the help of chemokines such as MCP-1. Initially, monocytes roll and adhere to adhesion molecules on the surface of activated ECs, including E-selectins and P-selectins via their receptors (1). This is followed by further binding to adhesion molecules ICAM-1 and VCAM-1 via LFA-1 and VLA-4 respectively that mediates firm adhesion (2). The monocytes then crawl (locomotion) on the endothelium to the nearest junction in a process mediated by ICAM1 and Mac-1 (3). Finally, JAMs mediate the transmigration of monocytes across the endothelium to the intima where they differentiate into macrophages (4). Macrophages uptake modified LDL and transform into lipid-laden foam cells, produce further chemokine and cytokines that subsequently sustain the recruitment of inflammatory cells. **Abbreviations:** MCP-1, monocyte chemotactic protein 1; M-CSF, macrophage colony stimulating factor; IL-8, interleukin 8; TNF-α, tumour necrosis factor alpha; ICAM1, intercellular adhesion molecule 1; VCAM1, vascular cell adhesion molecule 1; VLA-4, very late antigen-4; LFA-1, lymphocyte function-associated antigen-1; Mac-1, macrophage-1-antigen; JAM, junctional adhesion molecule. Image created with BioRender.com

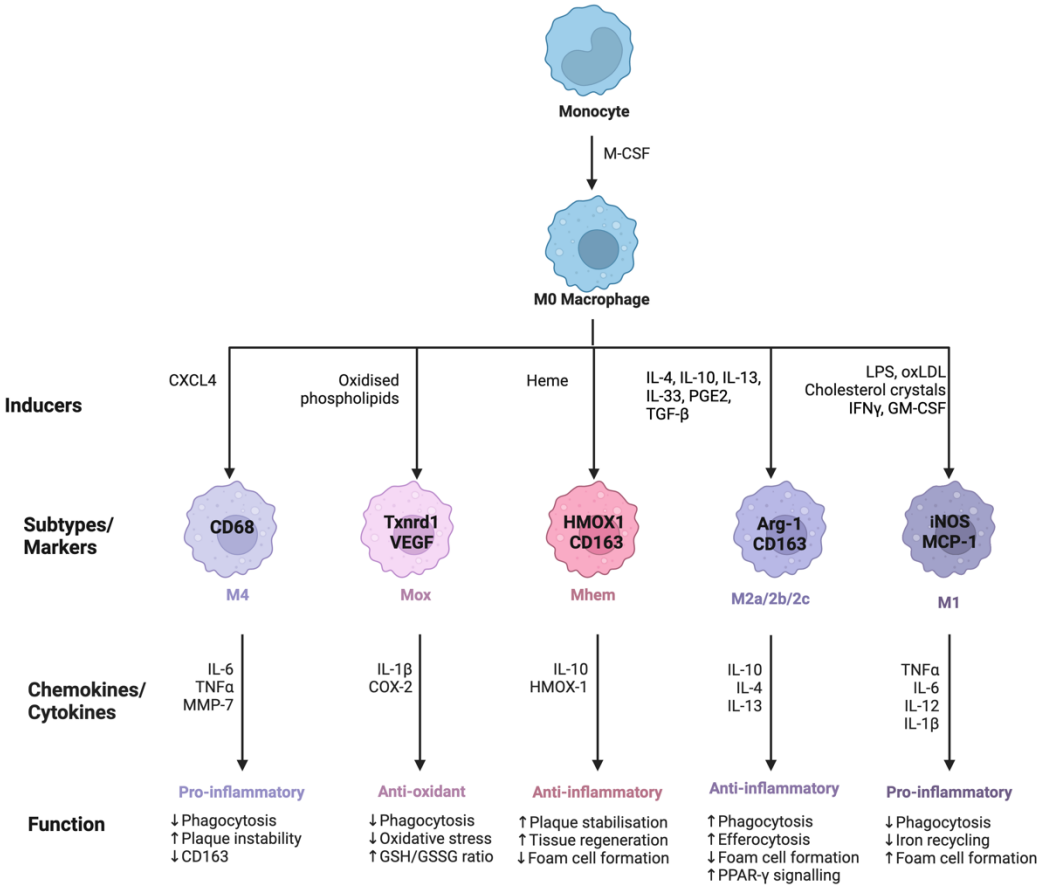

Figure 1.4 Macrophage polarised phenotypes in atherosclerotic plaques

Monocytes differentiate into M0 macrophages via M-CSF. They are then polarised to a particular subtype depending on local stimuli. The primary subtypes are M1 (pro-inflammatory) and M2 (anti-inflammatory) macrophages. However, multiple other subtypes have been identified including Mhem, Mox and M4. All of these subtypes have specific markers (shown in the middle of the cell), produce distinct chemokines and cytokines and have diverse roles in the atherosclerotic plaque. **Abbreviations:** M-CSF, macrophage colony-stimulating factor; LPS, lipopolysaccharide; ox-LDL, oxidised low-density lipoprotein; IFN- γ, interferon-gamma; GM-CSF, granulocyte-macrophage colony-stimulating factor; IL, interleukin; iNOS, inducible nitric oxide synthase; MCP-1, monocyte chemoattractant protein-1; Arg-1, Arginase 1; HMOX1, Heme oxygenase 1; *Txnrd1, t*hioredoxin reductase 1, VEGF, vascular endothelial growth factor; COX-2, Cyclooxygenase 2; TNF-α, tumour necrosis factor alpha; MMP-7, matrix metalloproteinases-7. Image adapted from BioRender template and created with BioRender.com.

Following the migration, monocytes differentiate into M1 macrophages in response to several stimuli, including IFN-γ, lipopolysaccharide (LPS) and GM-CSF, and contribute to the progression of atherosclerosis by producing pro-inflammatory cytokines and chemokines, including TNF-α, IL-1β, IL-6, IL-12 and MCP-1. These factors contribute together to induce the polarisation of naïve macrophages to M1 phenotype. The signal transducer and activator of transcription (STAT)-1 signalling, mediated by IFN-γ, along with NF-κB are the two major

pathways involved in M1 macrophage polarisation (Liu et al. 2014; Wang et al. 2014a; Yao et al. 2019; Yang et al. 2020). This phenotype of macrophages expresses pattern recognition receptors (PRRs), such as scavenger receptors (SRs), Toll-like receptors (TLRs) and nucleotide-binding oligomerisation domain (NOD)-like receptors (NLRs), that are implicated in foam cell formation and are responsible for inflammatory response stimulation against endogenous particles generated from damaged cells, termed damage-associated molecular patterns (DAMPs)(Takeuchi and Akira 2010). The cytokines generated by M1 macrophages induce further endothelial dysfunction by reducing eNOS and increasing oxidative stress by generation of ROS (Chan and Ramji 2022). Furthermore, M1 macrophages also contribute to T helper-1 (T_{h1}) responses (Mantovani et al. 2009). Interestingly, the large abundance of M1 macrophages within the plaque is believed to originate from local proliferation rather than from migrated monocytes that subsequently differentiate into macrophages (Groh et al. 2018; Chan and Ramji 2022). Many studies have shown that the local proliferation of macrophages contributes to the initiation and progression of atherosclerotic lesions, particularly advanced lesions (Sukhovershin et al. 2016; Yamada et al. 2018; Xu et al. 2019).

On the other hand, T_{h2}-type cytokines IL-4, IL-13 and M-CSF induce M2 macrophages, which possess athero-protective functions by releasing anti-inflammatory cytokines such as IL-10 and transforming growth factor- β (TGF-β) (Bai et al. 2017; Orekhov et al. 2019). Both M1 and M2 macrophages are present during the development of atherosclerotic lesions (Lee et al. 2018). However, the imbalance in the M1:M2 ratio plays a crucial role in plaque development where M1 macrophages represent the most abundant phenotype in plaque progression and M2 macrophage abundance is associated with plaque regression (Bobryshev et al. 2016; Lee et al. 2018).

More recently, VSMCs have been identified as a major cell type of atherosclerotic plaques that possesses substantially more heterogeneity in their morphology and gene expression than previously thought (Kong et al. 2022). VSMCs plasticity is driven by various local signals and stimuli from resident cells in the vessel. Most VSMCs in the arterial wall display a contractile phenotype to maintain vascular tone; however, under pathological conditions (as in atherosclerosis), they undergo a phenotypic switching process in which contractile VSMCs are transformed into an adverse proliferative synthetic phenotype (Petsophonsakul et al.

2019). The synthetic VSMCs are characterised by increased secretion of enzymes that mediate plaque rupture and facilitate further migration of these cells as well as contribute to local inflammation via secretion of extracellular vesicles (Petsophonsakul et al. 2019). Beside the synthetic phenotype, VSMCs transform into different phenotypes, such as pro-inflammatory macrophage-like phenotype, VSMCs-derived foam cells, mesenchymal stem cells and osteoblast cells (Figure 1.5)(Chan and Ramji 2022). The exposure of VSMCs to different stimuli such as cholesterol, oxidised phospholipids (oxPL) and platelet-derived growth factor (PDGF) stimulates their phenotypic transformation into macrophage-like cells under the regulation of Kruppel-like factor 4 (KLF-4) while exposure to ox-LDL induces foam-cell formation (Chistiakov et al. 2017; Cheng et al. 2021; Gui et al. 2022). However, the exact mechanisms underlying foam cell formation from VSMCs are not yet fully understood. The macrophage-like VSMCs act as nonprofessional phagocytes and contribute to chronic inflammation via the production of different cytokines, IL-1β, IL-8 and IL-6 and various adhesion and chemokine molecules. In addition, this phenotype expresses various SRs including LDL receptor-related protein 1 (LRP1), which enables the uptake of LDL and leads to foam cell formation (Sorokin et al. 2020). Recently, it has been found that about 40% of plaque macrophages are derived from VSMCs, which is the product of VSMCs phenotypic switching (Gui et al. 2022). Collectively, although the vast majority of foam cells arise from macrophages, a significant number (40% to 50%) are believed to be derived from VSMCs (Sun et al. 2016; Wang et al. 2019d; Ru et al. 2020).

1.3.4 Foam cell formation: a major hallmark of early-stage atherosclerotic lesions

1.3.4.1 Cholesterol uptake

After passing through ECs junctions, the trapped LDL particles are prone to numerous enzymatic and non-enzymatic modifications, such as glycation, aggregation or oxidation, by myeloperoxidases, lipoxygenases (LOX), ROS, peroxynitrite and NO (Bobryshev et al. 2016). The aggregated LDL (agLDL) can be internalised into macrophages via LRP1, phagocytosis or by patocytosis process, in which the agLDL particles sequestrate in the macrophages' surface-connected compartments and plasma membrane invaginations. These particles are digested by lysosomes and the products are secreted, leading to large accumulation of free (FC) and cholesterol esters (CE) in macrophages. Macrophages attempt to efflux the excess lipid;

however, over time this mechanism is rapidly overwhelmed, transforming macrophages into foam cells (Sanda et al. 2021). The oxidation of accumulated LDL within the intima is the most common modification process in which LDL undergoes progressive changes that ultimately results in ox-LDL formation (Sangle and Shen 2010; Bobryshev et al. 2016). This subsequently increases oxidative stress, triggers inflammatory cytokine production, reduces antioxidant enzymes activity and induces endothelial dysfunction (Sangle and Shen 2010).

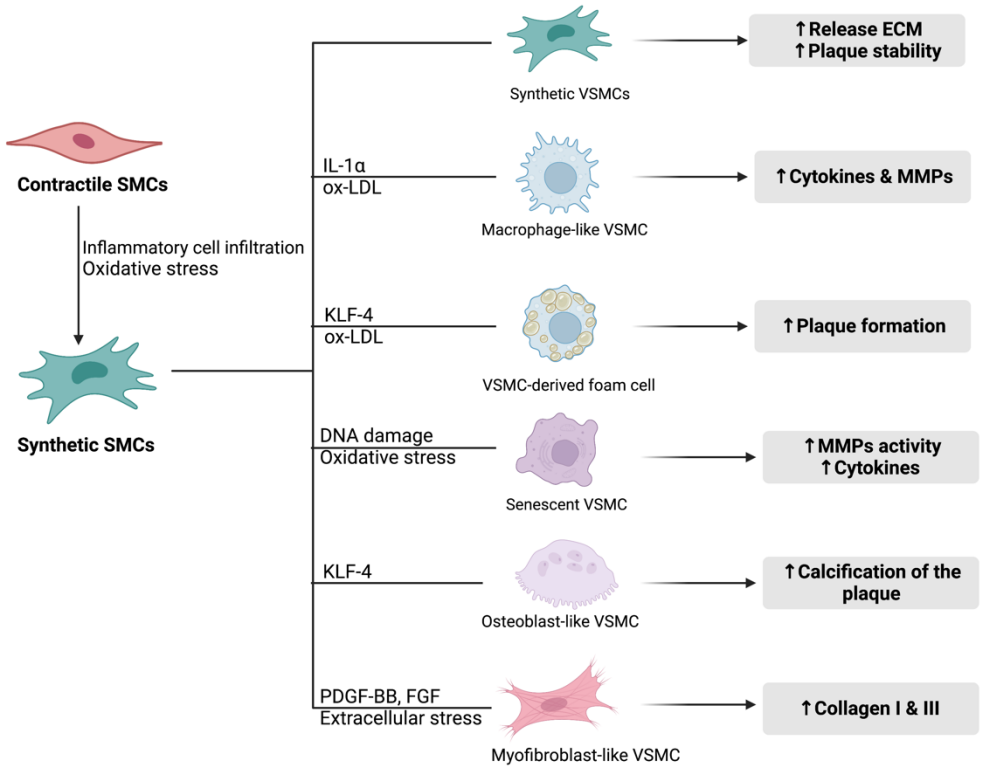

Figure 1.5 Vascular smooth muscle cell (VSMC) phenotypes and their role in atherosclerosis

VSMCs differentiate into a synthetic phenotype in response to inflammatory mediators. They are then transformed into different phenotypes depending on the local microenvironment. VSMCs with a macrophage-like phenotype act as inefficient non-professional phagocytes and contribute to inflammation via the secretion of chemokines, which attract circulating inflammatory cells. In addition, macrophage-like cells undergo diapedesis and mature into macrophages that uptake lipids and transform into foam cells. Myofibroblast-like and osteoblast-like cells play a role in promoting fibrous cap formation and calcification of plaque respectively. Finally, senescent VSMC exhibit susceptibility to apoptosis or undergo necroptosis, which contributes to the production of a pro-inflammatory environment. **Abbreviations:** SMC, smooth muscle cells; VSMC, vascular smooth muscle cells; ECM, extracellular matrix; IL, interleukin; ox-LDL, oxidised low-density lipoprotein; MMP, matrix metalloproteinase; KLF-4, Krüppel-like factor-4; PDGF, platelet-derived growth factor, FGF, Fibroblast growth factors. Image created with BioRender.com.

Indeed, trapped LDLs bind to proteoglycans, which then enhances their retention period, and thereby accumulation, leading to increased oxidation (Bobryshev et al. 2016; Kang et al. 2019). Minimally modified LDL (mmLDL) is not recognised by SRs, and hence cannot be taken up by macrophages and contribute to foam cell formation. However, it instigates endothelial dysfunction and triggers a chronic inflammatory response, resulting in the expression of several pro-inflammatory cytokines and chemokines, which mediate the recruitment of circulating monocytes and T-cells to the site of activation via PRRs such as TLR4. On contrary, fully/high oxidised LDL causes foam cell formation and subsequent inflammation (Bae et al. 2009; Wang and Butany 2017; Linton et al. 2019). The oxidation of LDL molecules leads to the formation of oxidation-specific neoepitopes (OSEs) which are present on ox-LDL and are capable of being recognised by PRRs such as macrophage SRs and proteins of the innate immune system such as CRP (Leibundgut et al. 2013; Binder et al. 2016). Furthermore, the presence and accumulation of modified LDL in the intima also promotes VSMC mitogenesis, necroptosis along with inflammation within the artery (Susser and Rayner 2022). Additionally, the ox-LDL particles bind to lectin-like ox-LDL receptor (LOX-1) on ECs, leading to the activation of cluster of differentiation (CD)40/CD40 ligand (CD40L) signalling. This signalling pathway encourages the production of chemokines and cell adhesion molecules by ECs, which promotes immune cell recruitment, adherence and infiltration (Zeya et al. 2016). Although T cells are not involved in foam cell formation, they participate in inflammatory responses via secretion of pro- or anti-inflammatory cytokines depending on their subsets. For example, T_{h1} cells produce cytokines such as IFN-γ, TNF-α and IL-2 which propagate inflammation, while T_{regs} secrete cytokines such as TGF-β and IL-10, which cause the resolution of inflammation (Ait-Oufella et al. 2011).

Besides ox-LDL uptake, macrophages are able to uptake native LDL via their LDL receptor (LDLR). Unlike SR-mediated uptake, this process is under a negative feedback mechanism which is strictly regulated by intracellular cholesterol levels (Zhang et al. 2016). Macrophages express a variety of SRs on their surfaces such as SR-A, SR- B, cluster of differentiation antigen 36 (CD36) and CD68 to uptake ox-LDL that subsequently triggers the release of IL-1β, TNF-α and other pro-inflammatory cytokines (Wu et al. 2017). In addition, the migrated VSMCs can adopt various phenotypes to contribute to foam cell formation as previously described in Section 1.3.3. Both Macrophages and VSMCs are able to uptake modified lipoproteins,

particularly ox-LDL via SR-mediated endocytosis, as well as macropinocytosis (receptor-independent endocytic pathway) or phagocytosis and transform into the characteristic lipid-laden foam cells (Wang et al. 2019a). However, among these mechanisms, SR-mediated endocytosis is often considered the main mechanism in foam cell formation. A significant amount of ox-LDL (75%-90%) is internalised into macrophages via SR-A and CD36, while LOX-1 is responsible for about 5%-10% of ox-LDL internalisation (Wang et al. 2019a; Xu et al. 2019).

Previous studies have shown that not only modified LDL, but also native LDL, can be taken up by macrophages via fluid-phase endocytosis (macropinocytosis and phagocytosis) that is mediated via phosphoinositide 3-kinase (PI3K), liver X receptors (LXRs), M-CSF, and protein kinase C activator, phorbol 12-myristate 13-acetate (PMA) (Kruth et al. 2005; Meyer et al. 2012). It has been also shown that internalisation via fluid-phase endocytosis contributes significantly to foam cell formation (Kruth et al. 2002; Michael et al. 2013; Ding et al. 2017a). Interestingly, the rapid and uncontrollable internalisation of ox-LDL into M2 macrophages induces their functional phenotype to shift towards a pro-inflammatory state and consequently triggers the release of pro-inflammatory cytokines. This shifting is attributed to a reduction in their expression of Kruppel-like factor 2 (KLF-2) (Stewart et al. 2010; Shirai et al. 2015). The excessive uptake of modified lipoproteins, particularly ox-LDL by macrophages along with decreased cholesterol efflux from foam cells leads to increased CE accumulation (Chistiakov et al. 2017). The accumulation of CE and ox-LDL within macrophages, along with lysosomal destabilisation and ROS activation, promotes inflammasome activation, by which NOD leucine-rich repeat and pyrin domain-containing protein 3 (NLRP3) inflammasome is activated and results in the cleavage and secretion of mature forms of IL-1β and IL-18, (Kelley et al. 2019).

1.3.4.2 Cholesterol efflux

The dysfunction in cholesterol efflux mechanisms “collaborate” with excessive ox-LDL uptake by macrophages resulting in the enhancement of foam cell formation and subsequent atherosclerosis (Chistiakov et al. 2016). Therefore, the balance between the three major mechanisms, involving lipid uptake, cholesterol esterification and cholesterol efflux is crucial in the regulation of foam cell formation. Every single mechanism is controlled by extracellular

factors such as cytokines via changes in the expression and/or activities of various enzymes, receptors and transporters (Wang et al. 2019a). Figure 1.6 shows the mechanism of cholesterol homeostasis and foam cell formation.

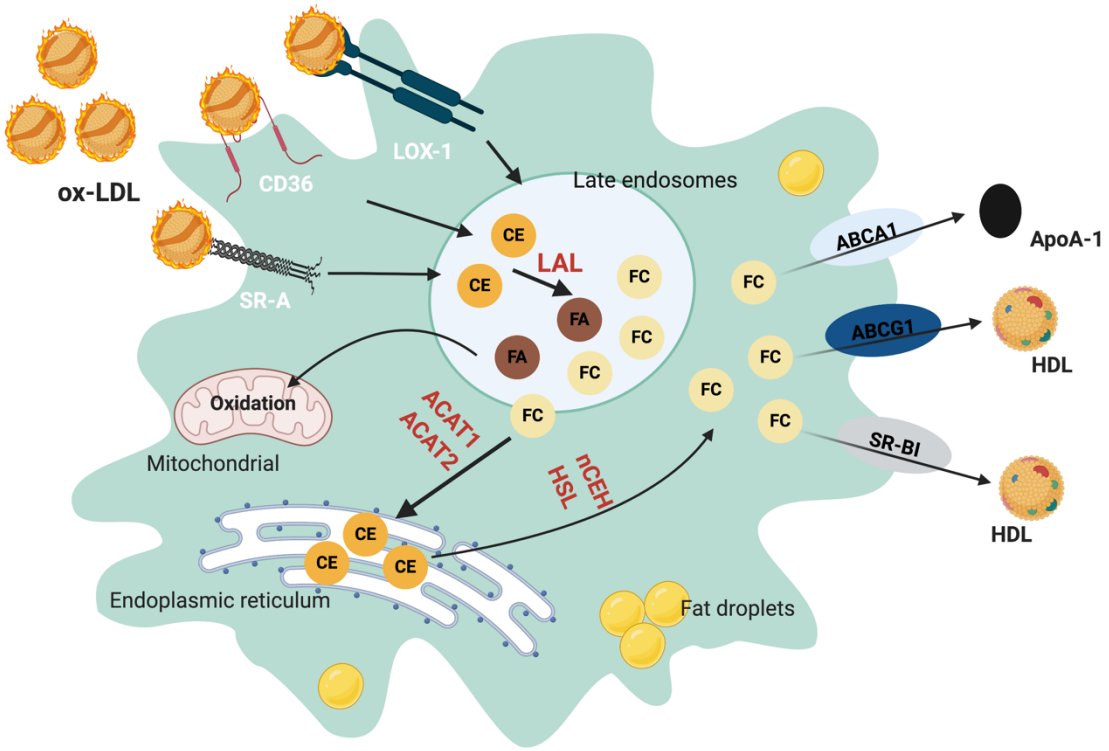

Figure 1.6 Macrophage foam cell formation.

Modified LDL particles, ox-LDL in particular, are taken up with the help of several SRs, including SR-A, CD36 and LOX-1, on the cell surface of differentiated macrophages. This process is unregulated that means that macrophages continuously uptake and accumulate modified LDL. The ox-LDL is internalised and transported to the late endosomes/lysosomes where the LAL hydrolyses the CE portion in LDL to FA and FC. The FA is transported to the mitochondria where they are oxidised to generate energy for the cell. On the other hand, FC is then either moved out of the cell through ABCA1 and ABCG1, as well as via SR-BI to ApoA1 or HDL, or delivered to the ER. In the ER, FC is esterified to CE via ACAT1/ ACAT2. CE is either stored as lipid droplets in the cytoplasm or digested to FC by NCEH and HSL, and then exported from the cell through ATP-binding cassette transporters. **Abbreviations:** LDL, low-density lipoprotein; ox-LDL, oxidised low-density lipoprotein; SRs, scavenger receptors; LOX-1, lectin-like ox-LDL receptor-; LAL, lysosomal acid lipase; CE, cholesterol ester; FA, free fatty acids; FC, free cholesterol; ABCA1/G1, ATP-binding cassette transporters A1/G1; SR-BI, scavenger receptor B; ApoA1, apolipoprotein A1; HDL, high-density lipoprotein; ER, endoplasmic reticulum; ACAT, acyl coenzyme A: cholesterol acyltransferase; NCEH, neutral cholesteryl ester hydrolases; HSL, hormone-sensitive lipase. Image created with BioRender.com.

Under normal conditions, cells protect against lipid overload via homeostatic mechanisms that induce cholesterol efflux and control the inflammatory response. This is carried out via several mechanisms such as conversion into a more transportable form or reverse cholesterol transport (RCT), the predominant pathway by which the excess cholesterol is removed from peripheral tissues and transported to the liver, where it may be reused there or by other organs, or excreted as bile through the gallbladder (Marques et al. 2018b). An overview of RCT is shown in Figure 1.7. The cholesterol derivatives and intermediate precursors such as oxysterols and desmosterol respectively can activate LXRs, resulting in increased expression of lipid efflux transporters, facilitating cholesterol transport from peripheral cells to extracellular acceptors via RCT. Additionally, the intracellular cholesterol pools within macrophages trigger autophagy, in which intracellular lipid contents are sequestered in autophagosome that is characterised by double-membrane vesicles. This autophagosome is then fused with the lysosome for CE degradation and the intracellular FC is then subjected to RCT (Robichaud et al. 2021; Gui et al. 2022). In RCT, macrophages efflux the excess intracellular FC out of the cell to HDL via hepatic transporters such as ATP binding cassette transporter (ABC) A1 or ABCG1 (Khera and Rader 2010; Phillips 2014). Both ABCA1 and ABCG1 are located at the plasma membrane and in intracellular compartments, cycling between these locations and facilitating a flow of intracellular cholesterol to the plasma membrane (Favari et al. 2015). Indeed, ABCA1 promotes efflux to lipid-poor ApoA-I (nascent HDL) while ABCG1 is responsible for efflux to mature HDL particles (Gui et al. 2022). The lipidation and maturation of HDL in the plasma are followed by hepatic uptake, where SR-B1 on hepatocyte binds to the mature HDL, and subsequent cholesterol removal via catabolism and excretion. Besides SR-B1, hepatocytes express LDLRs that endocytose LDL and thus remove LDL from the plasma (Trigatti et al. 2000a; Trigatti et al. 2000b).

In addition to ApoA-I and HDL, the endogenous production of apolipoprotein E (ApoE) is shown to play a crucial role in mediating cholesterol efflux. ApoE is synthesised mainly by hepatocytes; however, 5-10% of ApoE in the plasma is produced and secreted by macrophages in response to stimuli such as cytokines and lipid enrichment, and acts as a mediator for cholesterol efflux either from the macrophage that originally secreted it (autocrine effect) or from surrounding macrophages (paracrine effect)(Dove et al. 2005; Linton et al. 2019).

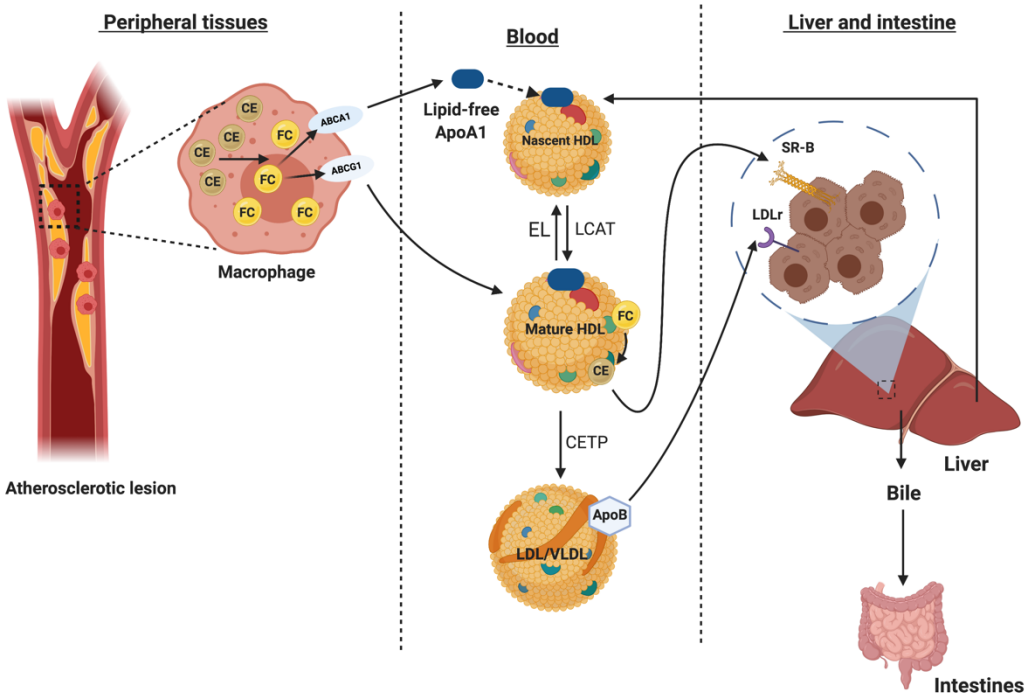

Figure 1.7 Pathway of reverse cholesterol transport (RCT)

RCT begins with FC that is removed from arterial macrophage foam cells. This step is considered as the rate-limiting step of RCT pathway that requires cholesterol efflux to FC acceptors such as nascent or mature HDL. Both the liver and the intestine produce lipid-poor ApoA-I and secrete it into the plasma. This lipid-poor ApoA-I promotes cholesterol efflux from macrophages via ABCA1/ABCG1. In the bloodstream, these particles bind with FC to form nascent HDL. In the presence of LCAT, the FC is esterified to CE on the surface of HDL particles, and as a result mature HDL is formed. These mature HDL particles act as an additional acceptor of cholesterol that efflux from macrophages. Cholesterol can then be transported to the liver either directly or indirectly. In the direct pathway, mature HDL transfers its cholesterol content via interaction with SR-B1 in the liver. The resulting HDL molecule starts re-circulation and repeats the RCT process. Alternatively, in an indirect way, CETP catalyses the transfer of cholesterol from mature HDL to Apo B-100 containing lipoproteins such as VLDL or LDL. These lipoproteins bind to their cognate receptors on hepatocytes and transfer their cholesterol content. Finally, cholesterol is excreted via bile in faeces. **Abbreviations:** FC, free cholesterol; HDL, high-density lipoprotein; ApoA-I, apolipoprotein A-I; ABCA1/G1, ATP-binding cassette transporters A1/G1; LCAT, lecithin cholesterol acyltransferase; CE, cholesterol ester; SR-B1, scavenger receptor B1; CETP, cholesteryl ester transfer protein; AopB-100, apolipoproteins B-100; VLDL, very low-density lipoprotein; LDL, low-density lipoprotein; Image created with BioRender.com.

Additionally, ApoE acts as a ligand for lipoprotein receptors, particularly those involved in the clearance of ApoB-containing chylomicrons and very low-density lipoproteins (VLDL) from the plasma and thus reducing plasma lipid levels (Getz and Reardon 2018). Many studies *in vivo* have found that ApoE knockout mice (ApoE$^{-/-}$) are associated with hypercholesterolemia and spontaneous atherosclerosis (Burnett et al. 2001; Lo Sasso et al. 2016; Oppi et al. 2019) while re-expression of the protein leads to a reduction in atherosclerotic lesions (Greenow et al. 2005). Bone marrow transplantation of wild-type mice into ApoE$^{-/-}$ mice showed

normalisation of plasma cholesterol concentration, promotion of lipoprotein elimination and protection from the adverse effects of a high-fat diet (HFD) (Davignon 2005). Therefore, both LDLR and ApoE are fundamental for circulating LDL-C clearance and maintaining cholesterol homeostasis, and hence are widely used as animal models in atherosclerosis studies (Olszanecki et al. 2005; Lo Sasso et al. 2016; Chen et al. 2022; Gisterå et al. 2022).

1.3.5 Necrotic core formation and an advanced lesion progression

After a while, foam cells undergo various pathways of cell death programmes, including apoptosis, autophagy, necroptosis and pyroptosis due to insufficient availability of needed nutrients in the surrounding medium, the toxic effects of intracellular cholesterol as well as a combination of other factors and processes such as oxidative stress, and the activation of death receptors by ligands that already exist in advanced plaques (McLaren et al. 2011; Moore and Tabas 2011b; Gui et al. 2022). In early atherosclerotic lesions, the efficient and rapid efferocytosis mechanism of apoptotic foam cells contributes to diminished inflammatory response and disease progression (Tajbakhsh et al. 2020). However, in advanced atherosclerotic lesions, impaired elimination of apoptotic macrophages due to defective efferocytosis encourages proinflammatory cytokine release from various cells that subsequently form a necrotic environment, enhancing cellular dysfunction and continued pro-inflammatory signalling. As a result, the necrotic core, a pocket of dead macrophages, intracellular debris and modified lipids, is formed (Tajbakhsh et al. 2020; Susser and Rayner 2022). This creates a negative loop as activated immune cells and pro-inflammatory signalling can impair cholesterol efflux from cells, increasing the formation and accumulation of foam cells, and their eventual death aggravates inflammation and stimulates pro-atherogenic processes (Tall and Yvan-Charvet 2015). For instance, IFN-γ that is produced by T_{h1} cells can inhibit the activation of LXR signalling, consequently inhibiting cholesterol efflux and stimulating cholesterol accumulation. Furthermore, the apoptotic cells undergo secondary necrosis and release DAMPs that act as endogenous signals to activate the innate immune system via interaction with PRRs (Roh and Sohn 2018; Bäck et al. 2019). At this stage of disease progression, the accumulation of apoptotic macrophages/VSMCs-derived foam cells, cellular debris and cholesterol as well as an inflammatory environment within the artery facilitates the progression towards fibroatheromas, a necrotic core encapsulated with a

fibrous cap (Otsuka et al. 2015). In addition to inflammatory signals released by apoptotic cells, resident foam cells and ECs release various cytokines, PDGF and fibroblast growth factor (FGF)-2 as well as matrix metalloproteinase (MMPs) that induce VSMCs proliferation and migration from the tunica media into the arterial intima (Rudijanto 2007). Intimal VSMCs undergo a phenotypic shift from a quiescent state and contractile function to a synthetic state, contributing to plaque stability by the formation of fibrous cap via secretion of extracellular matrix (ECM) proteins such as elastin and collagen where they accumulate between the endothelium and the necrotic core, protecting from blood in the lumen (Rohwedder et al. 2012; Björkegren and Lusis 2022). The plaque stability theory is supported by a recently multi-coloured VSMC lineage-tracing study in $ApoE^{-/-}$ mice that demonstrated that in the early stages of atherosclerosis, the necrotic core, as well as the fibrous cap, consists of an average of 70% VSMC-derived cells (Checkouri et al. 2021). The stable plaque is characterised by a thick fibrous cap with high levels of α-smooth muscle actin $(\alpha SMA)^{+}$, smooth muscle myosin heavy chain (SM-MHC, encoded by the *Myh11* gene) and collagen type I and III (Libby 2021; Susser and Rayner 2022). Therefore, it can be clearly seen that VSMCs can mediate negative and positive effects in regulating plaque progression and remodelling, depending on their phenotypic switching.

1.3.6 Plaque rupture

In the late stages of atherosclerosis, the stable plaque is transitioned to an unstable plaque (vulnerable plaque) that is characterised by a large lipid-rich necrotic core covered by a thin inflamed fibrous cap rich in monocytes, macrophages and T-lymphocytes (Libby 2021; Chan and Ramji 2022). The inflammatory cytokines within the necrotic core along with ROS stimulate macrophages and other resident cells (e.g. ECs and VSMCs) to secrete MMPs and other proteases that degrade ECM protein components of the fibrous cap, increasing plaque destabilisation and vulnerability and eventually rupture (Olejarz et al. 2020; Chan and Ramji 2022). The degradation and thinning of the fibrous cap are also orchestrated by inhibited expression of endogenous tissue inhibitors of MMPs (TIMPs) which attenuate VSMCs proliferation and promote their apoptosis (Chan and Ramji 2022). Furthermore, cell senescence is found to play a fundamental role in atherosclerosis, particularly plaque instability. For example, senescent VSMCs contribute to plaque instability and vascular

calcification via the regulation of expression of several genes such as osteopontin (*Opn*), mediating inflammation and ECM degradation (Wu et al. 2021a; Huang et al. 2022). VSMCs senescence in atherosclerosis is likely to be induced by multiple stimuli such as replicative exhaustion of the cellular lifespan as well as a result of external stress-induced premature senescence such as DNA-damaging agents and/or oxidative stress (Grootaert et al. 2018). It is noteworthy that some authors have proposed the role of calcification in contributing to plaque rupture. However, this relationship remains uncertain as other pieces of the literature demonstrated that calcification may protect against plaque rupture (Fishbein 2010; Björkegren and Lusis 2022). All of the factors detailed above collaborate to indue plaque weakening and degradation of the fibrous cap, leading to plaque instability and rupture. Indeed, the thinnest spot in the fibrous cap that contains fewer VSMCs and collagen content is more prone to rupture (Bentzon et al. 2014). Once lipid-rich necrotic core contents are released, a series of thrombotic reactions are activated. The coagulation proteins circulate in the plasma in an inactive form that are converted into an active form; and interact with plaque contents, resulting in platelet activation/adhesion and aggregation and subsequently thrombosis (Badimon and Vilahur 2014). Platelet aggregation causes impaired blood flow that can lead to low oxygen supply to vital organs such as the heart and consequently MI or stroke (Schrottmaier et al. 2020). Moreover, there is evidence indicating that fibrous cap rupture is not the only mechanism that could contribute to thrombosis as superficial erosion is found to be another possible mechanism (Luo et al. 2021). The plaque erosion is characterised by a discontinuity in the intimal ECs monolayer that lacks fibrous cap rupture and a necrotic core. Neutrophils play a key role in erosion via the secretion of neutrophil extracellular traps (NETs) that can boost EC stress and induce apoptosis and endothelial monolayer denudation (Partida et al. 2018). Thrombosis due to superficial erosion is dramatically different from those associated with fibrous cap rupture and is illustrated in Figure 1.8. A diagrammatic overview of the key processes involved in atherosclerosis pathogenesis is shown in Figure 1.9.

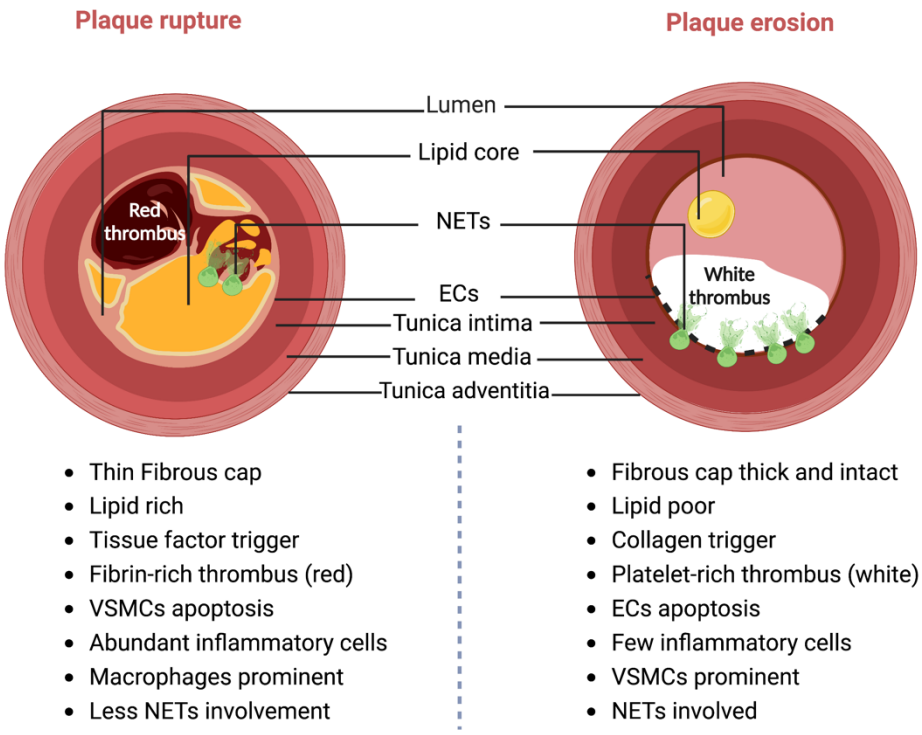

Figure 1.8 Contrasts between fibrous cap rupture and superficial erosion as causes of arterial thrombosis.

This diagram illustrates cross-sections of coronary arteries. The image on the left represents thrombosis due to plaque rupture along with plaque characteristics underneath. The right side of this illustration depicts thrombosis due to plaque erosion along with plaque characteristics underneath. **Abbreviations:** NETs, Neutrophil extracellular traps; ECs, endothelial cells. Image created with BioRender.com

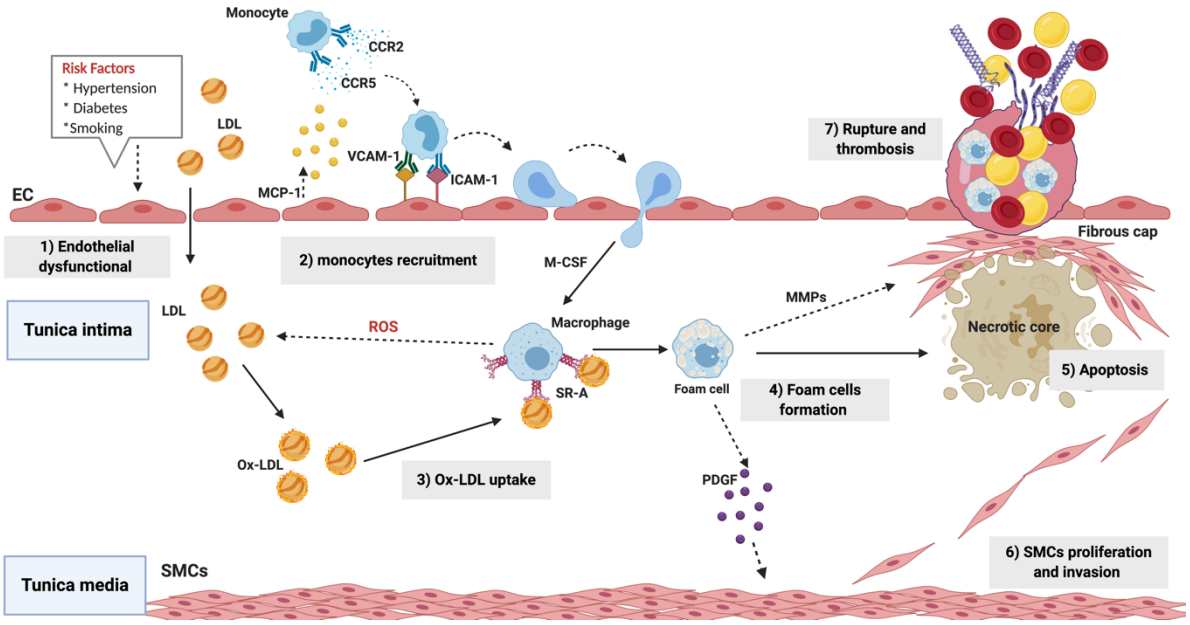

Figure 1.9 Overview of atherosclerosis disease development

CVDs risk factors such as diabetes, hypertension, smoking etc collaborate to trigger EC dysfunction resulting in increased endothelial membrane permeability. The activated ECs express a range of cell adhesion molecules, cytokines and chemokines, such as MCP-1, M-CSF, IL-8 and TNF-α, that facilitate recruitment and *trans*-endothelial diapedesis of circulating leukocytes. **2.** Monocytes are recruited to the site of inflammation (intima) through the adherence and rolling process in which monocytes roll and adhere to adhesion molecules on ECs such as E-selectins and P-selectins. This is followed by further binding to ICAM1 and VCAM1 to mediate firm adhesion. Then, monocytes undergo crawling to the nearest junction and migrate across the endothelium into the intima where they differentiate into macrophages by the action of M-CSF. **3.** As a result of increased endothelium permeability, LDL particles passively diffuse between cells junction and are retained in the subendothelial space where they are oxidised by ROS. In addition to passive diffusion, SR-B1 in ECs also promotes further LDL particles transport to the intima via transcytosis. Macrophages then uptake modified LDL via their SR-A and CD36 together with other processes such as macropinocytosis. **4.** This process occurs in an unregulated manner that coupled with ineffective efflux of cholesterol causes transformation of macrophages into lipid-laden foam cells. **5.** Foam cells undergo apoptosis and necrosis due to lack of nutrients and toxic effects of intracellular cholesterol accumulation that then causes release of their lipid contents into the surrounding environment. This leads to accumulation of lipids in the intima and formation of lipid-rich necrotic core. **6.** Foam cells release several cytokines and growth factors, such PDGF and FGF-2, that stimulate VSMCs proliferation and migration from tunica media into tunica intima. VSMCs secrete elastin and collagen that cover the necrotic core to form a fibrous cap. **7.** In advance plaques, apoptotic VSMCs and apoptotic foam cells release MMPs enzymes together with other proteases that lead to degradation of ECM components, including collagens and elastins, and subsequently plaque rupture. Once ruptured, the plaque contents are released into the lumen resulting in thrombosis. **Abbreviations:** ECs, endothelial cells; MCP-1, monocyte chemotactic protein 1; M-CSF, macrophage-colony stimulating factor; IL-8, interleukin 8; TNF-α, tumour necrosis factor alpha; ICAM1, intercellular adhesion molecule 1; VCAM1, vascular cell adhesion molecule 1; PDGF, platelet-derived growth factor; FGF-2, fibroblast growth factor-2; VSMCs, vascular smooth muscle cells; ECM, extracellular matrix; MMPs, matrix metalloproteinase. Image created with BioRender.com.

1.4 Non-alcoholic fatty liver disease and atherosclerosis

Non-alcoholic fatty liver disease (NAFLD) represents a spectrum of liver diseases ranging from hepatic steatosis through steatohepatitis (NASH) to fibrosis and irreversible cirrhosis and hepatocellular carcinoma (Guo et al. 2021)(Figure 1.10). It is characterised by lipid accumulation (steatosis) in > 5% of hepatocytes in the absence of excessive alcohol intake (Balta 2022). The global prevalence of NAFLD has increased over the last 11 years from 17.2%

to 32.4% (Riazi et al. 2022; Tang et al. 2022). Although 10% to 25% of NAFLD patients develop NASH, which can progress to cirrhosis, hepatocellular carcinoma, and eventually liver failure, the major cause of death in NAFLD patients is CVDs with a prevalence of at least 40% of total deaths in NAFLD (Przybyszewski et al. 2021; Duell et al. 2022). The precise causal mechanisms underlying the association between NAFLD and CVD are not fully understood; however, the coexistence of NAFLD and CVDs is attributed to overlapping risk factors, including hypertension, dyslipidemia, insulin resistance and abdominal obesity (Balta 2022). Moreover, a growing body of clinical evidences indicate that NAFLD is independently associated with CVDs and atherosclerosis progression; it has been found that NAFLD patients suffer from increased carotid intima media thickness (cIMT), impaired endothelial flow-mediated dilation (FMD) and increased prevalence of carotid atherosclerotic plaques (Balta 2022). Indeed, it hypothesised that NAFLD is not only a marker of CVDs, but may also contribute to the inflammatory CVD milieu and accelerate atherosclerosis progression by inducing oxidative stress, lipid peroxidation, inflammation, and fluctuation of adipokines such as TNFα, IL-6 and CRP (Xu et al. 2015). All of these markers orchestrate to induce arterial wall inflammation and plaque vulnerability (Kasper et al. 2021).

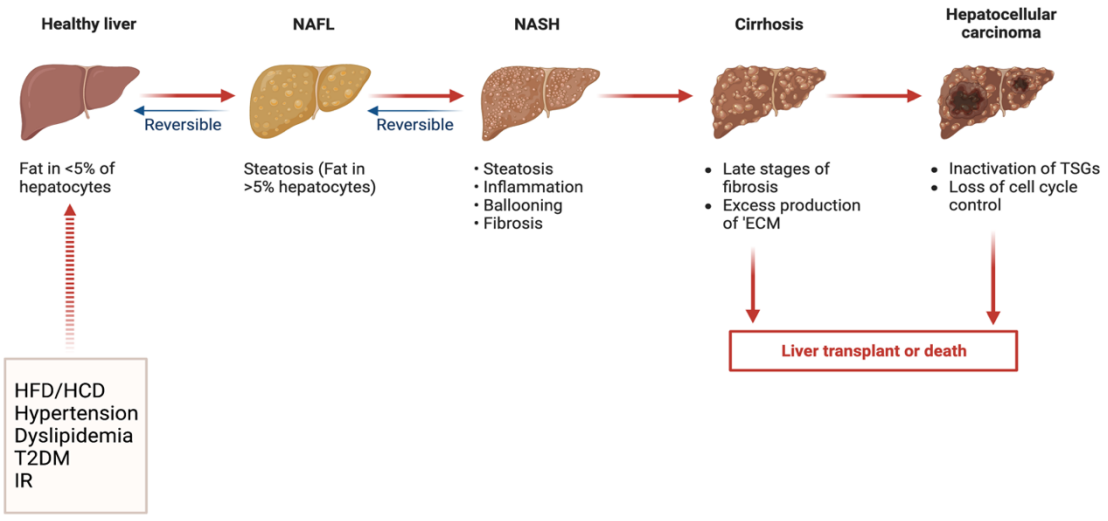

Figure 1.10 Schematic of progression of NAFLD

Abbreviations: NAFL, non-alcoholic fatty liver; NASH, non-alcoholic steatohepatitis; TSGs, tumour suppressor genes; HFD/HCD, high fat diet/high cholesterol diet; T2DM, Type 2 diabetes mellitus; IR, insulin resistance. Image adapted from BioRender template and created with BioRender.com

The atherogenic role of liver inflammation is confirmed by the fact that NASH patients have increased atherosclerosis compared to those with simple steatosis (Xu et al. 2015). NASH patients showed elevated plasma and hepatocyte expression levels of IL-6 and were found to be associated with the prevalence and severity of atherosclerosis (Simon et al. 2018; Fontes-Cal et al. 2021). Indeed, IL-6 induces macrophages to secrete MMPs, MMP-1 in particular, that plays a role in liver fibrosis and degradation of the fibrous cap, eventually causing plaque rupture. In addition to MMP, IL-6 induces mononuclear cells (MNCs) that participate in plaque formation, promote LDLR synthesis and cause influx of LDL into macrophages (Xu et al. 2015). The interplay between NAFLD and atherosclerotic is presented in Figure 1.11.

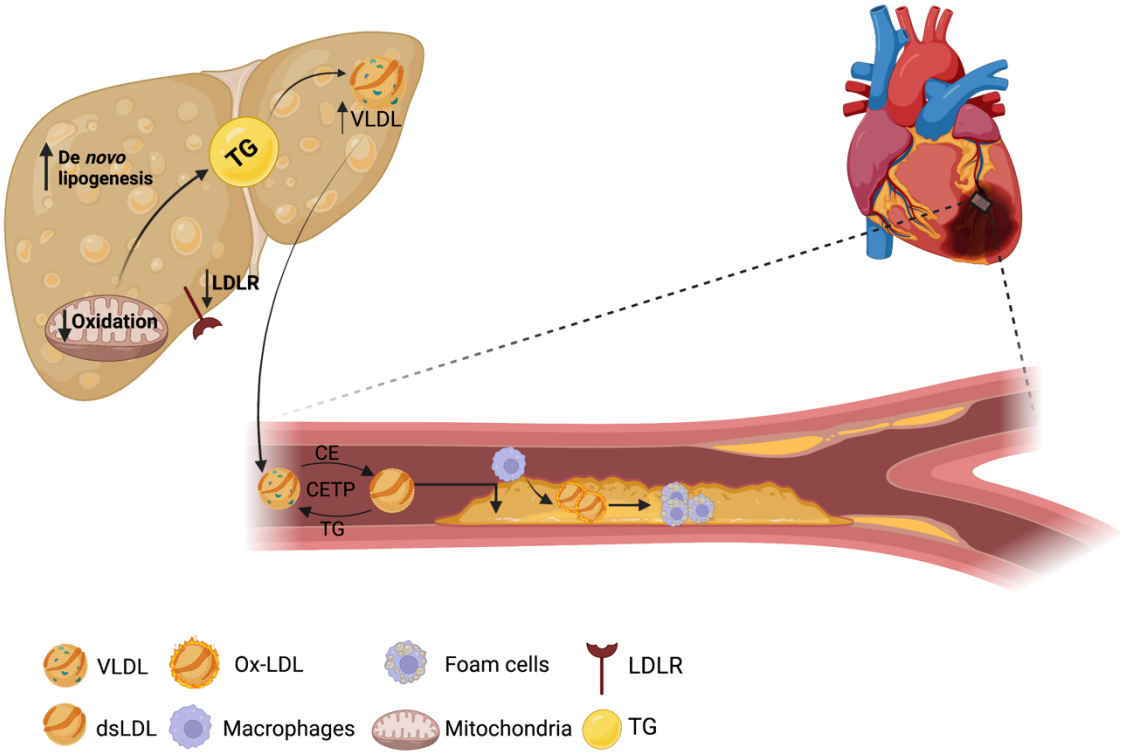

Figure 1.11 The interplay between NAFLD and atherosclerosis

During the development of NAFLD, increased production of TG in the liver leads to increased production and secretion of large TG-laden VLDL particles from the liver into the bloodstream. This is combined with a reduction in LDLR that facilitate TG-laden VLDL particles to undergo slow metabolism in the circulation as well as undergo CETP-mediated exchange process. In the exchange process, CE from the particles is replaced by TG between VLDL and LDL particles, resulting in sdLDL particles formation. These sdLDL particles have low affinity to LDLR, and hence cannot be recycled back to the liver. Instead, sdLDL particles migrate into the arterial wall due to its small size and are subjected to oxidation, leading to lipid-laden formation. **Abbreviations:** TG, triacylglycerol; LDLR, low density lipoprotein receptor; VLDL, very low density lipoprotein; sdLDL, small dense density lipoprotein; Ox-LDL, oxidised low density lipoprotein; CE, cholesterol ester; CETP, cholesteryl ester transfer protein. Image created with BioRender.com

1.5 Current and emerging pharmacotherapies for the treatment of atherosclerosis: options available

1.5.1 Statins and other strategies targeted to reduce LDL-C

Pharmaceutical medications are required when changes in lifestyle and diet together with increased physical activity and cessation of smoking are not sufficient to reduce CVDs risk. Lipid-lowering medication remains the gold standard for the management of atherosclerosis in addition to healthy lifestyles. The 3-hydroxy-3-methyl–glutaryl-coenzyme A (HMG-CoA) reductase inhibitors, known as statins, are the current and mainstay globally used cardiovascular medication. They are successful in combating hyperlipidaemia with a very good safety profile and low-cost (Bergheanu et al. 2017). They lower LDL-C levels by inhibiting HMG-CoA reductase activity, which leads to attenuation in the conversion of HMG-CoA to mevalonate, a key step in cholesterol biosynthesis. A consequence of this action is the stimulation of the expression of LDLR on hepatocytes surface because of reduced intracellular cholesterol levels, which causes increased uptake of LDL-C from blood and consequently decreased plasma concentration of LDL-C and apoB-containing lipoproteins, including TG-rich particles (Bergheanu et al. 2017; Kansu and Lang 2017). In addition, statins have pleiotropic effects such as anti-inflammatory activities (reducing TNFα, IL-1 and IL-6 in the plasma along with oxidative stress), reducing platelet activity and VSMCs proliferation, and improving endothelial cell dysfunction (Davignon and Ganz 2004; Pinal-Fernandez et al. 2018; Nasr and Huang 2021). Notwithstanding the unquestionable benefits of statins, they also cause some potential side effects such as liver and muscle diseases (Table 1.3).

In the light of side effects and limitations of statins, non-statin alternatives are imperative to reduce the risk of CVDs. Several statin co-therapies with non-statin agents have been developed recently. Ezetimibe has emerged as a potent complement to statins in decreasing LDL and lowering CVD risk during the last decade. It works by attenuating the absorption of cholesterol in the small intestine through binding to cholesterol transport protein Niemann Pick C1-like 1 protein (NPC1L1P) and inhibiting its functions (Pradhan et al. 2020). It is often prescribed alongside statins because they work in a different manner, so their combined effects add up to decrease cholesterol even more. Thus, previous studies demonstrated that the administration of ezetimibe alone can lower circulating plasma cholesterol in humans by

15-20%; however, the combination of ezetimibe and statins results in additive effects on LDL-C reduction (Garcia-Calvo et al. 2005). IMPROVE-IT (Improved Reduction of Outcomes: Vytorin Efficacy International Trial) and recent comparative meta-analysis reported that statin-ezetimibe co-therapy was more efficacious than statin monotherapy in lowering the risk of CVDs (Cannon et al. 2015; Miao et al. 2019; Pradhan et al. 2020). The limitations associated with ezetimibe are summarised in Table 1.3. Bempedoic acid is a new and the only approved inhibitor of adenosine triphosphate-citrate lyase (ACL) that has been combined with ezetimibe to successfully lower LDL-C and CRP (Brandts and Ray 2020). It works in a similar way to statins by targeting the cholesterol-synthesis pathway, resulting in a safe (not associated with adverse side effects) and effective reduction in LDL-C. Recently, the FDA has approved the use of bempedoic acid and its fixed-dose combination preparation with ezetimibe. However, additional clinical trials are required to confirm whether this fixed-dose combination can reduce cardiovascular risk (Brandts and Ray 2020).

In addition to the aforementioned medications, bile acid sequestrants (BASs), including cholestyramine, colestipol or colesevelam, have emerged as lipid-lowering agents that can be used in combination with statins or as a monotherapy (Lent-Schochet and Jialal 2019). BASs bind to bile acids, which contain cholesterol, in the intestine and form an insoluble complex that inhibits lipid solubilising activity and thus blocks cholesterol absorption and enhances lipid excretion in the faeces. They also reduce bile acid reabsorption (which is generally 95%), causing a reduction of the bile acid pool. In response to bile acid deficiency in the body, the liver produces more bile acids from cholesterol and as a consequence decreases plasma cholesterol levels. Cholesterol depletion enhances LDLR expression, which promotes LDL-C removal from the bloodstream (Mazidi et al. 2017). However, their side effects (summarised in Table 1.3) along with their interactions with other commonly prescribed medicines (e.g., Warfarin, anticoagulant and Digoxin, treatment for heart failure (HF)) restrict their usage (Brown et al. 2010; Lent-Schochet and Jialal 2019).

Proprotein convertase subtilisin/kexin type 9 (PCSK9)-inhibitors have also shown potential as efficient lipid-lowering agents. PCSK9 is a serine protease that is mainly secreted by the liver, as an inactive enzyme and is involved in cholesterol homeostasis. However, the actived PCSK9 binds to hepatic LDLR and induces their intracellular degradation. The inhibition of PCSK9

leads to the prevention of LDLR degradation and hence enhances LDL-C particle uptake by the liver, which consequently results in the lowering of plasma LDL-C levels (Liberale et al. 2017). Monoclonal antibodies targeting PCSK9, namely evolocumab and alirocumab, and small interfering RNA (inclisiran) have been used to inhibit PCSK9 function. Inclisiran is presently being studied in a large-scale clinical trial as part of the ongoing 'ORION' project to determine its safety and efficacy on cardiovascular outcomes (Stoekenbroek et al. 2018). Despite the fact that these strategies have shown efficacy in lowering plasma LDL-C levels and thus managing cardiovascular risk with a favourable safety profile and a low rate of adverse effects in various clinical trials, current prescription of PCSK9 inhibitors (evolocumab and alirocumab) is restricted to high-risk patients such as familial hypercholesterolemia (FH) due to their high costs and due to the requirement of repeated subcutaneous injection on a regular basis (Gürgöze et al. 2019; Chan and Ramji 2022).

1.5.2 Strategies targeted to elevate HDL-C

A range of alternatives to LDL-C lowering therapies have emerged such as HDL-C elevating agents and anti-inflammatory agents. Although there is a strong inverse correlation between high levels of HDL-C and CVDs, several studies on strategies that raise HDL levels, such as CETP inhibitors and niacin, have shown conflicting results in reducing CVDs mortality (Schmidt et al. 2021). None of the four CETP inhibitors, torcetrapib, dalcetrapib, evacetrapib and anacetrapib, that entered phase III cardiovascular outcome trials received FDA approval yet (Schmidt et al. 2021). The large clinical trials on the CETP inhibitor torcetrapib were found to increase HDL-C but also increase the risk of mortality from CVDs (Eyvazian and Frishman 2017; Tall and Rader 2018). As a result, the trials were terminated early due to increased risk to patients. Furthermore, in a phase III trial, dalcetrapib enhanced HDL-C concentrations but without a reduction of CVDs events while evacetrapib reduced LDL-C and increased HDL-C with no significant effect on CVDs events compared to placebo. Accordingly, subsequent trials on CETP inhibitors dalcetrapib and evacetrapib were terminated in the early stages due to a lack of efficacy in reducing CVDs events. (Tall and Rader 2018; Riggs and Rohatgi 2019). However, Randomized Evaluation of the Effects of Anacetrapib through Lipid modification (REVEAL) trials showed that anacetrapib is the only CETP inhibitor that can significantly diminish CVDs events when administrated in combination with statins but with no effect on

CVDs mortality (Filippatos et al. 2017; Group 2017; Tall and Rader 2018). Despite positive results, the pharmaceutical company has decided not to seek for approval for anacetrapib claiming that the outcome data was not strong enough. This trail was by far the largest and longest ever conducted using a CETP inhibitor and when compared to placebo, anacetrapib showed a moderate 9% reduction in the risk of major coronary events (Taylor 2017). Niacin (Nicotinic acid) has been shown to lower LDL-C and triglyceride levels while increasing HDL-C levels. According to one research, niacin can raise HDL levels by 25% to 35% (Farrer 2018). Although niacin was able to raise HDL-C levels and lower LDL-C levels, other research has revealed that niacin is ineffective. In a large randomised clinical trial, Treatment of HDL to Reduce the Incidence of Vascular Events (HPS2-THRIVE), niacin therapy was found to significantly reduce CVDs mortality or events but was also associated with serious adverse effects (Table 1.3) (McCarthy 2014; Farrer 2018). In a systematic review and meta-analysis published in 2019, only 17 out of 119 clinical trials showed niacin's effect on CVDs outcome and did not demonstrate that niacin overall reduces/prevents CVDs. Moreover, in a meta-analysis of 17 studies that included 35,760 patients with CVDs or dyslipidemia (17,105 patients receiving niacin), niacin showed no significant therapeutic effect on CV mortality (D'Andrea et al. 2019). Based on such conflicting results, the evidence against the hypothesis that high HDL-C levels can protect from CVDs is now accumulating and the hypothesis has been rightfully challenged as in certain conditions high levels of HDL-C become pro-inflammatory (Kosmas et al. 2018). It is likely that the activity of HDL in RCT is more important than its concentration.

1.5.3 Inflammation as a therapeutic target

Despite the effectiveness of strategies that aim to lower LDL-C levels, major adverse cardiovascular events (MACE) have been reported to occur in normolipidemic patients since CRP levels have been found to be elevated in some statin-treated patients, indicating the presence of chronic inflammation after treatment intervention (Puri et al. 2013; Thongtang et al. 2013; Ridker et al. 2018). Therefore, targeting inflammation along with hyperlipidaemia would be more effective to combat cardiovascular risk. Canakinumab is a monoclonal antibody that directly neutralises IL-1β, a potent pro-inflammatory cytokine that is crucial in stimulating the IL-6 signalling pathway (Ridker et al. 2017). In The Canakinumab Anti-inflammatory Thrombosis Outcome Study (CANTOS), canakinumab markedly diminished

levels of IL-6 and CRP in the plasma with no effect on LDL-C or HDL-C levels in patients on statins with high levels of the CRP; and most importantly reduced CVDs events (Ridker et al. 2017). Due to the high cost, lack of other confirming studies and adverse effects (Table 1.3), the European Medicines Agency advised against the use of Canakinumab (Pello Lázaro et al. 2021).

Despite the promising results of canakinumab, alternative anti-inflammatory drugs have had fewer promising results in clinical studies. One of these potential anti-inflammatory agents is methotrexate. Although methotrexate exerts anti-inflammatory effects and is used as a first line of treatment in rheumatoid arthritis, the CIRT (The Cardiovascular Inflammation Reduction Trial) revealed that methotrexate failed to reduce cardiovascular outcomes (Mullard 2018; Libby and Everett 2019). Another study with atherosclerotic patients who received low-dose methotrexate showed that it failed to reduce circulating levels of IL-1β, IL-6 or CRP, and therefore had no effect on inflammation and reduction of CVDs risk (Ridker et al. 2019). Moreover, it was associated with a modest increase in liver enzyme levels and infection (Ridker et al. 2019). Notwithstanding the clinical trials that did not provide sufficient evidence to support the use of methotrexate as an intervention for CVDs, it has been shown to combat CVDs events in rheumatoid arthritis patients (Sun et al. 2021). Colchicine is another agent that is extensively used to treat inflammatory conditions. It works by suppressing the release of pro-inflammatory cytokines and NLRP3 inflammasome activation, and consequently inhibiting the maturation of proinflammatory cytokines IL-1β and IL-18 (Libby and Everett 2019; Zhang et al. 2022a). In recent clinical trials, the incidence rate of cardiovascular death was significantly reduced by colchicine (0.5-1 mg/day) in patients with chronic CVDs (Nidorf et al. 2020; Imazio and Nidorf 2021). However, the use of colchicine as a therapeutic agent for CVDs remains restricted due to its side effects (Table 1.3) (Zhang et al. 2022a). Based on clinical trials, targeting the NLRP3 inflammasome pathway to treat CVDs patients remains an important area for future investigation.

Despite the fact that anti-inflammatory agents are potentially emerging as a promising pharmacological therapy for combating CVDs, alternatives are required until cost-effective anti-inflammatory medications are developed, and their long-term safety and efficacy are confirmed in large-scale clinical studies, particularly infections that are associated with

dampening inflammation. A summary of key therapies for atherosclerosis and CVD and their limitation are included in Table 1.3.

Table 1.3 Key therapies for atherosclerosis and CVD and their limitations

Category	Medication	Limitations	References
Cholesterol-lowering agent	Statins	• Increase the risk of mayopathy, myotoxicity as well as increased risk of T2DM, especially for patients who suffer from other risk factors for the disease such as high BMI, impaired fasting glucose or high levels of HbA1c. • Associated with liver dysfunction, renal disorders, memory loss and eye conditions. • Statins cannot be taken without precaution by patients who suffer from chronic liver problems, are pregnant or are breastfeeding mothers, and those with a family history of muscular disorders.	(Russo and Jacobson 2004; Kansu and Lang 2017; Pinal-Fernandez et al. 2018; Cai et al. 2021; Saha and Garg 2021)
	Ezetimibe	• Causes serious toxic hepatitis. • Elevation in liver enzyme levels, and gastrointestinal and musculoskeletal symptoms.	(Kanagalingam et al. 2021)
	Bile acid sequestrants	• Gastrointestinal side effects. • Exacerbation of peptic ulcer disease. • Abnormal hepatic function. • Increase in TG levels. • Deficiency of vitamin K or fat-soluble vitamins.	(Lent-Schochet and Jialal 2019)
	PCSK9 inhibitors	Need subcutaneous injection on a regular basis High costs.	(Chan and Ramji 2022)
Elevated HDL-C	Niacin	Causes peptic ulceration, myopathy, infection and gastrointestinal and intracranial bleeding.	(McCarthy 2014; Farrer 2018)
Anti-inflammatory	Canakinumab	Causes higher incidence of infection, thrombopenia and neutropenia, High cost.	(Pello Lázaro et al. 2021)
	Methotrexate	Fails to reduce inflammatory markers (IL-1β, IL-6 or CRP).	(Ridker et al. 2019)
	Colchicine	Causes gastrointestinal discomfort, liver and kidney function dysfunction and potential long-term toxicity.	(Zhang et al. 2022a)

Abbreviations: T2DM, diabetes mellitus (type 2); BMI, body mass index, HbA1c, high levels of haemoglobin A1c; TG, triglyceride.

1.6 Nutraceuticals: promising future agents for combating atherosclerosis

Nutraceuticals are nutritional compounds found in foods and herbs, which are associated with health benefits beyond their nutritional value (Ruchi et al. 2017). In recent years, research activity in the field of nutraceuticals has increased since such compounds have been identified as potential therapeutic agents for many diseases, including cancer, atherosclerosis and CVD (Ruchi et al. 2017). They represent promising alternatives to pharmaceuticals due to their wide availability, low cost and demonstrated long-term safety profile as well as having anti-inflammatory and antioxidant activities with the potential of improving CV health (Moss et al. 2018; Helal et al. 2019). Furthermore, nutraceuticals can be used in combination with pharmaceutical medicines or other lifestyle modifications due to their pleiotropic effects with the potential for inhibiting pro-atherogenic changes. In addition, nutraceuticals could be beneficial for individuals who are intolerant to medications (e.g. statins, ezetimibe), or who have serious concerns about side effects such as sarcopenia (Moss et al. 2018). Omega-3 and -6 polyunsaturated fatty acids (PUFAs), flavanols (catechins), and polyphenols (hydroxytyrosol and resveratrol) are all promising nutraceutical agents that have received substantial interest. Recent clinical trials have shown the potential of combining nutraceuticals with statins to reduce atherosclerosis. In the Reduction of Cardiovascular Events with Icosapent Ethyl-Intervention Trial (REDUCE-IT), the daily intake of 4 g of a purified ethyl ester of eicosapentaenoic acid (EPA; an omega-3 PUFA) (icosapent ethyl) in combination with statins by patients with CVDs, resulted in a significant reduction in the incidence of ischemic events as well as attenuation of plaque burden (Bhatt et al. 2019; Budoff et al. 2020). Therefore, nutraceuticals might be used in dual strategies together with pharmaceuticals to slow the progression of atherosclerosis and provide protection against MACE. The potential cardiovascular benefits of these nutraceuticals in preclinical studies are summarised in Table 1.4.

Several clinical trials have been conducted on these nutraceuticals and reported their anti-atherogenic effects; the major finding of these trials are summarised by Moss and Ramji (Moss and Ramji 2016). However, there is a dearth of literature delineating the precise processes through which these nutraceuticals lower the prevalence of CVD and mortality; hence, the underlying mechanisms are usually not fully understood (Moss and Ramji 2016).

Table 1.4 Potential cardiovascular benefits of nutraceuticals in preclinical studies

Nutraceutical	Source	CV health benefits	Experimental Models	References
Curcumin	*Curcuma longa*	• Reduced atherosclerotic plaque development. • Reduced TC, LDL and TG in plasma. • Reduced levels of CRP, ICAM-1 and VCAM-1 in plasma.	ApoE and LDLR double knockout mice fed with Western diet Rabbit fed HCD	(Olszanecki et al. 2005) (Majeed et al. 2021)
Quercetin	Apples, honey, raspberries and onions	• Reduced plaque size and lipid content. • Attenuated intestinal levels of lipid metabolites. • Improved human aortic endothelial cells' morphology in the presence of ox-LDL. • Decreased cell apoptosis and ROS production induced by ox-LDL. • Decreased lipid content in arterial lumina of $ApoE^{-/-}$ mice.	$LDLR^{-/-}$ mice fed HFD Human aortic endothelial cells *in vitro* $ApoE^{-/-}$ mice fed HFD	(Nie et al. 2019) (Marín-Aguilar et al. 2017; Jiang et al. 2020)
Berberine	European barberry, Oregon grape and tree turmeric	• Reduced plaque size and enhanced plaque stability via increase in α-SMCs actin and collagen content in plaques. • Attenuated MMPs, ICAM-1 and VCAM-1 expression in plaques.	$ApoE^{-/-}$ mice fed with a Western diet	(Chen et al. 2014)
Allicin	Garlic	• Decreased lipid accumulation and foam cell formation. • Enhanced cholesterol efflux.	THP-1 macrophages	(Lin et al. 2017)

		• Lowered plasma lipid levels.	cholesterol-fed Rabbits	(Sobenin et al. 2016)
Hydroxytyrosol	Olive oil	• Reduced expression of adhesion molecules (E-selectin, VCAM-1, MCP-1 and ICAM-1) in plaques. • Reduced levels of plasma TG, TC, and LDL-C and increased plasma HDL-C. • Induced expression of ABCA1, ApoA-I, and SR-BI in the liver.	$ApoE^{-/-}$ mice fed standard diet $ApoE^{-/-}$ mice fed with western diet	(Catalán et al. 2018) (Zhang et al. 2020c)
ω-3 PUFAs	Fish oils, flax seeds and nuts	• Inhibits development of atherosclerotic plaques. • Decreased plasma levels of TC and TG.	$ApoE^{-/-}$ mice $LDLR^{-/-}$ mice	(Moss and Ramji 2016; Takashima et al. 2016) (Gladine et al. 2014)
ω-6 PUFAs	Sunflower, corn oils, animal fat and rapeseed oils	• Reduced lipid content in arterial wall. • Reduced plasma lipid profile (TC and TG).	$LDLR^{-/-}$ mice	(Machado et al. 2012; Patterson et al. 2012)
Catechin	Fruits, green tea, and cocoa	• Inhibited activation of MMPs. • Attenuated SMC invasion and migration. • Decreased TC levels in aorta and plasma. • Enhanced cholesterol efflux by increased mRNA expression for ABCA1 and ABCG1 in the aorta as well as SR-B1 in the liver.	VSMCs Wistar rats fed HFD	(Maeda et al. 2003; Mangels and Mohler III 2017) (Susanti et al. 2019)

Abbreviations: ApoE, apolipoprotein E; LDLR, low-density lipoprotein receptor; TC, total cholesterol; TG, triglyceride; CRP, c-reactive protein; HCF, high cholesterol diet; ICAM-1, intercellular adhesion molecule-1; VCAM-1, vascular cell adhesion molecule-1; HFD, high-fat diet; ox-LDL, oxidised low-density lipoprotein; ROS, reactive oxygen species; SMC, smooth muscle

cell; MCP-1, monocyte chemoattractant protein-1; LDL-C, low-density lipoprotein cholesterol; HDL-C, high-density lipoprotein cholesterol; ApoA-I, apolipoprotein AI; ABCA1/G1, ATP-binding cassette transporter A1/G1; SR-BI, scavenger receptor BI; VSMC, vascular smooth muscle cell.

Furthermore, the availability of several nutrients within the same food, each of which may mediate the beneficial benefits in a somewhat different way, makes it more challenging to interpret the findings. Therefore, further study is necessary to determine the precise protective activities of individual dietary nutrients and their association with cardiovascular health.

1.7 Resveratrol: promising dietary polyphenol

Resveratrol (RSV, 3,5,4'-trihydroxy-*trans*-stilbene) is a natural polyphenol produced as a secondary metabolite by plants. This compound presents at high concentration in the skins of peanuts, red grapes, berries (mulberries, blueberries, cranberries and bilberries), soybeans, pomegranates, dark chocolate, pistachios, and *Polygonum cuspidatum* (Japanese knotweed) (Salehi et al. 2018; Zhang et al. 2021b). Naturally, it consists of two phenolic rings linked by a double styrene bond, and is found in two isoforms; *trans*- and *cis*-isomeric forms (Figure 1.12) (Zhang et al. 2021b). Among the two isoforms, the *trans*-isomer is more biologically active and stable, and this may be due to its non-planar conformation (Sutriyo 2019). In addition, the *trans*-isomer has been found to be the dominant natural form as the *cis*-isomerisation occurs only when the *trans*-isoform is exposed to artificial UV or natural daylight (Dull et al. 2019).

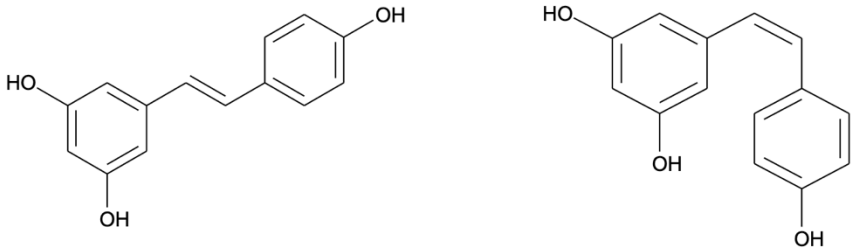

(A) *Trans*-resveratrol (B) *Cis*-resveratrol

Figure 1.12 *Trans*- and *cis*-resveratrol

RSV exists in two different isomeric forms in nature: *trans* and *cis*. Under UV light exposure, the *trans* isomer is transformed into the *cis* isomer, which is more stable and biologically active. Image created using ChemDraw®.

The synthesis of RSV occurs naturally in a variety of plants such as a phytoalexin, as part of their resistance mechanisms against pathogens such as fungi and bacteria, UV irradiation, and several abiotic stresses (Hasan and Bae 2017; Park et al. 2021). Its synthesis can either start with phenylalanine or tyrosine and involves four major enzymes, which are phenylalanine ammonia lyase (PAL)/ tyrosine ammonia lyase (TAL), cinnamate-4-hydroxylase (C4H), coumaroyl-CoA ligase (4CL), and stilbene synthase (STS)(Hasan and Baek 2013). Figure 1.13 illustrates the biosynthesis of RSV. Although some plants such as the root of *Polygonum cuspidatum* are rich in RSV, it is generally synthesised in low amounts as detailed in Table 1.5 (Thapa et al. 2019). However, due to its health-promoting properties and high commercial demand, a comparatively high amount of RSV is produced chemically by using different biotechnological approaches, such as hairy root culture and genetically modified transgenic plants, most of these technologies are summarised by Thapa (Thapa et al. 2019).

Dietary RSV is metabolised and biotransformed by the digestive enzymes and microbes within the gastrointestinal tract, which generally involves sulfation and glucuronidation; it is estimated that approximately 77-80% of RSV intake is absorbed in the intestine (Pannu and Bhatnagar 2019). The intestine recognises RSV as a xenobiotic, thereby allowing its penetration via the intestinal epithelium into the bloodstream through a transcellular pathway. The enterocytes are considered the first site of RSV metabolism where it undergoes sulfation and glucuronidation. A small fraction of RSV escapes conjugation and together with the conjugated RSV exits the small intestine's apical membrane to the large intestine where is metabolised by the action of the gut microbiota into dihydroresveratrol (DHR), lunularin (L) and 3,4’-dihydroxy-*trans*-stilbene. The metabolites and RSV that leave the enterocytes, enter the portal circulation and reach the liver where they undergo phase II drug metabolism, leading to further conjugation by liver enzymes. In addition, conjugated RSV and its metabolites move through enterohepatic circulation, leaving the liver to be reabsorbed in the intestine following hydrolysis, and then returning to the liver for further metabolism through the portal circulation. RSV sulfates are the major metabolites of RSV found in plasma and urine in humans, while RSV glucuronides are the major metabolites in pigs and rats (Catalgol et al. 2012; Springer and Moco 2019). RSV and its metabolites are finally absorbed by peripheral tissues such as adipose tissue after entering systemic circulation from the liver.

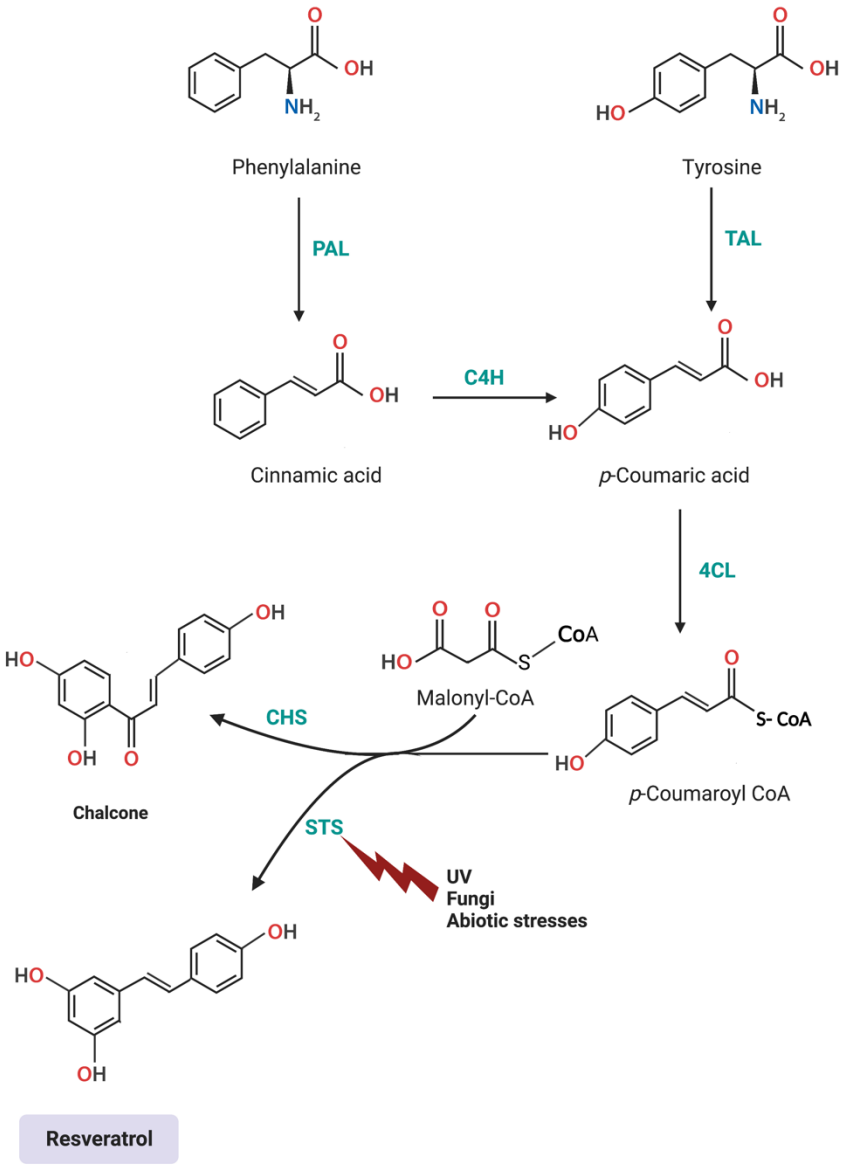

Figure 1.13 Biosynthesis of resveratrol

RSV is synthesised in plants from the aromatic amino acid phenylalanine or tyrosine via the sequential reaction of four enzymes. In the first step, phenylalanine is converted into *trans*-cinnamic acid via the deamination effect of PAL. Subsequently, *trans*-cinnamic acid is converted into *p*-coumaric acid by the action of C4H. In the case of tyrosine, this first transforms directly into *p*-coumaric acid by TAL. The *p*-coumaric acid then undergoes esterification with CoA and is converted into *p*-coumaroyl-CoA by 4CL. Finally, *p*-Coumaroyl-CoA is condensed with three molecules of malonyl-CoA through the sequential reaction of STS that competes with CHS to produce RSV. **Abbreviations:** PAL, phenylalanine ammonia lyase; TAL, tyrosine ammonia lyase; C4H, cinnamic acid 4-hydroxylase; CoA, coenzyme A; 4CL, 4-coumaroyl-CoA synthase; STS, stilbene synthase; CHS, chalcone synthase. Image created with BioRender.com.

Table 1.5 The amount of RSV found in natural foods

Source	RSV concentration	References
Dry grape skin	24 mg/g	(Zhang et al. 2021b)
Grapes	0.16 to 3.54 mg/g	
Cranberry juice	0.2 mg/l	
Dark chocolate	350 mg/kg	
Milk chocolate	100 mg/kg	
Peanuts	0.02–1.92 µg/g	(Mukherjee et al. 2010)
Boiled peanuts	~5.1 µg/g	
100% Natural peanut butter	~0.65 µg/g	
Blueberries	~0.32 ng/g	
Cranberry raw juice	~0.2 mg/l	
Grape juice	~0.5 mg/l	

The kidneys also play a role in RSV metabolism, resulting in the excretion of polar RSV metabolites (Springer and Moco 2019). RSV has been noted for its rapid metabolism along with rapid excretion since about 75% of absorbed RSV is excreted in the urine, and this results in low bioavailability (Pannu and Bhatnagar 2019). Despite its low bioavailability, RSV has been shown to be effective *in vivo* and in clinical trials. According to data in the literature, RSV mediates its effect through its metabolites and through accumulation at high concentrations in specific tissues such as intestinal tissue, kidney, liver and heart (Walle 2011; Gambini et al. 2015). Böhmdorfer *et al.* (2017) demonstrated that unconjugated RSV concentration was approximately 30 times higher in the heart of mice than in the plasma after 30 minutes of administration (via gavage). Furthermore, the concentration of the RSV metabolite (resveratrol-3-O-glucuronide) was approximately 10 times higher in the heart compared to the plasma following 30 minutes of administration (via gavage)(Böhmdorfer et al. 2017). In addition to that, results from clinical studies reveal that the highest concentrations of *trans*-RSV and its metabolites (about 1.8-2 µM) were found in the blood of healthy volunteers after around 1 hour of oral administration of 25 mg of *trans*-RSV (Walle et al. 2004). In another study, the concentration of *trans*-RSV was found to range from 0.3 µM to 2.3 µM in the plasma of healthy volunteers between 0.8 and 1.5 hours after receiving single ascending doses of RSV orally (i.e., 0.5 g, 1 g, 2.5 g, and 5 g). In contrast, the same study demonstrated that the when a higher dose of *trans*-RSV (5g) was orally administered, the levels of RSV conjugates in the plasma were found to be approximately 2 to 8 times higher than the levels of *trans*-RSV(Boocock et al. 2007). It has been also found that the receiving 1

g of *trans*-RSV daily can yield about 22 µM of resveratrol-3-O-sulfate (ranging from 8 to 32 µM) and about 7-8 µM for monoglucuronide conjugates (ranging from 2 to 18 µM)(Patel et al. 2013). Based on this, the RSV effect could be explained by the conversion of sulphates and glucuronides back to RSV in target organs such as the liver (Gambini et al. 2015). Beyond this, a co-administration of a variety of molecules, such as piperine and quercetin, has been demonstrated to increase RSV bioavailability (Smoliga and Blanchard 2014). In this regard, several methodological approaches have been developed to enhance RSV bioavailability, including improved delivery systems such as RSV encapsulation in lipid nanocarriers or liposomes and emulsion (Chimento et al. 2019). The suggested daily doses of RSV for therapeutic use based on animal studies range from hundreds of milligrams to several grams (Zhang et al. 2021b). However, RSV is available as a dietary supplement in the suggested daily dosages on the market. Several clinical studies suggest RSV can be supplemented at dosages up to 5 g/day with well tolerance and is highly safe (little to no side effects) (Zhang et al. 2021b).

In the last few decades, RSV has received a lot of scientific attention for its reported promising pharmacological potential (Cheng et al. 2020a; Zhang et al. 2021b; Chupradit et al. 2022). A large number of studies have revealed an association between RSV administration and improvement in a spectrum of diseases such as cancer, diabetes, neurological disorders, NAFLD and atherosclerosis-associated CVDs (Berman et al. 2017). Many studies have provided evidence that RSV has multifaceted salubrious properties, including anti-inflammatory, anti-oxidant, anti-carcinogenic, cardio-protective, anti-aging, anti-diabetic, anti-bacterial and neuroprotective activities (Berman et al. 2017; Zhang et al. 2021b). The key protective effects of RSV in different diseases as reported by human and animal studies are summarised in Figure 1.14. Furthermore, the role of RSV in CVDs is discussed in detailed in the following section.

1.7.1 Role of RSV in CVDs

Generally, a plethora of evidence shows that RSV may help reduce incidences of MACE and related CVDs mortality due to many therapeutic effects such as improving endothelial dysfunction, reducing inflammatory markers, diminishing platelet aggregation, reducing ROS

levels, as well as favourably modulating plasma lipid profile (Fardoun et al. 2020); however, questions regarding RSV underlying mechanisms remain unanswered. A comprehensive review of the role of RSV in major events in the pathogenesis of atherosclerosis is discussed in more detail in the next sections.

.

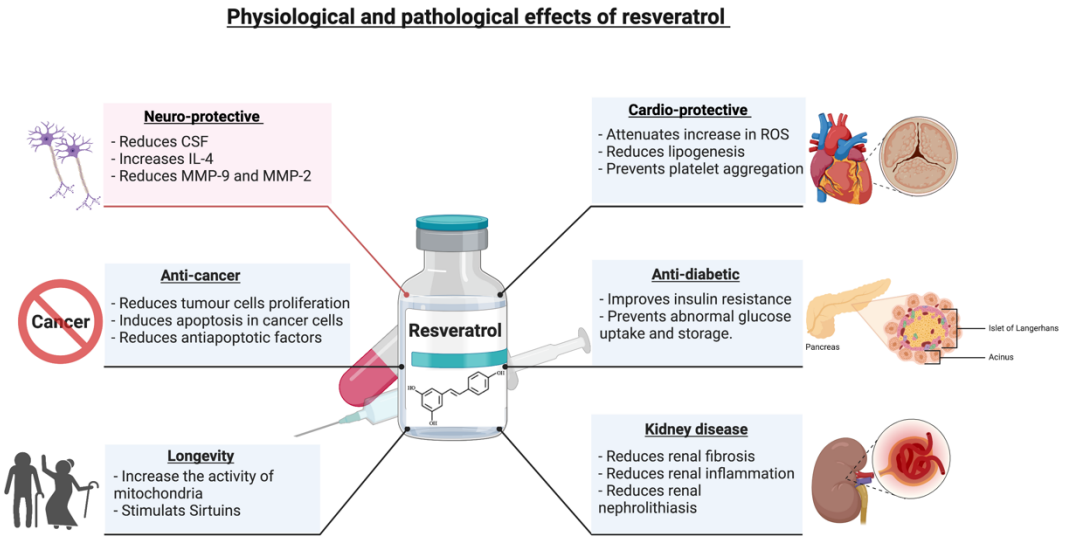

Figure 1.14 Physiological and pathological effects of RSV

An overview of the results of different studies indicating a positive effect of RSV on different pathological conditions. Image created with BioRender.com. **Abbreviations:** CSF, Cerebrospinal fluid; IL-4, Interleukin-4; MMP, Matrix metalloproteinase. Image created with BioRender.com

1.7.1.1 Role of RSV on endothelial dysfunction and ROS production

The role of endothelial dysfunction in disease initiation and progression has been discussed earlier in this chapter (section 1.3.1). The beneficial effects of RSV on modulation of endothelial function have been demonstrated in different model systems *in vitro*, *in vivo* and in clinical trials (Wallerath et al. 2002; Magyar et al. 2012; Li et al. 2019a). Improvement of endothelial function has been implicated, including upregulation of eNOS expression along with enhanced eNOS activity and prevention of eNOS uncoupling (Li et al. 2019a). These

effects, either singly or in combination, have been reported using different doses of RSV, route of administration as well as different treatment duration. For instance, oral treatment of RSV at 20 mg/kg/day improved endothelial function in HFD-fed and diabetic wild-type peroxisome proliferator-activated receptor delta (*Ppard)* mice by triggering NO production through increased peroxisome proliferator-activated receptor-delta (PPARδ) transcriptional activity (San Cheang et al. 2019). The same observation was seen in AopE^{-}/$^{-}$ mice fed HFD with the inclusion of 200 mg RSV/100 g diet for 8 weeks (Li et al. 2019b). Such observations have been also confirmed in different cell lines and primary cultures such as human umbilical vein endothelial cells (HUVEC), rat aortic endothelial cells (RAEC) and human coronary arterial endothelial cells (HCAEC) (Li et al. 2019a; Zhou et al. 2019b). In healthy individuals, the consumption of 400 mg of RSV/day for a month led to improved endothelial function by decreasing ICAM-1 and VCAM-1 expression (Agarwal et al. 2013). Patients with MI who received 10 mg RSV daily for 3 months had improvement in left ventricle diastolic function and endothelial function (Magyar et al. 2012). In addition to modulating NO production and activity to improve endothelial function, RSV is able to mediate its effect via its potent anti-oxidant property. In this regard, RSV has a dual function as an anti-oxidant in that it may both increase the activity of anti-oxidant enzymes and serve as a free radical scavenger (Izzo et al. 2021).). It has been demonstrated that the potent anti-oxidant activity of RSV depends upon the positioning of functional groups on its nuclear structure. As a result, the structure (a *trans* isomer of double bound, allowing a ligand-receptor interaction of a hydroxyl group), substitution (H-transfer capacity, in which the free radical removes a hydrogen atom from RSV and becomes a radical), and the total amount of hydroxyl groups all have a significant impact on numerous mechanisms of anti-oxidant actions, including scavenging of free radicals and metal ion chelation (Leopoldini et al. 2004; Salehi et al. 2018).

Multiple cellular models along with animal models have been used to examine RSV's anti-oxidant effects. For instance, in an earlier study, It was shown that RSV has anti-oxidant activity on rat aortic smooth muscle A10 cells (ASMCs) by inducing the cellular levels and activity of anti-oxidant enzymes, including superoxide dismutases (SOD), catalase, glutathione reductase (GR), glutathione S-transferases (GST) and NAD(P)H:quinone oxidoreductase 1(NQO1). In addition to cellular protein content, RSV upregulates mRNA levels of catalase, GSTA1 and NQO1 (Li et al. 2006). This study also revealed the ability of RSV

to reduce ROS accumulation in pre-treated ASMCs cells by 70% (Li et al. 2006). In addition, the reduction of protein and mRNA levels of SOD in HepG2 cells exposed to RSV is another example (Chen et al. 2016b). In animal models, it is generally believed that the anti-oxidant effects of RSV *in vivo* are mediated via the regulation of various anti-oxidant enzymes. For example, an increase in anti-oxidant enzymes activity in the heart of $ApoE^{-/-}$ mice (administrated RSV at doses of 30 or 100 mg/kg via gavage for 7 days) and a reduction in levels of MDA (i.e. lipid peroxidation) in the liver, heart, brain and testis of Wistar rat (fed 5g/kg RSV in standard diet)(Kasdallah-Grissa et al. 2006; Xia et al. 2010). Similar results of cardio-protection against ROS have been published using guinea pigs that were given oral administration of RSV (60 mg/l in tap water for 16 days)(Floreani et al. 2003). In a recent study that was performed using spontaneously hypertensive rats (SHRs) and malignantly hypertensive rats (MHRs), treatment with RSV for 4 weeks (10 mg/kg/day by gavage) showed a significant reduction in advanced oxidation protein products (AOPPs) together with thiobarbituric acid reactive substances (TBARSs). Additionally, superoxide anion radical (O_2^-) and pro-oxidative balance (PAB) were decreased in the treated group. Myeloperoxidase (MPO) activity level was also significantly reduced by RSV. MPO is produced and released by neutrophils and monocytes; and increased MPO levels is associated with vascular pathology and the production of ROS as well as oxidation of many biological molecules. The 4 weeks of RSV application to spontaneously hypertensive female rats significantly improved antioxidant enzymes, including SOD, catalase and GPx. In histopathological examination, RSV showed a significant decrease in cardiomyocyte damage score (Grujić-Milanović et al. 2021).

1.7.1.2 Role of RSV on macrophages and the inflammatory response

Based on the aforementioned facts (section 1.3), targeting the differentiation of monocytes to macrophages is considered as a potentially promising therapeutic avenue for treating atherosclerosis. The effect of RSV on monocyte differentiation and associated inflammation has been investigated using both *in vitro* and *in vivo* models, THP-1 monocytes and $ApoE^{-/-}$ mice, respectively (Vasamsetti et al. 2016). The study demonstrated that RSV stimulates 5' AMP-activated protein kinase (AMPK) activation that restores intracellular glutathione (GSH) levels that consequently results in reduced PMA-induced THP-1 monocyte to macrophage differentiation as well as expression of inflammation markers (i.e. mRNA levels of TNF-α, IL-

1β, and MCP-1). Additionally, RSV dose-dependently reduces the expression of CD-36, LOX-1 and SR-A1 scavenger receptors in these cells. Consistent with such changes, RSV significantly impairs the incidence of Ang-II-induced atheromatous plaque formation in $ApoE^{-/-}$ mice, which is an important phenomenon in atherosclerosis development. The outcome of the histological analysis revealed a reduction in plaque size in the thoracic and abdominal aorta and an increase in lumen size in RSV treated group (Vasamsetti et al. 2016). RSV also contributes to a reduction in the inflammatory response induced in macrophages, ECs and SMCs. In a study on the effect of RSV administration on the expression of VCAM-1 and ICAM-1, RSV prevented the adherence of monocytes to ECs by inhibiting ICAM-1 expression in mouse and bovine aortic ECs stimulated with LPS. In line with these findings, ICAM-1 expression was attenuated by RSV in endothelial-enriched RNA obtained from the left carotid artery (LCA) of C57BL/6J mice (Seo et al. 2019). This should contribute to a reduction in monocyte recruitment and subsequently the accumulation of macrophages in subendothelial space, and thereby decreasing inflammation. In a recently published study, the anti-inflammatory effect of RSV was shown *in vitro* and *in vivo* (Nallasamy et al. 2021). In addition to inhibiting the mRNA expression of adhesion molecules in the pre-treatment of ECs-stimulated with TNF-α *in vitro*, the *in vivo* finding showed the ability of RSV to reduce monocyte binding to aortic ECs as well as plasma concentrations of MCP-1, ICAM-1 and VCAM-1 in male C57BL/6J mice after administration of RSV followed by injection of TNF-α. Additionally, immunohistochemical staining of the aorta showed a reduction of NF-κB activation by RSV (Nallasamy et al. 2021). Several studies using *in vivo* and *in vitro* models have suggested that the anti-inflammatory effects of RSV involves down regulation of expression of various inflammatory markers such as ICAM-1, VCAM-1, E-selectin, TNF-α, IL-1β, IL-1-α, IL-2,IL-6, IL-8, IL-12 and IFN-γ in different model systems such as LPS- stimulated adhesion of THP-1 human monocytes, ECs, splenic lymphocytes and human peripheral blood mononuclear cells (PBMCs) (Gao et al. 2001; Boscolo et al. 2003; Wung et al. 2005; Song et al. 2013; Wakabayashi and Takeda 2013; Seo et al. 2019; Xie et al. 2019; Zhang et al. 2020d).

RSV exerts anti-inflammatory effects not only by inhibiting the expression of inflammatory cytokines but additionally by inducing the levels of several anti-inflammatory cytokines. For example, RSV increases the secretion of IL-10 and transforming growth factor-β1 (TGF-β1) in macrophages and mouse model systems (Palacz-Wrobel et al. 2017; Shabani et al. 2020; Zhou

et al. 2020). Furthermore, RSV enhances the deacetylation and activation of peroxisome proliferator-activated receptor gamma coactivator 1-alpha (PGC-1α), which is downregulated during atherosclerosis development and significantly contributes to an increased inflammatory response by inducing oxidative stress (Gal et al. 2021).

1.7.1.3 Role of RSV on foam cell formation and plasma lipid profile

RSV affects foam cell formation in several ways. As previously stated, RSV raises plasma HDL levels and reduces LDL levels in addition to its potent anti-oxidant effects that improves cholesterol efflux (Avellone et al. 2006; Berrougui et al. 2009). Moreover, RSV upregulates LXR-α in macrophages at mRNA and protein levels in addition to upregulation of mRNA levels of ABCA1 and ABCG1 that consequently leads to the removal of excess cholesterol from foam cells. Together with the downregulation of expression of lipoprotein lipase (LPL) and SR-A genes, RSV can modulate the expression of genes involved in foam cell formation (Sevov et al. 2006). Generally, it has been suggested that the anti-foam cells actions of RSV are due to its ability to activate AMPK and upregulate SIRT1 along with attenuating mRNA expression of inflammatory cytokines, MCP-1 in particular (Dong et al. 2014b). In two independent *in vivo* studies on HFD-fed ApoE^{-}/$^{-}$ mice, administrated RSV (10 mg/kg/day via gavage for 24 weeks), showed a reduction in plaque lipid content and lesion area (Ye et al. 2019; Ma et al. 2021b).

Regarding modulation of plasma lipid profile, several pre-clinical studies have been carried out to investigate the effect of RSV on lipids and lipoproteins levels. For instance, treatment of hypercholesterolemic rats with RSV at 20 mg/kg of body weight/day for 14 days or at 1 mg/kg body weight for 30 days resulted in a reduction in plasma TC, LDL-C and TG levels (Penumathsa et al. 2007; Rocha et al. 2009). In addition, the impact of RSV administration has been studied in mice deficient in ApoE and LDLR. The study lasted 8 weeks and found that administration of HFD supplemented with 96 mg/kg RSV in diet lowered plasma levels of TC and TG as well as dramatically suppressed atherosclerosis development in the aorta (Fukao et al. 2004). In a more recent study, daily intragastric injection of 5 mg/kg of body weight/day of RSV dispersed in 5% (v/v) sodium carboxymethyl cellulose solution for 20 weeks

ameliorated atherosclerosis induced by HFD plus LPS in ApoE$^{-/-}$ mice. The study showed that RSV reduced plasma levels of total cholesterol, TG and LDL and enhanced HDL concentrations after 20 weeks (Zhou et al. 2020). Similar results have been published using LDLR$^{-/-}$ mice, Chassot and his colleagues in 2018 investigated the effects of administration of RSV (0.83 mg/day) in the prevention and regression of atherosclerosis (Chassot et al. 2018). In the prevention group, mice were fed a standard diet for 8 weeks before switching to an atherogenic diet for the next 8 weeks, whereas in the regression study the converse was done. RSV showed a hypocholesterolemic effect in the prevention study by reducing TC, LDL-C, VLDL-C and HDL-C while no results were presented for LDL-C, TC or VLDL-C in the regression study. However, RSV reduced HDL-C in the regression group (Chassot et al. 2018).

In contrast to the abundance of pre-clinical research on RSV, there are a limited number of human clinical studies. A summary of the main findings from clinical trials is included in Table 1.6.

Table 1.6 Key observations in humans following RSV intake

Observations	References
Improve a plasma lipid profile	(Magyar et al. 2012; Zamora-Ros et al. 2012; Hoseini et al. 2019; Simental-Mendía and Guerrero-Romero 2019; Gal et al. 2020; Cao et al. 2022).
Reduce of inflammatory markers (e.g. TNF-α and hs-CRP levels)	(Timmers et al. 2011; Agarwal et al. 2013; Tomé-Carneiro et al. 2013; Shi et al. 2017; Koushki et al. 2018; Teimouri et al. 2022)
Induce of flow-mediated dilation and improve of endothelial function	(Wong et al. 2011; Magyar et al. 2012; Wong et al. 2013; Emamat et al. 2018; Marques et al. 2018a)
Reduce of blood pressure	(Wong et al. 2011; Biesinger et al. 2016; Theodotou et al. 2017)

Abbreviations: TNF-α, tumour necrosis factor α; hs-CRP, high-sensitivity C-reactive protein.

1.8 Project aims.

Atherosclerosis is the primary cause of CVD, which has become one of the world's major concerns due to a rise in prevalence and consequently morbidity and mortality, which impose a considerable economic cost. Currently available therapeutic strategies that mainly target hyperlipidaemia, such as statins, have limited effectiveness in combating cardiovascular risk and have other concerns, such as undesirable side effects (mentioned in Table 1.3). Indeed,

with the fact that MACE was observed in normolipidemic patients after statin medication, the importance of residual inflammation in generating clinical consequences has been brought to light. Targeting inflammation using anti-inflammatory drugs such as canakinumab that combat CVDs by inhibiting IL-1β showed new hope in the CANTOS trial. However, any immunotherapy raises concerns about increased infection risk and appropriateness for patients who are already immunocompromised. Due to these reasons, the requirement for alternatives that have well-known safety profiles, are widely available and are cost-efficient is vital. RSV among all nutraceuticals has been highlighted as a promising anti-atherogenic agent due to its demonstrated ability to modify a range of atherogenic risk factors, such as cholesterol homeostasis and plasma lipid levels together with its anti-oxidant and anti-inflammatory effects. Despite a number of studies that have been carried out on RSV, its effects on the full range of atherosclerotic processes are not fully understood along with the underlying molecular mechanisms. Therefore, there are a number of crucial questions that need to be answered and it is hypothesized that by answering these questions, significant insights will be gained:

- What are the athero-protective roles of RSV on the main cell types implicated in atherosclerosis progression (i.e., monocytes/macrophages, ECs and VSMCs) as well as another cell type that is indirectly involved in disease progression such as hepatocyte?
- What is the effect of RSV supplementation on atherosclerotic plaque progression and stability *in vivo*?
- What are the possible underlying mechanisms for the observed anti-atherogenic effects *in vivo*?
- What are the roles of RSV in NAFLD?

Firstly, the anti-atherosclerotic, anti-oxidative and anti-inflammatory effects of RSV were broadly investigated across a number of key cellular processes associated with the initiation and progression of atherosclerosis using a range of *in vitro* model systems and assays. These assays enable the study of the effect of RSV on cell viability and proliferation, monocytes migration, ROS production, foam cell formation (i.e. lipid uptake and efflux), MMP production and the expression of chemokine and adhesion molecules. The key results from THP-1 cells were confirmed in primary human macrophages (human monocyte-derived macrophages, HMDMs), to verify that observations were not specific to the cell line.

Secondly, the anti-atherosclerotic effect of RSV supplementation was investigated *in vivo.* This was carried out via the inclusion of RSV to HFD supplemented male LDLR knock-out (KO)/deficient mice. Use of mice with this kind of genetic modification is required since wild-type mice display mild or no atherosclerotic changes when fed a standard chow diet or even HFD, as cholesterol is carried in HDL particles due to lack of CETP protein that mediates the exchange of cholesterol between HDL and LDL particles in humans (Gisterå et al. 2022). The $LDLR^{-/-}$ mice were chosen over other species, in particular $ApoE^{-/-}$ mice, because they have several advantages. For instance, the development of atherosclerosis and induction of plaque formation in $LDLR^{-/-}$ mice requires feeding of an atherogenic diet whereas $ApoE^{-/-}$ mice can develop atherosclerosis spontaneously on a standard chow diet, resulting in hypercholesterolaemia associated with elevated circulating levels of LDL in $LDLR^{-/-}$ mice and VLDL in $ApoE^{-/-}$ mice (Gisterå et al. 2022). Other advantages had been addressed in Chapter 4, experimental aims section). During this study, the $LDLR^{-/-}$ mice were fed HFD with or without RSV (20 mg/kg/day) for 12 weeks in order to induce atherosclerosis. After that, the changes in mouse organs' weights, haematopoietic stem and progenitor cells within the bone marrow, immunophenotyping of peripheral blood cell populations and plasma lipid profile were investigated.

Thirdly, the research was extended *in vivo* to investigate whether RSV supplementation can attenuate atherosclerosis progression and induce plaque stabilisation. This was achieved via analysis of changes in plaque morphometry as well as immunohistochemical analysis of SMCs, macrophages and T-cells within atherosclerotic plaques.

Fourthly, the effect of RSV on transcriptomic profile of thoracic aorta from $LDLR^{-/-}$ mice that were fed HFD following supplementation with RSV was determined using RNA-sequencing to identify changes in gene expression and pathways involved in atherosclerosis development compared to HFD (control) group.

Finally, considering the strong correlation between NAFLD and atherosclerosis, the therapeutic effect of RSV on NAFLD was elucidated via staining of liver sections from $LDLR^{-/-}$ mice to evaluate cellularity/morphological changes and the degree of steatosis. Furthermore,

an *in vitro* model of NAFLD involving the HepG2 cell line was used to assess ROS production and lipid accumulation after RSV treatment *in vitro*. These studies provided mechanistic insights into the association between atherosclerosis and NAFLD.

Schematic diagrams of the project objectives for *in vitro* and *in vivo* studies are shown in Figure 1.15 and 1.16 respectively. Furthermore, a summary of the contents of thesis chapters is provided in Figure 1.17.

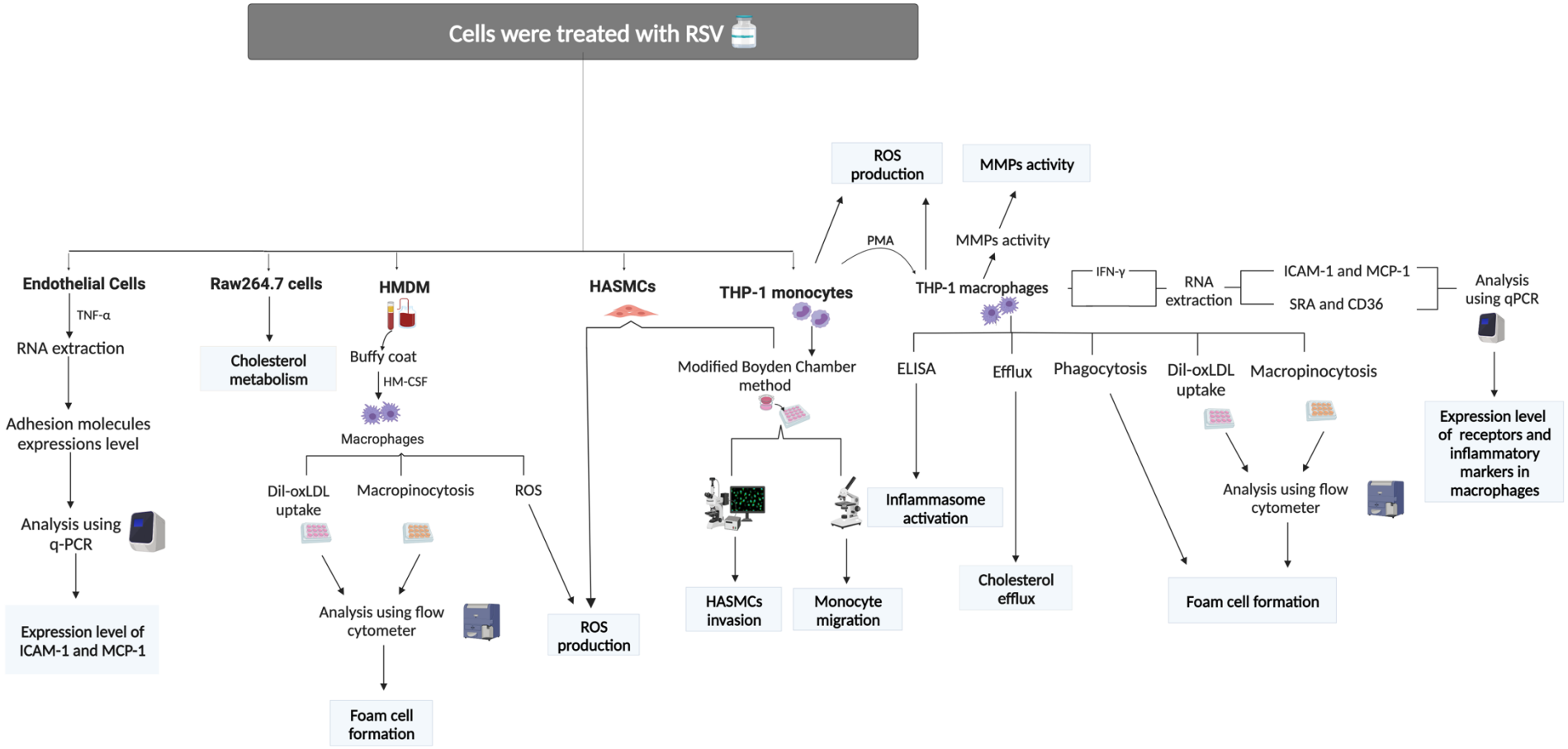

Figure 1.15 Experimental strategy used to assess the role of RSV on key cellular processes associated with the initiation and progression of atherosclerosis using a range of primary cells and cell lines *in vitro*.

Abbreviations: RSV, resveratrol; TNF-α, tumour necrosis factor-α; qPCR, quantitative polymerase chain reaction; HMDM, human monocyte-derived macrophages; HM-CSF, human macrophage-colony stimulating factor; ROS, reactive oxygen species; HAVSMCs, human aortic vascular smooth muscles cells; PMA, phorbol 12-myristate 13-acetate; MMPs, matrix metalloproteinase; ELISA, enzyme-linked immunosorbent assay; IFN-γ, interferon gamma; ICAM-1, intercellular adhesion molecule-1; MCP-1, monocyte chemoattractant protein-1; SR-A, scavenger receptor-A; CD36, cluster differentiation 36. Image created with BioRender.com.

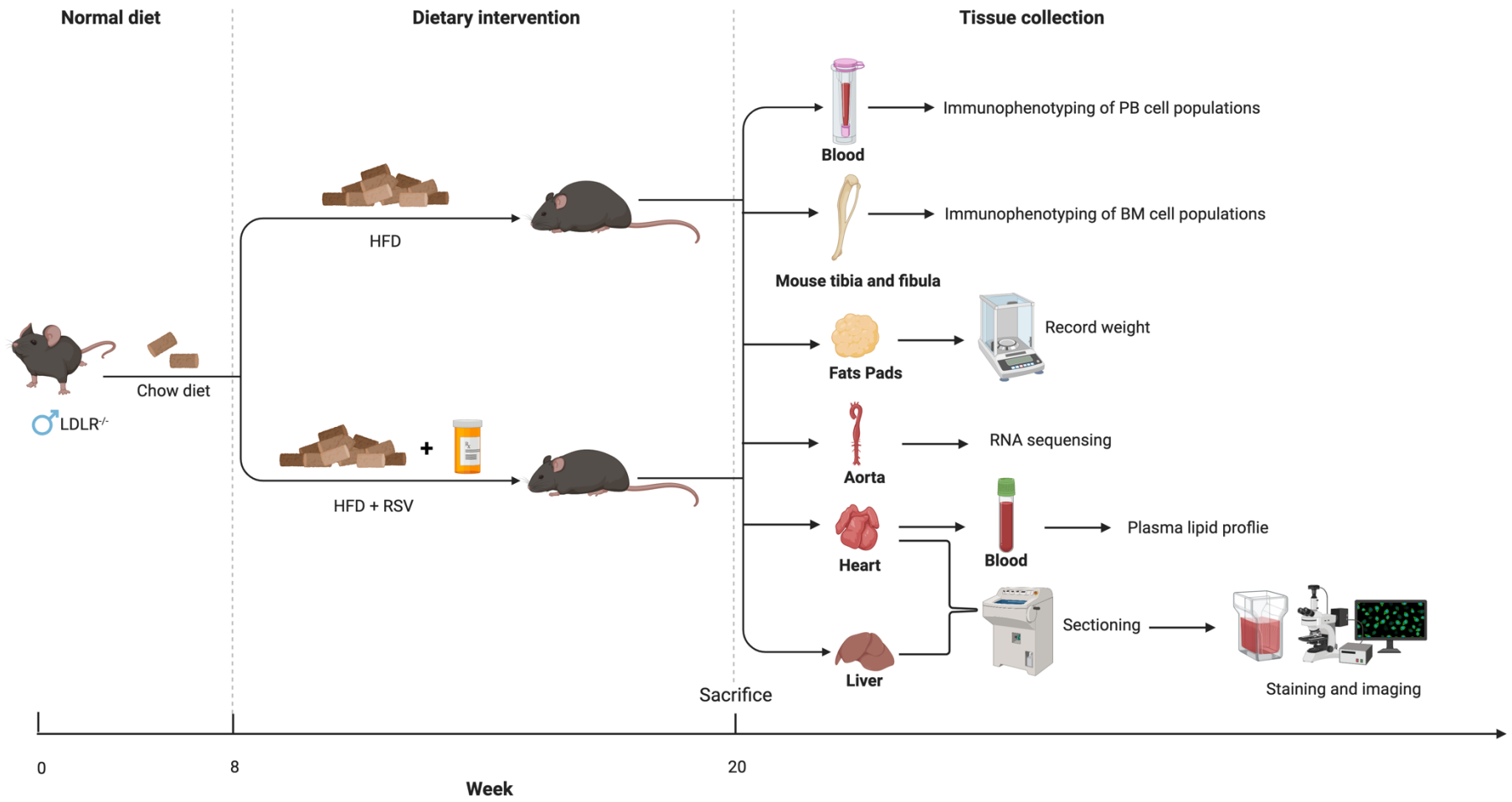

Figure 1.16 Strategy for the *in vivo* study

Eight-week-old male LDLR^{-}/$^{-}$ mice were divided randomly to one of two groups: HFD or HFD + RSV. The mice were then given the relevant dietary manipulations before being sacrificed after 12 weeks.
Abbreviations: LDLR^{-}/$^{-}$, Low-density lipoprotein deficient receptor; HFD, High fat diet; RSV, Resveratrol; PB, Peripheral blood; BM, Bone marrow. Image created with BioRender.com.

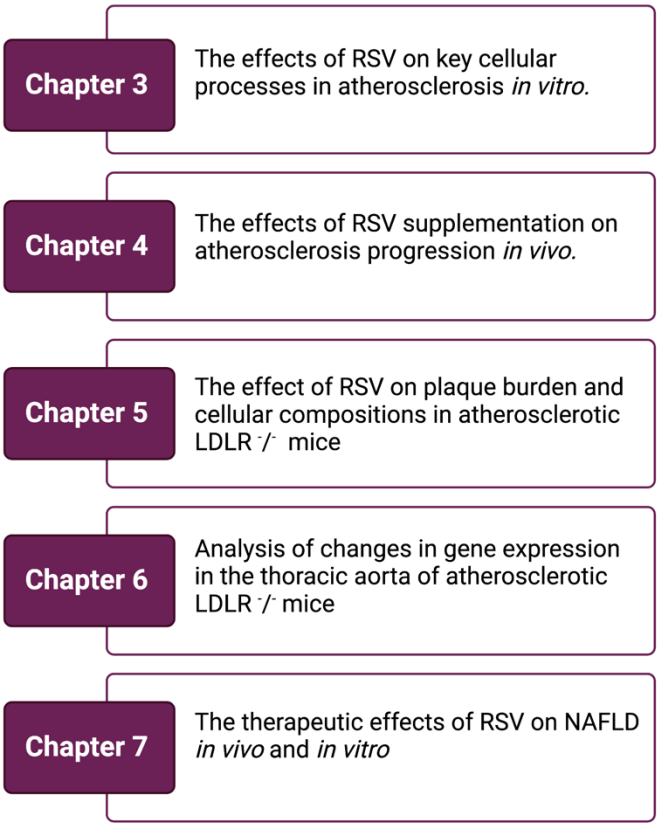

Figure 1.17 A summary of content of thesis chapters contents

Abbreviations: LDLR, low density lipoprotein receptor; NAFLD, non-alcoholic fatty liver disease.

CHAPTER 2

Materials and Methods

2.1 Materials

A list of all the materials that have been used in this project and their suppliers are outlined in Table 2.1.

Table 2.1 List of materials/reagents used and their suppliers

Suppliers	Materials/Reagents
Abcam, UK	DCFDA Cellular ROS Detection Assay Kit; Antibodies for immunofluorescence staining (see Table 2.9 for details); HDL and LDL/VLDL Cholesterol Assay Kit; MMP Activity Assay Kit (Fluorometric - Green); Triglyceride Quantification Assay Kit; Van Geison's solution
Alfa Aesar, UK	Acetylated LDL; DiI-labelled oxidised LDL; Heparin sodium salt (250 mg)
BD Bioscience, UK	40/70 µm sterile cell strainer; FITC-conjugated anti-mouse CD34 (553733)
Biolegend, USA	APC/Cy7-conjugated anti-mouse Sca-1 (108125); APC-conjugated anti-mouse c-Kit (105811); FITC-conjugated anti-mouse CD48 (103403); PE/Cy7-conjugated anti-mouse CD150 (115913); PE/Cy7-conjugated anti-mouse CD16/32 (101317); PE-conjugated anti-mouse CD127 (121111); PE-conjugated anti-mouse Sca-1 (108107); PE/Cy7 anti-mouse NK-1.1 (108714); PE anti-mouse CD115 (135505); PE/Cy7 anti-mouse Ly-6C (128018); FITC anti-mouse Ly-6G (127605); FITC anti-mouse/human CD45R/B220 (103206); PE anti-mouse CD3 (100206); APC anti-mouse/human CD11b (101212); PerCP anti-mouse CD4 (100537); APC/Cy7 anti-mouse CD8a (100714)
Helena Biosciences, UK	12- and 96-well tissue culture plates (for PBMCs seeding)
Jackson Laboratory, USA	$LDLR^{-/-}$ mice
Labtech, UK	Foetal bovine serum (South American origin)
Life Technologies, Paisley, UK	Phosphate buffered saline (PBS) pH 7.4 x1
Peprotech, UK	Recombinant human MCP-1; ICAM-1; GAPDH; M-CSF; PDGF-BB; TNF-α; IFN-γ
Perkin-Elmer, USA	[1,2-^{3}H(N)] cholesterol; Opti-FLUOR®; Scintillation analyser, 20 ml Super Polyethylene Vial with Quick Closure
Promega, UK	MMLV Reverse Transcriptase; MMLV RT 5x buffer; Random primers; RNasin® Ribonuclease Inhibitor

Qiagen, UK	RNeasy Mini Kit, 2mm stainless steel beads, TissueLyser
R&D system, UK	Human IL-1β DuoSet ELISA (DY201); DuoSet ELISA Ancillary Reagent Kit (DY008)
Sigma Cell Culture, USA	Sodium phosphate (Na_2HPO_4)
Sigma-Aldrich, UK	1, 2-Propanediol; 2-propanol (isopropanol); 12/24/96-well plates; 15 and 50 ml Falcon tubes; 5- Bromo-2'-deoxy-uridine Labeling and Detection Kit III; Acetone; Accuspin tubes; Apolipoprotein A-I; Aquamount (aqueous mounting medium); Bovine serum albumin (BSA); Chloroform; Crystal Violet; DAPI nuclear stain; Dulbecco's Modified Eagle Medium, high glucose (DMEM); Dulbecco's Modified Eagle Medium, low glucose (DMEM); Dulbecco's PBS; Dimethyl sulphoxide (DMSO); DPX mounting medium for histology; Ethidium bromide; Endothelial Cell Growth Culture Medium; Eosin solution; Hanks Balanced Salt Solution (HBSS); Harris Modified Haematoxylin Solution; Hexane; Human Aortic Smooth Muscle Cells (adult); Human Aortic Endothelial Cells (HAEC), Hydroxytyrosol; Isopropanol; Lucifer yellow (LY); Matrigel ECM gel; Methanol; Nalgene Mr. Frosty™ freezing container; Oil Red O solution (0.5% (w/v) in propylene glycol); Oil Red O solution (0.5% (w/v) in isopropanol; Pap pen for immunostaining; paraformaldehyde (PFA); Penicillin-streptomycin; Pasteur pipettes (plastic); Phorbol-12-myristate-13-acetate (PMA); Resveratrol (≥99%)100 mg; RPMI-1640 medium (with L-glutamine and sodium bicarbonate); Smooth Muscle Cell Growth Medium; SYBR Green Jumpstart Taq Readymix; Sodium hydroxide; Serum (goat and donkey); Stripettes (10 ml, 25 ml); Sudan Black B; THP-1 human acute monocytic leukemia cell line; Tris-borate EDTA (TBE); Xylene
Special Diets Services, UK	High fat diet [21% (w/w) pork lard and 0.15% (w/w) cholesterol]
Starlabs, UK	1.5 ml Eppendorf tubes; 25 and 75 cm^2 tissue culture flasks; 96-well PCR plates for Roche® Lightcycler®; 250 mm CytoOne cell scraper (with 10 mm pivoting blade); Polypropylene PCR sealing film strips; Reagent reservoirs
Stemcell Technologies, UK	Ammonium chloride solution; Lymphoprep™
ThermoFisher Scientific, UK	Agarose; Ambion™ nuclease-free water; Cryoprotected tissue freezing reagent (OCT); Diethyl ether; Nanodrop™ ND2000; Pierce™ LDH Cytotoxicity Assay Kit; Ribozol; RiboRuler high range RNA ladder; RNA loading dye (2X); *RNAlater*™ stabilisation

	solution; Trypsin-EDTA (0.05%); Sarstedt Microvette CB300 EDT; Shandon base cryomolds; Sodium hydroxide (NaOH); Vybrant® Phagocytosis Assay Kit; Invitrogen™ eBioscience™ Streptavidin eFluor™ 450 Conjugate
VWR Jencons, UK	Ethanol absolute; Feather microtome blades type S22; Falcon® 8 µm cell culture inserts with 12-well companion plates; Rectangular glass coverslips; Superfrost® microscope slides.

Abbreviations: DCFDA, 2'7'-dichlorofluorescin diacetate; ROS, reactive oxygen species; DiI, 1,1'-Dioctadecyl-3,3,3',3'-tetramethylindocarbocyanine perchlorate; HDL, high density lipoprotein; LDL/VLDL, low density lipoprotein/very-low density lipoprotein; MMP, matrix metalloproteinase; FITC, fluorescein isothiocyanate; APC, allophycocyanin; Cy7, cyanine7; PE, phycoerythrin; PerCP, peridinin-chlorophyll- protein; LDLR, LDL receptor; MCP-1, monocyte chemotactic protein-1; M-CSF, macrophage colony-stimulating factor; PDGF-BB, platelet derived growth factor (homodimeric form); TNF-α, tumour necrosis factor-α; IFN-γ, interferon-γ; MMLV, moloney murine leukaemia virus; ELISA, enzyme-linked immunosorbent assay; DAPI, 4', 6'-diamidino-2-phenylindole; RPMI, Roswell Park Memorial Institute; OCT, optimum cutting temperature; LDH, lactate dehydrogenase; EDTA, ethylenediaminetetraacetic acid.

2.2 Cell culture and maintenance

2.2.1 THP-1 monocytic cell line

The human acute monocytic leukaemia cell line THP-1 is extensively utilised in research on CVD. When the non-adherent THP-1 monocytes differentiate with phorbol 12-myristate 13-acetate (PMA) into macrophages, they mimic and display the physiological and biochemical activities of native human monocyte-derived macrophages (Auwerx 1991; Qin 2012). THP-1 monocytes were cultured in 75 cm^2 tissue culture flasks in RPMI-1640 tissue culture medium (containing L- glutamine and sodium bicarbonate), supplemented with 10% (v/v) heat-inactivated foetal bovine serum (HI-FBS; heated at 56°C for 1 hour), penicillin (100 U/ml) and streptomycin (100 µg/ml) (called complete medium hereafter) at 37°C in a humidified 5% (v/v) CO_2 incubator. In order to sub-culture cells, they were transferred from a flask to a 50 ml Falcon tube and centrifuged at 110 x g for 5 minutes at room temperature. The supernatant was then discarded, and the cell pellet was resuspended in 5 ml of complete medium. The cell suspension was then split into a ratio of approximately 1:30 and 20 ml fresh complete medium was added to each flask. For experimental use, cells between passage 4 and 10 were used.

THP-1 monocytes were differentiated into macrophages by incubating them with 0.16 µM PMA for 24 hours at 37°C, 5% (v/v) CO_2. In order to ensure that the differentiation had taken

place, the cells were examined under a microscope after 24 hours for changes in morphological features that are associated with the process. The PMA supplemented media was then aspirated, and the adherent cells washed once with 1X PBS before starting experiments.

2.2.2 RAW264.7 cell line

The RAW264.7 cell line is a mouse macrophage like cell line that is derived from BALB/c mice that had been injected with *Abelson leukaemia* virus (Kong et al. 2019). Since then, they have become a popular cellular model that is extensively employed in studies of different diseases, including atherosclerosis, due to their capability for performing macrophage functions, such as lipid uptake, gene expression and inflammatory response, associated with such diseases (Hu et al. 2020; Wan et al. 2021).

RAW264.7 is an adherent cell line that requires scraping to dislodge them from the flask surface. Cells were scrapped directly from the flask in the presence of old cell culture medium (about 20 ml of complete medium). The cell suspension was then transferred into a 50 ml Falcon tube and subjected to centrifugation at 110 x g for 5 minutes. After centrifugation, the pellet was resuspended in fresh complete RPMI-1640 tissue culture medium. Cells were then counted and seeded in cell culture plate and left to adhere in humidified incubator at 37°C for 24 hours before using them in experiments. The remaining cells were split at a ratio of 1:15 and 20 ml of fresh complete medium was added to each flask and allowed to adhere and reach confluence in approximately 3 days.

2.2.3 Human aortic smooth muscle cells (HASMCs) and human aortic endothelial cells (HAEC)

Primary human aortic smooth muscle cells (HASMCs) and human aortic endothelial cells (HAECs) are ideal model systems for studying parameters associated with atherosclerosis and CVD. Both models have been used extensively in research to delineate the mechanisms underlying atherosclerosis and atherosclerosis-related diseases (Liu et al. 2019a).

For cell maintenance, HASMCs were cultured in Smooth Muscle Cell Growth Medium and HAEC were cultured in Endothelial Cell Growth Culture Medium without adding FBS or

penicillin/streptomycin. Sub-culturing was carried out once cells had reached about 80% confluency.

Briefly to sub-culture or for experimental use, HASMCs or HAECs were firstly washed with Hank's Balanced Salt Solution (HBSS) or 1X PBS respectively, followed by incubation in 4 ml of 0.05% (w/v) trypsin-EDTA to dislodge the cells from the flask surface for 5 minutes in a 37^{o}C incubator with 5% (v/v) CO_2. In order to inactivate the trypsin enzyme, 5 ml of fresh culture medium was added. The cells were then pelleted by centrifugation for 5 minutes at 220 x g and resuspended in 3-5 ml of fresh culture medium depending on the pellet size. Cells between passage 4 and 10 were used. For experimental use, cells were seeded in cell culture plate at desired number (depending on experiments) and incubated at 37^{o}C incubator with 5% (v/v) CO_2 for a minimum of 1 hour and a maximum of 24 hours to allow cells to adhere before starting experimental protocols.

2.2.4 HepG2 cell line

HepG2 is a human liver cancer cell line that serves as a useful model for studying the pathogenesis of liver and liver-associated diseases. Numerous clinical observations and published research indicate that NAFLD increases the risk of atherosclerosis. HepG2 cell line is extensively used in research associated with NAFLD as seen during atherosclerosis and other metabolic disorders (Zhu et al. 2014; Han et al. 2020; Yu et al. 2021b).

HepG2 cells were seeded in 75 cm^2 tissue culture flasks in low-glucose DMEM medium supplemented with 10% (v/v) HI-FCS (heated at 56ºC for 1 hour) and Penicillin-Streptomycin (Pen-Strep) (100 U/ml) (called 'complete medium' from hereon) at 37°C in a humidified 5% (v/v) CO_2 incubator. The culture medium was replaced with fresh complete medium every other day and cells were sub-cultured when confluency reached about 70-80%.

To remove the cells from flasks either for experimental use or sub-culturing, the culture medium was discarded, and the cells were then washed with 1X PBS. Cells were then detached by trypsinisation using 5 ml of 0.05% (w/v) trypsin-EDTA for 5 minutes in a 37°C incubator. To inhibit trypsin activity, complete medium was added. The cells were then centrifuged at 110 x g for 5 minutes and the supernatant discarded. The resulting pellet was finally resuspended in 5 ml of fresh complete medium. For subculturing, cells were seeded in

new 75 cm^2 culture flasks at 2.1 x 10^6 cells in 15 ml of complete medium. On the other hand, for experimental processes, cells were seeded either in 24- or 96-well plates and only cells between passages 3-10 were used.

2.2.5 Freezing and thawing frozen cells

Only healthy cells that were passage 4 or less were frozen as stock. Once cells reached a minimum confluency of 80%, cells were harvested as previously mentioned (from Sections 2.2.1 to 2.2.4). The pellet was then resuspended in 10% (v/v) DMSO in HI-FCS. The cells were then counted and an amount of 1 ml, containing approximately 1 x 10^6 cells, were transferred into cryovials. Cells were then frozen by reducing the freezing temperature gradually by placing cryovials in a Nalgene Mr. Frosty™ freezing container. This step is vital to avoid cell shock associated with rapid freezing. The Nalgene Mr. Frosty™ freezing container was filled with isopropanol before being transferred to -80°C overnight. Cryovials were then either kept at -80°C for short-term storage or transferred to liquid nitrogen for long-term storage to be used as a stock.

For thawing, stock vails were defrosted in a 37°C water bath for a maximum of 1-2 minutes. Cells were then vigorously pipetted up and down to homogenise the cell suspension before being transferred into a 15 ml Falcon tube containing 10 ml of complete culture medium and centrifuged for 5 minutes at 110 x g to remove DMSO from the cells. The supernatant was discarded, and the pellet was resuspended in complete medium. Cell suspension was then transferred into culture flasks and placed into a humidified 37°C incubator containing 5% (v/v) CO_2. The flask was left undisturbed for 24 hours before changing culture medium to wash all traces of DMSO. Cell culture was maintained as detailed above (from Sections 2.2.1 to 2.2.4).

2.2.6 Culture of human monocyte-derived macrophages

THP-1 monocyte-derived macrophages have characteristics that are similar to those of primary human macrophages, and laboratory findings on THP-1 macrophages are often confirmed in primary human cells (McLaren et al. 2010). To rule out the possibility that the findings obtained in this study were due to the transformed nature of the THP-1 cell line, some key findings were confirmed using human monocyte-derived macrophages (HMDMs).

Buffy coats were supplied by the National Blood Service Wales who also granted ethical permission for their use in research. HMDMs were isolated from human buffy coats using the procedure summarised in Figure 2.1.

The blood from the buffy coat was transferred to 50 ml Falcon tubes and diluted with Dulbecco's PBS (1:1) at room temperature (RT). To obtain the peripheral blood mononuclear cells (PBMCs), 25 ml of diluted blood was then layered slowly over 15 ml of Lymphoprep^{TM} that was already placed at the bottom of 50 ml Accuspin tubes. Separation was achieved by centrifugation at 250 x g at RT for 30 minutes (no brake was applied during this centrifugation step). The upper plasma layer was then removed as much as possible and the PBMCs layer was then carefully transferred to a new 50 ml Falcon tube. The PBMCs were then incubated with 1 ml of ice-cold ammonium chloride solution (0.8% NH_4Cl in 0.1 mM EDTA in water buffered with $KHCO_3$ to achieve a final pH of 7.2-7.6) for 2-3 minutes to lyse the red blood cells. This was followed by centrifugation for 7 minutes at 250 x g at 4°C with the step repeated as required to remove red blood cells and get a clear pellet. In order to remove any platelet contamination, PBMCs were washed with 10 ml cold Dulbecco's PBS for 4-7 times. The final pellet was then resuspended in complete RPMI-1640 medium and seeded at desired numbers in Helena Bioscience 12- or 96-well tissue culture plates. Monocytes were finally differentiated into HMDMs by incubating them in RPMI-1640 complete medium containing human macrophage-colony stimulating factor (HM-CSF; 20 ng/ml) at 37°C, 5% (v/v) CO_2 for 4-6 days. Once differentiated, HMDM cells were washed extensively with complete RPMI to remove any non-adhering cells and then used in experiments.

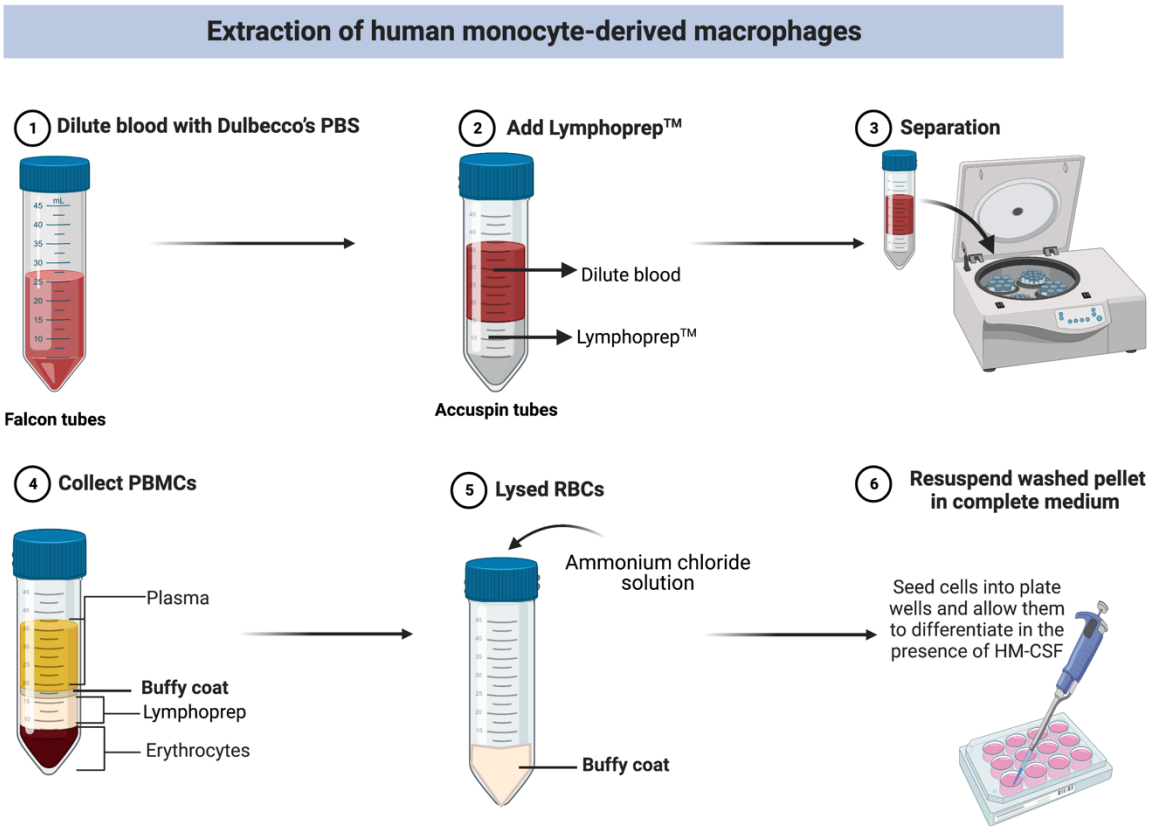

Figure 2.1 Isolation of human monocyte-derived macrophages

Blood was diluted with equal parts of Dulbecco's PBS (1), the diluted blood was then layered over the Lymphoprep™ (2). This was followed by centrifugation without brake to enable the separation of PBMCs, Lymphoprep™ and erythrocytes (3,4). The PBMCs layer was carefully transferred to new tube and incubated with ice-cold ammonium chloride solution to lyse red blood cell (5). After many washing steps to removing contaminating platelets, the pellet was resuspended in complete RPMI-1640 medium and seeded in Helena Bioscience tissue culture plates (6). **Abbreviations:** PBS, phosphate-buffered saline; PBMCs, peripheral blood mononuclear cells; RBCs, red blood cells; HM-CSF, human macrophage-colony stimulating factor. Image created with BioRender.com.

2.2.7 Cell counting

A haemocytometer was used to determine the number of cells in a suspension in order to seed the required number of cells for experiments. Haemocytometer was prepared by cleaning the chamber surface with 75% ethanol and drying well. A small volume (7.5 µl) of the cell suspension was placed on the haemocytometer and a glass cover slip was then used to cover the haemocytometer and to ensure even distribution of cells on a 5 x 5 grid (the central area of the counting chamber). Using hand tally counter, cells within the four corner and middle square of 5 x 5 grid were counted. The obtained number was then multiplied by

5. To determine the required volume (µl) of cell suspension to be seeded, the following formula was used: (number of cells required / cell count)/10.

2.3 Cell treatment

2.3.1 Preparation of RSV

RSV (≥ 99%) was dissolved in DMSO, which therefore served as a vehicle control, and a 43.8 mM stock was prepared. Stock solution was then aliquoted and stored at -20°C until use. For experiments, 1 mM working solution was freshly made up in appropriate tissue culture medium and further dilution was prepared according to experimental conditions in 0.1% (v/v) DMSO for all *in vitro* experiments.

2.3.2 Cell treatment

Depending on the experiment, treatment duration ranged from a minimum of 3 hours (short-term effect) to a maximum of 8 days (long-term effect). The incubation of cells with either RSV or vehicle control was carried out in a humidified 37^{o}C incubator containing 5% (v/v) $CO_{2.}$ In incubation time of over 24 hours, the cells were provided with a freshly made treatment solution in the appropriate culture medium every 24 hours. This was done due to the ability of RSV to be degraded over time (in days) at temperatures above 25°C (Navarro-Orcajada et al. 2022).

2.4 Preparation of glassware and solutions

Glassware and solutions were autoclaved (if necessary) for 20-30 minutes at 121°C (975kPa).

2.5 Cells-based assays

2.5.1 Cell viability

This assay was carried out firstly to verify that there was no cytotoxic effect of RSV on cells and to confirm that any findings were not a result of cell death. The Pierce^{TM} Lactate Dehydrogenase (LDH) Cytotoxicity Assay Kit was used for this purpose, and the assay was carried out according to the manufacturer's instructions (ThermoFisher Scientific).

Lactate dehydrogenase (LDH) is a cytoplasmic enzyme present in many cell types, which is rapidly released when the plasma membrane is damaged. It is frequently used to measure cytotoxicity. The released LDH catalyses a reaction involving the reduction of nicotinamide adenine dinucleotide (NAD) to NADH in a process of conversion of lactate to pyruvate. In this assay, the reduction of tetrazolium salt (yellow) by NADH into formazan (red) is measured at 590 nm. Extracellular LDH concentration is directly proportional to the number of damaged cells.

THP-1 macrophages (10^5 cells/well), HMDMs (10^5 cells/well), HAECs (10^4 cells/well), HASMCs (10^4 cells/well) or HepG2 cells (10^4 cells/well) were seeded into 96-well plate and incubated with RSV or DMSO vehicle control for 24 hours. As some experiments on HASMCs required incubation greater than 24 hours, the viability for HASMCs was assessed over a 8-day period. Following the manufacturer's instructions, 10 µl of lysis buffer (provided in the kit) was added to the positive control well and the same volume of H_2O was added to all the other wells. The plate was then returned to a humidified incubator at 37ºC for 45 minutes. Then, 50 µl of cell supernatants were transferred to a new 96-well plate and 50 µl of reaction mix (prepared by combining the substrate mix and the assay buffer provided in the kit) was added to all samples and incubated at 37ºC for 30 minutes. The reaction was then stopped by adding stop solution (provided in the kit) and the cellular LDH concentration was measured using a microplate reader at 570 nm absorbance. The results were expressed as a percentage to the DMSO vehicle control, which was arbitrarily assigned as 100%.

2.5.2 Cell proliferation

The remaining cells from the LDH assay were stained with 0.2% (w/v) crystal violet (CV) solution (in 10% (v/v) ethanol) and incubated for 5 minutes at room temperature. CV binds to the nucleic acid of adherent cells but not to those that have died or are detached. The cells were then washed 3 times with 100 µl of 1X PBS and the intracellular CV was dissolved using 0.1 M NaH_2PO_4 in 50% (v/v) ethanol. The absorbance was read at 570 nm, and the results were expressed as a percentage to the DMSO vehicle control, which was arbitrarily assigned as 100%.

2.5.3 HASMCs proliferation rate over 8 days

To confirm the significant changes observed in HASMCs proliferation using crystal violet staining, the rate of HASMCs proliferation was assessed using 5-Bromo-2'-deoxy-uridine Labeling and Detection Kit III (Sigma-Aldrich), in which uridine with a bromine substituted at the fifth carbon atom (BrdU) is incorporated into RNA within cells. These changes in RNA levels can be measured using standard enzyme-linked immunosorbent assay (ELISA) where high RNA levels indicates an increase in cell numbers and, therefore, increased cell proliferation rate. The BrdU is targeted with a monoclonal anti-BrdU labelled antibody with peroxidase, that after addition of the substrate, catalyses the formation of a coloured reaction product that can be detected at 405 nm.

HASMCs were seeded in a 96-well plate and incubated at 37°C, 5% (v/v) CO_2 with the vehicle control or RSV, and the proliferation rate was assessed over a 8-day period. The old medium was replaced with fresh culture medium every 2 days to maintain culture conditions. Following the incubation period, the proliferation rate was assessed using the BrdU Labeling and Detection Kit III following the manufacturer's instructions (Sigma-Aldrich). All reagents were provided in the kit and reconstituted according to the manufacturer's instructions. Following incubation with the treatment, 10 µM bromouridine labelling solution was added to the cells and the plate returned to the humidifier incubator for 3 hours for incorporation to occur. The media was then aspirated, and the cells washed twice using 250 µl of complete media. After the last wash, the media was carefully removed, and the cells were fixed by incubation with 200 µl of ice-cooled fixative (0.5 M HCl in 70% (v/v) ethanol) for 30 minutes at -20°C. Once fixed, the fixative was removed, and the cells were washed a further three times with 250 µl of complete media. Then, 100 µl of nucleases (provided in the kit) was then added to the cells and the incubation for 30 minutes in the absence of CO_2 (water bath). The cells were again washed 3 times in culture media, as described above, and incubated with 100 µl anti-BrdU-POD, Fab fragments solution (provided in the kit) for 30 minutes at 37°C, 5% (v/v) CO_2. The antibody conjugate was then removed, and the cells were washed with 250 µl washing buffer (provided in the kit) for 3 times before being incubated with 100 µl peroxidase substrate solution (provided in the kit) at room temperature in darkness for 30 minutes. A microplate reader was then used to measure the colour product at 405 nm with a secondary

reference wave-length at 490 nm. The results were expressed as a percentage to DMSO vehicle control, which was arbitrarily assigned as 100%.

2.5.4 Monocyte migration

This assay involved comparing the migration of THP-1 monocytic cells in response to the MCP-1 in the presence of the vehicle control or RSV. Migration was performed using the modified Boyden chamber method. In this assay, 8 µm pore Falcon® cell culture inserts and Falcon® 12-well companion plates were used, in which the cell culture inserts mimic the arterial endothelium (Figure 2.2).

THP-1 monocytes at a concentration of $1x10^6$ cells/ml were suspended in complete medium containing either RSV or DMSO and placed on top of cell culture inserts in the modified Boyden chamber. In the bottom chamber, 1 ml of complete media containing 20 ng/ml of MCP-1 was placed for all conditions except the negative control that had no chemokine. After 3 hours of incubation at 37^{o}C to allow cells to migrate, the remaining cells on the top of the insert membrane were removed. In order to ensure that all the migrating cells were captured, the membrane was washed using 0.5 ml of 1 X PBS. The remaining media was transferred into Falcon tubes and subjected to centrifugation at 110 x g for 5 minutes at room temperature. The cell pellet was resuspended in 1 ml of 1 X PBS. To facilitate cell counting, the haematocytometer was employed as described in Section 2.2.7 and the final value was expressed as a percentage in relation to the total input cells.

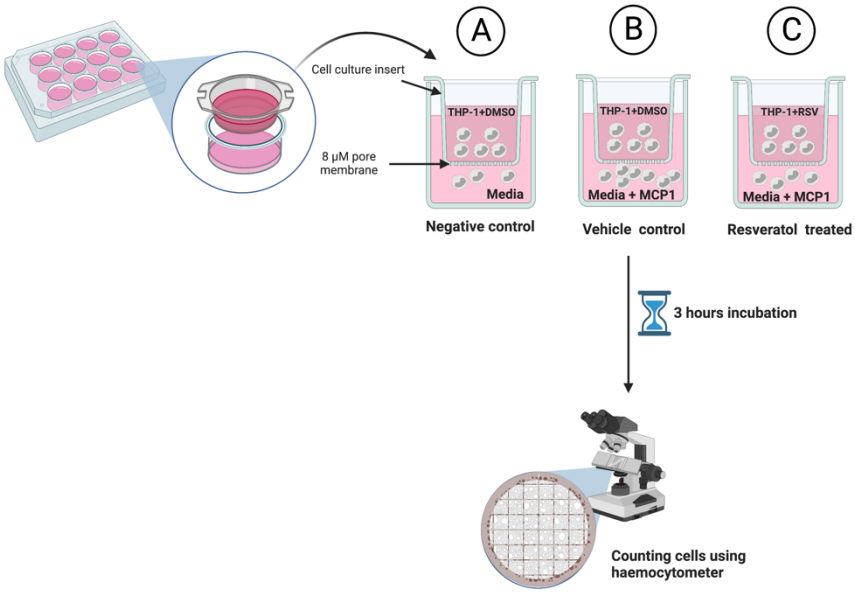

Figure 2.2 Illustration of the experimental set up for the monocyte migration assay using the modified Boyden chamber method.

THP-1 monocytes were suspended in either the vehicle control (DMSO) or RSV and then placed on top of a cell culture insert with 8 µm pores (upper chamber). Cells were then incubated for 3 hours to allow migration of the cells to the lower chamber in response to the chemoattractant stimulus (MCP-1). Migrated cells in the lower chamber were then counted using a haemocytometer. (A) represents negative control where the assay was carried out in the absence of MCP-1 in the lower chamber (media only), as a result limited migration should be seen. (B) representing vehicle control (positive control) where the assay was carried out in the presence of MCP-1 in the lower chamber. High number of migrated cells are expected in the bottom chamber. (C) representing treatment conditions, cells were suspended in media containing RSV and placed in the upper chamber and media plus MCP-1 in the lower chamber. The effective treatment should result in a reduction in the number of migrated cells in the bottom chamber if anti-atherogenic. **Abbreviations:** MCP-1, monocyte chemoattractant protein-1. Image created with BioRender.com.

2.5.5 Smooth muscle cell invasion

The effect of RSV on the invasion of SMCs was investigated using HASMCs in a modified Boyden chamber set up similar to that used for monocyte migration. Instead of the MCP-1 chemoattractant in monocyte migration, human platelet-derived growth factor-BB (PDGF-BB; homodimeric form of PDGF) was used to stimulate HASMC invasion. Firstly, Matrigel extracellular matrix (ECM) gel (from Engelbreth-Holm-Swarm murine sarcoma) was prepared. Stock Matrigel vial was kept at -20°C and thawed at 4°C just before use as recommended by the manufacturer (Sigma-Aldrich). The Matrigel was kept on ice to avoid gel solidification. The Matrigel was then diluted with ice-cold DMEM at a ratio of 2:1. Falcon® cell culture inserts with 8 µm pore were then coated with 300 µl of diluted Matrigel solution using pre-cooled

pipette tips. Excess gel solution was then quickly removed using a pipette. The plate was then left undisturbed in a 37°C humified incubator for 30 minutes to allow the gel to set.

Once set, the cells at a concentration of 1 x 10^5 cells/insert in 500 µl of DMEM complete medium were added to the upper chamber and returned to the incubator for 1-2 hours to allow the cells to adhere. After incubation, the culture media was then replaced with 500 µl of serum-free DMEM, and the plate returned to the incubator for a further 48 hours to induce quiescence. After 48 hours, the serum-free DMEM was replaced with 500 µl of either vehicle control or RSV in serum-free DMEM. In the bottom of the chamber, 1 ml of DMEM complete medium was added either alone in negative control wells or with PDGF-BB (20 ng/ml) in vehicle control and RSV wells. The plate was incubated for a further 4 hours at 37°C, 5% (v/v) CO_2 to allow invasion to occur. Medium was then removed from the inserts and the cells on the upper side of the membrane were removed using cotton swabs. The inserts were then carefully removed using a scalpel and the cells on the underside of the membrane were mounted on slides with Fluoroshield™ mountant containing DAPI. The number of cells that migrated through the membrane in different fields of view were counted and an average taken over 5 high power fields (HPF) using an Olympus BX61 microscope (x20 magnification) with a DAPI filter (Figure 2.3). The results were expressed as a percentage to PDGF-BB vehicle control which was arbitrarily set as 100%.

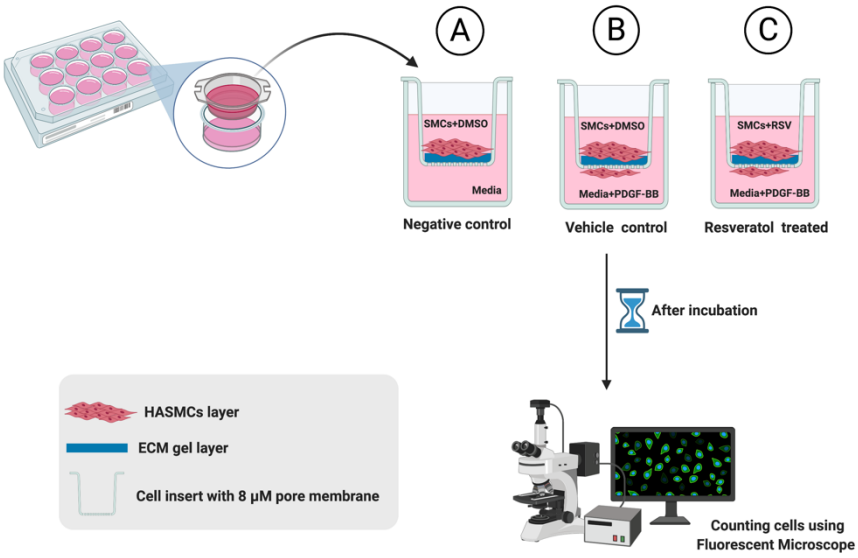

Figure 2.3 Diagrammatic representation of the set up for the HASMCs invasion assay using the modified Boyden chamber method.

HASMCs were suspended in either the vehicle control (DMSO) or RSV and then placed on the cell culture insert with 8 µm pores (upper chamber) coated with the ECM gel. Cells were then allowed to invade through the ECM gel layer to the downside of the insert in response to the chemoattractant stimulus (PDGF-BB). The inserts were removed and mounted on slides with Fluoroshield™ mountant containing DAPI. Cells were then counted, and an average taken over 5 high power fields (HPF) using an Olympus BX61 microscope with a DAPI filter. (A) representing negative regulation, with cells containing vehicle in the upper chamber and media alone in the lower chamber, indicating unstimulated invasion to the underside of the membrane. (B) representing vehicle control (positive control) where the assay was carried out in the presence of PDGF-BB in the lower chamber and cells plus vehicle in the upper chamber. (C) representing treatment well; cells were suspended in media containing resveratrol and placed in the upper chamber and media plus PDGF-BB in the lower chamber. **Abbreviations:** SMCs, smooth muscle cells; PDGF, platelet-derived growth factor; ECM, Matrigel extracellular matrix. Image created with BioRender.com.

2.5.6 Reactive oxygen species (ROS) microplate assay

To measure ROS production/activity, the 2', 7'–dichorofluorescin diacetate (DCFDA) cellular ROS detection kit was used, and the procedures were carried out according to the manufacturer's instructions (Abcam). The main components in the kit are DCFDA and Tert-Butyl Hydrogen Peroxide (TBHP). TBHP causes the production of ROS that then oxidises DCFDA to 2', 7' –DCF, where DCF is a fluorescent compound that can be measured using a plate reader. THBP was therefore used to induce ROS levels in the cells and the effect of RSV or vehicle on this was analysed.

THP-1 monocytes (1.5 x 10^5 cells/ml), THP-1 macrophages (1 x 10^5 cells/ml), HASMCs (1.5 x 10^4 cells/ml) or HMDMs (3x10^5 cells/well) were used. The densities of cells used were based on previous optimisation in the laboratory to account for cell size variations and the maximum increase in ROS production induced by TBHP observed. Cells were resuspended in the 20 µM DCFDA stain for THP-1 monocytes or macrophages and HepG2 cells, 25 µM for HASMCs and 40 µM for HMDMs (again based on previous optimisation experiments in the laboratory). They were then incubated for 45 minutes at 37°C in a humidified incubator containing 5% CO_2 in darkness. The cells were then washed twice using 1 X dilution buffer (provided in the kit) to remove the stain. In case of THP-1 monocytes, the cells were centrifuged at 110 x g for 5 minutes at room temperature to remove the stain and then washed twice using 1 X dilution buffer. After this washing step, the cells were treated with the required concentration of resveratrol or the DMSO vehicle in complete medium. In addition, TBHP solution at a final concentration of 50 µM (75 µM for HMDMs) was added to all cells except the negative control. The cells were then incubated for 3 hours at 37°C in a humidified incubator containing 5% CO_2 in darkness. The fluorescence was then measured at Ex458/Em535 using Infinite f Nano$^+$ microplate reader. The fluorescent readings were standardised to the TBHP control, which was arbitrarily set at 100%.

2.5.7 Fatty acids-induced ROS production in HepG2 cells

Intracellular production of ROS was also assessed in HepG2 hepatic steatosis model. In which HepG2 cells were incubated with 1mM of oleic acid (OA) and palmitic acid (PA) at a ratio of 2:1 to induce hepatic steatosis. Furthermore, optimisation experiments in the laboratory showed that OA and PA at a ratio of 2:1 are capable of inducing ROS production.

HepG2 cells (1.5 x 10^4 cells/well) were seeded in 96-well plate and left to adhere overnight. The complete medium was then changed to a serum-free medium and incubation continued in a 37°C humidified incubator for 24 hours. Cells were then washed twice with 1X dilution buffer (provided in the kit) and stained with 20 µM DCFDA by incubation for 45 minutes at 37°C in a humidified incubator. The DCFDA solution was removed, and the cells were washed again and treated with RSV or DMSO in the presence of OA:PA (treatments were prepared in 1% (w/v) fatty acid free BSA culture medium) for 24 hours at 37°C in a humidified incubator

containing 5% CO_2. The fluorescence was then measured at Ex458/Em535 using a plate reader.

2.5.8 Mitochondrial ROS production

In mammalian cells, mitochondria are a major intracellular source of ROS. Excess production of mitochondrial ROS (mitoROS) results in oxidative damage to mitochondrial proteins, membranes, and DNA, thereby causing impaired metabolic functions and limiting mitochondria's capacity to generate ATP. Consequently, this oxidative damage of the mitochondria contributes to a wide range of pathologies such as atherosclerosis (Murphy 2009). To investigate the effect of RSV on mitoROS production, MitoSOX™ Red mitochondrial superoxide indicator kit was used due to its high selectivity to detect ROS in the mitochondria of live cells. MitoSOX^{TM} Red reagent is a fluorogenic dye that is permeable to living cells and targets mitochondria rapidly and specifically. Once in the mitochondria, it is oxidised by superoxide to produce red fluorescence.

THP-1 monocytes ($8x10^4$ cells/well) were seeded into a 96-well plate and treated with RSV or vehicle (DMSO) for 24 hours in a humidified 37°C incubator containing 5% (v/v) CO_2. Next day, 5 µM MitoSOX^{TM} Red working reagent was prepared in HBSS according to the manufacturer's instructions (ThermoFisher Scientific). The cells were washed with 1X PBS and stained with 5 µM MitoSOX^{TM} Red reagent by incubation for 30 minutes in a 37°C incubator containing 5% (v/v) CO_2. The cells were then washed with fresh HBSS and 100 µl of HBSS was added to the wells and fluorescence was measured in a microplate reader at Ex510/Em580 nm. Results were standardised to the vehicle that was stained with MitoSOX^{TM} Red (positive control), which was set arbitrarily as 100%.

2.5.9 Oil Red O staining to evaluate lipid accumulation in HepG2 cells

ORO solution is a red fat-soluble lysochrome that is commonly used in research for quantitative and qualitative measurement of lipid droplets in the sample. The ORO solution can only stain the neutral lipid components in the cell such as cholesterol esters and

triglycerides without staining amphiphilic lipids in cell membranes such as phospholipids (Mehlem et al. 2013).

HepG2 cells at a density of $15x10^5$ cells/well were seeded in 24-well plates and left to adhere overnight. The complete medium was then changed to serum-free medium and returned to a 37°C humidified incubator containing 5% (v/v) CO_2 for 24 hours. In this assay and other assays involving analysis of lipids, the complete medium was replaced by culture medium supplemented with 0.2% (w/v) fatty acid-free BSA because of the ability of HI-FCS to stimulate cholesterol efflux from the cells and therefore affecting the accuracy of the assay (Gallagher 2016).

Cells were then treated with RSV or vehicle control (DMSO) in the presence of a combination of 1mM of OA and PA at a ratio of 2:1 that was prepared in DMEM medium containing 1% (w/v) fatty acid-free BSA. Negative vehicle control was included with no OA and PA. After incubation for 24 hours, the overlying medium was discarded, and adherent cells were then washed gently with 1X PBS. Cells were then fixed by incubation with 4% paraformaldehyde (PFA) for 10 minutes at room temperature. The PFA was then aspirated, and the excess was removed by washing the cells twice using 1XPBS. To stain the neutral lipids, the cells were incubated with 250 µl of Oil Red O solution (ORO; 0.5% (w/v) in isopropyl alcohol) for 20 minutes at room temperature in darkness. In order to remove background staining, the cells were washed three times with deionised distilled water (ddH_2O). Intracellular stained lipid content was then extracted by incubation of the cells with 250 µl of 60% isopropanol for 10 minutes at room temperature in darkness. The extracted ORO (100 µl) was then transferred to a 96-well plate and the absorbance measured at 540 nm using a microplate reader. Results were standardised to the positive vehicle control, which was arbitrarily assigned as 100%.

2.5.10 Foam cell formation assays

2.5.10.1 Dil-oxLDL uptake

The uptake of modified lipoproteins such as oxLDL is an important step in atherosclerosis lesion progression (Xia et al. 2013). In addition to macrophages, VSMCs contribute significantly to foam cell formation via their scavenger receptors (Chellan et al. 2016;

Basatemur et al. 2019). 1,1'-diocadecyl-3-3-3',3'-tetramethyl indocarbocyanine perchlorate (Dil) is a lipophilic dye that is capable of diffusing into the hydrophobic part of LDL particles without affecting their ability to bind to apolipoprotein B or their cognate cell surface receptors (Raniolo et al. 2016; Gu et al. 2017). The labelling of oxLDL with Dil (Dil-oxLDL) is extensively used in lipid uptake assays because it is recognised by scavenger receptors such as SR-A and CD36 in macrophages and VSMCs. The level of oxLDL uptake can then be determined by flow cytometry.

THP-1 macrophages (1×10^6 cells/well), HASMCs ($1.5X10^4$ cells/well) or HMDMs (5×10^5 cells/well) were incubated with RSV or the vehicle control (DMSO) in the presence of Dil-oxLDL (5 µg/ml; except negative vehicle control cells, which has no Dil-oxLDL) in appropriate culture medium supplemented with 0.2% (w/v) fatty acid-free BSA for 24 hours at 37°C in a humidified incubator containing 5% (v/v) CO_2.

In order to collect the cells, the medium was aspirated, and the cells removed by incubation with 0.05% (v/v) trypsin for 5 minutes in a 37°C humidified incubator before deactivation of the enzyme by adding an equal volume of complete culture medium. Cells were then collected in 1.5 ml Eppendorf tubes and subjected to centrifugation at 9,000 x g for 5 minutes. The pellet was resuspended in 2% (w/v) PFA and Dil-oxLDL uptake was quantitated by using BD LSRFortessa ™ cell analyser. At least 10,000 events were counted for each sample. DMSO with Dil-oxLDL was used as a positive control and the results were arbitrarily assigned as 100%.

2.5.10.2 Macropinocytosis

In addition to their scavenger receptors, both macrophages and VSMCs uptake lipids and lipoproteins by macropinocytosis. This is an important pathway by which macrophages and VSMCs uptake cholesterol during foam cell formation (Rivera et al. 2013). Lucifer yellow (LY) is one of the most employed fluorescent tracers in research that can enter cells via macropinocytosis. It can be internalised by the cell from the surrounding medium without toxic effect on cells (Swanson and Silverstein 1988; Hanani 2012). Consequently, measuring the LY signal within macrophages and VSMCs can be used as a marker for the level of macropinocytosis, which has occurred within the cells (Lim and Gleeson 2011).

THP-1 macrophages (1 ×10^6 cells/well), HASMCs (1.5X10^4cells/ml) or HMDMs (5 ×10^5 cells/well) were treated with RSV or the DMSO vehicle in the presence of 100 µg/ml of LY for 24 hours at 37°C in a humidified incubator containing 5% (v/v) CO_2. The overlying medium was then discarded, and the cells removed from the plastic surface by treatment with 0.05% (v/v) trypsin for 5 minutes in a 37°C humidified incubator before deactivation of the enzyme by adding an equal volume of complete culture medium. The cell suspension was then collected in 1.5 ml Eppendorf tubes and centrifuged at 9,000 x g for 5 minutes to pellet the cells. The resulting pellet was resuspended in 2% PFA and the LY uptake was analysed using the FACS Canto flow cytometer, counting a minimum of 10,000 events for each sample. DMSO with LY was used as a positive control and values were arbitrarily assigned as 100%.

2.5.10.3 Cholesterol efflux

The assay was carried out following the manufacturer's instruction (Abcam) with some modifications. THP-1 macrophages (150 x 10^5 cells /well) were labelled with labelling medium mix (provided in the kit and prepared by mixing with serum-free RPMI medium) by incubation for 1 hour at 37°C in a 5% (v/v) CO_2 incubator. After labelling, a mixture of equilibration buffer (provided in the kit) and ac-LDL (25 µg/ml) was prepared immediately before adding to the cells. The plate was returned to a 37°C, 5% (v/v) CO_2 incubator for incubation for 24 hours. The next day, the equilibration medium was gently aspirated, and the cells were washed with phenol red-free, serum-free RPMI-1640 culture medium. Cells were then incubated at 37°C, 5% (v/v) CO_2 incubator for 3-4 hours in vehicle and LXR agonist (TO-901317) (negative control), with vehicle plus LXR agonist (TO-901317, 2µM) plus apoA1 (10 µg/ml; vehicle control), or with RSV plus apoA1 (10 µg/ml) plus LXR agonist (TO-901317). The LXR agonist was used to induce ABCA1 and ABCG1 expression in macrophages, thus promoting cholesterol efflux. At the end of the incubation period, the supernatant was transferred to a white 96-well plate (with opaque, flat-bottom wells) and the fluorescence was measured at Ex458/Em535. The adherent cells were then solubilised with cell lysis buffer (provided in the kit) with shaking for 30 minutes at room temperature. Finally, the cell lysate was transferred to another white 96-well plate (with opaque, flat-bottom wells) and the fluorescence at Ex458/Em535 was measured. Cholesterol efflux was calculated by dividing the fluorescence intensity from the supernatant by the sum of the fluorescence intensity of the supernatant and cell lysate. The obtained value was then multiplied by 100 to get % of cholesterol efflux.

2.5.10.4 Phagocytosis

This assay was carried out to assess the effect of resveratrol on phagocytic capability of macrophages using the Vybrant® Phagocytosis Assay Kit according to the manufacturer's instructions (ThermoFisher Scientific). The principle of this assay is based on the internalisation of fluorescein-labelled killed *E. coli* (K-12 strain) cells. In addition to the lyophilised *E. coli*, trypan blue solution is used to quench the fluorescence from particles that were not internalised as described in the manufacturer's protocol.

THP-1 macrophages (15 $\times 10^4$ cells/well) were seeded in a 96 well plate and incubated with either the vehicle (DMSO) or RSV for 3 hours at 37°C, 5% (v/v) CO_2 (Negative control wells with media and DMSO only were also included). After three hours incubation, the supernatant was replaced with *E. coli* BioParticles® and the plate was then transferred back to the incubator for a further 2 hours. The *E. coli* BioParticles® were then aspirated and trypan blue (provided in the kit) was added to all the wells followed by incubation at room temperature for 1 minute to stain the cells and to limit fluorescence from non-internalised BioParticles. Excess trypan blue was then removed, and fluorescence was determined using a microplate reader at Ex/Em 480/520 nm. Net phagocytosis was calculated after subtracting the average fluorescence intensity from negative-control wells. The data were presented as a percentage in relation to the vehicle control, which was arbitrarily assigned as 100%.

2.5.11 Cholesterol metabolism

The incorporation of [^{14}C] acetate into major lipid classes was measured to determine the effect of RSV on intracellular cholesterol metabolism. RAW264.7 macrophages had been chosen to carry out this assay based on previous work within the laboratory that has demonstrated the ability of RAW264.7 to produce much greater quantities of intracellular lipids, particularly sterol esters, compared to THP-1 macrophages.

2.5.11.1 Lipid extraction

RAW264.7 macrophages (2 x 10^6 cells/well) were seeded in 6-well plate for 24 hours in culture medium at 37°C in 5% (v/v) CO_2 to allow the cells to adhere. Once adhered, the cells were then incubated with either the vehicle plus [^{14}C] acetate (1 µCi/ml; negative control),

vehicle plus [^{14}C] acetate (1 µCi/ml) and 25 µg/ml acLDL (vehicle positive control) or RSV plus [^{14}C] acetate (1 µCi/ml) and 25 µg/ml acLDL for a further 24 hours. The lipids were then extracted following Folch's method (Folch et al. 1957). After aspirating the overlying medium, the adherent cells were washed with 1X PBS and removed from the culture plate by scraping. The cell suspension was then transferred to Eppendorf tubes and centrifuged for 5 minutes at 9,000 xg. The pellet was then resuspended in 1ml of dH_2O to induce phase separation and transferred to glass tubes with 2 ml of chloroform: methanol (2:1) solution. Samples can be stored at -20°C in Sparkfree freezers (Sparkfree freezers have to be used to avoid any chance of igniting flammable liquids) and are stable for a week. Samples were then vortexed and lipid separation was achieved by centrifugation of the samples for 5 minutes at 220 x g. The upper aqueous phase contains polar molecules, the interphase contains precipitated proteins, and the lower phase (chloroform layer) contains lipids. The lower layer was then collected carefully without disturbing the interphase layer using a glass pipette into a new clean glass tube, evaporated under nitrogen gas and reconstituted in 50 µl of chloroform. The solution was then transferred into 2 ml glass chromatography vial and stored at -20°C in Sparkfree freezers.

2.5.11.2 Thin layer chromatography (TLC)

One-dimensional TLC was performed to separate different lipid classes. This allows separation of the following lipid classes: total polar lipids (TPL), triglycerides (TG), free fatty acids (FFA) and cholesterol esters (CE). The extracted lipids were applied on a silica gel G Merck plate (10 X 10) that was then placed vertically in a glass tank containing a shallow layer of solvent mixture of hexane: diethyl ether: acetic acid (80:20:1, v/v/v). The glass tank was covered to ensure that the atmosphere in the tank was fully saturated with solvent vapour. To allow maximum separation, the solvent was left to rise until it reached the top of the plate (about 2 mm). The plate was then removed from the tank and left to dry at room temperature. Once dry, the plate was sprayed with a 0.05% (v/v) solution of 8- anilino-4-naphthosulphonic acid (ANSA) in methanol to allow detection of lipid fractions under UV light. The position of the separated lipid fractions on the plate was then marked using a pencil. Subsequently, the plate was sprayed with water for scraping regions of interest, which were transferred immediately into individual scintillation vials. OptiFluor® scintillation fluid (10 ml) was added to each

sample before measuring the radioactivity in each lipid fraction using liquid scintillation counter. The assay was conducted as illustrated in Figure 2.4.

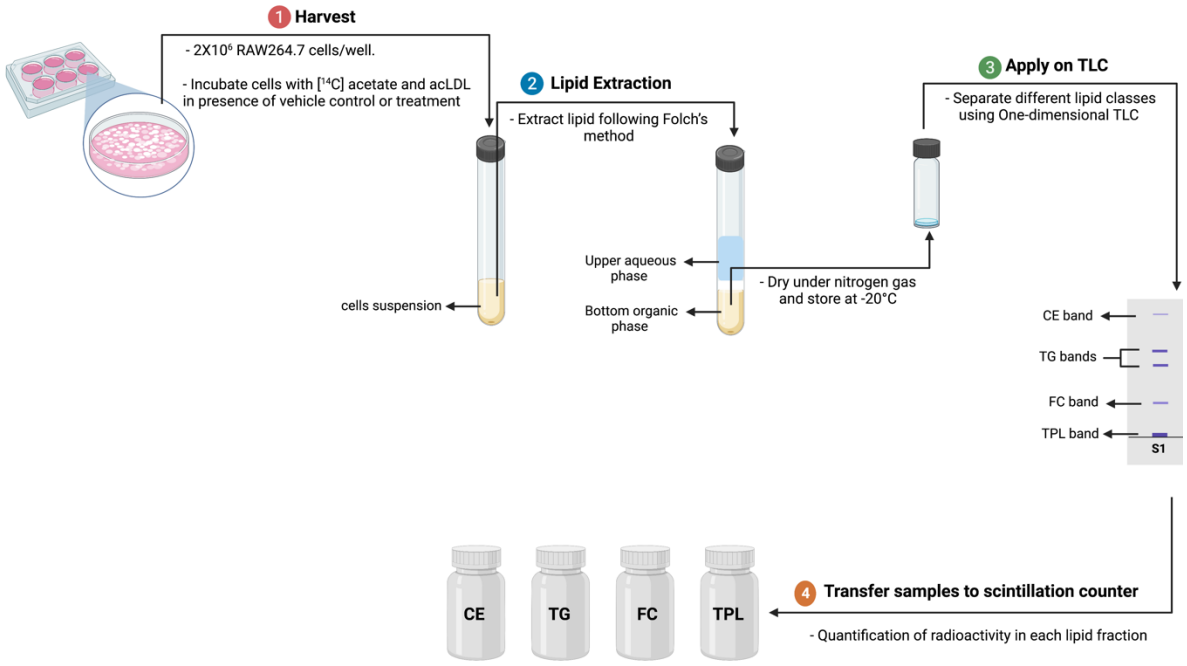

Figure 2.4 Experiment set-up for [^{14}C] acetate incorporation

In the first step, RAW 264.7 cells were incubated with [^{14}C] acetate, acLDL and treatments for 24 hours. Cell suspension was then collected, and the lipids were extracted following Folch's method. Extracted lipids were applied on TLC plates to separate different lipid classes. Finally, each lipid fraction was then transferred into scintillation vail and radioactivity was measured using scintillation counter. **Abbreviations:** TLC, thin layer chromatography; CE, cholesterol ester; TG, triglyceride; FC, free cholesterol; TPL, total polar lipid. Image created with BioRender.com.

2.5.12 Molecular techniques

2.5.12.1 Stimulation of THP-1 macrophages and endothelial cells with cytokines

To assess the effect of RSV on ICAM-1 and MCP-1 gene expression under inflammation conditions, both THP-1 macrophages and endothelial cells were stimulated using appropriate cytokines. THP-1 macrophages were incubated with IFN-γ (250 U/mL) while HAECs were stimulated with TNF-α (50 ng/ml), both for 24 hours at 37°C in a 5% (v/v) CO_2 incubator.

2.5.12.2 RNA extraction

RNA was extracted from THP-1 macrophages and HAECs for gene expression analysis following protocols adapted from those previously optimised in the laboratory (Moss 2018). RNA was isolated using RiboZol™, single-phase phenol that homogenises cells and inhibits RNase activity, according to the manufacturer's instructions (VWR International). All RNA extraction steps were performed on ice to reduce RNase activity.

HAECs at a density of 3×10^5 cells/well were seeded in 6-well plates and left to grow for two days until about 85% confluency was reached and the culture medium was changed daily. Cells were then stimulated with TNF-α in the presence of the vehicle control or RSV; negative control was also included (vehicle control without TNF-α). For THP-1 macrophages (1×10^6 cells/ml), two different experimental approaches were used. Firstly, THP-1 macrophages were treated with vehicle control or RSV in the absence of cytokines to investigate the effect of RSV on scavenger receptors (SRA and CD36) gene expression. Secondly, THP-1 macrophages were stimulated with IFN-γ to determine ICAM-1 and MCP-1 expression levels in the presence of vehicle control or RSV; negative control was also included.

The same RNA extraction protocol was applied to both stimulated and unstimulated cells. The cells were washed with 1X PBS before being suspended in 1 ml of cold RiboZol™ for overnight at 4°C for cell lysis to occur. After vigorous mixing, the cell lysate suspensions were transferred to Eppendorf tubes and 200 µl of chloroform was added. Samples were then shaken vigorously for 15 seconds and incubated for 3 minutes at room temperature. Tubes were then centrifuged for 15 minutes (12,000 x g at 4°C), which creates a lower phenol-chloroform phase, a white interphase, and an upper aqueous phase. The upper aqueous phase, containing the RNA, was carefully transferred to new Eppendorf tubes without disturbing the interphase. The RNA was then precipitated by adding 500 µl of cold isopropanol and incubation overnight at -80°C. RNA was then pelleted (10 minutes, 12,000 x g, 4°C), and washed three times with cold 75% (v/v) ethanol and pelleted again (5 minutes, 7,500 x g, 4°C). Following the final wash, the supernatant was removed, and the pellet was left to air dry. Finally, the RNA pellet was dissolved in 15-20 µl of nuclease-free water and incubated for 10

minutes at 56°C to completely dissolve the RNA. The concentration of RNA samples was then measured and then kept at -80°C until further use.

2.5.12.3 RNA quality assessment

The purity and concentration of RNA samples were determined using a NanoDrop™ ND2000 spectrophotometer. The absorbance ratios A260/A280 and A230/A260 were used to assess RNA purity where the A260/A280 ratio is an indication of the level of protein contamination and the A230/A260 ratio is an indication of DNA contamination in the sample. The values of A260/A280 should be between 1.8 to 2.0 and the value of A230/A260 should be greater than 1.7 for good quality RNA. In addition, the integrity of RNA was assessed by size-fractionation of a small aliquot using agarose gel electrophoresis as described in Section 2.5.12.4. The quality was judged as good intact RNA when two distinct bands of 28S and 18S rRNA were visible. In addition, the 28S band should be twice as intense of 18S band as shown in Figure 2.5.

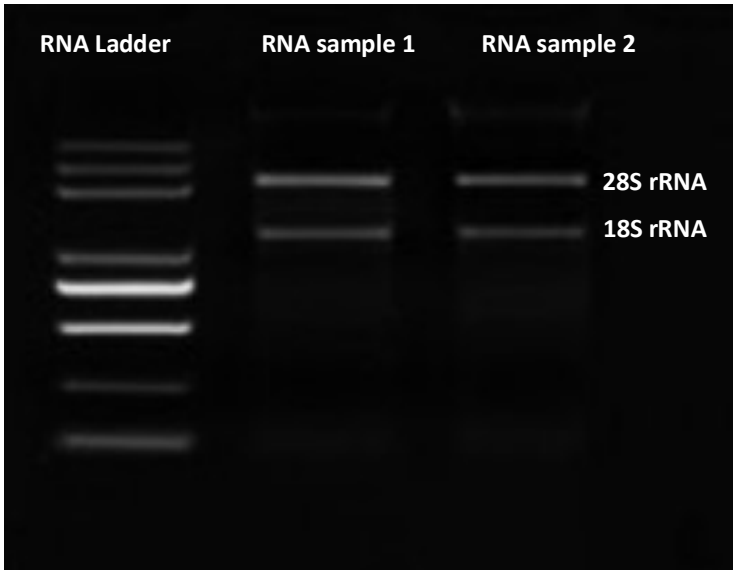

Figure 2.5 Agarose gel electrophoresis to assess the quality of RNA by size fractionation

Example of agarose gel electrophoresis to check the quality of RNA samples. The gel shows the two ribosomal RNA bands (28S and 18S). The 28S band should have twice the intensity of the 18S band for good quality RNA.

2.5.12.4 Agarose gel electrophoresis

A 1.5% (w/v) gel was prepared by dissolving agarose powder in 1X Tris-borate-EDTA (TBE; 89 mM Tris-borate, 89 mM boric acid, 2 mM EDTA, pH 8.3) buffer followed by heating it in a microwave until it had completely dissolved. In order to visualise the RNA bands under UV light, 20 µM of nucleic acid stain, ethidium bromide (EtBr), was added before the gel was left to cast in a horizontal gel tray. The gel was then loaded with RNA samples that had been already mixed with 2X RNA loading dye (ThermoFisher Scientific) in equal volume. Electrophoresis was carried out in a horizontal gel tank at 100 V for around 50 minutes in 1X TBE. The gel was then visualised under UV light using a Sygene Gel Documentation system.

2.5.12.5 Reverse transcriptase polymerase chain reaction (RT-PCR)

To investigate the effect of RSV on gene expression, RNA was reverse transcribed into complimentary DNA (cDNA) by the process of RT-PCR. For this, 200 pmol of random hexamer primers were added to 1 µg of purified RNA and made up to a total volume of 14 µl with nuclease-free water. The samples were then incubated at 70°C for 5 minutes and immediately placed on ice to prevent RNase activity. The cDNA master mix listed in Table 2.2 was then added to a final volume of 20 µl and the samples then incubated for 1 hour at 37°C followed by a final incubation for 5 minutes at 90°C for enzyme inactivation and then cooling to 4°C. Finally, nuclease-free water (80 µl) was added to the cDNA samples to achieve a final concentration of 10 µg/ml. The cDNA samples were then kept at -80°C for use in subsequent gene expression analysis.

Table 2.2 Composition of cDNA master mix used in the reverse transcription process

Reagent	Master mix (X1) (µl)
100 mM dNTP mix (dATP, dGTP, dCTP, dTTP)	1.0
M-MLV buffer (5X)	4.0
RNase inhibitor (40 U/µL)	0.5
M-MLV reverse transcriptase (200 U/µL)	0.5
Total	**6**

* All reagents obtained from Promega

2.5.12.6 Real time quantitative PCR (qPCR)

The effect of RSV on the mRNA expression level of SRA, CD36, ICAM-1 and MCP-1 was quantified using RT-qPCR reaction on a Roche light cycler. This assay was performed using SYBR Green Jumpstart Taq Readymix that intercalates into double-stranded DNA and therefore the fluorescent emission at the end of each cycle is measured and recorded. The signal strength is proportional to the amount of cDNA template. Threshold (C_T) values for genes under investigation were compared to the values of housekeeping gene GAPDH that was used as a reference gene. GAPDH was chosen based on previous studies in the laboratory (Gallagher 2016). The qPCR reaction mix, primers sequence and amplification conditions that were used in this study are shown in Tables 2.3, 2.4 and 2.5 respectively.

Table 2.3 Composition of 1X master mix used in qPCR reaction

Reagent	qPCR volume (µl)
SYBR Green Jumpstart™ Taq Readymix™	12.5
Forward primer (2.5 µM)	0.5
Reverse primer (2.5 µM)	0.5
cDNA (10 ng/µL)	1
Nuclease-free H_2O	10.5
Total	**25**

Table 2.4 Intron-spanning primer sequences used in qPCR

Target gene	Forward Sequence (5'-3')	Reverse Sequence (5'-3')
GAPDH	CTTTTGCGTCGCCAGCCGAG	GCCCAATACGACCAAATCCGTTGACT
SR-A	GTCCAATAGGTCCTCCGGGT	CCCACCGACCAGTCGAAC
CD36	AGCCATTTTAAAGATAGCTTTCC	AAGCTCTGGTTCTTATTCACA
ICAM	GACCAGAGGTTGAACCCCAC	GCGCCGGAAAGCTGTAGAT
MCP-1	CGCTCAGCCAGATGCAATCAATG	TGGTCTTGAAGATCACAGCTTCTTTGG

Abbreviations: GAPDH, glyceraldehyde 3-phosphate dehydrogenase; SR-A, scavenger receptor-A; MCP-1, monocyte chemotactic protein-1; ICAM-1, intercellular adhesion molecule-1.

Table 2.5 Amplification steps for qPCR reaction

PCR step	Temp (°C)		Time (s)
Pre-incubation	94		120
Melting	95	X40	30
Annealing	60		60
Extension	70		60

2.5.13 Analysis of SRA, CD36 and LDLR cell surface expression of proteins using flow cytometry

THP-1 macrophages were incubated with the vehicle control or RSV for 24 hours. Following incubation, the overlying medium was aspirated, and the cells were washed with 500 µl of 1XPBS. The cells were then detached using 500 µl of 1XPBS and cell scraper. The suspension was then subjected to centrifugation for 5 minutes at 9,000 x g to pellet the cells. The resulted pellet was resuspended in preprepared antibodies mix in 2% PBS-FCS (v/v) and incubated at 4°C for 30 minutes. Negative control without antibodies mix was also included. Following staining, the cells were washed with 2% PBS-FCS (v/v) and centrifuged as above. The cells were then resuspended in 500 µl of 2% PBS-FCS (v/v) and were ready for FACS analysis. Gating of cell populations was carried out according to cell specific markers: PE Mouse Anti-Human MSR1; Anti-Human LDLr APC Conjugated Mouse IgG1; and FITC Mouse Anti-Human CD36 clone (CLB-IVC7) (BD Biosciences). The analysis of cell populations was performed using the FlowJo v.10 software.

2.5.14 Inflammasome activation

2.5.14.1 Preparation of cholesterol crystals

Cholesterol was dissolved in 95% (v/v) ethanol at a final concentration of 12.5 g/l. Solution was then heated to 60°C and filtered through a Whatman paper to remove any undissolved cholesterol. For crystallisation, the solution was left to dry overnight at room temperature. The crystals were collected and autoclaved. Finally, the cholesterol crystals were ground using a homogeniser to unify crystal size and stored at -20°C for use in experiments.

2.5.14.2 Enzyme linked immunosorbent assay (ELISA)

Activation of NLRP3 in response to a pro-inflammatory stimulus can be evaluated by the level of IL-1β production, which can be determined using standard ELISA methods. The inflammasome activation *in vitro* requires a primer, such as lipopolysaccharide (LPS), followed by a second hit, such as cholesterol crystal. In the current study, PMA, which was used in differentiation of THP-1 monocytes to macrophages, acts as the first stimulus, and hence LPS was not required.To determine the effect of RSV on the activation of the NLRP3 inflammasome, THP-1 monocytes were cultured in 24 well plates at a density of 5 x 10^5 cells per well in RMPI media containing 0.2% (w/v) fatty acid-free BSA and PMA to differentiate the monocytes to macrophages. The macrophages were then treated for 24 hours at 37°C, 5% (v/v) CO_2 with either the vehicle (DMSO) or RSV in the presence of cholesterol crystals (0.5 mg/ml). Negative control was included without cholesterol crystals. Supernatant was then transferred to Eppendorf tubes and subjected to centrifugation at 9,000 x g for 5 minutes to remove any crystals. The concentration of IL-1β was then determined in the supernatant using a standard ELISA protocol according to manufacturer's instructions (R&D Systems).

All reagents were reconstituted in reagent diluent (provided in the kit) following the manufacturer's instructions (R&D Systems). Firstly, the ELISA plate was coated with human IL-1β capture antibody (4 µg/ml) and left for incubation overnight at room temperature. The plate was then washed 3 times with 1X wash buffer (provided in the kit) before incubation with block buffer for 1 hour at room temperature. Washing of the plate was repeated 3 times. Samples and a series of IL-1β standards with concentrations from 0 to 250 pg/ml were then prepared using reagent diluent and 100 µl added to the plate. Samples and standards were then incubated for 2 hours. Washing of the plate was repeated as above before the addition of the IL-1β human detection antibody (150 ng/ml) to plates for 2 hours. Washing steps were repeated, and 100 µl streptavidin-HRP was then added for 20 minutes and protected from light by covering the plate with an aluminum foil. The plate was then washed with 1X wash buffer and 100 µl of substrate solution (provided in the kit) was added and incubated for a further 20 minutes. Finally, 50 µl stop solution (provided in the kit) was added and absorbance measured on a plate reader at 450 nm with correction at 540 nm. The standard curve was prepared using absorbance values of the IL-1β standards. Unknown IL-1β concentrations of samples were determined using the standard curve.

2.5.15 MMP activity

The MMP Activity Assay Kit was used according to the manufacturer's instructions (Abcam). The substrate solution (provided in the kit) contains a fluorescent resonance energy transfer (FRET) peptide that is composed of two components, an emitter and a quencher. In intact situation, the quencher prevents the emitter from releasing a fluorescent signal while after cleavage into two separate fragments of the emitter and quencher by MMPs, the fluorescence of the emitter is recovered. Accordingly, reducing MMP activity will result in more FRET peptides remaining intact and low fluorescent signal detected.

THP-1 macrophages (1 x 10^5 cells/well) were incubated with complete RPMI media that contains either the vehicle control (DMSO) or RSV for 3 or 24 hours at 37°C, 5% (v/v) CO_2. These time points were chosen to assess both short- and long-term effects of RSV on MMP activity. After the desired incubation time, 50 µl of the media was transferred to a new plate and an equal volume of MMP green substrate solution (provided in the kit) was added to each well (except the negative control wells). For the negative control, 50 µl of assay buffer (provided in the kit) was added. The plate was then covered with foil to keep it away from the light and left for incubation for 30 minutes at room temperature. The fluorescence was then measured in a fluorescence microplate reader, with Ex/Em 490/525 nm. The results were expressed as a percentage to the DMSO vehicle control, which was arbitrarily assigned as 100%.

2.6 *In vivo* methods

2.6.1 Housing and husbandry of mice

The effect of RSV was investigated on 8-week-old male $LDLR^{-/-}$ mice homozygous for the $LDL^{rtm1Her}$ mutation and backcrossed to the C57BL/6J strain (obtained from the Jackson Laboratory). All procedures for animal experiments were approved by The Cardiff University Institutional Ethics Review Committee and the UK Home Office and all experiments were performed in compliance with the Handbook for the Care and Use of Laboratory Animals (NIH Publication No. 85–23, updated 1996; Experimental License 30/3365).

The mice were expanded locally in a pathogen-free environment. All mice were housed in a conventional open top cage in a light and temperature-controlled facility (12-hour light/dark cycle, 22°C) with free access to water and food. A total of 40 mice were randomly distributed between two groups (20 per group). In the study, the first group was fed high fat diet (HFD) [21 % (w/w) pork lard and 0.15 % (w/w) cholesterol], where the second group was fed HFD supplemented with RSV (20 mg/kg/day). RSV has low water solubility and hence the RSV powder was mixed with HFD (to avoid using toxic DMSO in animals) and kept at -20°C until use. The study was carried out for a period of 12 weeks. This duration time had been chosen based on previous research in the host laboratory. Additionally, the RSV dose was based upon a previously published study on apoE-deficient mice (Chang et al. 2015a).

Mouse body weight was measured at the start of the study and body weight was recorded each time during the feeding period (2 days/week). In addition, the weight of the supplied food together with that remaining was recorded for monitoring purpose.

2.6.2 Tail vein blood sampling (non-surgical)

One day before the mice were sacrificed, peripheral blood was collected from the lateral tail vein for subsequent immune-phenotyping assay in order to investigate the populations of circulating myeloid and lymphoid cells. For this, the mouse was placed in a plastic Tailveiner Restrainer. Anesthesia was then induced by spraying the tip of the tail with a local anesthetic (ethyl chloride) from about 10 cm followed by waiting for approximately 15 seconds or until the mouse tail skin turned white. Using a sterile scalpel blade, no more than 1 mm of tail was removed, and blood flow was encouraged by applying a gentle massage on the tail with fingertip of the thumb and index finger from the beginning to the end of the tail. Blood drops were then collected (25-50 µl) into EDTA microvette tubes. Blood flow was stopped by applying finger pressure to the soft tissue at the site of blood sampling for 30-45 seconds. Mice were finally closely observed to verify the bleeding had stopped and there were no adverse effects before returning them to their original cage.

2.6.3 Blood and tissue collection

At the end of the study, all mice were sacrificed by increasing CO_2 levels in a chamber (inhalation overdose) and death was confirmed by the absence of a pulse. Blood from cardiac puncture was then collected directly into Eppendorf tubes containing heparin (50 U/mL) to prevent blood clotting and kept at room temperature until plasma separation. Plasma was obtained by centrifugation of the blood sample for 10 minutes at 12,000 x g at 4°C. Plasma was then transferred to a new Eppendorf tube and kept at - 80^{o}C until use.

To collect organs, the mice were placed on a surgical board in supine position. Both legs and arms were then pinned outwardly using syringe needles. Forceps and scissors were then used to cut and pinch the external layer of the fur and skin. Subcutaneous and inguinal fat was collected before using the fine scissors to create a midline incision in order to expose the abdominal cavity. In addition, the rib cage was cut to expose the thymus, heart and lungs. For perfusion, 1X PBS bottle was attached with a 26G needle via plastic pipes and valve to control dripping speed. The 1X PBS bottle was then placed 100-120 cm above the mouse (to ensure sufficient perfusion pressure). A small cut in the left ventricle was then made and a 26G needle was inserted into the apex of the left ventricle to gradually perfuse the organs. Approximately 10-25 ml of 1X PBS was used for each mouse and the pale colour of the liver was used as an indicator of good perfusion. Once this was carried out, the fat pads, including gonadal fat, renal fat and brown fat together with spleen and thymus, were dissected. Moreover, the intestine from three different sections at consistent intervals and the faeces were collected. The heart (after cutting away about 1/3 of the ventricular mass), brachiocephalic artery and a small section of the liver were removed and mounted on Shandon base cryomolds in optimum cutting temperature (OCT) formulation and snap frozen immediately either on dry ice or in liquid nitrogen. The aorta and the remaining parts of the liver were isolated and kept in *RNAlater*™ Stabilisation Solution and snap frozen immediately to avoid RNA degradation to be used for gene expression analysis. All organs were weighed and snap frozen on dry ice before finally storing at - 80^{o}C until use. Finally, rear legs were removed and stored in 1X PBS supplemented with 2% (v/v) HI-FCS for subsequent analysis of cell populations in the bone marrow.

2.6.4 Immunophenotyping of peripheral blood

The effects of RSV on lymphoid and myeloid populations were carried out using peripheral blood samples that had been collected from the tail vein (as described in Section 2.6.2). The assay was carried out in collaboration with Mrs. Sarab Taha at the European Cancer Stem Cell Research Institute (ECSCRI). The samples were processed immediately after blood collection within four hours maximum to limit cell death.

Briefly, 12 µl of mixed blood was transferred to two Eppendorf tubes (for myeloid and lymphoid cell analysis). Red blood cells were then lysed by incubating the samples with 600 µl of 1X ammonium chloride (0.8% NH_4Cl, 0.1 mM EDTA in water buffered with $KHCO_3$ to achieve a final pH of 7.2-7.6), for around 8 minutes. Then, white blood cells were obtained by centrifugation for 10 minutes at 500 x g at 4°C to pellet the cells. The cells were then resuspended in 50 µl of antibody mix (listed in Table2.6) and incubated for 30 minutes at 4°C. Cells were again washed with 1ml of PBS (1x, pH 7.4) which was supplemented with 2% (v/v) HI-FCS (referred to as 2% PBS-FCS from here on), pelleted by centrifugation for 5 minutes at 500 xg and resuspended in 300 µl of 2% PBS-FCS. Solutions were then transferred to round-bottom polystyrene tubes and kept on ice. Finally, the DAPI nuclear stain was added immediately before analysing the samples on a BD FACS Forsseta flow cytometer to identify viable cells. In addition, single stain samples were prepared simultaneously for sample compensation (i.e. adjust cells population to reduce spill-over between channels). Samples were analysed until 20,000 counts were reached. Gating of the cell populations was carried out according to cell specific markers as detailed in Table 2.6 and samples with a cell viability of 85% or more were used for statistical analysis, otherwise samples were excluded. Analysis of cell populations was performed using FlowJo v.10 software. The strategy of gating that was utilised for the identification of lymphoid and myeloid cells populations are shown in Figure 2.6 and Figure 2.7 respectively. Backgating strategy was applied to ensure the accuracy of the gating. This is done by overlaying the final gated population over the preceding parent populations.

Table 2.6 Markers used in the immunophenotyping of peripheral blood cell populations

Class	Cell type	Antibody	Fluorochrome
Myeloid	Monocytes	CD115	PE
		Ly6C	PE-Cy7
	Granulocytes	Ly6G	FITC
Lymphoid	T cells	CD3	PE
		CD4	PerCP
		CD8	APC-Cy7
	Natural killer cells	NK1.1	PE-Cy7
	B cells	B220	FITC

Abbreviations: FITC, fluorescein isothiocyanate; APC, allophycocyanin; PE, phycoerythrin; Cy7, cyanine-7; PerCP, peridinin-chlorophyll- protein.

2.6.5 Immunophenotyping of bone marrow cell populations

Previous studies have demonstrated that a HFD can alter the proportion of haematopoietic stem/progenitor cells in the bone marrow (Chan et al. 2012; Adler et al. 2014; Hermetet et al. 2019). This assay was carried out to determine if RSV can prevent HFD induced changes in haematopoietic cell populations. This was done using a previously employed method in the host laboratory (Moss 2018; O'Morain 2019; Chan 2021) and in collaboration with Sarab Taha. Summary of the protocol is described in Figure 2.8.

The day after collection of the rear legs, the tibia and femur were crushed using a mortar with 10 ml of 2% PBS-FCS. The homogenised marrow was then passed through a sterile 70 µm filter into a Falcon tube and the filter washed twice with 2% PBS-FCS to make up to a final volume of 30 ml. The number of cells were then determined using Via1-Cassette™ and either 10 or 8 million cell suspensions were transferred to separate FACS tubes to analyse the signaling lymphocytic activation molecule (SLAM) and progenitor cell populations respectively. The cells were then pelleted by centrifugation for 5 minutes at 500 x g at 4°C.

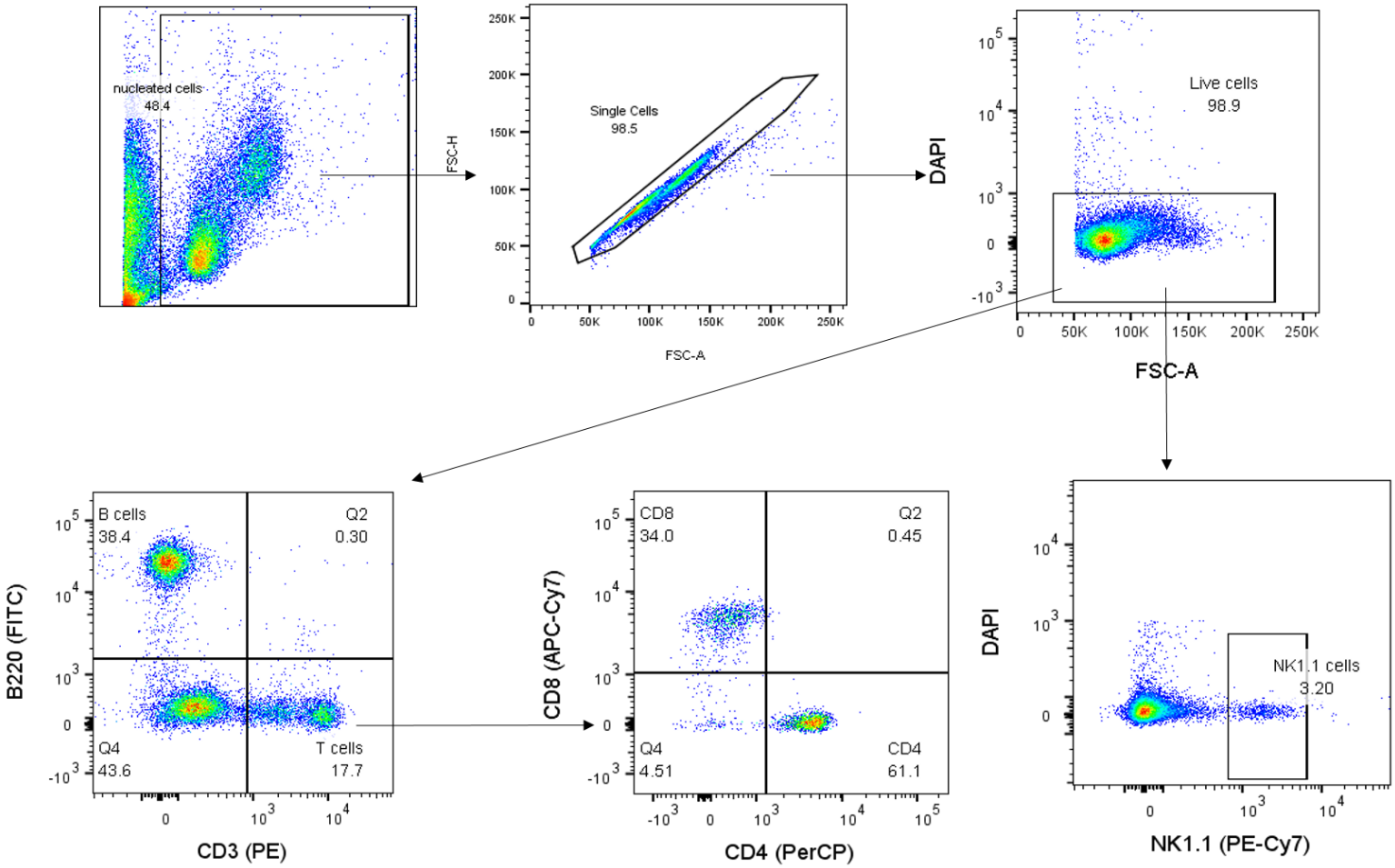

Figure 2.6 Sequential plots for fluorescent activating cell sorting (FACS) showing the gating strategy for identification of lymphoid cell populations

The graph illustrates the gating strategy for the identification of lymphoid cells in the peripheral blood. Live cells, which are DAPI negative were used to identify NK cells, B cells and T cells. The latter was used to determine the frequency of CD8 and CD4. **Abbreviations:** SSC, side scatter; FSC, forward scatter; DAPI, 4', 6'-diamidino-2-phenylindole; NK, natural killer.

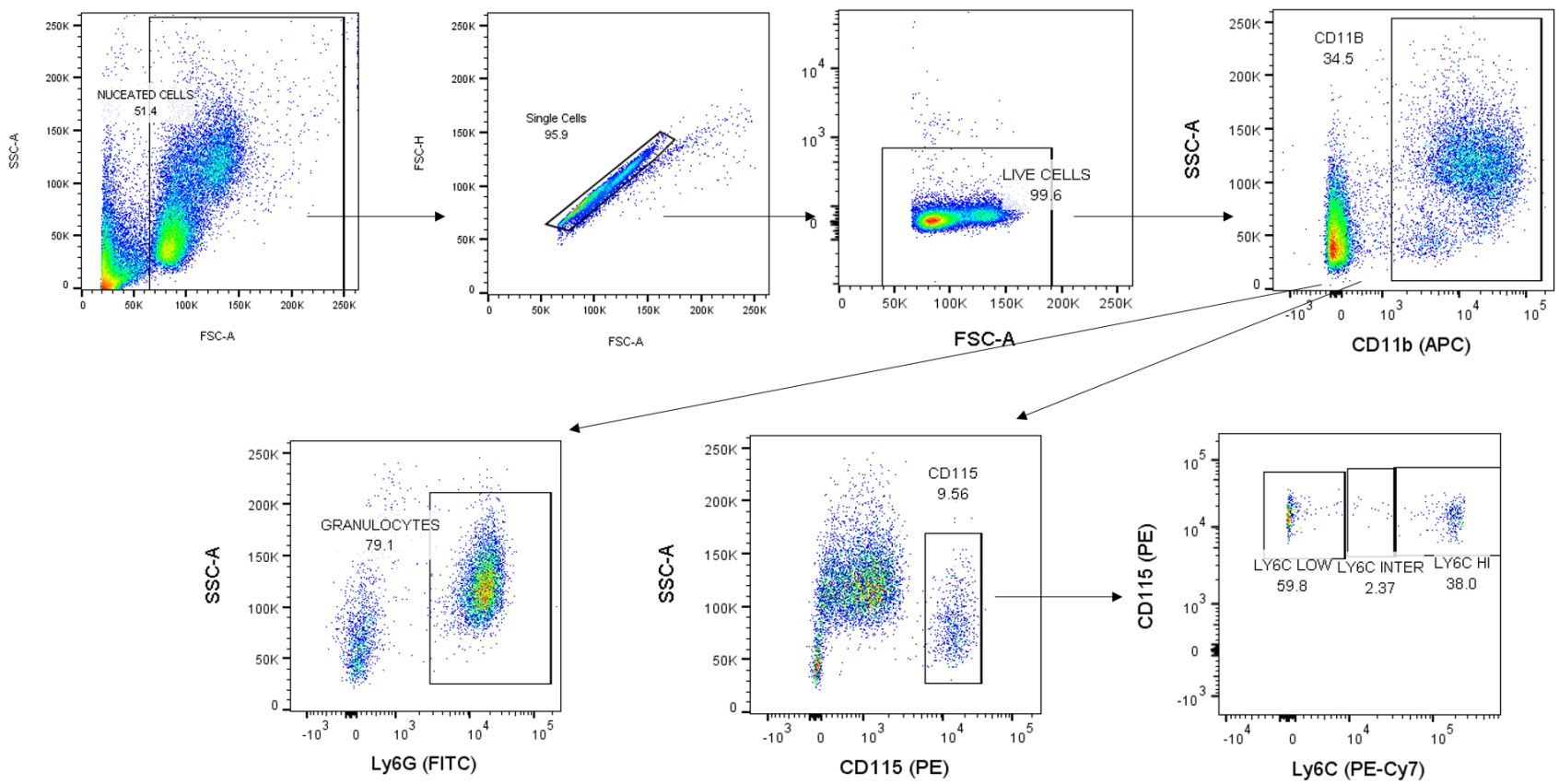

Figure 2.7 Sequential plots fluorescent activating cells sorting (FACS) showing the gating strategy for the identification of myeloid cell populations

The graph illustrates the gating strategy for the identification of myeloid cells in the peripheral blood. Live cells, which are DAPI negative were used to identify CD11b^{+} that was then used then to determine granulocytes and monocytes (CD115^{+}). Monocytes were used to distinguish between the two subpopulations of monocytes Ly6C^{high} (inflammatory monocytes) and Ly6C^{low} (nonclassical monocytes). **Abbreviations:** SSC, side scatter; FSC, forward scatter; DAPI, 4', 6'-diamidino-2- phenylindole.

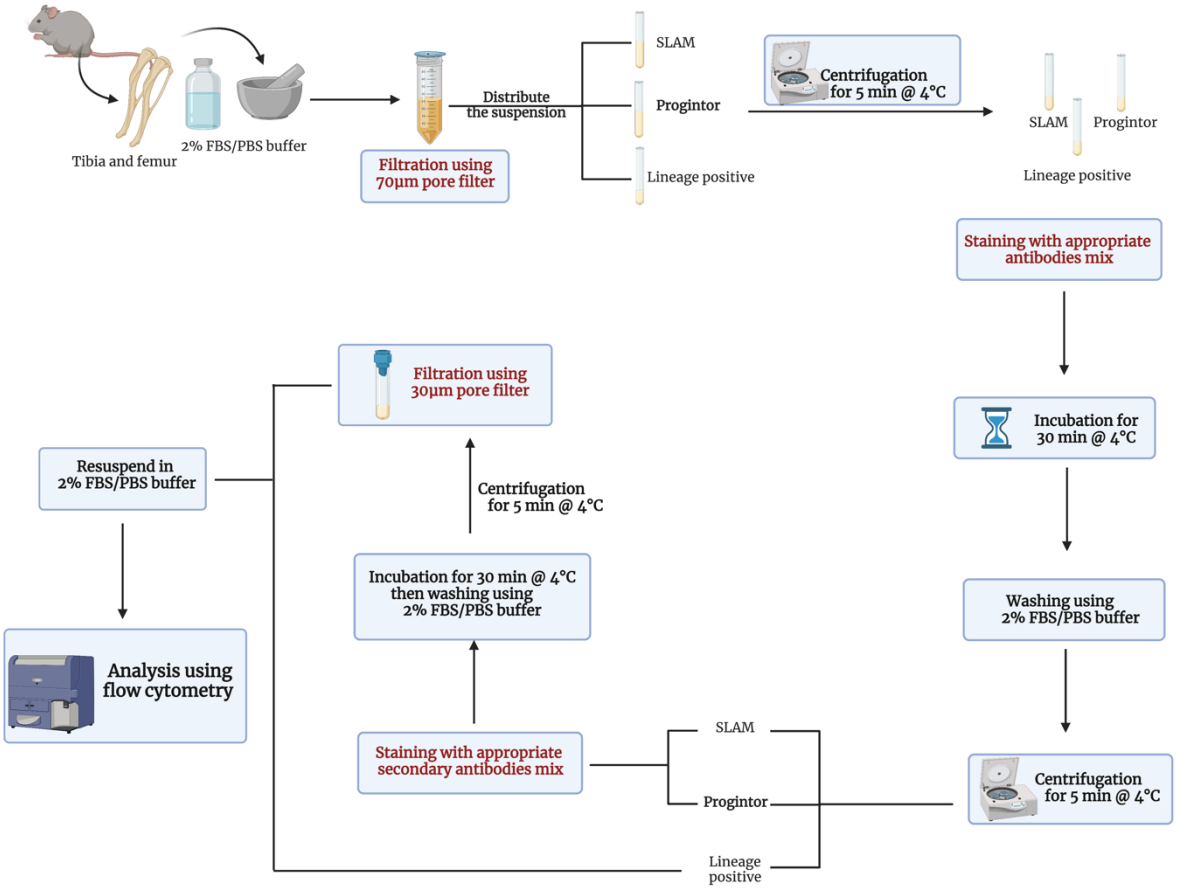

Figure 2.8 Procedure for immunophenotyping of bone marrow cell populations

Both tibia and fibia from LDLR$^{-/-}$ mice were placed in a mortar along with 2% FBS/PBS and crushed until homogenised. The mixture was then filtrated using 70 µm pore filter. After counting the cells, the desired cell numbers were placed in a FACS tube to analyse the SLAM, progenitor and lineage positive populations. Cells were then pelleted by centrifugation and the resulting pellets were stained for 30 minutes at 4°C with appropriate antibodies mix. After initial staining, the cells were washed and centrifuged for 5 minutes. The lineage positive populations, after resuspending in 2% FBS/PBS, were now ready to be analysed by FACS. For SLAM and progenitor cells, incubation was carried out with secondary antibodies mix for a further 30 minutes at 4°C. Before analysing by flow cytometry, the samples were filtered into FACS tubes using sterile 40 µm pore filters and resuspended in 2% FBS/PBS. **Abbreviation:** SLAM, signalling lymphocytic activation molecule. Image created with BioRender.com.

This centrifuge setting was used for all centrifugation steps throughout the procedure unless stated otherwise.

Cells were then stained at 4°C for 30 minutes with a biotinylated mix of lineage marker antibodies present within the SLAM and progenitor cells as detailed in Table 2.7. After initial staining, the

cells were washed with 2% PBS-FCS. Cells were then resuspended in 100 µl of streptavidin (0.2 mg/ml) and incubated for a further 30 minutes at 4°C. Samples were then washed with 2% PBS-FCS and resuspended in 500 µl of 2% PBS-FCS. Finally, the samples were filtered into FACS tubes using sterile 40 µm filters.

Table 2.7 Composition of antibody cocktails used in immunophenotyping of bone marrow cell populations.

Class	Antibody	Fluorochrome
SLAM	Ly-6A/E (Sca-1)	PE
	CD48	FITC
	CD150	PE/Cy7
	CD117 (c-Kit)	APC
	Lineage cocktail	-
	2% PBS-FCS	-
	FC block (added separately per tube)	-
Progenitor	Ly-6A/E (Sca-1)	APC/Cy7
	CD34	FITC
	CD16/32	PE/Cy7
	CD127	PE
	CD117 (c-Kit)	APC
	Lineage cocktail	
	2% PBS-FCS	
Lineage	Ly-6G/Ly-6C (Gr-1)	PE/Cy7
	CD11b (Mac-1)	PE
	CD45R/B220	APC
	CD3	FITC
	TER-119	APC/Cy7
	2% PBS-FCS	-
Lineage cocktail	Biotin CD3	-
	Biotin CD4	-
	Biotin CD8a	-
	Biotin Ly-6G/Ly-6C (Gr-1)	-
	Biotin CD11b	-
	Biotin CD45R/B220	-
	Biotin TER-119	-
	2% PBS-FCS	-

Abbreviations: SLAM, signalling lymphocyte activation molecule; FITC, fluorescein isothiocyanate; APC, allophycocyanin; PE, phycoerythrin; Cy7, cyanine-7; PerCP, peridinin-chlorophyll- protein.

For the preparation of lineage cell populations, 75 µl of cell suspension was placed in new FACS tube and incubated with lineage marker antibodies as detailed in Table 2.7 for 30 minutes at 4°C. Cells were then washed with 2% PBS-FCS and centrifuged as above. The cells were then resuspended in 300 µl of 2% PBS-FCS for FACS analysis. In addition to SLAM, progenitor and lineage cell populations, single stain samples were prepared for use in the calibration of fluorochromes during FACS analysis. For this, 75 µl of cell suspension was incubated with 50 µl of appropriate single antibody marker representing each fluorochrome (plus DAPI that stains dead cells, and unstained cells as controls).

Once all of SLAM, progenitor, lineage and single cell fluorochrome preparations were completed, samples were analysed on a BD FACS Fosseta flow cytometer. To identify the percentage of live cells in each sample, 20 ng/ml of the DAPI nuclear stain was added to SLAM, progenitor, lineage and DAPI control samples immediately prior to analysis.

For SLAM and progenitor cell populations, samples were analysed until 3 million counts were reached. Lineage samples and single cell stains were analysed until 20,000 and 2000 counts respectively were reached. Compensation was done for each sample to avoid cross-over between fluorochromes using single cell fluorochrome stains. All markers of the haematopoietic cell populations analysed in this study are presented in Table 2.8.

Gating of cell populations was then carried out according to cell specific markers as detailed in Table 2.8 and illustrated in Figure 2.9 and 2.10. The back gating strategy was applied to ensure the accuracy of the gating. This was carried out by overlaying the final gated population over the preceding parent populations to decide if all target cells were correctly isolated. Analysis of cell populations was carried out using FlowJo v.10 software.

Table 2.8 Markers used in the immunophenotyping of bone marrow cell populations

Class	Cell type	Identifier
SLAM	**Lineage -**	
	LSK	Lin^- $Sca\text{-}1^+$ $c\text{-}Kit^+$
	HSC	$CD150^+$ $CD48^-$
	MPP	$CD150^-$ $CD48^-$
	HPC I	$CD150^-$ $CD48^+$
	HPC II	$CD150^+$ $CD48^+$
Progenitor	**Lineage -**	
	LK	Lin^- $Sca\text{-}1^-$ $c\text{-}Kit^+$
	CMP	$CD34^+$ $CD16/32^-$
	MEP	$CD34^-$ $CD16/32^-$
	GMP	$CD34^+CD16/32^+$
	CLP	$CD127^+$
Lineage	**Lineage +**	
	MDSC	$GR1^+$ $Mac1^+$
	Macrophages	$GR1^-$ $Mac1^+$
	B-Cell	$B220^+$
	T-Cell	$CD3^+$
	Erythroid cells	$Ter\text{-}119^+$

Abbreviations: SLAM, signalling lymphocyte activation molecule; HSC, haematopoietic stem cell; MPP, multipotent progenitors; HPC, heamatopoietic progenitor cell; CMP, common myeloid progenitor; MEP, megakaryocyte-erythroid progenitor; GMP, granulocyte-macrophage progenitor; CLP, common lymphoid progenitor; MDSC, myeloid-derived suppressor cells.

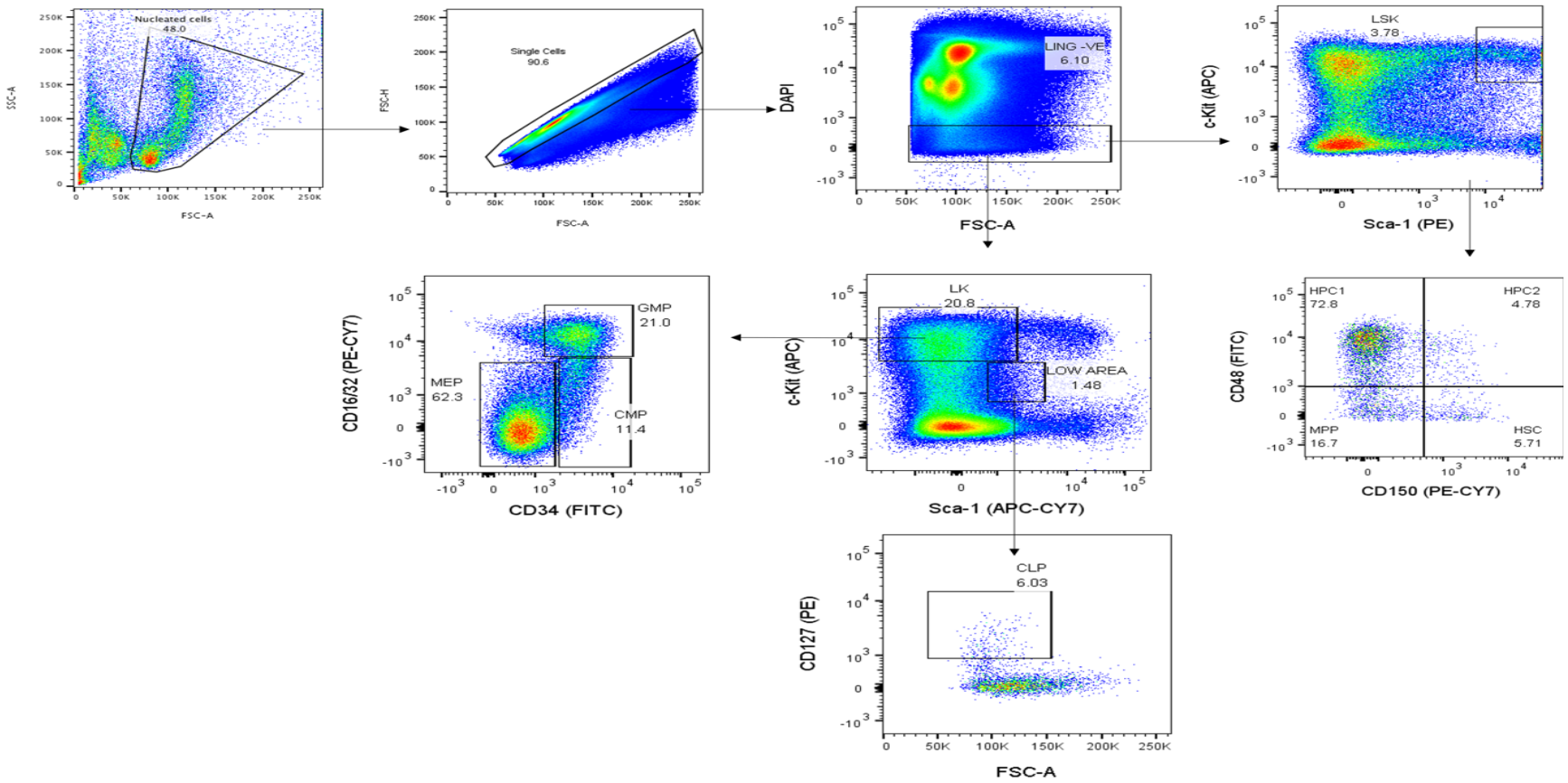

Figure 2.9 Sequential gating to identify SLAM and progenitor cell populations in the bone marrow.

The graph represents flow plots outlining the gating strategy that was used in the analysis of SLAM and progenitor cell populations by FlowJo v.10 software. The FSC-A allows to discriminate the cells size by measuring the amount of light that passes around the cell. SSC-A is proportional to cell granularity by determining the amount of light which is reflected by particles within the cells. Different filters and gating were applied to identify populations of interest. In the first plot, debris and nucleated RBCs were excluded. Then single cells were gated from WBCs to exclude doublets. DAPI negative populations were defined as live cells. LSK and LK population was then gated from live cells, which were then used to determine its compartment frequency. **Abbreviations:** FSC-A, forward scatter; SSC-A, side scatter; RBC, red blood cell; WBCs, white blood cells, LIN-, lineage negative; HPC, haematopoietic progenitor cell; MPP, multipotent progenitor; HSC, haematopoietic stem cell; GMP, granulocyte-macrophage progenitor; CMP, common myeloid progenitor; MEP, megakaryocyte-erythroid progenitor; CLP, common lymphoid progenitor.

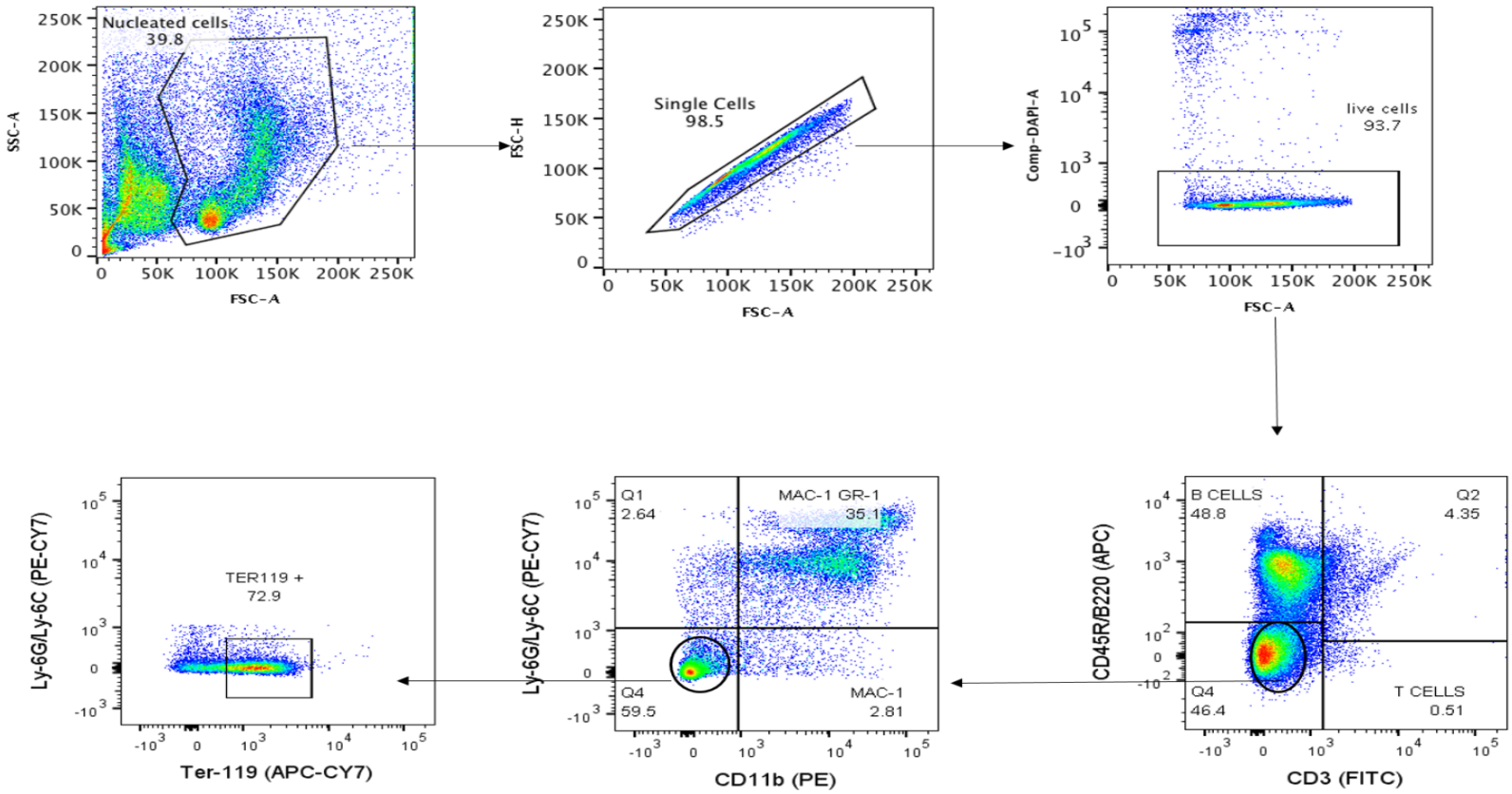

Figure 2.10 The gating strategy used to identify and quantify the lineage positive cell populations within the bone marrow of LDLR$^{-/-}$ mice.

The arrows demonstrate identification of each cell population from the previous gating strategy. The axis represents the various stains used to distinguish populations of cells. MAC-1 GR-1 represents myeloid-derived suppressor cells (MDSC); MAC-1 represents macrophages population and Ter-119 represents the erythroid cells within the bone marrow.

2.6.6 Plasma lipid quantification

2.6.6.1 Measurement of plasma triglyceride (TG) levels

TG concentrations in isolated mouse plasma was measured using the Abcam Triglyceride Quantification Assay Kit according to the manufacturer's instructions. In the protocol, TGs are first converted to free fatty acids and glycerol via incubation with a master mix solution containing lipase. The glycerol is then oxidised into a product that reacts with the target probe to produce a detectable colour at 570 nm. In the first step of the protocol, TG standards (provided in the kit) were prepared (0 – 10 nmol) and the samples diluted to fit within the range of the standards. The dilution factor of the samples was determined based on a previous pilot experiment. Samples and standards were then incubated with the lipase for 20 minutes at room temperature with constant agitation. Background samples (control well) were also included and incubated with the assay buffer (provided in the kit). After that, a reaction mix containing the assay buffer, probe and enzyme mix (all provided in the kit) was prepared and added to the standard, samples and background control wells. The plate was then left for incubation for 1 hour in darkness. The absorbance was then measured using a microplate reader at 570 nm. The absorbance values for the TG standards were used to construct a standard curve from which the TG concentration in the samples was calculated after subtracting the background value.

2.6.6.2 Measurement of plasma cholesterol and lipoprotein levels

Cholesterol concentration in the isolated mouse plasma was determined using the Abcam HDL and LDL/VLDL Cholesterol Assay Kit according to the manufacturer's instructions. In the assay protocol, total (TC) and free cholesterol (FC) was determined directly from the plasma after dilution (dilution factor based on previous pilot experiments) while precipitation steps were required for HDL and LDL/VLDL fractions (Figure 2.11). To separate HDL and LDL/VLDL fractions, a small volume of plasma (7.5 µl) was incubated with 43 µl of precipitation buffer (provided in the kit) for 10 minutes at room temperature, before centrifugation at 2,000 x g for 10 minutes. The supernatant (containing the HDL fraction) was transferred to a new Eppendorf tube while the pellet (containing LDL/VLDL fraction) was re-centrifuged again to ensure removal of any remaining HDL. The pellet was then resuspended in 1XPBS. Following

the separation, total cholesterol reaction mix (including cholesterol esterase) was prepared according to the manufacturer's instructions and added to TC, HDL, LDL/VLDL as well as the standards while the free cholesterol reaction mix (without cholesterol esterase) was added to FC samples only. The samples were then incubated for 1 hour at room temperature and protected from light. The change in colour (absorbance) was measured at 570 nm on a microplate reader. The standard curve was produced from the absorbance values of standards from which cholesterol and cholesterol fractions concentrations were calculated.

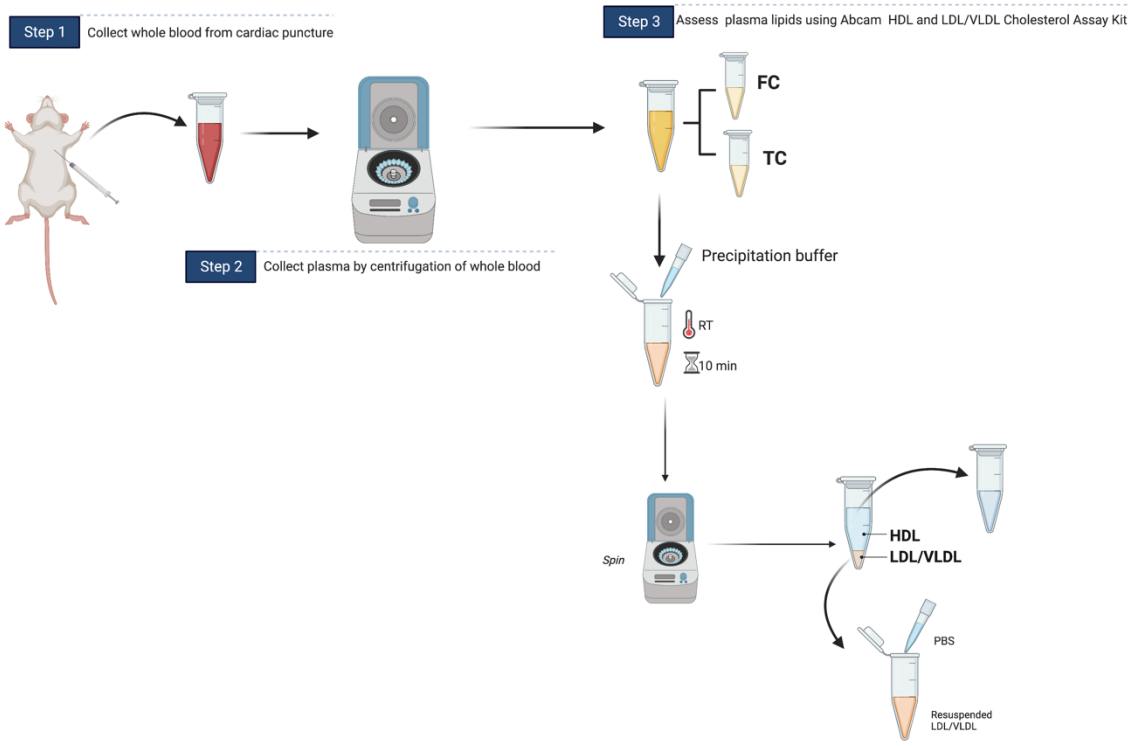

Figure 2.11 A diagram of lipid fractions obtained for total cholesterol, free cholesterol, HDL and LDL/VLDL using Abcam HDL and LDL/VLDL Cholesterol Assay Kit.

In the beginning, blood was collected directly from mouse's heart in heparin containing tubes. Plasma was then collected by centrifugation of the whole blood that was then used directly for TC and FC quantification. To obtain HDL and LDL fractions, the plasma was mixed with precipitation buffer and incubated for 10 minutes at room temperature before centrifugation for 10 minutes at 2,000 x g. The HDL fraction was then transferred to a new tube and the remaining LDL/VLDL (pellet) fraction resuspended in 1X PBS. **Abbreviations:** HDL, hight density lipoprotein; LDL/VLDL, low/very low-density lipoprotein; FC, free cholesterol; TC, total cholesterol. Image created with BioRender.com.

2.6.7 Morphometric analysis of atherosclerotic plaques and liver sections

2.6.7.1 Sectioning

Morphometric analyses of plaque and liver were carried out to determine the impact of RSV on HFD-induced changes. For morphometric analyses of the plaque, the frozen heart in OCT with the aortic root was sectioned at three valves. In addition, the liver sample in OCT was sectioned to study hepatocyte morphology and lipid accumulation associated with steatosis. Serial microtome-cryostat sectioning was carried out at -20°C and -14°C for heart and liver, respectively. Samples with 7-10 µm thickness were then prepared and three sections were collected on one Superfrost® microscope slide. The collection of heart samples was started when all three valves were visible and continued until the three valves disappear. On the other hand, the liver sections were collected when the tissue texture was good and without any cracks. All sections were air-dried for about 1 hour before storage at -80°C until use in staining.

2.6.8 Histological staining

2.6.8.1 Oil Red O staining (ORO)

ORO was chosen to quantify the lipid content in atherosclerotic plaque area because of its highly selectivity, cost-effectiveness and rapid time for detection.

Frozen heart sections were left to thaw at room temperature for 5-10 minutes before fixing in ice-cold 4% (w/v) PFA for 5 minutes. The fixed sections were then rinsed in distilled water (dH_2O) for three times for 5 minutes (15 minutes in total). After washing, the sections were counterstained with Harris Modified Haematoxylin solution (Sigma-Aldrich) for 3 minutes. The excess Haematoxylin stain was then rinsed in tap wate by subjecting the slide to indirect water stream until clear water was observed. Sections were then dipped in dH_2O before placing them in coplin staining jar containing absolute propylene glycol for 5 minutes to dispel water. To stain the lipid content, sections were immersed and incubated with ORO solution (0.5% (w/v) in propylene glycol; preheated at 65^{o}C for 1 hour before use) for 30 minutes at 65^{o}C, followed by incubation with 85% (v/v) propylene glycol for 5 minutes. Finally, sections were mounted with Aquamount (fluoromount G) immediately, coverslip applied, and edges

sealed with clear nail polish. Slides were then allowed to dry at room temperature for a few hours. Images of each section in the slide were captured using a Leica DMRB brightfield microscope at X5 magnification (2.5 objective). ImageJ software was then used to analyse plaque area and lipid content in stained sections.

For liver ORO staining, frozen sections were thawed for 5-10 minutes at room temperature and PAP pen was then used to draw a hydrophobic circle around each individual sections. Following this, the ORO solution was added directly to each section (~85 µl) and incubated for 20 minutes at room temperature. The excess ORO solution was then removed by gently tapping the slides. The slides were then placed in a coplin staining jar filled with Harris Modified Haematoxylin solution (Sigma-Aldrich) and incubated for 2 minutes. The excess Haematoxylin stain was then rinsed in tap water by subjecting the slide to indirect water stream until clear water was observed. Sections were finally mounted with Aquamount (fluoromount G) and the coverslip edges sealed with clear nail polish. Images were then captured under a Leica DMRB brightfield microscope using x20 magnification (2.5 objective). Images were finally analysed using ImageJ software.

2.6.8.2 Haematoxylin & Eosin staining

Hematoxylin and eosin (H&E) is the most common and widely used counterstain in histology to study morphological changes (Fischer et al. 2008; Chan 2014). Hematoxylin is a basic dye with positive charge that is used to stain acidic structures in the cells such as DNA in the nucleus which produces a purple colour. On the other hand, Eosin, eosin Y (eosin yellowish) in particular, is an acidic dye with negative charge that results in staining of basic cell organelles (e.g. cytoplasm and extracellular matrix) that appear as pink colour (Andrés-Manzano et al. 2015).

This protocol was used with sections from the liver only. Thawed sections were rinsed 2-3 times in tap water before incubating them with Harris Modified Haematoxylin solution (Sigma-Aldrich) for 5 minutes. Following the removal of the excess haematoxylin solution (as described in Section 2.6.8.1), sections were dipped in a coplin jar filled with 95% (v/v) ethanol and counterstained with eosin solution for 10 minutes. The sections were then dehydrated by passing the slides through 95% (v/v) ethanol twice, 100% (v/v) ethanol thrice and 100%

xylene thrice for 5 minutes each. Slides were then mounted using the DPX mounting medium for histology and coverslip was then placed. Gentle pressure was applied to ensure no air bubbles remained (no nail polish was used in this case). Slides were left to dry at room temperature for a few hours before capturing images under a Leica DMRB brightfield microscope using X20 magnification (2.5 objective). Images were finally analysed using the ImageJ software.

2.6.8.3 Collagen staining

Van Gieson's solution for collagen staining (provided in Elastic Stain Kit by Abcam) was used to analyse collagen content present within atherosclerotic plaques. After the slides were thawed for 10 minutes at room temperature, sections were fixed in ice-cold 4% (w/v) PFA solution for 5 minutes. Slides were then placed in dH2O for 5 minutes followed by incubation with Harris Modified Haematoxylin solution (Sigma-Aldrich) for 3 minutes. The excess haematoxylin was rinsed in tap water by subjecting the slide to indirect water stream until clear water was observed. Slides were then stained with Van Gieson's solution for 5 minutes before being dehydrated in 100% (v/v) ethanol for 5 minutes. The slides were then placed with xylene for 15 minutes in a fume hood. Finally, the DPX mounting medium was used to mount the sections and the slides were sealed by applying a gentle pressure on the coverslip (no nail polish was applied). Images of the sections were captured using a Leica DMRB microscope under x5 magnification for analysis. Resulting images were analysed using ImageJ software.

2.6.8.4 Immunofluorescence staining (IF)

Immunofluorescence (IF) staining is a powerful technique that has been used extensively in research that allows visualisation and localisation of various components in any tissue or cell type (Im et al. 2019). In this technique, specific antibodies with fluorescent dyes are used to detect their antigen (i.e., epitopes) typically on the surface of the cell of interest. To assess the effect of RSV on changes in the cellular content in $LDLR^{-/-}$ mice fed a HFD for 12 weeks, indirect immunofluorescence was used due to its high sensitivity (Figure 2.12).

The IF staining of aortic valve sections was carried out to analyse plaque cellularity and inflammation using several markers to detect key cell types and subtypes in atherosclerotic plaques such as macrophages, M1 macrophages, T cells and alpha smooth muscle actin (αSMA)-SMCs. Details of the antibodies used are detailed in Table 2.9. The final concentrations used were based on previous optimisation experiments in the host laboratory.

All antibodies (as well as isotype controls) that were used in this procedure were diluted in 0.1% (w/v) BSA in PBS according to previous optimisation in the laboratory. In addition, blocking buffers were prepared in 1X PBS supplemented with 5% (v/v) serum (dependent on the species that the secondary antibody is raised in) and 5% (w/v) BSA and stored at -20 °C until used.

Sections were thawed for 10 minutes at room temperature before fixing in ice-cold acetone for 10 minutes and then washed twice with 1X PBS to remove residual acetone. PAP pen was then used to carefully create a hydrophobic barrier around individual sections. Slides were then transferred to the slide staining tray (black tray) and about 85 µl of appropriate blocking serum (see Table 2.9) was added to each section (the entire section was submersed) and incubated at room temperature for 30 minutes in darkness. The blocking serum chosen depends on the species to which the secondary antibody was raised to reduce any non-specific binding and to improve the sensitivity of the assay. The blocking buffer was then removed by tapping and the sections incubated with the isotype control or primary antibody overnight at 4 °C. Isotype control was included as a negative control to confirm the specificity of primary antibody binding.

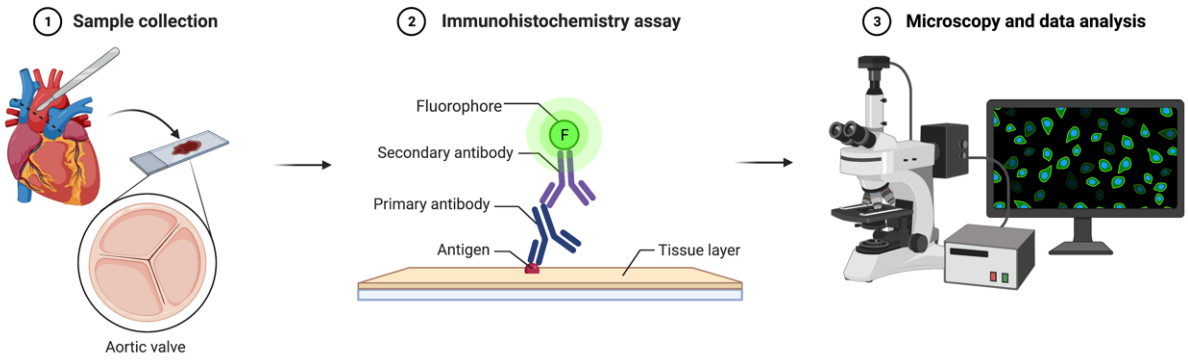

Figure 2.12 Illustration of the basic principle of immunofluorescence (IF) staining

The aortic valve sections were stained directly with appropriate antibodies. After incubation for an optimised time to allow the antibody to bind to its antigen, the unbound antibody was washed away, and the marked secondary antibody was added. The resulting images were then captured using fluorescence microscope. Image created with BioRender.com

Table 2.9 Details of antibodies used for immunofluorescence staining.

Cell type	Blocking Serum	Isotype	Primary	Secondary
		Rat IgG2b (ab18541)	Rat anti-mouse MOMA2 (ab33451)	Goat anti-rat IgG (AF488) (ab150157)
Macrophages	Goat	Stock: 0.5 mg/ml Working dilution: 1:100	Stock: 0.5 mg/ml Working dilution: 1:100	Stock: 2 mg/ml Working dilution: 1:500

M1 macrophages	Goat	Rabbit IgG (ab171870) Stock: 0.5 mg/ml Working dilution: 1:100	Rabbit anti-mouse iNOS (ab15323) Stock: 0.2 mg/ml Working dilution: 5:200	Goat anti-rabbit IgG H&L (AF488) (ab150077) Stock: 2 mg/ml Working dilution: 1:500
SMCs	Donkey	Rabbit IgG (ab171870) Stock: 1 mg/ml Working dilution: 1:500	Rabbit anti-mouse αSMA (ab5694) Stock: 0.2 mg/ml Working dilution: 1:100	Donkey anti-rabbit IgG (AF488)(ab150073) Stock: 2 mg/ml Working dilution: 1:500
T cells	Donkey	Rabbit IgG (ab171870) Stock: 1 mg/ml Working dilution: 1:500	Rabbit anti-mouse CD3 (ab5690) Stock: 0.2 mg/ml Working dilution: 1:100	Donkey anti-rabbit IgG (AF488)(ab150073) Stock: 2 mg/ml Working dilution: 1:500

The next day, sections were washed twice with 1X PBS and incubated with secondary antibody for 1 hour at room temperature in the dark. Sections were then counterstained in 0.3% (w/v) Sudan Black in 70% (v/v) ethanol for 20 minutes at room temperature to reduce auto-fluorescence. Sudan black solution was then removed by tapping the edge of the slide. Finally, sections were mounted in DAPI with Fluoroshield™ (one drop to each section) and sealed with a coverslip and nail polish. Slides were kept away from light and images were captured as soon as possible using an Olympus BX61 microscope with x4 magnification. DAPI and FITC filters were applied for visualisation. All secondary antibodies that have been used in this assay are conjugated with Alexa Fluor 488 (AF488), which can be visualised using the FITC filter. All images were captured using consistent exposure, intensity and contrast setting

of the same batch to ensure consistent analysis and analysed using ImageJ software by threshold adjustment to quantify areas of fluorescence (i.e., positive staining) within plaques.

2.6.9 Image analysis

All image analysis was conducted using ImageJ (Fiji) in a blinded manner where possible. The image analysis protocol has been developed in the host laboratory and the detailed steps were published in Methods in Molecular Biology in Atherosclerosis (Chan et al. 2022a; Chan et al. 2022b). For ORO-stained aortic root sections images, outlines around plaque, lumen and vessel area were drawn as accurately as possible using the selection brush tool and saved separately as templates. The size of each template (plaque, lumen, and vessel) was measured after the scale bar was set (conversion of pixels into mm^2). To quantify areas of ORO positive staining, the 'colour deconvolution' function in ImageJ was used to separate the red (ORO) from the purple (haematoxylin) staining. The 'FastRed FastBlue' vector, which has been found as the most appropriate vector to detect the red staining, was then applied. The ImageJ then creates three different versions of the original image. The reddish/ pinkish version (a version that picks up the ORO (red) staining) was then chosen for analysis. To achieve consistency and less subjectivity, a threshold generated automatically by the software was applied. Data was shown in terms of plaque, lumen and vessel size (mm^2), occlusion (plaque size/lumen size x 100), plaque content (plaque size/vessel size x 100) and lipid content (ORO positive staining area/ plaque area x 100). On the other hand, for collagen and immunofluorescence-stained aortic root sections, the plaque area was only required to outline. In order to quantify positively stained areas, the threshold was adjusted manually after converting the image to 8-bit format, and the same threshold was applied to all images as possible, otherwise a range of ± 5 was used.

For ORO-stained liver sections, the intensity of the red colour was analysed in these images as the contrast between the red ORO and the purple haematoxylin is much less pronounced than in those of the aortic root. Therefore, it was impossible to reliably detect neutral lipids in hepatocytes using the colour deconvolution method. Subjectivity and bias are limited since there is no need to outline any regions of interest or no adjustment of the threshold is required. The intensity analysis involved dividing the image into three separate colour

channels (red, blue, and green) and then intensity measurement performed using the software. To analyse H&E-stained liver sections, the 'colour deconvolution' function in ImageJ was used to achieve consistency and less subjectivity. The 'H&E' vector was then applied as it has been found to be the most appropriate vector. The purple version was then chosen for analysis as it has been found to be the most accurate version.

2.6.10 Calculation of plaque necrosis and stability

To quantify plaque necrosis, the ORO-stained aortic root sections were used with the following method employed in the host laboratory and as described by (Solanki et al. 2017; Chan 2021). Plaque necrosis was presented as a percentage. The plaque stability index was calculated using the formula described by (Liu et al. 2019b) as follows: (VSMC area + collagen area)/(macrophage area + lipid area), all values used in this formula were percentage positive staining of plaques.

2.6.11 RNA-sequencing

RNA-sequencing (RNA-seq) is an important tool in molecular biology that uses capabilities of high-throughput sequencing technologies (Next generation sequencing, NGS) to analyse differential gene expression (DGE) in biological samples (Stark et al. 2019). The workflow includes different steps starting with RNA extraction, followed by total RNA qualification, mRNA enrichment, double strand cDNA synthesis, the addition of end repair, poly A and adaptor, followed by fragments selection and PCR, library quality assessment. Finally, the samples are analysed on Illumina HiSeq™ for sequencing (Figure 2.13).

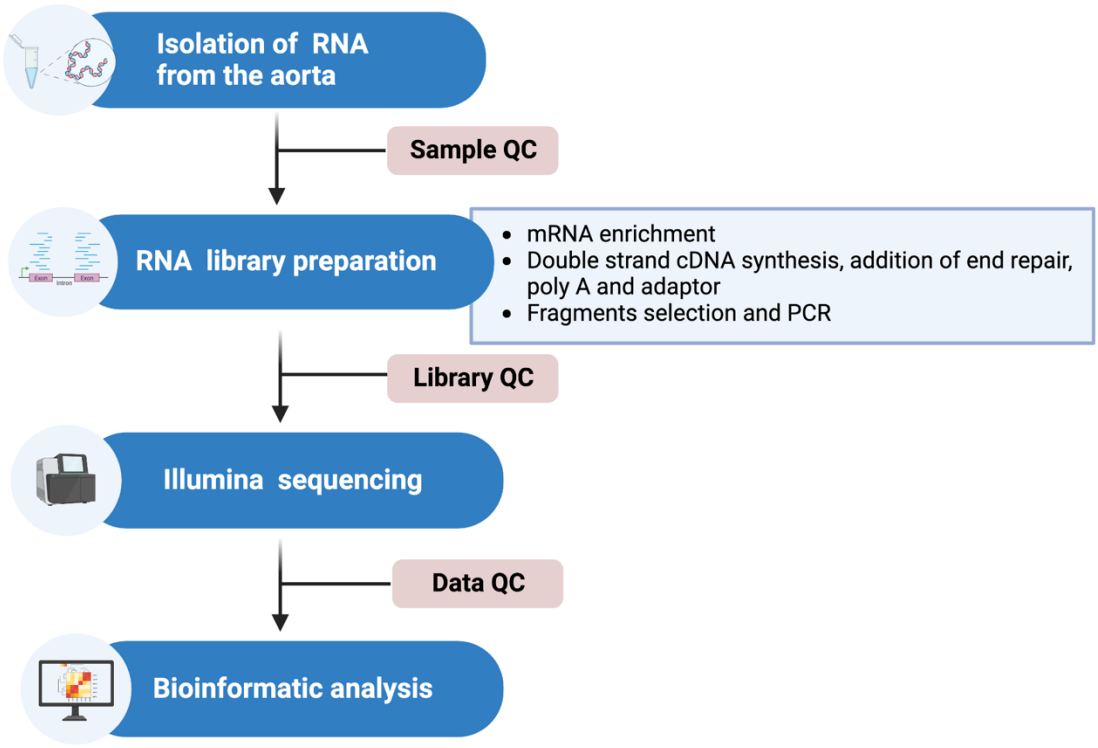

Figure 2.13 RNA-sequencing workflow

The project workflow starts with RNA extraction in the host laboratory followed by sample quality control (Sample QC) which was done in the host laboratory and by Novogene to ensure that samples meet the criteria of the RNA-Seq technique. After that, the library was prepared and subsequently tested for its quality (library QC). Then, a 150 bp paired-end sequencing strategy was used for sequencing the samples and the quality of obtained data was checked (Data QC). Finally, bioinformatic analyses were carried out. **Abbreviation:** QC, quality control; mRNA, messenger ribonucleic acid; cDNA, complementary DNA; PCR, polymerase chain reaction

2.6.11.1 RNA sample preparation

The first step in RNA-seq is isolation of RNA from biological samples. RNA was extracted from the thoracic part of mouse aorta that had been previously stored in *RNAlater*™ stabilisation solution at -80°C. The extraction was carried out using RNeasy Mini Kit from Qiagen and following the manufacturer's instructions with some modification to improve concentration and quality.

The whole process of RNA extraction was performed under sterile conditions and at room temperature (according to manufacturer's instructions) unless otherwise stated. The thoracic aorta was placed in a sterile petri dish on the ice-cold pack and the adjacent adipose tissue

was carefully removed quickly to prevent RNA degradation. All subsequent steps were performed at room temperature. The TissueLyser II from Qiagen at Central Biotechnology Services (CBS) in Cardiff University was used for homogenisation of the tissue for RNA extraction to provide rapid and efficient disruption. The clean aorta was placed in round bottom 2 ml Eppendorf tube that contained one 2 mm stainless steel beads (complementary to the machine) and 600 µL RLT buffer (provided in the kit). The tubes were then transferred to TissueLyser Adapter and homogenised at 25 Hz for 1 minute. The samples and racks were then rotated and the TissueLyser was operated again at the same setting for another 1 minute. Samples were then centrifuged briefly in a microcentrifuge to collect any remnants from the side of the tubes and the solution was then transferred directly to a new 1.5 ml Eppendorf tube for subsequent steps in the RNeasy kit procedure.

The samples were centrifuged for 3 minutes at maximum speed in a microcentrifuge. The supernatant was then transferred carefully to a new Eppendorf tube containing 600 µl of ice-cold, freshly prepared 70% ethanol. The mixture was then transferred to RNeasy spin column placed in a 2 ml collection tube (supplied in the kit) and centrifuged for 30 seconds at 9,000x g. Samples were washed by adding 350 µl of RW1 buffer directly to the RNeasy spin column and centrifuged for 30 seconds at 9,000x g. All washing steps in this protocol were carried out twice and the tubes orientation were changed each time before centrifugation (i.e., hinge of the tube's lid facing the outer or inner rim of the centrifuge) to ensure washing of the entire column for 30 seconds at 9000x g. The flow-through was then discarded before incubation of the samples with 80 µl of DNase I mix (Qiagen) for 15 minutes to remove any contamination DNA in samples. The DNase I mix was prepared directly before adding to the sample by mixing 10 µl prepared DNase I stock solution to 70 µl of buffer RDD (per sample). Both reagents (DNase I and RDD buffer) are not provided in the RNeasy Mini Kit. The samples were then first washed with 350 µl of RW1 buffer and then with 700 µl of RW1 buffer. Washing steps were continued by the addition of 500 µl Buffer RPE (supplied in the kit) to the RNeasy spin column and repeated three times. For the last wash, 500 µl of Buffer RPE was added and centrifuged for 2 minutes at 9,000x g. To ensure that no RPE buffer was carried over during RNA elution, the spin column membrane was placed in a new 2 ml collection tube and centrifuged for 1.5 minutes at maximum speed in a microcentrifuge for drying purposes. This was repeated at the same speed and time with changing the tube orientation. The RNeasy spin column was

then placed in a 1.5 ml Eppendorf tube and 30 µl of RNAse-free water added directly to the spin column membrane. Tubes were placed on ice and samples were incubated for 15 minutes for optimal yield and stability. The samples were then centrifuged for 1 minute at 9,000x g. The RNA concentrations and purity was then checked using NanoDrop™ One/One^{C} Microvolume UV-Vis Spectrophotometer facility in CBS.

Different criteria were applied before sending the samples to further check RNA quality. The samples concentrations should not be less than 400 ng (20 ng/ µl) and for RNA purity, the OD260/280 was about 2-2.2 and OD260/OD230 was about 1.8-2. Once this was achieved, each sample was aliquoted into two tubes, one (5 µl) for assessing integrity and the other (10 µl) for RNA sequencing if required. The aliquoting was carried out to minimise the potential degradation of RNA by repeated freeze-thaw cycles.

2.6.11.2 Determining RNA quality in the samples

RNA samples (5 µl aliquot) were passed to Dr Amanda Redfern in CBS, Cardiff university to check RNA quality before sending samples to Novogene for RNA-seq. The samples were analysed on Agilent 2100 Bioanalyzer following the manufacturer's instructions. Agilent 2100 Bioanalyzer is a microfluidics-based automated electrophoresis based on traditional gel electrophoresis principles that have been adapted into a chip format. This chip is formatted to reduce separation time significantly and reduce sample volume. Before loading samples on the chip, the chip micro-channels were filled with mixture of Agilent RNA 6000 Nano gel matrix and RNA 6000 Nano dye concentrate (provided with the kit) in order to prepare the chip to be an integrated electrical circuit. RNA 6000 Nano marker was then added to samples and ladder (provided with kit) before loading them in appropriate wells (according to manufacturer's instructions). The chip was then placed on the bioanalyser. Samples were then separated by size. Dye molecules intercalate into RNA which then allows detection by laser-induced fluorescence. Data were then translated into gel-like images (densitometry plot) and peaks images (electropherograms).

This assay provides reliable and precise results together with RNA integrity number (RIN) between 1 and 10 for each sample where 10 shows the highest quality. According to

Novogene, the RIN value should be equal or more than 6.8 to be sufficient to generate a library for sequencing.

2.6.11.3 Library Construction and quality controls (QC)

Library construction and RNA-seq processes were carried out by Novogene, UK. Once samples were delivered to them, the quality was checked again before library construction steps were done to ensure high quality data. Samples were passed through the following three quality control steps: Nanodrop, Agarose Gel Electrophoresis and Agilent 2100.

Briefly, After the QC procedures, mRNA was purified from total RNA using poly T-oligo-attached (dT) magnetic beads before cDNA library construction. After that, the mRNA was fragmented randomly using a specific fragmentation buffer and cDNA was synthesised using random hexamer primers. This was followed by second strand synthesis by using dTTP for non-directional library. After cDNA purification, terminal repair, A-tailing and ligation of sequencing adapters, size selection and PCR enrichment were carried out (Figure 2.14).

The QC for library construction was then quantified using a Qubit 2.0 fluorometer (Life Technologies), and the insert size was checked on an Agilent 2100 before the final quantification using quantitative PCR (q-PCR) for greater accuracy.

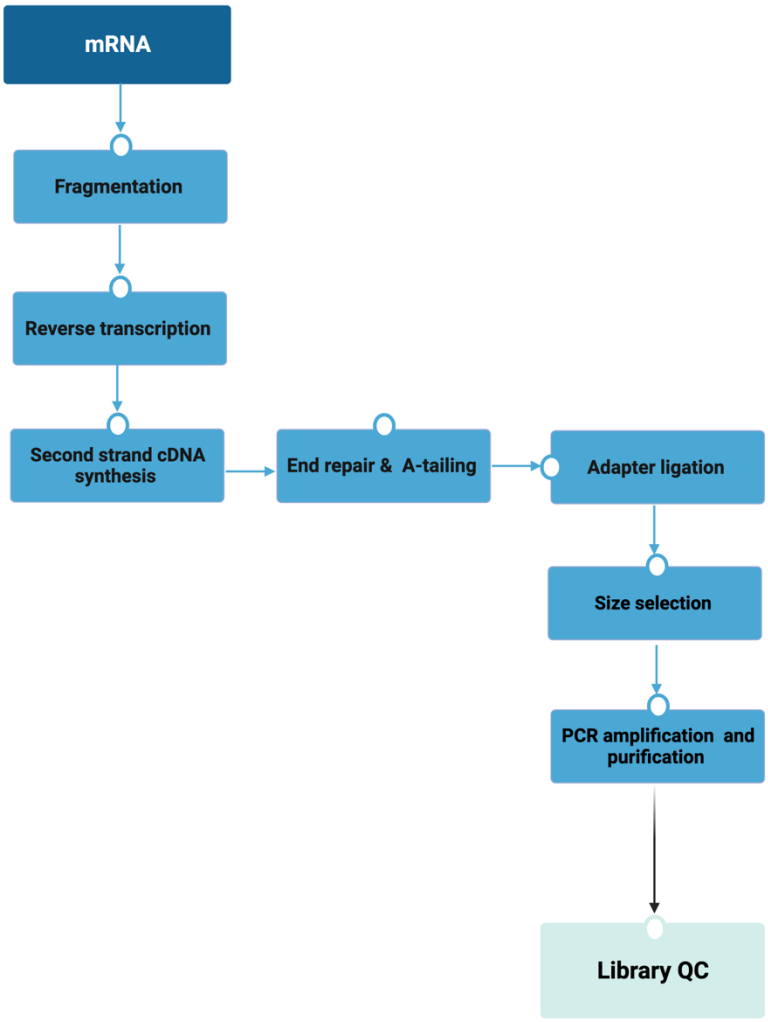

Figure 2.14 Library construction workflow

Abbreviations: mRNA, messenger RNA; QC, quality control.

2.6.11.4 Clustering and sequencing

Following the clustering of the index-coded samples, libraries were loaded onto HiSeq Illumina sequencers and paired-end reads were generated.

2.6.11.5 Data analysis

Primary analysis was performed by Novogene (Figure 2.15). First, the raw data (raw reads) of FASTQ format were processed. During this step, reads containing adapter or containing ploy-N and low-quality reads from raw data were removed to obtain clean data (clean reads).

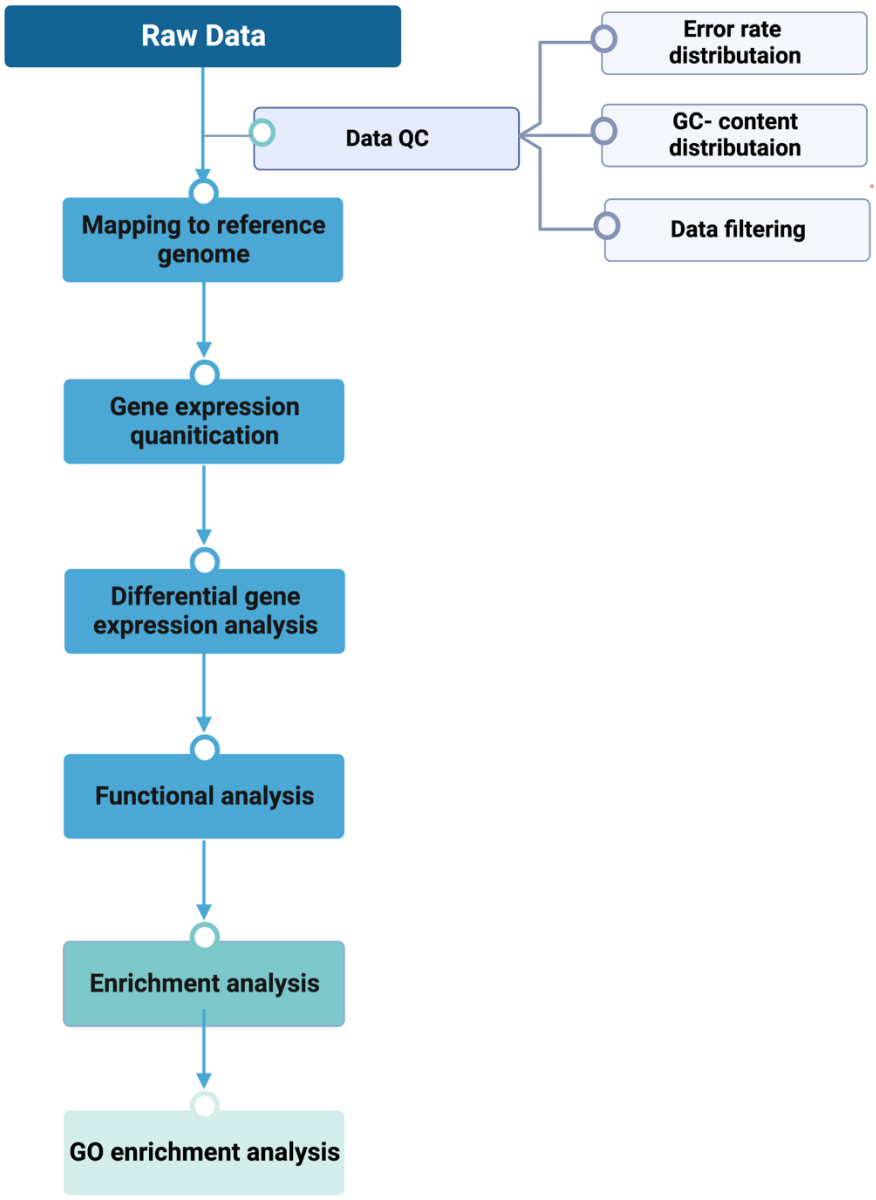

Figure 2.15 Analysis pipeline utilised by Novogene for RNA-seq data

Abbreviations: QC, quality control; GC-content, guanine cytosine-content; GO, gene ontology.

2.6.11.6 Mapping reads to the reference genome

Mapping the clean data to the reference genome was performed in which HISAT2 v2.0.5 was used as the mapping tool. This was used to build the index of the reference genome and for alignment of paired-end clean data to the reference genome.

2.6.11.7 Quantification of gene expression levels

The abundance of transcript reflects the gene expression level directly, hence in the next step, the reads numbers mapped to each gene were counted using a software program, featureCounts v1.5.0-p3. After that, the expected number of Fragments Per Kilobase of transcript sequence per Millions base pairs sequenced (FPKM), which is the most common method of estimating gene expression levels, of each gene was calculated.

2.6.11.8 Differential gene expression analysis

Following the quantification of gene expression, statistical analysis of the expression data was carried out to identify genes whose expression levels were significantly different in different conditions. This was performed using the DESeq2Rpackage and involved 3 steps: normalisation of the read count; use of the statistical model to calculate p-values; and applying multiple hypothesis test corrections to obtain false discovery rate (FDR values) (FDR < 0.05). This approach was used to determine adjusted p-values for each gene.

In addition to the above-mentioned analyses that were performed by Novogene, Qiagen Ingenuity Pathway Analysis (Qiagen IPA) software was used for a more in-depth analysis. The padj <0.05 filter was used in the analysis where transcripts with adjusted p values <0.05 were considered as significantly differentially expressed. The use of IPA helps to identify the affected canonical pathways, diseases and function and up-stream regulators. Furthermore, the list of the genes associated with the canonical pathways were considers but not taken in detail in the analysis. Then, genes implicated in the top affected diseases and function were presented as heatmap using heatmapper online software (http://www.heatmapper.ca/expression/). For a more comprehensive analysis, the changes in interesting biological pathways associated with atherosclerosis and inflammation were explored using searching tools in the IPA followed by overlay analysis tool that allows visualisation of the affected genes in the pathway.

2.6.11.9 Enrichment analysis of differentially expressed genes

Gene Ontology (GO) enrichment analysis was performed by Novogene using clusterProfiler R package software. It is considered as a fundamental bioinformatics categorisation system that allows to annotate genes to biological processes, cellular locations and molecular functions that are affected by the studied condition. GO terms with padj < 0.05 are significant enrichment.

2.6.12 Statistical analysis

All data were presented as mean fold change/percentage +/- standard error of the mean (SEM) after outliers (data values outside two standard deviations from the mean) were removed. Normality of the data sets was then tested using Shapiro-Wilk test. Statistical analysis for multiple groups (more than two groups) with normally distributed data was carried out by one-way analysis of variance (ANOVA) followed by either a Tukey's (for equal variances) or Dunnett's (for unequal variances) post-hoc test. On the other hand, for data with two groups only, unpaired t-test (for normally distributed data) or Mann-Whitney U test (for not normally distributed data) was performed. Significance was defined as * $p < 0.05$, ** $p < 0.01$ and *** $p < 0.001$. Data were subjected to statistical analysis only if a minimum of three independent experiments had been completed and were carried out using GraphPad Prism 9 software.

Chapter 3

The effects of resveratrol on key cellular processes in atherosclerosis *in vitro*

3.1 Introduction

RSV is a well-known polyphenolic compound present in various plants, including grapes, peanuts, dark cocoa and different species of berries (Zhang et al. 2021b). It has long been associated with various health beneficial effects such as in the prevention of chronic diseases where oxidative stress plays an important role, including diabetes, kidney disorders, neurodegeneration, cancer and CVDs, and therefore it has been a subject of interest for many *in vitro*, *in vivo* and clinical studies (Malaguarnera 2019). Despite its cardioprotective effects to improve pathological conditions related to CVDs and their associated risk factors that have been highlighted previously in Chapter 1, as well as in many *in vitro* and *in vivo* studies (Prasad 2012; Gal et al. 2021) such as antioxidant, anti-inflammatory and anti-apoptotic effects, further investigation on RSV actions *in vitro* in the context of the key cellular processes in different key cell types implicated in atherosclerosis is still required.

3.1.1 Experimental aims

The main aim of all the studies presented in this chapter was to investigate the effect of RSV treatment on a range of key cellular processes associated with atherosclerosis development in order to provide an initial assessment of its potential anti-atherogenic effects. For this purpose, a range of experiments were carried out *in vitro* using different cell lines and primary cell cultures, including THP-1 monocytes, macrophages, HASMCs and HAECs that were treated with RSV. To rule out the possibility that the findings in THP-1 macrophages were due to the cell line utilised, the major key studies were repeated in primary cultures of HMDMs.

The initial experiments were performed using different doses in order to identify the lowest effective concentration of RSV, with the aim of selecting a single optimal concentration. Investigations were then continued using the single optimal concentration. *In vitro* experimental strategy to identify the effective dose of RSV on key cellular processes associated with atherosclerosis progression is illustrated in Figure 3.1.

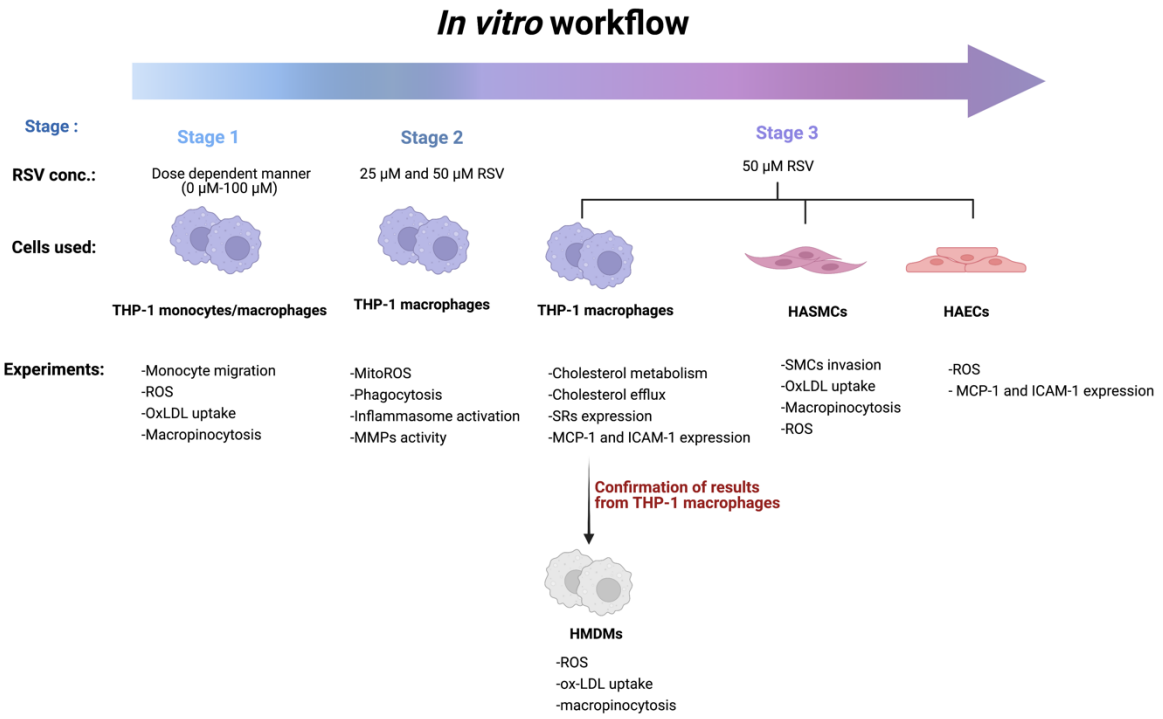

Figure 3.1 *In vitro* experimental strategy to identify the effective dose of RSV on atherosclerosis progression.

Initially, experiments were performed in dose-response manner using THP-1 monocytes/macrophages (stage 1). After then, two concentrations were chosen (stage 2) before the single effective dose was determined and utilised for further investigations (stage 3). **Abbreviations:** ROS, reactive oxygen species; MitoROS, mitochondrial reactive oxygen species; SRs, scavenger receptors, MCP-1, monocyte chemoattractant protein-1; ICAM-1, intercellular adhesion molecule-1; HASMCs, human aortic smooth muscle cells; HAECs, human aortic endothelial muscle cells; HMDMs, human monocyte-derived macrophages. Image created with BioRender.com

3.1.2 Key processes in atherosclerosis

3.1.2.1 Monocyte recruitment and migration

Monocyte recruitment and migration is a finely organised process involving the expression of chemokines and adhesion molecules by activated ECs (Čejková et al. 2016). MCP-1 is the pivotal pro-inflammatory chemokine that is secreted by a variety of immune or non-immune cell types such as macrophages, ECs, SMCs, fibroblasts, etc. However, in early atherosclerotic lesions, macrophages and ECs are the main sources of MCP-1 (Zhang et al. 2011b; Mirzaei et al. 2017). MCP-1 is also known as CCL2 and mediates its effects by binding to circulating monocytes and T cell receptor, CCR2 (Mirzaei et al. 2017; Georgakis et al. 2022). Previously in two independent pre-clinical studies on ApoE$^{-/-}$ and LDL$^{-/-}$ mice deficient in CCR2

demonstrated a significant reduction in atherosclerotic lesions and macrophage accumulation in the aortic wall (Boring et al. 1998; Gu et al. 1998). Similar results have been observed with human ApoB transgenic mice with deficiency of MCP-1 (Gosling et al. 1999) while high expression levels of MCP-1 in atherosclerotic plaques have been shown by many *in vivo* studies (Gonzalez-Quesada and Frangogiannis 2009). In addition, clinical study of patients with atherosclerosis found increased levels of plasma MCP-1 (Mirzaei et al. 2017). Targeting the expression of MCP-1 in ApoE^{-}/$^{-}$ mice as a therapeutic strategy for combating atherosclerosis showed a reduction in atherosclerosis development as well as macrophages and lipid accumulation in the plaque (Inoue et al. 2002). Therefore, attenuation of monocyte migration in the presence of MCP-1 by RSV represents a potential anti-atherogenic effect and formed the focus of this investigation.

3.1.2.2 HASMCs invasion

VSMCs are the predominant cells in the media layer of arteries that are critical for the maintenance of the arterial wall structure and function (Jaminon et al. 2019). They have an ability to switch from a contractile phenotype to a synthetic phenotype when they have migrated from the tunica media into the arterial intima in response to various cytokines, chemokines and growth factors such as PDGF. The migrated VSMCs secrete ECM proteins that provide plaque stability and hence protect against plaque rupture (Louis and Zahradka 2010; Hu et al. 2019; Jaminon et al. 2019). This migration and proliferation of VSMCs is essential and normal response to injury. However, pathogenic vascular remodelling and generation of intimal vascular lesions following VSMCs invasion results in case the migrated and proliferated VSMCs fail to switch back to the contractile phenotype (Louis and Zahradka 2010). In this study, the ability of RSV to attenuate PDGF-stimulated migration of HASMC was investigated using modified Boyden chamber method.

3.1.2.3 ROS production

Cellular redox homeostasis is a crucial and dynamic process that ensures the function of the vascular system. The imbalance in cellular redox is caused by elevations in ROS levels that ultimately result in oxidative stress. Although ROS at appropriate baseline is important for proper cell signalling, severe oxidative stress can be deleterious and associated with the

development of many pathological conditions such as atherosclerosis-associated risk factors such as (e.g. CVDs, diabetes and obesity) (Niemann et al. 2017; Nowak et al. 2017). In atherosclerotic plaques, among a group of highly reactive oxygen derivatives, hydrogen peroxide (H_2O_2) is a major type of ROS generated mainly by macrophages and VSMCs as well as other sources such as local injured cells (Chien et al. 2004; Armstrong et al. 2011). H_2O_2 contributes to a key process of atherogenesis development, modification of LDL to ox-LDL by oxidation, and hence endothelial dysfunction, thereby stimulating an inflammatory response (Negre-Salvayre et al. 2020). In fact, H_2O_2 plays a crucial role as a key modulator in the activation of pro-inflammatory genes regulated by NF-κB, including ICAM-1, MCP-1 and TNF-α, as well as induces MMPs production that contributes to vascular dysfunction and plaque rupture (Jayakumar et al. 2014; Poznyak et al. 2021; Zhang et al. 2022b). Therefore, in this study, the ability of RSV to attenuate H_2O_2-induced ROS activity was measured in all investigated cell types.

3.1.2.4 Mitochondrial ROS (mitoROS) production

Mitochondria are not only a major site of ROS production, but they are also vulnerable to oxidative damage caused by ROS (Burtenshaw et al. 2019). Under normal conditions, metabolism of mitochondria generates harmful ROS that are normally neutralised by opening of the mitochondrial permeability transition pore (mPTP), resulting in the maintenance of mitochondrial homeostasis (Burtenshaw et al. 2019). However, under pathological conditions, impairment in the antioxidant system in addition to excessive production of ROS leads to mitochondrial oxidative stress (Sena et al. 2018). The mitochondrial oxidative stress contributes to mitochondrial DNA damage (mtDNA), ROS production and decreased mitochondrial respiration (Shemiakova et al. 2020). It has been reported that damage of mtDNA correlates with the pathogenesis of atherosclerosis, including inflammation, further ROS production, apoptosis of cells and plaque vulnerability (Shemiakova et al. 2020). Multiple lines of *in vivo* experimental evidence have revealed that increased atherosclerosis progression is strongly linked with excessive mitoROS levels within the vasculature. A study in ApoE$^{-/-}$ mice that are deficient in SOD2, a mitochondrial antioxidant enzyme, showed accelerated progression of atherosclerosis at arterial branching points by increasing mtDNA damage (Ballinger et al. 2002). The same study demonstrated that mtDNA damage is considerably higher in human atherosclerotic arterial specimens than in normal human

arterial tissue (Ballinger et al. 2002). Another study on hypercholesterolemic LDLr$^{-/-}$ mice showed increased ROS production by mitochondria in various tissues compared to wild type controls (Oliveira et al. 2005). Furthermore, oxidative damage to mtDNA is linked to the severity of atherosclerosis in humans and mice (Dorighello et al. 2016). Therefore, blockade of mitoROS production may serve as a potential therapeutic avenue for combating atherosclerosis progression. An aim of this study was to evaluate the effect of RSV on mitochondrial superoxide production in THP-1 macrophages.

3.1.2.5 Foam cell formation

3.1.2.5.1 Macropinocytosis

Macrophages and VSMCs uptake unmodified and modified lipids via macropinocytosis and transform into foam cells. Macropinocytosis is a receptor-independent endocytosis pathway in which large amount of fluid in the surrounding environment are non-specifically internalised into large endocytic vesicles known as macropinosomes (Lin et al. 2020). In contrast to other endocytic mechanisms, such as receptor-mediated endocytosis and phagocytosis, internalisation of molecules by macropinocytosis does not require molecules binding to cell surface receptors or contacting with the cell surface. It is an actin-dependent mechanism in which the actin filament polymerises at the plasma membrane to produce membrane ruffles. These ruffles catch solutes (e.g., lipids) into macropinosomes where the membranes undergo several fusion and fission steps before passing to other organelles in the endolysosomal system (Lin et al. 2020). In this study, the effect of RSV on macropinocytosis was assessed in THP-1 macrophages, HMDMs and HASMCs using Lucifer yellow (LY), a fluorescent tracer widely used to monitor macropinocytosis due to its ability to internalise into cells via macropinocytosis with harmless effects on the cells.

3.1.2.5.2 Dil-oxLDL uptake and scavengers receptors expression

Differentiated macrophages in the arterial wall uptake ox-LDL via a range of scavenger receptors, including SR-A and CD36, and consequently transform into foam cells. In addition to macrophages, VSMCs transform into foam cells through the uptake of ox-LDL via their scavenger receptors (Chellan et al. 2016). Indeed, it has been demonstrated that VSMCs constitute at least 50% of total foam cell population in the human plaque (Dubland and

Francis 2016). Formation of foam cells promote the secretion of pro-inflammatory cytokines that induce monocyte and T cells recruitment as well as secretion of ECM that promotes LDL retention in the intima (Linton et al. 2019; Davra and Galluzzi 2020).

SR-A and CD36 belong to class A and class B scavenger receptors, respectively. SR-A can bind a broad range of ligands, including acLDL, oxLDL, some types of collagens, ECM components and apoptotic cells. It has a high affinity for modified LDL but not for native LDL (Yi et al. 2009; Kzhyshkowska et al. 2012). In contrast to SR-A, CD36 can recognise and internalise certain ligands such as thrombospondin-1, oxidised phospholipids (oxPL), ox-LDL, long-chain fatty acids as well as native HDL, LDL and VLDL (Calvo et al. 1998; Park 2014). Several lines of evidence have shown the role of SR-A and CD36 overexpression in excessive lipid internalisation, foam cell formation, and, ultimately, atherosclerosis development. Inhibition of foam cell formation and scavenger receptors in atherosclerotic lesions had been studied and identified as a promising approach for combating atherosclerosis progression (Stephen et al. 2010; Wang et al. 2019a; Liu et al. 2020; Tian et al. 2020; Javadifar et al. 2021). Therefore, the ability of RSV to attenuate foam cell formation via the inhibition ox-LDL uptake was assessed in THP-1 macrophages, HMDMs and HASMCs, as well as the effect of RSV on SR-A and CD36 expression at the mRNA and protein levels using qPCR and flow cytometry respectively.

3.1.2.5.3 Phagocytosis

Macrophages are phagocytic cells that are capable of engulfing debris, dead cells as well as LDL, VLDL and ox-LDL by phagocytosis. They can uptake lipoproteins from dying cells easily and thereby contribute to foam cell formation (Remmerie and Scott 2018). Additionally, it has been reported in several studies that agLDL, which is formed in the intima either as a result of oxidation of LDL molecules or as a results of exposure of native LDL to sphingomyelinase and phospholipase A2 and retention by proteoglycans of the ECM , can be engulfed via phagocytosis and contribute to foam cell formation (McLaren et al. 2011; Lu and Gursky 2013; Sukhorukov et al. 2020). In the early stage of plaque development, internalisation of large self-associated modified LDL molecules induces the secretion of pro-inflammatory cytokines that facilitates the recruitment of monocytes and T-cells to the intima and, therefore, stimulates of inflammatory response (Orekhov et al. 2020). This study aims to elucidate the

long- (24 hours) and short-term (3 hours) effect of RSV on phagocytosis in THP-1 macrophages.

3.1.2.5.4 Cholesterol efflux

The impairment in cholesterol metabolism (i.e. increase in cholesterol uptake due to endothelial dysfunction and upregulation of scavenger receptors and decrease in cholesterol efflux from macrophages (as well as VSMCs)) leads to foam cell formation (Volobueva et al. 2018). Under normal physiological conditions, there is a tightly regulated cellular mechanism to ensure cholesterol homeostasis by reduction of cholesterol uptake and enhancement of cholesterol efflux (Ouimet and Marcel 2012). There are a number of mechanisms involved in cholesterol efflux such as active diffusion that is mediated by ABCA1 and ABCG1, and passive diffusion or SR-B1-mediated efflux (Marques et al. 2018b; Westerterp and Tall 2020). A study carried out to measure cholesterol efflux capacity in familial hypercholesterolemia (FH) patients demonstrated that cholesterol efflux is inversely associated with atherosclerosis risk (Ogura et al. 2016). A recent systematic review and meta-analysis of 20 studies found that high cholesterol efflux capacity was related to a 37% decreased risk of adverse CVDs (Lee et al. 2021). From these studies and much other solid evidence, stimulating cholesterol efflux is considered to be a therapeutic target for preventing atherosclerosis. The ability of RSV to attenuate foam cell formation by enhancing cholesterol efflux from human macrophages was hence investigated.

3.1.2.5.5 Intracellular cholesterol metabolism

The regulation of lipid homeostasis is tightly regulated with mechanisms regulating the influx, synthesis, storage, metabolism, and efflux of cholesterol. In atherosclerotic lesion development, disruption in cholesterol storage and metabolism plays an important role that leads to the accumulation of intracellular lipids and consequently foam cell formation (Sukhorukov et al. 2020). As discussed in detail in chapter 1, particularly Section 1.3.2, the CE contained within the modified LDL particles is unesterified into free cholesterol and free fatty acids. This free cholesterol is re-esterified to CE that is then either stored as lipid droplets in the cytoplasm or degraded to FC by nCEH enzymes followed by efflux from macrophages (Sukhorukov et al. 2020). In atherosclerosis, the imbalance in cycle of CE synthesis and hydrolysis results in an excess of CE stored in cytoplasmic lipid droplets and consequently

foam cell formation. Study was therefore carried out to evaluate the effect of RSV on the formation of CEs and other major lipid classes in macrophage foam cells by measuring the incorporation of [^{14}C] acetate into major lipid classes.

3.1.2.6 Inflammation in atherosclerosis development

3.1.2.6.1 Inflammasome activation

Inflammasome activation in macrophages occurs by, for example, phagocytosis of cholesterol crystals found in the plaque necrotic core. The activation of inflammasomes causes damage to the lysosomal system and promotes inflammatory response and foam cell formation (Bobryshev et al. 2016). The NLRP3 inflammasome is the most well-known inflammasome and a critical regulator of atherosclerosis inflammation (Jin and Fu 2019). It is responsible for the secretion of proinflammatory IL-1β and IL-18 by converting pro- to mature- forms (Grebe et al. 2018). IL-1β is a key cytokine released by the NLRP3 inflammasome and therefore measuring IL-1β secretion can be used as an indirect way of measuring inflammasome activation (Hoseini et al. 2017). Evidence has found that the protein and mRNA levels of IL-1β positively correlate with atherosclerosis severity (Mai and Liao 2020). IL-1β impacts all stages of atherosclerosis, including induction of expression of adhesion molecules and chemokines, promotion of inflammatory cell accumulation and stimulation of an inflammatory response (Mai and Liao 2020). A study to determine the expression level of NLRP3 in aorta samples taken from patients with CVD showed a strong correlation between increased expression of NLRP3 and enhanced severity of CVDs and atherosclerosis risk (Zheng et al. 2013). Moreover, gene silencing of NLRP3 in ApoE^{-}/$^{-}$ mice fed HFD showed inhibition of plaque development and proinflammatory cytokines secretion as well as improved plaque stability (i.e. increased SMCs and collagen content, reduced macrophages and lipid content)(Zheng et al. 2014). Furthermore, the CANTOS trial has offered targeting of IL-1β using canakinumab as a new promising anti-inflammatory therapy that significantly reduced CVDs events (Ridker et al. 2017). Therefore, the anti-inflammatory effect of RSV via attenuating IL-1β production was elucidate using THP-1 macrophages.

3.1.2.6.2 Expression of MCP-1 and ICAM-1

In all stages of atherosclerotic lesion development, inflammation takes place "hand-in-hand" with lipid accumulation in the vessel wall. Cytokines are small protein mediators released by a range of cells, including monocytes, macrophages, ECs, SMCs and T-cells, that play a key role with an interplay between pro- and anti-inflammatory cytokines influencing plaque formation and stability (Buckley and Ramji 2015; Fatkhullina et al. 2016). Among several cytokines, IFN-γ is considered a master regulator in the development of atherosclerosis that is capable of inducing the expression of around a quarter of genes expressed in macrophages (Moss and Ramji 2015). This includes chemokines (e.g., MCP-1) and adhesion molecules (e.g., ICAM-1 and VCAM-1) (Moss and Ramji 2015). In addition to IFN-γ, TNF-α induces inflammation and atherosclerosis development by promoting the interaction between monocytes and ECs via upregulation of expression of adhesion molecules ICAM-1 and VCAM-1 (Tousoulis et al. 2016). Several lines of evidence demonstrate a correlation between inhibition of IFN-γ and attenuation of inflammation in atherosclerosis. A study in hypercholesterolemic mice demonstrated that hypercholesterolemia induces T-cells adhesion to ECs; however, this effect is decreased in IFN-γ deficient mice (Stokes et al. 2003). Other studies on atherosclerotic mice, such as $ApoE^{-/-}$ and $LDLR^{-/-}$ reported a reduction in atherosclerotic lesions in mice with genetic ablation of IFN-γ or the IFN-γ receptors (Whitman et al. 2002; Buono et al. 2003; Koga et al. 2007). MCP-1 and ICAM-1 are both robust inflammatory markers and their upregulated expression by these cytokines contributes significantly to atherosclerosis progression. Therefore, attenuation of MCP-1 and ICAM-1 represents a promising avenue to inhibit lesion development. This study investigates the effect of RSV treatment on IFN-γ- and TNF-α-induced expression of inflammatory markers MCP-1 and ICAM1 in THP-1 macrophages and HAECs respectively.

3.1.2.7 MMPs activity

The fibrous cap stability in atherosclerosis is determined by a balance of VSMCs and ECM proteins such as collagen and elastin, as well as collagen fibrils degradation by enzymes such as MMPs and collagenases (Lust et al. 2021; Yurdagul Jr 2022). Macrophages release collagen fibril degrading enzymes during inflammatory responses that is also accompanied by apoptosis of SMCs, which then changes the balance towards ECM degradation and consequently plaque instability and rupture (Van Vré et al. 2012; Newby 2016). MMPs are a

family of zinc-dependent endoproteases enzymes that are secreted by various inflammatory and vascular cells such as macrophages, fibroblasts, neutrophils, SMCs, and ECs. They effect plaque rupture by modulating cellular and signalling pathways that are responsible for atherosclerosis development (Olejarz et al. 2020). Various studies have reported correlation between increase in MMPs activity and increased development of atherosclerotic lesions (Galis et al. 1994; Newby 2008,2016). A clinical study also demonstrated that overproduction of MMPs in CVDs patients increases the risk of CV events (Olejarz et al. 2020). In animal models, atherosclerosis is reduced significantly in Western diet-fed MMP8^{-}/$^{-}$/ApoE^{-}/$^{-}$double knockout mice with a reduction in macrophages and an increase in collagen content in the aorta (Laxton et al. 2009). These findings support MMPs as potential biomarkers for plaque instability, and that they can be targeted for atherosclerosis therapeutic interventions. In this study, MMP activity was measured after short- (3 hours) and long- (24 hours) term treatment with RSV in human macrophages.

3.2 Overview of experimental strategies

A summary of experimental strategies for each assay involved in this chapter is illustrated in Figures 3.2, 3.3 and 3.4. Details of specific methodologies for each experiment are detailed in Chapter 2.

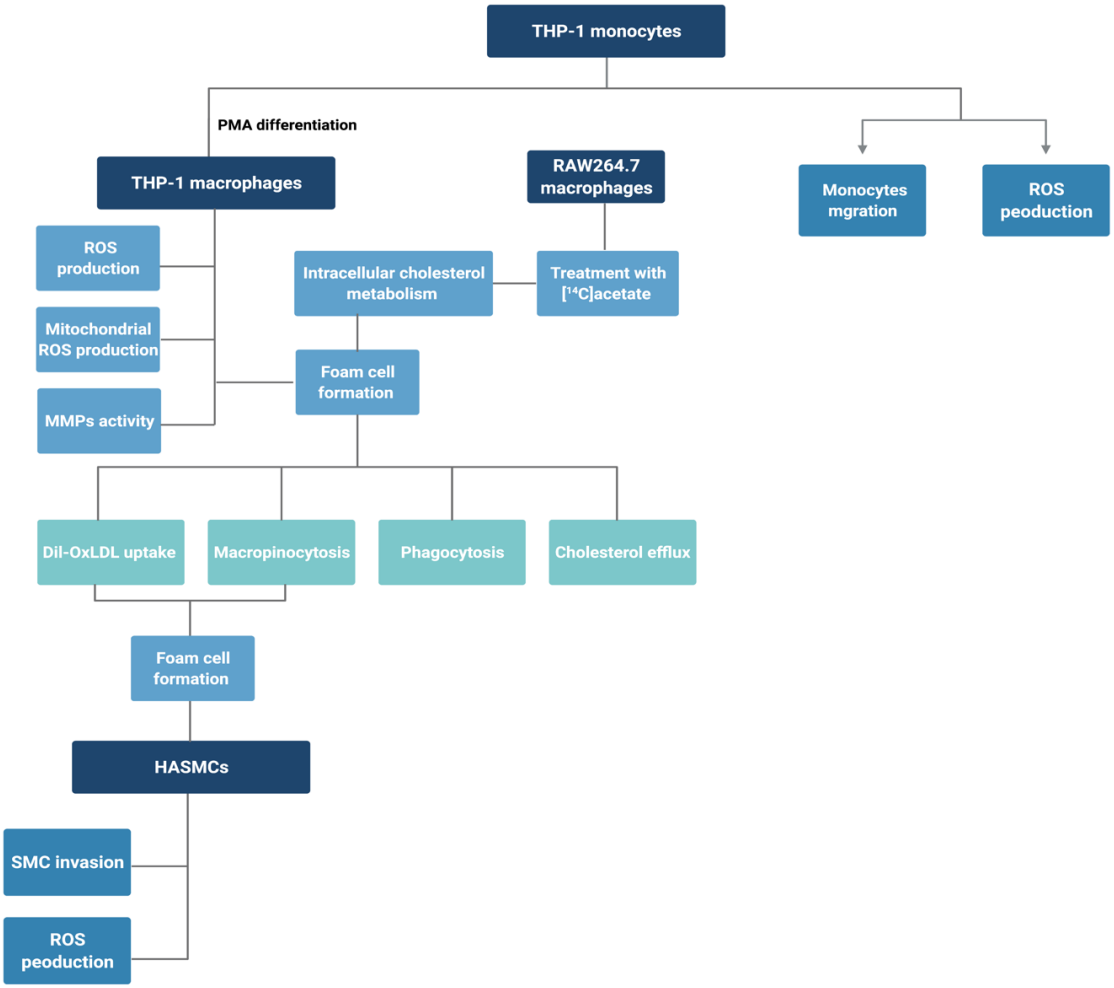

Figure 3.2 Experimental strategy used to investigate the effects of RSV on key cellular processes in atherosclerosis using key cell types involved in disease progression.

Abbreviations: ROS, reactive oxygen species; MMPs, matrix metalloproteinases; HASMCs, human aortic smooth muscle cells; SMC, smooth muscle cells. Image created with BioRender.com.

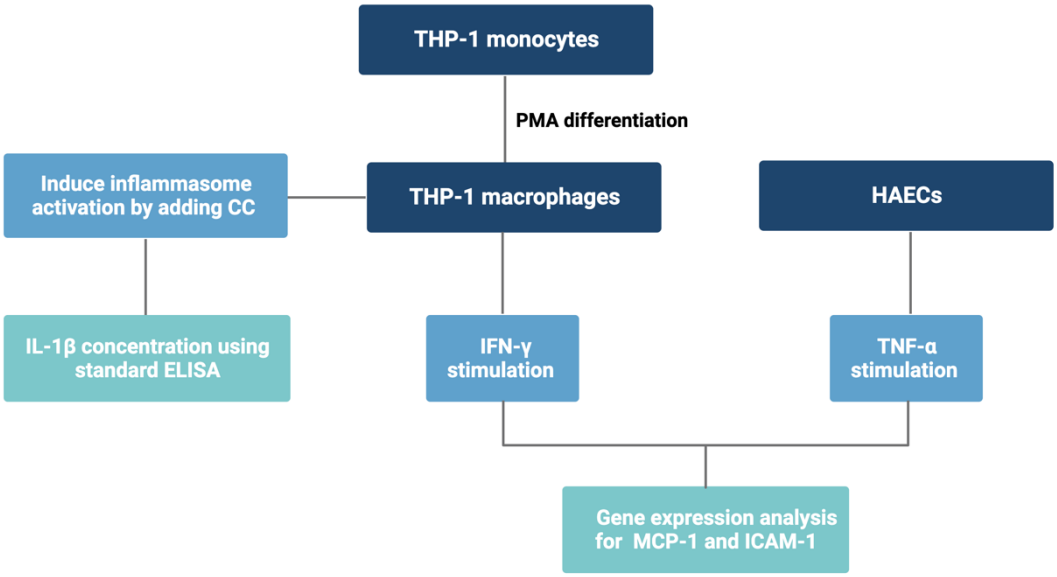

Figure 3.3 Experimental strategy for investigation of the anti-inflammatory effect of RSV

Abbreviations: PMA, Phorbol 12-myristate 13-acetate; CC, Cholesterol crystals; LPS, Lipopolysaccharide; IFN-γ, Interferon gamma; TNF-α, Tumour necrosis factor alpha; IL-1β, Interleukin-1beta; ELISA, Enzyme-linked immunosorbent assay; MCP-1, Monocyte chemoattractant protein-1; ICAM-1, Intercellular adhesion molecule-1. Image created with BioRender.com

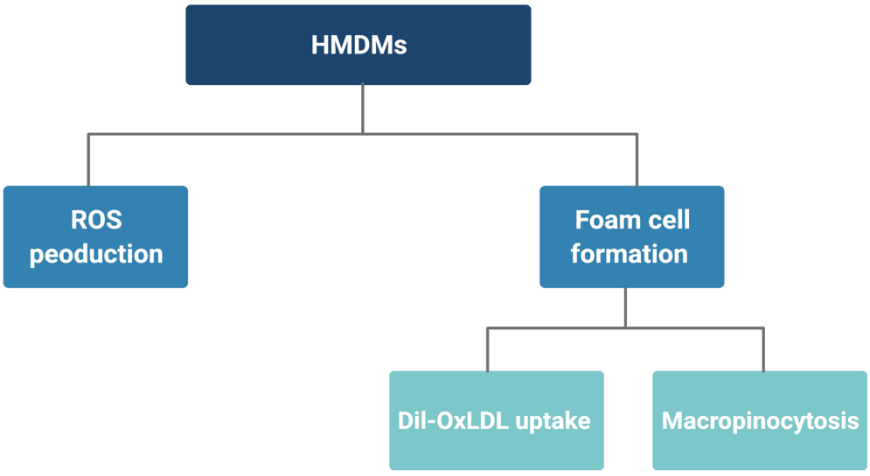

Figure 3.4 Experimental strategy using HMDMs to confirm findings in THP-1-macrophages

Abbreviations: HMDMs, human monocyte-derived macrophages; ROS, reactive oxygen species. Image created with BioRender.com

3.3 Results

3.3.1 Initial assays carried out on THP-1 monocytes/macrophages for determination of the optimal concentration of RSV

3.3.1.1 RSV has no detrimental effects on cell viability of human macrophages at all tested concentrations

Prior to performing any *in vitro* assays, the effect of RSV on cell viability was assessed for all investigated cell culture model systems that were used in the study. This was carried out to ensure that was no significant cytotoxic impact of RSV on cells as well as to verify that any findings were not due to compromised cell viability. Initially, dose response experiments were carried out on the viability of THP-1 macrophages and HMDMs as these cells were used to identify optimal concentration on atherosclerosis-associated processes that can subsequently be used for further studies in these cells and other cell culture model system (HASMCs and HAECs). As shown in Figure 3.5, no significant effects on cell viability were observed following treatment of the cells with RSV when compared to the vehicle control in THP-1 macrophages and HMDMs.

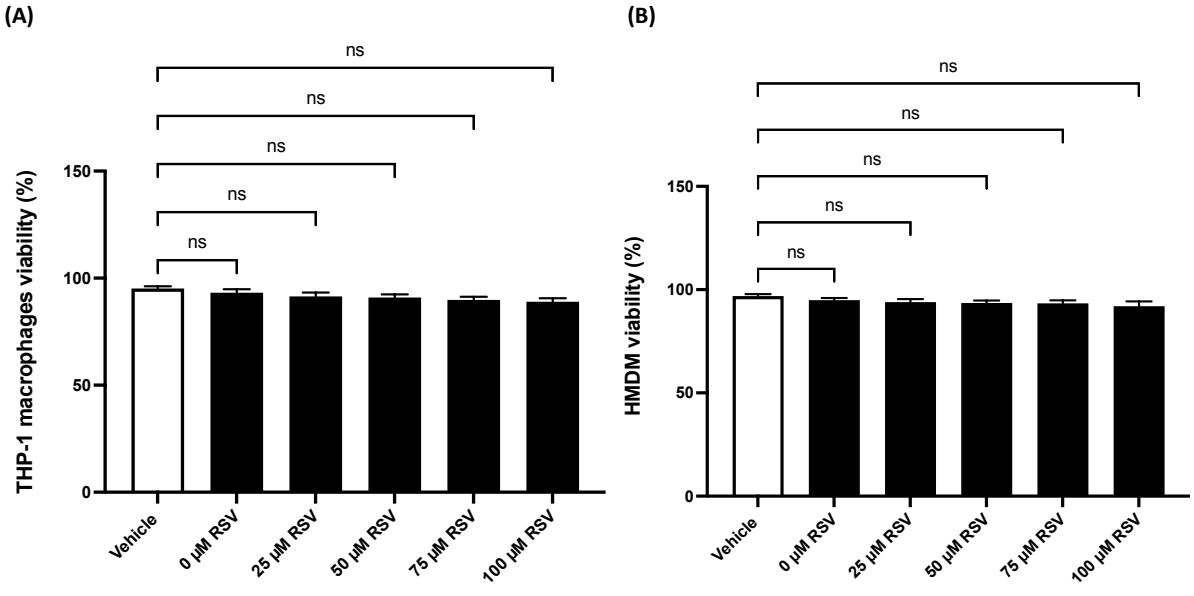

Figure 3.5 RSV has no detrimental effects on cell viability on the cell types used for *in vitro* studies.

THP-1 macrophages (A) and HMDMs (B) were treated with the vehicle control or the indicated concentration of RSV for 24 hours. LDH assay kit was then used to assess cell viability. Data are represented to the vehicle control that has been arbitrarily assigned as 100%. Data are presented as mean fold change ± SEM. Statistical analysis was performed using one-way ANOVA with Dunnett (A) or Tukey's post-hoc analysis (B). **Abbreviations:** HMDMs, human monocyte-derived macrophages; ns, not significant.

3.3.1.2 RSV no effect on cell proliferation of human macrophages

Figure 3.6 shows that no significant changes were seen in all investigated cells (THP-1 macrophages and HMDMs) after 24 hours treatment with RSV when compared to the vehicle control.

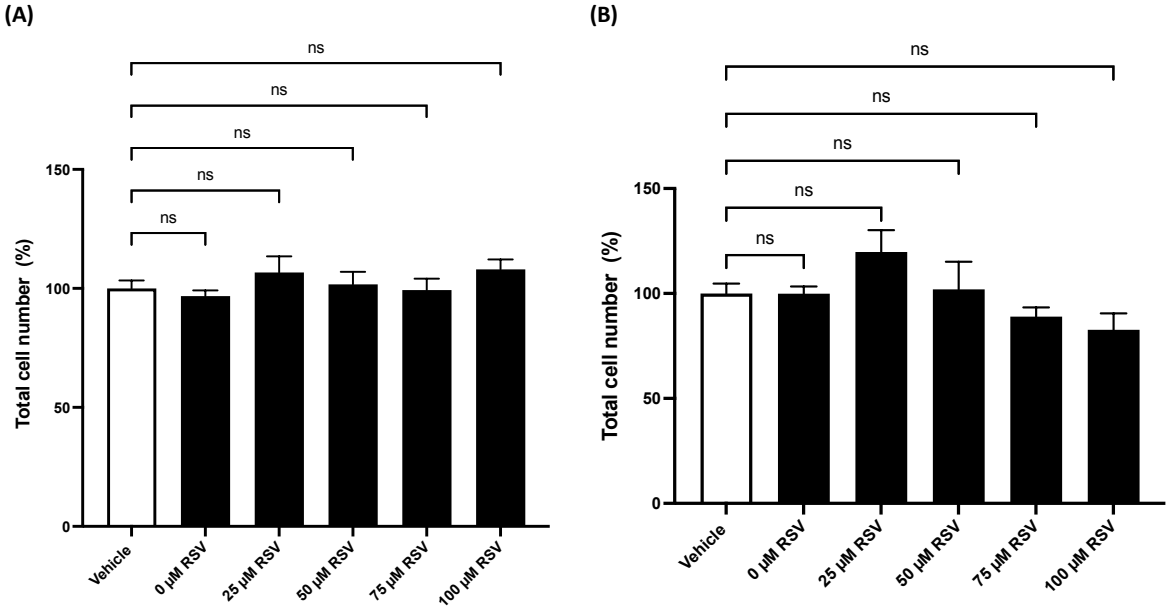

Figure 3.6 RSV has no effect on proliferation of human macrophages after 24 hours.

THP-1 macrophages (A) and HMDMs (B) were treated with the vehicle control or RSV for 24 hours, CV staining of adherent cells was then used to assess cell proliferation. Data were normalised to the vehicle control that was arbitrarily assigned as 100%. Data are presented as mean ± SEM from three or four independent experiments. Statistical analysis was performed using a one-way ANOVA followed by Tukey's (A) or Dunnett (B) post-hoc analysis. **Abbreviations:** HMDMs, human monocyte-derived macrophages; ns, not significant.

3.3.1.3 RSV significantly inhibits the MCP-1-induced migration of THP-1 monocytes

As shown in Figure 3.7, monocyte migration was significantly induced by 50% ($p \leq 0.001$) in the presence of MCP-1 when compared to vehicle alone (no MCP-1). At all concentrations, treatment of cells with RSV inhibits MCP-1-driven migration with 50 µM, 75 µM and 100 µM producing reduction by around 27% ($p = 0.001$), 37% ($p \leq 0.001$) and 30% ($p \leq 0.001$) respectively. In addition, a trend towards reduction was observed following treatment with 25 µM RSV ($p = 0.055$).

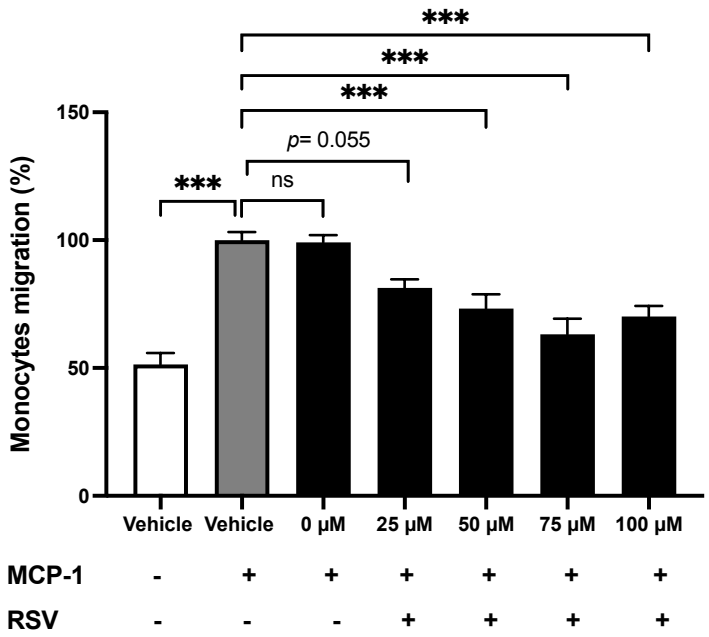

Figure 3.7 RSV significantly inhibits the MCP-1-induced migration of THP-1 monocytes.

THP-1 monocytes were incubated with vehicle alone or MCP-1 (20 ng/ml) with the indicated concentration of resveratrol for 3 hours. The proportion of migrated cells were expressed as a percentage of total input cells and displayed as a percentage of migration relative to the vehicle control which was arbitrarily set to 100%. The graph presents data as the mean ± SEM from four independent experiments. Statistical analysis was performed using one-way ANOVA with Tukey's post-hoc analysis, where *** $p \leq 0.001$. **Abbreviations:** MCP-1, monocyte chemoattractant protein-1; ns, not significant.

3.3.1.4 RSV significantly reduces ROS production in monocytes and macrophages

In this experimental series, the antioxidant effects of RSV on ROS production were evaluated in multiple cell types, including THP-1 monocytes, THP-1 macrophages and HMDMs. In all cases, the ROS production was significantly induced in the presence of TBHP compared to vehicle alone (no TBHP). In THP-1 monocytes, treatment with RSV attenuates ROS production by 20% ($p \leq 0.001$), 22% ($p \leq 0.001$), 23% ($p \leq 0.001$) and 24%($p \leq 0.001$) with concentrations of 25 µM, 50 µM, 75 µM and 100 µM respectively (Figure 3.8A). Similarly, treatment of THP-1 macrophages with RSV resulted in a similar degree of inhibition in ROS production across all concentrations tested showing a reduction by 36% ($p \leq 0.001$), 38% ($p \leq 0.001$), 39% ($p \leq 0.001$) and 40% ($p \leq 0.001$) with 25 µM, 50 µM, 75 µM and 100 µM RSV respectively (Figure 3.8B). These finding were confirmed in HMDMs. Thus, the TBHP-induced ROS production was significantly reduced following treatment with 25 µM, 50 µM, 75 µM and 100 µM RSV by 35% ($p \leq 0.001$), 41% ($p \leq 0.001$), 37% ($p \leq 0.001$) and 40% ($p \leq 0.001$) respectively (Figure 3.8C).

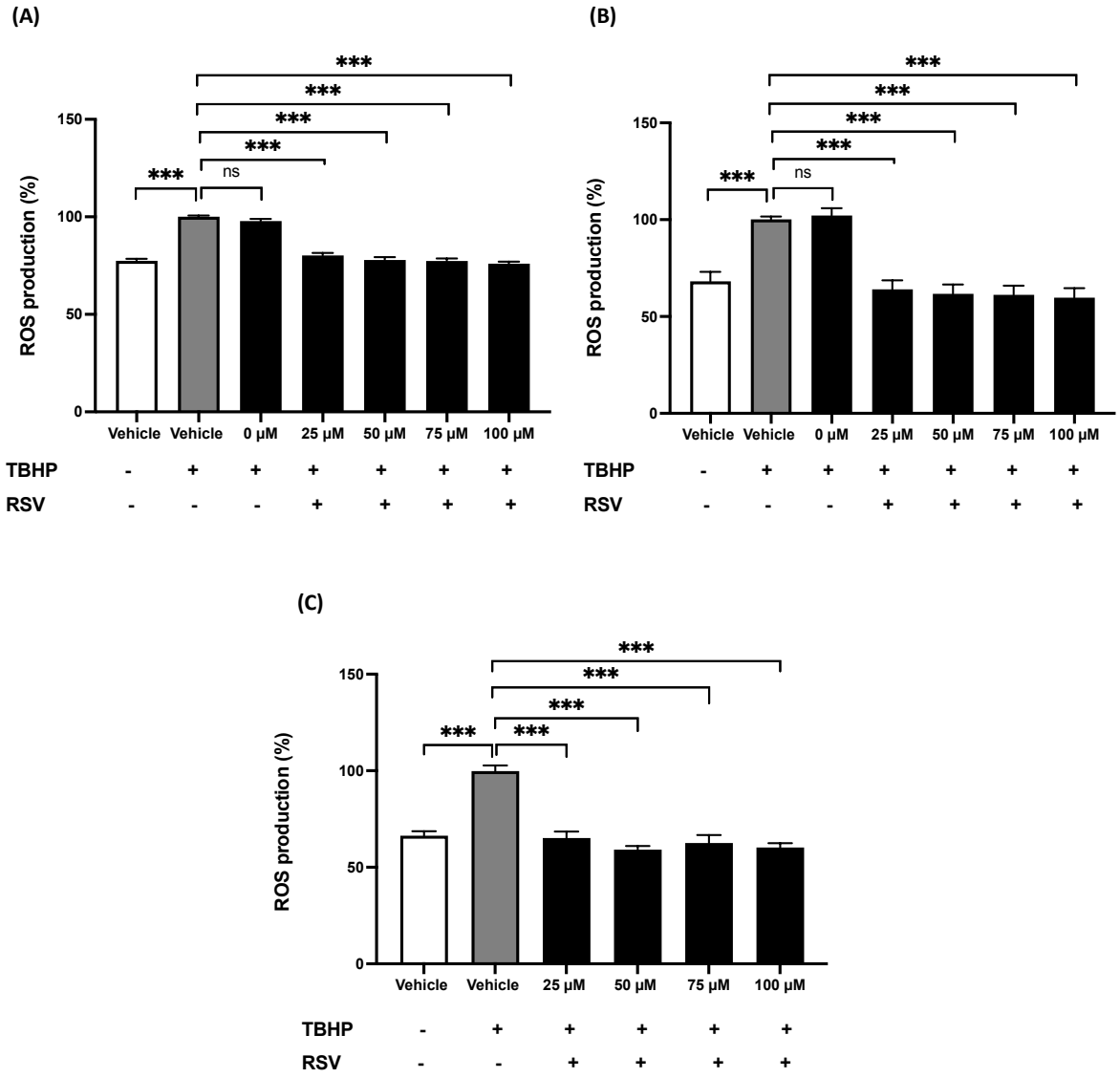

Figure 3.8 Treatment with RSV significantly inhibits the TBHP-induced ROS production in THP-1 monocytes and macrophages as well as HMDMs.

The effect RSV on TBHP-induced ROS production was assessed in human monocytes and macrophages and in a concentration dependent manner using the DCFDA Cellular ROS Detection Assay Kit. THP-1 monocytes (A), THP-1 macrophages (B) and HMDMs (C) were treated with TBHP and either vehicle (control) or RSV. Cells treated with vehicle in the absence of TBHP were also included for comparative purposes (No TBHP control). ROS production is displayed as percentage to the vehicle control which was arbitrarily set to 100%. Data are presented as mean ± SEM from four independent experiments. Statistical analysis was performed using a one-way ANOVA with Tukey's post hoc test for THP-1 monocytes and HMDMs while Dunnett post hoc test was used for THP-1 macrophages where ***$p \leq 0.001$. **Abbreviations:** HMDMs, human monocyte-derived macrophages; TBHP, tert-butyl hydroperoxide; ROS, reactive oxygen species; ns, not significant.

3.3.1.5 Effect of RSV on foam cell formation

3.3.1.5.1 Macropinocytosis was significantly attenuated following treatment with RSV in THP-1 macrophages.

To measure the effect of RSV on macropinocytosis in THP-1 macrophages, LY uptake was evaluated using flow cytometry. Macropinocytosis was significantly decreased following treatment of the cells with 25 µM and 50 µM RSV by 24% ($p \leq 0.001$) and, 46% ($p \leq 0.001$) respectively. The greater effect was obtained following treatment with higher concentrations of RSV (namely 75 µM and 100 µM) by an average of ~60% ($p \leq 0.001$) (Figure 3.9).

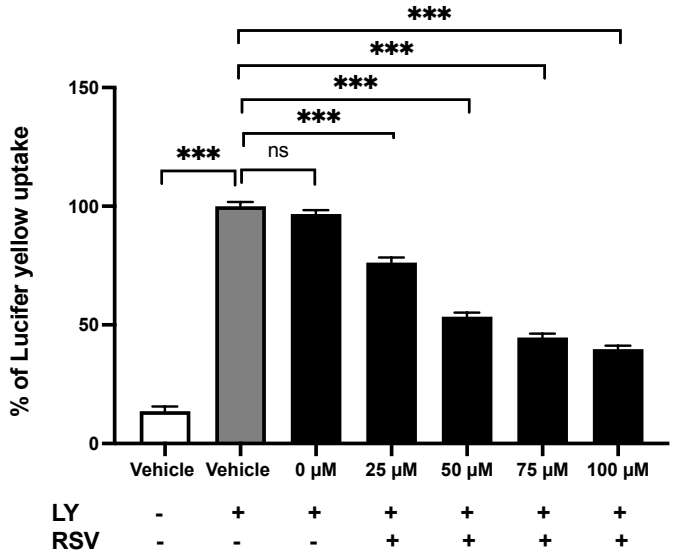

Figure 3.9 RSV inhibits LY uptake by macropinocytosis in THP-1 macrophages.

The effect of RSV on macropinocytosis was determined in THP-1 macrophages that were incubated with the indicated concentration of RSV or the vehicle (Vehicle control) for 24 hours. LY uptake was then measured using a FACS Canto flow cytometer and macropinocytosis was determined as a percentage relative to the vehicle control which was arbitrarily set to 100%. Data are presented as the mean ± SEM from four independent experiments. Statistical analysis was performed using one-way ANOVA followed by Tukey's post-hoc analysis, *** $p \leq 0.001$. **Abbreviations:** Ly, Lucifer yellow; ns, not significant.

3.3.1.5.2 RSV significantly inhibits Dil-oxLDL uptake in THP-1 macrophages

Dil-oxLDL uptake was investigated, as this is another key event in foam cell formation. RSV was found to significantly reduce Dil-oxLDL uptake seen in vehicle-treated THP-1 macrophages across all concentrations tested by around 20% ($p \leq 0.001$) (Figure 3.10).

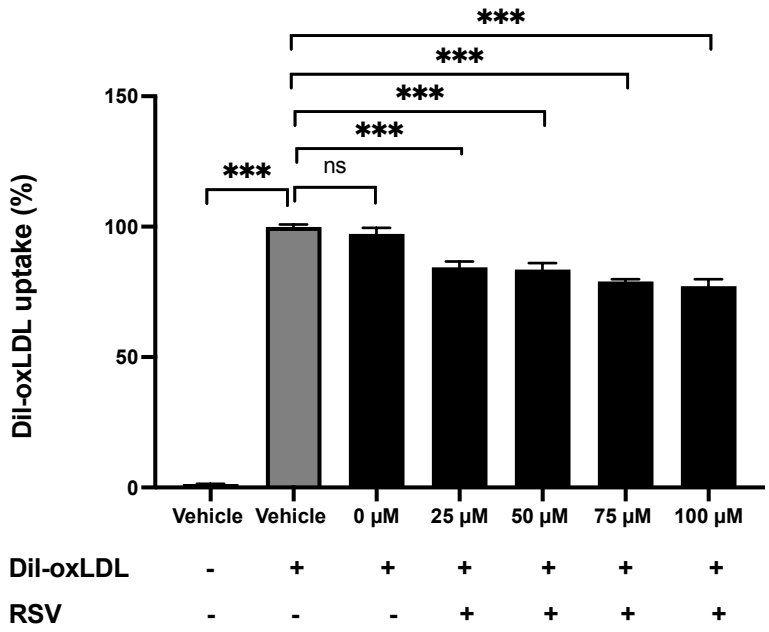

Figure 3.10 RSV significantly attenuates Dil-oxLDL uptake by human macrophages.

THP-1 macrophages were incubated with RSV or vehicle control plus Dil-oxLDL for 24 hours. Negative control without Dil-oxLDL was also included for comparative purposes. Cells were then collected, resuspended in 2% (v/v) PFA and uptake was measured using FACS analysis. Treatment with vehicle in the presence of Dil- oxLDL was used as a positive control and arbitrarily assigned as 100%. Graph indicates the average uptake as the mean ± SEM from four independent experiments. Statistical analysis was performed using one-way ANOVA and Dunnett post hoc, where *** $p \leq 0.001$. **Abbreviations:** ns, not significant.

In light of the results obtained so far, two concentrations of RSV (25 µM and 50 µM) were taken forward for subsequent studies.

3.3.2 Assays were carried out using two concentrations to further delineate the optimal concentration

3.3.2.1 RSV significantly attenuates macrophage mitoROS production

RSV significantly attenuates mitochondrial superoxide production by 16% ($p \leq 0.001$) in THP-1 macrophages treated with 50 µM RSV for 24 hours compared to the vehicle control. However, no significant change was seen with 25 µM RSV treatment (Figure 3.11).

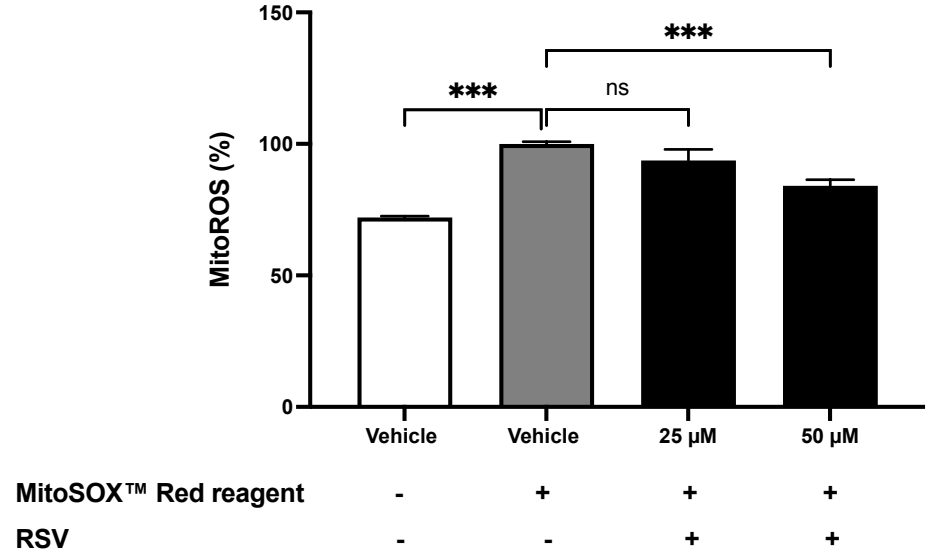

Figure 3.11 Treatment with RSV significantly inhibits mitoROS production in THP-1 macrophages.

The effect of RSV on mitoROS production in THP-1 macrophages was investigated using MitoSOX^{TM} Red staining in which mitochondrial superoxide production was measured in THP-1 macrophages treated with RSV for 24 hours. Data are presented as mean +/- SEM from three independent experiments and displayed as percentage to the vehicle control which was arbitrarily set to 100%. Statistical analysis was performed using a one-way ANOVA and Dunnett post-hot test where *** $p \leq 0.001$. ns, not significant.

3.3.2.2 Treatment with RSV significantly decreased phagocytic activity of THP-1 macrophages

The effect of RSV on phagocytosis activity was assessed in THP-1 macrophages. As shown in Figure 3.12, both RSV concentrations significantly decrease the phagocytic activity in THP-1 macrophages. The 25 μM RSV reduces phagocytosis by 42% (p=0.043) while a greater reduction was seen with 50 μM concentration by 49% (p=0.018).

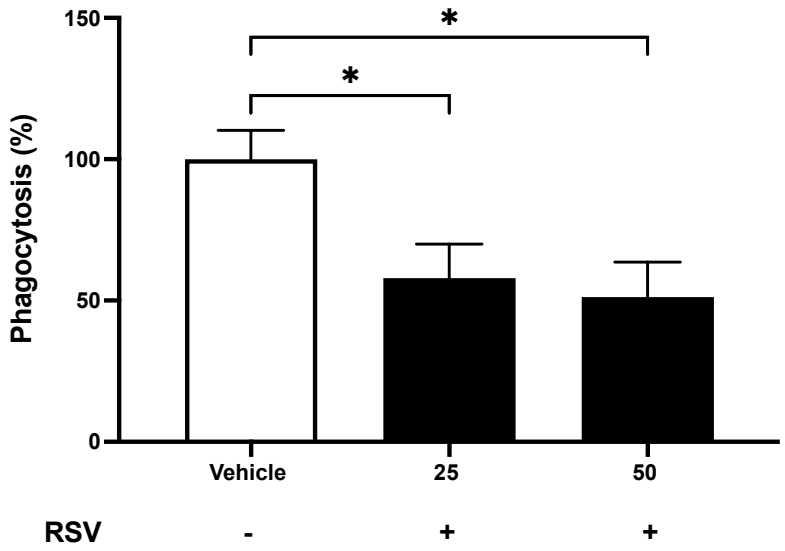

Figure 3.12 RSV significantly inhibits phagocytosis in THP-1 macrophages.

The effect of RSV on macrophage phagocytic activity was assessed using the Vybrant Phagocytosis Assay Kit. Phagocytosis was calculated as a percentage to the vehicle control after background subtraction and presented relative to vehicle which was arbitrarily set to 100%. Data are presented as mean ± SEM from four independent experiments. Statistical analysis was performed using a one-way ANOVA and Tukey's post hoc test where *$p \leq 0.05$.

3.3.2.3 Activation of the NLRP3 inflammasome was significantly attenuated in the presence of RSV

To assess the effect of RSV on NLRP3 inflammasome activation, THP-1 macrophages were treated with either the vehicle or RSV at 25 µM or 50 µM concentration. Data are presented in Figure 3.13 and showed that treatment with 25 µM or 50 µM RSV resulted in a significant attenuation in IL-1β production by 35% ($p \leq 0.001$) and 29% ($p \leq 0.001$) respectively.

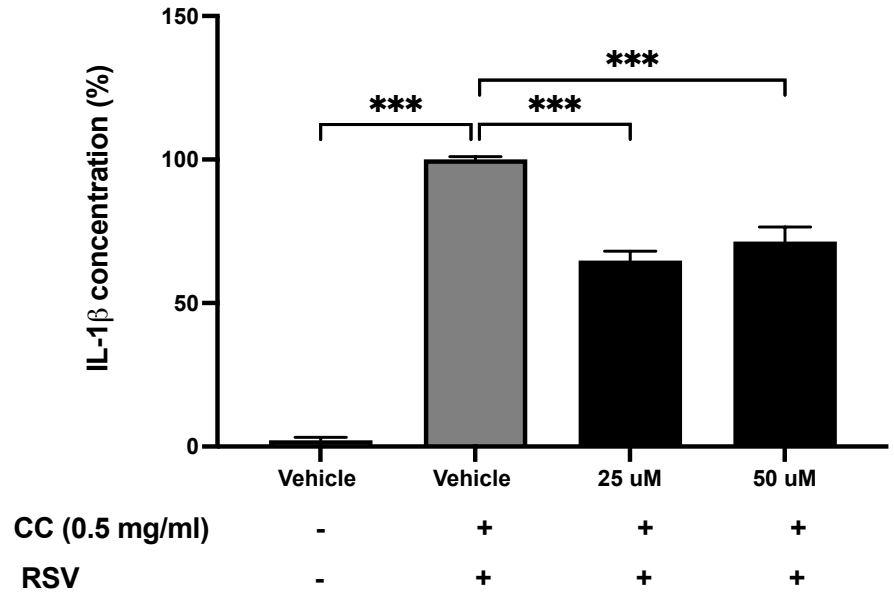

Figure 3.13 Inflammasome activation was significantly attenuated in the presence of RSV.

THP-1 macrophages were stimulated with cholesterol crystals and treated with vehicle or RSV for 24 hours. IL-1β concentration was determined by standard ELISA and expressed as a percentage to the vehicle control that was arbitrarily set to 100%. Data are presented as mean ± SEM from three independent experiments. Statistical analysis was performed using a one-way ANOVA with Dunnett post-hoc test where *** $p \leq 0.001$. **Abbreviations:** IL-1β, interleukin-1β; CC, cholesterol crystal.

3.3.2.4 RSV reduces MMP activity in human macrophages after 3 hours of treatment

The effects of RSV on MMP activity in THP-1 macrophages were investigated at both 3 and 24 hours to determine both short-term and long-term actions. As shown in Figure 3.14A, the MMP activity of THP-1 macrophages was reduced by 21% (p=0.004) after 3 hours of treatment with 50 µM RSV while no effect was seen after 24 hours when compared to the vehicle control cells (Figure 3.14B). No significant changes were observed after treatment of cells with 25 µM RSV either in short- or long-term investigation.

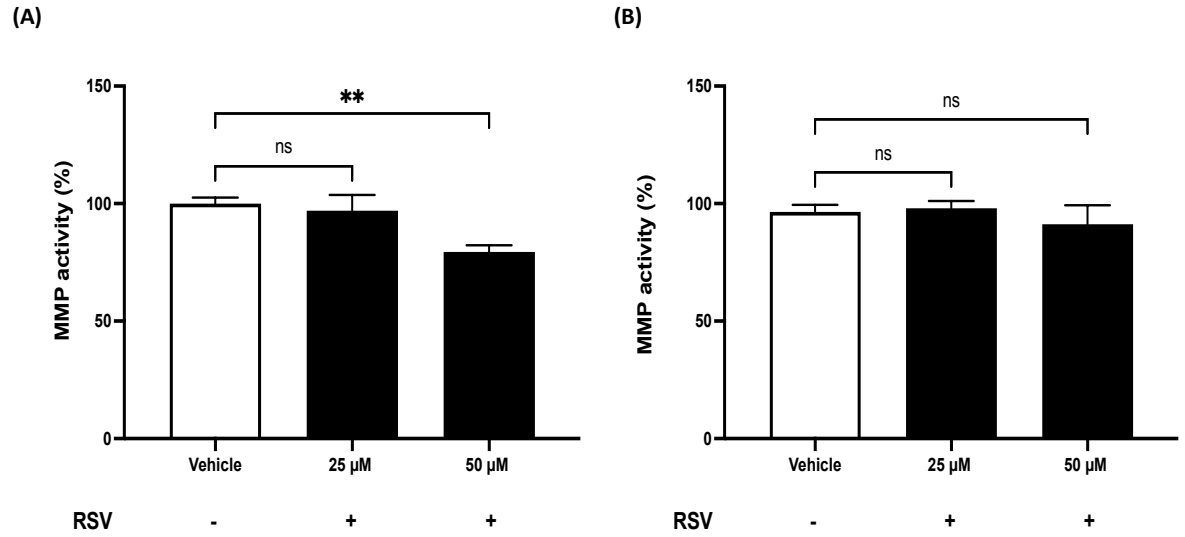

Figure 3.14 RSV inhibits MMP activity in human macrophages after 3 hours.

THP-1 macrophages were treated with either the vehicle or RSV for either 3 or 24 hours to evaluate MMP activity. MMP activity was determined as a percentage to the vehicle control which was set to 100%. The data are presented as a mean ± SEM from five independent experiments and statistical analysis was performed using one-way ANOVA with Dunnett post-hoc test where ** $p \leq 0.01$. **Abbreviations:** MMP, matrix metalloproteinase; ns, not significant.

On the basis of studies detailed above, 50 µM RSV was found to impact most of the responses studied and was hence used for all subsequent studies.

3.3.3 Assays carried out using 50 µM concentration, the optimal concentration, using different cell model systems

3.3.3.1 RSV has no detrimental effects on cell viability of the cell types used for further *in vitro* studies

In addition to THP-1 macrophages and HMDMs, cell viability was assessed in other cell culture model system utilised in this study, HASMCs and HAECs. As some experiments on HASMCs were required more than 24 hours, the viability for HASMCs was also assessed over a 8-day period. No significant effects on cell viability were observed following treatment of the cells with RSV when compared to the vehicle in both HASMCs and HAECs (Figure 3.15 and 3.16 respectively).

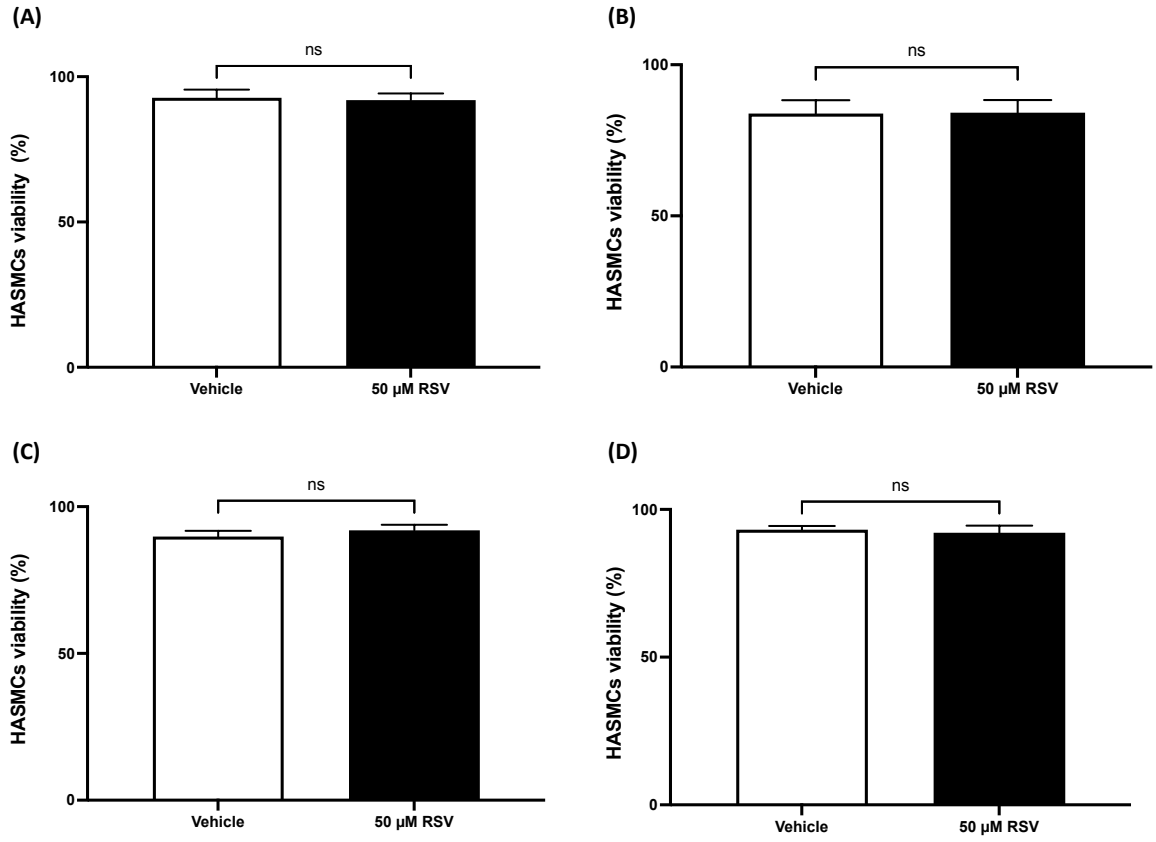

(E)

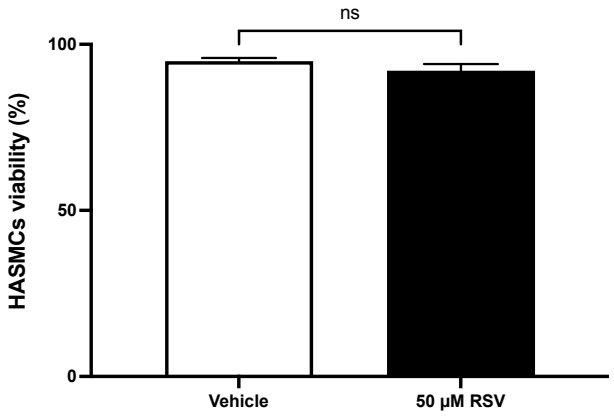

Figure 3.15 RSV has no detrimental effects on cell viability of HASMCs over a 8-day period.

HASMCs were treated with the vehicle control or 50 µM RSV for (A) 0 hour, (B) 24 hours, (C) 2 days, (D) 4 days and (E) 8 days. Cell viability was then assessed for each time point using the LDH assay kit. The results are presented as mean ± SEM relative to the vehicle control, which was set to 100% from three independent experiments. Statistical analysis was performed using an unpaired Student's t-test (A; B; C; D) or Mann Whitney U test (E). **Abbreviations:** HASMCs, human aortic smooth muscle cell; ns, not significant.

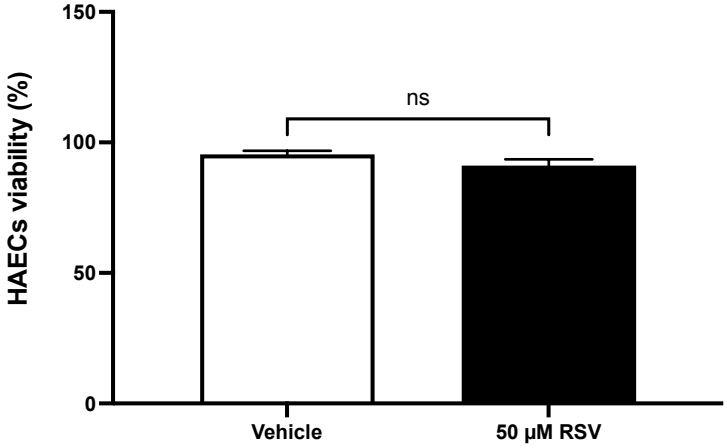

Figure 3.16 RSV has no detrimental effects on cell viability of HAECs after 24 hours.

HAECs were treated with the vehicle control or 50 µM RSV for 24 hours, LDH assay kit was then used to assess cell viability. Data were normalised to the vehicle control that has been arbitrarily assigned as 100%. Data are presented as mean ± SEM. Statistical analysis was performed using an unpaired Student's t-test was used for HAECs. **Abbreviations:** HAECs, human aortic endothelial cells; ns, not significant.

3.3.3.2 RSV has varying impacts on cell proliferation depending on the cell types being used for *in vitro* studies

Along with cell viability, proliferation of HASMCs and HAECs was assessed. Figure 3.17 shows that there were no significant changes in HASMCs proliferation at days 0, 1 and 4. However, proliferation was increased significantly at days 2 and 8 after RSV treatment by 14% (p=0.017) and 34% (p=0.002) respectively. To confirm these findings, BrdU Labeling and Detection Kit III was used for monitoring proliferation rate of HASMCs. Figure 3.18 shows the fold change in cell proliferation over 8-day period, where treatment of cells with RSV resulted in 8% (p=0.034) increase in cell proliferation at day 8. On the other hand, the proliferation of HAECs was not affected by RSV after 24 hours (Figure 3.19).

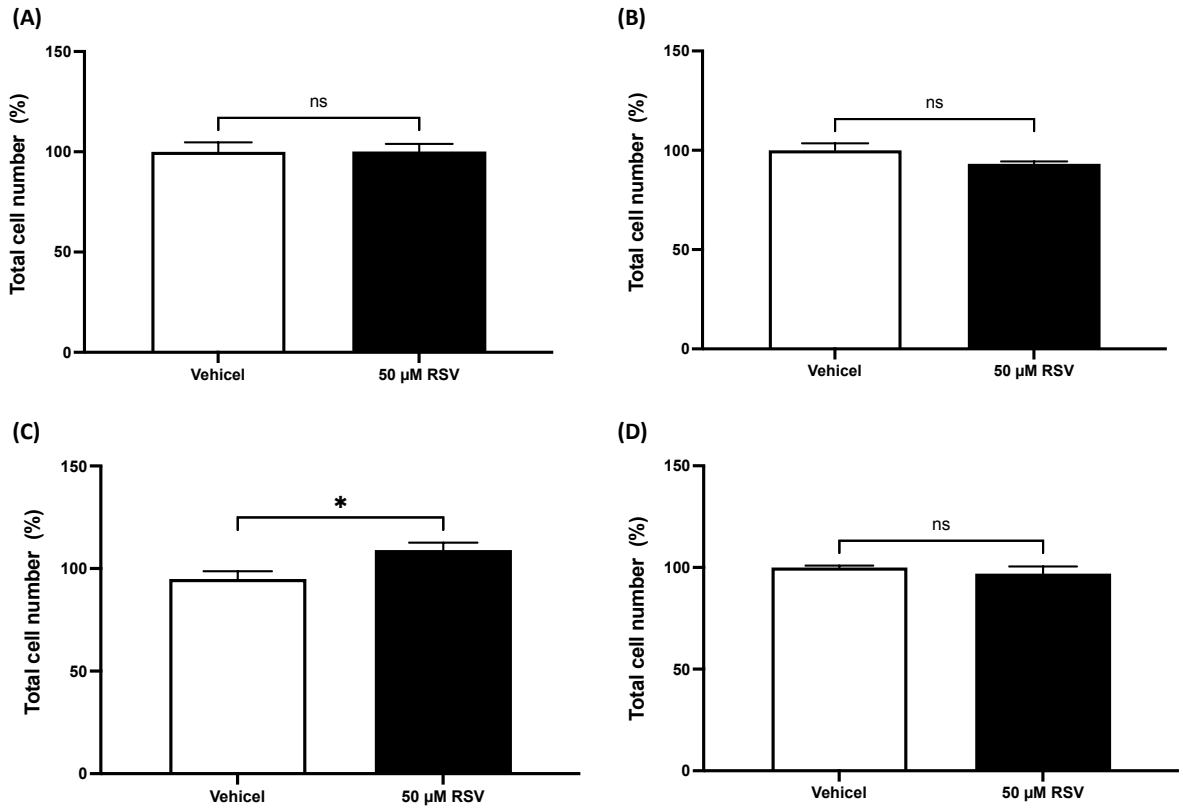

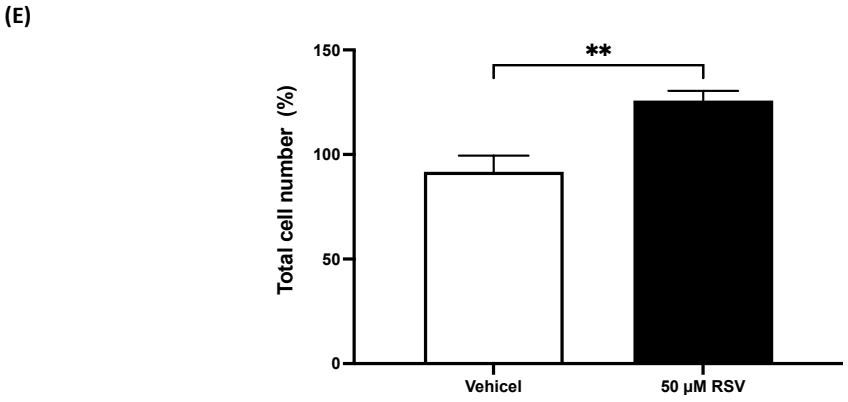

Figure 3.17 Proliferation of HASMCs was increased significantly after RSV treatment at days 2 and 8.

HASMCs were treated with the vehicle control or 50 µM RSV for (A) 0 hour, (B) 24 hours, (C) 2 days, (D) 4 days and (E) 8 days. Cell Proliferation was then assessed for each time point using CV staining. The results are presented as mean ± SEM relative to the vehicle control, which was set to 100% from three independent experiments. Statistical analysis was performed using an unpaired Student's t-test (A; C; D; E) or Mann Whitney U test (B) where * $p \leq 0.05$ and ** $p \leq 0.01$. Abbreviations: HASMCs, human aortic smooth muscle cell; ns, not significant.

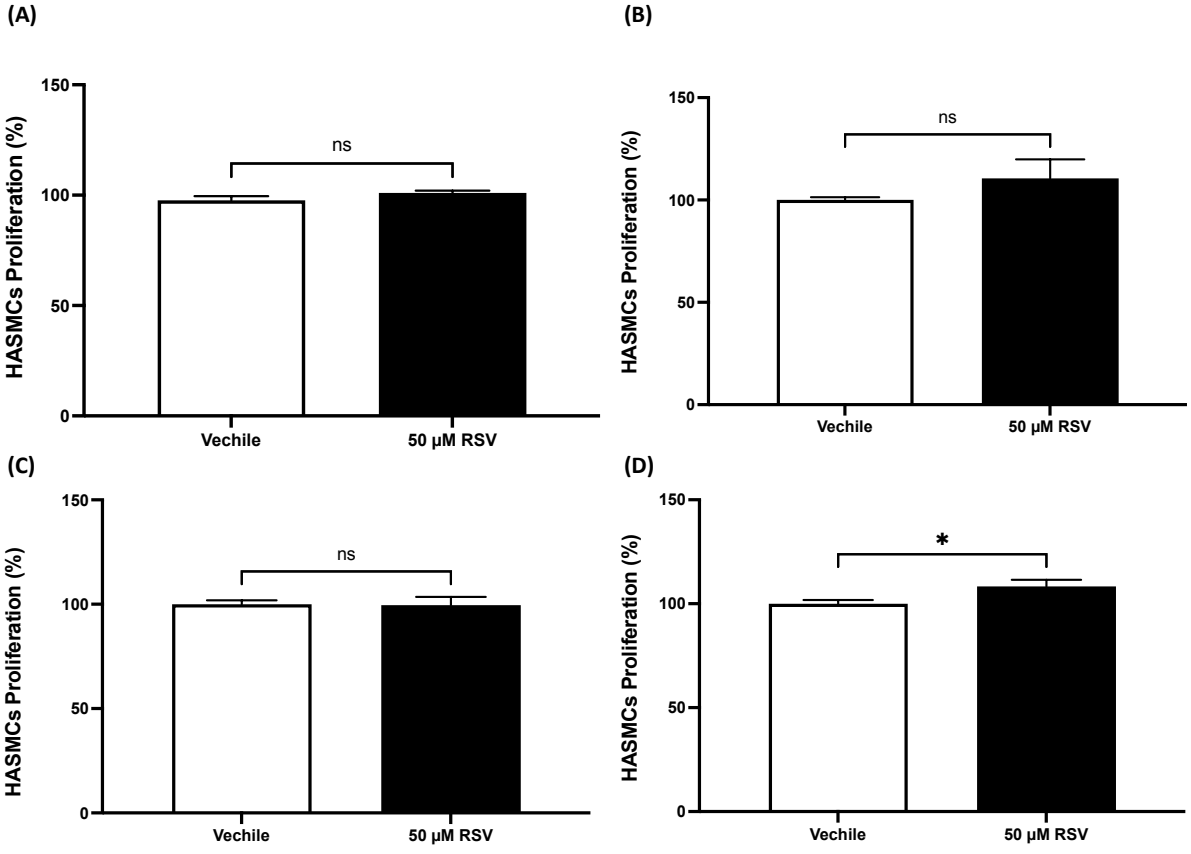

Figure 3.18 RSV enhances HASMCs proliferation rate at day 8.

HASMCs were treated with the vehicle control or 50 µM RSV for (A) 0 hour, (B) 2 days, (C) 4 days and (D) 8 days. Cell Proliferation was then assessed for each time point using the BrdU Labeling and Detection Kit, where results are presented as percentage relative to the vehicle control, which was set to 100%. Data are presented as mean ± SEM from three independent experiments. Statistical analysis was performed using an unpaired Student's t-test where * $p \leq 0.05$. **Abbreviations:** HASMCs, human aortic smooth muscle cells; ns, not significant.

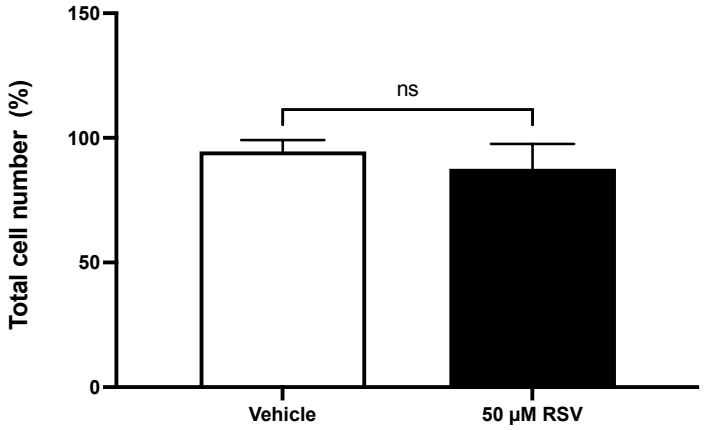

Figure 3.19 RSV has no detrimental effects on cell proliferation after 24 hours.

HAECs were treated with vehicle control or 50 µM RSV for 24 hours, CV staining of adherent cells was then used to assess cell proliferation. Data were normalised to the vehicle control that was arbitrarily assigned as 100%. Data are presented as mean ± SEM from three independent experiments. Statistical analysis was performed using an unpaired Student's t-test. **Abbreviations:** HAECs, human aortic endothelial cells; ns, not significant.

3.3.3.3 RSV significantly attenuates PDGF-induced invasion of HASMCs

The assessment of quiescent HASMCs migration towards PDGF showed that this growth factor induced the migration of HASMCs by 85% ($p \leq 0.001$). However, RSV significantly attenuated this by 36% ($p \leq 0.001$) (Figure 3.20).

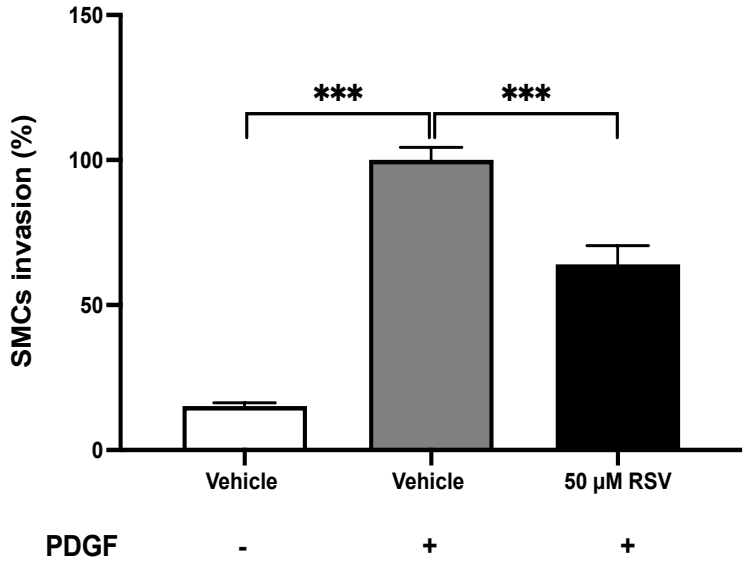

Figure 3.20 Invasion of HASMCs was significantly attenuated in the presence of RSV.

The effect of RSV on the invasion of SMCs was assessed using HASMCs incubated with PDGF-BB and either the vehicle control (Vehicle) or RSV. Cells incubated with the vehicle in the absence of PDGF-BB (No PDGF) were included for comparative purposes. The number of migrated cells were counted and averaged per five HPF and presented as a percentage to the vehicle control which was arbitrarily set to 100%. Data are presented as mean ± SEM from three independent experiments. Statistical analysis was performed using a one-way ANOVA with Dunnett post-hotc test where *** $p \leq 0.001$. **Abbreviations:** PDGF, platelet-derived growth factor; SMCs, smooth muscle cells; ns, not significant.

3.3.3.4 RSV significantly reduces ROS production in various cell types.

The ROS assay was performed with 50 µM RSV in HASMCs and HAECs. In both cases, the ROS production was significantly induced in the presence of TBHP compared to the vehicle alone (no TBHP). However, treatment of HASMCs and HAECs with 50 µM RSV attenuates TBHP-induced ROS production by 62% ($p \leq 0.001$) and 84% ($p \leq 0.001$) respectively (Figure 3.21A and B).

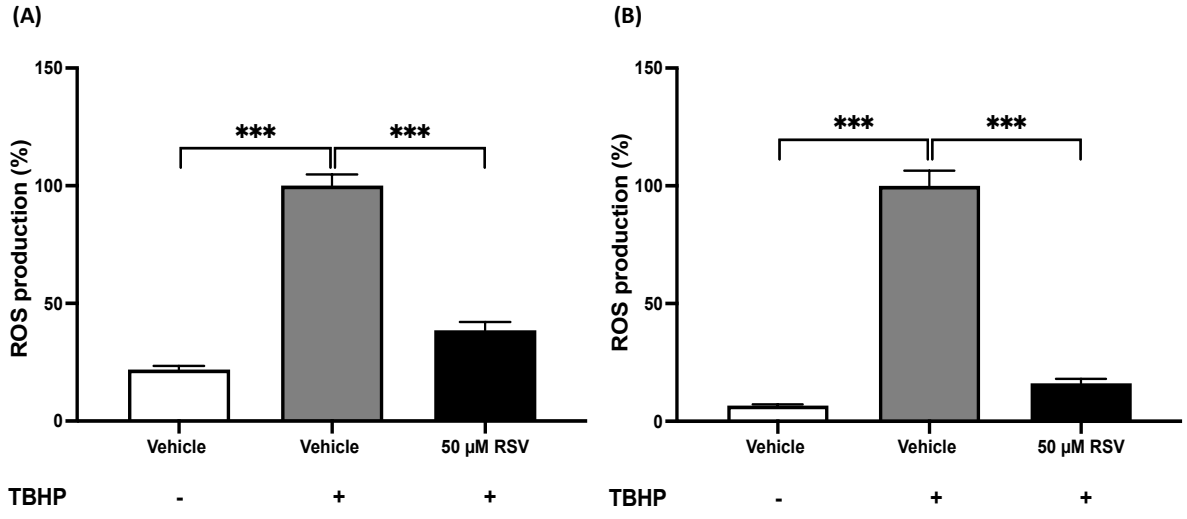

Figure 3.21 Treatment with RSV significantly inhibits the TBHP-induced ROS production in HASMCs and HAECs.

The effect RSV on TBHP-induced ROS production was assessed using the DCFDA Cellular ROS Detection Assay Kit. HASMCs (A) and HAECs (B) were treated with TBHP and either vehicle (control) or 50 µM RSV. Cells treated with vehicle in the absence of TBHP were included for comparative purposes (No TBHP control). ROS production is displayed as a percentage to the vehicle control which was arbitrarily set to 100%. Data are presented as mean ± SEM from three independent experiments. Statistical analysis was performed using a one-way ANOVA and Dunnett post-hot test where *** $p \leq 0.001$. **Abbreviations:** HASMCs, human aortic smooth muscle cell; HAECs, human aortic endothelial cells; TBHP, tert-butyl hydroperoxide; ROS, reactive oxygen species.

3.3.3.5 Effect of 50 µM RSV on foam cell formation

3.3.3.5.1 RSV significantly enhances the efflux of cholesterol from THP-1 macrophage foam cells

In addition to macropinocytosis and Dil-oxLDL uptake, cholesterol efflux was measured in THP-1 macrophages for better understanding of the mechanism of action of RSV in reducing foam cells formation. As shown in Figure 3.22, cells treated with vehicle plus LXR agonist plus ApoA1 showed an increase in cholesterol efflux compared to the vehicle by 14% (not statistically significant). However, treatment with 50 µM RSV plus LXR agonist plus ApoA1 significantly increased cholesterol efflux by 29% (p=0.045).

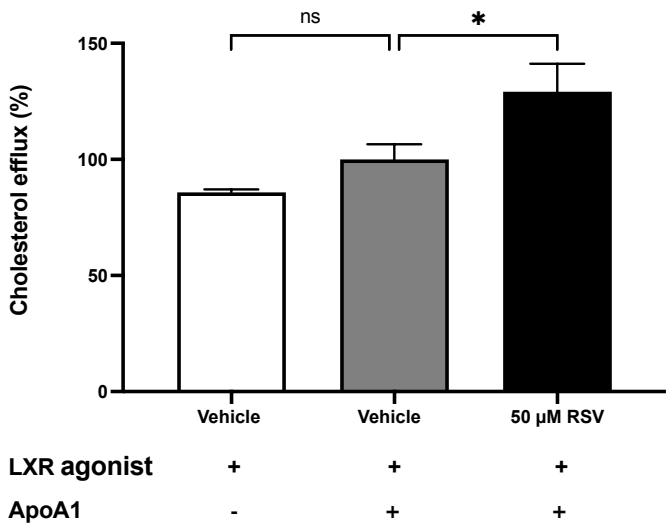

Figure 3.22 RSV significantly enhances the efflux of cholesterol from THP-1 macrophage foam cells.

THP-1 macrophages were labelled with labelling medium followed by incubating with equilibration buffer and ac-LDL (25 µg/ml) for 24 hours. Cells were then incubated with ApoA1 plus LXR agonist and either vehicle control (Vehicle) or 50 µM RSV. Cells treated with vehicle and LXR agonist in the absence of ApoA1 were included for comparative purposes (No ApoA1). Cholesterol efflux was calculated as a percentage relative to the vehicle control which was arbitrarily set to 100%. Data are presented as mean ± SEM from three independent experiments. Statistical analysis was performed using a one-way ANOVA and Dunnett post-hoc test where *$p \leq 0.05$. **Abbreviations:** LXR agonist, liver X receptor agonist; ApoA-1, apolipoprotein A-1; ns, not significant.

3.3.3.5.2 Macropinocytosis was significantly attenuated following treatment with RSV in human macrophages and HASMCs

The ability of RSV to attenuate macropinocytosis was measured in HMDMs and HASMCs. Treatment with 50 µM RSV resulted in a significant reduction by 40% (p=0.010) and 46% ($p \leq 0.001$) in both of HMDMs and HASMCs respectively (Figure 3.23A and B).

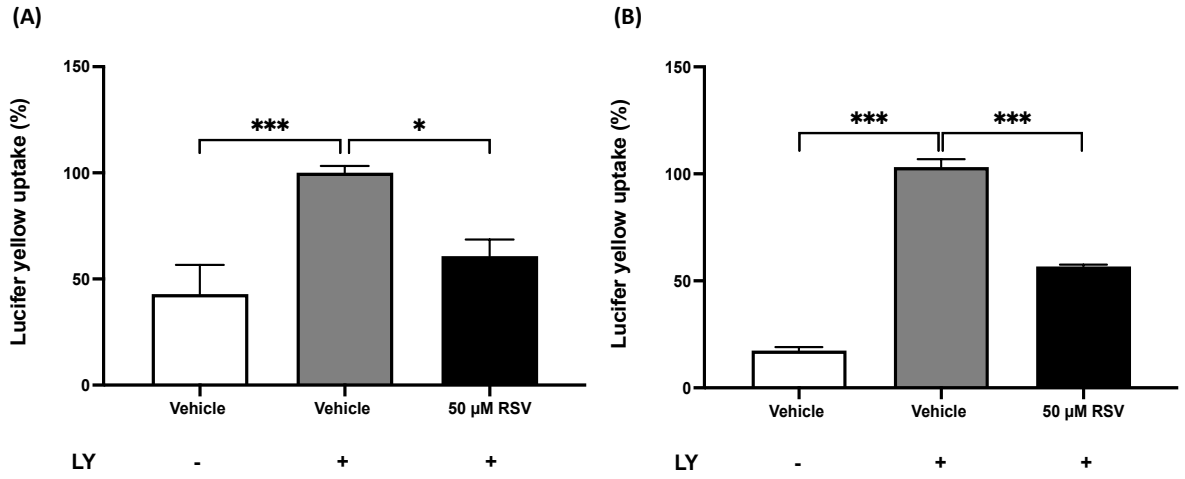

Figure 3.23 RSV inhibits LY uptake by macropinocytosis in human macrophages and HASMCs.

The effect of RSV on macropinocytosis was determined in HMDMs (A) and HASMCs (B) that were incubated with 50 µM RSV or the vehicle (Vehicle control) for 24 hours. LY uptake was then measured using a flow cytometer and macropinocytosis was determined as a percentage to the vehicle control which was arbitrarily set to 100%. Data are presented as the mean ± SEM from four independent experiments. Statistical analysis was performed using one-way ANOVA and Dunnett post hoc, where * $p \leq 0.05$ and *** $p \leq 0.001$. **Abbreviations:** Ly, Lucifer yellow; HASMCs, human aortic smooth muscle cell; HMDMs, human monocyte-derived macrophages.

3.3.3.5.3 RSV significantly inhibits Dil-oxLDL uptake in human macrophages and HASMCs.

In addition to THP-1 macrophages (Figure 3.10), the experiment was repeated in HMDMs and HASMCs. The results show that in the presence of 50 µM RSV, the uptake of Dil-oxLDL was significantly attenuated in HMDMs and HASMCs by 34% ($p \leq 0.001$) and 73% ($p \leq 0.001$) respectively (Figure 3.24A and B).

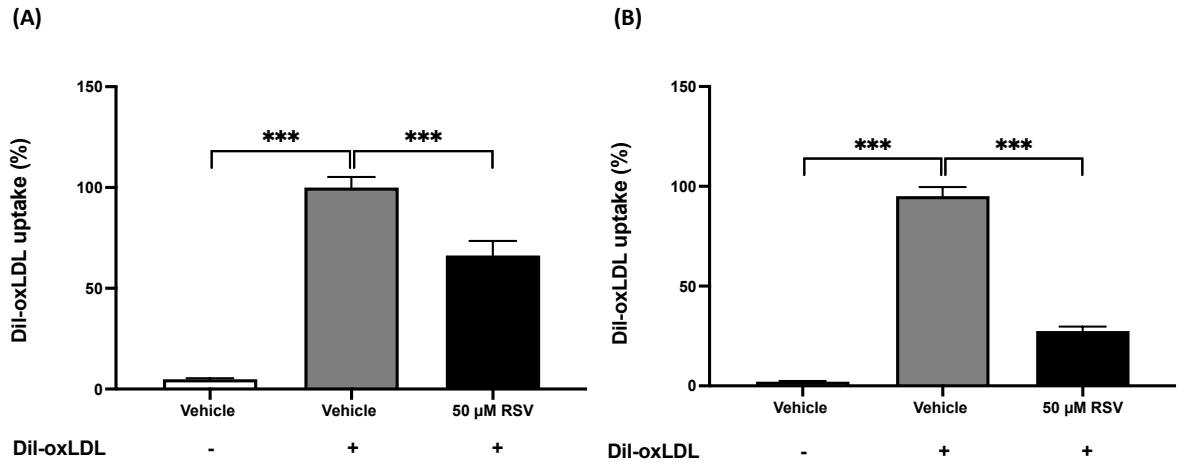

Figure 3.24 RSV significantly attenuates Dil-oxLDL uptake by human macrophages and HASMCs

HMDMs (A) and HASMCs (B) were incubated with RSV or the vehicle control (0.1%DMSO) plus Dil-oxLDL for 24 hours in independent experiments. Negative control without Dil-oxLDL was also included for comparative purposes. Cells were then collected, resuspended in 2% (v/v) PFA and uptake was measured using FACS analysis. Vehicle in the presence of Dil-oxLDL was used as a positive control and arbitrarily assigned as 100%. Graph indicates the average uptake as the mean ± SEM from four (A) or three (B) independent experiments. Statistical analysis was performed using one-way ANOVA and Dunnett post hoc, where *** $p \leq 0.001$. **Abbreviations:** HASMCs, human aortic smooth muscle cell; HMDMs, human monocyte-derived macrophages.

3.3.3.5.4 Treatment with RSV significantly enhances cholesterol metabolism in RAW264.7 macrophages.

All extracted lipid fractions, total polar lipids (TPL), triglycerides (TG), free cholesterol (FC) and cholesterol esters (CE), were measured using a liquid scintillation counter in order to measure the incorporation of [^{14}C] acetate into individual fractions and calculated as a percentage of total lipids. Results are shown in Figure 3.25. Treatment with 50 µM RSV resulted in an increase in the synthesis of TPL by around 21% ($p \leq 0.001$). On the other hand, the total cellular content of TG was significantly reduced in the presence of RSV by about 31% ($p = 0.018$). In addition, treatment with RSV resulted in a significant decrease in CE and in ratio of CE/FC by around 52% and 63% ($p \leq 0.001$) respectively, compared to the vehicle control. There was no significant change in FC fraction following RSV treatment.

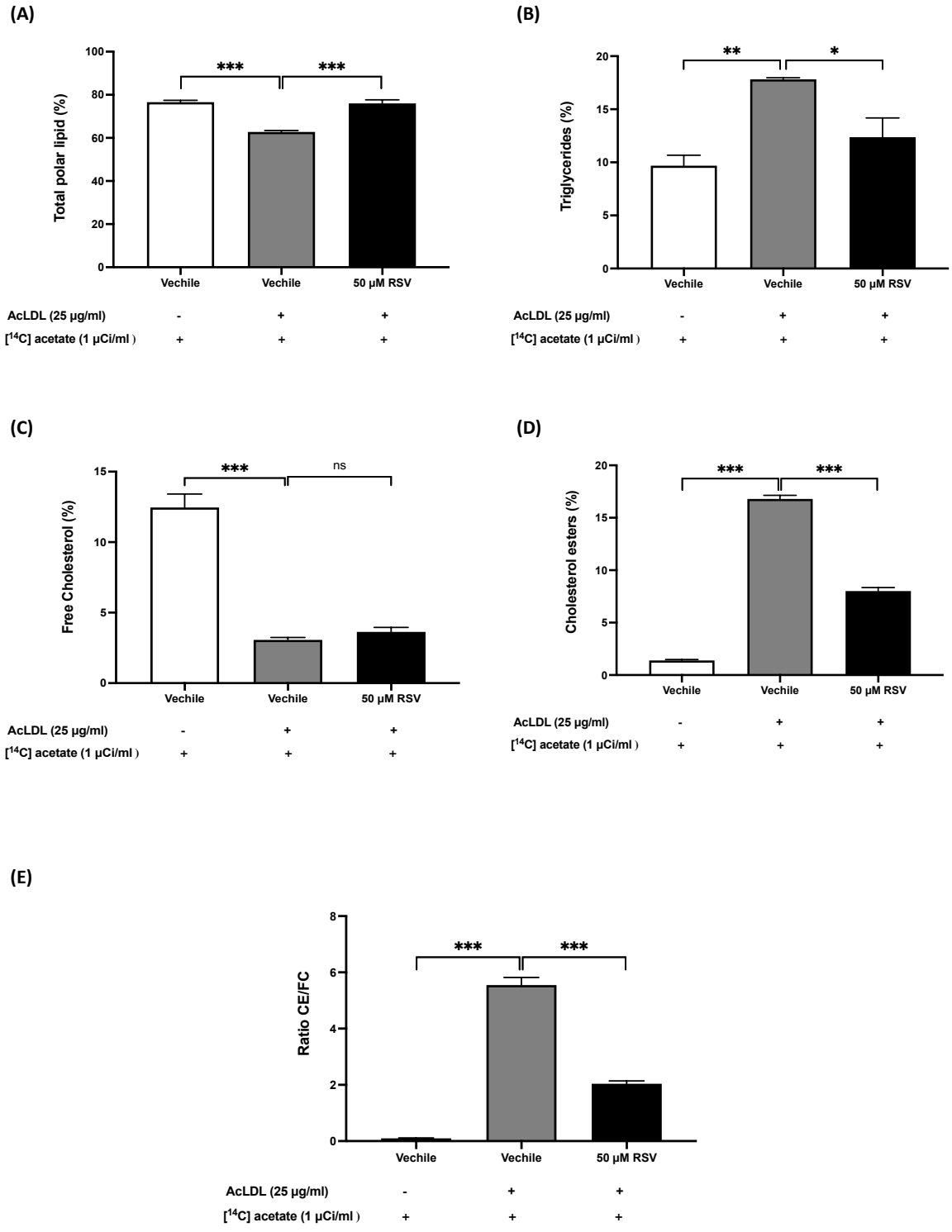

Figure 3.25 RSV treatment reduces lipid accumulation within RAW264.7 macrophages.

RAW264.7 macrophages were loaded with [^{14}C] acetate in the presence or absence of acLDL. Cells were treated either with vehicle (negative control), vehicle and acLDL (vehicle control) or RSV and acLDL. Lipid classes were separated by TLC and the incorporation of [^{14}C] acetate measured by using a scintillation counter. Graph presents the data as a percentage of the total lipids extracted from three independent experiments. Statistical analysis was performed using one-way ANOVA followed by Tukey's post hoc test for TPL (A) or Dunnett post hoc test for TG (B), FE(C), CE (D) and CE/FC (E) where* $p \leq 0.05$, ** $p \leq 0.01$ and *** $p \leq 0.001$. **Abbreviations:** AcLDL, acetylated low density lipoprotein; CE, cholesterol ester; FC, free cholesterol, ns, not significant.

3.3.3.6 Macrophage scavenger receptors were affected following treatment with RSV

The effect of RSV on key genes involved in modified LDL uptake, particularly SR-A and CD36 were investigated in THP-1 macrophages at the mRNA level using real-time qPCR. As shown in Figure 3.26, the expression of SR-A and CD36 was significantly upregulated in the presence of RSV by about 22% ($p \leq 0.001$) and about 174% ($p \leq 0.001$) compared to the vehicle control respectively.

In addition, changes in cell-surface expression of macrophage scavenger receptors SR-A and CD36 were also determined. Furthermore, LDLR was also included as it is involved in native LDL uptake. In contrast to mRNA expression, the surface expression of SR-A was significantly reduced in the presence of RSV by 31% ($p \leq 0.001$). On the other hand, the surface expression of both CD36 and LDLR was significantly increased after treatment with RSV by about 97% times and 47% compared to the vehicle ($p \leq 0.001$) (Figure 3.27).

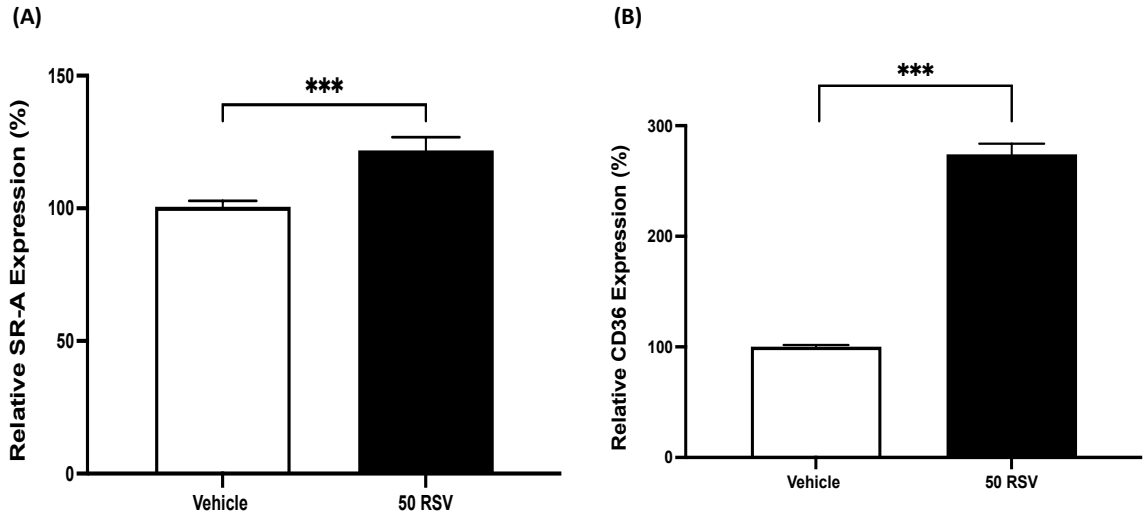

Figure 3.26 RSV significantly stimulates SR-A and CD36 mRNA expression.

THP-1 macrophages were incubated with 50 µM RSV or vehicle for 24 hours prior to RNA extraction. RNA was then subjected to reverse transcription and qPCR with primers specific for SR-A, CD36 or GAPDH control. Data are presented as mean ± SEM. Graphs display the effect of RSV on the average expression of scavenger receptors SR-A (A) and CD36 (B) as percentage compared to the vehicle control (arbitrarily assigned as 100%) from five independent experiments. Statistical analysis was performed using an unpaired student's t-test where *** $p \leq 0.001$. **Abbreviations:** SR-A, scavenger receptor-A; CD36, cluster of differentiation 36.

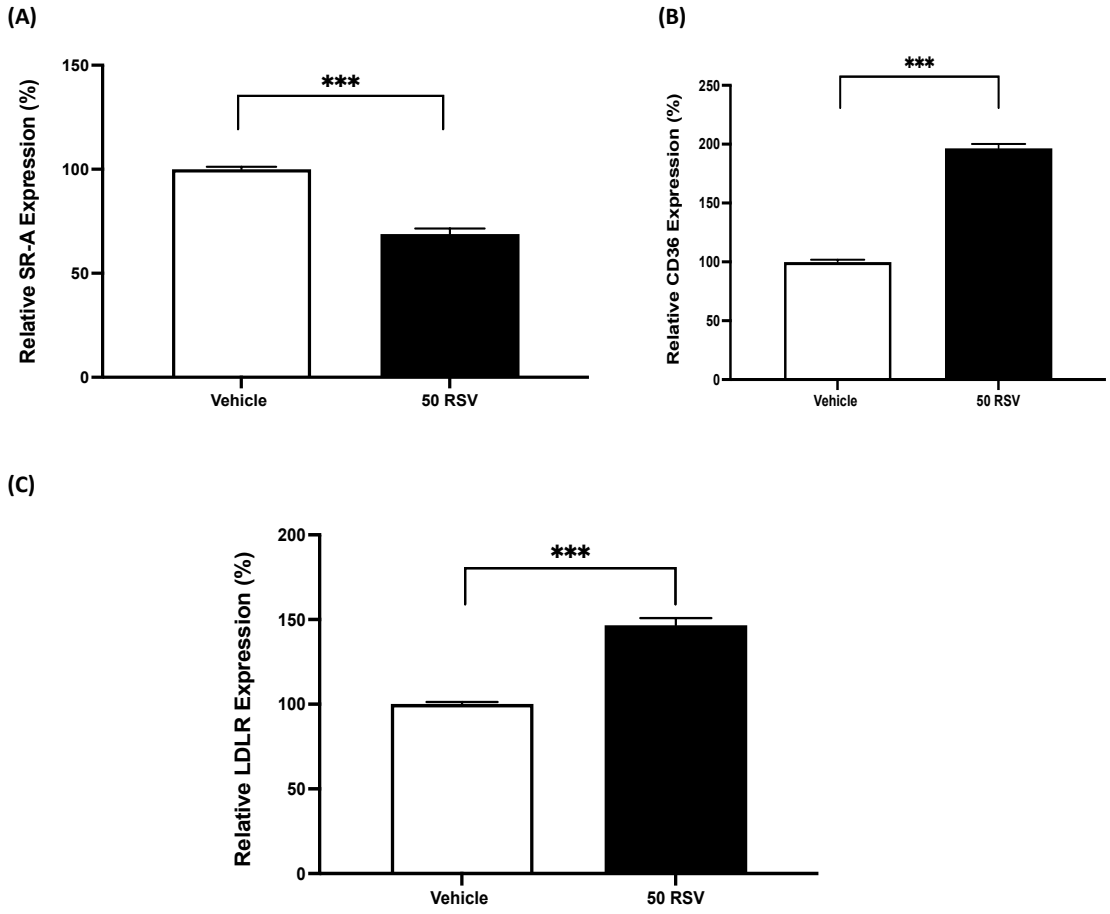

Figure 3.27 The effect of resveratrol on the cell surface expression of SR-A and CD36

The cell surface expression of SR-A and CD36 were determined using flow cytometry after treatment of THP-1 macrophages with either the vehicle control or 50 µM RSV for 24 hours. Data are presented as the mean ± SEM from three independent experiments and displayed as a percentage to the vehicle control which was arbitrarily set to 100%. Statistical analysis was performed using an unpaired Student's t-test (A and C) or Mann-Whitney test (B) where *** p ≤00.001. **Abbreviations:** SR-A, scavenger receptor-A; CD36, cluster of differentiation 36; LDLR, low density lipoprotein receptor.

3.3.3.7 Pro-inflammatory gene expression in cytokine stimulated human macrophages and HAECs was significantly changed after RSV treatment

The effect of RSV treatment on pro-inflammatory gene expression was assessed in THP-1 macrophage and HAECs stimulated with IFN-γ (250 U/mL) and TNF-α (50 ng/ml) respectively. The concentration of both cytokines was based on published literature as well as previous optimisation experiments in the host laboratory (Moss 2018; Gallagher et al. 2019; O'Morain 2019; Chan 2021).

The data in Figure 3.28A and B show that stimulation of macrophages with IFN-γ resulted in a significant increase in the expression of MCP-1 and ICAM-1 by 98% ($p \leq 0.001$) and about 73% ($p \leq 0.001$) compared to vehicle alone respectively. Treatment of IFN-γ-stimulated macrophages with RSV resulted in a significant reduction in MCP-1 expression by about 56% ($p \leq 0.001$) while the no significant change was observed in ICAM-1 expression.

For HAECs, following stimulation with TNF-α, both the MCP-1 and ICAM-1 expression was increased by 98.5% ($p \leq 0.001$) compared to vehicle alone. In the presence of RSV, the TNF-α-induced expression of MCP-1 was significantly attenuated by about 32% ($p = 0.007$) whereas a significant upregulation was observed in ICAM-1 expression by 87.7% ($p \leq 0.001$) (Figure 3.28C and D).

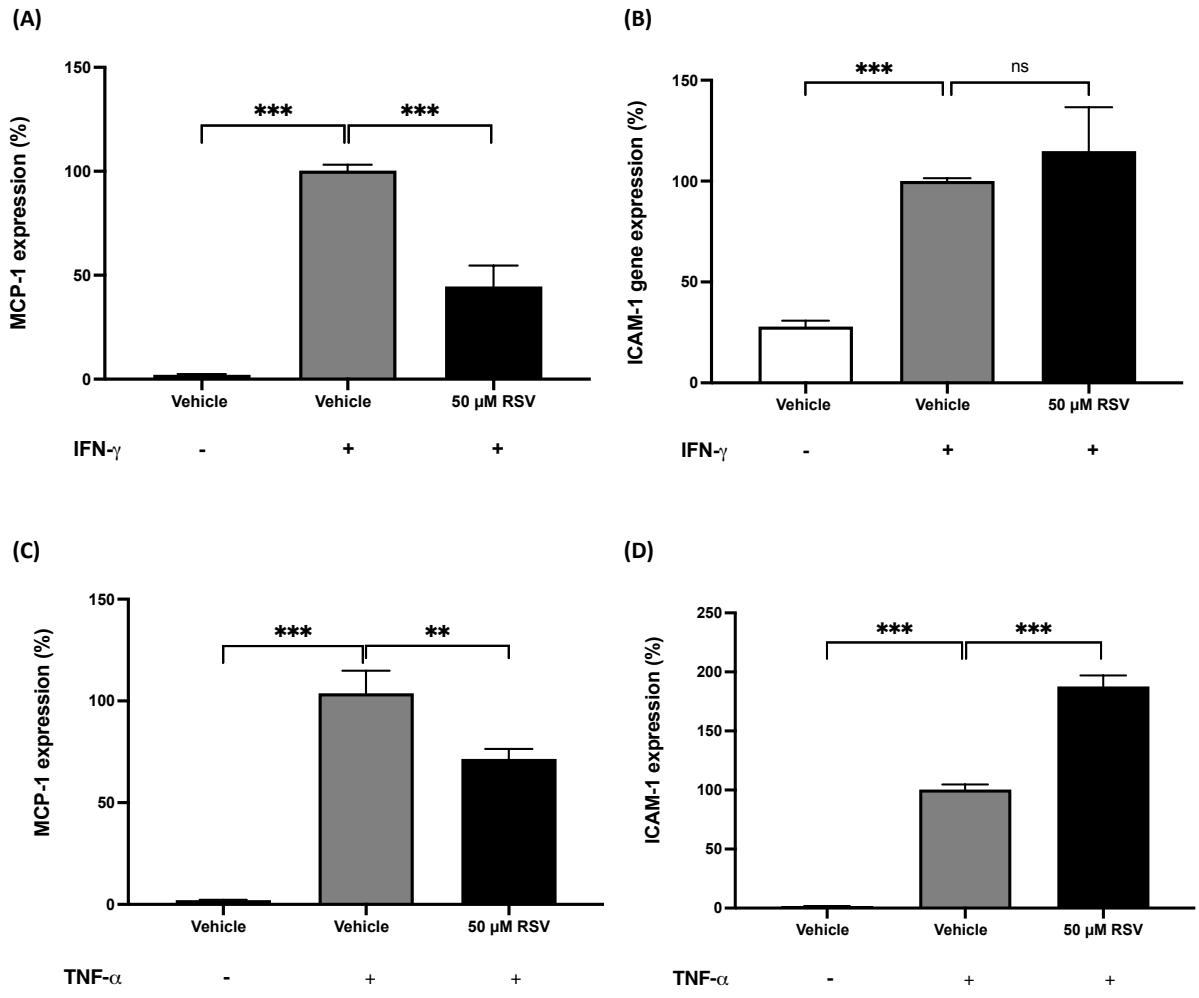

Figure 3.28 Pro-inflammatory gene expression in cytokine stimulated human macrophages and HAECs was significantly affected by RSV treatment

The expression of MCP-1 and ICAM-1 was assessed in IFN-γ-stimulated THP-1 macrophages (A and B) and TNF-α-stimulated HAECs (C and D) that were either treated with vehicle (vehicle control) or 50 µM RSV for 24 hours. For comparative purposes, unstimulated cells with vehicle only were included. Gene expression levels were determined by qPCR using a comparative ΔΔCT method and normalised to the housekeeping gene (GAPDH) with values from cells treated with vehicle (positive control) arbitrary assigned as 100%. Statistical analysis was performed using a one-way ANOVA with Dunnett post-hoc test from three (C and D) and five (A and B) independent experiments where ** $p \leq 0.01$ and *** $p \leq 0.001$. **Abbreviations:** IFN-γ, interferon-γ; TNF-α, tumour necrosis factor-α; MCP-1, monocyte chemoattractant protein-1; ICAM-1, intercellular adhesion molecule-1; ns, not significant.

3.4 Discussion

Despite the increase in published studies on the anti-atherogenic properties of RSV, its effects on the full range of atherosclerotic processes in key cell types implicated in the disease such as, monocytes/macrophages, ECs and SMCs *in vitro,* are not fully understood, and thus form the aim of studies in this chapter. Although multiple studies on RSV have validated its safety profile, the effects of RSV on cell viability and proliferation were verified prior to start of any further assays to ensure that any findings observed were due to RSV rather than altered cell viability. Furthermore, the initial experiments were performed in dose response manner to determine the lowest optimum dose of RSV. Following on from the dose response data, two concentrations were chosen (25 µM and 50 µM) to confirm that the 50 µM concentration is the optimal dose that was then used for further investigations. Results of the studies presented in this chapter demonstrate strong anti-oxidative, anti-inflammatory, and anti-atherogenic activities of RSV (50 µM in particular) *in vitro*. Results for the key findings are summarised in Table 3.1.

Table 3.1 An overview of 50 μM RSV effects on various atherosclerosis-associated cellular processes *in vitro*.

Model system used	Cellular processes	Percentage	*p*-value
THP-1 monocytes/ macrophages	Monocyte migration	↓ 27%	=0.001 (***)
	ROS production (monocytes)	↓ 22%	≤0.001(***)
	ROS production (macrophages)	↓ 38%	≤0.001(***)
	MitoROS production	↓ 16%	≤0.001(***)
	Macropinocytosis	↓ 46%	≤0.001(***)
	Dil-oxLDL uptake	↓ 20%	≤0.001(***)
	SR-A expression (qPCR)	↑22%	≤0.001 (***)
	CD36 expression (qPCR)	↑174%	≤0.001(***)
	SR-A levels (FACS)	↓31%	≤0.001(***)
	CD36 levels (FACS)	↑97%	≤0.001(***)
	LDLR level (FACS)	↑47%	≤0.001(***)
	Phagocytosis	↓ 49%	=0.018 (*)
	Cholesterol efflux	↑ 29%	=0.045(*)
	IFN-γ induced MCP-1 expression	↓ 56%	≤0.001(***)
	IFN-γ induced ICAM-1 expression	NC	NS
	NLRP3 inflammasome activation	↓ 29%	≤0.001(***)
	MMP activity (after 3 hours incubation)	↓ 21%	=0.004(**)
RAW264.7 macrophages	Cholesterol metabolism- TPL	↑ 21%	≤0.001(***)
	Cholesterol metabolism- TG	↓ 31%	=0.018(*)
	Cholesterol metabolism- CE	↓ 52%	=0.001(***)
	Cholesterol metabolism- FC	NC	NS
	Cholesterol metabolism- CE/FC	↓ 63%	≤0.001(***)
HMDMs	ROS production	↓ 41%	≤0.001(***)
	Macropinocytosis	↓ 40%	=0.01 (*)
	Dil-oxLDL uptake	↓ 34%	≤0.001(***)
HASMCs	SMCs invasion	↓ 36%	≤0.001(***)
	ROS production	↓ 62%	≤0.001(***)
	Macropinocytosis	↓ 46%	≤0.001(***)
	Dil-oxLDL uptake	↓ 73%	≤0.001(***)
HAECs	ROS production	↓ 84%	≤0.001(***)
	TNF-α induced MCP-1 expression	↓32%	=0.007(**)
	TNF-α induced ICAM-1 expression	↑87.7%	≤0.001(***)

Abbreviations: NS, not significant effect; ↓decrease; ↑increase; NC, no change; ROS, reactive oxygen species; MMP, matrix metalloproteinase; IFN-γ, interferon-γ; TNF-α, tumour necrosis factor-α; MCP-1, monocyte chemoattractant protein-1; ICAM-1, intercellular adhesion molecule-1; TPL, total polar lipids; TG, triglycerides; CE, cholesterol esters; FC, free cholesterol; HMDMs, human monocyte-derived macrophages; HASMCs, human aortic smooth muscle cells; HAECs, human aortic endothelial cells.

3.4.1 RSV reduces MCP-1-stimulated monocyte migration

The vital role of MCP-1 in monocyte recruitment to the endothelium and subsequently initiation and progression of the disease was previously highlighted in Chapter 1 and this chapter. Because of this, it was of interest to determine whether RSV could inhibit the role of MCP-1 in inducing monocyte migration across a barrier that mimics arterial endothelial cells. Results from this study show that the migration of monocytes toward MCP-1 was significantly inhibited across all tested concentrations, except for 25 µM where there was a trend towards reduction (Figure 3.7). These data suggest the role of RSV in inhibiting an early and important step in the inflammatory response that leads to atherosclerosis initiation.

Much *in vivo* evidence demonstrated that genetic deletion of MCP-1 or its receptor in atherosclerotic mouse models is atheroprotective and represents a promising therapeutic target (Gu et al. 1998; Inoue et al. 2002; Combadière et al. 2008). For instance, in a study conducted in atherosclerotic $LDLR^{-}/^{-}$ mice that either express wild type MCP-1 or are genetically deficient for MCP-1, the LDLR/MCP-1 deficient mice showed fewer macrophages and lipid accumulation in the aortic wall (Gu et al. 1998). In a similar study, Boring, et al. (1998) found that $ApoE^{-/-}$ mice that are deficient in CCR2 had significantly decreased atherosclerotic lesion size, as well as a decrease in monocytes and macrophages in the aortas (Boring et al. 1998). The results obtained from this study are in line with previously reported observation about the ability of RSV to attenuate THP-1 monocyte migration as well as MCP-1 expression in the presence of LPS stimuli (Zhang et al. 2021c). Moreover, Cullen and colleagues demonstrated that RSV treatment inhibits ^{125}I-MCP-1 binding to CCR2 on THP-1 monocytes without affecting the affinity of MCP-1 for its CCR2 receptor as well as inhibition of CCR2 mRNA and protein expression levels (Cullen et al. 2007).

3.4.2 RSV attenuates PDGF-stimulated SMCs migration with increased cell proliferation rate

The proliferation of VSMCs is well-known to have a role in atherogenesis. However, the exact roles of these cells in the initiation of lesions are less known as most studies are focused on endothelial and inflammatory cells in the initiation of lesions while the role of VSMCs is discussed largely in the context of late atherosclerosis when they contribute to fibrous cap

formation and plaque stabilisation. Previous studies suggested the antiproliferative effects of RSV in VSMCs (Poussier et al. 2005; Ekshyyan et al. 2007; Li et al. 2019a). However, treatment of RSV in this study was found not to significantly affect the cell proliferation rate until 4 days of incubation and then significantly increased by day 8 (Figure 3.17 and 18). This finding implies that RSV treatment may potentially have a beneficial effect on plaque stability.

SMCs migration is a critical mechanism in the pathophysiology of atherosclerosis, and this process is tightly controlled and mediated by growth factors, such as PDGF-BB, synthesised and released by resident cells of the vessel wall (Michael et al. 2012). It is stimulated by the binding of PDGF-BB to PDGF receptor beta (PDGFRβ) whose expression is upregulated in human atherosclerotic plaques (Tanizawa et al. 1996; Yu et al. 2003). Therefore, the inhibition of PDGF-BB will reduce migration and proliferation of SMCs, and subsequently atherosclerotic lesion size. Indeed, a previous study has shown that treatment of diabetic ApoE$^{-/-}$ mice with the tyrosine kinase inhibitor (known as Imatinib) is associated with a reduction in PDGF-BB expression and phosphorylation of PDGFRβ as well as reduction in lesion area (Lassila et al. 2004). This study found that RSV in the presence of PDGF-BB stimulus significantly attenuates the migration of HASMCs by 36% relative to the vehicle control (Figure 3.20). These data are compatible with published observation that RSV (or vitisin B, RSV tetramer) attenuated PDGF-BB and eventually HASMCs migration, and suggested that the reduction in SMCs invasion was due to an attenuation of PDGFR phosphorylation via an increase in protein tyrosine phosphatase activity and consequently the inhibition of downstream kinase cascades(Venkatesan et al. 2008; Choi et al. 2010; Ong et al. 2011).

Thus, overall, RSV has anti-migratory impact on THP-1 monocytes and HASMCs towards MCP-1 and PDGF-BB respectively. However, investigation of RSV treatment on PDGFR expression would be important for delineating potential mechanisms.

3.4.3 RSV inhibits ROS production in various cell types

Excessive ROS production and associated oxidative stress has been observed in all stages of atherosclerosis development and has been linked with key signalling pathways involved in inflammation in the disease. In this study, RSV significantly attenuated TBHP-induced ROS

production in THP-1 monocytes and macrophages, HMDMs, HASMCs and HAECs at all tested concentrations. This is not surprising as RSV is a well-known antioxidant. Findings reported in several *in vitro* and *in vivo* studies demonstrate that the antioxidative property of RSV is due to its radical scavenging and metal ion chelation abilities as well as its ability to induce antioxidant enzymes (Jia et al. 2008; Cheng et al. 2014; Liu et al. 2015b; Lou et al. 2018; Kim et al. 2019b). For example, a previously published *in vitro* study showed that RSV is capable of delaying oxidative stress-induced apoptosis in a variety of cell types, including human umbilical vein endothelial cells (HUVECs), RAW264.7 cells, and THP-1 macrophages (Guo et al. 2014; Liu et al. 2017c; Sun et al. 2017). Additionally, it has been reported that treatment of AopE^{-}/$^{-}$ mice with RSV resulted in induction of antioxidant enzymes and a reduction of NADPH oxidases (Xia et al. 2010).

The attenuation of ROS production and oxidative stress subsequently contributes to the inhibition of endothelial dysfunction and associated pro-inflammatory signalling, lipid peroxidation and foam cell formation. A previous study found that RSV attenuates lipid peroxidation in human lymphocytes from healthy volunteers by inducing the activity of GSH, GPX and GR in addition to inhibition of catalase activity (Yen et al. 2003). Furthermore, the addition of RSV to human LDL inhibits LDL oxidation induced by copper ion incubation. This effect has been suggested to be due to copper ion chelation activity of RSV (Frankel 1993; Delmas et al. 2005). An interesting study that analysed LDL samples from human volunteers noted that RSV was incorporated into human LDL particles following consumption due to its lipophilic character, and suggested that this way its protects LDL particles from oxidation (Urpí-Sardà et al. 2005). In addition, feeding rat and mice with HFD and RSV led to increased SOD levels and thus a reduction in LDL oxidation (Rocha et al. 2009; Sun et al. 2017). In conclusion, the data obtained in the present study, when combined with previous studies, reveal an antioxidant activity of RSV as a potentially potent mechanism for protecting against CVDs.

3.4.4 Inhibition of mitoROS production by RSV

As previously highlighted in section 3.1.2.4, there is a high correlation between mitoROS/ mitochondrial oxidative stress (mitoOS) and human atherosclerosis severity. Increased mitoROS production and low NADPH/NADP+ ratio have been reported in

hypercholesterolemic LDLR^{-}/$^{-}$ mice compared to control group that consequently promotes inflammation and oxidative stress (Dorighello et al. 2016). In this study, incubation of macrophages with 50 µM RSV resulted in a significant reduction in mitoROS production by 16% ($p \leq 0.001$) while there was a lack of any effect seen with 25 µM RSV (Figure 3.11).

In a previous *in vitro* study, pre-treatment of HUVECs with RSV significantly attenuated the TBHP-induced oxidative damage by enhancing cell viability, reducing apoptosis, suppressing mitochondrial membrane potential, and lowering mitoROS generation (Zhou et al. 2014). The mitoROS scavenging activity of RSV could potentially be due to enhancement of silent mating-type information regulation 2 homolog 3 (Sirt3) pathway, a key pathway in the regulation of mitoROS homeostasis (Zhou et al. 2014).

Research that investigated the effect of suppressing mitoROS in atherosclerotic LDLR^{-}/$^{-}$ mice noted a significant reduction in aortic root lesion area as well as a reduction in macrophages and infiltration of monocytes to inflammatory lesion sites. In addition, the same study reported a reduction in MCP-1 expression and down-regulation of the proinflammatory NF-κB pathway (Wang et al. 2014b). Furthermore, treatment of mice suffering from pressure-overload-induced heart failure (HF) with RSV improves both cardiac- and non-cardiac symptoms. Most interestingly, it has been reported that treatment of HF-mice with RSV restored levels of mitochondrial oxidative phosphorylation complexes as well as restored AMP-activated protein kinase activation (AMPK) (Sung et al. 2015). It has been suggested that treatment with RSV could improve mitochondrial function through either direct or indirect mechanisms. In the direct mechanism, RSV interacts with Sirtuin 1 (SIRT1), causing deacetylation of liver kinase (LKB 1), and this subsequently phosphorylates and activates AMPK. On the other hand, in the indirect pathway, RSV activates SIRT 1 by inhibiting cAMP-degrading phosphodiesterase (PDE) leading to the accumulation of cAMP effector protein, enhancement of intracellular Ca^{2+} levels and activation of subsequent down-stream pathways. In both schemes, the activation of AMPK results in phosphorylation of PPAR gamma co-activator 1 alpha (PGC-1α) that is then deacetylated by SIRT 1. PGC-1α is a master regulator of mitochondrial oxidative metabolism and biogenesis (Bastin and Djouadi 2016; Gligorijević et al. 2021)(see Figure 3.29). In a recent study, RSV showed the ability to

ameliorate mitochondrial dysfunction in rats that are in the early phase of status epilepticus (Folbergrová et al. 2021).

Owing to the strong link between mitoROS/mitoOS and atherosclerosis progression, it would be valuable to repeat mitoROS production assay using different cell types such as HMDMs, HASMCs and HAECs to confirm the effect of RSV on mitoROS using THP-1 macrophages is not due to the cell line utilised. Additionally, more focus should be placed on mitochondrial bioenergetic profile using various mitochondrial-based assays (e.g. Agilent Seahourse Technology).

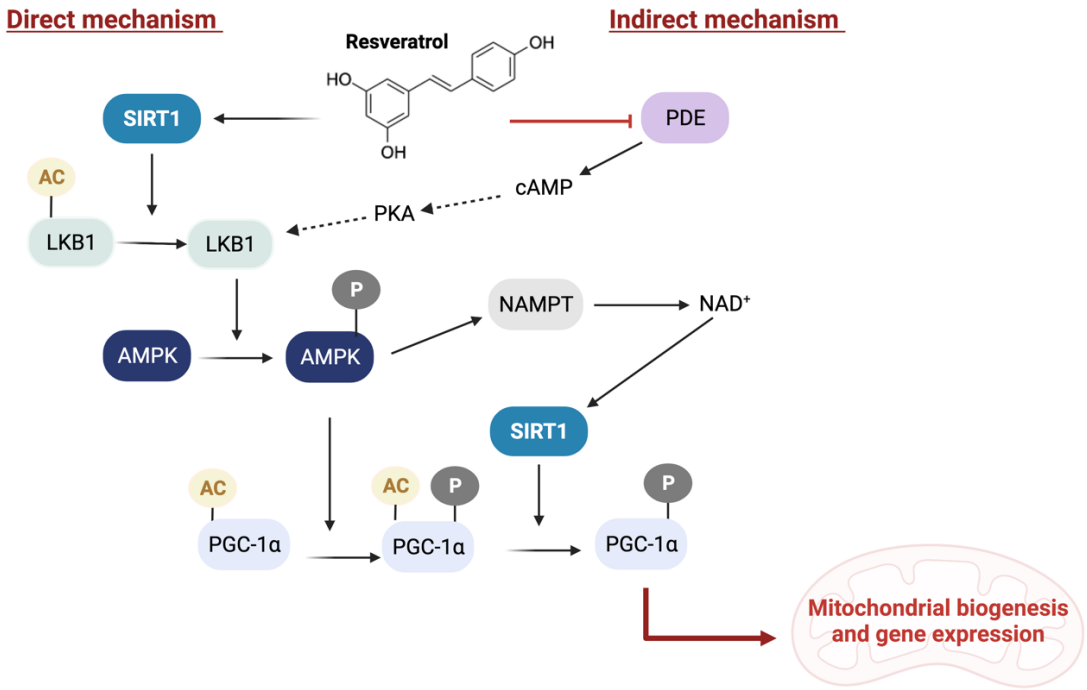

Figure 3.29 Putative signalling pathways involving SIRT1, AMPK and PDE in the actions of resveratrol.

One of the proposed mechanisms (direct mechanism) is that RSV would act as a powerful activator of SIRT1 that leads to deacetylation/activation of LKB1. The LKB1 then activates AMPK via phosphorylation. In the other proposed mechanism (indirect), RSV activates SIRT1 indirectly by blocking PDE activity. Both mechanisms eventually result in the activation of PGC-1α, a key regulatory of mitochondrial oxidative metabolism and biogenesis. **Abbreviations:** SIRT1, Sirtuin1; AMPK, AMP-activated protein kinase; PDE, phosphodiesterase; cAMP, cyclic AMP; PKA, protein kinase A; LKB1, liver kinase B1; PGC-1α, PPAR gamma co-activator 1 alpha. Figure adapted from (Gligorijević et al. 2021) and created with BioRender.com.

3.4.5 Foam cell formation

3.4.5.1 Attenuation of macropinocytosis in human macrophages and HASMCs

Macropinocytosis is one of the key mechanisms utilised by macrophages and SMCs to uptake both modified LDL and unmodified LDL and therefore transform into foam cells. As stated in section 3.1.2.5.1, inhibition of LY uptake, and thereby macropinocytosis, by either macrophages or HASMCs represents a putative mechanism for the reduction of intracellular cholesterol levels and hence reduction in foam cell formation. Several investigations have supported this. Thus, treatment of M-CSF stimulated HMDMs with a macropinocytosis inhibitor showed a 40% reduction in LDL uptake (Anzinger et al. 2010). In a study using time-lapse video phase-contrast microscopy and time-lapse digital confocal-fluorescence microscopy with fluorescent DiI-LDL to monitor macropinocytosis in HMDMs revealed that the macropinocytosis inhibitors LY294002 inhibits macrophages macropinocytosis by completely blocking PMA-activated macrophage fluid-phase endocytosis (Kruth et al. 2005). Similar results have been published using different cell types such as RAW264.7 and THP-1 macrophages (Yao et al. 2009; Michael et al. 2013). Additionally, lipid accumulation was significantly inhibited by 50% in BMDM from $LDLR^{-/-}$ and wild-type mice after treatment with macropinocytosis inhibitors LY294002 or wortmannin (Anzinger et al. 2012; Barthwal et al. 2013). Furthermore, previous studies observed that incubation of VSMCs with unmodified serum lipids resulted in excessive accumulation of lipids in VSMCs and their transformation into foam cells, which was inhibited in the presence of macropinocytosis inhibitors such as LY294002 (Rivera et al. 2013).

Notably, in the current study treatment of THP-1 macrophages, HMDMs and HASMCs with 50 µM RSV shows about a similar degree of reduction in all investigated cells (~ 40%) (Figure 3.9 and 3.23). The effect of RSV treatment on macropinocytosis has previously not been studied in macrophages nor HASMCs. However, the obtained results indicate that RSV had a comparable effect to macropinocytosis inhibitors utilised in previously mentioned studies (Anzinger et al. 2010; Anzinger et al. 2012; Barthwal et al. 2013; Michael et al. 2013). These findings provide a possible mechanism for the attenuation of foam cell formation by RSV.

3.4.5.2 Inhibition of Dil-oxLDL uptake in human macrophages and HASMCs.

In addition to macropinocytosis, both macrophages and SMCs uptake modified LDL via receptors such as SR-A, CD36 and LOX-1 to transform into foam cells. The effect of RSV on Dil-oxLDL uptake was investigated in THP-1 macrophages, HMDMs and HASMCs. Uptake of Dil-oxLDL was significantly inhibited by around 20%- 30% in human macrophages while greater inhibition of more than 70% was seen in HASMCs (Figure 3.10 and 3.24). In contrast to macropinocytosis, the ability of RSV to attenuate oxLDL uptake in macrophages has been shown in previous literature (Voloshyna et al. 2013). Voloshyna and his colleagues explored the atheroprotective effect of RSV treatment on foam cell formation. This study demonstrated that RSV attenuates oxLDL uptake and consequently lipid accumulation in cultured cholesterol-loaded THP-1 macrophages. Moreover, in the same study, ORO staining of macrophages pre-treated with oxLDL showed a significant reduction in foam cell by 40% in RSV-treated cells (Voloshyna et al. 2013). These results build on the previous finding of Park et al. who indicated that RSV decreases foam cell formation in macrophages induced by LPS (Park et al. 2009a). Most of the other literature have focused on parameters that contribute to lipid uptake such as AMPK activity, MCP-1 expression and ROS production and confirmed the anti-foam cell formation activity of RSV (Park et al. 2009a; Dong et al. 2014b; Guo et al. 2014).

In terms of foam cell formation in SMCs, this is the first study to investigate the effect of RSV treatment on oxLDL uptake in HASMCs. It is possible that RSV reduces oxLDL uptake by downregulating SRA expression. Under normal condition, human SMCs do not express their scavenger receptors. However, oxidative stress caused by ROS enhances their expression (Mietus-Snyder et al. 2000). One possible mechanism is that RSV downregulates SR-A expression by inhibiting ROS production. The other possible mechanism is through modulation of the activity of SMC COX-2. The inhibition of COX-2 leads to inhibition of PGE2 production and consequently reduced SR-A expression (Mietus-Snyder et al. 2000). However, further studies are required to elucidate the effect of RSV on SMCs scavenger receptors expression.

To provide more insight into the mechanism of action of RSV in attenuating oxLDL uptake, the expression of scavenger receptors (namely SR-A and CD36) in macrophages after RSV

treatment was investigated in this study and will be discussed in the next section. However, expanding this study to HASMCs would be highly informative and valuable due to lack of research in this area.

3.4.5.3 SR-A and CD36 expression in THP-1 macrophages.

Macrophages were identified with high affinity binding site receptors that can bind and endocytose only modified (acLDL or oxLDL) but not native LDL, that subsequently leads to lipid-enriched foam cell formation (Goldstein et al. 1979; Cuthbert et al. 2020). Among the different scavenger receptors classes, SR-A and CD36 were widely studied due to their centrally implicated role in this lipid uptake process. Previous studies have revealed that inhibition of either CD36 or SR-A1 alone had atheroprotective effects in hyperlipidaemic $LDLR^{-/-}$ mice and reduced lipid accumulation in $ApoE^{-/-}$ macrophages via reducing modified LDL uptake and binding (Kunjathoor et al. 2002; Moore et al. 2005; Mäkinen et al. 2010). In addition to SR-A and CD36, LDLR on macrophages facilitates foam cell formation and, therefore, contributes to atherosclerosis (Herijgers et al. 2000).

However, the results obtained in this study were somewhat unexpected. Although there was a significant reduction in oxLDL uptake, the mRNA levels of both SR-A and CD36 was significantly increased following RSV treatment (Figure 3.26). For expression of proteins, the levels of SR-A were significantly decreased while CD36 increased after RSV incubation (Figure 3.27). These results are in line with a previous study that demonstrated that treatment with RSV had significant and concentration dependent effect on CD36 expression in both THP-1 macrophages and in HAECs. On the other hand, treatment of THP-1 macrophages and HAECs with RSV had no significant change on SR-A expression; the authors noted that increase RSV concentration tends to upregulate SR-A expression (Voloshyna et al. 2013). However, only one study indicated inhibition of SR-A II and LPL in THP-1-derived macrophages after RSV treatment (Sevov et al. 2006). However, although the mRNA level of SR-A, the protein level was significantly reduced which is most important for receptor function.

While RSV had no beneficial effect on CD36 and LDLR expression, it should be noted that there are several other scavenger receptors, such as CD68, LOX-1, and SR-PSOX that are expressed

in human atherosclerotic lesions, and their role in lipid uptake and foam cell formation needs to be investigated further. Studying the effect of RSV treatment on the expression of these receptors would be worthwhile.

3.4.5.4 Phagocytic activity of macrophages

As previously discussed, phagocytosis is well known to be one of the earliest events in innate immune response. In addition to facilitating the recruitment of monocytes and T-cells, the excessive uptake of cholesterol esters via phagocytosis results in inflammasome activation that can then cause damage to the lysosomal system (Bobryshev et al. 2016).

In this study, the phagocytic activity of macrophages was significantly inhibited with 25 µM and 50 µM RSV by more than 40% (Figure 3.12). Previous studies have reported both stimulating and suppressive effects of RSV treatment on macrophage phagocytosis activity. The results obtained from this study are in accordance with previous findings that demonstrated that treatment with RSV inhibits, in a dose-dependent manner, the phagocytosis of *Escherichia coli* and of *Staphylococcus aureus* by THP-1 cells and RAW264.7 cells via inhibition of NF-κB activation (Iyori et al. 2008). In a separate study, treatment with RSV increased the phagocytic activity of THP-1 cells and U937 human promonocytic cell line (Bertelli et al. 1999; Zunino et al. 2018). Overall, the effect of macrophage phagocytotic activity in terms of atherosclerosis and foam cell formation remains poorly understood and needs more investigation. While a previous study correlated increased phagocytosis to decreased oxLDL uptake and atherosclerotic plaque in ApoE^{-}/$^{-}$ mice(Laguna-Fernandez et al. 2018), other studies indicated that phagocytosis could potentially induce pro-atherogenic effects via uptake of lipoproteins, erythrocytes, and platelets (Schrijvers et al. 2007). Further studies are required on the effect of decreased phagocytosis on oxLDL uptake as well as the clearance of apoptotic cells and debris.

3.4.5.5 Cholesterol efflux from THP-1 macrophage foam cells

In this study, treatment with ApoA1 induced efflux by 14% (not statistically significant); however, additional treatment with RSV resulted in a significant increase in cholesterol efflux by 29% (Figure 3.22).

A previous study measured cholesterol efflux from THP-1 macrophages to AopA1 in the presence of RSV treatment and demonstrated that at low concentration (10 µM and 25 µM), RSV enhanced cholesterol efflux by up to 4.67% (Voloshyna et al. 2013). Similarly, several other studies have shown the ability of RSV to induce cholesterol efflux from cholesterol-loaded macrophages using different cell types such as J774 and RAW 264.7 macrophages (Berrougui et al. 2009; Allen and Graham 2012; Chang et al. 2012). Notably, RSV was able to enhance cholesterol efflux in a concentration dependent manner (Berrougui et al. 2009; Voloshyna et al. 2013). One mechanism postulated for this effect is that RSV increases the expression of the major proteins responsible for cholesterol efflux: ABC transporters (ABCA1 and ABCG1) and LXR-α. For example, the efflux of cholesterol induced by RSV was associated with a corresponding increase in the expression of ABCA1, ABCG1 and LXR-α, and their upregulation was in concentration-dependent manner (Sevov et al. 2006; Berrougui et al. 2009; Voloshyna et al. 2013). Moreover, it has also been reported that the effect of RSV on cholesterol efflux is PPARγ-dependent (i.e. RSV increased the expression of PPAR-γ). The blocking of PPARγ by either gene silencing or PPARγ antagonist GW9662 prevented upregulation of ABCA1 by RSV (Hai et al. 2012; Voloshyna et al. 2013; Ye et al. 2019).

An earlier study showed that suppressing LXRα-mediated, ABCA1/ABCG1-dependent cholesterol efflux from macrophages results in increased atherosclerotic lesion area and plaque lipid accumulation in $ApoE^{-}/^{-}$ mice (Jin et al. 2018). The same study indicated that LXR activator (T0901317) upregulated the expression of ABCA1 and ABCG1 both *in vitro* and *in vivo*, consequently decreasing foam cell formation and atherosclerotic lesion area in THP-1 macrophages and $ApoE^{-}/^{-}$ mice respectively (Jin et al. 2018). However, RSV treatment showed its ability to upregulate the expression of induced LXRα at mRNA and protein levels in human macrophages and potentially reduce lipid accumulation (Sevov et al. 2006).

Therefore, as increased ABC transporters A1/G1 represents a possible mechanism by which RSV treatment enhances cholesterol efflux from macrophages, investigation of their expression at the molecular and cellular level is required to delineate the mechanisms of RSV actions. In addition, future studies could extend to investigation of the roles of several other pathways in the literature, such as increased expression of ABC transporters, PPAR-γ/LXR-α pathway, and Janus kinase 2 (JAK2)/signal transducer and activator of transcription 3 (STAT3) pathway, particularly in relation to stimulating ABCA1 expression (Fu et al. 2014a).

3.4.5.6 Cholesterol metabolism in macrophages

Along with lipid uptake mechanisms, it was important to investigate the role of RSV treatment in the metabolism of internalised cholesterol in macrophages.

Figure 3.25 shows that TPL fractions were increased significantly while the fractions of TG, CE and CE/FC ratio were reduced significantly after treatment with RSV. However, no observed change in FC content was seen. These data indicate a role of RSV in the inhibition of CE accumulation. These findings, along with the inhibition of macrpoinocytosis, oxLDL uptake, phagocytosis, and stimulation of cholesterol efflux, reveal mechanisms by which RSV suppresses formation of foam cells. It had been previously published that incubation of RAW264.7 cells with oleic acid triggers TC and CE accumulation in macrophages that is inhibited in the presence of RSV. This effect was suggested to be due to activation of PPARα and PPARγ signalling (Ye et al. 2019). Other mechanisms could potentially be involved such as reduction in the activity of ACAT1 or increase in the activity of nCEH. As previously mentioned, the formation of CE in macrophages is catalysed by the action of ACAT enzymes that are expressed in both human atherosclerotic lesions and in cultured macrophages (Miyazaki et al. 1998). Inhibition of ACAT to reduce intracellular accumulation of cholesterol in macrophages was a target for preventing or treating atherosclerosis in several studies (Matsuda 1994; Matsuo et al. 1995; Nicolosi et al. 1998; Pal et al. 2013). ACAT1$^{-/-}$ macrophages treated with acLDL showed an increase in acLDL efflux and increase in FC (Ghosh et al. 2010). Therefore, inhibition of ACAT1 is most likely to reduce the development of atherosclerosis by inhibiting CE formation and storage as well as increase in FC efflux (Ghosh et al. 2010). Partial inhibition of ACAT1 and ACAT2 in ApoE$^{-/-}$ mice on western diet

showed anti-atherogenic effects via reduced lesion size and macrophages in lesion area (Kusunoki et al. 2001). A previous study that investigated the effect of RSV and *Polygonum cuspidatum* water extract (PCWE), which has RSV at higher concentration than in grapes, on lipid metabolism in addition to ACAT enzyme activity indicated that both RSV and PCWE significantly reduced the activity of ACAT in a dose-dependent manner by 50% (Park et al. 2004). Furthermore, the CE content was significantly attenuated in HepG2 cells after incubation with PCWE while no changes were observed in the FC content. The authors suggest that RSV might be responsible, at least in part, for the inhibitory effect of PCWE (Park et al. 2004). Notwithstanding the promising effect of inhibiting ACAT1 to prevent CE accumulation and foam cell formation, disruption of the ACAT gene in atherosclerotic mouse models has proved controversial. For example, hypercholesterolemic LDLR null mice reconstituted with $ACAT1^{-/-}$ macrophages displayed increased atherosclerotic plaque size compared to control $LDLR^{-/-}$ mice as well as increased FC accumulation in the arterial wall (Fazio et al. 2001). Future studies should investigate the mechanisms underlying the ability of RSV to diminish CE formation and storage. This could include investigation of the effect of RSV on the expression of ACAT1, ACAT2 and nCEH at the mRNA and protein level.

3.4.6 Anti-inflammatory effects in atherosclerosis

3.4.6.1 Inflammasome-mediated IL-1β secretion

Treatment of cholesterol crystal-stimulated THP-1 macrophages with RSV resulted in a significant attenuation in IL-1β secretion, suggesting inhibition of the NLRP3 inflammasome and anti-inflammatory effect of RSV (Figure 3.13).

The results presented in this study are in agreement with a previous study which demonstrated the ability of RSV to inhibit NLRP3 inflammasome and thereby protect against oxidative damage and proinflammatory cytokine production via inhibition of NF-κB signalling and activation of AMPK and Sirt1 pathways (Tufekci et al. 2021). Recently published work has indicated that RSV is capable of inhibiting NLRP3 inflammasome in mice by dephosphorylation of serine/threonine kinase (AKT1), a mechanism that is responsible for stimulating NLRP3 inflammasome activation in cardiomyocytes (Wang et al. 2022). Another suggested mechanism behind the activity of RSV to ameliorate the inflammasome was via suppression

of mitoROS production (Chang et al. 2015b). RSV treatment was demonstrated previously in this chapter to significantly decrease mitoROS generation, suggesting one of the putative mechanisms of RSV activity to suppress the NLRP3 inflammasome. According to Kepp et al. (2011), excessive production of mitoROS induces mitochondrial permeability allowing cytosolic release of mitochondrial DNA, which activates the NLRP3 inflammasome and the production of IL-1β (Kepp et al. 2011). From data in this study and with support of previous studies, the anti-inflammatory activity of RSV against activation of NLRP3 inflammasome can be concluded. However, due to several suggested mechanisms for the action of RSV, further investigation to determine the exact mechanism is required.

3.4.6.2 Inflammatory gene expression in cytokine stimulated macrophages and HAECs

The effect of RSV on cytokine- induced expression of key inflammatory markers, namely MCP-1 and ICAM1, in THP-1 macrophages and HAECs was investigated. The anti-inflammatory activity of RSV has been reported previously (Liu et al. 2015a; Wang et al. 2020a; Meng et al. 2021). However, no previous studies have investigated the effect of RSV on MCP-1 and ICAM-1 induced by IFN-γ or TNF-α in human macrophages or HAECs, which are more relevant to atherogenesis.

Treatment with RSV resulted in a significant decrease in MCP-1 expression in both IFN-γ-stimulated THP-1 macrophages and TNF-α- stimulated HAECs by 56% and 32% respectively (Figure 3.28). This observation is in line with many previous studies. For example, pre-treatment of human primary monocytes with RSV showed a reduction in LPS-triggered MCP-1 and TNF-α production, which corresponded to a reduction in the migration of these cells in the same study (Wang et al. 2020a). In addition, a previous investigation aimed to determine the expression of MCP-1 in the presence or absence of TNF-α showed that RSV was able to inhibit MCP-1 production in 3T3-L1 adipocytes only under inflammatory conditions, which was suggested to be due to inhibition of NF-κB activation (Zhu et al. 2008). In addition to TNF-α and MCP-1, the ability of RSV to reduce IFN-γ levels as well as inhibition of IFN-γ-mediated inflammation has been shown in *in vitro* and *in vivo* studies (Boscolo et al. 2003; Zang et al. 2011; Ding et al. 2021; Saleh et al. 2021). RSV caused a dose-dependent inhibition of IFN-γ-stimulated levels of MCP-1 in human coronary artery smooth muscle cells

(HCASMCs)(Wakabayashi and Takeda 2013). Therefore, targeting MCP-1 represents a promising therapeutic target and RSV impacts this.

In contrast to MCP-1, the expression levels of ICAM-1 were stimulated in response to RSV treatment (Figure 3.28). This finding contradicts several lines of evidence from previous investigations that RSV in a concentration-dependent manner ameliorates upregulation of expression of ICAM-1 and others adhesion molecules in different cell types following TNF-α stimulation, such as bone marrow-derived endothelial progenitor cells, HUVECs and ECs from aorta of TNF-α-treated mice, via inhibition of NF-κB activation (Park et al. 2009b; Liu et al. 2017a; Zhang et al. 2020d). In LPS-stimulated HUVECs, the expression of ICAM-1, VCAM-1 and MCP-1 was decreased by RSV via increased SIRT1 expression (Wang et al. 2020b). However, it must be mentioned that in all these studies, cells were pre-treated with RSV before being stimulated with either TNF-α or LPS to induce ICAM-1 expression, which is not the case in the current work.

Taken together, although treatment with RSV had no beneficial effect on ICAM-1 expression, the inhibition of MCP-1 may represent one potential mechanism by which RSV may exert anti-inflammatory effects. It should be highlighted that there are several pro-inflammatory cytokines and inflammatory markers implicated in disease progression that need be investigated before drawing any firm conclusions.

3.4.7 MMPs activity

The accumulated macrophage-derived foam cells within atherosclerotic plaques are the major source of MMPs, which directly degrade ECM protein constituents of the fibrous cap leading to cap degradation and consequently plaque instability (Olejarz et al. 2020). This study found that treatment of THP-1 macrophages with RSV significantly attenuated MMP activity after 3 hours while no effect was seen after 24 hours (Figure 3.14).

In previously published research, RSV showed the ability to attenuate the activities/expression of a wide range of MMPs, namely MMP-1, MMP-2, MMP-3, MMP-9 and MMP-13 using different cell lines such as MM cell line and VSMCs (Sun et al. 2006; Pandey et al. 2015; Farrokhi et al. 2018; Kang et al. 2018). An *in vitro* study conducted on oxLDL- and

LPS-treated HUVECs found a suppression in the expression and secretion of MMP3 and MMP9 following RSV treatment while *in vivo* investigations showed a reduction in plasma levels of MMP-9 in C57BL/6 mice fed HFD with RSV intervention (Zhang et al. 2019). Additionally, RSV at all tested concentrations inhibited MMP-9 expression at mRNA and protein levels in H_2O_2-induced VSMCs after 24 hours; however, the RSV concentrations were higher than the concentration utilised in this study. It has been also reported in the same study that RSV increased the expression of the tissue inhibitors of metalloproteinases (TIMPs) after 48 hours (Farrokhi et al. 2018). Gweon and Kim (2014) support the previous study by reporting the suppression of MMP-2 and -9 expression in a time- and dose-dependent manner following RSV treatment at concentrations of 10, 20, 30, 40 and 50 μM in chondrosarcoma cells (Gweon and Kim 2014). In additional investigations, RSV inhibited TNF-α induced expression of MMP-1 and MMP-3 in human dermal fibroblasts and expression of MMP-9 in VSMCs (Lee and Moon 2005; Lu and Chen 2021).

Notably, the majority of the previously performed research focused on the expression of particular MMPs such as MMP-2 and -9 in the context of atherosclerosis. However, it would be more relevant and valuable to investigate the effect of RSV on the activity of specific MMPs in the presence of individual inhibitors. Furthermore, assessing the expression of TIMPs in addition to MMPs would provide a better indication of potential ECM degradation.

3.5 Future directions

This study has identified various beneficial effects of RSV on the development atherosclerotic lesions *in vitro*. However, several further experiments should be performed to cement the observed results as well as shed light on the mechanisms underlying RSV activities associated with these findings. Because RSV has been shown in this chapter to reduce lipid accumulation within macrophages and HASMCs, the research might be expanded to investigate the effect of RSV on other scavenger receptors involved in lipid uptake at mRNA and protein levels. Other experiments such as the expression levels of ABCA1/G1, LXRα, LXRβ, ACAT1, and nCEH should be carried out to allow a more complete understanding of RSV effects on foam cell formation. Furthermore, to delineate the anti-inflammatory actions of RSV, extensive

research on the expression of a wide variety of inflammatory markers in the presence of RSV should be conducted.

Beyond this, investigation of the effect of RSV on bioenergetics and mitochondrial function has not yet been studied. For this purpose, Seahorse Technologies that had previously been optimised in the host laboratory can be utilised (O'Morain 2019; Chan 2021). Using this approach, the effect of RSV treatment on mitochondrial function can be investigated by evaluating several parameters such as basal respiration, maximal respiration, spare respiratory capacity, ATP production and others.

To investigate the actions of RSV further, its effects on several parameters associated with endothelial dysfunction such as NO production and eNOS expression could be studied. In addition, changes in macrophage efferocytosis and apoptosis of macrophages, HASMCs and HAECs following RSV treatment could be investigated. Finally, the effect of RSV treatment on HASMCs gene expression regarding to phenotypic markers is intriguing. This could be accomplished utilising RNA-sequencing (RNA-seq) to investigate how RSV affects the overall cellular transcriptome.

Taken together, these studies provide a valuable insight into RSV activities as well as contribute to the development of knowledge of its mechanism of action in the context of atherosclerosis.

3.6 Conclusions

The aim of this chapter was to gain comprehensive insights into the effects of RSV treatment on key processes in atherosclerosis. Data presented in this chapter reveal that RSV has anti-atherogenic actions *in vitro* in various key cell types implicated in all stages of atherosclerosis development. In particular, RSV attenuates monocyte migration and HASMCs invasion towards MCP-1 and PDGF respectively. Additionally, RSV exhibits antioxidant activities in all investigated cell types at all tested concentrations by inhibiting ROS and mitoROS production. Furthermore, treatment with RSV also exerts a number of highly desirable effects on human macrophage activity. In foam cell formation, results from this study show different mechanisms by which RSV reduces this that includes attenuation of oxLDL uptake, with a

corresponding attenuation in scavenger receptors SR-A at the protein level, as well as inhibition in macropinocytosis, phagocytosis and CE accumulation. Additionally, RSV treatment resulted in a significant enhancement in the efflux of cholesterol to Apo-A from lipid-laden macrophages. As previously highlighted VSMCs also contribute to foam cell formation, this study is the first that investigated the effect of RSV on HASMCs transformation into foam cells. Treatment of HASMCs with RSV showed the ability of RSV to reduce lipid accumulation within HASMCs and consequently inhibit their transformation into foam cells. Taken together, RSV exhibits potent anti-foam cell formation activity in both human macrophages and VSMCs.

Finally, the anti-inflammatory effect of RSV was not as extensive as anti-oxidant or anti-foam cell formation but it must be considered that several other inflammatory markers should be investigated before drawing firm conclusions. However, RSV was capable of mitigating inflammasome-mediated IL-1β secretion and and MCP-1 expression after cytokine-induced inflammatory responses. Figure 3.30 summarises the anti-atherogenic properties of RSV from this study.

Based on these findings, it was concluded that RSV represents a promising candidate capable of suppressing atherogenesis. Therefore, the research progressed to investigate the effect of RSV supplementation on atherosclerosis progression in atherosclerotic $LDLR^{-/-}$ mice, which are presented and discussed in the next chapter.

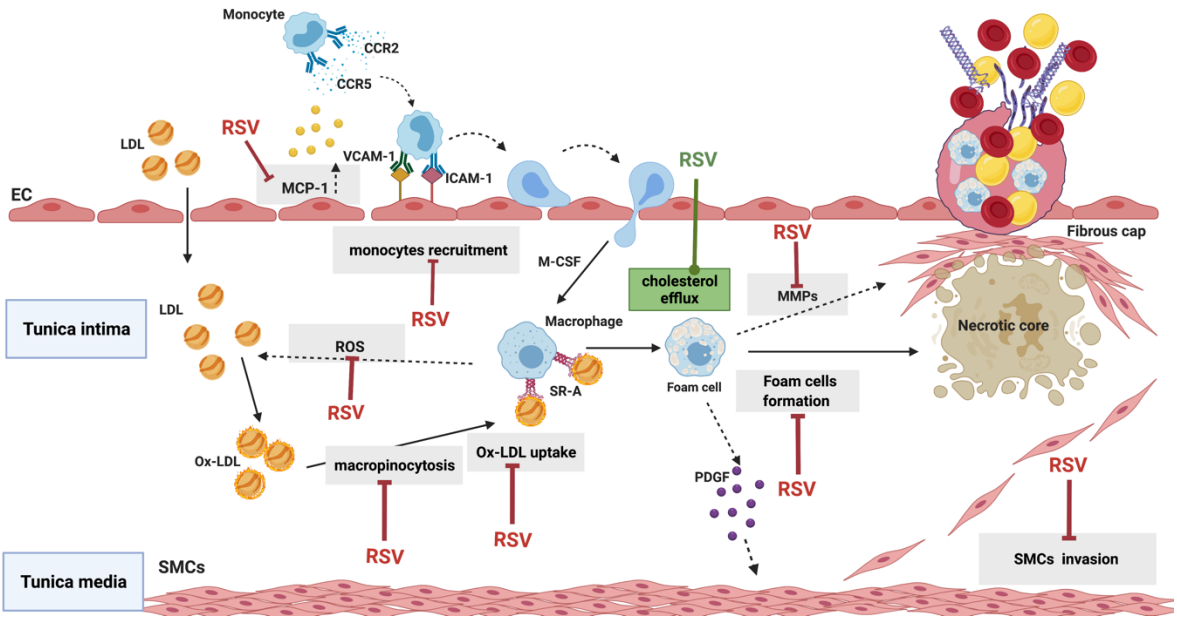

Figure 3.30 Summary of the anti-atherogenic properties of RSV

The events inhibited in atherosclerosis disease progression after RSV treatment are marked with red arrows whereas those increased by RSV are marked with green arrows. **Abbreviations:** MCP-1, monocyte chemotactic protein 1; M-CSF, macrophage colony stimulating factor; ICAM1, intercellular adhesion molecule 1; VCAM1, vascular cell adhesion molecule 1; ROS, reactive oxygen species; PDGF, platelet-derived growth factor; SMCs, smooth muscle cells; MMPs, matrix metalloproteinase. Image created with BioRender.com

CHAPTER 4

The effects of RSV supplementation on atherosclerosis progression *in vivo*

4.1 Introduction

Results from studies presented in the previous chapter support the potential of RSV as an anti-atherogenic agent for atherosclerosis via attenuation of monocyte migration and SMCs invasion, reduction of ROS production by various cell types and inhibition of foam cell formation in human macrophages and HASMCs. Although the results from *in vitro* studies are valuable and highly informative, the requirement for validation through *in vivo* study is crucial given that atherosclerosis involves the action of many different cell types that interact with each other. Mouse models are predominantly used in atherosclerosis because of several advantages such as a well-known genetic background, being easy to breed and look after, cost effectiveness, and when evaluating specific pharmacological agents in studies where cost or availability is a concern, mice would require less amount of the agent than equivalent experiments conducted in larger animals such as pigs (Whitman 2004; Lin et al. 2015). Among the different mouse models, LDLR- and ApoE- deficient mice have been extensively used in atherosclerosis research. Such genetic modifications are essential for the development of atherosclerosis as wild-type mice are inherently resistant to developing atherosclerotic lesions because the circulating cholesterol in mice, unlike humans, is transported via HDL particles (Lin et al. 2015). Various studies have been conducted in these mouse models and revealed key mechanistic insights into the aetiology of the disease and potential therapeutic avenues. For example, in previous studies, supplementation of RSV has been found to improve plasma lipid profile and atherosclerosis-associated risk factors in AopE^{-}/$^{-}$ mice through reduction of plasma TC and LDL-C levels along with elevation in the plasma levels of HDL-C after 20 weeks (Do et al. 2008). Furthermore, feeding AopE^{-}/$^{-}$ mice HFD with RSV showed anti-obesity and hypolipidemic effects in addition to modulation of lipid metabolism in the liver and white adipose tissues after 12 weeks of supplementation compared to AopE^{-}/$^{-}$ mice fed HFD with lovastatin (Jeon et al. 2014). In addition, a reduction in T cells (CD4) proliferation and activation was observed in AopE^{-}/$^{-}$ mice after 20 weeks of administration HFD plus RSV (Zhou et al. 2020). Despite the number of *in vivo* studies that have investigated the impact of RSV intervention on atherosclerosis progression or its associated risk factors, there have been no detailed studies on RSV in LDLR^{-}/$^{-}$ mice. Furthermore, in previous studies, RSV was administrated intragastrically or orally (via gavage) which is better in terms of delivery of the agent and not the case in this study due to several disadvantages of using these

techniques such inadvertent tracheal administration, suffocation and death as well as stressful for mice for long duration.

4.1.1 Experimental aims

The studies presented in this chapter aimed to explore the effect of RSV supplemented HFD feeding on atherosclerosis progression in male LDLR^{-}/$^{-}$ mice by investigating the changes in mouse organs weight, plasma lipid profile, bone marrow haematopoietic stem cells (HSCs), and peripheral blood immune cells population compared to mice fed HFD alone. The LDLR^{-}/$^{-}$ mice exhibit more advantages compared to ApoE^{-}/$^{-}$ mice and were therefore chosen for studies described in this chapter. Firstly, while the ApoE^{-}/$^{-}$ mice are hyperlipidaemic and develop atherosclerosis spontaneously on a standard chow diet, the LDLR^{-}/$^{-}$ mice require atherogenic diet feeding to initiate atherogenesis. In addition, cholesterol in LDLR^{-}/$^{-}$ mice is carried in the plasma as LDL particles which results in hypercholesterolaemia and has a plasma lipid profile comparable to that of dyslipidaemic humans. Thirdly, unlike ApoE^{-}/$^{-}$ mice where the ApoE protein is known to have anti-inflammatory properties, the absence of LDL receptor has no effect on inflammation and the mice also exhibit features of human familial hypercholesterolaemia (FH). Finally, it is well known that ApoE^{-}/$^{-}$ mice develop more severe atherosclerosis lesions compared to LDLR^{-}/$^{-}$ mice (Veseli et al. 2017; Oppi et al. 2019).

During this study, the LDLR^{-}/$^{-}$ mice were fed for 12 weeks HFD alone or with 20 mg/kg/day RSV. The 12 weeks of feeding duration was based on previously optimised studies in the host laboratory. The RSV powder was mixed with HFD before use, which hence avoids the use of toxic DMSO in animals, and the concentration was chosen based upon a previously published study in ApoE deficient mice (Chang et al. 2015a).

4.1.2 Adiposity and CVDs

Adipose tissue is comprised of highly heterogeneous cellular populations such as adipocytes, macrophages, lymphocytes and ECs (Zhang et al. 2020a). Over the decades, our understanding of adipose tissue functions has evolved from an inactive storage site for surplus lipids to a metabolically active endocrine organ involved in the regulation of non-shivering thermogenesis, glucose and lipid metabolism, vascular endothelial function, and

inflammatory response (Kwok et al. 2016). It has been categorised into two classes: white or brown adipose tissues that differ in morphology and function. Anatomically, the white adipose tissue depot resides mainly in the subcutaneous area (under the skin) and in the visceral region (around internal organs)(Choe et al. 2016; Kwok et al. 2016). The key physiological functions of white adipose tissue are insulation and storage of energy for organs. However, an imbalance between energy intake and expenditure as well as excessive consumption of HFD leads to the accumulation of white adipose tissue and consequently obesity in human and animals (Schrauwen and Westerterp 2000; Buettner et al. 2007; Hariri and Thibault 2010; de Moura e Dias et al. 2021). Intriguingly, each anatomical depot of white fat adipose tissue has various metabolic and hormonal characteristics, as well as physiological functions that result in different clinical implications. For example, the excessive accumulation of white fat in the abdomen is highly corelated with CVDs. Indeed, obesity causes adipose tissue dysfunction that consequently stimulates the production and secretion of various hormones, cytokines and pro- and anti-inflammatory adipokines, which can directly act on cardiovascular tissues to induce disease initiation (Kwok et al. 2016). There are several adipokines involved in CVDs development such as CRP, TNF-α, MCP-1, leptin, IL-10, and IL-6. It has been found that up to 35% of circulating IL-6 is produced by the white adipose tissue (Landecho et al. 2019; Wueest and Konrad 2020). Unlike the white adipose tissue, the brown adipose tissue is predominantly localised around the scapular of rodents and infant humans and appears brown due to the abundance of mitochondria. Brown adipose tissue is implicated in non-shivering thermogenesis via lipid oxidation to produce energy (Choe et al. 2016; Kwok et al. 2016). Furthermore, in contrast to white adipose tissue, they are positively correlated with improvement in body metabolism and protection against weight gain (i.e., resists HDF-induced obesity) as a result of higher energy consumption and insulin sensitivity (Kwok et al. 2016). Due to the strong correlation between obesity and CVDs, the effect of RSV supplementation on HFD-induced obesity and accumulation of adipose tissue was investigated.

4.1.3 Plasma lipid profiling

Plasma lipid profiling is often carried out to uncover lipidomic biomarkers that are associated with CVDs. As previously highlighted in Chapter 1, elevated levels of classical lipid markers, such as TC, LDL-C, and TG, as well as a decrease in HDL-C, all lead to an increased risk of CVDs. LDL-C is the predominant lipoprotein that carries cholesterol, and an increase in circulating levels of LDL-C has long been known to be a major contributor to the development of atherosclerosis since they have the propensity to accumulate within macrophages and VSMCs (forming lipid-loaded foam cell) in the wall of arteries to initiate an inflammatory response via release of various pro-inflammatory cytokines (Björkegren and Lusis 2022). In contrast to LDL-C, plasma levels of HDL-C are negatively associated with atherosclerosis progression. HDL-C particles mediate cholesterol removal from peripheral tissues to the liver via RCT. This, in turn, inhibits ECs activation thereby preventing inflammatory cell infiltration and atherosclerosis development (Björkegren and Lusis 2022). Furthermore, an increase in HDL-C and reduction in LDL-C levels are associated with a decrease in haematopoiesis and circulation of leukocytes. It has been reported that hyperlipidaemia enhances haematopoiesis by affecting cholesterol efflux pathways and this effect is abolished via the functions of ABCA1 and ABCG1, and an increase in HDL-C. Therefore, LDL-C has been labelled as the main pro-atherogenic lipoprotein while HDL-C has been implicated as anti-atherogenic (Björkegren and Lusis 2022). A meta-analyses have identified that a reduction in LDL-C by 1 mmol/l corresponds to a reduction in the risk of coronary heart disease mortality by 19% (Baigent et al. 2005) while another study reported that an increase in HDL-C by 1 mg/dl would correspond to about 2-3% reduction in risk of mortality from coronary heart disease (Gordon et al. 1989; Cui et al. 2001). Among various medications targeting hyperlipidaemia, statins are considered as cornerstone therapy for CVD and this is due to the fact that statins not only suppress cholesterol synthesis and enhance hepatocyte LDL uptake, but also have anti-inflammatory, anti-oxidant and other pleiotropic activities (Kim et al. 2019a). Despite this, there is still a significant residual risk of atherosclerotic cardiovascular disease even when hyperlipidaemia has been successfully treated with statins (Wong et al. 2017). Several clinical investigations have shown that residual inflammatory risk after statin therapy is not an uncommon occurrence as evidenced by rise in plasma levels of IL-1β, IL-6 and CRP (Ridker 2017; Aday and Ridker 2019). In addition to statins, different therapeutic approaches aimed to decrease LDL-

C are available and used in clinical lipid-lowering therapy such as inhibitors of intestinal cholesterol absorption (known as ezetimibe) and inhibitors of PCSK9 that act as inducer of LDL uptake via prevention of degradation of LDL-receptors (Dayar and Pechanova 2022). Despite the effectiveness of these agents in decreasing LDL-C, many individuals are affected by their major adverse side effects (Dayar and Pechanova 2022). There is also substantial evidence that evaluating plasma LDL-C or HDL-C levels independently does not necessarily correlate with cardiovascular health and the LDL:HDL ratio is a better clinical risk marker of CVDs and sudden cardiac death (Millán et al. 2009; Chen et al. 2016a; Kunutsor et al. 2016). Therefore, in the current study, in addition to quantifying the concentration of major plasma lipid parameters following RSV supplementation, their ratios were calculated to acquire a more comprehensive perspective of the potential impact of changes in lipid profile.

4.1.4 Profiling of haematopoietic stem, progenitor and immune cell status

Haematopoiesis is a tightly regulated and efficient mechanism by which all mature blood and immune cells are produced to maintain the whole immune system. The primary site of haematopoiesis is the bone marrow (Dragoljevic et al. 2018). A heterogeneous population of haematopoietic stem and progenitor cells (HSPCs) are mainly responsible for mature blood and immune cell production, and maintain lifelong haematopoiesis due to their ability to self-renew and differentiate into mature cell lineages (Hurwitz et al. 2020). Within the HSPCs population, there are two subpopulations of haematopoietic stem cell populations (HSCs), which are long-term HSCs (LT-HSCs) and short-term HSCs (ST-HSCs). The former has long-term self-renewal ability while the latter has limited self-renewal capacity (Seita and Weissman 2010). The LT-HSCs differentiate into ST-HSCs that then give rise to multipotent progenitors (MPPs), which no longer possess self-renewal ability. The MPPs then differentiate into either the common lymphoid progenitor (CLP) that can then differentiate into all types of lineage lymphocytes or to the common myeloid progenitor (CMP), which can differentiate into megakaryocyte-erythrocyte progenitors (MEPs) and granulocyte-macrophage progenitors (GMPs). MEPs and GMPs finally differentiate into myeloid lineage cells (Kondo 2010; Seita and Weissman 2010; Cheng et al. 2020b). Figure 4.1 illustrates the hierarchical model system of haematopoietic stem cell differentiation from the bone marrow.

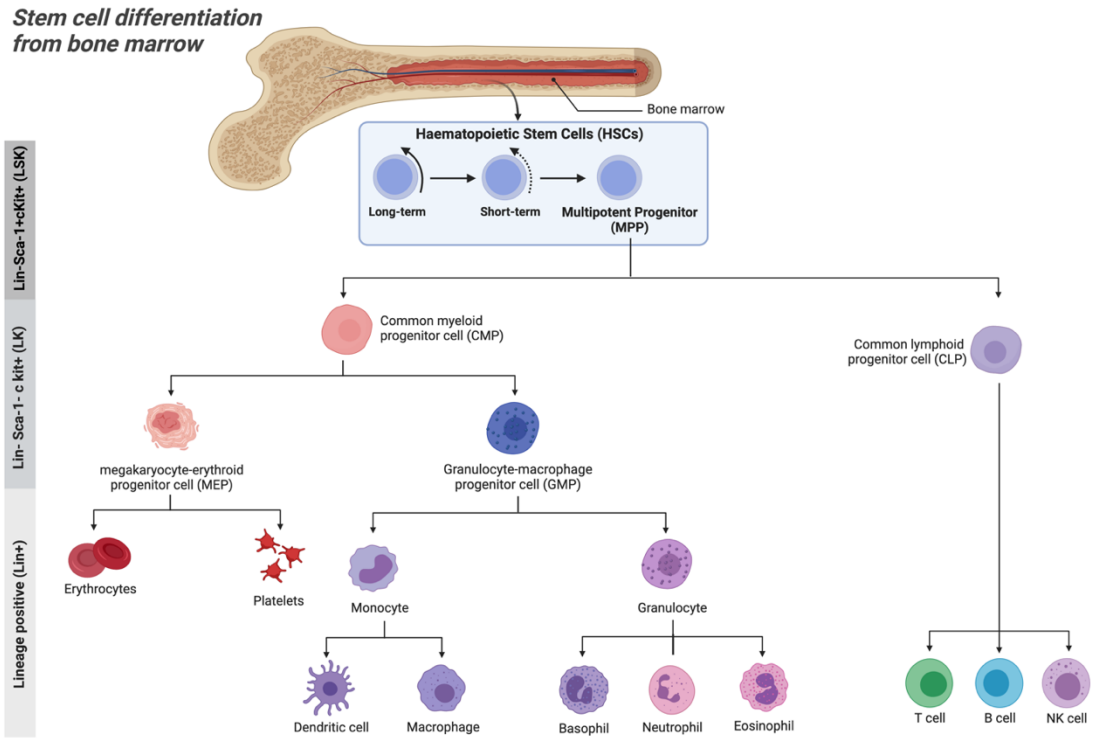

Figure 4.1 The hierarchical system model of haematopoietic stem cell differentiation from the bone marrow.

HSCs are divided into LT-HSCs that are characterised by long-term self-renewal activity. The LT-HSCs that reside on the highest tip of hierarchy then differentiate into ST-HSCs, and subsequently, into MPPs with limited self-renewal activity. Further downstream, MPP, CMP or CLP are produced that express lineage negative markers. The CMP then give rise to MEP and GMP. At the end, CLP, MEP and GMP differentiate to mature blood cells (lineage positive) in peripheral blood, such as T cells, B cells, NK cells, erythrocytes, platelets, granulocytes and monocytes. **Abbreviations:** HSCs, Haematopoietic Stem Cells; LT-HSCs, Long-Term HSCs; ST-HSCs, Short-Term HSCs; MPPs, Multipotent Progenitors; CMP, Common Myeloid Progenitor; CLP, Common Lymphoid Progenitor; MEP, Megakaryocyte-Erythroid Progenitor; GMP, Granulocyte-Macrophage Progenitor; NK, Natural Killer. Image created with BioRender.com.

Changes in bone marrow cell populations is highly associated with excessive HFD consumption (hypercholesterolaemia) along with sedentary lifestyle, and these alterations have been suggested to contribute to atherosclerosis progression (Devesa et al. 2022). A growing body of research has demonstrated that diet-induced hypercholesterolemia in rodents is associated with a significant alteration in haematopoiesis that results in skewing of mature cell production towards the myeloid lineage (Lang and Cimato 2014; Ma and Feng 2016; Vanhie et al. 2020). In atherosclerosis, the persistent activation of the haematopoietic system in the most common atherosclerotic mouse model (ApoE$^{-/-}$) has been shown to be associated with elevation in HSPCs and monocytosis (Swirski et al. 2007; Tacke et al. 2007; Murphy et al. 2011). The increase in haematopoietic activity in the bone marrow has also been observed in human atherosclerosis patients (Van der Valk et al. 2017). Along with the

activation of the haematopoietic system, increases in monocytosis or leukocytosis in atherosclerotic animal models as well as in humans have been demonstrated (Averill et al. 1989; Feldman et al. 1991; Madjid et al. 2004; Murphy et al. 2011; Madjid and Fatemi 2013; Heyde et al. 2021). Large meta-analyses reported an association between the presence of clonal haematopoiesis with increased incidence of atherosclerotic mortality and cardiovascular conditions (Jaiswal et al. 2014; Jaiswal et al. 2017; Evans et al. 2020; Min et al. 2020).

A variety of leukocytes contribute to the pathogenesis of atherosclerosis via secretion of pro-inflammatory cytokines and other mechanisms. Circulating monocytes are a heterogeneous population that accounts for 4% and 10% of nucleated blood cells in mice and humans respectively (Tahir and Steffens 2021). They can be distinguished based on their expression of surface antigens into two major populations in mice and humans: classical (Ly6-C^{hi} monocytes in mice analogous to $CD14^{+}$ $CD16^{-}$ monocytes in humans) and non-classical monocytes (Ly6-C^{low} monocytes in mice analogous to $CD14^{low}$ $CD16^{+}$ monocytes in humans)(Wolf et al. 2019). These different monocyte types differ not only in their phenotype but also in their function in atherosclerotic plaque formation and rupture. The classical monocytes are the most abundant subtype found in atherosclerotic plaques with potent pro-inflammatory activity; they account for 50% and 95% of the whole monocytes pool in mice and humans respectively (Kang et al. 2021). These monocytes adhere to activated ECs and are recruited to inflammation sites through their high expression of CCR-2 receptor, where they differentiate into macrophages (in particular M1 macrophages) or dendritic cells depending on the local cytokine environment (Kratofil et al. 2017; Kang et al. 2021). They act as highly phagocytic and scavenger cells (Mehu et al. 2022). The increase in the proportion of classical monocytes correlates with atherosclerosis severity in mice and humans (Swirski et al. 2007; Tacke et al. 2007; Kologrivova et al. 2020). On the other hand, the non-classical monocytes (with no expression of CCR-2) are patrolling cells that account for about 2–11% of circulating monocytes that monitor for endothelium injury in the context of homeostasis and vascular inflammation. In addition, they are considered as precursor cells of M2 macrophages and contribute to the resolution of inflammation by phagocytosising apoptotic M1 macrophages as well as tumour cells and viruses from the circulation. They have been widely

viewed as anti-inflammatory cells that promote tissue repair via stimulation of secretion of collagen (Kang et al. 2021; Tahir and Steffens 2021).

Besides monocytes and macrophages, atherosclerotic plaques contain a variety of other pro-inflammatory immune cells, such as neutrophils, NK cells, T cells, and B cells, which all play a key role in the inflammatory response. Neutrophils, such as granulocytes, have been found in early and advanced lesions (Döring et al. 2015). During the early stages of atherosclerosis, neutrophils move from the circulation to the arterial wall, where they roll on the endothelium and subsequently migrate into the intima and start to discharge their granules (Mehu et al. 2022). In the later stages, neutrophils undergo apoptosis which reduces inflammation. However, if the engulfment capacity of macrophages is overloaded and they cannot phagocytise the apoptotic neutrophils, the neutrophils become necrotic and contribute to inflammation. The neutrophil-to-lymphocyte ratio has recently attracted interest as an inflammation marker; increased neutrophils and decreased lymphocytes is a predictable marker for the occurrence, progression, and apoptosis in atherosclerosis lesions. The abundance of neutrophils correlates positively with macrophage abundance and lipid-rich necrotic core, and correlates negatively with collagen and smooth muscle cells (Murphy and Tall 2016; Mehu et al. 2022). Indeed, they play a crucial role in plaque destabilisation by inducing SMC death (Mehu et al. 2022). The depletion of neutrophils via repetitive injections of $ApoE^{-/-}$ mice with the Ly6G antibody showed a significant reduction in lesion burden (Döring et al. 2015). The NK cells have also been detected in advanced atherosclerotic plaques in human and mice as well as in the bloodstream (Palano et al. 2022). They can infiltrate to the arterial wall and contribute to atherosclerosis progression via production of perforin and granzyme B and/or cytokines such as IFN-γ, and hence promote plaque instability and atherothrombosis (Selathurai et al. 2014; Palano et al. 2022). A previous study performed in $ApoE^{-/-}$ mice that depleted NK cells observed a significant reduction in atherosclerotic lesion size (Selathurai et al. 2014). T cells and B cells are two other types of lymphocytes that have also received attention for decades because of their important roles as major drivers and modifiers of atherosclerotic lesion progression. T cells are key regulators of the adaptive immune system that are commonly identified by CD3 expression on their surface (Winkels and Wolf 2021). $CD4^+$ T or T helper cells (T_h) cells are one of the major subtype of T cells that when activated produce and release multiple cytokines such as IFN-γ, TNF-α and IL-2, and

hence contribute to atherosclerosis development (Mehu et al. 2022). In humans as well as in animal models, T_{h1} cells have been found to be the predominant type of T cells in atherosclerotic plaques, with a large body of evidence supporting their pro-atherogenic role (Baidya and Zeng 2005). It has been reported that T_{h1} cells are induced in the presence of IL-12 and IL-18 secreted by macrophages, resulting in the production IFN-γ (Tse et al. 2013). In addition to T_{h1} cells, Th_{17} cells have been observed in atherosclerotic plaque; it has been reported that differentiation of Th_{17} cells is driven by IL-6 and is characterised by IL-17 production (Chen et al. 2010). It has been suggested that Th_{17} cells modulate plaque inflammation and promote plaque rupture by inhibiting collagen expression. However, the exact role of Th_{17} cells is still being debated (Mehu et al. 2022). As Th_{17}, the role of T_{h2} cells in the development of atherosclerosis is under dispute with no clear role and opposite results from several studies (Mallat et al. 2009; Cardilo-Reis et al. 2012; Bartlett et al. 2019). In addition to T_h cells, $CD8^+$ T cells or cytotoxic T cells are the second subtype of T cells, they regulate monopoiesis and macrophage accumulation in early stages of atherosclerosis as well as being involved in macrophage death and necrotic core formation (Schäfer and Zernecke 2020). On the other hand, B cells exert pro- and anti-atherogenic activities that are dependent on their subsets and functional targeting (Schiller et al. 2002).

Collectively, there is no doubt that analysing the bone marrow stem, progenitor and differentiated lineage cell populations as well as circulating lymphoid and myeloid cell populations in the peripheral blood will shed light on the inflammatory status and severity of the disease. In the current study, the effect of RSV supplementation on haematopoietic activity along with circulating leukocytes was investigated using immunophenotyping.

4.1.5 Overview of experimental strategies

The experimental strategy used in this chapter is illustrated in Figure 4.2. Details of specific methodolgies for each experiment are detailed in Chapter 2.

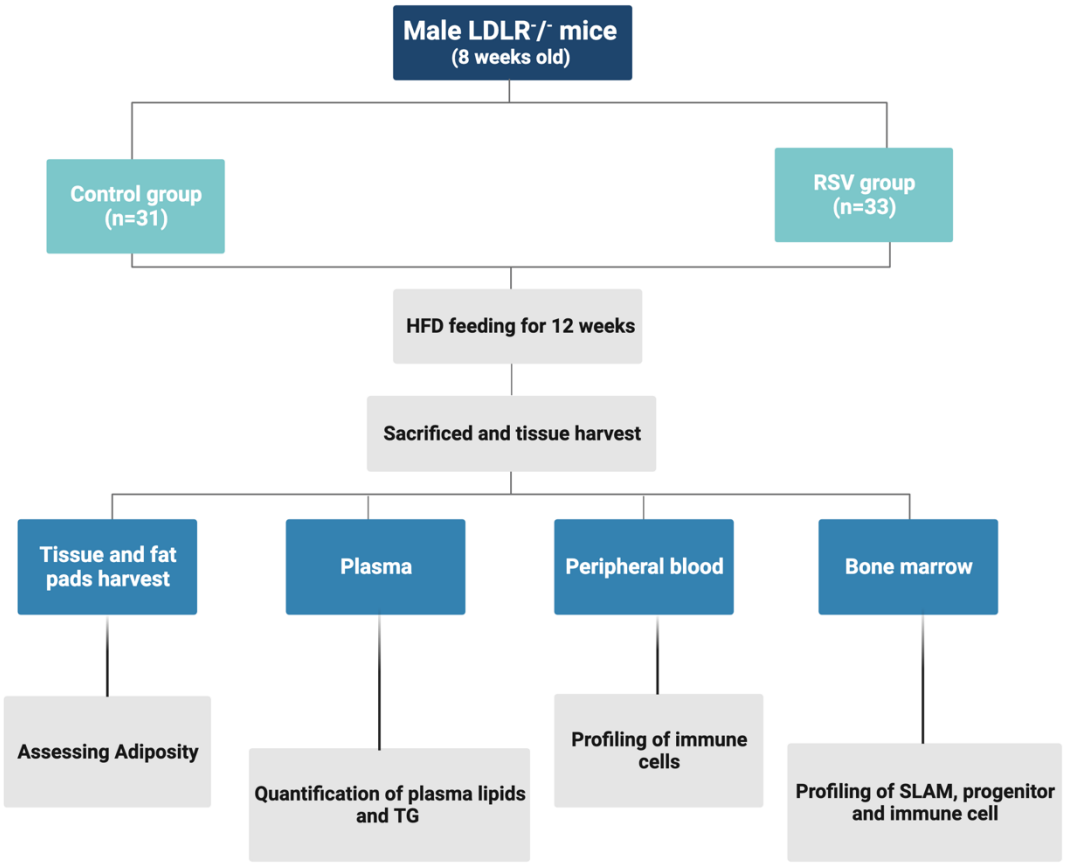

Figure 4.2 Experimental strategy used to investigate the effect of RSV on adiposity, lipid profile and immune cells *in vivo.*

Abbreviations: HFD, high fat diet; TG, triglyceride; SLAM, signaling lymphocyte activation molecules.

4.2 Results

4.2.1 RSV supplementation had no effect on the body weight and fat pads of LDLR$^{-/-}$ mice fed a HFD

Throughout the study, both mouse weight and HFD consumption were monitored and recorded every 2-3 days. This was performed to evaluate the change in mouse weight and amount of food consumed, in addition, to ensure that the mouse health was not affected and there were no issues related to the palatability of the HFD. As shown in Figure 4.3, there were no significant difference in either the final mouse weight or weight gained as well as no significant change in mouse weight change over the study period (i.e., rate of weight gain) between the RSV and control group. Additionally, there was no difference in the estimated amount of HFD consumption between the two groups (data not shown).

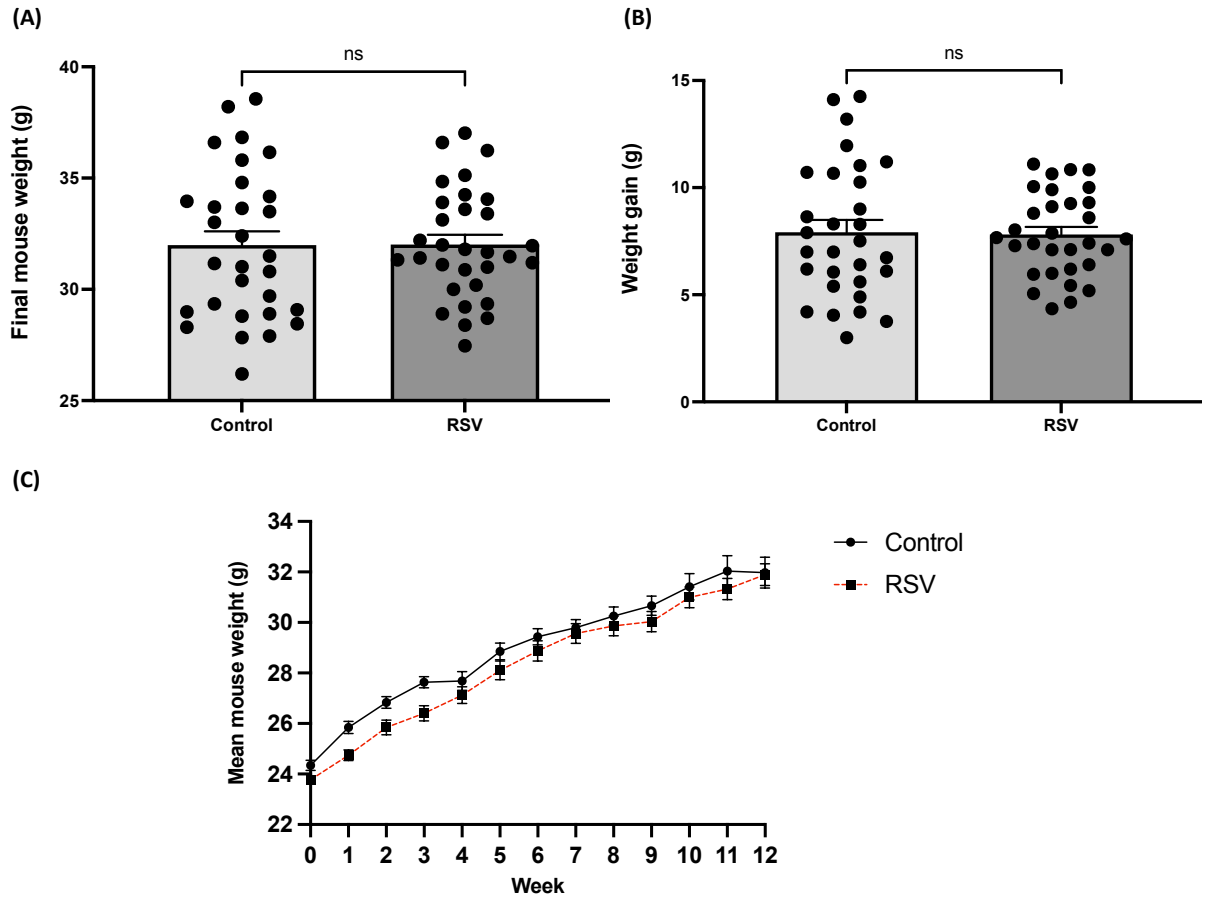

Figure 4.3 RSV supplementation had no effect on mouse body weight compared to the control group.

Male LDLR$^{-/-}$ mice were fed either HFD (Control) or HFD supplemented with 20 mg/kg/day RSV (RSV) for 12 weeks and mouse weights were recorded twice a week. The final mouse weight is shown in (A) while the mouse weight gain calculated from study start and end point is shown in (B). Data are presented as mean ± SEM from n= 30 control group and n=31 for RSV group. The rate of mouse weight gain per week is shown in (C). Statistical analysis was performed using an unpaired Student's t-test for (A and B) and linear regression for (C). **Abbreviations:** ns, not significant.

To investigate adiposity, the white fat pads (i.e., subcutaneous, inguinal, gonadal, and renal) in addition to brown fat were harvested and weighed at the end point. Due to the variances in mouse weight, all the measurements were standardised to the final body weight. As shown in Figure 4.4, there were no significant differences in either individual white fats or total white fats between the two groups. Additionally, RSV supplementation had no significant change on interscapular brown fat, total fat weights and ratio of brown to white fats (Figure 4.5).

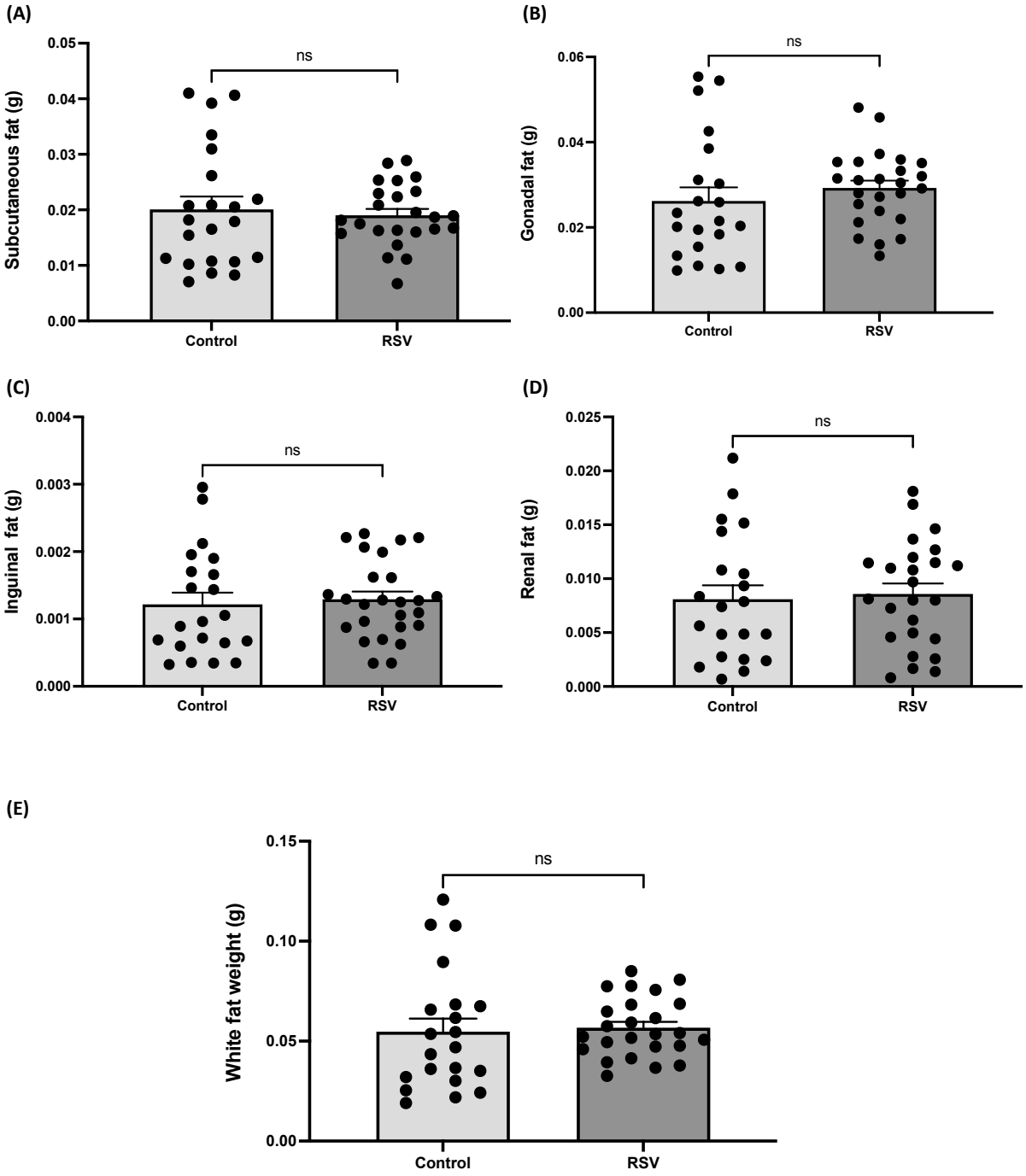

Figure 4.4 No significant changes were observed in weight of white fats following RSV intervention.

Male LDLR$^{-/-}$ mice were fed either HFD (Control) or HFD supplemented with RSV (RSV) for 12 weeks. The mice were then sacrificed and the subcutaneous (A), gonadal (B), inguinal (C) and renal (D) adipose tissue were harvested and weighed. The total of white adipose tissue was calculated as sum of subcutaneous, gonadal, inguinal, and renal fat. Data are presented as mean ± SEM from n=22 (A) or n= 21 (B, C, D or E) for control and n=24 (A), n=25 (B, D, or E) or n=26 (C) for RSV, and then standardised to final body weight. Statistical analysis was performed using Mann Whitney U test (A, B, C or E) or unpaired Student's t-test (D). **Abbreviations:** ns, not significant.

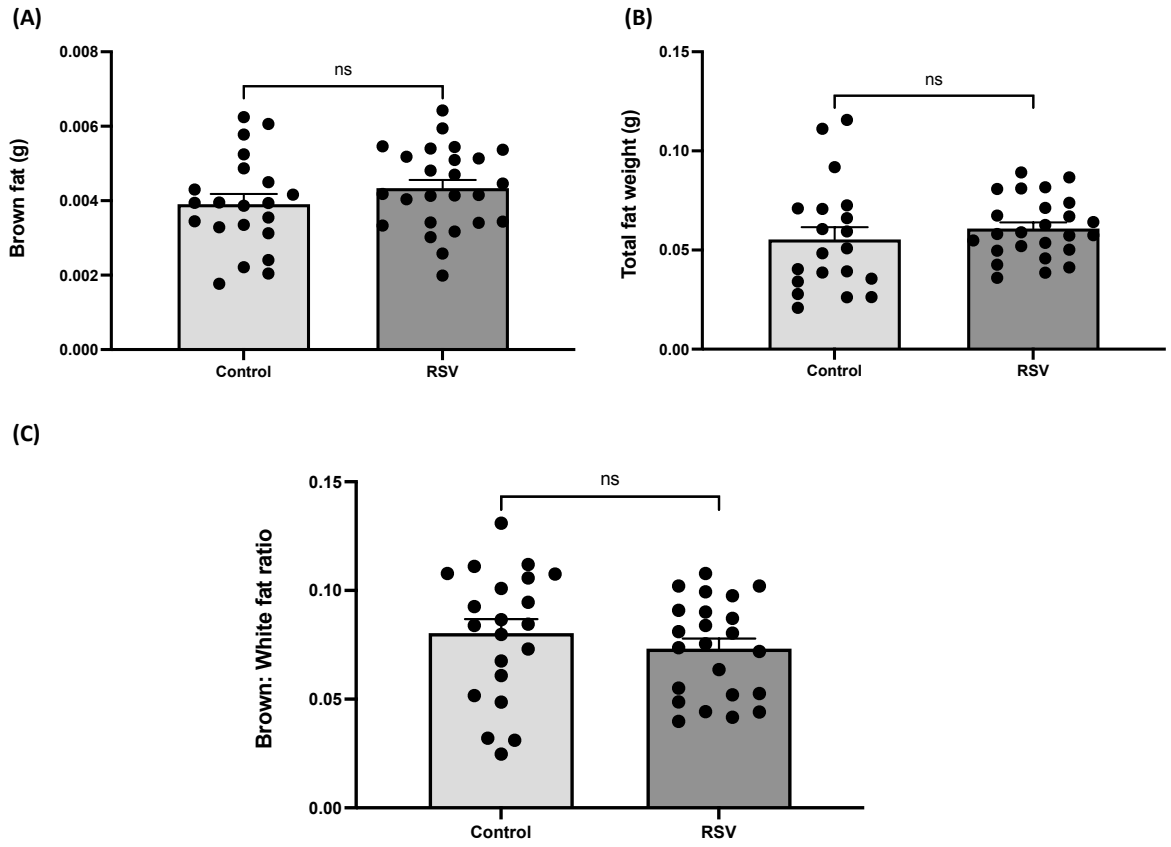

Figure 4.5 Mouse brown fat and total fat weights recorded at the end of the study.

Male LDLR$^{-/-}$ mice were fed either HFD (Control) or HFD supplemented with RSV (RSV) for 12 weeks. The mice were then sacrificed, and brown fat was harvested and weighed, and the measurements were standardised to final body weight. Total fat was calculated as a sum of all white and brown adipose tissue (C). Data are presented as mean ± SEM from n=21 (A and C) or n=20 (B) for control and n=25 (A, B or C) for RSV. Statistical analysis was performed using an unpaired Student's t-test. **Abbreviations:** ns, not significant.

4.2.2 RSV supplementation significantly reduced liver weight and produced a trend towards reduced heart weight in LDLR$^{-/-}$ mice fed a HFD

The weight of other key organs, including heart, liver, spleen, and thymus, were also determined to evaluate any abnormalities such as splenomegaly and cardiac hypertrophy in addition to any indication of other disorders such as NAFLD. There were no significant changes seen in the weight of the spleen and thymus between the RSV and the control group (Figure 4.6). However, the liver weight was significantly decreased in the RSV group compared to the control group by around 6% (p=0.003). There was a trend towards reduction of the heart weight in the RSV group by around 9% compared to the control group (p=0.054; Figure 4.6). Moreover, the cardiac hypertrophy index was calculated by dividing the heart weight (mg) with the tibia length (mm) determined at the time of bone marrow extraction.

Supplementation with RSV had no significant effect on the cardiac hypertrophy index (Figure 4.7).

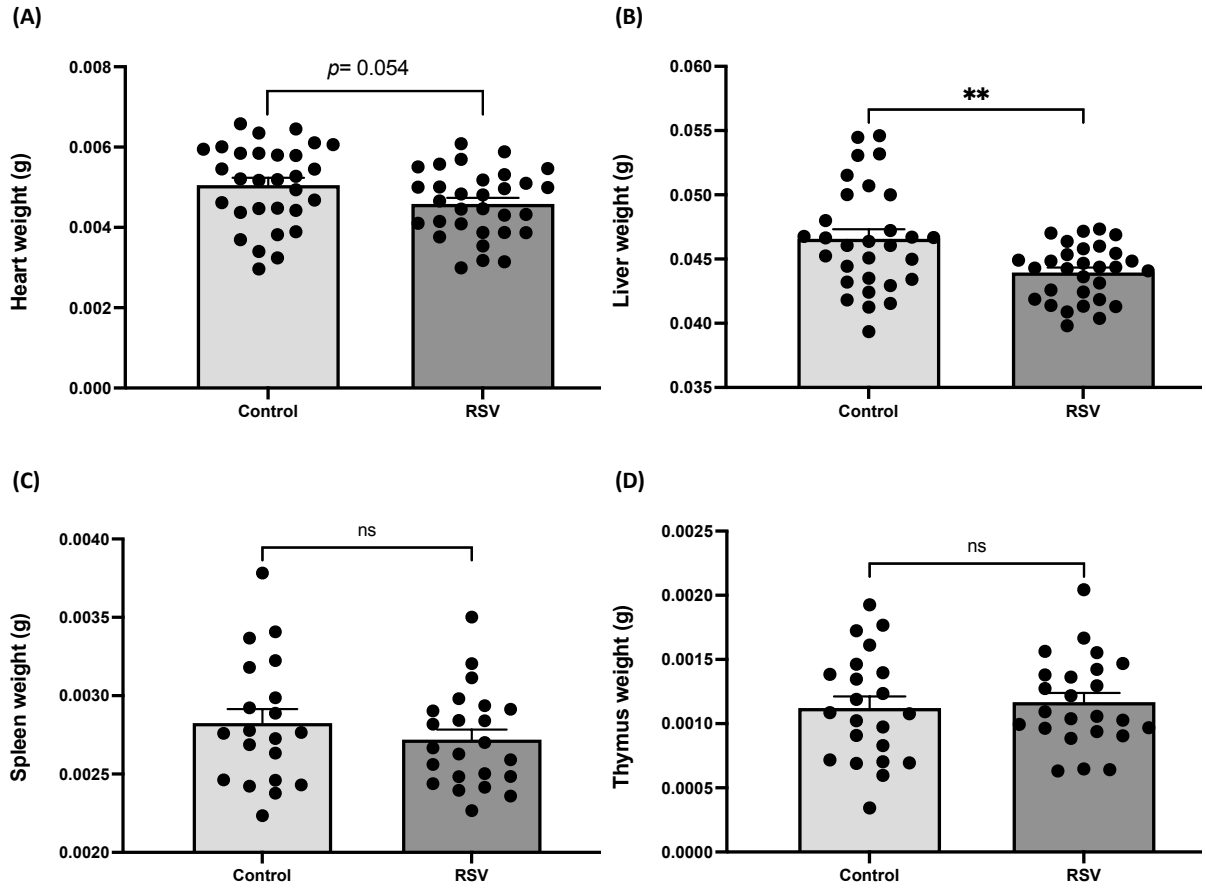

Figure 4.6 RSV supplementation significantly reduced liver weight and produced a trend towards reduction of heart weight.

Male LDLR^{-}/$^{-}$ mice were fed either HFD (Control) or HFD supplemented with RSV (RSV) for 12 weeks. The major organs were harvested and weighed at the end of study; all measurements have been standardised to the body weight. Data are from n=30 (A and B), n=20 (C) or n=22 (D) for control, and n=31 (A), 30 (B), 23 (C) or 24 (D) for RSV and are presented as mean ± SEM. Statistical analysis was via an unpaired Student's t-test where **$p \leq 0.01$. **Abbreviations:** ns, not significant.

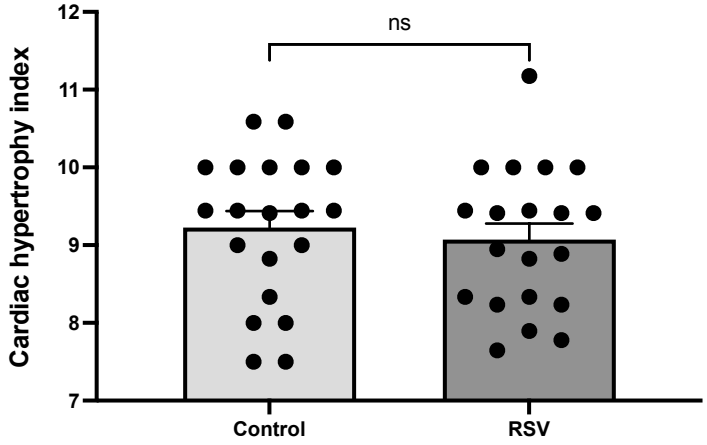

Figure 4.7 Cardiac hypertrophy index.

Cardiac hypertrophy index was calculated from male LDLR^{-}/$^{-}$ mice that were fed either HFD (Control) or HFD supplemented with RSV (RSV) for 12 weeks by dividing the heart weight (mg) over the tibia length (mm). Data are from n=20 for control and RSV group and are presented as mean ± SEM. Statistical analysis was via an unpaired Student's t-test. **Abbreviations:** ns, not significant.

4.2.3 RSV supplementation has beneficial effects on plasma cholesterol levels of LDLR^{-}/$^{-}$ mice fed a HFD

4.2.3.1 Lipid profile

The plasma was separated from the blood collected via cardiac puncture and used for plasma lipid profiling. Results presented in Figure 4.8B and F demonstrate a significant 23.2% reduction in plasma LDL/VLDL cholesterol ($p \leq 0.001$), in addition to a significant 45.2% ($p \leq 0.001$) decrease in CE levels in the RSV group compared to the control group. Furthermore, treatment with RSV showed a trend towards reduction in plasma levels of TC (Figure 4.8C) by 10% ($p=0.069$). The RSV group also showed an increase in HDL-C levels by around 20% though this was not significant (Figure 4.8A). The FC and TG levels were not affected by RSV intervention compared to the control group (Figure 4.8D and E).

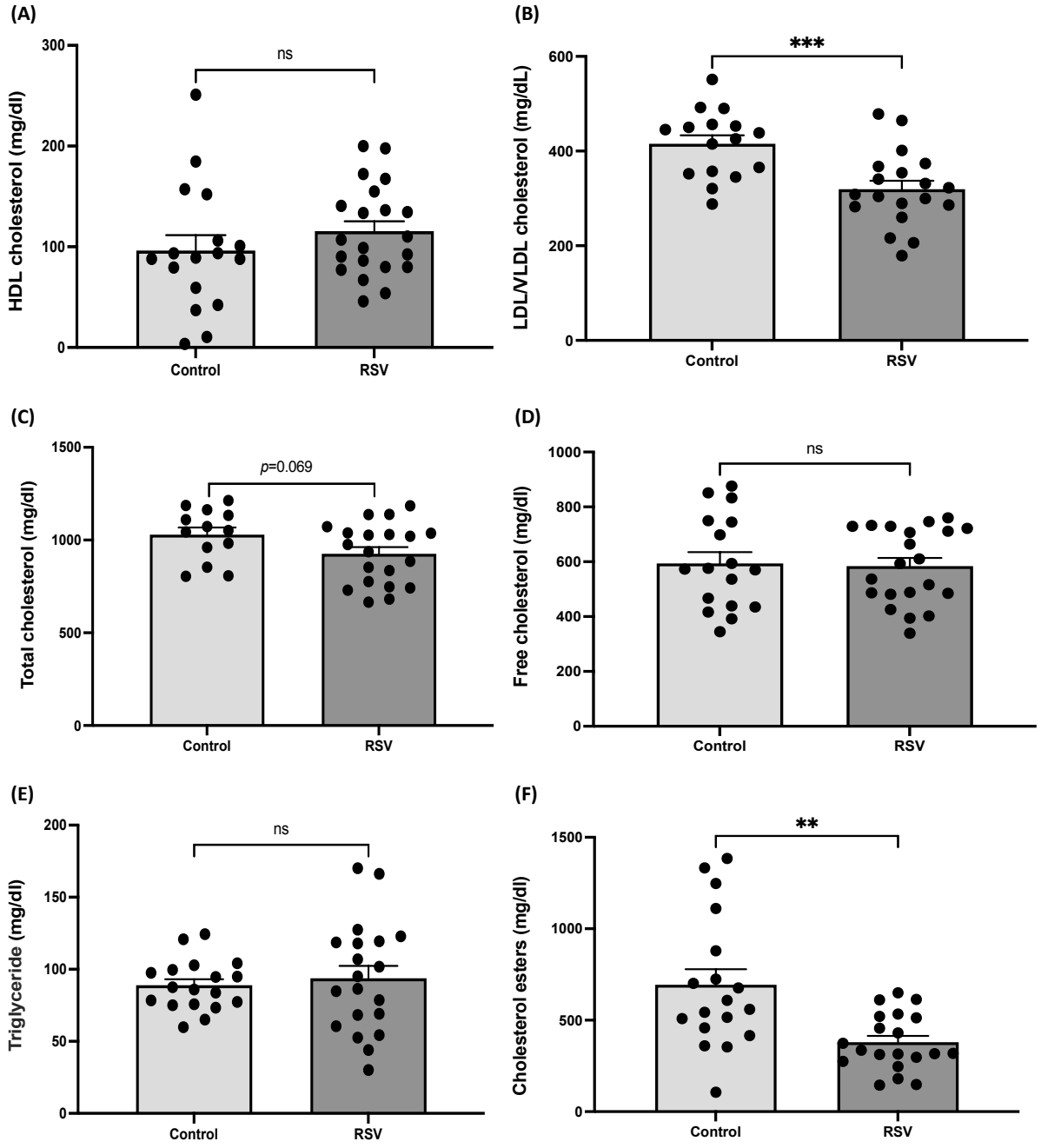

Figure 4.8 RSV supplementation has beneficial effects on plasma lipid profile.

Male LDLR$^{-/-}$ mice were fed either HFD (Control) or HFD supplemented with RSV (RSV) for 12 weeks. The plasma levels of HDL-C, LDL-C, TC and TG were measured using colorimetric assay kits. CE levels were calculated as the difference between the total and free cholesterol. Data are presented as mean ± SEM from n=17 (A and D), 16 (B), 13 (C) or 18 (E and F) for control group and n=21 (A and D), 19 (B) or 20 (C, E or F) for RSV group. Statistical analysis was performed using an unpaired Student's t-test for A, B, C, E and F with Mann Whitney U test used for C where $^{**}p \leq 0.01$ and $^{***}p \leq 0.001$. **Abbreviations:** ns, not significant.

4.2.3.2 Plasma lipid ratios

In addition to lipid levels in the plasma, their clinically relevant ratios were also determined. As shown in Figures 4.9A and C, the RSV group had a trend towards reduction in the ratio of LDL-C to HDL-C and TC to HDL-C by around 44% (p=0.082) and 23.3%(p=0.073) respectively. There were no significant changes seen in the other ratios.

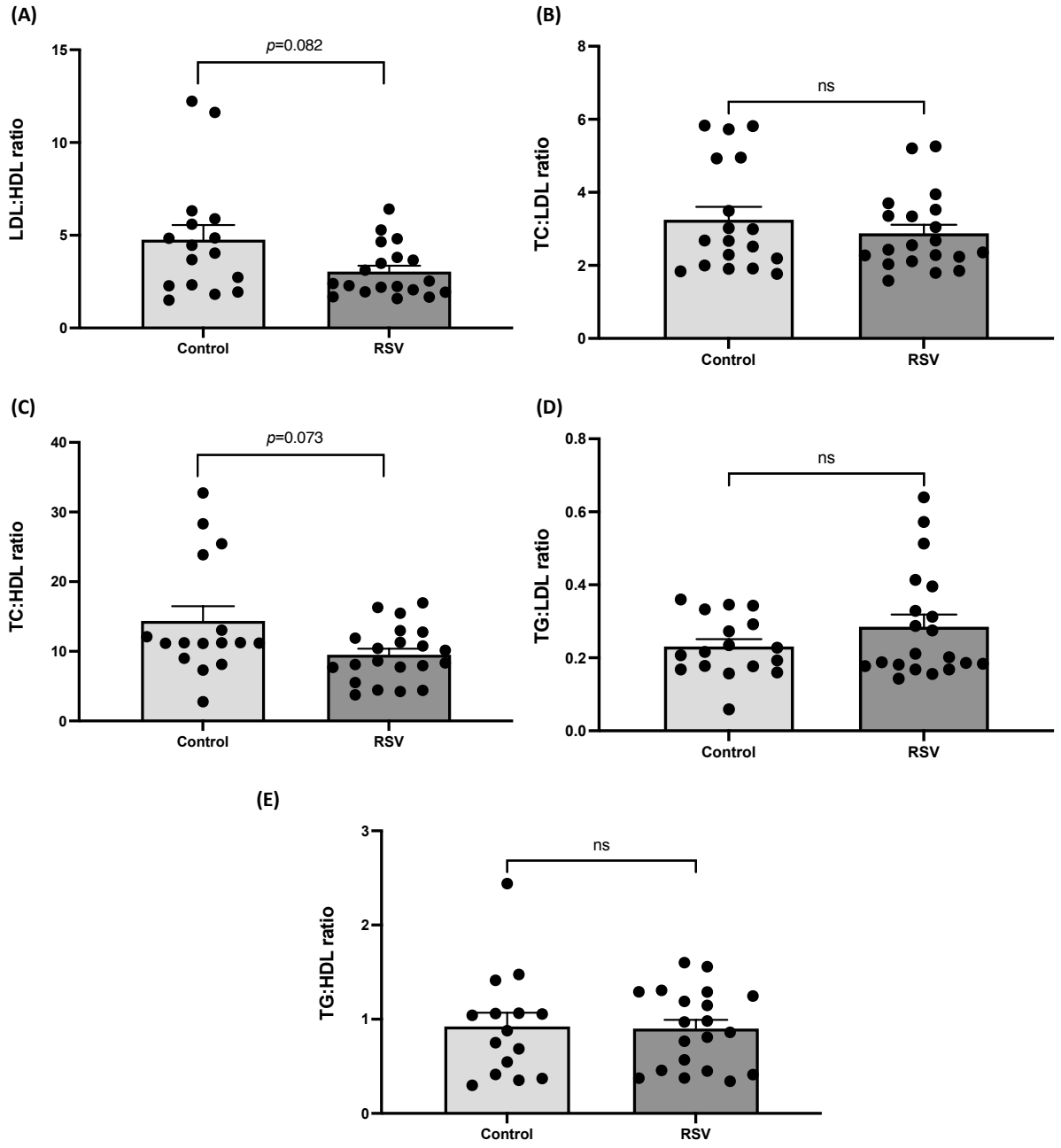

Figure 4.9 RSV supplementation has beneficial effects on lipid ratios compared to the control.

Male LDLR$^{-/-}$ mice were fed either HFD (Control) or HFD supplemented with RSV (RSV) for 12 weeks. The plasma levels of HDL-C, LDL-C, TC and TG were measured using colorimetric assay kits. Ratios were calculated using data presented in

Figure 4.8. Data are presented as mean ± SEM from n=16 (A and C), 18 (B) or 17 (D, E or F) for control group and n=19 (A), 20 (B, D, E or F) or 21 (C) for RSV group. Statistical analysis was performed using Mann Whitney U test (A - C) or unpaired Student's t-test (F). **Abbreviations:** LDL, low density lipoprotein; HDL, high density lipoprotein; TC, total cholesterol; TG, triglyceride; ns, not significant.

4.2.4 Bone marrow stem, progenitor, and immune cell population analysis

The inflammation condition of an individual can be detected within the bone marrow by measuring the number of white blood cells (WBCs) (Madjid and Fatemi 2013). Thus, the number of WBCs within the bone marrow was measured before starting immunophenotyping of the stem, progenitor, and immune cell populations. A shown in Figure 4.10, RSV produced a significant reduction in the number of WBCs in the bone marrow by approximately 40% ($p \leq$ 0.001) when compared to the control group. Because of the significant change in total WBCs count between the control and the treated group, the absolute cell number of each subsequent cell population was then determined rather than their frequency.

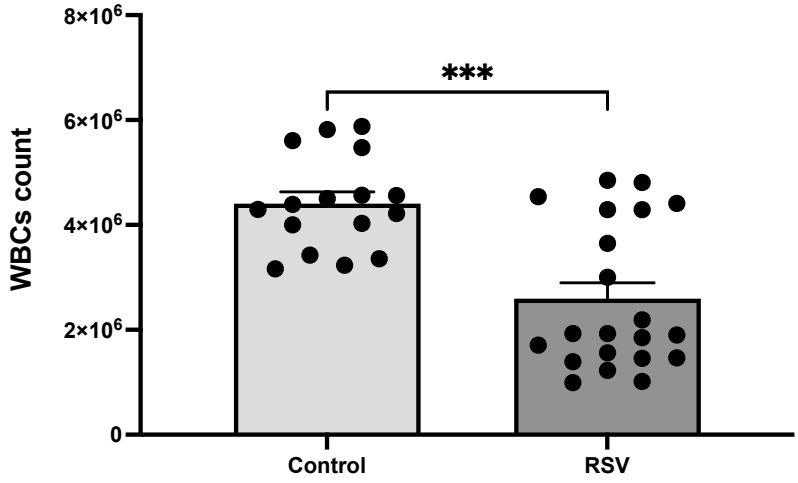

Figure 4.10 RSV significantly reduces WBCs count in the bone marrow of male LDLR^{-}/$^{-}$ mice fed HFD.

The total number of WBCs in the bone marrow of LDLR^{-}/$^{-}$ mice after receiving HFD alone (Control) or supplemented with RSV (RSV) was assessed using the Via1-Cassette™. Graph represents the total count of WBCs counts in 1 ml from the control and treated groups. Data are presented as mean ± SEM from 16 control and 21 RSV group. Statistical analysis was performed using Mann Whitney U test where *** $p \leq 0.001$.

4.2.4.1 RSV supplementation reduces the populations of stem cells within the bone marrow of LDLR^{-}/$^{-}$ mice fed a HFD

The stem cell populations (LSK, Lin^{-} Sca-1^{+} c-Kit^{+}), including HSCs, MPPs and haematopoietic progenitor cell I and II (HPC I and II), were then determined. Results for LSK and their compartments are shown in Figure 4.11B-F. Inclusion of RSV to HFD resulted in a significant attenuation in LKS (p= 0.003), HPC1(p= 0.002), HPC2($p\leq$ 0.001), HSCs ($p\leq$ 0.001) and MMP (p= 0.023) by more than 50% compared to the control group.

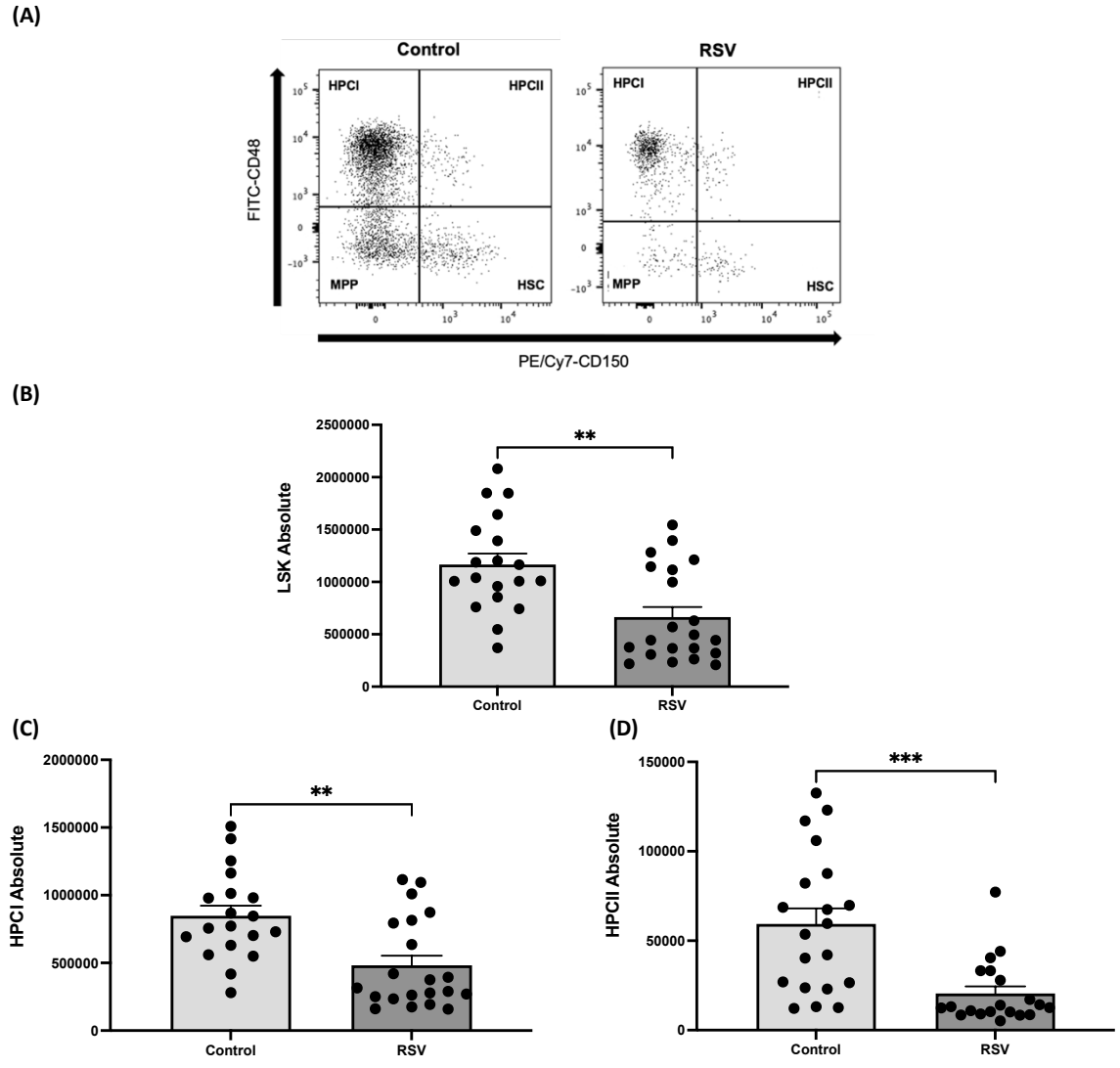

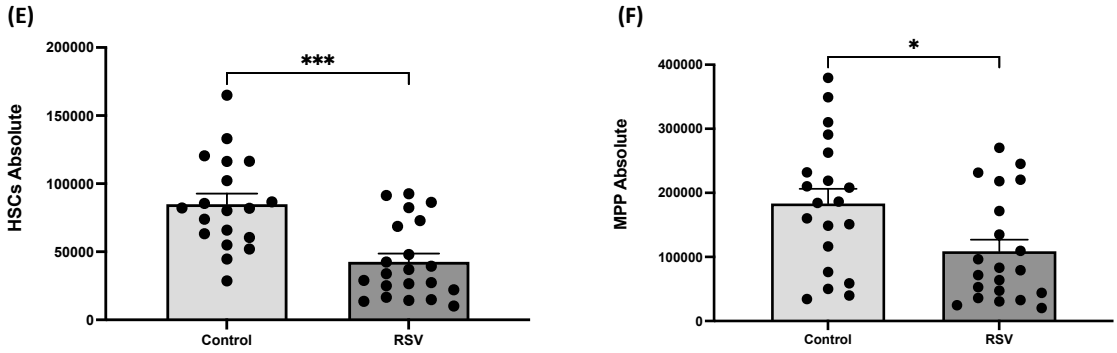

Figure 4.11 RSV supplementation significantly reduces stem cell populations in the bone marrow.

Immunophenotyping of bone marrow SLAM cell populations from LDLR^{-}/$^{-}$ mice was performed following 12 weeks feeding with either HFD (Control) or HFD supplemented with RSV (RSV). Representative dot plots along with the gating strategy are shown in panel A with graphs showing absolute numbers of LSK (B); HPC I (C); HPC II (D); HSCs (E); and MPP (F) populations. Data are presented as mean ± SEM from n=20 (B, D or F) or 19 (C or E) for control and n=21 (B, C, E or F) or 20 (D) for RSV group. Statistical analysis was performed using Mann Whitney U test where * $p \leq 0.05$, ** $p \leq 0.01$ and *** $p \leq 0.001$. **Abbreviations:** FITC, fluorescein isothiocyanate; PE/Cy7, phycoerythrin/cyanine7; LSK, Lin^{-} Sca-1^{+} c Kit^{+}; HPC, haematopoietic progenitor cell; HSC, haematopoietic stem cell; MPP, multipotent progenitors.

4.2.4.2 RSV supplementations decreases the populations of progenitor cells within the bone marrow of LDLR^{-}/$^{-}$ mice fed a HFD

The Lin^{-} Sca-1^{-} c-kit^{+}, universally known as LK cell population, was assessed within the bone marrow of LDLR^{-}/$^{-}$ mice fed HFD (control group) or treated with RSV. The levels of LK and their progeny, CLP, CMP, MEP and GMP, were found to be significantly affected in the presence of RSV when compared to the control mice. Thus, treatment with RSV significantly attenuates LK population by around 58% ($p \leq 0.001$) (Figure 4.12B), CMP by about 41% ($p \leq 0.001$), CLP by about 56% (p=0.001), MEP by about 66% ($p \leq 0.001$) and GMP by about 59% ($p \leq 0.001$) (Figure 4.12 C, D, E and F respectively).

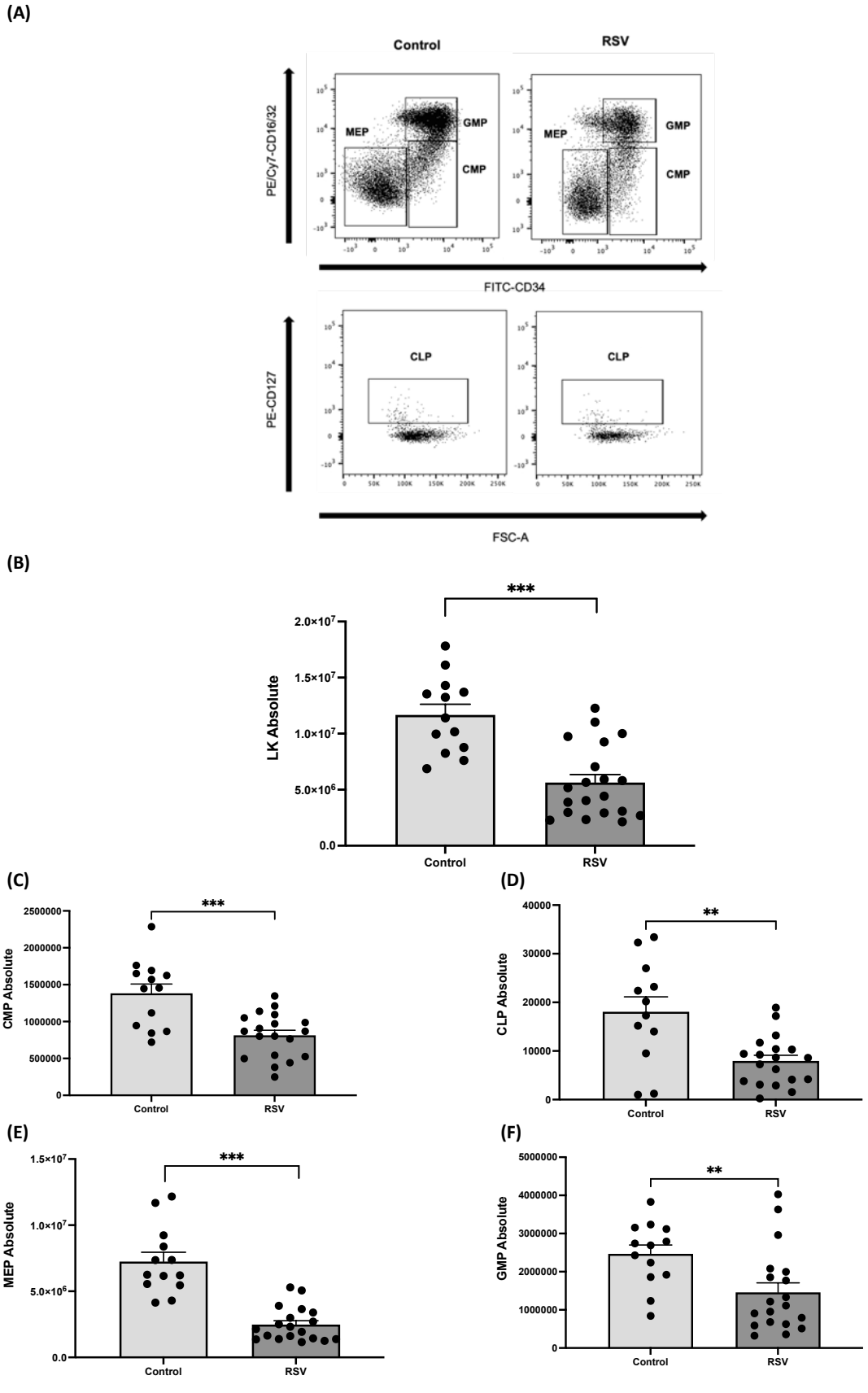
(A)
Control
RSV
PE/Cy7-CD16/32
MEP
GMP
CMP
FITC-CD34
PE-CD127
CLP
FSC-A
(B)
LK Absolute
***
Control
RSV
(C)
CMP Absolute
***
(D)
CLP Absolute
**
(E)
MEP Absolute
***
(F)
GMP Absolute
**

Figure 4.12 RSV supplementation significantly reduces progenitor cell populations within the bone marrow.

Immunophenotyping of bone marrow progenitor cell populations from LDLR^{-}/$^{-}$ mice was performed following 12 weeks feeding with either HFD (Control) or HFD supplemented with RSV (RSV). Representative dot plots along with the gating strategy are shown in panel A with graphs showing abosulte numbers of LK (B); CMP (C); GMP(D); MEP(E); and CLP (F) populations. Data are presented as mean ± SEM from n=13 (B, C, D or E) or 12 (F) for control and n=20 (B) or 19 (C, D, E or F) for RSV group. Statistical analysis was performed using Mann Whitney U test (B, D or E) and unpaired Student's t-test (C, F) where $^{**}p \leq 0.01$ and $^{***}p \leq 0.001$. **Abbreviations:** FITC, fluorescein isothiocyanate; PE, phycoerythrin; PE/Cy7, phycoerythrin/cyanine7; LK, Lin^{-} Sca-1- c Kit^{+}; CMP, common myeloid progenitor; CLP, common lymphoid progenitor; MEP, megakaryocyte-erythroid progenitor; GMP, granulocyte- macrophage progenitor.

4.2.4.3 RSV supplementation decreases the populations of lineage^{+} cells within the bone marrow of hypercholesterolemic LDLR^{-}/$^{-}$ mice

For the lineage^{+} class of cells, five populations were assessed in the bone marrow of male LDLR^{-}/$^{-}$ after 12 weeks of receiving HFD alone or supplemented with RSV: macrophages (Mac1^{+}); myeloid-derived suppressor cells (MDSC; Mac1^{+}/Gr1^{+}); B cells (B220^{+}); T cells (CD3^{+}); and erythroid cells (Ter119^{+}) (Figure 4.13). Inclusion of RSV to HFD resulted in a significant reduction in the levels of macrophages, MDSC and erythroid cells by about 52%, 64%, and 60% respectively ($p \leq 0.001$ in all cases). In addition, the levels of both lymphoid B cells and T cells were significantly attenuated by RSV by about 44% (p=0.002) and by about 53% (p=0.005) respectively.

(A)

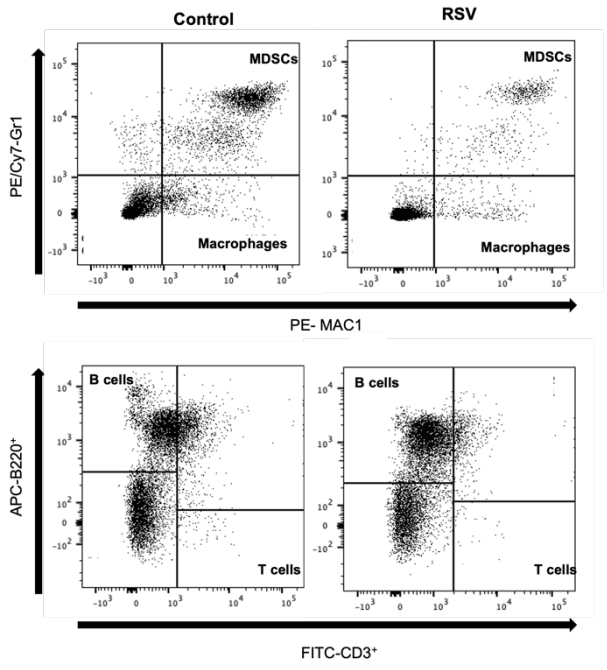

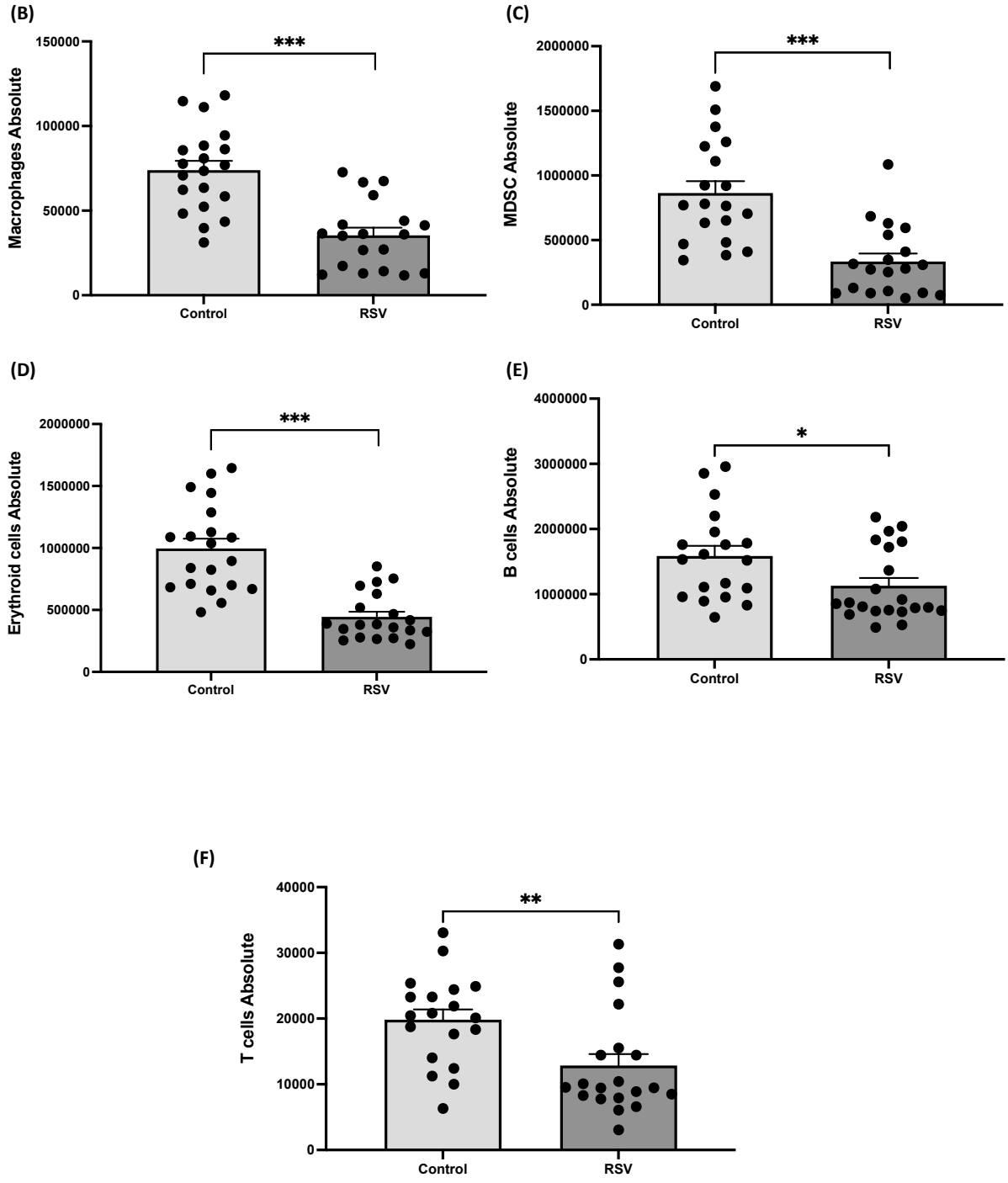

Figure 4.13 RSV supplementation significantly reduces lineage positive cell populations within the bone marrow.

Immunophenotyping of bone marrow lineage positive cell populations from LDLR^{-}/$^{-}$ mice was performed following 12 weeks feeding with either HFD (Control) or HFD supplemented with RSV (RSV). Representative dot plots along with the gating strategy are shown in panel A with graphs displaying absolute numbers of macrophages (B); MDSC (C); B cells (D); T cells (E); and erythroid cells (F). Data are presented as mean ± SEM from n=20 (B or F) or 19 (C, D or E) for control and n=19 (B or C), 21 (D) or 20 (E or F) for RSV group. Statistical analysis was performed using unpaired Student's t-test (B) or Mann Whitney U test (C, D, E or F) where *$p \leq 0.05$, **$p \leq 0.01$ and ***$p \leq 0.001$. **Abbreviations:** PE, phycoerythrin; PE/Cy7, phycoerythrin/cyanine7; FITC, fluorescein isothiocyanate; APC, allophycocyanin; MDSC, myeloid-derived suppressor cells

4.2.5 Analysis of peripheral blood immune cell populations

4.2.5.1 RSV produced a trend towards reduction of some lymphoid cell populations in peripheral blood of LDLR^{-}/$^{-}$ mice fed a HFD

From the analysis of the lymphoid cell population, RSV produced a trend towards reduction in the proportion of B cells by about 5% (p=0.068) (Figure 4.14D), and CD3^{+} T cells and CD8^{+} T cells by about 12% (p=0.082) and 13% (p=0.089) respectively (Figure 4.1E and 4.1F respectively). However, RSV produced no significant changes in the proportion of CD4^{+} T cells and NK cells (Figure 4.14G and H).

(A)

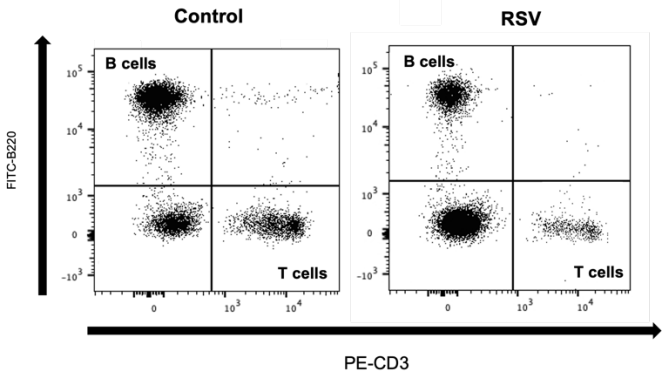

(B)

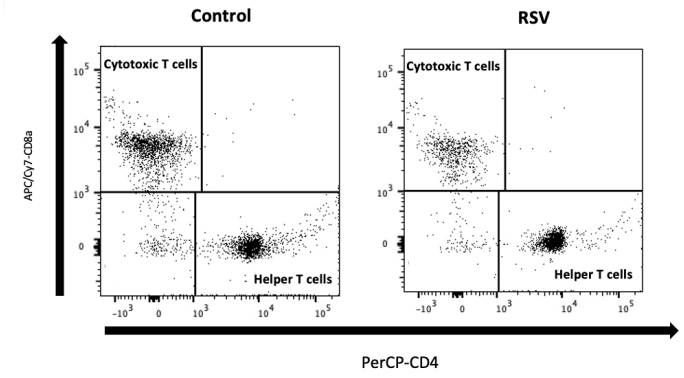

(C)

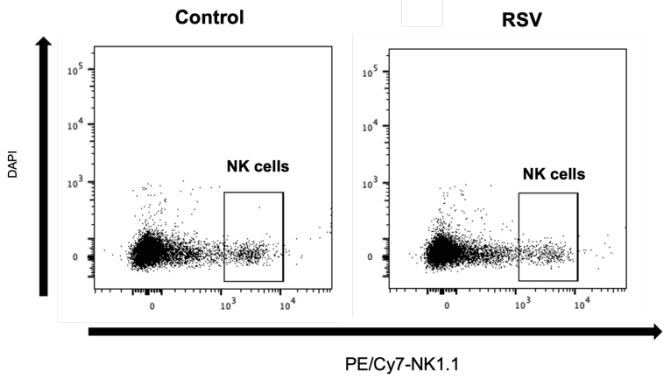

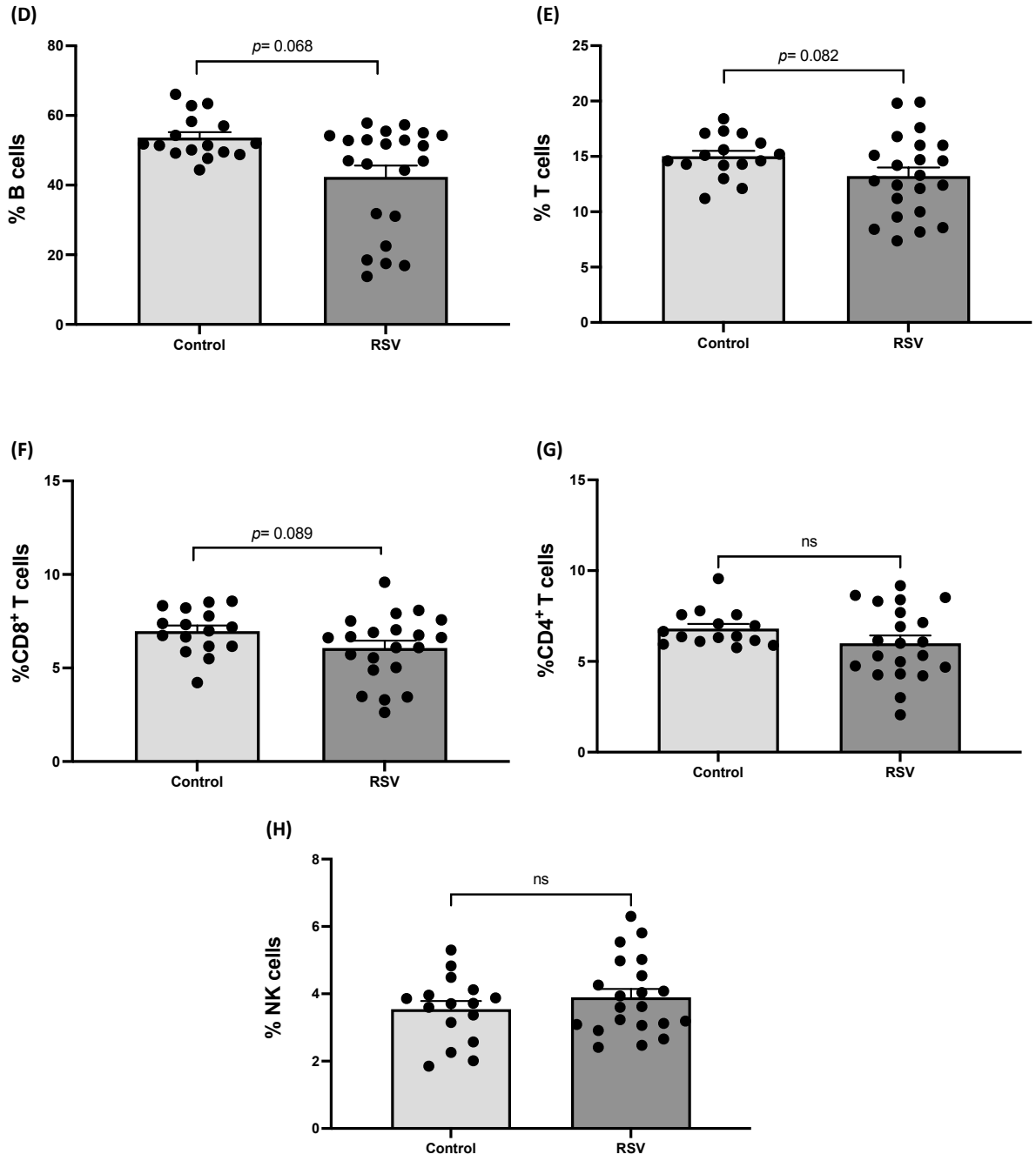

Figure 4.14 Effect of RSV supplementation on lymphoid cell populations in the peripheral blood.

Immunophenotyping of lymphoid cell populations in the peripheral blood from LDLR$^{-/-}$ mice was performed following 12 weeks feeding of either HFD (Control) or HFD supplemented with RSV (RSV). Representative dot plots along with the gating strategies for FITC- B220^{+} (B cells) and PE-CD3^{+} (T cells) (A); PerCP-CD4^{+} T cells and APC/Cy7-CD8^{+} T cells (B); and PE/Cy7-NK1.1^{+} (NK cells) (C) are displayed. Data are calculated as percentage of total white blood cells and presented as mean ± SEM for different cell populations as indicated from n=16 (D, E, F or H) or 15 (G) for control and n=22 (D or E) or 21 (F, G or H) RSV group. Statistical analysis was performed using unpaired Student's t-test (E, F or H) or Mann Whitney U test (D or G). **Abbreviations:** FITC, fluorescein isothiocyanate; PE, phycoerythrin; PerCP, peridinin-chlorophyll-protein; APC/CY7, allophycocyanin/cyanine7; NK, natural killer; ns, not significant.

4.2.5.2 RSV has no significant effect on myeloid cell populations

Analysis of the myeloid cell populations in the peripheral blood includes granulocytes and monocytes as well as monocyte subsets (Ly6C^{high} monocytes and Ly6C^{Low}monocytes) (Figure 4.15). RSV produced no significant changes in the populations of granulocytes (Figure 4.15D), monocytes (Figure 4.15E) or the subsets of Ly6C^{high} monocytes (Figure 4.15F) and Ly6C^{Low}monocytes (Figure 4.15G) compared to the control.

(A)

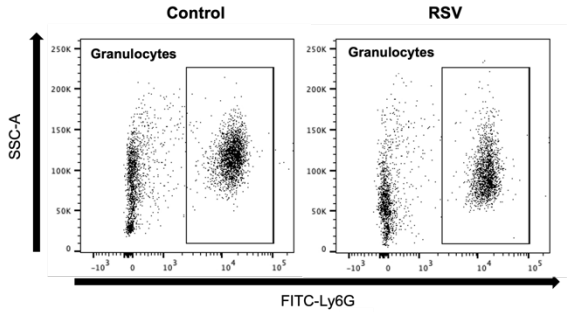

(B)

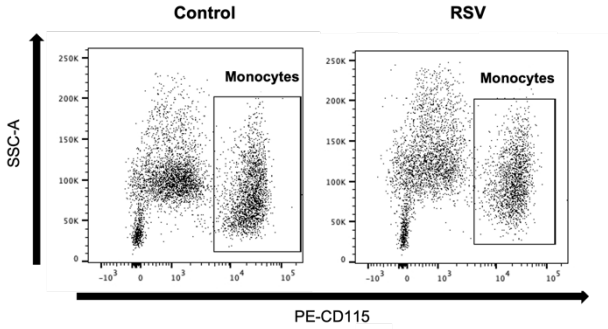

(C)

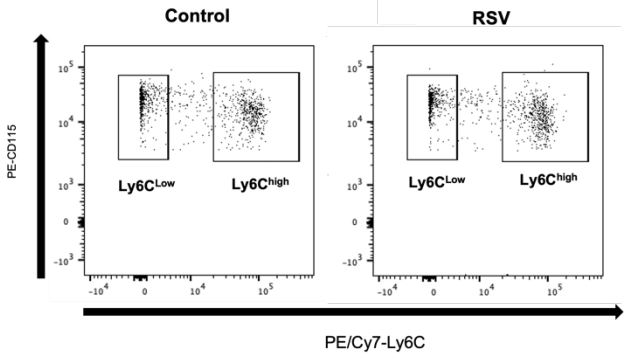

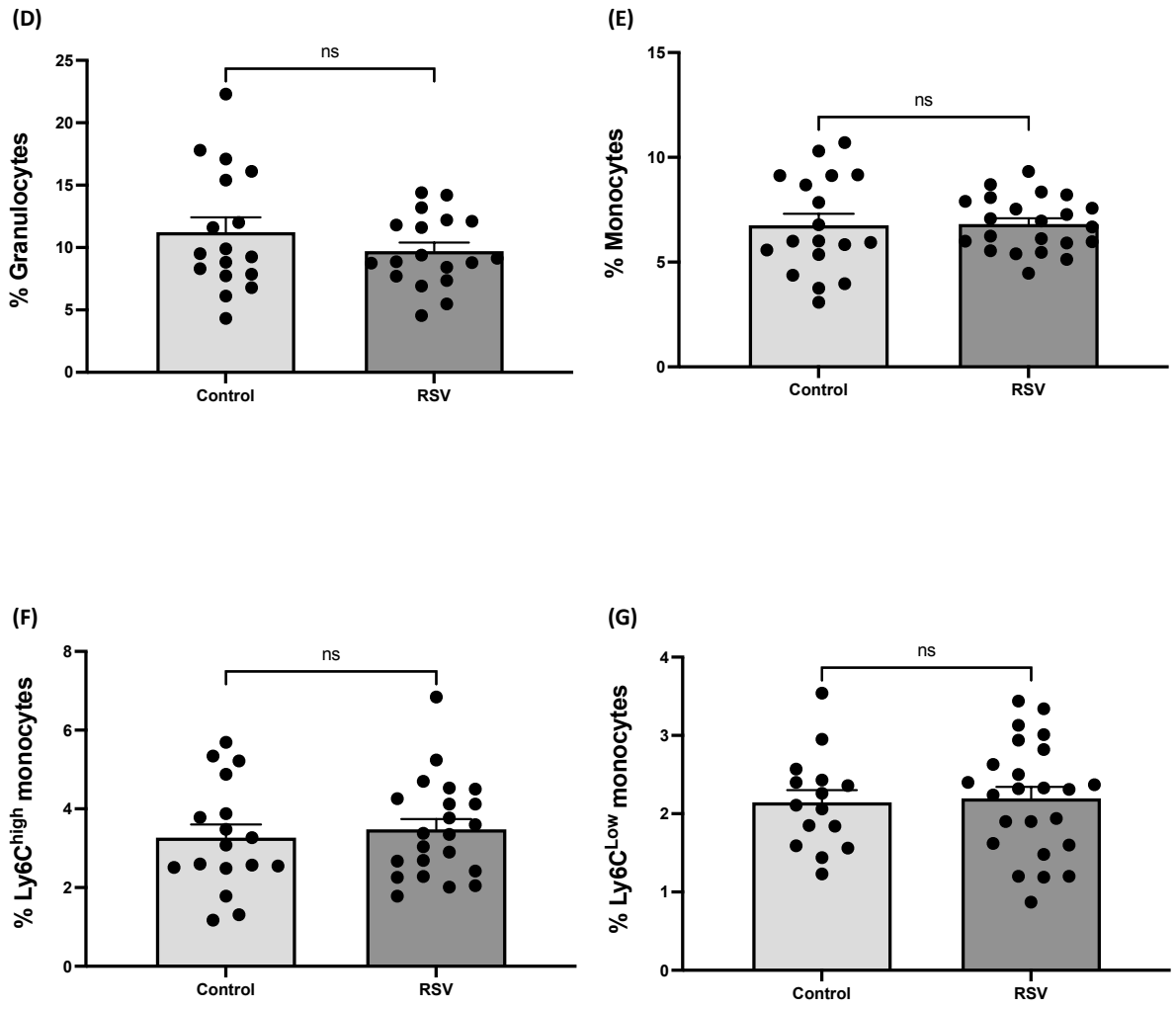

Figure 4.15 RSV has no significant effect on myeloid cell populations.

Immunophenotyping of lymphoid cell populations in the peripheral blood from LDLR$^{-/-}$ mice was performed following 12 weeks feeding of either HFD (Control) or HFD supplemented with RSV (RSV). Representative dot plots along with the gating strategies for FITC- Ly6G^{+} granulocytes (A), PE-CD115^{+} monocytes (B) and PE/Cy7- Ly6C$^{low/high}$ monocytes are shown. Data for different myeloid cell populations are calculated as percentage of total white blood cells and presented as mean ± SEM from n=17 (D or F), 18 (E) or 15 (G) for control and n=18 (D), 22 (E or F) or 24(G) for RSV group. Statistical analysis was performed using unpaired Student's t-test. **Abbreviations:** FITC, fluorescein isothiocyanate; PE, phycoerythrin; PE/CY7, phycoerythrin/cyanine7; ns, not significant.

.

4.3 Discussion

In light of the promising findings obtained from *in vitro* studies (presented and discussed in Chapter 3), the project continued to *in vivo* studies to explore the effect of RSV supplementation in a mouse model system. The ability of RSV to affect atherosclerosis and its associated factors have been shown by several studies in different animal models (Prasad 2012). However, no study has yet reported the potential effect of RSV to prevent atherogenesis or disease development in detail using the $LDLR^{-/-}$ mouse model system; hence, the aims of this chapter was to fill this gap in research. Mice receiving RSV (20 mg/kg/day) for 12 weeks demonstrated multiple beneficial changes in relation to atherosclerosis and its associated risk factors. For instance, a reduction in the plasma levels of LDL/VLDL-C and CE in addition to LDL:HDL and TC:HDL ratios were observed. Furthermore, several favourable changes were seen in LSK and LK cell populations and their progenies along with mature immune cells within the bone marrow. In the peripheral blood, administration of RSV was found to exhibit a tendency towards reducing lymphoid cells, in particular B cells, $CD3^+$ T cells and $CD8^+$ T cells. The findings of the research so far strongly suggest potential anti-atherosclerotic function of RSV and support the potential of RSV as a promising candidate for supressing atherogenesis. Table 4.1 shows a summary of data presented in this Chapter (significant changes or changes with a trend towards significance are highlighted).

Table 4.1 Summary of changes produced in male LDLR^{-}/$^{-}$ mice fed HFD with RSV

Effects of RSV on the progression of atherosclerosis				
	Male			
	Control Mean	RSV Mean	Change	Significance
Overall weight gain (g)	7.92	7.81	NC	NS
Body fat (mg) – normalised				
Total	0.055	0.06	NC	NS
Total white fat	0.055	0.057	NC	NS
Brown fat	0.003	0.004	NC	NS
Brown: white ratio	0.080	0.073	NC	NS
Subcutaneous	0.02	0.019	NC	NS
Gonadal	0.026	0.029	NC	NS
Inguinal	0.001	0.001	NC	NS
Renal	0.008	0.008	NC	NS
Cardiac hypertrophy index	9.22	9.07	NC	NS
Organ weights (mg) -normalised				
Heart	0.005	0.004	↓Trend	p=0.054
Liver	0.047	0.044	↓	p=0.003
Spleen	0.003	0.002	NC	NS
Thymus	0.001	0.001	NC	NS
Plasma lipoproteins (mg/dL)				
TG	88.5	93.8	NC	NS
TC	1029.3	925.7	↓Trend	p=0.070
FC	593.9	583.8	NC	NS
HDL cholesterol	96.3	115.5	NC	NS
LDL/VLDL cholesterol	412.6	319.3	↓	$P \leq 0.001$
CE	693.7	379.7	↓	p=0.001
Plasma lipid ratios				
LDL:HDL	7.1	3.0	↓Trend	p=0.080
TC:HDL	14.4	9.5	↓Trend	p=0.070
TC:LDL	3.3	2.9	NC	NS
TG:LDL	0.23	0.29	NC	NS
TG:HDL	1.5	0.88	NC	NS
WBCs count				
Total WBCs	$4.4x10^6$	$2x10^6$	↓	$p \leq 0.001$
SLAM cells in bone marrow (Absolute)				
LSK	$1.2x10^6$	$6.6x10^5$	↓	p=0.002
HPC1	$8.5x10^5$	$4.8x10^5$	↓	p=0.002
HPC2	$5.9x10^4$	$1.8x10^4$	↓	$p \leq 0.001$
HSCs	$8.5x10^4$	$4.3x10^4$	↓	$p \leq 0.001$
MPP	$1.8x10^5$	$1.1x10^5$	↓	p=0.023
PROG cells in bone marrow (Absolute)				
LK	$7.6x10^6$	$5.6x10^6$	↓	$p \leq 0.001$
CMP	$8.9x10^5$	$8.1x10^5$	↓	$p \leq 0.001$
GMP	$1.6 x10^6$	$1.5 x10^6$	↓	p=0.005
MEP	$4.7x10^6$	$2.5x10^6$	↓	$p \leq 0.001$
CLP	$1.1x10^4$	$7.9x10^3$	↓	p=0.001

Lineage$^+$ cells in bone marrow (Absolute)				
B cells	$1.6x10^6$	$1.1x10^6$	↓	p=0.017
T cells	$1.9x10^4$	$1.3x10^4$	↓	p≤0.001
Macrophages	$7.3x10^4$	$3.5x10^4$	↓	p≤0.001
MDSCs	$8.6x10^5$	$3.3x10^5$	↓	p=0.005
Erythroid	$9.9x10^5$	$4.4x10^5$	↓	p≤0.001
Peripheral blood – Lymphoid cells (frequency of nucleated cells)				
B cells	53.5	42.3	↓Trend	p=0.068
T cells	15	13.2	↓Trend	p=0.080
CD4	6.8	5.9	NC	NS
CD8	6.9	6	↓Trend	p=0.090
NK cells	3.5	3.9	NC	NS
Peripheral blood – Myeloid cells (frequency of nucleated cells)				
Monocytes (CD115$^+$)	6.8	6.8	NC	NS
Ly6C ^{High} monocytes	3.3	3.5	NC	NS
Ly6C ^{Low} monocytes	2.1	2.2	NC	NS
Granulocytes	11.2	9.7	NC	NS

Significance was defined as p≤0.05 while trend of significance was defined as 0.1<p<0.05. Significant changes or changes with a trend towards significance are highlighted.

Abbreviations: NC, no change; NS, not significant; ↓, decrease; TG, triglycerides; TC, total cholesterol; FC, free cholesterol; CE, cholesterol esters; HDL, high density lipoprotein; LDL, low density lipoprotein; LSK, Lin$^-$ Sca-1$^+$ c Kit$^+$; HPC, haematopoietic progenitor cell; HSC, haematopoietic stem cell; MPP, multipotent progenitors; **:** LK, Lin$^-$ Sca-1$^-$ c Kit$^+$; CMP, common myeloid progenitor; CLP, common lymphoid progenitor; MEP, megakaryocyte-erythroid progenitor; GMP, granulocyte- macrophage progenitor; MDSC, myeloid-derived suppressor cells; NK, natural killer.

4.3.1 The effect of RSV on mice adiposity

RSV supplementation had no significant effect on the final body weight or gain of weight (Figure 4.3) as well as weight of adipose tissue depots (Figure 4.4 and 4.5) compared to the control group. A previous study using HFD-fed ApoE^{-}/$^{-}$ mice demonstrated a suppression of HFD-induced weight gain and fat accumulations after administration of 0.02% RSV in diet for 12 weeks (Jeon et al. 2014). Similar findings were reported in HFD-fed C57BL/6J and C57BL/6C mice after receiving RSV via gavage at different concentrations for 16 and 10 weeks respectively (Chang et al. 2016; Wang et al. 2020c). Contrary to this, further studies in 50 KM mice and C57BL/6RJ mice fed HFD noted no change in mice body weight after injection of RSV either intragastrically (10, 20, and 40 mg/kg for 6 weeks) or intraperitoneally (24 mg/kg for 8 weeks) respectively (Xie et al. 2014; Pallauf et al. 2019). Such differences in results could potentially be because of several factors, including RSV dosage, duration of intervention, way of administration (e.g., gavage or IP injections) and mouse strain used. In this study, no changes were also observed in the weights of the spleen and thymus; however, liver and heart

weights were significantly decreased or showed a trend towards reduction respectively in RSV-treated group compared to the control (Figure 4.6). Increase in liver weight has been associated with hepatic steatosis that consequently causes NAFLD and contributes to increased risk of preclinical atherosclerosis (Zhou et al. 2018b; Pilling et al. 2021). The result is in agreement with a systematic review that showed the ability of RSV to act as a hepatoprotective agent by reducing hepatic steatosis and several other associated mechanisms *in vivo* and *in vitro* (Faghihzadeh et al. 2015). In this context, further investigations on RSV intervention on the liver were carried in this project and are described in Chapter 7. In relation to heart weight, an increase has been reported in obese animals and humans due to the accumulation and infiltration of lipids (particularly TG) (Lucas et al. 2016; Bruder-Nascimento et al. 2017). Compelling evidence from the literature indicates a strong correlation between increased lipid accumulation in cardiac tissue and cardiac dysfunction such as cardiac hypertrophy. The data obtained in this study suggest a beneficial effect of RSV against HFD-induced changes in the heart though significant changes in cardiac hypertrophy were not seen (Figure 4.7). However, further investigations such as extraction of total lipids and fatty acids from the heart tissue should shed light to the mechanisms underlying the potential beneficial effects of RSV on the heart.

4.3.2 The effect of RSV on plasma lipid profile

Supplementation with RSV resulted in a significant reduction in LDL/VLDL cholesterol, TC and CE levels and a non-significant increase in HDL-C while no change was observed in TG and FC levels (Figure 4.8). These data are consistent with various other studies that have reported the ability of RSV to decrease plasma levels of TC and LDL-C in animal models and humans (Fukao et al. 2004; Rivera et al. 2009; Xie et al. 2014; Simental-Mendía and Guerrero-Romero 2019; Zhou et al. 2020; Ji et al. 2022). Recently, a significant reduction was observed in atherosclerotic lesion size in ApoE^{-}/$^{-}$ mice along with the reduction in plasma lipid profile after treatment with RSV (Ji et al. 2022). In contrast to these aforementioned studies, RSV failed to show a change in lipid profile in ApoE^{-}/$^{-}$/LDLR^{-}/$^{-}$ mice and New Zealand rabbits; however, this did not influence the ability of RSV to significantly suppress atherosclerotic lesion size (Wang et al. 2002; Fukao et al. 2004; Wang et al. 2005). The lack of reduction in TG levels and a non-significant increase in HDL-C following RSV treatment are similar to previous studies using rats

receiving a HFD as well as a recent meta-analysis in patients with metabolic syndrome, where no effect was seen in TG and HDL-C after RSV intervention (Wang et al. 2005; Akbari et al. 2020).

The current study showed a trend towards reduction in LDL:HDL and TC:HDL ratios (Figure 4.9). These results are in line with previous studies that demonstrated a reduction in LDL:HDL ratio with higher or no change in HDL-C levels (Chen et al. 2012; Chang et al. 2015a). Collectively, reduction in LDL-C, TC and CE along with LDL-C and TC to HDL-C ratio seen in this study are promising findings.

4.3.3 The effect of RSV on stem, progenitor and immune cells in the bone marrow

Previous studies have shown a strong relationship between the levels of an individual's WBCs and CHDs where the total number of WBCs can be used as an indicator of severity of CHDs as well as atherosclerosis progression (Ates et al. 2011; Kim et al. 2017; Mozos et al. 2017). In the current study, a significant reduction in count of WBCs was observed following 12 weeks of feeding HFD supplemented with RSV compared to the control group (Figure 4.10). This result is consistent with a previous study that demonstrated attenuation of inflammation in rats after RSV administration via reduction in WBCs and other inflammatory markers (Hişmioğulları et al. 2013). The potential of RSV as an anti-inflammatory agent was also suggested by the levels of stem, progenitors and lineage cell population being significantly decreased in RSV-treated group compared to the control (Figure 4.11-13).

Based on previous studies, elevation in HSPCs is highly associated with hypercholesterolaemia while reducing cholesterol levels results in a reduction in hypercholesterolaemia-induced proliferation of HSPCs (Feng et al. 2012; Lang and Cimato 2014; Ma and Feng 2016). Moreover, hypercholesterolaemia enhances proliferation of HSCs, their mobilisation into the bloodstream and their differentiation into inflammatory monocytes that then participate in an inflammatory response (Lang and Cimato 2014; Ma and Feng 2016; Vanhie et al. 2020). In contrast to the results obtained in this study, an earlier study investigating the effect of RSV on HSPC compartments in the bone marrow of C57BL/6 mice showed a significant increase in the frequency and total number of LSK cells and multipotent progenitor cells after 3 weeks of

administration (Rimmelé et al. 2014). In addition, this study showed that the effect of RSV is strongly associated with both the dose and the duration of the treatment (Rimmelé et al. 2014).

Similar to LSK and their progenies, the LK population usually expands during disease progression and relocates to the spleen where they differentiate into monocytes and macrophages (Robbins et al. 2012). A previous study demonstrated that HFD is capable of stimulating an expansion of the CMP and GMP populations (Gao et al. 2014; Singer et al. 2014). Results from this study indicated the ability of RSV to protect against HFD induced LK cell population and their compartments (i.e., CMP, CLP, MEP and GMP) (Figure 4.12).

The reduction in GMP, MEP and CLP are highly correlated to a reduction observed in lineage^{+} cell populations (Figure 4.13). The increase in bone marrow macrophages, MDSCs, B cells and T cells have previously been observed in obese mice (Singer et al. 2014). Previous studies have also shown that macrophages and MDSCs have pro-atherogenic and inflammation modulatory function and their accumulation and activation is associated with chronic inflammation in atherosclerosis (Moore and Tabas 2011a; Wang et al. 2015). Therefore, a reduction in their numbers and activity could potentially contribute to attenuation of disease progression. However, the role of the MDSCs population during atherosclerosis development remains unclear; though, accumulating evidence from several mouse models and clinical studies suggests a correlation between increased frequency of MDSCs with their ability to suppress T cell proliferation (in particular T_{h1} and T_{h17} cells) (Wang et al. 2015; Foks et al. 2016; Zhou et al. 2018a). Interestingly, it is worth noting that despite a decrease in MDSCs population, the T cells population was also attenuated following RSV treatment. These findings indicate that RSV intervention may cause a reduction in both MDSCs and T cell populations via separate mechanisms. Furthermore, it has been previously found that angiogenesis is promoted by MDSCs. Angiogenesis in atherosclerosis results in destabilisation and progression of plaque, and hence the reduction observed in MDSCs population in this study may result in enhanced plaque stability (Camaré et al. 2017). Therefore, further investigations into the role MDSCs during atherosclerosis progression are required to fully evaluate and decipher the consequences of RSV treatment in reducing this population.

It has been reported that MDSCs also inhibit B cell proliferation in mice and humans (Lelis et al. 2017). However, the frequency of B cells in the current study was also decreased (Figure 4.13E). Numerous lines of evidence demonstrate the presence of B cells in atherosclerotic lesions with their roles dependent on the subset involved (Ma et al. 2021a). For instance, B1 cells and marginal zone B cells exert athero-protective effects while follicular B cells and innate response activator B cells show the opposite effects (Ma et al. 2021a). In an earlier study, B cell deficiency in hypercholesteraemic $LDLR^{-}/^{-}$ mice was associated with an increase in atherosclerotic lesions by 30% to 40% (Major et al. 2002). In contrast, studies in hypercholesteraemic $ApoE^{-}/^{-}$ and $LDLR^{-}/^{-}$ mice lacking both B and T cells demonstrated a significant reduction in atherosclerotic plaque formation, supporting their pro-atherogenic function (Daugherty et al. 1997; Reardon et al. 2001; Song et al. 2001). Due to these contrasting data, further investigations to identify which subsets of B cells had changed following RSV treatment is necessary to determine whether the reduction observed in B cell population in this study is beneficial or detrimental.

In conclusion, reduction in bone marrow cell populations following RSV treatment appear to be generally anti-atherogenic. The findings suggest that RSV could protect against HFD-induced proliferation of HSPCs and generation of pro-inflammatory immune cells.

4.3.4 The effect of RSV on peripheral blood immune cells

Apart from the reduction in the circulating B cells and $CD3^{+}$ T cells and $CD8^{+}$ T subsets, RSV failed to affect the actions of HFD on circulating lymphoid ($CD4^{+}$ T cells and NK cells) and myeloid immune cells (Figures 4.14 and 4.15). This suggests that RSV is less efficacious in attenuating inflammatory cells in peripheral blood compared to the bone marrow.

The reduction in the frequency of B cells in the peripheral blood is likely to be a consequence of their reduction in the bone marrow. The potential implication of reducing B cells following RSV treatment on atherosclerosis has been discussed in detailed in the previous section (Section 4.3.4). With regards to T cells, no previous research has been carried out to define the effects of RSV supplementation on $CD3^{+}$ T cells. However, it has been mentioned that $CD3^{+}$ T cells account for the second majority of leukocytes after monocytes/macrophages

in mouse and human atherosclerotic plaques, and hence their reduction will potentially protect against lesion development (discussed in detailed in the next chapter in relation to changes in immune cells in plaques). Furthermore, the effect of RSV on cytotoxic $CD8^+$ T cells in the context of atherosclerosis progression, has not been previously investigated. Previous studies noted that depletion of $CD8^+$ T lymphocytes in hyperlipidaemic $ApoE^{-/-}$ and $LDLR^{-/-}$ mice resulted in a reduction in both atherosclerotic plaque burden and macrophage accumulation in the plaque (Kyaw et al. 2013; Cochain et al. 2015). However, the transfer of $CD8^+$ T cells to $ApoE^{-/-}$ mice contributes to necrotic core formation and vulnerable atherosclerotic plaques (Kyaw et al. 2013). Interestingly, it also has been observed that depletion of $CD8^+$ T cells in hypercholesteraemic $LDLR^{-/-}$ mice results in a reduction in mature monocytes and GMP in the bone marrow and spleen of these mice (Cochain et al. 2015). Taken together, the data obtained in the current study suggest that the reduction observed in $CD8^+$ T cells in the peripheral blood could correlate to the reduction observed in GMP levels in the bone marrow along with observed reduction in macrophage content in plaque and increased plaque stability (discussed in the next chapter). Overall, the results from bone marrow and peripheral blood indicate that RSV is potentially capable of inducing an anti-inflammatory state within male $LDLR^{-/-}$ mice receiving a HFD. Future studies to investigate changes in the spleen and the thymus after RSV supplementation would be informative.

4.4 Future directions

The results obtained in this chapter highlighted various beneficial effects of RSV supplementation on atherosclerosis-associated risk factors. As heart weight was reduced, so further investigation of the underlying mechanisms should be carried out. For example, extraction of total lipids and fatty acids from the heart of mice as well as analysis of expression of key genes that affect free fatty acid and TG metabolism in cardiac myocytes and heart such as heart-specific fatty acid binding protein (hFABP), fatty acid transport protein (FATP) and CD36 should be carried out. Furthermore, several lines of evidence from both human and animals studies demonstrate the ability of short chain fatty acids to reduce plasma cholesterol levels and foam cell formation in plaques together with anti-inflammatory actions (Aguilar et al. 2014; Richards et al. 2016). The ability of RSV to promote short chain fatty acids production has been studied in relation to inflammatory bowel disease (Li et al. 2022b). Therefore,

analysing the concentration of short chain fatty acids in the faeces collected from mice fed HFD supplemented with RSV using several analytical techniques, such as gas or liquid chromatography, would provide more valuable insights. Further studies investigating both long and short chain fatty acids in the plasma would also be informative. Finally, the implication of RSV intervention on plasma cytokines has not been studied so could form an additional future avenue.

4.5 Conclusions

RSV produced several anti-atherogenic activities by modulating many atherosclerosis-associated factors, such as reducing LDL/VLDL-C, TC and CE and increase HDL-C (not statistically significant) in plasma, as well as reducing LDL:HDL and TC:HDL ratios. Furthermore, RSV exerts anti-inflammatory actions by reducing stem, progenitor, and mature cell populations within the bone marrow and by trend towards reducing the frequency of circulating T cells and B cells in the peripheral blood. While these initial assessments are encouraging, the research continued to assess the effect of RSV on plaque burden and compositions, which are presented in the next chapter.

CHAPTER 5

Evaluation of the effect of RSV on plaque burden and composition in atherosclerotic LDLR$^{-/-}$ mice

5.1 Introduction

The inclusion of RSV to HFD in male LDLR^{-}/$^{-}$mice showed this polyphenol as a promising nutraceutical candidate for protecting against risk factors associated with atherosclerosis development. Thus, RSV inhibited several key processes associated with atherosclerosis development *in vitro* (Chapter 3), as well as producing a favourable plasma lipid profile and exhibiting anti-inflammatory properties by reducing stem, progenitors and mature cells in the bone marrow and decreasing B cells and T cells in the peripheral blood *in vivo* (Chapter 4). Given these beneficial effects, it was decided to study the effect of RSV supplementation on the development of atherosclerosis and composition of plaques. Atherosclerotic plaques often develop at branching point of the artery such as the aortic root and brachiocephalic artery, where the blood flow is slowed and more turbulent (low shear stress), which contributes to endothelial dysfunction (Warboys et al. 2011; Lin et al. 2015). However, since the aortic root in mice has the highest susceptibility to lesion development, most of the research focusses on plaque development at this site to determine the severity of the disease in mice. This is can be achieved via assessment of lesion size and plaque composition (Lin et al. 2015). Indeed, the atherosclerotic plaque is a heterogeneous structure composed of lipid-rich core, inflammatory cells (e.g. macrophages and T cells), SMCs and fibrous elements (e.g. collagen). Importantly, the presence of these components in variable proportions is responsible for plaque stability (Sirol 2005).

5.1.1 Experimental aims

The main aim of the studies presented in this chapter was to investigate the effect of RSV supplementation on atherosclerotic plaque progression in male LDLR^{-}/$^{-}$ male fed HFD for 12 weeks. This was achieved via assessment of plaque burden and composition in sections from the aortic root taking advantage of several staining techniques that had already been optimised in the host laboratory. Analysis of plaque development and burden was achieved by measuring several parameters in stained sections, including plaque and vessel size, and occlusion as well as lipid content while immunohistochemical analysis was carried out to determine plaque composition, particularly content of macrophages (MOMA-2), T cells (CD3^{+}) and SMC (αSMA^{+}).

5.1.2 Plaque burden and lipid content

Analysis of plaque size within the vessel, vessel size, plaque occlusion and lipid content within the plaque are all considered to be informative data that reflect the severity of atherosclerosis. Thus, increase in plaque size over vessel size correlates to a decrease in lumen size (occlusion) and this is due to the encroachment of plaque upon the arterial lumen, consequently leading to arterial obstruction and impaired blood flow. Accumulation of lipids within the plaque is an indicator of the abundance of lipid-laden foam cells. It is well known that plaques rich in lipids and pro-inflammatory cells with a thin fibrous cap are more prone to rupture (Chan et al. 2022a). However, although plaque rupture is a hallmark of the disease in humans, it is rarely seen in mouse models. It has been suggested that this is potentially related to the small diameter of the mouse vessels and an increase in vessel surface tension (Veseli et al. 2017). Therefore, in the current study, evaluation of plaque burden, content of lipids and pro-inflammatory cells, and plaque stability following RSV treatment were carried out to assess disease severity.

5.1.3 Plaque composition

Monocytes/macrophages and T cells are the most abundant immune cells in atherosclerotic plaques and their infiltration into the artery wall is stimulated by several inflammatory cytokines and chemokines expressed and secreted by ECs and macrophages/foam cells (McLaren et al. 2011; Ilhan and Kalkanli 2015). During inflammation, circulating monocytes are recruited into the intima and differentiate into macrophages that polarise mainly to either M1 macrophages (pro-inflammatory) or M2 macrophages (anti-inflammatory) depending on local microenvironment of cytokines (Lin et al. 2021). M1 macrophages, which are the predominant phenotype in unstable plaques, are polarised in response to T_{h1} cytokines (e.g. IFN-γ and TNF-α) or LPS, and they contribute to disease progression and plaque vulnerability via secretion of high levels of pro-inflammatory cytokines such as IL-1β, IL-6, IL-12, and TNF-α as well as ROS (Chinetti-Gbaguidi et al. 2015; Lin et al. 2021). Indeed, the accumulation of cholesterol crystals triggers the activation of the NLRP3 inflammasome that results in the secretion of IL-18 and IL-1β, stimuli for M1 macrophage polarisation. In addition, ox-LDL accumulation in the intima promotes macrophage M1 polarisation (Chinetti-Gbaguidi et al. 2015). After macrophages, M1 in particular, T cells represent the second most abundant

immune cells found in atherosclerotic plaques (Bullenkamp et al. 2016). Although, they can not transform into foam cells, they play a key role in the inflammatory response in atherosclerosis development via their activity as mediators of numerous pro-inflammatory processes as discussed in Chapter 4. Thus, in this chapter, specific antibodies targeting MOMA-2, iNOS and CD3 were employed to assess the abundance of macrophages, M1 macrophages and T cells respectively in atherosclerotic plaques to evaluate disease severity.

5.1.4 Plaque Necrosis and stability

During lesion progression, VSMCs undergo phenotypic switching characterised by a transition from a contractile to proliferative state, and migrate from the tunica media into the intima. Like macrophages, VSMCs in the intima transform into foam cells via the uptake of lipid particles; however, they also play a crucial role in plaque stability. Apoptosis of foam cells suppress efferocytosis and this adds to plaque burden and leads to secondary necrosis and further inflammation (Björkegren and Lusis 2022). The accumulation of apoptotic cells, cell debris and cholesterol within the artery wall gives rise to fibroatheromas, necrotic core covered by a fibrous cap (Björkegren and Lusis 2022). The atherosclerotic plaque stability depends on fibrous cap thickness and degree of inflammation, i.e. the fibrous cap in a stable plaque is characterised by enrichment of VSMC-derived αSMA^{+} cells and low-grade inflammation (Halvorsen et al. 2008; Basatemur et al. 2019). Indeed, VSMCs contribute to plaque stability by secreting ECM proteins such as elastin and collagen (Bennett et al. 2016). Collagens are the most important ECM proteins in the vascular wall and their amount and distribution correlates with plaque stability. Among their different types, collagen I and III are the predominant types in the stable plaque (Nadkarni et al. 2009). Thus, VSMCs may exert positive and negative activities on plaque progression and remodelling (Basatemur et al. 2019). Therefore, in the current study, plaque stability was determined by staining for VSMCs and collagen content within the plaque following RSV treatment. The plaque stability was then calculated as (sum of plaque VSMC and collagen content) / (sum of plaque macrophage and lipid content). In addition, plaque necrosis was determined via quantification of acellular regions (holes present within plaques) of the ORO-stained sections. Measuring plaque stability and necrosis provides a comprehensive perspective of the atherosclerosis severity.

5.1.5 Experimental strategies

The experimental strategy is illustrated in Figure 5.1.

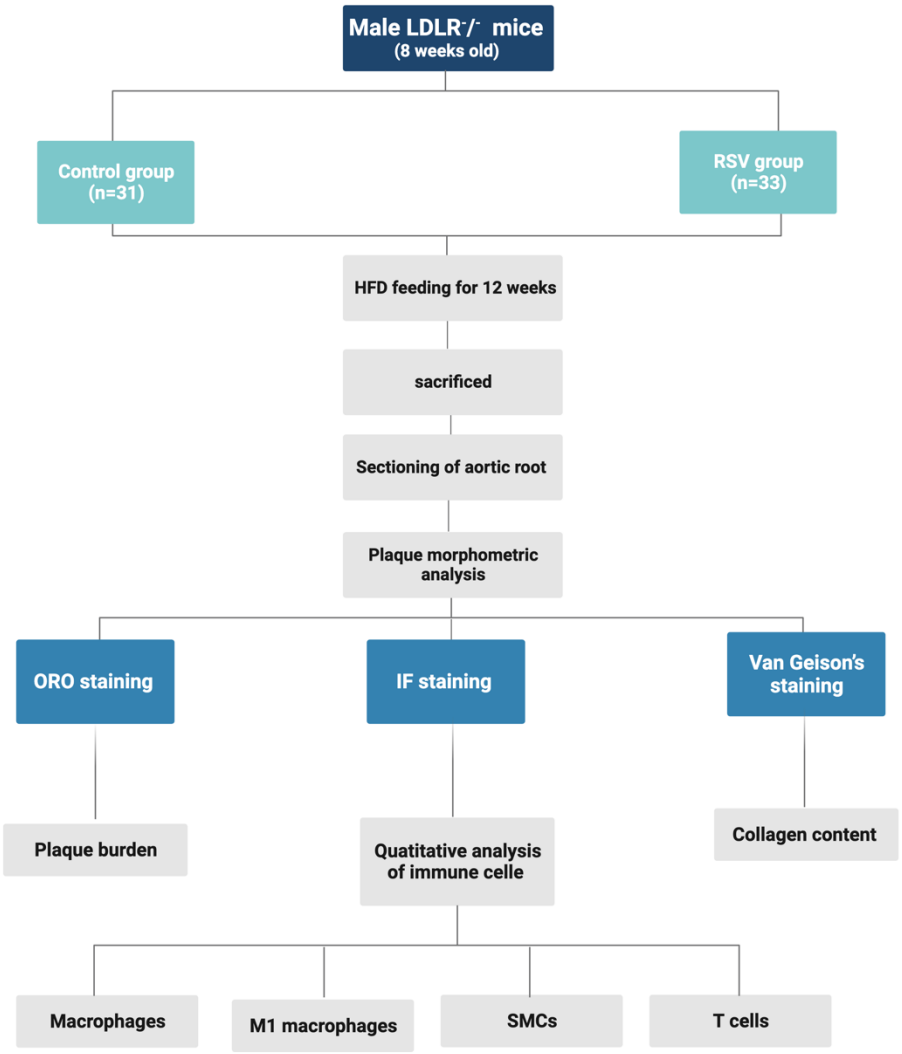

Figure 5.1 Experimental strategy used to assess the effect of RSV supplementation on atherosclerotic plaque progression *in vivo*.

Abbreviations: HFD, High fat diet

5.2 Results

5.2.1 Inclusion of RSV in HFD has no impact on atherosclerotic plaque burden and lipid content in LDLR^{-}/$^{-}$ mice

The aortic root sections stained with ORO were used to assess atherosclerotic plaque burden. There were no statistically significant changes seen in the RSV group in the measured parameters, including lipid content, plaque content, occlusion, plaque size, vessel size and lumen size (Figure 5.2).

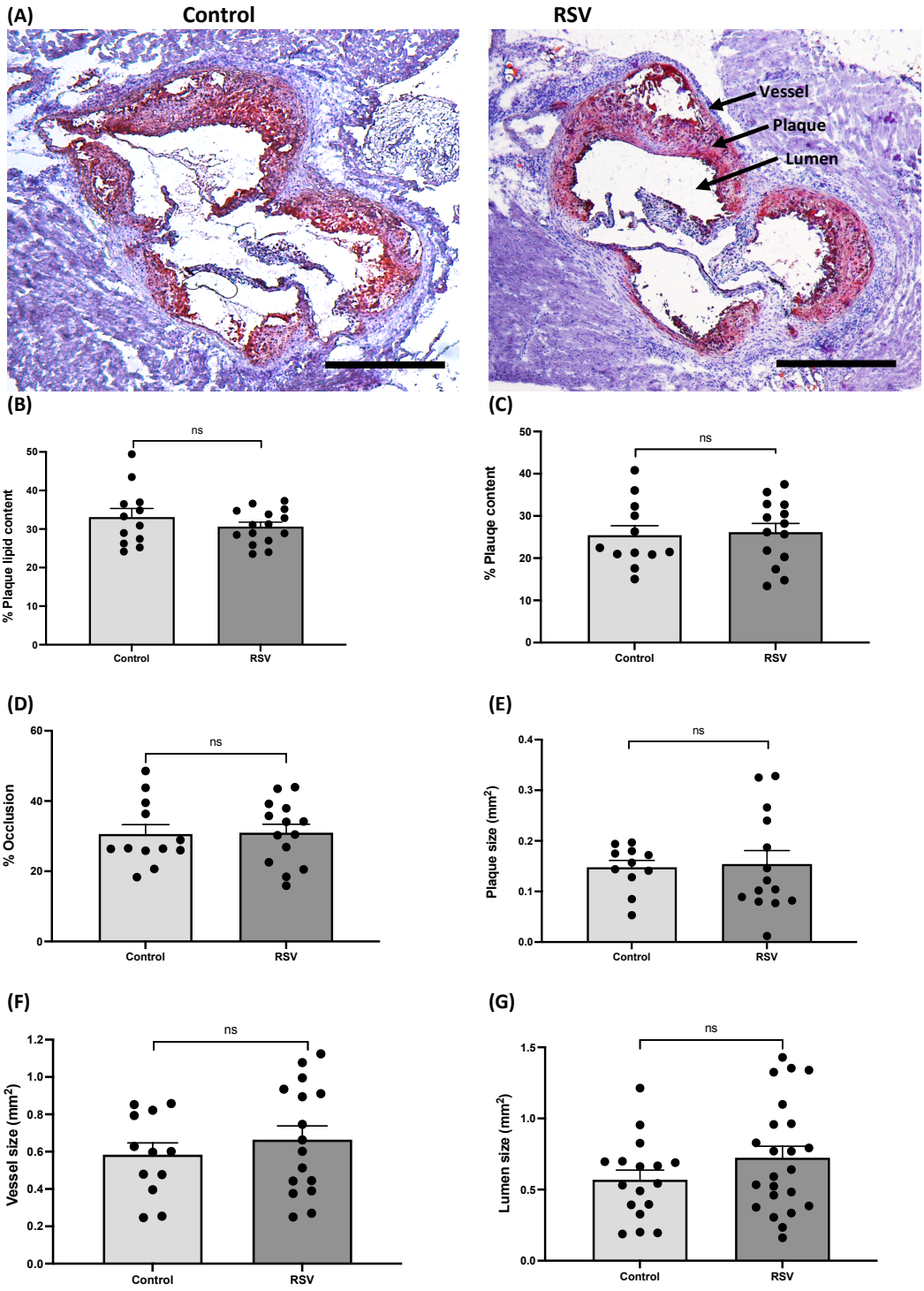

Figure 5.2 RSV supplementation has no effect on plaque burden and lipid content in LDLR$^{-/-}$ mice fed a HFD

Male LDLR$^{-/-}$ mice were fed either HFD or HFD supplemented with RSV for 12 weeks. The aortic root at the three valve cusps was sectioned and stained with ORO. Images were then captured using Leica DMRB microscope under x5 magnification. Images were then analysed using ImageJ software in a blinded manner. Representative images are shown in panel A (scale bar of 400 µm) and graphs show lipid content (determined as percentage ORO^{+} staining; B), plaque content (calculated as percentage plaque area of vessel area; C), occlusion (calculated as percentage plaque area of lumen area; D), plaque size (E), vessel size (F), and lumen size (G). Data are presented as mean ± SEM from n=12 (B; C; D; F), 11(E) or 17 (G) control and n=15 (B), 14 (C; D; E), or 16 (F) or 23 (G) RSV group. Statistical analysis was performed using an unpaired Student's t-test. **Abbreviations:** ns, not significant; OCT, optimum cutting temperature; ORO, Oil red O.

5.2.2 Macrophages were significantly reduced in the aortic root of LDLR$^{-/-}$ mice-treated with RSV

Analysis of the intensity of immunofluorescence staining to detect MOMA-2^{+} macrophages showed that RSV intervention for 12 weeks significantly reduced macrophage content within atherosclerotic plaques by 55% ($p \leq 0.001$) compared to the control group (Figure 5.3).

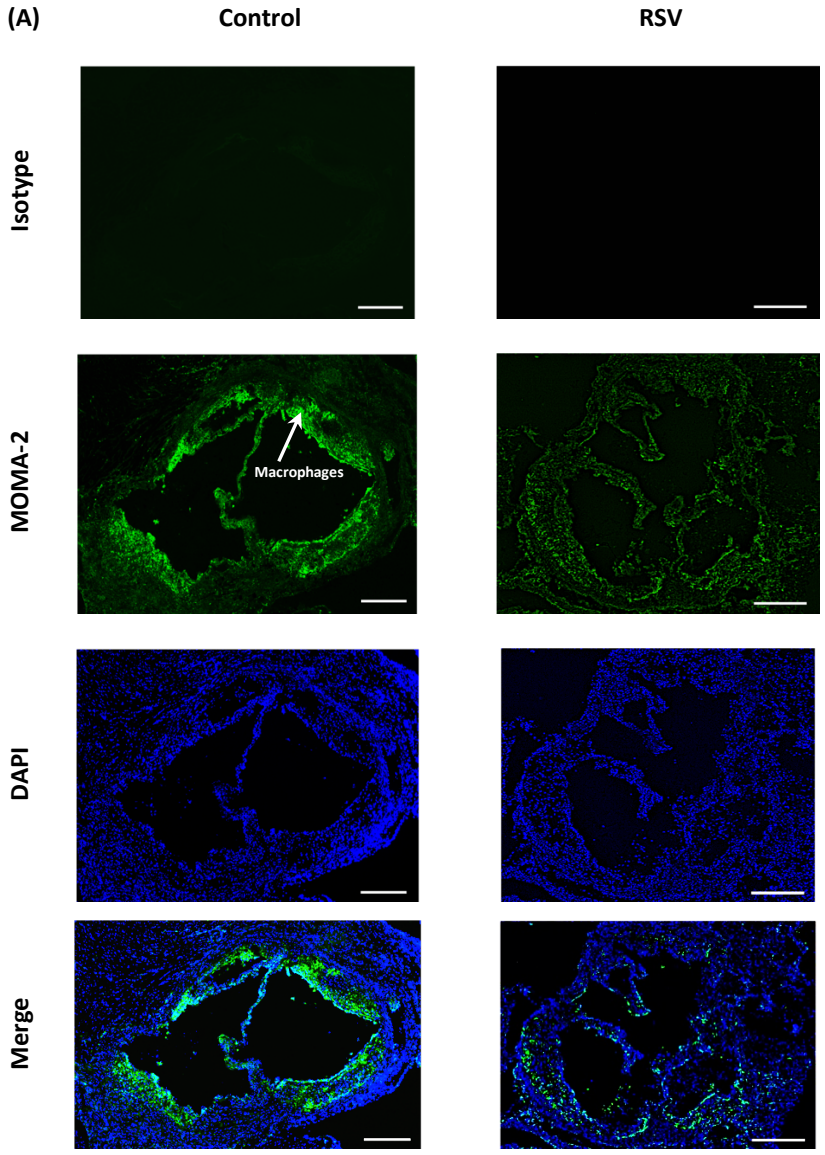

Figure 5.3 Macrophage content was significantly reduced in the aortic root of LDLR^{-}/$^{-}$ mice-treated with RSV

Following 12 weeks of feeding male LDLR^{-}/$^{-}$ mice either HFD or HFD supplemented with RSV, immunofluorescence staining of sections of the aortic root was carried out to detect MOMA-2^{+} macrophages. Images were then captured using an Olympus BX61 microscope under x4 magnification and the intensity of staining within the plaque was quantified using the ImageJ software in a blinded manner. Representative image with scale bar 400 µm is shown A) with graphs displaying the percentage of MOMA-2^{+} macrophages in the plaque (B). Data are presented as mean ± SEM from n=13 control and n=14 RSV group. Statistical analysis was performed using an unpaired Student's t-test where ***$p \leq 0.001$. **Abbreviations:** OCT, optimum cutting temperature.

5.2.3 The percentage of pro-inflammatory M1 macrophages were significantly attenuated following RSV treatment.

Immunofluorescence staining with an $iNOS^{+}$ antibody was performed in order to determine M1 macrophage content within the plaque. M1 macrophage content was significantly attenuated by around 38% (p =0.002) in the RSV group compared to the control group (Figure 5.4B).

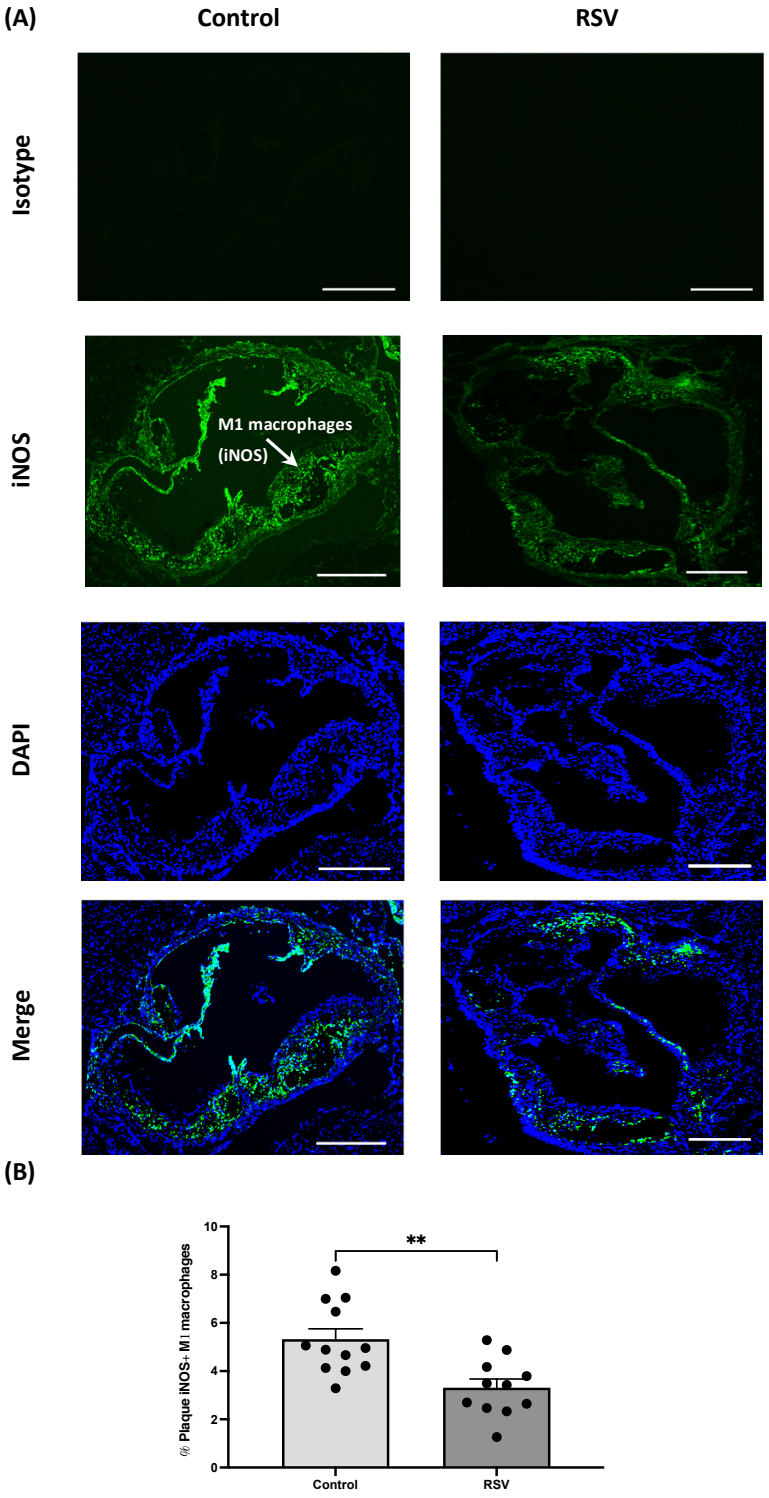

Figure 5.4 RSV supplementation significantly reduced M1 macrophages in the aortic root of LDLR-/- mice

Male LDLR$^{-/-}$ mice were fed either HFD or HFD supplemented with RSV for 12 weeks. Immunofluorescence staining of sections from the aortic root was carried out to detect M1 macrophages using iNOS+ antibody. Images were then captured using an Olympus BX61 microscope under x4 magnification and analysed using ImageJ software in a blinded manner. Images with scale bar of 400 µm are shown (A) with graphs displaying percentage of M1 macrophages within the plaque(B). Data are presented as mean ± SEM from n=12 control and n=11 RSV group. Statistical analysis was performed using an unpaired Student's t-test where ** $p \leq 0.01$. Abbreviations: iNOS, inducible nitric oxide synthase.

5.2.4 T cells were significantly reduced in the aortic root of LDLR^{-}/$^{-}$ mice-treated with RSV

The RSV group had significantly reduced proportion of CD3^{+} T cells in the plaques (p=0.036) (Figure 5.5B) by 38.2% compared to the control group.

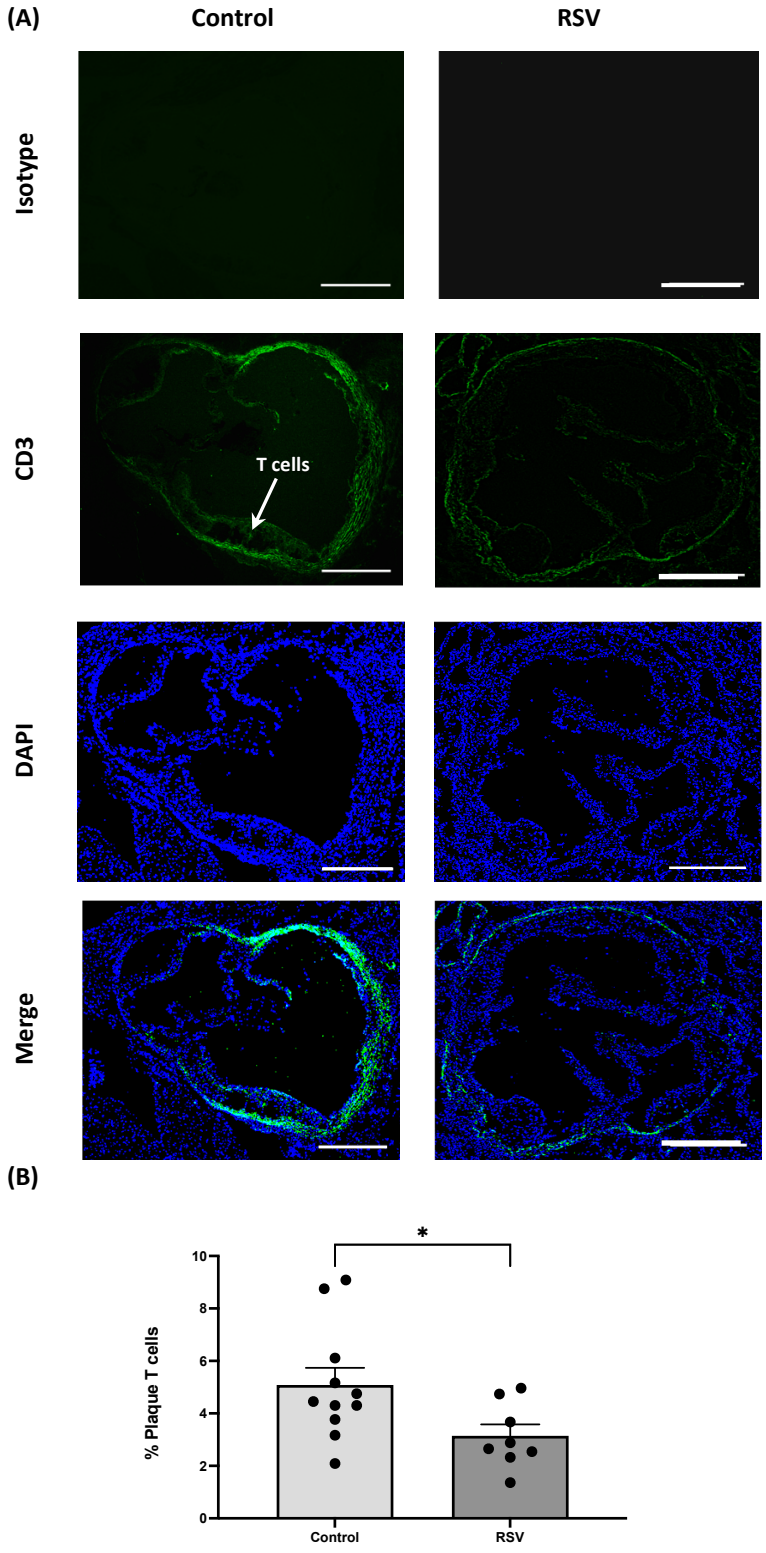

Figure 5.5 T cells were significantly reduced in the aortic root of LDLR$^{-/-}$ mice-treated with RSV

Following 12 weeks of feeding male LDLR$^{-/-}$ mice either HFD or HFD supplemented with RSV, the aortic root sections were subjected to immunohistochemical analysis to detect CD3+ T cells. Image were then captured using Olympus BX61 microscope under x4 magnification. Images analysis was conducted using the ImageJ software in a blinded manner. Representative images are shown with scale bar of 400 µm (A) and graphs display percentage of T cells within the plaque(B). Data are presented as mean ± SEM from n=11 control and n=8 RSV group. Statistical analysis was performed using an unpaired Student's t-test where * $p \leq 0.05$.

5.2.5 Plaque stability and necrosis

5.2.5.1 Treatment with RSV significantly increased αSMA$^+$ VSMCs in plaques of atherosclerotic LDLR^{-}/$^{-}$ mice

αSMA$^+$ VSMCs in plaques were stained by immunofluorescence and the RSV group had significantly increased levels in the plaque (p=0.015) by around 41% compared to the control group (Figure 5.6).

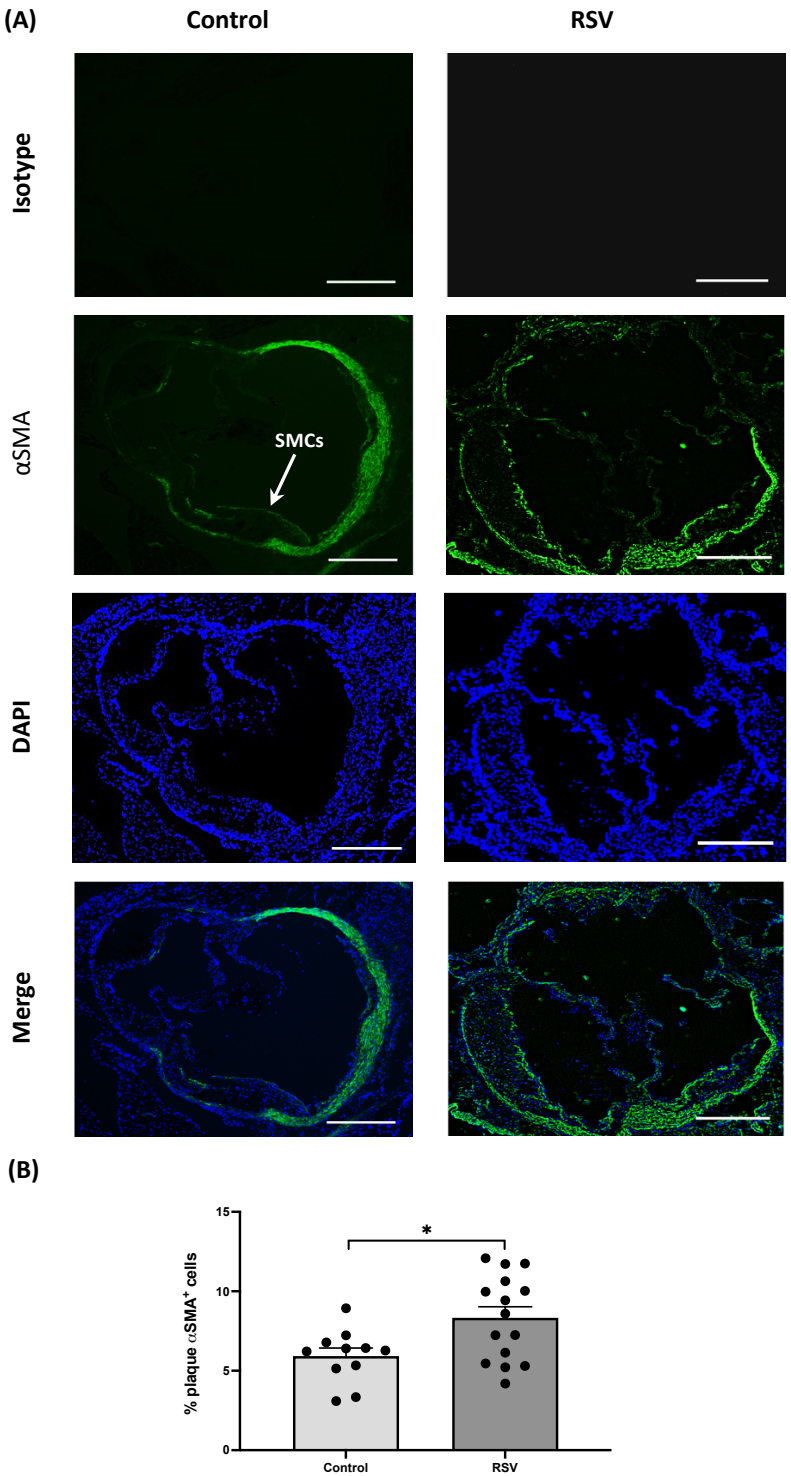

Figure 5.6 Treatment with RSV significantly increases SMCs in the aortic root of LDLR^{-}/$^{-}$ mice

Following 12 weeks of feeding male LDLR^{-}/$^{-}$ mice either HFD or HFD supplemented with RSV, sections from the aortic root were subjected to immunofluorescence staining to detect SMCs. Images were then captured using Olympus BX61 microscope under x4 magnification. Image analysis was performed using ImageJ software in a blinded manner. Representative images with scale bar of 400 µm are shown (A) with graphs displaying percentage αSMA+ cells within the plaque (B). Data are presented as mean ± SEM from n=11 control and n=15 RSV group. Statistical analysis was performed using an unpaired Student's t-test where *p ≤0.05. Abbreviations: αSMA, alpha-smooth muscles actin.

5.2.5.2 RSV supplementation significantly increased the collagen content in plaques of atherosclerotic LDLR^{-}/$^{-}$ mice

The plaque collagen content was also increased significantly in the RSV group by around 81% ($p \leq 0.001$) compared to the control group (Figure 5.7).

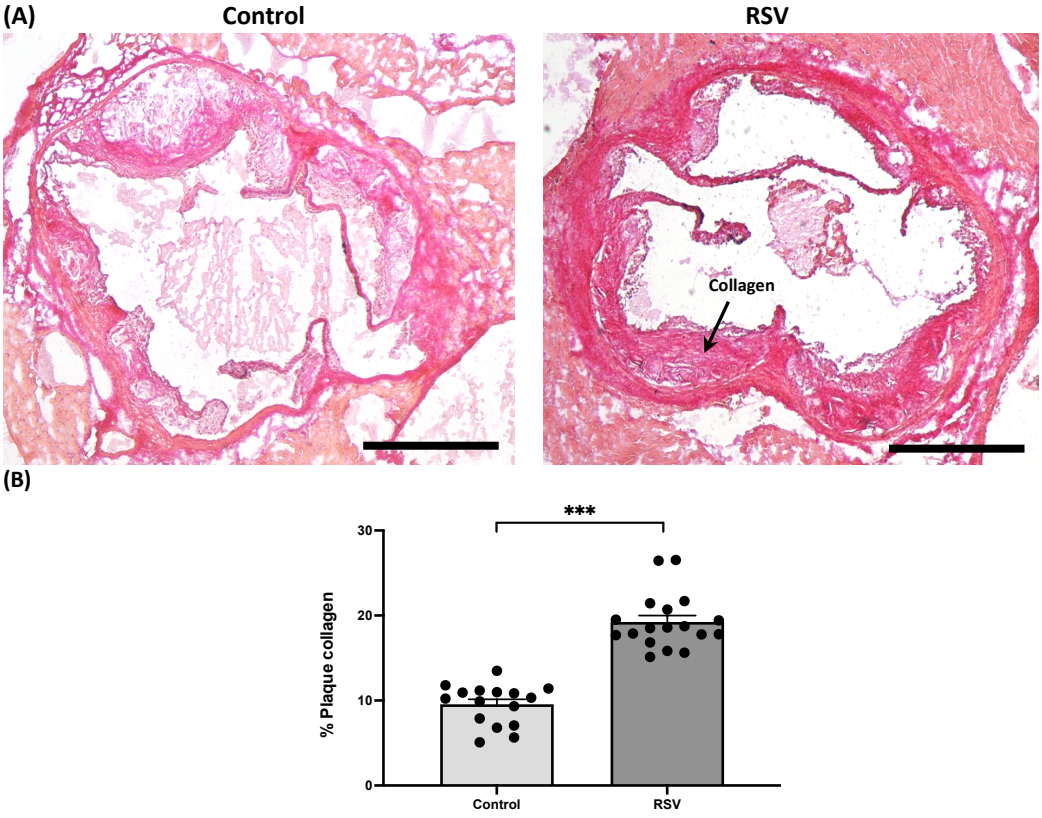

Figure 5.7 Treatment with RSV significantly increases the collagen content within aortic root of LDLR-/- mice

Male LDLR-/- mice were fed either HFD or HFD supplemented with RSV for 12 weeks and sections from the aortic root were subjected to Van Gieson's staining to determine the collagen content within the plaque. Images were captured using Leica DMRB microscope under x5 magnification and analysed using ImageJ software in a blinded manner. Representative images with scale bar of 400 µm are shown (A) with graphs displaying percentage of collagen content within the plaque (B). Data are presented as mean ± SEM from n=16 control and n=18 RSV group. Statistical analysis was performed using an unpaired Student's t-test where ***$p \leq 0.001$.

5.2.5.3 Plaque stability and necrosis

As a result of increase in content of SMCs and collagen in the plaque along with a reduction in macrophages, it was found that there was a 73.17% increase in plaque stability index in the RSV group compared to the control group ($p \leq 0.001$) (Figure 5.8). However, no significant changes were found in plaque necrosis between the two groups (Figure 5.9).

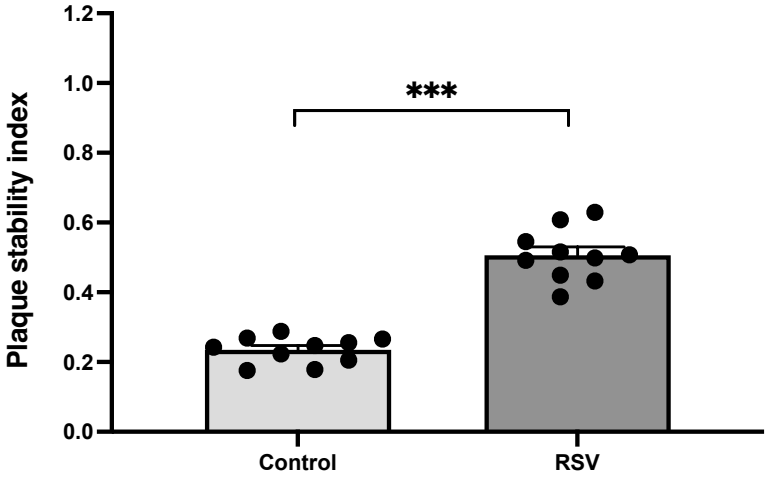

Figure 5.8 RSV supplementation significantly increases the plaque stability index in LDLR^{-}/$^{-}$ mice

Male LDLR^{-}/$^{-}$ mice (8 weeks old) were fed HFD or HFD supplemented with RSV for 12 weeks. The plaque stability index was calculated after all the required staining were performed as (smooth muscle cells + collagen) / (macrophages + lipids) from n=10 control and n=10 RSV groups. Data are presented as mean ± SEM and Statistical analysis was performed using an unpaired Student's t-test where ***$p \leq 0.001$.

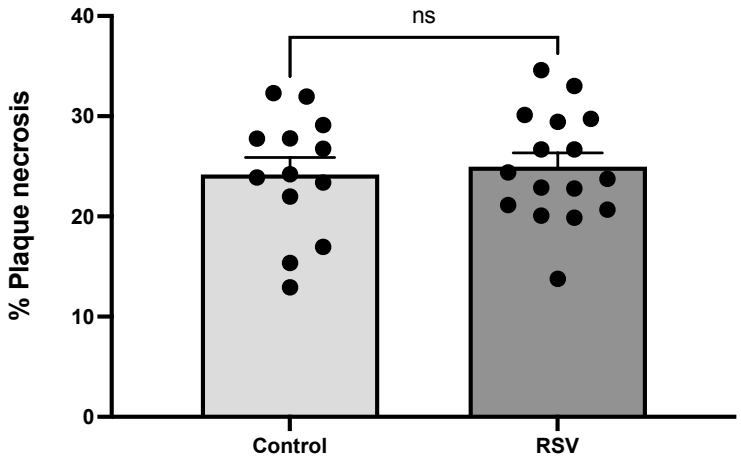

Figure 5.9 RSV supplementation has no effect on plaque necrosis in LDLR^{-}/$^{-}$ mice

Following 12 weeks of feeding of male LDLR^{-}/$^{-}$ either HFD or HFD supplemented with RSV, aortic root sections were stained with ORO. Images were then captured using Leica DMRB microscope under x5 magnification. Images were then analysed using ImageJ software in a blinded manner. Data are presented as mean ± SEM from n=12 control and n=14 RSV group. Statistical analysis was performed using an unpaired Student's t-test. **Abbreviations:** ORO, Oil red O.

5.3 Discussion

Treatment with RSV has been found to be beneficial in modulating several atherosclerosis-associated risk factors in various animal studies; its effects in reducing atherosclerotic lesions has been shown in ApoE^{-}/$^{-}$ mice and ApoE^{-}/$^{-}$ / LDLR^{-}/$^{-}$ mice (Fukao et al. 2004; Do et al. 2008). A far as we are aware, only one study had been performed in male LDLR^{-}/$^{-}$ mice to investigate the effect of RSV in plaque progression (Chassot et al. 2018). However, no details about changes in plaque and plaque composition were provided in this study, and hence this was the aim of studies presented in this chapter. Mice receiving RSV orally with HFD demonstrated numerous favourable changes in plaque progression, particularly plaque compositions. Indeed, the presence of pro-inflammatory immune cells (macrophages and T cells) was significantly attenuated in the RSV group while plaque stability parameters (VSMCs and collagen content) were increased significantly. Table 5.1 provides a summary of data presented in this chapter where the significant changes are highlighted.

Table 5.1 Summary of changes in atherosclerotic plaque progression produced by inclusion of RSV in HFD in male LDLR^{-}/$^{-}$ mice

	Control Mean	RSV Mean	Change	Significance
Plaque burden and lipid content				
Lipid content (%)	33.11	30.63	NC	NS
Plaque content (%)	25.43	26.17	NC	NS
Plaque size (mm^2)	0.15	0.15	NC	NS
Vessel size (mm^2)	0.58	0.66	NC	NS
Lumen size (mm^2)	0.57	0.72	NC	NS
Occlusion (%)	30.61	30.97	NC	NS
Plaque composition				
Plaque macrophages (%)	40.72	18.29	↓	$P\leq$ 0. 001 (***)
Plaque M1 macrophage (%)	5.32	3.31	↓	p=0.002(**)
Plaque T cells (%)	5.09	3.14	↓	p=0.036(*)
Plaque VSMCs (%)	5.93	8.33	↑	p=0.015(*)
Plaque collagen (%)	10.32	18.74	↑	$P\leq$0.001(***)
Necrosis and stability				
Plaque stability index	0.24	0.51	↑	$P\leq$0.001(***)
Plaque necrosis (%)	0.03	0.03	NC	NS

Significance was defined as p≤0.05.
Abbreviations: NS, not significant; NC, no changes; VSMCs, vascular smooth muscle cells.

5.3.1 Effects of RSV on plaque burden and composition

Although RSV significantly reduced plasma LDL, TC and CE levels (data presented and discussed in Chapter 4), no significant changes in plaque burden and lipid content were seen in the current study (Figure 5.2). These data are consistent with previous literature reporting no changes in plaque burden in LDLR^{-}/$^{-}$ mice treated with RSV although a reduction in plasma levels of LDL and VLDL were seen (Chassot et al. 2018), emphasising that changes seen in plasma. lipid profile don't always correlate with lipid content in atherosclerotic plaques. However, significant changes were found in plaque inflammation and stability. Analysis of immune cells, particularly macrophages and T cells, in plaques following RSV intervention showed a significant reduction in macrophages and iNOS^{+} M1 proinflammatory macrophages as well as a reduction in CD3^{+} T cells. These data are in part similar to a previous study in atherosclerotic ApoE^{-}/$^{-}$ mice that reported a significant reduction in macrophage infiltration (about 40%) and other inflammatory markers in plaques after the inclusion of RSV to HFD (Chang et al. 2015a). In addition, the combination of RSV with catechin and caffeic acid showed a similar reduction in macrophage content within plaques of ApoE^{-}/$^{-}$ mice as well as

a reduction in T cells (Norata et al. 2007). However, caution should be applied when iNOS results are interpreted as the protocol was optimised for cell surface proteins, not for intracellular proteins. This could probably explain why iNOS macrophages were significantly less than total macrophages in the plaque. The decrease in T lymphocytes in the plaque is likely to be attributable to a decrease found in the bone marrow and peripheral blood (Chapter 4). It is well known that these T cells release IFN-γ, an important cytokine in monocyte differentiation to macrophages. Therefore, it can be suggested that a reduction observed in macrophages in the plaque could be contributed by a reduction of T cells via IFN-γ as no changes were observed in $Ly6C^{high}$ monocytes levels in the peripheral blood (Chapter 4) and RSV had no effect on the expression of ICAM-1 (Chapter 3). Indeed, a previous study demonstrated that depletion of IFN-γ in $ApoE^{-}/^{-}$ mice resulted in a decrease in macrophages as well as an increase in collagen content, thereby preventing plaque progression and enhancing stability while exogenously administered IFN-γ showed an opposite effect (Gupta et al. 1997; Whitman et al. 2000; Koga et al. 2007; De Meyer et al. 2012). Further investigation on the expression of IFN-γ and adhesion molecules, such as ICAM-1 and VCAM-1, in plaques would be informative. Furthermore, determination of M2 macrophage content using cell surface staining markers, such as arginase I and CD206 as well as T cells subsets, in particular T_{h1} ,T_{h17} and $CD8^{+}$T cells (as $CD8^{+}$ decreased in peripheral blood; Chapter 4), would provide additional insights.

5.3.2 Effects of RSV on plaque stability and necrosis

The combination of increase in VSMCs and collagen content in the plaque along with a reduction in macrophages after 12 weeks of inclusion of RSV to HDF resulted in a marked increase in atherosclerotic plaque stability index (73.17%) despite no significant changes in lipid content of plaques. Furthermore, there were no differences in plaque necrosis between the two groups (Figure 5.9). In fact, RSV increased VSMCs proliferation *in vitro*, but decreased their migration towards PDGF (Chapter 3). Thus, it can be suggested that RSV in the early stages may have the ability to delay atherosclerosis progression, but in advanced lesions it may promote proliferation and consequently encourage fibrous cap formation and plaque stability. This proposition is also supported by the marked reduction in ROS production by all investigated cells as well as reduction in MMP activity (Chapter 3). Furthermore, the reduction

in $CD8^+$ T cells in peripheral blood may also play a role in plaque stability as a previous study demonstrated necrotic core formation and vulnerable atherosclerotic plaques after transfer of $CD8^+$ T cells to $ApoE^{-/-}$ mice (Kyaw et al. 2013). However, staining of $CD8^+$ T cells in plaque should be carried out before drawing any firm conclusions. Previously, supplementation of RSV was found to increase plaque stability by increasing collagen content to macrophage ratio in ApoE*3-Leiden.CETP mice fed a HFD (Berbée et al. 2013). The study also reported an increase in plaque SMCs and decrease in macrophage content although no effect was seen in the number of adhering monocytes to the endothelium (Berbée et al. 2013). Therefore, for a more comprehensive analysis, several staining for VSMCs should be carried out. For example, staining of VSMCs using osteopontin (OPN), a marker of synthetic VSMCs (Zhao et al. 2020) together with markers of contractile VSMCs, such as myosin heavy chain 11 (MYH11) and myocardin (Bennett et al. 2016). In addition, it would be valuable to determine the degree of vascular calcification. It has been reported that the area of calcification can be seen using ^{18}F-sodium fluoride tracer (Fayad and Robson 2021). Moreover, Von Kossa staining is considered as the gold standard tool to detect calcium salt in atherosclerotic plaque and has been used by several studies (Rattazzi et al. 2005; Relucenti et al. 2010; Schlieper et al. 2010).

5.4 Future directions

In this study, RSV shows the ability to attenuate atherosclerotic plaque progression. Therefore, further staining using the aforementioned markers would provide more mechanistic insights. However, due to a limited number of sections available, any staining performed must provide key additional insights in order to avoid wasting valuable sections. As previously mentioned, atherosclerotic plaques have heterogeneous structures that vary depending on its anatomical location and hence, comprehensive plaque morphometric investigations should also be carried out in the brachiocephalic artery to validate the changes seen in the aortic root. Moreover, since RSV treatment shows several beneficial effects on VSMCs (*in vitro* and *in vivo*), further investigation using RNA-seq could be carried out on VSMCs *in vitro* to provide more insights on the underlying mechanism of RSV action. Beyond this, it seems reasonable for proceeding on to further investigations to determine whether RSV is capable of promoting the regression of established plaques using male $LDLR^{-/-}$ mice as this will provide more insight into the therapeutic potential of RSV. Furthermore, the

differences between male and female LDLR^{-}/$^{-}$ mice in atherosclerotic plaque progression and severity has been observed with other nutraceuticals (catechin and hydroxytyrosol) in the host laboratory. Therefore, investigation of the ability of RSV supplementation to attenuate atherosclerosis progression in female LDLR^{-}/$^{-}$ mice should be investigated. Indeed, male LDLR^{-}/$^{-}$ were chosen for this study due to their enhanced vulnerability to diet-induced metabolic syndrome as well as several investigations on inflammation that found significant differences in male mice compared to female either for LDLR^{-}/$^{-}$ or ApoE^{-}/$^{-}$ models (Engelbertsen et al. 2012; Matsumoto et al. 2016; Zhang et al. 2018; Chen et al. 2020a).

5.5 Conclusions

When considered together, the results presented in this chapter and Chapter 4 have established a strong foundation in investigation of the effects of RSV supplementation on the progression of atherosclerosis and its associated risk factors *in vivo*. In male LDLR^{-}/$^{-}$ mice, RSV attenuates plaque progression by reducing macrophages, M1 macrophages in particular, and infiltration of T cells. Furthermore, plaque stability was also increased via VSMCs and collagen content. With no significant changes in lipid accumulation in plaque, it can be suggested that the observed effects on the plaque are mainly due to its anti-inflammatory functions, demonstrating that it may serve as a preventative agent for atherosclerotic lesions formation that could be supplemented with current pharmacological therapies. To shed more light and uncover further the mechanism of action of RSV, RNA-seq from the descending thoracic aorta was carried out to analyse whole transcriptome changes, which form the aim of studies in the next chapter.

CHAPTER 6

Analysis of changes in gene expression in the thoracic aorta of atherosclerotic LDLR $^{-}/^{-}$ mice

6.1 Introduction

RSV is a promising nutraceutical candidate for the prevention of atherosclerosis progression. This has been evidenced by its ability to supress several key pro-atherogenic processes in various cell types implicated in the initiation and progression of the disease (Chapter 3), in addition to data obtained from the *in vivo* studies presented in Chapters 4 and 5. Results from the *in vivo* studies showed that supplementation of RSV alleviates numerous factors associated with the development of the disease. The broad effects of RSV include decreased LDL/VLDL-C, TC, CE and LDL/HDL ratio, inflammation via reduced WBCs count compared to the control group and decreased progenitor, stem and mature immune cells in the BM and a trend toward reduction in the frequency of T cells, B cells and granulocytes in PB. Furthermore, analysis of atherosclerotic plaque showed significant reduction in plaque macrophages and T cells and an increase in plaque stability (increase VSMCs and collagen). Understanding the mechanisms underlying these changes is vital and will provide valuable insight into the molecular basis of RSV actions as well as aiding in the generation of hypothesis for future experiments. There has been a recent increase in the number of studies that have used high throughput next generation sequencing (RNA-seq) either at tissue or single cell level, in order to obtain more in-depth mechanistic insights (Xi et al. 2017; Baron et al. 2018; Paik et al. 2020; Zhao et al. 2021). Using RNA-seq provides an alternative method to microarray for obtaining mRNA expression profiles with exceptional sensitivity and precision. There are a number of advantages of choosing RNA-seq over other techniques, such as microarray and qPCR (Xi et al. 2017). Firstly, unlike microarray, which is limited to detecting pre-designed sequences, RNA-seq is an unbiased strategy that allows for the detection of all sequences in a high-throughput manner while utilising less starting RNA (Xi et al. 2017; Nevado et al. 2022). In addition, it has a high sensitivity to detect gene expression either at a low or very high level. Thirdly, there is lack of cross-hybridisation issue that other methods have because DNA sequences can be mapped to specific regions in the genome. Finally, it is capable of detecting both known and novel transcripts (Xi et al. 2017). Although previously published literature identified changes in gene expression induced by HFD supplementation (in leptin-deficient mice, ApoE^{-}/$^{-}$ and C57BL/6J mice) (Townsend et al. 2008; Yokota et al. 2016; He et al. 2020), there is no study to date that has investigated the impact of HFD on global gene expression in LDLR^{-}/$^{-}$ mice. Most importantly, there is no previous research before

this study that assessed the changes in global transcriptomics profile in mice after RSV supplementation.

6.1.1 Experimental aims

The aim of studies presented in this chapter was to determine the whole transcriptome-level changes in gene expression in the aorta of male LDLR^{-}/$^{-}$ mice after feeding RSV for 12 weeks in comparison to the control group using RNA-seq. Using this approach helps to identify dysregulated genes involved in atherosclerosis and atherosclerosis-associated risk factors. Furthermore, it aids in the discovery of biological pathways impacted by RSV intervention, regardless of whether the sequence or biological function of the gene is known and contributes to the advancement in the understanding of pathways that lead to atherosclerosis. This was achieved via extraction of RNA from the mouse aorta and subjecting the samples to several quality control assessments before sending them to Novogene. Furthermore, once samples arrived at Novogene, they underwent another quality control check by the experts there before starting the RNA-seq process. Finally, the project results with standard bioinformatics analysis were sent back to the host laboratory for further analysis of regulated genes using Ingenuity Pathway Analysis (IPA) software from Qiagen.

6.1.2 Experimental strategy

The experimental strategy is illustrated in Figure 6.1.

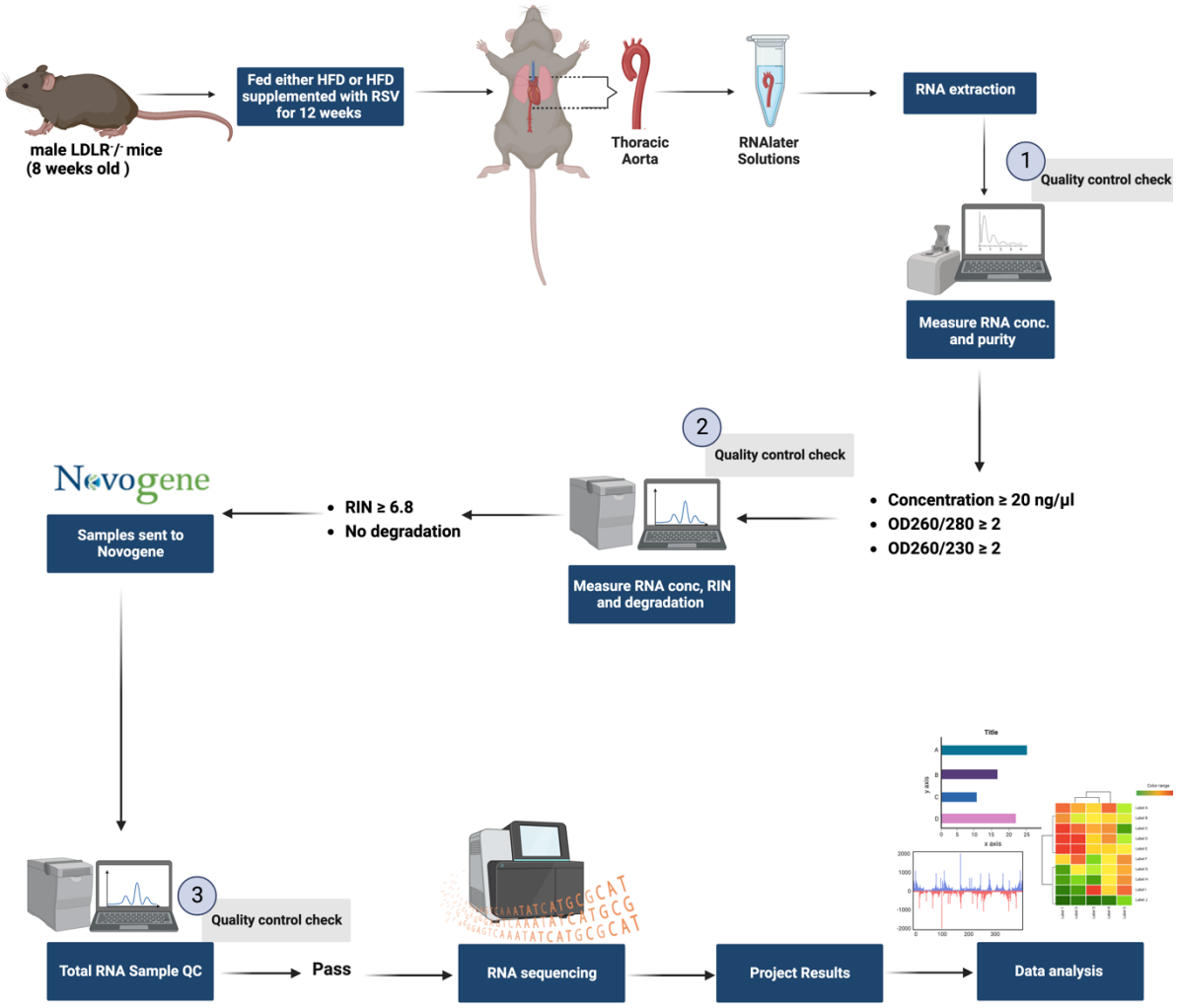

Figure 6.1 Experimental strategy for RNA-sequencing.

Abbreviations: HFD, High fat diet; OD, Optical density; RIN, RNA integrity number; QC, Quality control.

6.2 Results

6.2.1 RNA quality control (QC) check

6.2.1.1 Assessment of RNA integrity for aorta samples in the host laboratory

The use of intact RNA is crucial for successful RNA-seq analysis. Therefore, Agilent 2100 bioanalyser system was used to assess the RIN. The analysis of RIN for RNA samples using Eukaryote Total RNA Nano kit showed that all RNA samples from either HFD (8 samples) or RSV (8 samples) achieved the required RIN ($\geq$ 6.8) to be used for sequencing (data not shown), the RIN for the vast majority of processed samples were 10 while the lowest RIN was 9.7. Figure 6.2A shows an example of an "electrophoresis file run summary" for some samples involved in this study. Representative electropherograms for HFD and RSV groups are shown in Figure 6.2B and C respectively.

(A)

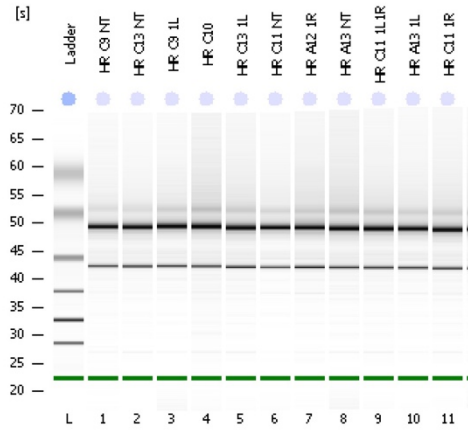

(B)

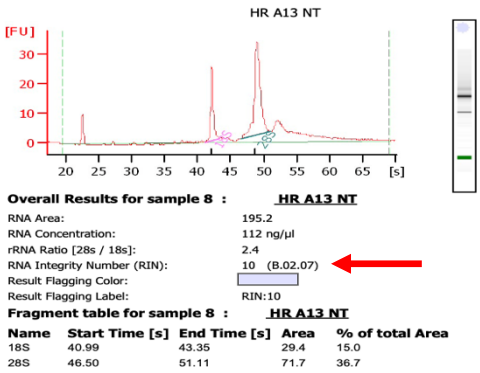

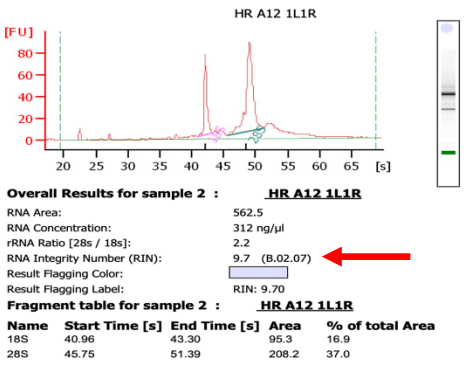

(C)

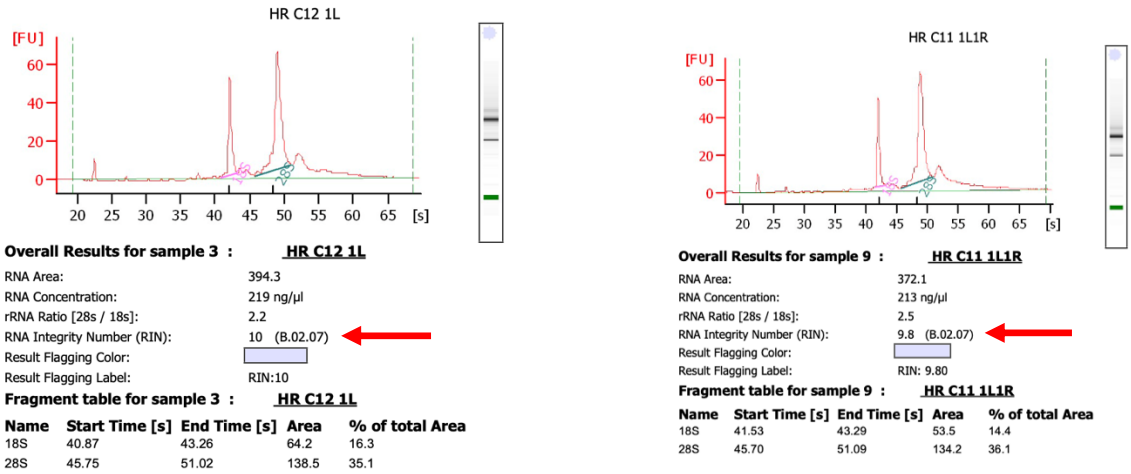

Figure 6.2 Representative images of quality of RNA samples from HFD and RSV groups

Thoracic aorta from LDLR$^{-/-}$ mice fed HFD or HFD supplemented with RSV were collected and kept in RNAlater solution. RNA extraction was carried out using RNeasy mini kit following the manufacturer's instructions. Only RNA samples with concentration of 20 ng/µl or more were passed to be tested for integrity. RIN was assessed using Agilent 2100 bioanalyser system. (A) representative electrophoresis image, (B) representative electropherograms from HFD group and (C) representative electropherograms from RSV group. All images represent samples with high RNA quality. Red arrows indicate RIN.

6.2.1.2 Second QC check for aorta samples at Novogene.

A comprehensive evaluation was carried out by Novogene using several QC methods to ensure that the samples met the required criteria and qualified for library preparation. This was to ensure that the quality of the samples was not affected during the transportation process. All RNA samples from both groups passed the QC and qualified for RNA-seq. Figure 6.3 shows the QC results summary provided by Novogene.

	No.	Sample Name	Nucleic Acid ID	Concentration(ng/ul)	Volume(ul)	Total amount(ug)	RIN	Sample QC Results	Sample QC Memo
Control	1	HRA13_1L	EKRN210022899-1A	215.00	7	1.50500	7.5	Pass	N/A
	2	HRA12_NT	EKRN210022900-1A	449.00	7	3.14300	7.0	Pass	N/A
	3	HRA12_1L1R	EKRN210022901-1A	437.00	6	2.62200	7.4	Pass	N/A
	4	HRA3_1L	EKRN210022902-1A	255.00	7	1.78500	8.0	Pass	N/A
	5	HRA2_1R	EKRN210022903-1A	235.00	7	1.64500	7.9	Pass	N/A
	6	HRA8_NT	EKRN210022904-1A	250.00	7	1.75000	7.5	Pass	N/A
	7	HRA10_NT	EKRN210022905-1A	340.00	6	2.04000	7.4	Pass	N/A
	8	HRA1_1R	EKRN210022906-1A	276.00	7	1.93200	8.1	Pass	N/A
RSV	9	HRC13_NT	EKRN210022907-1A	344.00	7	2.40800	8.3	Pass	N/A
	10	HRC9_1L	EKRN210022908-1A	109.00	7	0.76300	8.3	Pass	N/A
	11	HRC11_1L1R	EKRN210022909-1A	251.00	6	1.50600	7.8	Pass	N/A
	12	HRC13_1L	EKRN210022910-1A	288.00	7	2.01600	7.9	Pass	N/A
	13	HRC12_1R	EKRN210022911-1A	188.00	6	1.12800	7.6	Pass	N/A
	14	HRC12_1L	EKRN210022912-1A	352.00	6	2.11200	7.4	Pass	N/A
	15	HRC11_1L	EKRN210022913-1A	407.00	5	2.03500	7.2	Pass	N/A
	16	HRC11_NT	EKRN210022914-1A	418.00	5	2.09000	7.2	Pass	N/A

Figure 6.3 Summary of QC results provided by Novogene

Thoracic aorta from LDLR^{-}/$^{-}$ mice fed HFD or HFD supplemented with RSV were collected and kept in RNAlater solution. RNA extraction was carried out using RNA mini kit following the manufacturer's instructions. Only RNA samples that met the RNA-seq requirements were sent to Novogene. Second QC check, including gel electrophoresis, Nanodrop and Agilent 2100 was performed, and QC results' report was generated. The test conclusion was based on the "RNA Samples QC Criteria" that reveals if the testing sample fulfils the library construction requirements. Pass indicates that the samples completely fulfil the criteria for library construction and sequencing. **Abbreviations:** RSV, resveratrol; RIN, RNA integrity number; N/A, not available.

6.2.2 Principal component analysis (PCA)

The principal component analysis (PCA) was performed by Novogene. It is frequently employed to assess intragroup variations and summarise the information in large data tables. It was carried out using the gene expression value (Fragments Per Kilobase of transcript sequence per Millions base pairs sequenced, FPKM) of all samples. Figures 6.4 and 6.5 show the distribution of samples before and after removing the outliers. Based on the data distribution shown in Figures 6.4, control 1, 2 and 3 and treated 2 samples were considered outliers as they are far from other samples in the same group which may affect the data accuracy. As clearly seen in Figure 6.5, the samples between the two groups (control and treated) are dispersed while samples within the same group are clustering, indicating optimal condition.

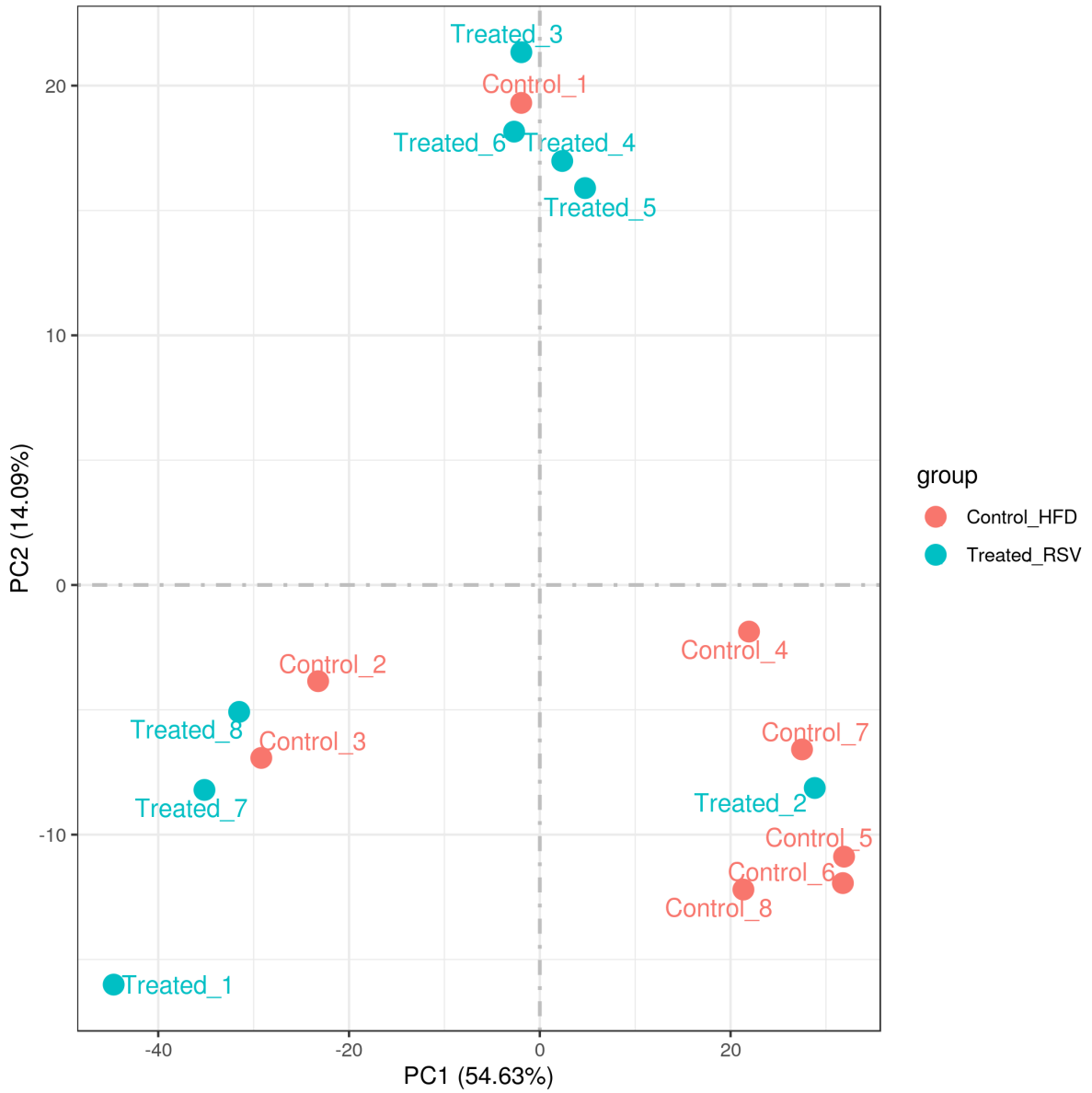

Figure 6.4 Principal component analysis (PCA) for all 16 samples from control and RSV group.

The graph shows the PCA of the entire data (8 samples from the control group and 8 samples from the RSV group) before removing the outliers. The red dots represent the control group while green dots represent the RSV group.

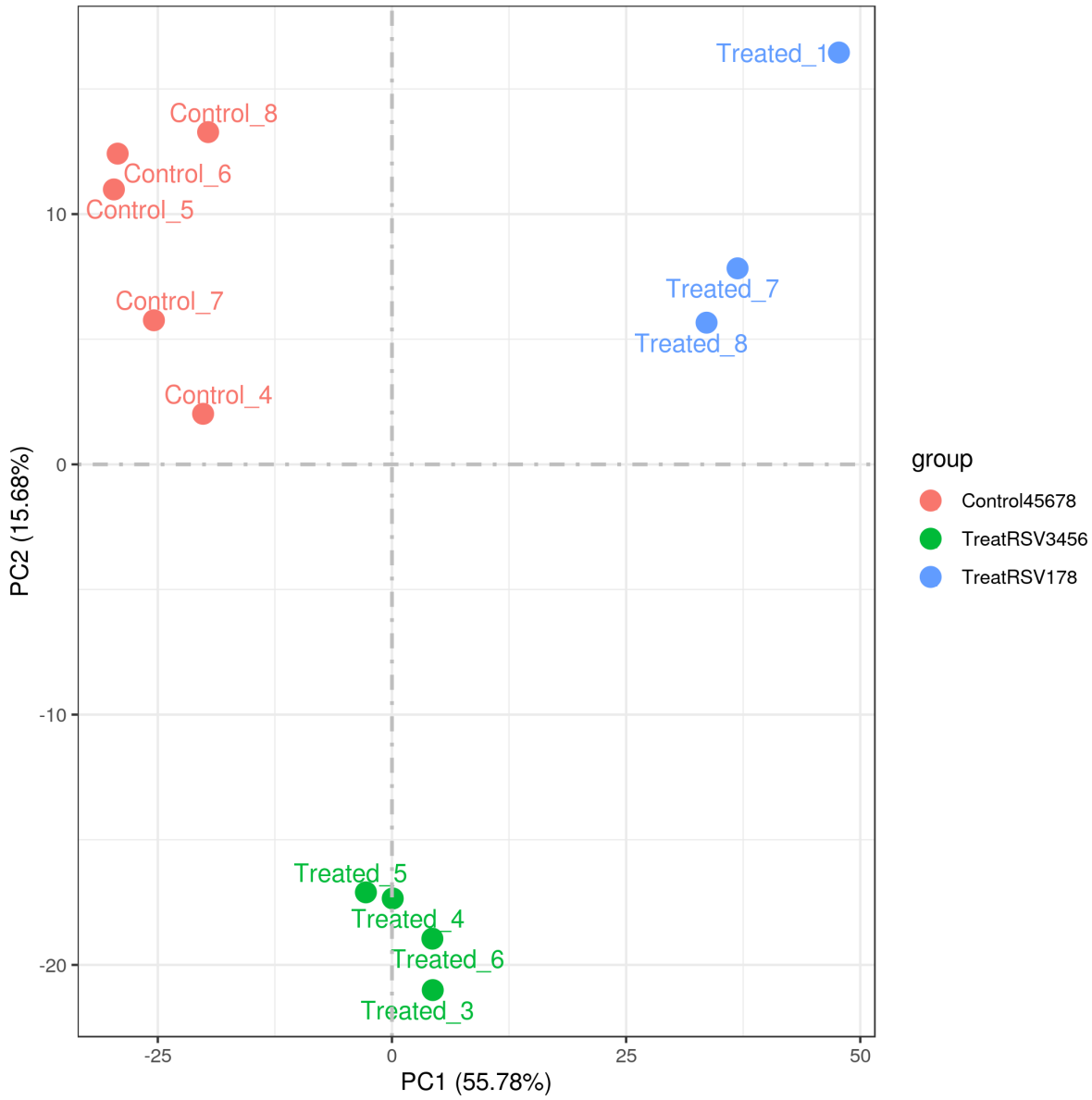

Figure 6.5 Principal component analysis (PCA) after removing the outliers from both groups.

The graph shows the difference between the two groups after removing the outliers. The dot represents sample for each group, red dots represent the control group while green and blue dots represent the RSV group.

6.2.3 Data analysis

Two analysis options were generated by Novogene based on data distribution seen in Figure 6.5. In the first file, a comparison between control samples 4, 5, 6, 7, 8 versus RSV samples 3, 4, 5, 6, while in the second file comparison between control samples 4, 5, 6, 7, 8 versus RSV samples 1, 7, 8, was performed. The analysis of both files shows a lot of similarity in the majority of the comparison aspect, including the affected canonical pathways and top affected molecular and cellular functions. However, the data from the first file (control 4, 5, 6, 7, 8 versus RSV 3, 4, 5, 6) was chosen to be presented in this Chapter due to more samples in the treatment group. Data from the second file (control 4, 5, 6, 7, 8 versus RSV 1, 7, 8) are presented in the appendix.

6.2.3.1 The effect of RSV intervention on gene expression

The transcriptome analysis of RNA samples from both groups showed that there are 419 genes in the control group versus 1,031 genes in the RSV group only that are uniquely expressed in each group while there are 11,888 overlapping genes between the two groups (Figure 6.6).

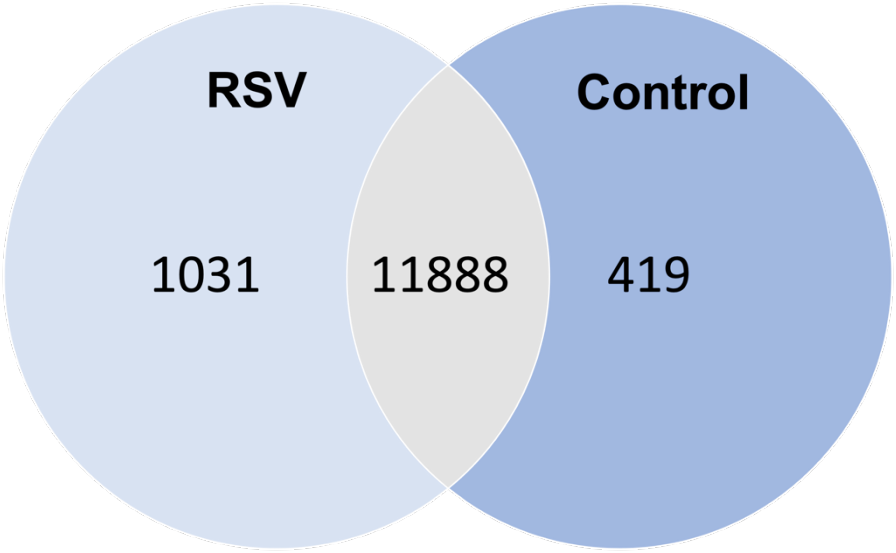

Figure 6.6 Venn diagram showing numbers of genes expressed in the two groups.

The co-expression Venn diagram shows the number of genes that are expressed uniquely within each group, with overlapping areas (grey) indicating the number of genes that are expressed in both groups.

6.2.4 Effect of RSV intervention on differentially expressed genes (DEGs)

The significant and non-significant DEGs were plotted as a volcano plot using NovoSmart from Novogene as shown in Figure 6.7. The statistically significant DEGs are shown above the horizontal dotted lines; with adjusted *p* value <0.05. There are 5178 DEGs significantly different between the two groups ($p < 0.05$) with 2,100 downregulated and 3,078 upregulated genes (Figure 6.8). A list of the top 20 significant up-regulated and top 20 significant down-regulated DEGs are displayed in Table 6.1 and 6.2 respectively.

In addition to identifying the DEGs, gene ontology (GO) enrichment analysis was performed using NovoSmart from Novogene with adjusted *p* value <0.05 to annotate genes according to their biological processes (BP), cellular components (CC) and molecular functions (MF). From the GO enrichment analysis results, the top 30 most significant terms that were represented in each of the three GO categories are shown in Figure 6.9. The GO enrichment analysis revealed that significant genes were associated with mitochondrial organisation, fatty acid oxidation and lipid oxidation. Figure 6.10. shows the number of genes involved in each GO term.

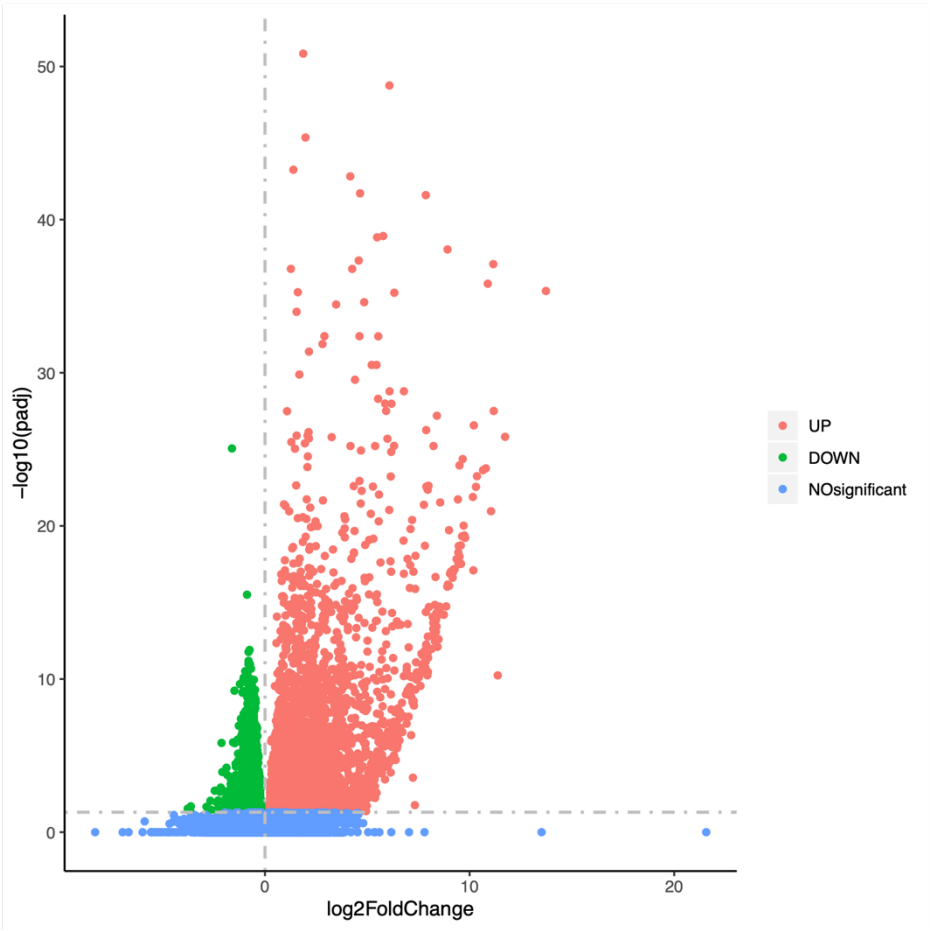

Figure 6.7 Volcano plot shows the upregulated and downregulated DEGs.

The x-axis represents log2Fold change while the y-axis represents −log 10 (adjusted P-value<0.05). The blue dots represent non-significant DEGs, red dots represent significantly upregulated DEGs while green dots represent significantly downregulated DEGs.

.

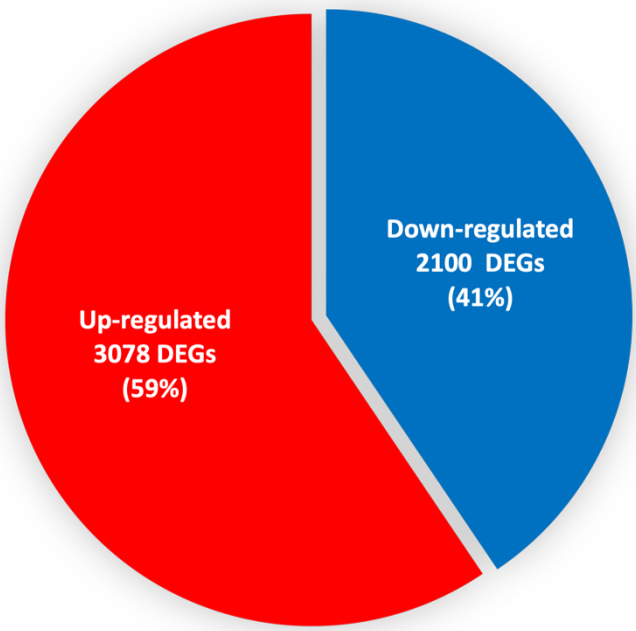

Figure 6.8 Venn diagram for significant DEGs.

The graph represents the number and percentage of significantly up-regulated DEGs (red) and down-regulated DEGs (blue) in RSV group after 12 weeks of feeding HFD compared to the control group.

Table 6. 1 List of top 20 significant up-regulated DEGs

Gene ID	Gene name	log2FoldChange	padj	Function	References
ENSMUSG00000054986	Sec14l3	13.7321262	4.54E-36	Has tumor-suppressive role	(Zhu et al. 2022)
ENSMUSG00000024653	Scgb1a1	11.7350869	1.52E-26	Influencing the inflammatory and immune responses of alveolar macrophages and helps to alleviate excessive cytokine surges in the lungs.	(Xu et al. 2020b)
ENSMUSG00000027483	Bpifa1	11.3777132	5.76E-11	Exhibits immunomodulatory properties in the context of airway inflammation	(Saferali et al. 2020)
ENSMUSG00000070306	Ccdc153	11.1815604	3.12E-28	Specific marker for ependymal cells	(Shu et al. 2022)
ENSMUSG00000027485	Bpifb1	11.1606842	8.04E-38	Contributing to innate immune response	(Li et al. 2020a)
ENSMUSG00000020159	Gabrp	11.0494518	1.10E-21	Act as an inhibitory neurotransmitter in the brain	(Petryshen et al. 2005)
ENSMUSG00000066108	Muc5b	10.8895913	1.52E-36	Has protective function in the normal lung	(Lachowicz-Scroggins et al. 2016)
ENSMUSG00000038791	Scgb3a2	10.7952908	1.74E-24	An emerging growth factor that plays a significant role in lung tissue.	(Kurotani et al. 2008)
ENSMUSG00000061527	Krt5	10.6578439	2.29E-24	Provides instructions for making fibrous proteins that form the structural framework of cells that make up the skin.	(Gholizadeh et al. 2020)
ENSMUSG00000021789	Sftpa1	10.3626256	5.70E-24	Has essential role in lung homeostasis and in the defence against respiratory diseases	(Nathan et al. 2016)
ENSMUSG00000021795	Sftpd	10.3122412	2.81E-23	Part of the innate immune response, protecting the lungs	(Leth-Larsen et al. 2005)
ENSMUSG00000005547	Cyp2a5	10.2087802	2.72E-27	Mediate regulation of testosterone homeostasis and the expression of salivary androgen-binding protein	(Zhou et al. 2011)
ENSMUSG00000040412	5330417C22Rik	10.1844118	7.97E-18	The precise function is not known	-
ENSMUSG00000047021	Cfap65	10.1610224	1.29E-22	Involve in spermiogenesis	(Wang et al. 2021)

ENSMUSG00000020062	Slc5a8	9.78199033	6.05E-20	Mediate the Wnt signaling pathway	(Zhang et al. 2020b)
ENSMUSG00000043164	Tmem212	9.7495765	4.21E-20	Predicted to contribute to the innate architecture of face processing	(Brown et al. 2012)
ENSMUSG00000064057	Scgb3a1	9.70962412	9.60E-21	It is anti-inflammatory and immunoregulatory mediators in airway diseases	(Mootz et al. 2022)
ENSMUSG00000054146	Krt15	9.66439725	4.28E-25	Biomarker of epidermal stem cells	(Bose et al. 2013)
ENSMUSG00000053153	Spag16	9.63234783	4.78E-20	Play an essential role in normal spermatogenesis and sperm motility	(Alciaturi et al. 2019)
ENSMUSG00000040728	Esrp1	9.58095391	3.01E-18	Suppress cancer cell motility	(Ishii et al. 2014; Willemsen and de Winther 2020)

Abbreviations of name of genes are listed in the appendix

Table 6.2 List of top 20 significant down-regulated DEGs

Gene ID	Gene name	log2FoldChange	padj	Function	References
ENSMUSG00000102833	Gm9694	-3.7762734	0.02890846	The precise function is not known	-
ENSMUSG00000107624	Gm44005	-3.7665275	0.03592688	The precise function is not known	-
ENSMUSG00000033063	Cntnap3	-3.6372881	0.04536434	Regulates mice social behaviors	(Tong et al. 2019)
ENSMUSG00000072972	Adam4	-3.6251437	0.02046171	Mediates inflammatory cells recruitment	(Van der Vorst et al. 2012)
ENSMUSG00000109931	Gm39929	-2.858631	0.02191331	The precise function is not known	-
ENSMUSG00000040808	S100g	-2.6682455	0.00890868	Involves in the development of atherosclerosis.	(Xiao et al. 2020)
ENSMUSG00000050423	Ppp1r3g	-2.6538171	0.03343438	Regulates glucose homeostasis during fasting	(Zhang et al. 2014)
ENSMUSG00000028655	Mfsd2a	-2.4541045	0.00195836	Suppress ECs transcytosis and maintain blood-retinal barrier	(Wang et al. 2020d)

ENSMUSG00000022066	Entpd4b	-2.3934877	0.03711833	Implicated in cell adhesion, proliferation and apoptosis	(Al-rashida and Iqbal 2014)
ENSMUSG00000113856	Gm10790	-2.3597655	0.01133276	The precise function is not known	-
ENSMUSG00000004552	Ctse	-2.2895025	0.04334212	Enhance the inflammatory process in atherosclerosis	(Zhao and Herrington 2016)
ENSMUSG00000107296	Gm43500	-2.2840553	0.00836291	The precise function is not known	-
ENSMUSG00000028009	1700061I17Rik	-2.2430635	0.011188	The precise function is not known	-
ENSMUSG00000106568	Gm42814	-2.2093334	0.00201351	The precise function is not known	-
ENSMUSG00000017868	Sgk2	-2.195767	0.00228925	Promotes renal cancer via mediating the phosphorylation of ERK 1/2 and AKT/PKB	(Liu et al. 2019c)
ENSMUSG00000110256	Gm45412	-2.1620337	0.00121022	The precise function is not known	-
ENSMUSG00000069456	Rdh16	-2.1565738	0.0185548	Regulates vitamin A function	(Duester 2000)
ENSMUSG00000111013	Gm32468	-2.1242367	1.48E-06	The precise function is not known	-
ENSMUSG00000049109	Themis	-2.0925128	0.04483984	Involves in T cell development	(Lesourne et al. 2009)
ENSMUSG00000001657	Hoxc8	-2.0864545	0.00011743	Marker of adipose tissue browning	(Fain et al. 2013)

Abbreviations: ERK, extracellular regulated protein kinases; AKT/PKB, protein kinase B; see appendix for list of abbreviation of gene.

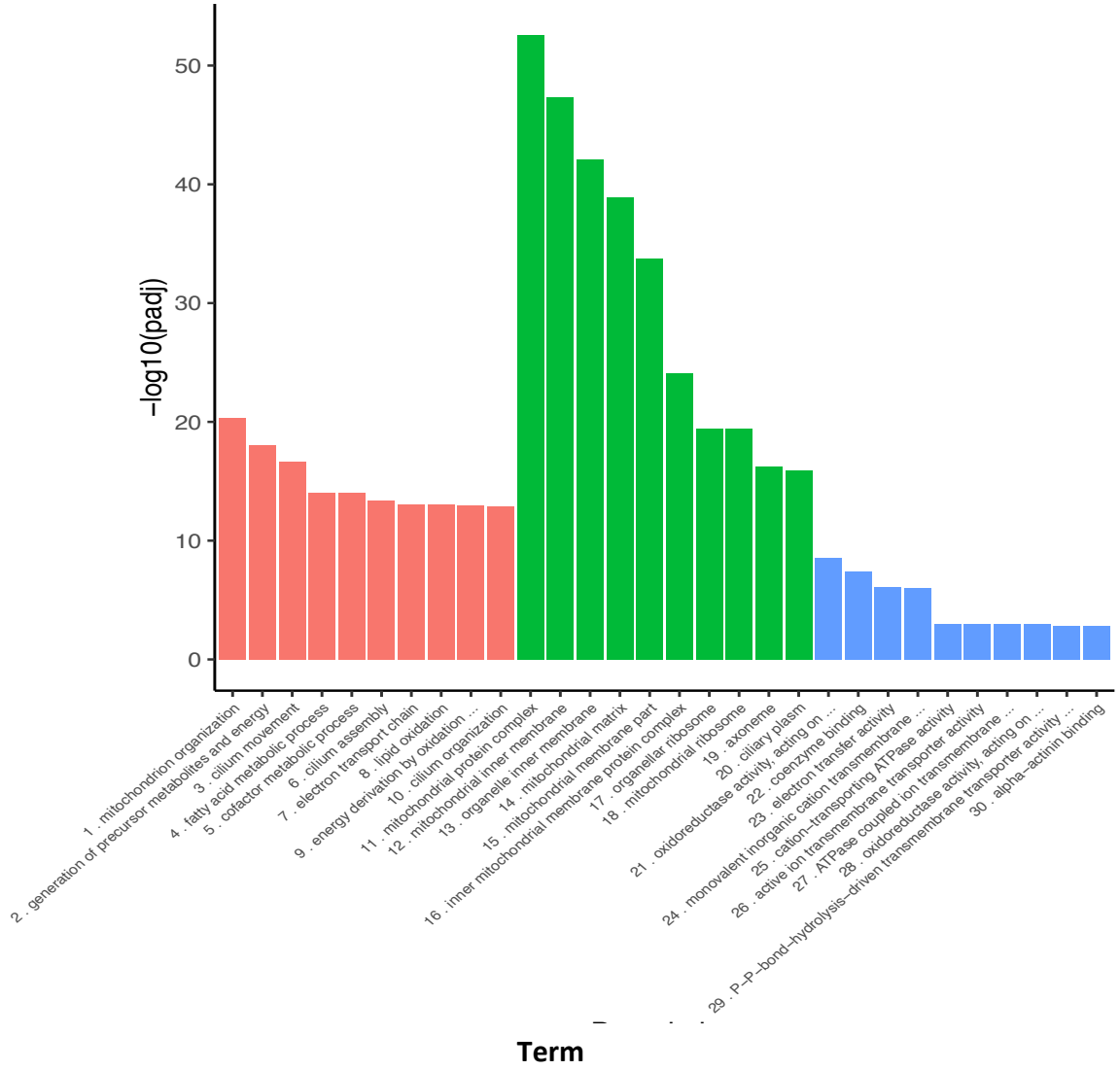

Figure 6. 9 The most enriched GO terms bar chart.

Bars in the figure with different colours correspond to different GO categories. Red bar represented biological process, green bar represented cellular component, and blue represented molecular function.

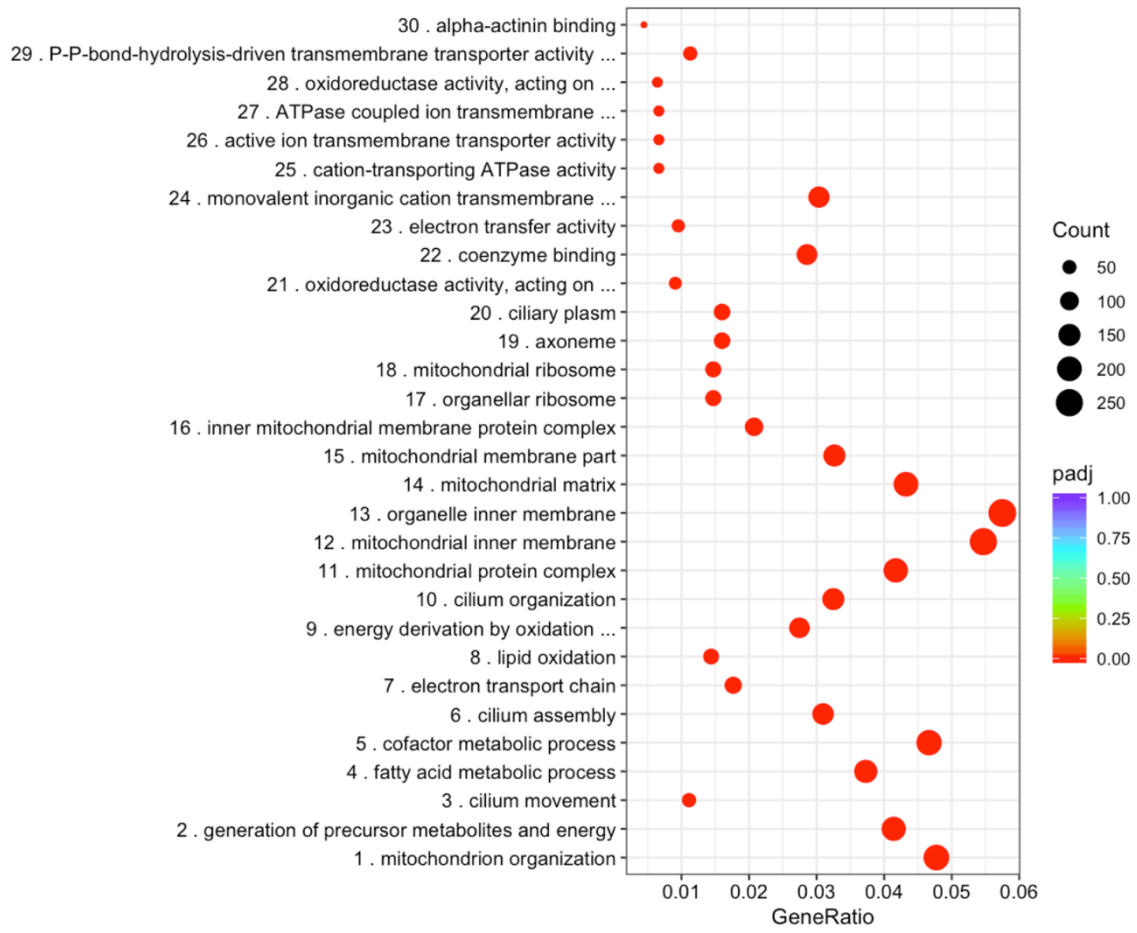

Figure 6.10 GO enrichment analysis dot plot shows the affected terms by RSV intervention.

The abscissa in the graph is the ratio of the differential gene number to the total number of differential genes on the GO term, and the ordinate is the top 30 significant GO enrichment terms. The colour of dots represents the significant level of enrichment while the size of the dots represents the number of genes annotated to a specific GO Term.

6.2.4.1 Effect of RSV treatment on canonical pathways in hypercholesterolemic LDLR^{-}/$^{-}$ mice

The IPA software was utilised to identify the canonical pathways for transcripts that are differentially activated or inhibited in the RSV group versus the control group with adjusted *p* <0.05. The top 20 canonical pathways affected by RSV are displayed in Figure 6.11. However, the top 20 potential pathways involved in the pathogenesis of atherosclerosis and may have an impact on the presented data in this study are shown in Figure 6.12. It can be clearly seen that the inclusion of RSV to HFD down-regulates several pathways such as oxidative phosphorylation (OXPHOS), valine and tryptophan degradation, fatty acid β-oxidation,

tricarboxylic acid (TCA) cycle, TG and cholesterol biosynthesis, ketogenesis, glycolysis and necroptosis signalling pathways. On the other hand, RSV intervention up-regulates white adipose tissue browning pathway, integrin-linked kinase (ILK) signalling, nitric oxide signalling (NO) and glutathione-mediated detoxification. In addition, although mitochondrial dysfunction emerges on the top of the canonical pathways list that was altered by RSV, IPA cannot predict if it is up-or down-regulated.

Furthermore, the vertical stacked bar chart was used to present the number of genes enriched in each potentially important canonical pathway (Figure 6.13) and the names of genes, including the *p*-value, are presented in Table 6.3. The IPA revealed mitochondria dysfunction as the top significantly enriched canonical pathway (p = 7.24E-23). Of the 160 genes implicated in this pathway, there are 127 genes (79.4 %) down-regulated and 32 genes (20%) up-regulated while one gene that does not overlap with the dataset. Following the mitochondria dysfunction pathway, oxidative phosphorylation was the second significantly enriched canonical pathway and the first significantly inhibited pathway by RSV (p = 2.43E-21). For 102 genes mapped, there were 91 DEGs down-regulated (89.2%) and 10 DEGs up-regulated (9.8%) while there is one gene that does not overlap with the dataset. All of the proteins encoded by these genes are located in the inner mitochondrial membrane and function as enzymes or transporters for mitochondria. The effect of RSV on genes attributed to mitochondria OXPHOS pathway is shown in Figure 6.14.

The sirtuin signalling pathway emerged as the third significantly enriched canonical pathway and the first significantly activated pathway by RSV (p = 1.32E-18). Of the 269 genes that are curated for this pathway, 189 genes (70.3%) are down-regulated, 77 (28.6%) genes are up-regulated and 3 genes in the pathway do not overlap with the dataset.

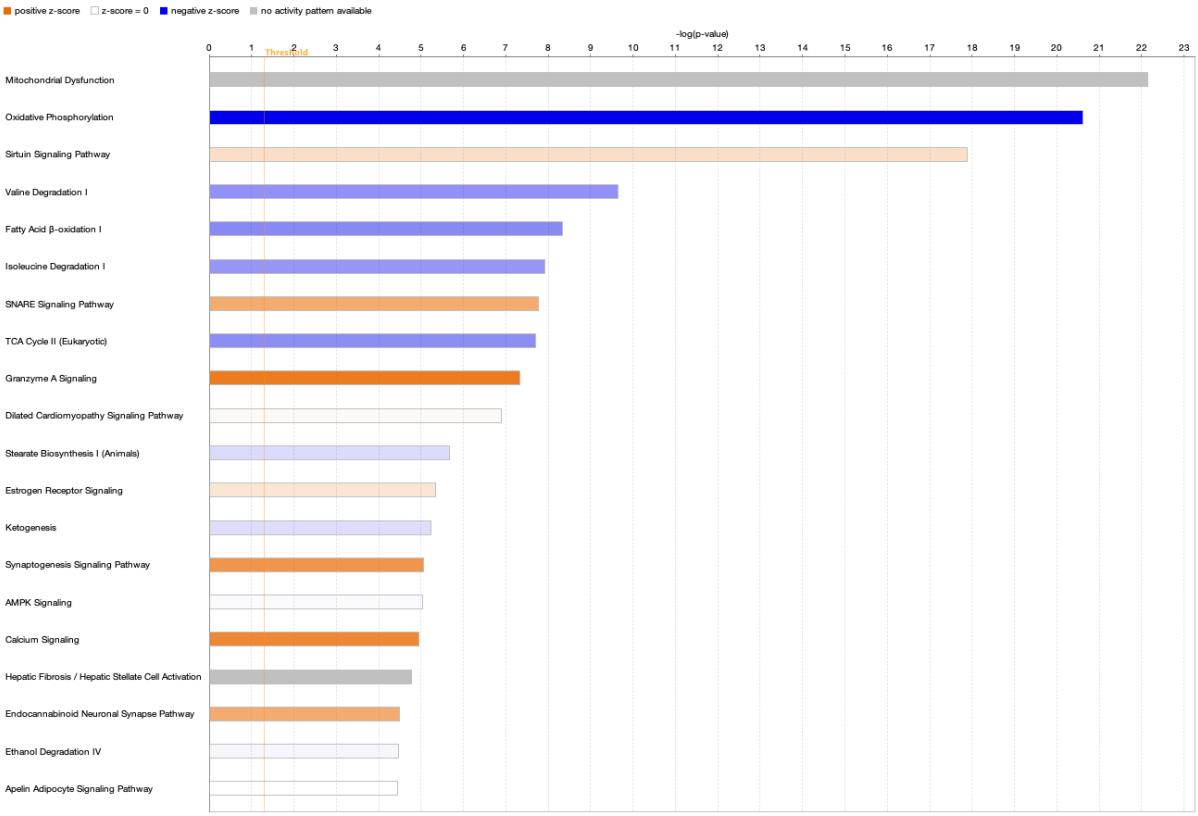

Figure 6. 11 Top 20 significantly affected canonical pathways by RSV intervention.

Flowing IPA "Core Analysis," several canonical pathways emerged. However, only the top 20 most significant canonical pathways across the entire dataset are displayed. The names of the pathways are displayed on the y-axis while the x-axis displays the -log of p-value that is calculated by the right-tailed Fisher's Exact Test. The taller the bars, the more significant the pathway. The blue and orange-coloured bar represents an overall negative z-score (predicted downregulated) and positive z-score (predicted upregulated), respectively. The grey bar indicates pathway that IPA is unable to make a prediction while the white bar shows the pathway with a z-score of zero or close to zero. The thin orange vertical line represents the ratio that is calculated as number of genes in a given pathway that meet cut-off criteria/the total number of known genes that make up that pathway and found in the IPA reference gene set. **Abbreviations:** TCA, tricarboxylic acid cycle; SNARE, soluble N-ethylmaleimide-sensitive factor attachment protein receptor; AMPK, AMP-activated protein kinase. Image generated by the IPA program.

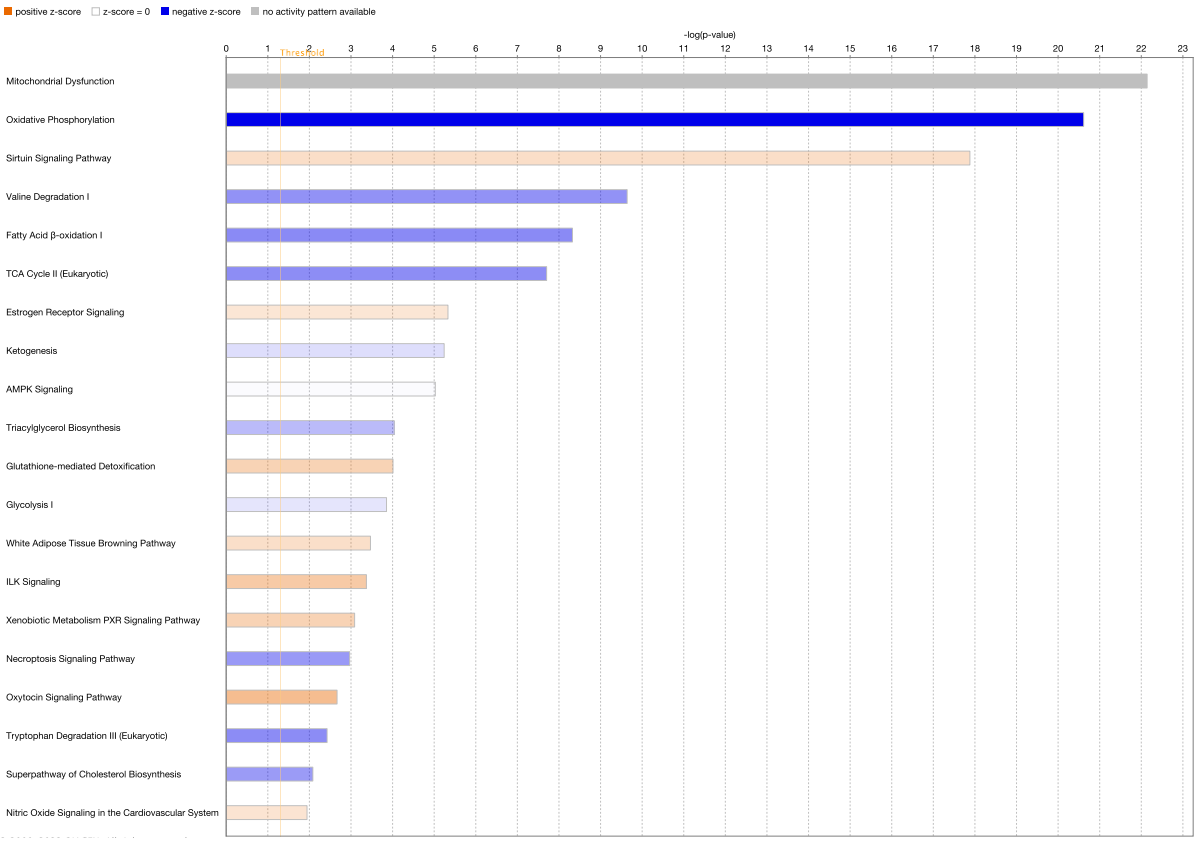

Figure 6.12 The top 20 potential canonical pathways involved in atherosclerosis pathogenesis

Following IPA "Core Analysis," several canonical pathways emerged. Among them, only the top 20 most significant canonical pathways across the entire dataset associated with atherosclerosis and/or may have an impact on the results in this study are shown. The names of the pathways are displayed on the y-axis while the x-axis displays the -log of p-value that is calculated by the right-tailed Fisher's Exact Test. The taller the bars, the more significant the pathway. The blue and orange-coloured bar represents an overall negative z-score (predicted downregulated) and the positive z-score (predicted upregulated), respectively. The grey bar indicates pathway that IPA is unable to make a prediction while the white bar shows the pathway with a z-score of zero or close to zero. The thin orange vertical line represents the ratio that is calculated as number of genes in a given pathway that meet cut-off criteria/the total number of known genes that make up that pathway and found in IPA reference gene set. **Abbreviations:** AMPK, AMP-activated protein kinase; ILK, integrin-linked kinase; TCA, tricarboxylic acid cycle. Image generated by the IPA program.

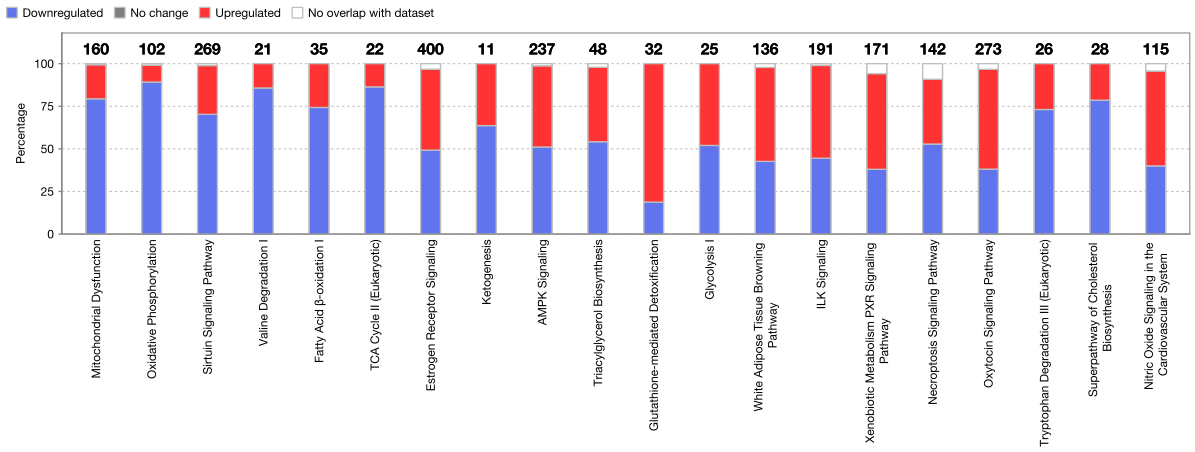

Figure 6.13 Stacked bar chart for the up- and down-regulated genes involved in each canonical pathway.

The chart displays the proportions of up-regulated (red) and down-regulated (blue) genes within each canonical pathway. The white area of the bar represents genes involved in the pathway but are not in the dataset. The most significant canonical pathways are listed on the x-axis (bottom) while the percentage of genes in a specific canonical pathway is shown on the y-axis. The numerical value above each bar represents the total number of genes in the pathway. Image generated by the IPA program.

Table 6.3 Ingenuity canonical Pathways with involved genes and p-value

Ingenuity Canonical Pathways	P-value	Z-score	Genes
Mitochondrial Dysfunction	7.24E-23	NaN	*Aco1,Aco2,Aifm1,App,Atp5e,Atp5f1a,Atp5f1b,Atp5f1d,Atp5mc1,Atp5mc3,Atp5mf,Atp5mg,Atp5pb,Atp5pf,Atpaf2,Bace2,Casp3, Cat,Cox10,Cox15,Cox17,Cox4i1,Cox5a,Cox6a1,Cox6a2,Cox6b1,Cox6c,Cox7a1,Cox7a2,Cox7b,Cox8a,Cox8b,Cpt1b,Cyb5b,Cyc1, Cycs, Dhodh, Glrx2, Gpd2,Gpx4,Hsd17b10,Htra2,Mapk10,Mapk12,Mt-Atp6,Mt-Nd1,Mt-Nd2,Mt-Nd3,Mt Nd6,Ndufa1,Ndufa10,Ndufa2,Ndufa3,Ndufa4,Ndufa6,Ndufa7,Ndufa8,Ndufa9,Ndufab1,Ndufaf1,Ndufb1, Ndufb11, Ndufb3, Ndufb4, Ndufb5, Ndufb6, Ndufb8,Ndufb9,Ndufs1,Ndufs2,Ndufs3,Ndufs4,Ndufs6,Ndufs8,Ndufv1, Ndufv2, Ndufv3,Ogdh,Pdha1,Prdx3,Rhot2,Sdha,Sdhb,Sdhc,Sdhd,Sod2,Surf1,Txn2,Txnrd2,Ucp2,Uqcr10,Uqcrb,Uqcrc1,Uqcrc2,Uqcrfs1,Uqc rq,Vdac1*
Oxidative Phosphorylation	2.43E-21	-7.344	*Atp5e,Atp5f1a,Atp5f1b,Atp5f1d,Atp5mc1,Atp5mc3,Atp5mf,Atp5mg,Atp5pb,Atp5pf,Atpaf2,Cox10,Cox15,Cox17,Cox4i1, Cox5a,Cox6a1,Cox6a2,Cox6b1,Cox6c,Cox7a1,Cox7a2,Cox7b,Cox8a,Cox8b,Cyb5b,Cyc1,Cycs,Mt-Atp6,Mt-Nd1,Mt-Nd2,Mt Nd3,Ndufa1,Ndufa10,Ndufa2,Ndufa3,Ndufa4,Ndufa6,Ndufa7,Ndufa8,Ndufa9,Ndufab1,Ndufb1,Ndufb11,Ndufb3,Ndufb 4,Ndufb5,Ndufb6,Ndufb8,Ndufb9,Ndufs1,Ndufs2,Ndufs3,Ndufs4,Ndufs6,Ndufs8,Ndufv1,Ndufv2,Ndufv3,Sdha,Sdhb,Sdhc ,Sdhd,Surf1,Uqcr10,Uqcrb,Uqcrc1,Uqcrc2,Uqcrfs1,Uqcrq*
Sirtuin Signalling Pathway	1.32E-18	1.363	*Abca1,Acadl,Acss2,Agtrap,App,Atg101,Atg12,Atg2a,Atg3,Atg4b,Atg4d,Atg7,Atg9b,Atp5f1a,Atp5f1b,Atp5f1d,Atp5mc1, Atp5pb,Atp5pf,Cdh1,Cpt1b,Cyc1,Dot1l,Foxo3,G6pd,Gabarapl1,Gabpa,Gadd45b,Gls,Glud1,Got2,H3-3a/H3-3b,Hif1a,Ldha,Ldhb,Ldhd,Mapk12,Mapk15,Mlycd,Mt-Atp6,Mt-Nd1,Mt-Nd2,Mt-Nd3,Mt Nd6,Mtor,Nampt,Ndufa1,Ndufa10,Ndufa2,Ndufa3,Ndufa4,Ndufa6,Ndufa7,Ndufa8,Ndufa9,Ndufab1,Ndufaf1,Ndufb1,N dufb11,Ndufb3,Ndufb4,Ndufb5,Ndufb6,Ndufb8,Ndufb9,Ndufs1,Ndufs2,Ndufs3,Ndufs4,Ndufs6,Ndufs8,Ndufv1,Ndufv2,N dufv3,Nqo1,Nr1h2,Nr1h3,Pam16,Parp1,Pck1,Pdha1,Pfkfb3,Pfkm,Pgam1,Pgam2,Pgk1,Polr1a,Polr1d,Ppara,Pparg,Ppif,Pr kaa2,Scnn1a,Sdha,Sdhb,Sdhc,Sdhd,Sirt3,Slc25a4,Slc25a5,Slc2a1,Sod1,Sod2,Sod3,Timm10,Timm13,Timm17a,Timm22,Ti mm23,Timm44,Timm50,Timm8a,Timm8b,Timm9,Tomm20,Tomm22,Tomm40,Tomm5,Tomm7,Tomm70,Tp53bp1,Tspo, Tuba1a,Tuba3e,Tuba4a,Ucp2,Uqcrc2,Uqcrfs1,Vdac1,Xrcc5,Xrcc6*
Valine Degradation I	2.29E-10	-3.153	*Abat,Acad8,Acadsb,Aldh6a1,Auh,Bcat2,Bckdha,Bckdhb,Dbt,Dld,Echdc3,Echs1,Ehhadh,Hadha,Hadhb,Hibadh,Hibch,Hsd1 7b4,Sds*
Fatty Acid β-oxidation I	4.73E-09	-3.411	*Acaa1,Acaa1b,Acaa2,Acadm,Acsf2,Acsl1,Acsl5,Acsl6,Acsm1,Auh,Echdc3,Echs1,Eci1,Eci2,Ehhadh,Hadh,Hadha,Hadhb,Hs d17b10,Hsd17b4,Scp2,Sds,Slc27a1,Slc27a2,Slc27a6*
TCA Cycle II (Eukaryotic)	1.98E-08	-3.3	*Aco1,Aco2,Cs,Dld,Dlst,Fh,Idh3a,Idh3b,Idh3g,Mdh1b,Ogdh,Ogdhl,Sdha,Sdhb,Sdhc,Sdhd,Sucla2,Suclg1*
Estrogen Receptor Signalling	4.66E-06	1.043	*Adcy1,Adcy10,Adcy2,Adcy3,Agt,Akt2,Atf2,Atp5f1a,Atp5f1b,Atp5f1d,Atp5mc1,Atp5pb,Cacna1b,Cacna1c,Cacna1d,Cacna 1s,Cacna2d1,Cacna2d2,Cacna2d3,Cacnb1,Cacnb2,Ccnd1,Cdk8,Cfl2,Creb3,Creb3l1,Creb3l2,Cyc1,Egf,Eif2b4,Eif4ebp1,Fbx o32,Foxa1,Foxo3,Foxo6,Gna13,Gna14,Gnai1,Gnas,Gnb1,Gng2,Gng3,Grb2,Gsk3a,Gucy1a1,Hes1,Hif1a,Igf1,Igf1r,Igf2r,Ja k3,Lepr,Limk2,Mmp11,Mmp14,Mmp15,Mmp19,Mmp2,Mmp9,Mt-Atp6,Mt-Nd1,Mt-Nd2,Mt-Nd3,Mt-Nd6,Mtor,Myl1,Myl12b,Myl3,Myl4,Myl6b,Myl7,Ncor2,Ndufa10,Ndufa2,Ndufa3,Ndufa4,Ndufa6,Ndufa7,Ndufa8,Ndufa9, Ndufab1,Ndufaf1,Ndufb1,Ndufb11,Ndufb3,Ndufb4,Ndufb5,Ndufb6,Ndufb8,Ndufb9,Ndufs1,Ndufs2,Ndufs3,Ndufs4,Nduf s6,Ndufs8,Ndufv1,Ndufv2,Ndufv3,Notum,Nr0b2,Pak1,Pgf,Pik3c2b,Pik3r2,Pik3r3,Plcb4,Plch1,Plch2,Plcl1,Ppp1r12b,Prkaa 2,Prkab2,Prkaca,Prkar1b,Prkar2a,Prkar2b,Prkca,Prkcz,Prkd1,Rala,Rasd2,Rbfox2,Rock2,Rps6kb1,Sdha,Sdhb,Sdhc,Sdhd,S od2,Tfam,Trim63,Uqcrc2,Uqcrfs1,Vegfa,Zdhhc7*
Ketogenesis	5.75E-06	-1	*Acaa2,Acat1,Acat2,Bdh1,Bdh2,Hadha,Hadhb,Hmgcl,Hmgcll1,Hmgcs1*
AMPK Signalling	9.39E-06	-0.14	*Acaca,Acacb,Adipoq,Adra1a,Adra1b,Adrb3,Ak1,Ak2,Ak3,Ak6,Ak7,Ak8,Ak9,Akt2,Atf2,Ccnd1,Chrna10,Chrna2,Chrna3,Chr nb4,Ckm,Cpt1b,Cpt2,Creb3,Creb3l1,Creb3l2,Eif4ebp1,Fasn,Foxo3,Foxo6,Gna13,Gna14,Gnai1,Gnas,Gnb1,Gng2,Gng3,Gys*

			1,Gys2,Hltf,Lipe,Mapk12,Mapk13,Mapk14,Mlycd,Mtor,Pfkfb1,Pfkfb2,Pfkfb3,Pfkl,Pfkm,Pfkp,Pik3c2b,Pik3r2,Pik3r3,Ppat,Ppm1a,Ppm1e,Ppm1j,Ppm1k,Ppm1m,Ppp2r1b,Ppp2r2b,Ppp2r2c,Ppp2r2d,Ppp2r3a,Ppp2r5a,Prkaa2,Prkab2,Prkaca,Prkar1b,Prkar2a,Prkar2b,Ptpa,Rab27a,Rab2a,Rab3a,Rab7a,Rps6kb1,Slc2a1,Smarca2,Smarcb1,Smarcc2,Smarcd1,Smarcd3,Stim1,Tbc1d1
Triacylglycerol Biosynthesis	9.12E-05	-1.964	*Abhd5,Agpat1,Agpat2,Agpat3,Aspg,Crls1,Dbt,Dgat1,Dgat2,Elovl6,Gpam,Gpat4,Lpcat2,Lpcat3,Lpin1,Mboat1,Mboat2,Mboat7,Mogat1,Osgepl1,Plpp1,Plpp3,Plpp6,Porcn*
Glutathione-mediated Detoxification	9.77E-05	1.807	*GSTA3,Gsta4,GSTA5,GSTM1,GSTM2,GSTM5,Gstm6,GSTO1,GSTO2,Gstt1,GSTT2/GSTT2B,Gstt3,GSTZ1,MGST1,MGST2,MGST3,Nat8f3 (Includes Others),Nat8f4*
Glycolysis I	1.40E-04	-0.775	*Aldoa,Aldoc,Eno1,Eno2,Eno3,Eno4,Fbp2,Gpi,Pfkl,Pfkm,Pfkp,Pgam1,Pgam2,Pgk1,Pkm*
White Adipose Tissue Browning Pathway	3.40E-04	1.313	*Adcy1,Adcy10,Adcy2,Adcy3,Adrb3,Atf2,Cacna1b,Cacna1c,Cacna1d,Cacna1g,Cacna1h,Cacna1s,Cacna2d1,Cacna2d2,Cacna2d3,Cacnb1,Cacnb2,Creb3,Creb3l1,Creb3l2,Fgfr3,Fndc5,Gnas,Gucy1a1,Itpr2,Klb,Ldha,Ldhb,Ldhd,Lipe,Mapk12,Mapk13,Mapk14,Nppa,Plin1,Ppara,Pparg,Prkaa2,Prkab2,Prkaca,Prkar1b,Prkar2a,Prkar2b,Prkg1,Rarg,Runx1t1,Rxrb,Slc16a1,Ucp1,Vegfa,Vgf*
ILK Signalling	4.26E-04	2.177	*Actg2,Actn2,Akt2,Atf2,Casp3,Ccnd1,Cdh1,Cfl2,Creb3,Creb3l1,Creb3l2,Dsp,Flnc,Gsk3a,Hif1a,Irs3,Itgb4,Itgb6,Itgb8,Krt18,Mapk10,Mapk12,Mmp9,Mtor,Myh14,Myh6,Myh7,Myh8,Myl1,Myl3,Myl4,Myl6b,Myl7,Myo10,Myo18a,Myo18b,Myo1h,Parva,Parvb,Pgf,Pik3c2b,Pik3r2,Pik3r3,Ppm1j,Ppp1r14b,Ppp2r1b,Ppp2r2b,Ppp2r2c,Ppp2r2d,Ppp2r3a,Ppp2r5a,Ptgs2,Ptpa,Pxn,Rac3,Rhobtb1,Rhobtb2,Rhod,Rhof,Rhoj,Rhoq,Rhot1,Rhot2,Rhou,Rhov,Tesk1,Vegfa*
Xenobiotic Metabolism PXR Signalling Pathway	8.18E-04	1.807	*Abcb1,Abcc3,Aldh18a1,Aldh1a1,Aldh1b1,Aldh1l1,Aldh1l2,Aldh3a1,Aldh3b1,Aldh4a1,Aldh6a1,Aldh9a1,Camk2a,Camk2d,Camk2g,Cat,Cdk2,Cdk5,Ces1,Ces1e,Chst11,Dnajc7,Gal3st2,Gsta3,Gsta5,Gstm1,Gstm2,Gstm5,Gstm6,Gsto1,Gsto2,Gstt2/Gstt2b,Gstz1,Hs6st2,Mgst1,Mgst2,Mgst3,Ncor2,Nr1i2,Ppm1a,Ppp1ca,Ppp1r14b,Ppp1r14c,Ppp1r3a,Ppp1r3d,Prkaca,Prkar1b,Prkar2a,Prkar2b,Prkca,Prkcz,Prkd1,Smox,Sult1c2,Sult1c3,Sult1d1,Sult1e1,Sult4a1,Ugt1a6,Ugt2b10*
Necroptosis Signalling Pathway	1.08E-03	-2.941	*Axl,Camk2a,Camk2d,Camk2g,Capn11,Capn2,Capn6,Capns1,Chp1,Dapk1,Glud1,Glul,Ifnar1,Ngfr,Pam16,Pla2g12a,Pla2g2e,Pla2g4a,Pla2g4e,Pla2g5,Pla2g6,Ppif,Pygl,Rb1,Rbck1,Rbl2,Slc25a13,Slc25a3,Slc25a4,Slc25a5,Timm10,Timm13,Timm17a,Timm22,Timm23,Timm44,Timm50,Timm8a,Timm8b,Timm9,Tlr3,Tnfrsf11b,Tomm20,Tomm22,Tomm40,Tomm5,Tomm7,Tomm70,Tspo,Tyro3,Vdac1*
Oxytocin Signalling Pathway	2.16E-03	2.712	*Abcb8,Akt2,Atf2,Atp2b1,Atp2b2,Atp2b4,Cacna1b,Cacna1c,Cacna1d,Cacna1s,Cacna2d1,Cacna2d2,Cacna2d3,Cacnb1,Cacnb2,Calm1,Cd36,Chp1,Creb3,Creb3l1,Creb3l2,Gna13,Gnai1,Gnb1,Gng2,Gng3,Grb2,Gucy1a1,Gucy2d,Hspb2,Hspb3,Hspb7,Itpr2,Kcnt2,Lipe,Lpl,Mapk10,Mapk12,Mapk13,Mapk14,Mapk15,Mef2c,Myh14,Myh6,Myh7,Myh8,Myl1,Myl3,Myl4,Myl6b,Myl7,Myo10,Myo18a,Myo18b,Myo1h,Nppa,Npr2,Pik3c2b,Pik3r2,Pik3r3,Pla2g12a,Pla2g2e,Pla2g4a,Pla2g4e,Pla2g5,Pla2g6,Plcb4,Pnpla2,Ppara,Pparg,Ppp1r12b,Prkaa2,Prkab2,Prkaca,Prkar1b,Prkar2a,Prkar2b,Prkca,Prkcz,Prkd1,Prkg1,Ptgfr,Ptgs2,Rala,Rasd2,Rock2,Smarcc2*
Tryptophan Degradation III (Eukaryotic)	3.75E-03	-3.317	*Acaa2,Acat1,Acat2,Cyp2s1,Ehhadh,Gcdh,Hacd2,Hadh,Hadha,Hadhb,Hsd17b10,Hsd17b4,L3hypdh*
Superpathway of Cholesterol Biosynthesis	8.28E-03	-2.887	*Acaa2,Acat1,Acat2,Cyp51a1,Dhcr7,Hadha,Hadhb,Hmgcs1,Hsd17b7,Idi1,Lss,Nsdhl,Pmvk*
Nitric Oxide Signalling in the Cardiovascular System	1.14E-02	1.095	*Adrb3,Akt2,Atp2a2,Cacna1b,Cacna1c,Cacna1d,Cacna1s,Cacna2d1,Cacna2d2,Cacna2d3,Cacnb1,Cacnb2,Calm1,Chrm1,Flt1,Flt4,Gucy1a1,Gucy2d,Itpr2,Kng1,Npr2,Pde1c,Pde2a,Pde3b,Pgf,Pik3c2b,Pik3r2,Pik3r3,Prkaca,Prkar1b,Prkar2a,Prkar2b,Prkca,Prkcz,Prkd1,Prkg1,Ryr2,Slc7a1,Vegfa*

Abbreviations: NaN, no activity pattern is available (z-score could not be calculated by IPA); see appendix for the list of abbreviations of genes.

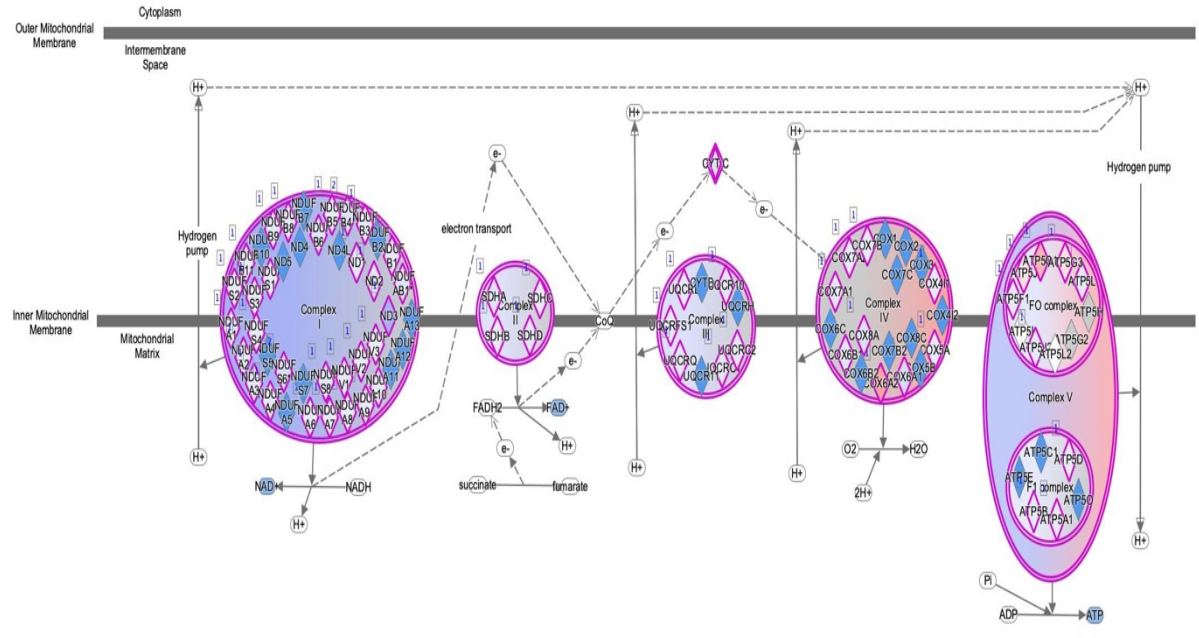

Figure 6.14 Schematic representation of oxidative phosphorylation pathway (OXPHOS) affected by RSV treatment.

The OXPHOS emerged as the most significantly enriched pathway inhibited by RSV. The inner mitochondrial membrane hosts five multi-subunit enzyme complexes (Complex I-V) and two electron carriers – coenzyme Q10 (CoQ10) and cytochrome C. The five complexes contain NADH: ubiquinone oxidoreductase (complex I), succinate: ubiquinone oxidoreductase (complex II), ubiquinol: ferrocytochrome c oxidoreductase (complex III), ferrocytochrome c: oxygen oxidoreductase or cytochrome c oxidase (complex IV), and ATP synthase (complex V). In the pathway, complex I catalyses the transfer of electrons from NADH to coenzyme Q (ubiquinone) that carries electrons from complex I to complex III. Complex II receives electrons from TCA cycle intermediate, succinate, and catalyses the transporter of electrons to FADH2 and then to coenzyme Q (ubiquinone) subsequently transferring electrons to complex III. In complex III, electrons transfer from ubiquinol to cytochrome C that brings electrons to complex IV. Finally, complex IV uses these electrons to reduce oxygen to water. The complex V is the final enzyme in the oxidative phosphorylation pathway and uses the energy stored in a proton gradient generated by respiratory chain to produce ATP from ADP. The genes in blue are those whose expression is suppressed while the genes in red are those whose expression is induced. Node intensity colour reflects the degree of significance whereases bright colour is less significant. Image generated by the IPA program.

6.2.4.2 Effect of RSV treatment on inflammatory signalling pathways involved in atherosclerosis.

Using the IPA software, the effect of RSV on important inflammatory signalling pathways implicated in atherosclerosis was searched in the database and the significant DEGs were overlayed on the pathway to visualise how the significantly up-and down-regulated genes in the dataset impact pathway activation. It was found that RSV significantly inhibits NF-κB signalling pathway (Figure 6.15). Furthermore, the effect of RSV on several other important pathways involved in inflammation, such as T cell receptor, NLRP3 inflammasome and Wnt/β-catenin pathway, was also investigated. As shown in Figures 6.16 and 6.17, both T cell receptor and NLRP3 inflammasome were predicted to be inhibited by RSV. On the other hand, the canonical Wnt/β-catenin pathway was predicted to be activated (Figure 6.18).

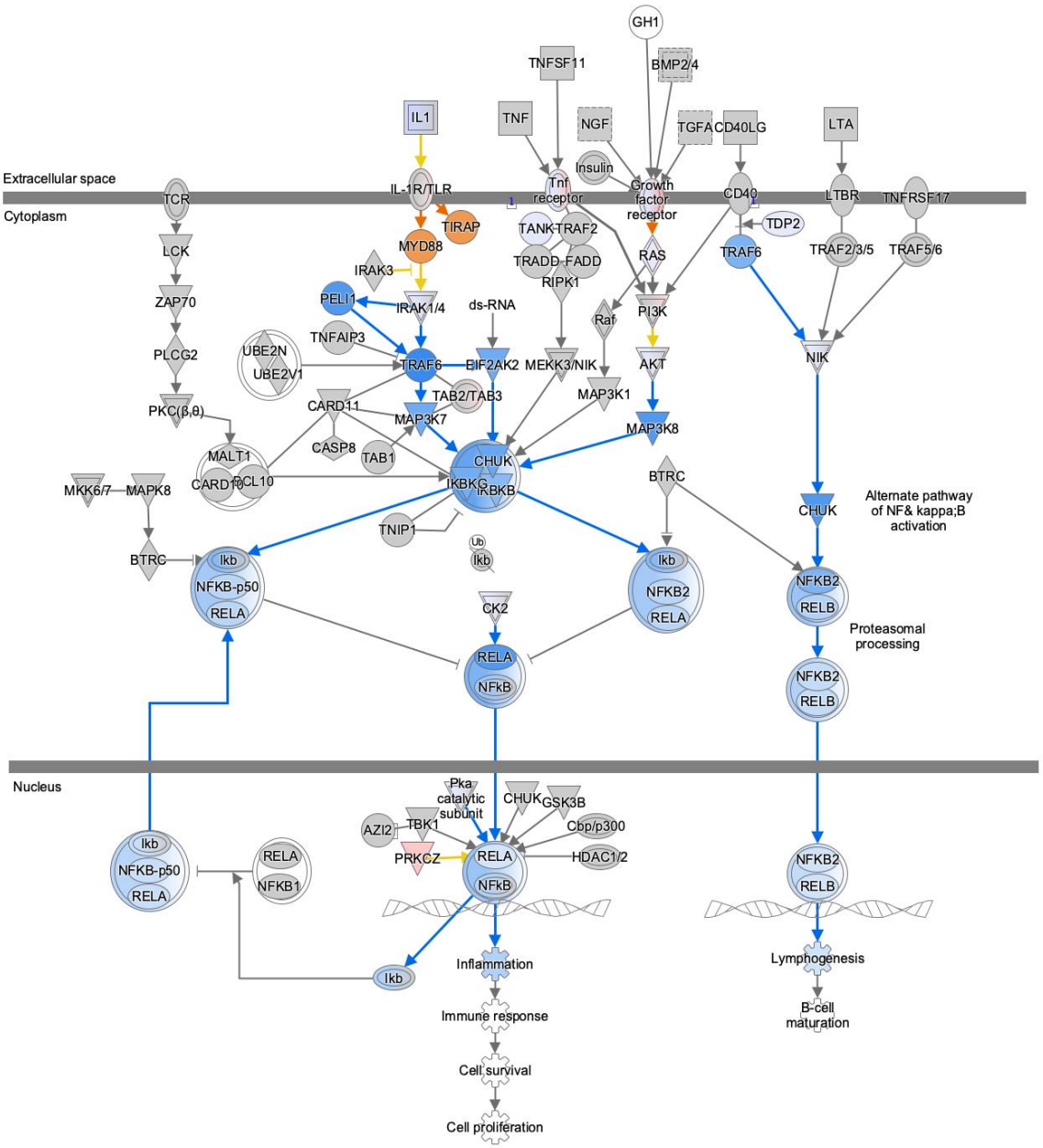

Figure 6.15 The NF-κB pathway was predicted to be inhibited by RSV.

The graph displays the NF-κB signalling pathway in which the genes in the data set were overlapped to visualise the effect of RSV intervention on genes implicated in the pathway and consequently pathway activation. The nodes in blue represent down-regulated genes while the red/orange nodes represent up-regulated genes. Genes in blue and red/orange colour are in the data set and are significantly dysregulated ($P<0.05$) while genes in gray colour are also in the data set but they are not significantly changed ($P\geq0.05$). **Abbreviations:** NF-κB, nuclear factor-kappa B; see appendix for the list of abbreviations of genes.

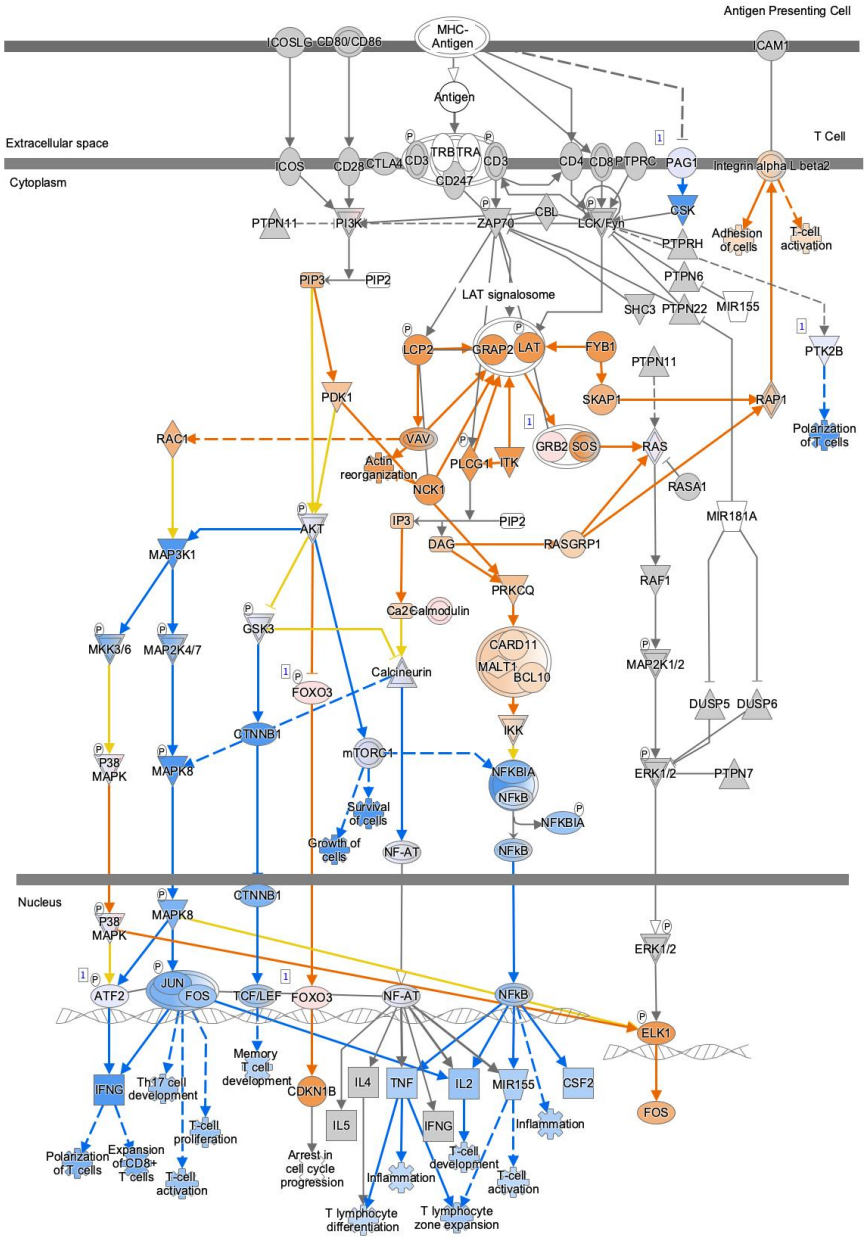

Figure 6.16 T cell signalling pathway was predicted to be inhibited by RSV.

The graph displays T cell signalling pathway in which the genes in the data set were overlapped to visualise the effect of RSV intervention on genes implicated in the pathway and consequently pathway activation. The nodes in blue represent down-regulated genes while the red/orange nodes represent up-regulated genes. Genes in blue and red/orange colour are in the data set and are significantly dysregulated ($P<0.05$) while genes in grey colour are also in the data set but they are not significantly changed ($P\geq0.05$). The graph shows the reduction in inflammation, T cell polarisation and activation, and expansion of $CD8^+$ T cells. See appendix for the list of abbreviations of genes.

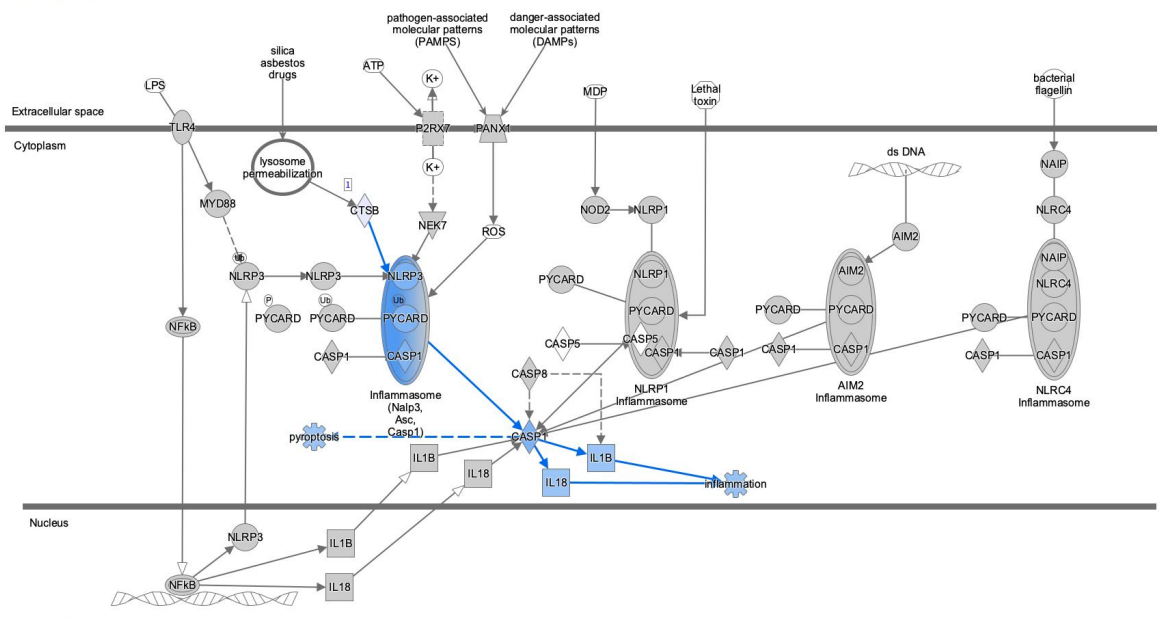

Figure 6.17 NLRP3 inflammasome activation was predicted to be inhibited by RSV intervention.

The graph displays the inflammasome activation pathway in which the genes in the data set were overlapped to visualise the effect of RSV intervention on genes implicated in the pathway and consequently pathway activation. The nodes in blue represent down-regulated genes. Genes in blue nodes are in the data set and they are significantly dysregulated ($P<0.05$) while genes in grey nodes are also in the data set, but they are not significantly changed ($P\geq0.05$). See appendix for the list of abbreviations of genes.

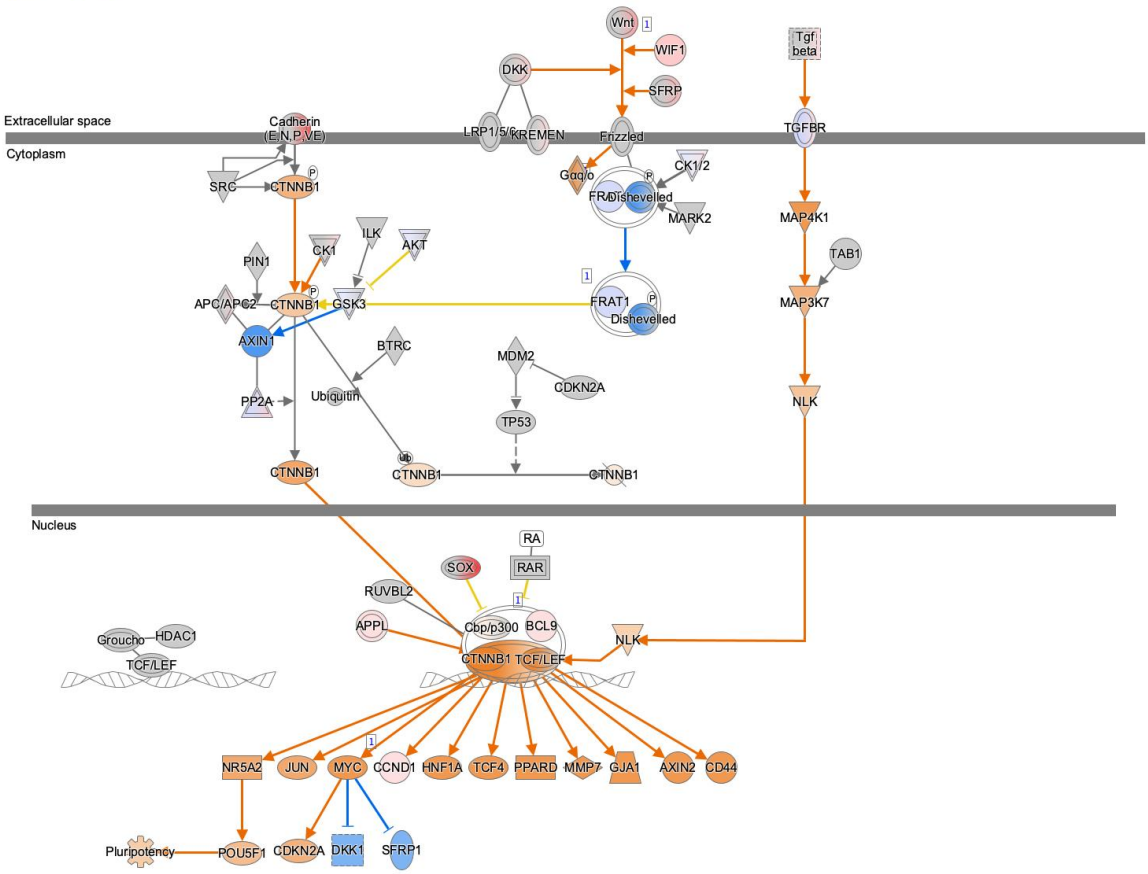

Figure 6.18 Wnt/β-catenin pathway was predicted to be activated by RSV.

The graph displays Wnt/β-catenin pathway in which the genes in the data set were overlapped to visualise the effect of RSV intervention on genes implicated in the pathway and consequently pathway activation. The nodes in blue and red/orange represent down-and up-regulated genes respectively. Genes in blue and red/orange nodes are in the data set and they are significantly dysregulated ($P<0.05$) while genes in grey nodes are also in the data set, but they are not significantly changed ($P\geq0.05$). See appendix for the list of abbreviations of genes.

6.2.4.3 Effect of RSV treatment on disease and functions in hypercholesterolemic LDLR$^{-/-}$ mice

Several diseases and biological functions are affected by RSV intervention, including organ morphology and development, lipid and carbohydrate metabolism and the cardiovascular system. Figure 6.19 shows the most affected biological processes associated with atherosclerosis development. Furthermore, by taking advantage of the Tox function tool in IPA, which helps to link experimental data to clinical pathology endpoints and consequently understand the pharmacological response and support the mechanism of action, it was found that RSV supplementation significantly affected several genes involved in glycolysis and lipid metabolism. This effect was predicted to result in a decrease in accumulation and concentration of TG, lipids and long-chain fatty acids, beta-oxidation of lipids and fatty acids

as well as lipid storage and an increase in lipolysis (Figure 6.20A and B) and decrease in glycolysis (Figure 6.20C). Furthermore, genes implicated in cardiac functions were also affected by RSV. For instance, there an inhibition was predicted in cardiac necrosis, fibrosis of the heart, heart failure, dysfunction of the heart, damage of heart muscles, tachycardia, bradycardia and LDH activity and quantity, in addition to activation in cardiogenesis (Figure 6.21). Moreover, several genes were affected that are predicted to reduce weight and obesity (Figure 6.22). In addition to the affected function and disease provided by IPA, the genes implicated in collagen synthesis and plaque stability were explored in the DEGs list and are presented in Figure 6.23.

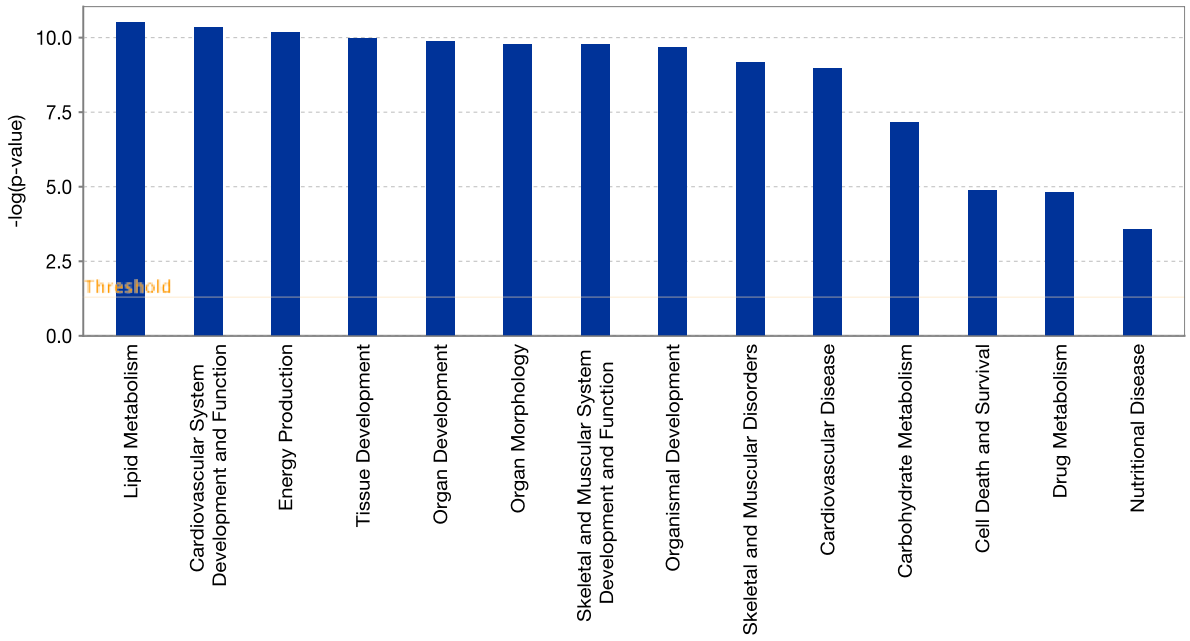

Figure 6.19 The most affected biological functions by RSV intervention.

The graph shows the most affected biological processes associated with atherosclerosis development. The orange line shows the default p-value significance threshold of 0.05. Abbreviations of name of genes are listed in the appendix.

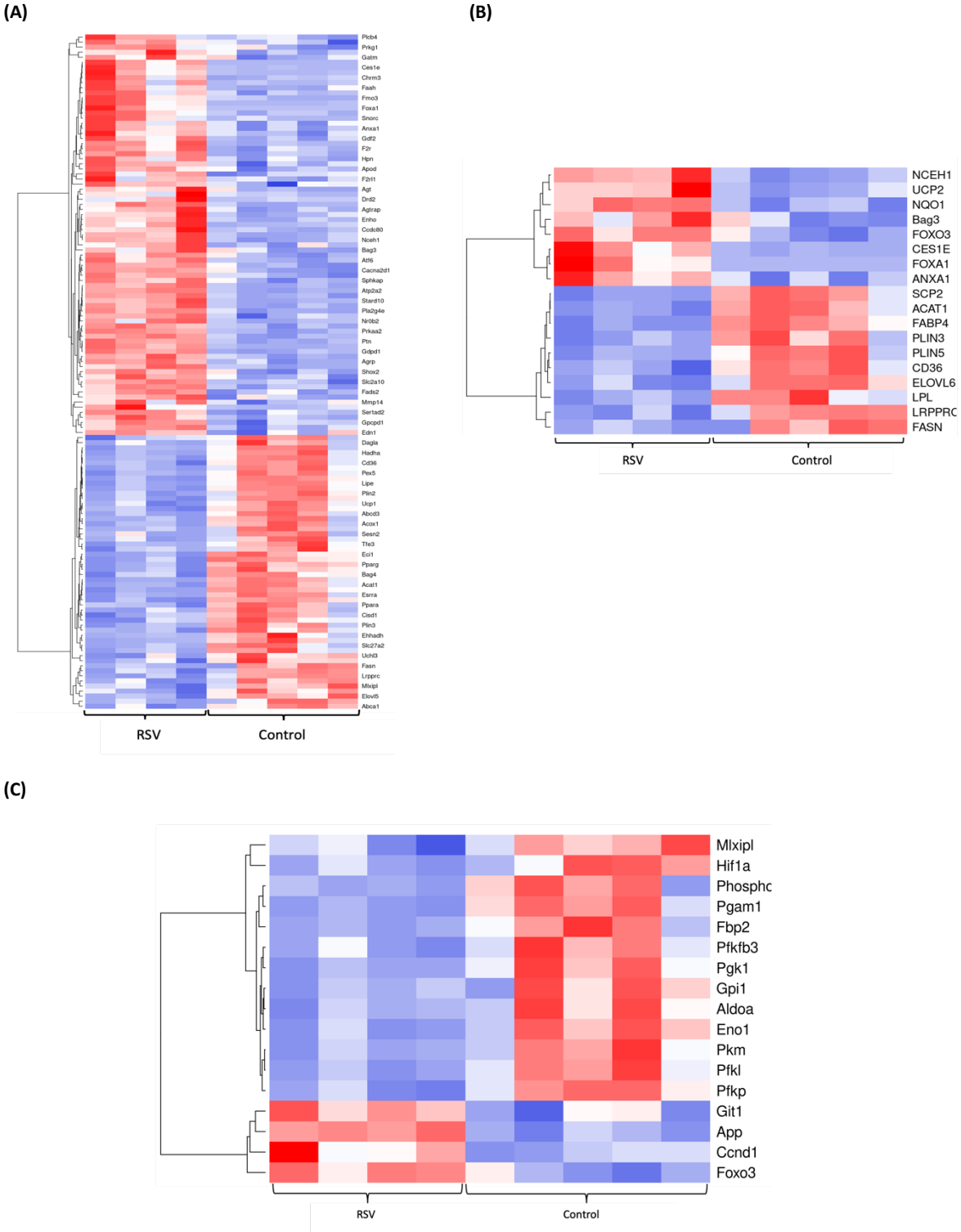

Figure 6.20 Heatmaps for genes implicated in lipid metabolism and glycolysis.

The IPA provides the list of genes that were significantly regulated and associated with a biological process or function. These genes were pre-ranked from lowest-to-highest log2FC and then inputted into Heatmapper software. (A) represents all genes in the data set that were implicated in the regulation of lipid metabolism, (B) represents genes of interest in lipid metabolism, that their role in lipid metabolism and macrophage foam cell formation is well known, while (C) displays genes implicated in down-regulation of glycolysis. Heatmaps were generated using http://www.heatmapper.ca/expression/. Abbreviations of the name of gene are listed in the appendix.

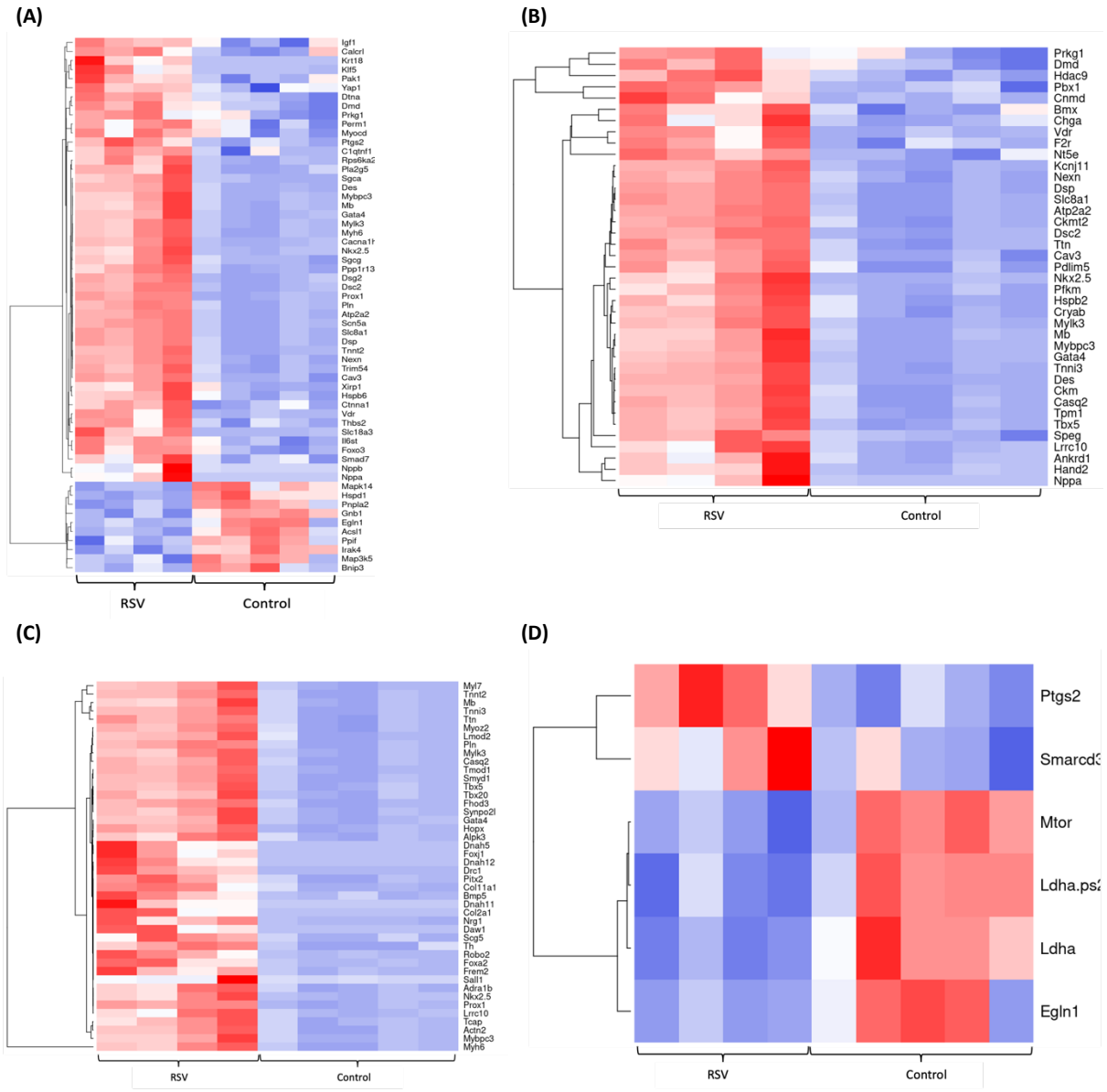

Figure 6.21 Heatmaps for genes involved in improvement of cardiac function.

The IPA provide the list of genes that were significantly regulated and associated with a biological process or function. These genes were pre-ranked from lowest-to-highest log2FC and then inputted into Heatmapper software. (A) represents all genes implicated in decrease of necrosis and fibrosis of cardiac muscle, (B) displays genes implicated in decrease in dysfunction of heart, (C) represents all genes involved in increase of cardiogenesis, and (D) represents all genes implicated in decrease in LDH quantity and activation. Heatmaps were generated using http://www.heatmapper.ca/expression/. See appendix for list of the abbreviations of genes.

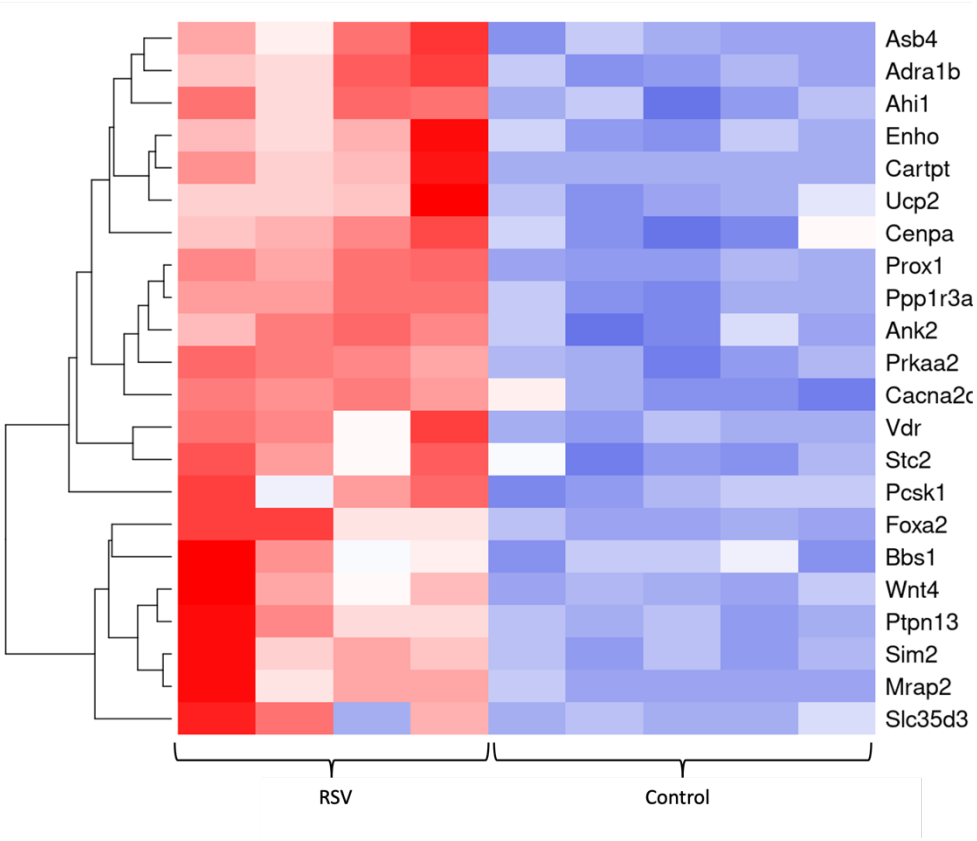

Figure 6.22 Heatmap for genes involved in reducing obesity and weight gain.

The heatmap shows significant downregulated and upregulated genes associated with reducing obesity and weight gain. These genes were pre-ranked from lowest-to-highest log2FC and then inputted into Heatmapper software (http://www.heatmapper.ca/expression/). See appendix for list of the abbreviations of genes.

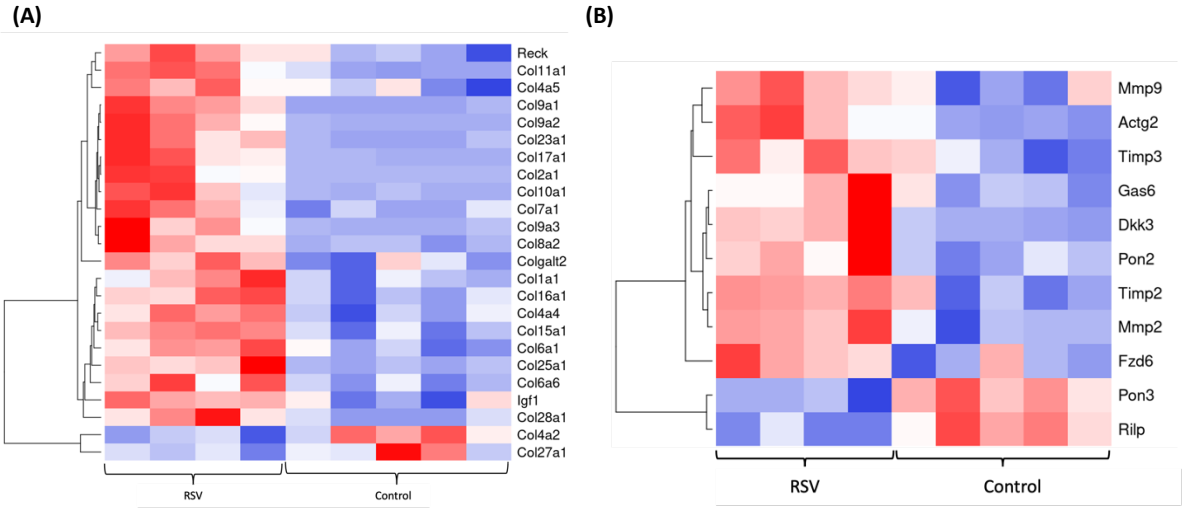

Figure 6.23 Heatmaps for genes implicated in collagen synthesis and atherosclerotic plaque stability.

Genes implicated in collagen synthesis and atherosclerotic plaque stability were explored in the list of significantly DEGs. These genes were pre-ranked from the lowest-to-highest Log2FC and then inputted into Heatmapper software (http://www.heatmapper.ca/expression/). (A) shows heatmap for collagen synthesis while (B) shows heatmap for plaque stability genes. **Abbreviations:** DEGs, differentially expressed genes; Abbreviations of genes name are listed in the appendix.

6.2.4.4 Effect of RSV intervention on upstream regulators

The upstream regulator analysis in IPA is an important tool in which the potential upstream regulators that are responsible for the changes observed in gene expression in the dataset were identified together with whether they are likely to be activated or inhibited. The activation state of each upstream regulator was predilected based on the activation z-score where predicted activated regulators have a positive z-score while predicted inhibited regulators have a negative z-score. The overlap *p*-value measures whether there is a statistically significant overlap between genes in the dataset and the genes that are regulated by transcriptional regulators. The top predicted upstream regulators are listed in Table 6.4. Furthermore, the IPA upstream regulator analysis can also be used to display each regulator as a network, showing the affected genes in the dataset. For in-depth analysis, grow tool in IPA allows visualisation of the relationship between those affected genes and diseases and functions. Thioredoxin reductase 1 (*Txnrd1*) was chosen as an example to be presented as a network since it has been found to play a role in liver lesions and may impact on the results presented in the next chapter (Figure 6.24).

Table 6.4 Top predicted upstream regulators affected by RSV

Upstream regulator	Molecule type	Predicted activation state	Activation z-score	*p*-value of overlap
Tead1	transcription regulator	Inhibited	-6.745	1.52E-28
Kdm5a	transcription regulator	Activated	3.976	2.03E-25
Map4k4	kinase	Activated	6.134	3.66E-24
Clpp	peptidase	Activated	6.733	3.79E-21
Tp53	transcription regulator	Activated	5.349	1.32E-18
Cpt1b	enzyme	Activated	6.589	7.92E-18
Slc27a2	transporter	Activated	5.274	6.07E-16
Insr	kinase	Inhibited	-5.383	2.7E-13
Esrra	transcription regulator	Inhibited	-2.161	1.31E-12
Ppargc1b	transcription regulator	Inhibited	-4.542	9.6E-12
Hba1/hba2	transporter	Inhibited	-3.536	1.01E-11
Klf15	transcription regulator	Inhibited	-4.027	1.06E-11
Nr4a1	ligand-dependent nuclear receptor	Activated	3.442	1.12E-10
Nrip1	transcription regulator	Activated	4.162	1.86E-10
Dmd	other	Activated	2.296	7.48E-10
Eif6	translation regulator	Activated	2.079	2.78E-09
Nrf1	transcription regulator	Inhibited	-2.683	2.99E-09

Ppargc1a	transcription regulator	Inhibited	-5.451	3.09E-09
Pitx2	transcription regulator	Inhibited	-2.498	8.39E-09
Por	enzyme	Activated	2.831	1.34E-08
Rictor	other	Activated	8.04	2.38E-08
Med13	transcription regulator	Activated	2.344	3.82E-08
Ctnnb1	transcription regulator	Activated	3.998	5.45E-08
Nampt	cytokine	Inhibited	-4.838	0.000000088
Flcn	other	Activated	4.25	0.000000157
Trib1	kinase	Inhibited	-3.514	0.000000223
Stk11	kinase	Inhibited	-5.896	0.000000413
Ppara	ligand-dependent nuclear receptor	Inhibited	-5.372	0.000000492
Ccnc	other	Inhibited	-4.155	0.00000087
Cidec	other	Activated	3.296	0.000000943
Fgf21	growth factor	Inhibited	-3.322	0.000000952
Ucp1	transporter	Inhibited	-4.473	0.00000177
Asxl1	transcription regulator	Activated	2.982	0.0000018
Nedd9	other	Inhibited	-4.536	0.00000376
Txnrd1	enzyme	Inhibited	-2.242	0.00000383
Gsr	enzyme	Inhibited	-2.198	0.00000383
Pparg	ligand-dependent nuclear receptor	Inhibited	-5.597	0.000008
Irs1	enzyme	Inhibited	-2.895	0.000008
Ehhadh	enzyme	Activated	3.45	0.0000108

All genes implicated in atherosclerosis either directly or indirectly are highlighted in yellow.

Abbreviations: *Map4k4*, mitogen-activated protein kinase kinase kinase kinase 4; *Clpp,* caseinolytic mitochondrial matrix peptidase proteolytic subunit; *Tp53*, tumor protein P53; Cpt1b, carnitine palmitoyltransferase 1b; *Slc27a2,* solute carrier family 27 member 2*; Insr,* insulin receptor; *Esrra,* estrogen-related receptor alpha; *Ppargc1b,* peroxisome proliferator-activated receptor gamma coactivator 1-beta*; Hba1/hba2,* hemoglobin subunit alpha 1 /2*; Klf15, krüppel-like factor 15; Nr4a1,* nuclear receptor subfamily 4 group a member 1; *Nrip1,* nuclear receptor interacting protein 1; *Dmd,* dystrophin*; Eif6,* eukaryotic translation initiation factor 6; *Nrf1,* nuclear respiratory factor 1**;** *Ppargc1a*, peroxisome proliferator-activated receptor gamma coactivator 1-alpha*; Pitx2, paired-like homeodomain transcription factor 2* ; *POR*, cytochrome p450 oxidoreductase**;** *Rictor,* RPTOR independent companion of mtor complex 2*; Med13,* mediator complex subunit 13*; Ctnnb1,* catenin beta-1; *Nampt,* nicotinamide phosphoribosyltransferase**;** *Flcn,* folliculin**;** *Trib1,* tribbles pseudokinase 1; *Stk11,* serine/threonine kinase 11**;** *Ppara,* peroxisome proliferator activated receptor alpha; *Ccnc,* cyclin c; *Cidec,* cell death-inducing dffa-like effector c; *Fgf21,* fibroblast growth factor 21; *UCP1*, uncoupling protein 1; *Nedd9,* neural precursor cell expressed, developmentally down-regulated 9**;** *Txnrd1,* thioredoxin reductase 1**;** *GSR*, glutathione-disulfide reductase**;** *Pparg,* peroxisome proliferator- activated receptor gamma**;** *IRS1*, insulin receptor substrate 1; *Ehhadh,* enoyl-coA hydratase and 3-hydroxyacyl coA dehydrogenase.

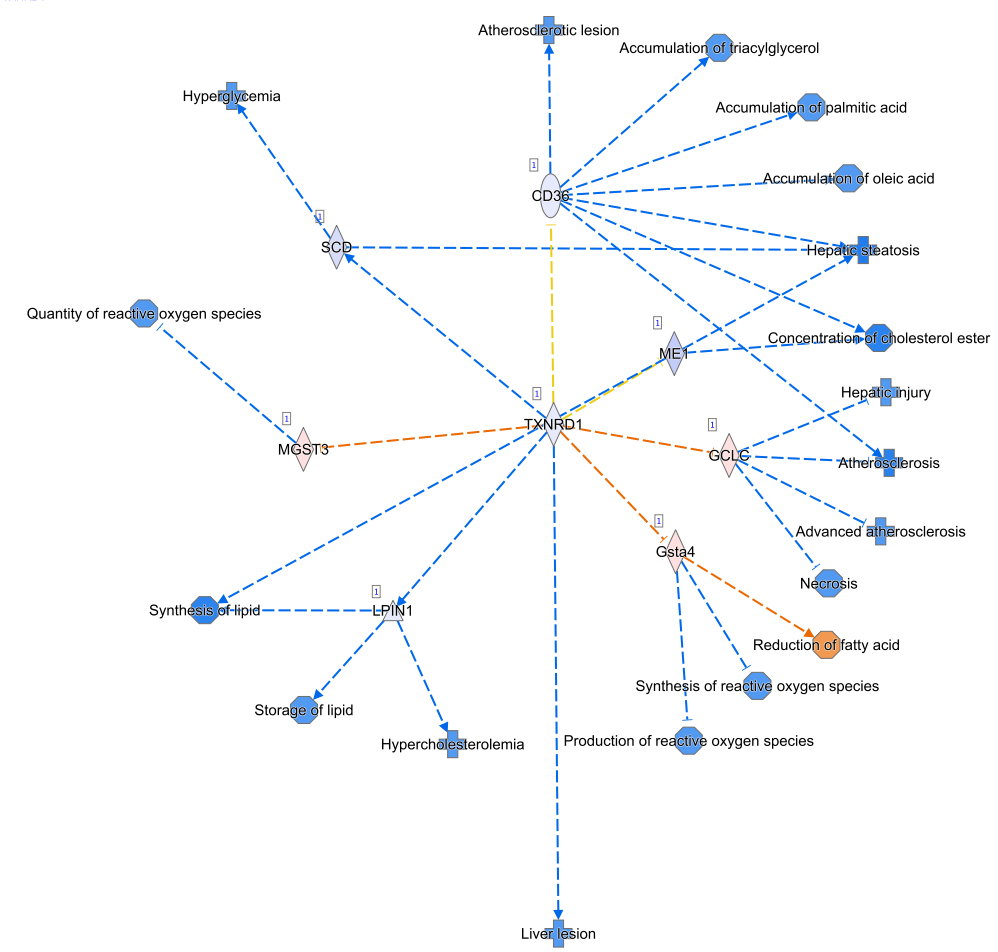

Figure 6.24 Graphical view of the relationships between *Txnrd1* upstream regulator and affected genes.

Graph displays the relationship between *Txnrd1* and its target genes that are associated with CV and liver diseases. The blue lines and nodes indicate predicted down-regulation effect while the orange and yellow lines and nodes indicate predicted up- regulation effect. Dotted lines indicate an indirect relationship (there is intermediate molecule or step).

6.3 Discussion

In this study, the effect of RSV intervention on gene expression of the thoracic aorta was investigated using the RNA-seq technique. Unless otherwise stated, no investigations on the relationship between these pathways/DEGs and RSV have been carried out before this study. However, even before any data analysis was carried out, it was clearly noticeable from the PCA (Figure 6.5) that RSV had an opposite effect to HFD on the pathways/DEGs, with RSV samples clearly separated from HFD samples.

6.3.1 Effects of RSV on canonical pathways implicated in atherosclerosis progression

6.3.1.1 OXPHOS pathway

The obtained results suggested that RSV affected several canonical pathways (Figure 6.11 and 6.12). The data showed that OXPHOS was inhibited by RSV. The inhibition of OXPHOS by RSV has been reported previously and it has been speculated that OXPHOS is a key target of RSV by which it potentially mediates various health benefits (Olivares-Marin et al. 2019). Indeed, the high consumption of HFD (or high carbohydrate/protein diet) that contains significant amounts of oxidisable substrates results in increased ATP availability that consequently enhances the activation of anabolic pathways such as lipid and cholesterol synthesis. However, intervention of RSV to HFD seems to mimic the effects of caloric restriction, that is used by several organisms to maintain health and to delay diseases such as CVDs, diabetes and cancer. The rationale is that inhibition of OXPHOS leads to a decrease in electrons passing through the ETC and hence reducing ATP generation. Although the exact location of electron sequestration by RSV is still unknown, it has been suggested that this may occur between complex I and III, the major sites for ROS production in mitochondria (Olivares-Marin et al. 2019; Tirichen et al. 2021). It has been reported that RSV competes with cellular oxygen for electrons released from complex III during OXPHOS, and this is attributed to its anti-oxidant activity (Pshenichnyuk and Komolov 2015). Figure 6.14 shows the OXPHOS pathway, and it can be seen that complex I to III are predicted to be inhibited by RSV.

6.3.1.2 Sirtuins signalling pathway

In addition to OXPHOS, sirtuins signalling pathway appears as the top significant canonical pathway that is affected by RSV intervention. Sirtuins serve as "metabolic sensors" since they depend on the availability of NAD^+ as a substrate to be activated. Indeed, the activation of sirtuins signalling pathway in response to energy deficit (e.g. ATP depletion due to inhibition of OXPHOS) triggers cellular adaptations to enhance metabolic efficiency (Srivastava 2016). Although Figure 6.14 shows a reduction in NAD^+ in OXPHOS, other NAD^+ precursors are also available in the body (Figure 6.25)(Winnik et al. 2015). The significant DEGs list in the dataset revealed a significant reduction in expression of poly ADP-ribose polymerases (PARP1), a key enzyme responsible for 85%-90% of PARP activity (Ke et al. 2019). It well known that PARP1 activation causes a depletion of cellular levels of NAD^+ by 50%–80% (Hurtado-Bagès et al. 2020); therefore, it can be hypothesised that the observed reduction in PARP1 might be responsible for NAD^+ abundance that in turn activates sirtuins signalling pathway. Furthermore, it has been found that nicotinamide mononucleotide adenylyltransferase 2 (NMNAT2), an enzyme that catalyses the formation of NAD^+, is significantly activated in the DEGs list. The activation of sirtuins pathway by RSV has been shown in several studies (Chao et al. 2017; Stacchiotti et al. 2018; Truong et al. 2018; Moraes et al. 2020), and discussed in Chapter 3 as a possible mechanism behind the observed attenuation of mitoROS production after RSV treatment (section 3.4.4). The beneficial effect of sirtuins has been shown on inflammation and lipid metabolism, slowing disease progression and many aspects of CVDs such as inhibition of oxidative stress, cell apoptotic pathways and ECs dysfunction (Grootaert and Bennett 2022).

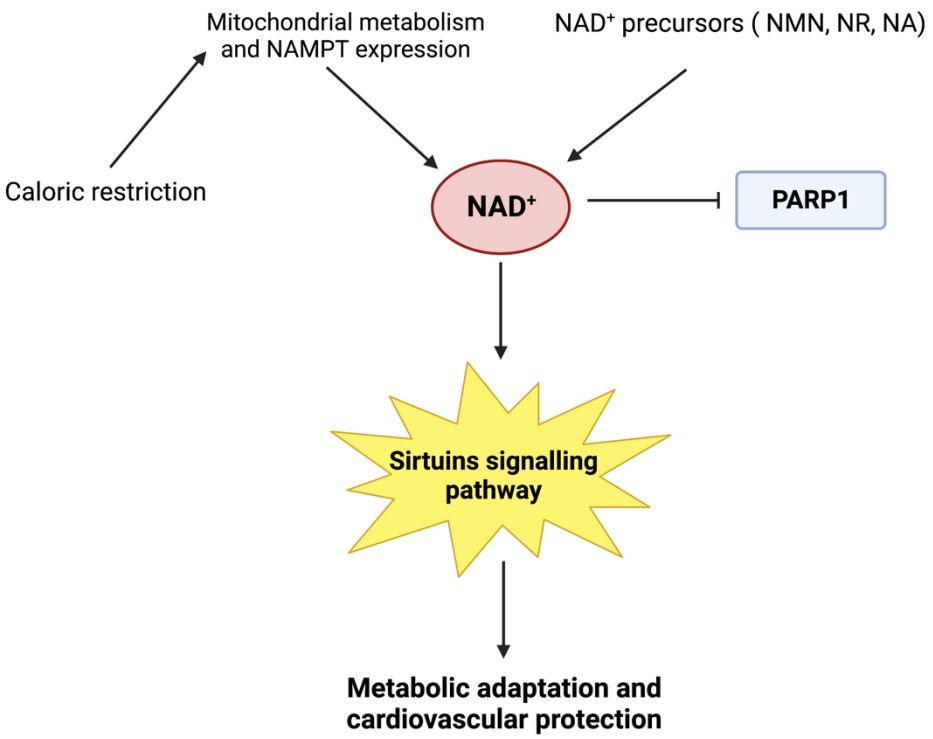

Figure 6. 25 Specific and unspecific sirtuin activation

One of the possible routes of sirtuin activation is via caloric restriction. This drives mitochondrial metabolism and expression of NAMPT. This results in the synthesis of NAD^+ that consequently activates sirtuins. Other routes of sirtuin activation are via supplementation of NAD^+ precursors, such as NMN, NR or NA, that mimic the effects of Sirt1; or through the inhibition of PARP1 activity. The activation of sirtuns at the end results in improvement of metabolic adaptation and/or cardiovascular protection. **Abbreviations:** NAMPT, nicotinamide phosphoribosyltransferase; NAD^+, nicotinamide adenine diphosphate; NMN, nicotinamide mononucleotide; NR, nicotinamide riboside; NA, nicotinic acid; PARP1, poly-adenosine diphosphate-ribose-polymerases 1. Figure adapted from (Winnik et al. 2015) and created with BioRender.com.

6.3.1.3 NO and ILK signalling pathway

Improving ECs function is also mediated by the activation of NO signalling pathway and ILK signalling (Figure 6.12). Most of the NO in the vascular system is generated by ECs, and hence called eNOS. The production of eNOS results in various favourable effects, including inhibition of ROS production, lipid peroxidation and infiltration of inflammatory cells (Wang et al. 2018). In addition to ECs, other vascular cells express iNOS that generates significant amount of NO that under inflammatory condition results in vascular dysfunction (Wang et al. 2018).

The production of NO via iNOS is negatively correlated with ILK signalling (i.e., decrease in iNOS results in increased ILK signalling). Collectively, it can be concluded from the data in this

chapter and previous chapter (Chapter 5) that the reduction observed in the infiltration of inflammatory cells (macrophages and T-cells; Figure 5.3 and 5.5) as well as iNOS (although further optimisation is required, Figure 5.4) could be a result of stimulation of sirtuins, NO and ILK signalling pathways.

6.3.1.4 Tryptophan degradation

The reduction in T-cells and macrophages by RSV in this study could be associated with inhibition of tryptophan degradation (Figure 6.12). To our knowledge, no previous studies have revealed the effect of RSV on amino acid metabolism (tryptophan in particular). However, among the different amino-acids, tryptophan has emerged as an important regulator of immune and inflammatory responses and considerable attention has been directed towards its association with CVDs (Mangge et al. 2014; Polyzos and Ketelhuth 2015; Melhem and Taleb 2021). In fact, it has been found that IFN-γ, released by activated T-lymphocytes, activates the indoleamine 2,3-dioxygenase (IDO) enzyme in monocyte-derived macrophages, dendritic and other cells, which in turn increases tryptophan catabolism into kynurenine and consequently increases serum kynurenine to tryptophan ratios (KYN/TRP) and incidence of CVDs (Wirleitner et al. 2003; Mangge et al. 2014; Yu et al. 2017; Konje et al. 2021). Therefore, it can be suggested that the reduction in T-cell infiltration in this study potentially resulted in decrease in IFN-γ, which in turn leads to suppression of macrophage activation and tryptophan degradation, thereby delaying disease progression.

On plasma lipid levels, it has been shown that administration of kynurenine pathway inhibitor to $LDLR^{-/-}$ mice fed HFD reduced plasma TC and TG associated with reduced inflammation and lesion size in the aorta (Zhang et al. 2012). Furthermore, data from a human study noticed that plasma Kyn/Trp ratio was found to be positively correlated with plasma LDL-C and TG levels as well as carotid intima-media thickness in advanced atherosclerosis (Eussen et al. 2015). Previously in this study (Chapter 4), RSV intervention was found to significantly reduce plasma LDL levels and produce a trend towards reduction in TC (Figure 4.8). Therefore, a reduction in tryptophan degradation could be a potential mechanism underlying the observed results. Taken together, tryptophan represents an intriguing player in atherosclerosis progression and therefore understating of its metabolism after RSV intervention is essential.

6.3.1.5 Oxytocin and estrogen receptor signalling pathway

In addition to aforementioned canonical pathways, several other pathways that have favourable effect on atherosclerosis were predicted to be activated by RSV. These include: activation of oxytocin signalling that is well known for its protective role via reducing inflammation (Wang et al. 2019c; Buemann and Uvnäs-Moberg 2020), activation of estrogen receptor signalling that has been proven to play a role in attenuating HFD from inducing lipid accumulation and inflammation in female as well as male ApoE and LDLR knock out mice (Nofer 2012) and activation of glutathione-mediated detoxification that reduces oxidative stress (Pahwa et al. 2017). As this is the first study that has shed light on the effect of RSV on such pathways, future research should investigate their roles in atherosclerosis and CVD in more detail.

6.3.1.6 Glycolysis, ketogenesis and TCA cycle

Glycolysis, ketogenesis and TCA cycle were predicted to be inhibited by RSV (Figure 6.12). The impact of HFD in inducing glycolysis, ketogenesis and TCA cycle has been published previously (Sikder et al. 2018; Perrotta et al. 2020; Ye et al. 2020; Li et al. 2022a). Although glycolysis is an important biological process, abnormalities in glycolysis flux have been shown to accelerate atherosclerosis progression. Indeed, during inflammation, both dysfunctional ECs and macrophages use glycolysis as their primary energy source. VSMCs also show high glycolytic capacity as they need it for their proliferation and migration (Li et al. 2022a). Furthermore, an increase in glycolysis was found to be associated with an increase in atherosclerotic plaques in $ApoE^{-/-}$ mice fed with a Western diet (Sarrazy et al. 2016). However, the inhibition of glycolysis has been reported to inhibit the inflammatory function of M1 macrophages, including ROS production and the secretion of pro-inflammatory cytokines (Viola et al. 2019). Therefore, regulating glycolysis could be a promising new strategy for anti-atherosclerosis therapy. The effect of RSV on glycolysis or the expression of genes in the context of atherosclerosis has not been reported yet. However, in this study, RSV was predicted to inhibit glycolysis by modulating several key genes implicated in its activation (Figure 6.20). Among all genes affected by RSV in this study, HIF-1a and PFKFB3 have been reported in previous studies as targeting molecules to regulate glycolysis (Li et al. 2022a; Thomas et al. 2022). Their blocking effect is not only restricted to reducing glycolysis but can

also inhibit inflammation, cholesterol and TG synthesis as well as ECs dysfunction, and decreasing disease progression and promoting plaque stability in LDLR$^{-/-}$, ApoE$^{-/-}$ mice and in *in vitro* studies (Nishizawa and Bornfeldt 2012; Akhtar et al. 2015; Poels et al. 2020; Li et al. 2022a). In addition to glycolysis, ketogenesis was found to be associated with heart failure (Cotter et al. 2013; Sikder et al. 2018), while reducing TCA cycle metabolites resulted in a decrease in NO and ROS levels in LPS-, TNFα- or IFNγ-stimulated macrophages (Liang et al. 2022). In the current study, it has been found that ketogenesis was predicted to be inhibited by RSV via down-regulation of *Acat1*, *Acat2*, *Acaa2* and *Hmgcs1* genes while the predicted inhibition of the TCA cycle was associated with down-regulation of key genes involved in TCA activation including *Aco1* and *Idh3a.*

6.3.1.7 White adipose tissue browning pathway

One of the potential pathways that was predicted to be activated by RSV in this study was the white adipose tissue browning. Several lines of evidence have demonstrated the browning of the white adipose tissue as a potential therapeutic approach in the fight against obesity and atherosclerosis (Hu et al. 2018; Jack et al. 2019; Roth et al. 2021). The results of the current study and a great deal of other evidence suggests that RSV has anti-obesity effects on HFD-fed mice, with browning of white adipose tissue identified as a potential mechanism underlying these effects and this effect is mediated by modulation of the composition of the gut microbiota and their metabolites as well as the activation of sirtuins signalling pathway (Qiao et al. 2014; Jung et al. 2016; Liao et al. 2018; Zhou et al. 2019a; Li et al. 2020b; Zu et al. 2021). The induction of browning exerts many beneficial effects, including increasing lipolysis as well as reducing obesity and weight gain (detected using IPA and presented in Figure 6.20 and Figure 6.22 respectively), although there were no changes observed in mouse body weight in this study (Chapter 4). However, more studies are required on the crosstalk between the gut microbiota and white adipose tissue browning. For example, analysis of the concentration of anti-inflammatory and anti-atherogenic short-chain fatty acids in the faeces and plasma of mice would provide more valuable insights.

6.3.1.8 Cholesterol and TG biosynthesis

Given the regulatory role of RSV in controlling TC and TG, IPA predicted that administration of RSV resulted in a reduction in cholesterol and TG biosynthesis (Figure 6.12). Previously in this study (Chapter 3), it was shown that RSV can reduce cholesterol metabolism *in vitro* (RAW264.7 cells treated with acLDL that resulted in a reduction in CE and TG accumulation). One potential mechanism is inhibition of Acat1 activity that leads to decreased esterification, and thereby, storage of cholesterol. In this chapter, IPA predicted downregulation of cholesterol metabolism based on the data set that showed *Acat1/2* and 3-hydroxy-3methylgutaryl-CoA synthase (*Hmgcs1*) are significantly inhibited by RSV. The atheroprotective role of complete or partial inhibition of *Acat* in mouse models has been discussed in depth in Chapter 3 (Section 3.4.5.6 in particular).

6.3.1.9 Fatty acid β-oxidation

The atheroprotective role of RSV was also predicted via reduced rate of cardiac fatty acid β-oxidation. Numerous experimental studies have shown that increased rate of myocardial fatty acid β-oxidation in different rodent strains fed HFD is accompanied by heart failure (Buchanan et al. 2005; Zhang et al. 2011a; Sankaralingam et al. 2015). Furthermore, it has been reported that switching to a low-fat diet or caloric restriction could result in a reduction in fatty acid β-oxidation, and hence protection from heart failure. The therapeutic effect of RSV to prevent or slow down the progression of heart failure in humans and animals has been reported previously (Sung and Dyck 2015; Riba et al. 2017; Gal et al. 2020; Zhang et al. 2021a). Therefore, based on the data from this study, it can be proposed that such an effect can potentially be mediated via a reduction in cardiac fatty acid β-oxidation.

6.3.1.10 Necroptosis signalling pathway

The atheroprotective role of RSV was predicted in the inhibition of necroptosis signalling pathway. The connection between the necroptotic pathway and atherosclerosis (in particular, plaque instability) has been shown in animal and human studies (Karunakaran et al. 2016; Kavurma et al. 2017; Zhe-Wei et al. 2018). In a previously published study, injection of hypercholesteraemic ApoE^{-}/$^{-}$ mice with a necroptotic inhibitor resulted in a reduction in both atherosclerotic plaque size and plaque instability markers as well as attenuation of further

progression of established lesions, confirming the role of necroptosis in plaque instability (Karunakaran et al. 2016). Thus, it can be suggested that inhibition of necroptotic pathway may play a role in the enhancement markers of plaque stability of LDLR^{-}/$^{-}$ mice seen in this study (data presented in Chapter 5). This result is in agreement with the previous study indicating that RSV intervention can attenuate necroptosis after ischemia-reperfusion in rats (Hu et al. 2021). Moreover, taken together it can be suggested that RSV may have had a comparable effect as a necroptotic inhibitor.

6.3.2 Effects of RSV on key inflammation-associated signalling pathways implicated in atherosclerosis progression

6.3.2.1 NF-κB pathway

The crucial role of NF-κB, a key regulator of inflammation, in the initiation and progression of atherosclerosis either directly or indirectly is widely known (Bonomini et al. 2015; Liu et al. 2017b; Li et al. 2022c). It has been shown that the activated form of NF-κB is found in human atherosclerotic plaques, and modulation of its activity limits disease progression in ApoE knockout mice (Wong and Tergaonkar 2009; Mallavia et al. 2013; Bonomini et al. 2015). This activation mediates the induction of pro-inflammatory cytokines, chemokines and adhesion molecules, including VCAM-1, ICAM-1, MCP-1 and IL-8, and thereby promotes disease progression (Bonomini et al. 2015; Liu et al. 2017b). Targeting NF-κB using an inhibitor in ApoE^{-}/$^{-}$ mice fed HFD showed a beneficial effect on the initiation and progression of atherosclerosis, including fewer macrophages (M1 subtype in particular) together with increased SMCs and collagen indicating more stable plaque (Mallavia et al. 2013). The inhibition of NF-κB signalling pathway by RSV in this study is consistent with previous studies both *in vitro* (HUVECs and HMDMs) and *in vivo* (C57BL/6 mice injected intraperitoneally with TNF-α)(Buttari et al. 2014; Pan et al. 2016; Nallasamy et al. 2021). Although all the aforementioned studies suggested that RSV mediates its effect via down-regulated TNF-α expression, the data results from this study showed the expression of TNF-α was not affected by RSV and it can be suggested that inhibition of TNF-α is not required to block the pathway.

6.3.2.2 T cell signalling pathway

T cell signalling is important for T cell activation and development. It has been demonstrated that activation of NF-κB signalling pathway is required for the induction of T cell signalling, and hence T cell activation and differentiation (Liu et al. 2017b). Under pathological conditions (i.e. inflammation as in atherosclerosis), T cells are considered the second most active and abundant inflammatory cells within atherosclerotic plaques after macrophages (Bullenkamp et al. 2016). Thus, inhibition of pro-atherogenic T cell activation via blocking its signalling could be used as a therapeutic strategy in combating atherosclerosis. Previously in this study, T cells were significantly reduced in the plaque of hypercholestermic $LDLR^{-}/^{-}$ mice after RSV intervention (Figure 5.5). Inhibition of T cell activation has been shown in DBA/1J mice after RSV intervention that consequently prevents autoimmune disease progression (Xuzhu et al. 2012). In the context of atherosclerosis, $ApoE^{-}/^{-}$ mice fed HFD with LPS (as an injection) and RSV (intragastric administrated daily) inhibited the proliferation and activation of $CD4^{+}$ T cells (Zhou et al. 2020). One of the other possible mechanisms underlying the inhibition of T cell activation by RSV, in addition to the inhibition of NF-κB, is through the activation of sirtuins pathway (Malaguarnera 2019). Taken together, it can be suggested that the reduction in T cells in plaques seen in this study may potentially be attributable to a decrease in T cell infiltration as well as the inhibition of activation of the T cell signalling pathway.

6.3.2.3 NLRP3 inflammasome

The NLRP3 inflammasome signalling pathway was predicted to be inhibited by RSV. This is not surprising as the anti-inflammatory effect of RSV, which is mediated by inhibiting the NLRP3 inflammasome activation, was shown previously in this study *in vitro* (Figure 3.13). These results are in line with a previous study that revealed that RSV inhibits NLRP3 inflammasome via inhibition of NF-κB signalling and activation of sirtuin pathways (Ma et al. 2018; Tufekci et al. 2021). The association between inflammasome and disease progression has been discussed previously in Chapter 3. Notwithstanding, studies in $ApoE^{-}/^{-}$ mice have shown contrasting results. For instance, in one study, $ApoE^{-}/^{-}$ mice-fed a western diet and treated with NLRP3 inhibitor MCC950 showed a reduction in atherosclerotic progression (Van der Heijden et al. 2017) while another study suggested that the progression of atherosclerosis in

these mice is independent of the NLRP3 inflammasome (Menu et al. 2011). However, there are no data yet, as far as we are aware, regarding LDLR^{-}/$^{-}$ mice. The inhibitory effect of RSV on NLRP3 inflammasome has been revealed by several studies on different diseases/pathophysiological changes, such as brain injury, cancer and NAFLD (Yang and Lim 2014; Zou et al. 2018; Maayah et al. 2021). In regard to atherosclerosis, rats fed a high-cholesterol diet combined with vitamin D2 and RSV, where vitamin D was used to aggravate injury by inducing calcium deposition in the vascular wall, showed a reduction in NLRP3 inflammasome and this was associated with upregulation of Sirt1 expression and downregulation of NF-κB p65 and p38 MAPK expression (Deng et al. 2015). With a lack of previous research on RSV intervention in LDLR^{-}/$^{-}$ mice, this study is the first to give insight into the possible mechanism underlying the anti-inflammatory effect of RSV *in vivo*. Therefore, more investigation is required on this link such as measuring IL-1β in plasma and immunofluorescence staining for aortic roots to detect the expression of NLRP3 inflammasome activation markers as well as its upstream mediator, NIMA-related kinase 7 (Nek7)(Zeng et al. 2021).

6.3.2.4 Wnt/β-catenin pathway

Beyond the effect of the Wnt/β-catenin on the regulation of cell differentiation and proliferation, its role in lipid storage and homeostasis has also been reported (Boucher et al. 2020). Thus, it has been reported that activation of Wnt1 and Wnt10b inhibits adipocyte differentiation whereas their overexpression in mouse models (FVB mice) resists obesity and improves glucose tolerance and insulin sensitivity (Boucher et al. 2020). Furthermore, inhibition of Wnt/β-catenin genes is highly correlated with an increased risk of atherosclerosis via elevation of cholesterol and TG synthesis and increased plasma TG and LDL levels in animals and human studies (Boucher et al. 2020). The effect of RSV on Wnt/β-catenin signalling activity has been studied widely in cancer research (Ji et al. 2013; Fu et al. 2014b; Dai et al. 2018; Pashirzad et al. 2021). It has been shown that RSV inhibits the pathway and consequently reduces the proliferation of cells and cancer metastases (Ji et al. 2013; Fu et al. 2014b; Dai et al. 2018; Pashirzad et al. 2021). However, no study has so far found a relationship between RSV and Wnt/β-catenin activity in regard to atherosclerosis development. In the current study, Wnt/β-catenin pathway was predicted to be activated by

RSV (Figure 6.18). In addition, IPA predicted inhibition in Dickkopf-1(*Dkk1*), an inhibitor of Wnt signalling pathway. Several clinical and pre-clinical (in hypercholesteraemic ApoE$^{-/-}$mice) studies have demonstrated the role of *Dkk1* in promoting inflammation, inducing plaque vulnerability and disease severity (Wang et al. 2013; Di et al. 2017). Therefore, activation of Wnt/β-catenin via inhibition of *Dkk1*expression could be one of the underlying mechanisms responsible for diminished inflammation and increased plaque stability seen in this study (Chapter 5) and hence, targeting the Wnt signalling pathway by RSV may provide novel therapeutic approaches for atherosclerosis. However, confirming these findings, for example, via measuring the plasma levels of *Dkk1*, is crucial before drawing any firm conclusion.

6.3.3 Effect of RSV treatment on disease and functions predicted by IPA

6.3.3.1 Improving lipid metabolism

Using IPA functional analysis, a sophisticated technique for associating biological functions and diseases to data sets, it was discovered that the DEGs from this study were mostly enriched in various biological processes (Figure 6.20 -23). On the top of affected functions is lipid metabolism. Data from this study demonstrated that RSV intervention caused upregulation of *Nceh1* and downregulation of *Cd36* and *Acat1*, well-known genes implicated in cholesterol uptake and metabolism. The role of these genes during atherosclerosis progression has been discussed previously in chapter 1 and chapter 3. In addition, other genes were found to be upregulated such as *Ucp-2, Ces1e, Foxo3, Foxa1, Anxa1, Bag3* and *Nqo1* while others such as *Elovl6*, *Fasn*, *Pilin3*, *Pilin*5, *Fabp4* were down-regulated (roles of these genes in lipid metabolism are summarized in Table 6.5). Interestingly, the roles of these genes in atherosclerosis are beyond the improvement of lipid metabolism. For example, overexpression of *Ucp-2* was found to protect against mitochondrial dysfunction through a reduction in mito-ROS (Tian et al. 2018) while bone marrow transplantation from *Ucp-2*$^{-/-}$ mice into LDLR$^{-/-}$ mice-supplemented with an atherogenic diet increased plaque content of macrophages and decreased collagen content, suggesting potentially more vulnerable plaques and protective role of *Ucp-2* (Blanc et al. 2003). Furthermore, upregulation of *Ces1* in human macrophages reduces atherosclerosis in LDLR$^{-/-}$ mice by stimulating CE hydrolysis and elimination (Bie et al. 2013). On the other hand, bone marrow transplantation from ELOVL6$^{-/-}$ mice or LPL$^{-/-}$ into LDLR$^{-/-}$ mice resulted in diminished macrophage infiltration and lesion

size (Babaev et al. 2000; Saito et al. 2011; Yvan-Charvet and Ivanov 2020). *Fasn* deficiency protects against inflammation, reduces macrophage infiltration in the adipose tissue, and decreases cholesterol accumulation (Bie et al. 2013). Taken together, the ability of RSV to ameliorate dysfunctional lipid metabolism in the current study was not surprising as the ability of RSV to improve plasma lipid profile as well as to modulate genes involved in lipid metabolism has been reported previously by other studies in addition to the current study (Chapter 3 and 4).

Table 6.5 Roles of genes in improvement of lipid metabolism

Gene	Role in lipid metabolism	References
Ucp-2	The precise role has not been reported. However, its expression levels in the aorta are strongly inversely correlated with lipid accumulation (seen in BATIRKO mice)	(Gómez-Hernández et al. 2014)
Ces1e	Catalyses neutral lipid (TG and CE) hydrolysis	(Jones et al. 2013)
Foxo3	• Regulates LDL-C homeostasis • Regulates hepatic TG metabolism via regulation of sterol regulatory-element binding protein 1c expression	(Tao et al. 2013; Wang et al. 2019b)
Foxa1	• Reduces fatty acid transporter protein and fatty acid uptake • Induces the breakdown of fatty acids	(Moya et al. 2012)
Anxa1	Plays a role in cholesterol transport via increase in ABCA1 expression	(Shen et al. 2020)
Bag3	The precise role has not been reported	-
Nqo1	Down-regulates lipid synthesis and increases lipid break down	(Gaikwad et al. 2001)
Elovl6	Regulates lipogenesis and lipolysis	(Junjvlieke et al. 2020)
Fasn	Catalyses de novo lipogenesis	(Jensen-Urstad and Semenkovich 2012)
Pilin3	Implicated in intracellular lipid droplet formation by acting as a transporter protein for free fatty acids	(Fan et al. 2013)
Pilin5	Facilitates delivery of fatty acids that are produced by lipolysis to mitochondria for oxidation	(Wu et al. 2021b)

Abbreviations: *UCP-2*, uncoupling protein 2; *Ces1e,* carboxylesterase 1E; *Foxo3*, forkhead Box A3; *Foxo1*, forkhead Box A1; *Anxa1*, annexin A1; *Bag3*, B cell lymphoma 2-associated athanogene 3; *Nqo1*, NADPH quinone oxidoreductase 1; *Elovl6*, elongation of long-chain fatty acids family member 6*; Fasn* fatty acid synthase; *Pilin3,* perilipin 3; *Pilin5,* perilipin 5.

6.3.3.2 Improving cardiac function and body weight

The improvement of cardiac functions by RSV is potentially mediated via up- and down-regulation of several genes (Figure 6.21). These DEGs were found to be enriched in decreased necrosis and fibrosis of cardiac muscle, dysfunction of heart, LDH levels and activation, and increased cardiogenesis (Figure 6.21). Cardiac functions have been seen to improve in patients and animal models with CVDs, including heart failure and myocardial infarctions, after receiving RSV (Dong et al. 2014a; Riba et al. 2017; Matsumura et al. 2018; Dyck et al. 2019; Gal et al. 2020; Zhang et al. 2021a). Furthermore, reduction of cardiac fibrosis by RSV has been demonstrated and attributed to the ability of RSV to inhibit NF-κB signalling pathway in animal models (Olson et al. 2005; Liu et al. 2019d; Yu et al. 2021a). In the current study, changes observed in these genes may have potential impact in the data obtained in this study (Chapters 4 & 5). For instance, *Cav3* has been reported to play an important role in SMCs phenotypic switch between contractile and synthetic states as it increases the expression of contractility markers such as SM α-actin (Gutierrez-Pajares et al. 2015). *Igf1* overexpression is associated with reduced plaque macrophages in AopE^{-}/$^{-}$ mice (Snarski et al. 2022). Moreover, *Vdr* expression has a protective role in LDLR^{-}/$^{-}$ mice. The ablation of VDR in LDLR^{-}/$^{-}$ mice exhibited increases in the expression of adhesion molecules and proinflammatory cytokines in the aorta (Szeto et al. 2012). Myoglobin (*Mb*) also has a cardioprotective role as it protects heart from hypoxia and modulates mitochondrial function. Furthermore, the deletion of *Mb* resulted in induced lipid accumulation in the myocardium of *Mb*$^{-}$/$^{-}$ mouse hearts (Hendgen-Cotta et al. 2017). Interestingly, in this study, RSV was predicted to trigger cardiogenesis. Many studies revealed that stimulating cardiomyocyte self-renewal (cardiogenesis) is a new paradigm for therapies against heart disease following myocardial infarction (Martin et al. 2017; Heallen et al. 2019). According to Srivastava and colleagues, the activation of 2 key genes is crucial for cardiogenesis, *Nkx2.5* and *Gata4* (Srivastava 2006). These 2 genes were found to be significantly activated by RSV; however, their role is not restricted to inducing cardiogenesis. For example, *Nkx2.5* has been found to play a role in regulating MMPs and TIMPS and thus induce plaque stability. Besides that, *Nkx2.5* has been also found to modulate ECs function by inhibiting leukocyte adhesion to the endothelium in ApoE^{-}/$^{-}$ mice (Du et al. 2016). The overexpression of *Gata4* has also been reported to improve ECs function by increasing NO production in HUVECs (Xu et al. 2018). Finally, it can be suggested that reducing

LDH levels and activation by RSV could potentially be highly correlated with its ability to protect from heart dysfunction and induce cardiogenesis.

Although no significant changes in mouse body weight were observed in RSV compared to HFD group (Chapter 4), bioinformatics analysis of RNA-seq showed the ability of RSV to affect different genes implicated in obesity and controlling body weight. The available data regarding RSV and obesity is controversial and discussed in Chapter 4.

6.3.3.3 Improving markers of plaque stability

In the previous chapter, the inclusion of RSV in HFD resulted in enhanced atherosclerotic plaque stability (Figure 5.5). Therefore, it was of interest to look in-depth for the expression of genes that are well-known to be implicated in plaque stabilisation. It was found that RSV significantly affected genes enriched in collagen synthesis and plaque stability (Figure 6.23). *Reck* is one of the genes that was upregulated because of RSV intervention. Increase in ECM components has been attributed to *Reck* deficiency (Meng et al. 2008). *Rilp* was reported as a key gene that can be used as a marker for plaque instability (Xu et al. 2020a); the expression of *Rilp* was down-regulated in RSV group compared to HFD, consistent with plaque stability. Based on the currently available data, *Mmp2*, *Mmp9* and *Timp2* were upregulated in RSV samples. It could be suggested that although RSV could not inhibit MMPs activity, it can induce activation of their inhibitors. This can be seen in heatmaps (Figure 6.23B) that shows down-regulation of TIMP inhibitor in HFD compared to RSV samples while both group shows increase in MMPs activation.

6.3.4 Effect of RSV intervention on upstream regulators

IPA suggested several upstream regulators that were affected upon RSV intervention. These upstream regulators could potentially be responsible for the changes observed in the expression of genes in the experimental datasets (Table 6.4). These upstream regulators have been implicated in the pathophysiology of many immune and metabolic diseases. Among them, *Txnrd1* was selected for presentation as it shows a link between atherosclerosis and liver disease that may have an impact on the results obtained and discussed in the next chapter. TXNRD1, standing for thioredoxin reductase 1, was predicted to have inhibited expression. The *Txnrd1* gene, which codes for an enzyme involved in cellular redox control and antioxidant

defence, was found to be highly expressed in the thoracic plaque (Okuda et al. 2001; Furman et al. 2004). It has also been found to be increased specifically by ox-LDL as other factors such as IL-1β, IL-6 and LPS failed to induce its expression in HMDMs (Furman et al. 2004). Interestingly, it has been reported that about a two-fold increase in *Txnrd1* expression level was found in atherosclerotic plaques relative to the surrounding healthy areas from an artery of the same patient (Furman et al. 2004). Furthermore, enhanced expression of *Txnrd1* resulted in increased ROS production, NF-κB activity and release and expression of MCP-1 in human endothelial-like EAhy926 cells (Liu and Shen 2009). The role of *Txnrd* in liver diseases has been reported previously in the literature (Sun et al. 2014). As in atherosclerosis, *Txnrd* activity showed higher activity levels in the liver of male BALB/c mice where fibrosis was induced and in liver cancer patients. Its expression in the liver is considered as a molecular tumour marker for diagnosis and evaluation of malignancies (Jiao et al. 2021; Wu et al. 2021c). However, to our knowledge, no previous study has reported the effect of RSV inclusion to HFD on *Txnrd* expression in the context of atherosclerosis or other diseases.

6.4 Future directions

This was an exploratory study and the first to be carried out with RSV in atherosclerosis. Using such a technique generates a huge dataset and it's not logical to present and discuss all of them. Therefore, defining specific questions to answer was the strategy used to present the data. In this chapter, the question was "what are the molecular mechanisms that might be responsible for the results demonstrated *in vivo*?". However, the obtained data so far is promising and hence, "digging" more in the data set would provide more valuable insights and can be used then to build up new hypothesis. In addition, the activation of white adipose tissue browning pathway is one of the top potential pathways. Therefore, RNA-seq from white or brown adipose tissue could be carried out to analyse whole transcriptome changes.

6.5 Conclusions

Results from this study are promising, and when considered in conjunction with previously demonstrated effects of RSV, they highlight the potential benefits of RSV supplementation as a potential anti-inflammatory and anti-atherosclerosis agent. The main conclusion from this study is that RSV has the potential to modulate pathways, biological processes, and

expression of genes which provides valuable insights into the mechanism of action of RSV, especially as the majority of them have no previously reported data. Interestingly, the anticipated inhibition of *Txnrd1* by RSV showed to produce favourable effects on atherosclerosis and liver disease. When combined with the change recorded in liver weight of RSV-treated mice, it was of interest to continue the research investigating the effect of RSV administration on NAFLD in male $LDLR^{-}/^{-}$ mice which forms the focus of the aim of the next chapter.

CHAPTER 7

Evaluation of the therapeutic effects of RSV on NAFLD *in vivo* and *in vitro*

7.1 Introduction

The inclusion of RSV to HFD has demonstrated various atheroprotective effects in $LDLR^{-/-}$ mice. The results obtained from this project demonstrate the ability of RSV to reduce inflammatory cell infiltration into plaque the and improve markers of plaque stability along with many others beneficial effects (Chapter 5). Importantly, a substantial reduction in liver weight and LDL-C and TC in the plasma of mice was seen after RSV administration (Chapter 4). It can hence be hypothesised that RSV may be able to reduce liver weight and improve plasma lipid profile via improved hepatic structure and function. This hypothesis is supported by the central role of liver in lipid homeostasis as well as atherosclerosis development. Overconsumption of HFD in the absence of significant alcohol intake results in NAFLD, the most prevalent chronic liver disease worldwide that is associated with obesity, lipid metabolism disorders, hypertension, and hyperglycaemia. Due to these shared risk factors, atherosclerosis is found to be intimately associated with NAFLD (Balta 2022). The lipid-lowering medication, such as a statins, has a significant influence on CVD and NAFLD; nevertheless, it may have deleterious effects in certain individuals with myalgia and myopathy, as well as an increased incidence of diabetes with high dosage of statin and interference with liver function (Ramkumar et al. 2016). Due to the limitations of statin therapy, there is a considerable need for alternative treatments for NAFLD and CVDs. The hepatoprotective effect of RSV against HFD induced NAFLD development and progression has been investigated in *in vivo* animal models such as C57BL/6NIA mice (Baur et al. 2006), C57BL6/J mice (Ahn et al. 2008; Kim et al. 2011; Cho et al. 2012) and different rat models (Shang et al. 2008; Gómez-Zorita et al. 2012; Khaleel et al. 2018). In several HFD-induced NAFLD models, the inclusion of RSV to HFD reduces hepatic steatosis, cholesterol and TG accumulation, suppresses lipogenesis and inflammatory cell infiltration together with insulin resistance (Shang et al. 2008; Gómez-Zorita et al. 2012; Jeon et al. 2012; Alberdi et al. 2013). Despite the number of conducted studies on RSV effect on NAFLD *in vivo,* its ability to ameliorate NAFLD along with atherosclerosis development together with the underlying mechanisms have not yet been studied in detail.

7.1.1 Experimental aims

Taking the strong correlation between lipid metabolism and cholesterol homeostasis in liver and atherosclerosis, the aim of studies presented in this chapter was to investigate the effect of RSV administration on NAFLD in male LDLR^{-}/$^{-}$ mice. This was achieved by investigating the changes in liver cellularity and lipid contents *in vivo* via staining and analysing liver sections of the same mice that were used for atherosclerosis studies. The ability of LDLR^{-}/$^{-}$ mice to develop atherosclerosis and hepatic steatosis, and eventually NAFLD, after feeding HFD has been revealed by several studies (Tang et al. 2018; Milasan et al. 2019; Lu et al. 2020). Furthermore, to confirm the *in vivo* findings and to further investigate the effect of RSV on the underlying mechanisms, an additional approach *in vitro* was undertaken using the HepG2 cell model system. Indeed, HepG2 cells are widely used *in vitro* in the study of NAFLD due to their ability to imitate liver morphology and function and their ease of culture. They were therefore used to assess the effect of RSV treatment on lipid accumulation and ROS production.

7.1.2 Hepatic cellularity and steatosis

Hepatic steatosis is the earliest recognisable stage of NAFLD in which hepatocytes start to accumulate fat without inflammation or damage to the hepatocellular architecture at this stage (Sattar et al. 2014). However, hepatic steatosis can progress and lead to more serious damage in the liver, including NASH, cirrhosis, and eventually liver carcinoma if left untreated (Sattar et al. 2014). H&E and ORO are frequently used to assess hepatic cellularity and steatosis respectively because they are fast and cheap. Therefore, sections of the liver from LDLR^{-}/$^{-}$ mice were taken at 10 µm intervals and stained with these dyes to allow observation of liver changes. This study along with that in, Chapters 4 and 5, on plaque staining, plasma lipid profile and immunophenotyping of stem, progenitors and mature cells should provide a detailed overview of the impact of RSV and HFD administration on atherosclerosis severity and NAFLD. Furthermore, the HepG2 model system allows robust conclusions on the action of RSV treatment on liver steatosis in the absence of any potential confounding factors present *in vivo*.

7.1.3 Oxidative stress and NAFLD

As in atherosclerosis, oxidative stress plays a crucial role in the pathogenesis of NAFLD. It is believed that the “two-hit” hypothesis explains the progression of NAFLD (Giorgio et al. 2013; Fernández-Quintela et al. 2018). The “first hit” is represented by insulin resistance that results in TG accumulation in the cytoplasm of hepatocytes as lipid droplets (steatosis). However, until an additional cellular processes, such as mitochondrial dysfunction, pro-inflammatory cytokine secretion and/or oxidative stress occur (“second hit”), the disease does not progress (Giorgio et al. 2013; Fernández-Quintela et al. 2018). Increased ROS production in the liver is tightly involved in lipid peroxidation and inflammation (Balta 2022). Indeed, the elevation in ROS levels modulates the expression and activity of vital enzymes involved in lipid metabolism that consequently results in dysregulation of lipid metabolism and accumulation in the liver. In turn, these accumulating hepatic lipids contribute to ROS generation by inducing mitochondrial dysfunction, endoplasmic reticulum stress, and NADPH oxidase activation (Chen et al. 2020b). In addition to the initiation of the disease, increased ROS production represents an important mediator in the progression of NAFLD (steatosis) to NASH which is characterised by inflammation and hepatocellular ballooning along with fat accumulation (Bovi et al. 2021; Balta 2022). Therefore, in this study, the ability of RSV to attenuate H_2O_2- and oleic and palmitic acids (OA/PA)-induced ROS activity in HepG2 cells was determined.

7.1.4 Overview of experimental strategies

The experimental strategy used in this chapter is illustrated in Figure 7.1. Details of specific methodologies for each experiment are detailed in Chapter 2.

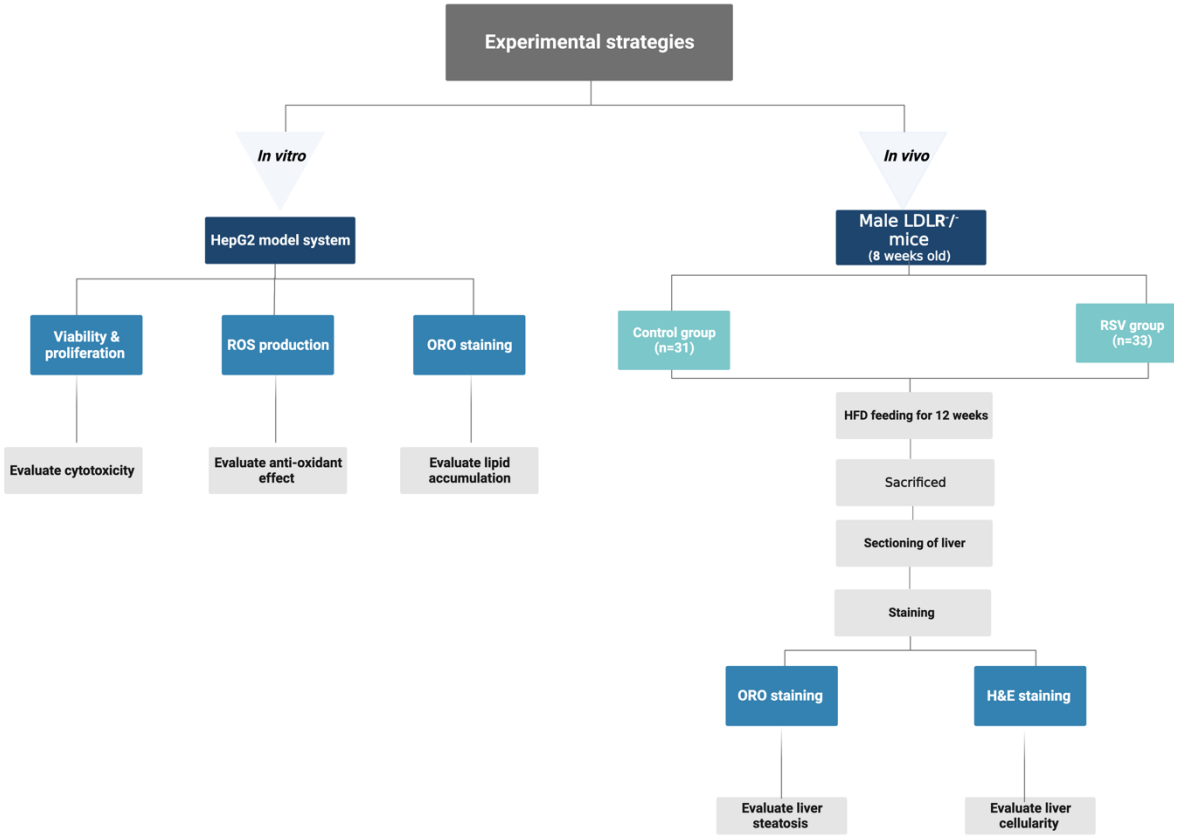

Figure 7.1 Experimental strategy used to investigate the effects of RSV on NAFLD associated with atherosclerosis *in vitro* and *in vivo*

Abbreviations: NAFLD, non-alcoholic fatty liver disease; ROS, reactive oxygen species; ORO, oil red O. Image created with BioRender.com.

7.2 Results

7.2.1 *In vivo* investigation of the effect of RSV on hepatic cellularity and steatosis

7.2.1.1 Resveratrol supplementation improves hepatic cellularity of LDLR^{-}/$^{-}$ mice fed HFD

H&E staining for liver sections showed that the inclusion of RSV to HFD for 12 weeks resulted in a significant increase in hepatic cellularity by 8.5% (p= 0.017) as shown in Figure 7.2B. Representative images are shown in Figure 7.2A.

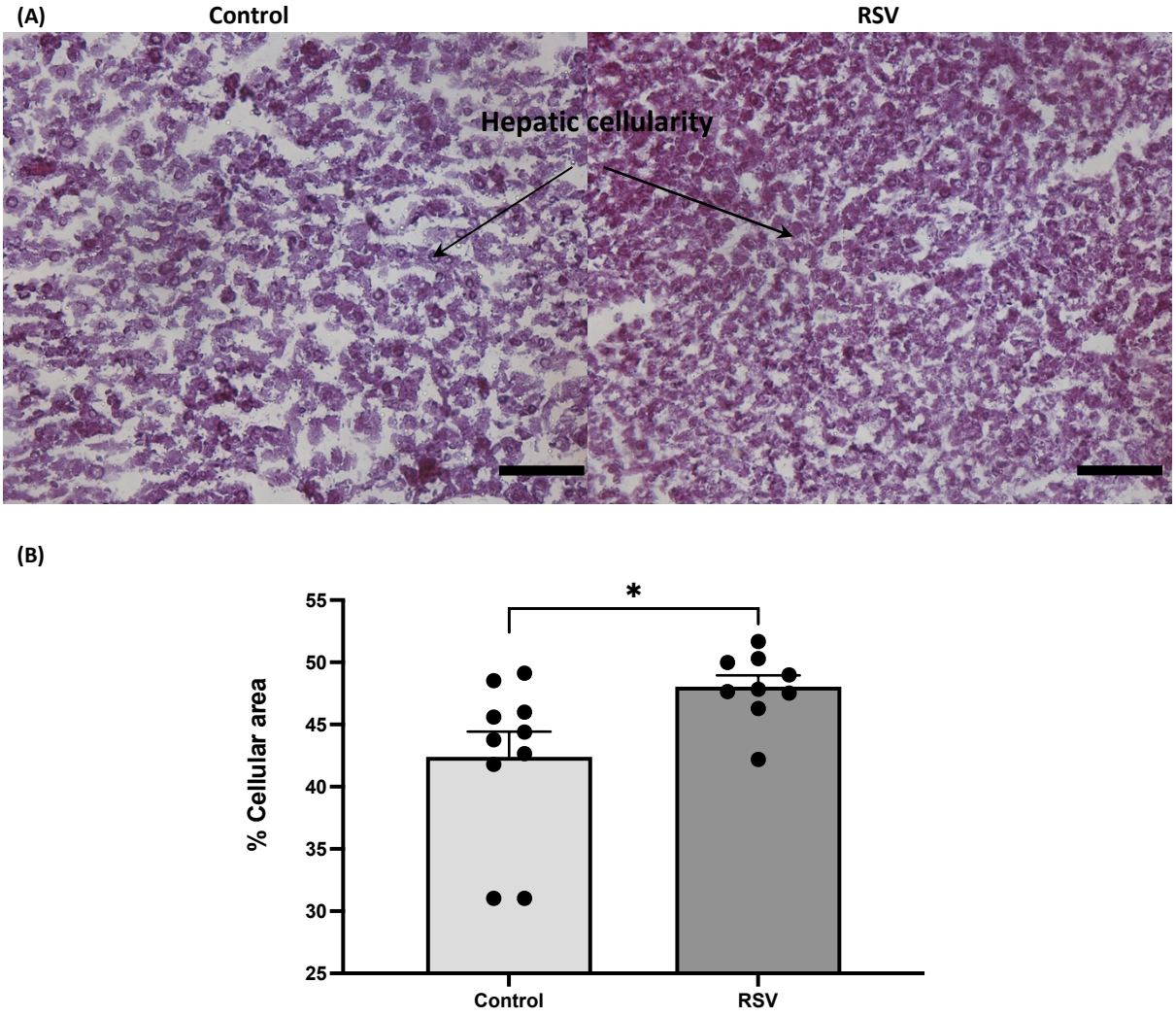

Figure 7.2 RSV significantly improves hepatic cellularity in atherosclerotic LDLR^{-}/$^{-}$ mice

Following 12 weeks of feeding male LDLR^{-}/$^{-}$ mice either HFD or HFD supplemented with RSV, the mice were sacrificed and part of the liver mounted in OCT. Sections of the liver were then taken and stained with H&E. Images were then captured using a Leica DMRB microscope under x20 magnification. Images were analysed using ImageJ software in a blinded manner. Graphs show representative images with scale bar of 80 µm (A). Data are presented as mean ± SEM from n=10 control and n=9 RSV group (B). Statistical analysis was performed using Mann-Whitney U test where *$P \leq 0.05$. **Abbreviations:** OCT, optimum cutting temperature; H&E, haematoxylin and eosin.

7.2.1.2 RSV treatment reduces intracellular lipid accumulation (steatosis) in the liver of LDLR^{-}/$^{-}$ mice.

The analysis of liver sections stained with ORO showed a significant reduction in intracellular lipid accumulation in the liver of LDLR^{-}/$^{-}$ mice fed HFD supplemented with RSV for 12 weeks by 10% (p= 0.012) as shown in Figure 7.3B. Representative images for both groups are shown in Figure 7.3A.

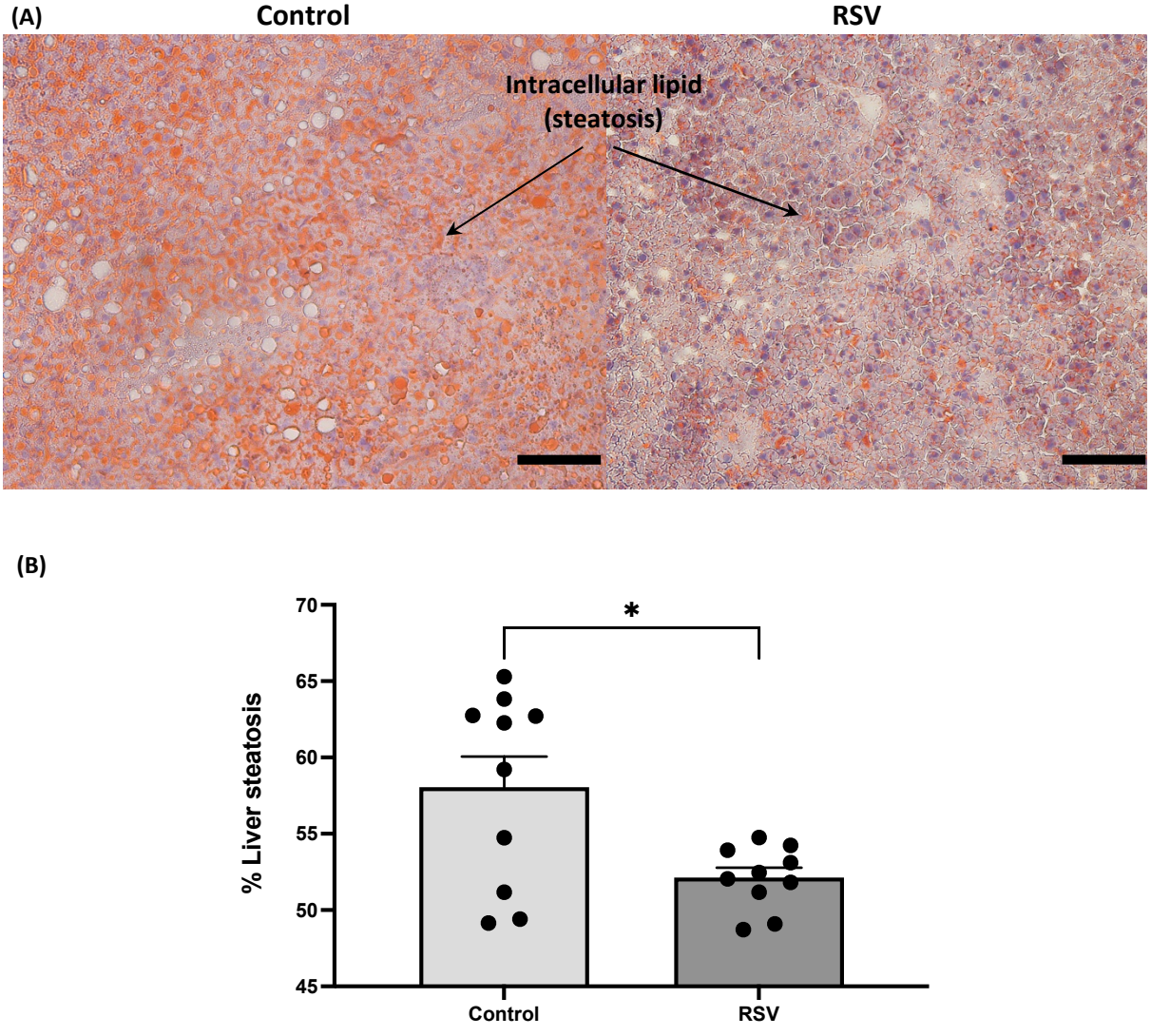

Figure 7.3 RSV significantly decreases liver steatosis in LDLR^{-}/$^{-}$ mice fed HFD.

Following 12 weeks of feeding male LDLR^{-}/$^{-}$ mice either HFD or HFD supplemented with RSV, the mice were sacrificed and part of the liver was mounted in OCT. Sections of liver were then taken and stained with ORO. Images were then captured using a Leica DMRB microscope under x20 magnification. Images were analysed using ImageJ software in a blinded manner. Graphs show representative images with scale bar of 100 µm (A). Data are presented as mean ± SEM from n=10 control and RSV group (B). Statistical analysis was performed using an unpaired Student's t-test where *$P \leq 0.05$. **Abbreviations:** OCT, optimum cutting temperature; ORO, oil red O.

7.2.2 *In vitro* investigation of the mechanisms underlying RSV-mediated changes in hepatic steatosis.

7.2.2.1 Resveratrol has no detrimental cytotoxicity effects on HepG2 cells in the absence of OA and PA

To confirm that RSV has no cytotoxicity effects on HepG2 cells, the LDH assay kit and CV staining were used to evaluate cell viability and proliferation respectively. After 24 hours of incubation, RSV had no effect on either cell viability or proliferation compared to the vehicle control, which was set arbitrarily as 100% (Figure 7.4).

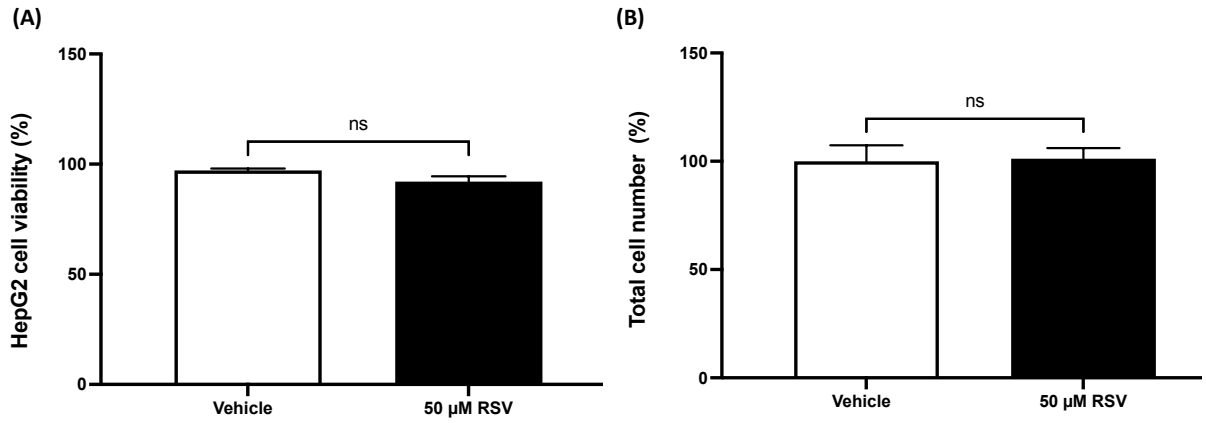

Figure 7.4 RSV has no cytotoxicity effects on HepG2 hepatocytes in the absence of OA and PA.

HepG2 hepatocytes were treated with the vehicle control or 50 µM RSV for 24 hours. Then, 50 µl of culture media was transferred to a new plate and LDH assay kit was used to assess cell viability. The adherent cells were stained with CV to assess cell proliferation. Data were normalised to the vehicle control that was arbitrarily assigned as 100%. Data are presented as mean ± SEM from three independent experiments. Statistical analysis was performed using an unpaired Student's t-test where ns, not significant.

7.2.2.2 Resveratrol has no detrimental cytotoxicity effects of HepG2 cells in the presence of OA and PA

To confirm that RSV has no cytotoxicity effects on HepG2 cells when combined with a mixture of OA and PA, the LDH assay kit and CV staining were used to evaluate cell viability and proliferation respectively. After 24 hours of incubation, RSV had no effect in either HepG2 cell viability or proliferation compared to the vehicle control (Figure 7.5).

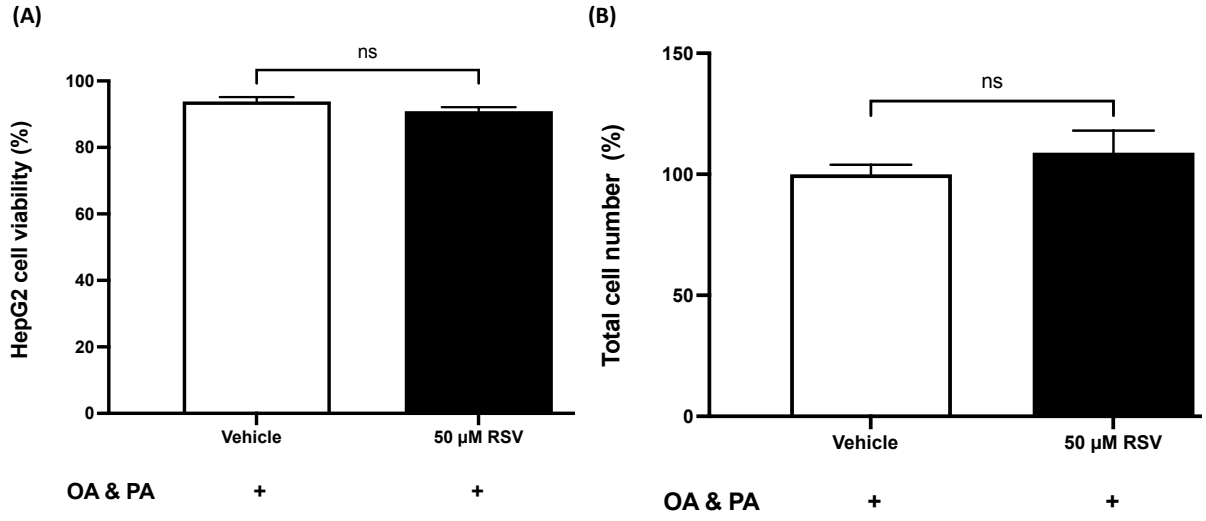

Figure 7.5 RSV has no cytotoxicity effects on HepG2 hepatocytes in the presence of OA and PA.

HepG2 hepatocytes were treated with vehicle control or 50 µM RSV with a combination of OA and PA for 24 hours. Then, 50 µl of culture media was transferred to a new plate and LDH assay kit was used to assess cell viability. The adherent cells were stained with CV to assess cell proliferation. Data were normalised to the vehicle control that was arbitrarily assigned as 100%. Data are presented as mean ± SEM from three independent experiments. Statistical analysis was performed using an unpaired Student's t-test where ns, not significant. **Abbreviations:** OA, oleic acid; PA, palmitic acid

7.2.2.3 Resveratrol treatment significantly reduces intracellular lipid accumulation in HepG2 induced by treatment with OA and PA

The incubation of HepG2 cells with 1 mM of OA:PA at a ratio of 2:1 resulted in significant intracellular lipid accumulation in HepG2 cells by 80% ($p \leq 0.001$) compared to cells treated with 1% BSA only (negative vehicle control) as shown in Figure 7.5. However, treatment with RSV produced a significant reduction by around 71% ($p \leq 0.001$) in comparison to the OA:PA alone (vehicle control) (Figure 7.6).

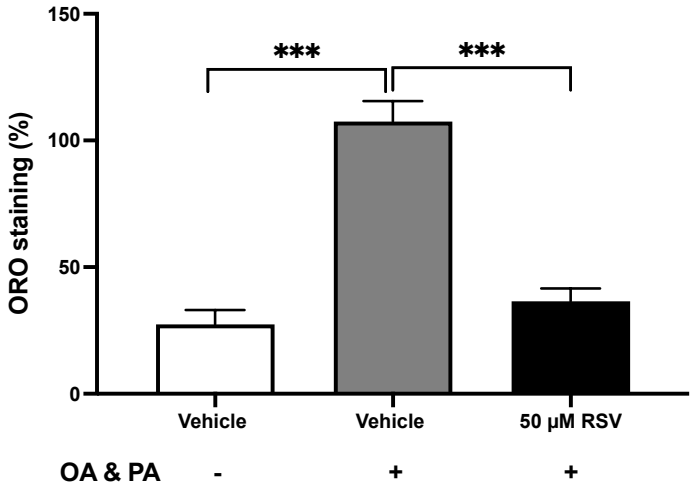

Figure 7.6 RSV treatment significantly reduces intracellular lipid content in HepG2 hepatocytes induced by OA and PA.

HepG2 hepatocytes were treated for 24 hours with 50 µM RSV or the vehicle control in the presence 1 mM of a combination of OA and PA at a ratio of 2:1 that were prepared in media containing 1% BSA. The culture media was then removed, and the cells were stained with ORO to determine hepatic intracellular fat accumulation. Intracellular lipid content was then extracted using 60% isopropanol. Data were normalised to the vehicle control that was arbitrarily assigned as 100%. Data are presented as mean ± SEM from three independent experiments. Statistical analysis was performed using one-way ANOVA with Tukey's post-hoc test where *** $P \leq 0.001$. **Abbreviations:** OA, oleic acid; PA, palmitic acid; ORO, oil red O.

7.2.2.4 Resveratrol significantly attenuates ROS production stimulated either by TBHP or OA/PA in HepG2 cells

The antioxidant activity of RSV on HepG2 cells was assessed in the presence of either TBHP or a combination of fatty acids (OA and PA). As shown in Figure 7.7A, RSV significantly attenuates the TBHP-induced ROS production after 3 hours of incubation by around 18% ($p \leq 0.001$). Furthermore, the OA/PA-stimulated ROS production was also measured in HepG2 cells. As shown in Figure 7.7B, a combination of OA and PA-induced ROS production by about 300.4 % ($p \leq 0.001$) compared to the vehicle control (No OA and PA). However, the addition of RSV resulted in the attenuation of ROS production by 31% ($p \leq 0.001$) compared to the vehicle control with OA and PA (Figure 7.7B).

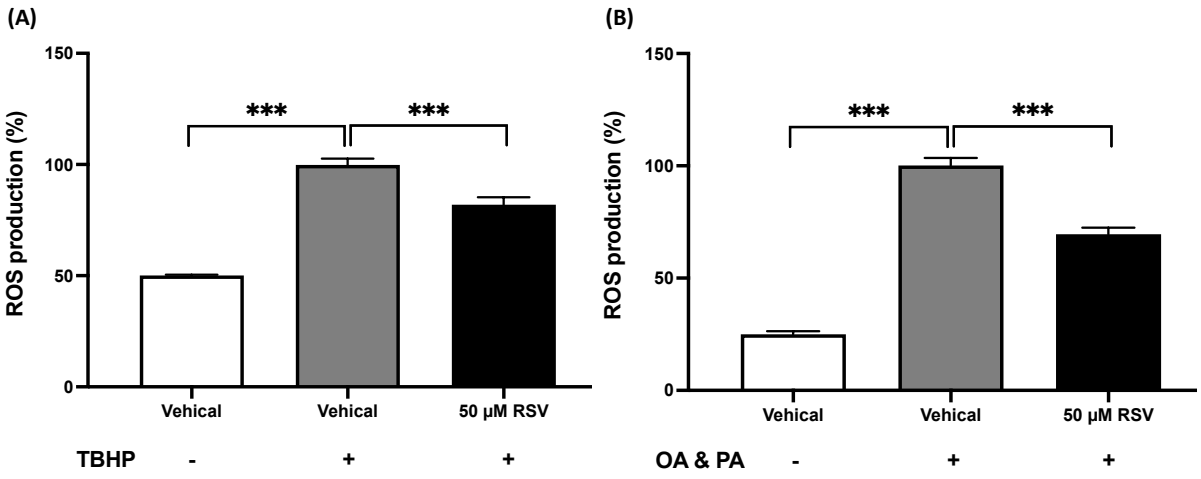

Figure 7.7 RSV treatment significantly reduces ROS production stimulated either by TBHP or OA and PA in HepG2 cells.

HepG2 cells were incubated for 3 hours with the vehicle control or RSV in the presence of TBHP (A) or 24 hours with 1 mM of combination of OA and PA at ratio of 2:1 (B). ROS production is displayed as a percentage to the vehicle control, which was arbitrarily set to 100%. Data are presented as mean ± SEM from three independent experiments. Statistical analysis was performed using a one-way ANOVA with either Tukey's post-hoc test (A) or Dunnett post-hot test(B) where *** $p \leq 0.001$. **Abbreviations:** ROS, reactive oxygen species; TBHP, tert-butyl hydroperoxide; OA, oleic acid; PA, palmitic acid.

7.3 Discussion

The results presented in this chapter support several research articles that demonstrate a strong link between atherogenic lipids and fatty liver diseases, NAFLD in particular. This association is increased with elevations in atherosclerosis risk factors such as and dyslipidaemia, hypertension, inflammation, oxidative stress and endothelial dysfunction (Targher et al. 2020). Data presented in this study show the ability of RSV to modulate NAFLD *in vivo* by increasing hepatic cellularity (Figure 7.2) and reducing ORO-stained lipid accumulation, indicating a reduction in hepatic steatosis (Figure 7.3) in LDLR^{-}/$^{-}$ mice receiving HFD supplemented with 20 mg/kg/day RSV. Furthermore, in this study fatty acids (OA and PA) were used to induce steatosis in HepG2 cells to mimic human NAFLD *in vitro.* Treatment of HepG2 cell line with 50 µM RSV exhibited several positive changes, including attenuation in intracellular lipid accumulation (Figure 7.5) and reduction in TBPH- and OA/PA-induced ROS production (Figure 7.6A and 7.6B respectively).

7.3.1 The effect of RSV on hepatic cellularity and steatosis

Several *in vivo* and *in vitro* studies reveal evidence for the potential therapeutic function of RSV as a hepatoprotective agent (Table 7.1). In this study, analysis of staining of liver sections showed a significant reduction in hepatic cellularity along with an increase in hepatic steatosis in the HFD group. These findings are in line with a previous study that found that HFD consumption in LDLR^{-}/$^{-}$ mice resulted in exacerbated hepatic macrophage infiltration, apoptosis, fibrosis, hepatic injury, steatosis and inflammation (Subramanian et al. 2011). Such changes are not restricted to the LDLR^{-}/$^{-}$ mouse strain only; they have been also reported with several other animal models such as C57BL/6J and catalase knock-out (CKO)mice (Guo et al. 2016; Piao et al. 2017; Nanizawa et al. 2020; Tsuru et al. 2020). In the current study, the addition of RSV to HFD attenuated hepatic injury induced by HFD by inducing hepatic cellularity and reducing hepatic steatosis. Several mechanisms underlying the antisteatotic effects of RSV have been proposed in previous studies. For example, Xin *et al.* (2013) concluded that the effect of RSV against HFD-induced hepatic steatosis is via upregulation of SR B type I (SR-BI) gene expression (Xin et al. 2013). In addition, reduction in lipid concentrations in liver could be another possible explanation showed by a study conducted on hypercholesterolaemic rats (Kopeć et al. 2013). In another study, feeding HFD

supplemented with a low-dose of RSV (0.005 %) in C57BL/6J mice showed a reduction in hepatic TG and cholesterol levels and this observation was attributable to changes in levels and/or activities of several enzymes in the liver and epididymal adipose tissue, including the suppression of fatty acid synthase, glucose-6-phosphate dehydrogenase, and phosphatidate phosphohydrolase in addition to activation of fatty acid oxidation (Cho et al. 2012). Focusing the attention on the molecular mechanisms underlying the hepatosteatosis protective effect of RSV, it has been found that intervention of RSV to HFD is mediated by the activation of the AMPK/SIRT1 pathway (Alberdi et al. 2013; Ding et al. 2017b). In addition to *in vivo* staining, this study also indicated a decrease in intracellular lipid accumulation *in vitro* (HepG2 cells). This observation verified the *in vivo* observation and is consistent with earlier published studies using HepG2 cells (Shang et al. 2008; Izdebska et al. 2017; Koushki et al. 2020). Treatment with RSV results in the upregulation of carnitine palmitoyltransferase 1A (CPT-1a) gene (implicated in fatty acid oxidation) in HepG2 cells and the liver of mice fed HFD-supplemented with RSV (Koushki et al. 2020). In addition to the aforementioned mechanisms, the potent antioxidant property of RSV also plays an important role in delaying the progression of liver steatosis (Bujanda et al. 2008; Fernández-Quintela et al. 2018). However, with a number of possible mechanisms resulting in reduced hepatic steatosis and consequently induced hepatic cellularity in this study, further investigation at the molecular and cellular level is necessary to elucidate the exact pathways underlying the observed protective effects.

Table 7.1 Preclinical studies conducted *in vivo* an *in vitro* to test the hepatoprotective effect of RSV

	Improvement	**Model**	**Dosage**	**Role of RSV**	**Reference**
In vivo	Liver Steatosis	Wistar Rats	10 mg	Reduces FA deposition in the liver	(Bujanda et al. 2008)
			100 mg/kg bw/day		(Shang et al. 2008)
		Zucker rat	10 mg/kg bw/day	Reduces liver TG and cholesterol content	(Rivera et al. 2009)
		C57BL/6N mice	30 mg/kg bw/day	Reduces in hepatic fat content	(Kang et al. 2012)
		C57BL/6J mice	50 mg/kg bw/day or 100 mg/kg bw/day	- Reduces in TG and LDL-C - Reduces lipid accumulation in the liver and ballooning degeneration	(Du et al. 2021)

	Oxidative stress and inflammation	C57BL/6J mice	0.4% w/w	Reduces ROS levels and lipid peroxidation	(Yuan et al. 2022)
		Wistar Rats	10 mg	Stimulates antioxidant enzymes (SOD, GPx and catalase) and decreases nitric oxide synthase in the liver	(Bujanda et al. 2008)
	Liver fibrosis	Wistar male albino rats	20 mg/kg bw/day	Prevents collagen deposition, lymphocytic infiltration and necrosis	(Abdu and Al-Bogami 2019)
In vitro	Oxidative stress and inflammation	HepG2 cells	0–100 µM	Reduces H_2O_2- mediated oxidative stress in a dose-dependent manner	(Pan et al. 2017)
		Primary hepatocytes from C57BL/6 mice	50 and 100 µM	Decreases expression levels of several inflammatory markers (IL-1β, IL-6, and TNF-α)	(Tian et al. 2016)
	Steatosis	HepG2 cells	- 10, 25, and 50 µM -15, 45 and 135 µM -20–80 µM	Reduces lipid accumulation and hepatocyte TG content	(Shang et al. 2008; Zhang et al. 2015; Tang et al. 2016)

Abbreviations: FA, fatty acid; TG, triglyceride; LDL-C, low-density lipoprotein- cholesterol; ROS, reactive oxygen species; SOD, superoxide dismutase; GPx, glutathione peroxidase; IL-1β, interleukin 1-beta; IL-6, interleukin-6; TNF-α, tumour necrosis factor-alpha.

7.3.2 The effect of RSV on oxidative stress

The significant reduction observed in this study on ROS production induced either by TBHP or fatty acids in HepG2 cells treated with RSV is not surprising. The potent antioxidant activity of RSV has been proven in this project on different cell models (Chapter 3) and also by several other studies (Zhang et al. 2015; Pan et al. 2017; Huang et al. 2020). The incubation of HepG2 cells with 1 mM of OA and PA at a ratio of 2:1 in order to develop *in vitro* steatosis model system that mimics human NAFLD was optimised previously in the host laboratory. Furthermore, the choice of OA and PA in particular was based on their prevalence as the most abundant unsaturated and saturated fatty acids, respectively, in liver TG of healthy individuals and NAFLD patients (Gomez-Lechon et al. 2007). In addition, the ability of OA and PA at concentrations and proportion used to induce ROS without any cytotoxic effects was shown in the laboratory by another researcher (data not shown) before starting the experiments.

The ability of RSV to dimmish ROS production is reflective of its ability to inhibit the "second hit" and consequently reduce lipid accumulation and delay disease progression. The results seen are in agreement with previous published study that indicated an increase in oxidative stress levels induced by OA and PA and their mixture in HepG2 cells without affecting cell viability (Izdebska et al. 2017). This observed effect may be associated with the ability of RSV to induce hepatic antioxidant enzyme activity, such as SOD, CAT, GPx and GSH, and reduce malondialdehyde (MDA) and nitric oxide synthase levels (Bujanda et al. 2008; Rubiolo et al. 2008; Franco et al. 2013; Chupradit et al. 2022). Due to the strong correlation between reduction in the oxidative stress and hepatic steatosis, further investigation to measure the effect of RSV on hepatic antioxidant enzymes using liver from $LDLR^{-}/^{-}$ mice used in this study as well as HepG2 cells is required to provide full insight into the exact antioxidant mechanisms behind the observed results.

7.4 Future direction

The primary investigations in this study provide encouraging results that can be used as foundation for further investigations to gain more mechanistic insights on the impact of RSV intervention in NAFLD development in the context of atherosclerosis. To gain more mechanistic insights of the action of RSV, RSN-seq from liver could be carried out to evaluate genome-wide, whole transcriptome-level changes in gene expression mediated by RSV supplementation. However, RNA extraction from liver tissue stored in RNAlater stabilisation solution was done and sent to Novogene at the end of this project. The data, which remain to be analysed in detail will provide valuable insights into how RSV intervention produces favourable effects on liver steatosis and cellularity. Beyond this, due to the sex differences as male shows more susceptibility to diet-induced metabolic syndrome compared to female, investigation of RSV to reduce NAFLD progression in female $LDLR^{-}/^{-}$ mice should be performed. Such sex-specific differences have been shown in the host laboratory during investigation of other nutraceuticals such as HT and catechin and other published studies (Lonardo et al. 2019; Lonardo and Suzuki 2020; Man et al. 2020). Furthermore, owing to the well-known anti-oxidant and anti-inflammatory actions of RSV, the effect of RSV on the expression of pro-inflammatory cytokines, such as TNF-α, IL-1α, IL-1β and IL-6, along with the previously mentioned antioxidant enzymes and other oxidative stress markers should be

studied *in vivo* (liver sections) and *in vitro* (OA/PA-induced HepG2). In addition, the infiltration of inflammatory cells in the liver is considered as a hallmark for the progression of NAFLD, NASH in particular (Miura et al. 2012). Like in atherosclerosis, macrophages uptake lipid and transform into foam cells that produce pro-inflammatory cytokines and consequently progress the disease towards steatohepatitis (Carpino et al. 2016). Aside from macrophages, $CD8^+$ T cells and NK cells were detected in liver of HFD mice and were demonstrated to influence further inflammatory reactions (Bhattacharjee et al. 2017). Therefore, IF staining for liver sections for these inflammatory cells will provide a comprehensive view on liver inflammatory status after RSV intervention.

7.5 Conclusions

The data obtained as part of this project support RSV as a potential promising nutraceutical capable of delaying the progression of NAFLD. The inclusion of RSV to HFD in male $LDLR^{-/-}$ mice for 12 weeks showed a delay in NAFLD progression via reduction in lipid accumulation and enhancement in liver cellularity. Furthermore, *in vitro* assays using HepG2 cells confirm these finding as well as demonstrate the potent antioxidant activity of RSV by reducing ROS production. Therefore, it can be concluded that the antisteatotic effect of RSV might be mediated, at least partly, via its anti-oxidant action. Together with its anti-atherogenic effects, including reduction in macrophages and T cells accumulation in the plaque, increase in plaque stability, improvement in plasma lipid profile as well as reduction in inflammation (i.e., beneficial changes in BM and PB cell populations), RSV exhibits a promising treatment avenue for NAFLD that should be investigated further to gain deeper insights into its mechanism of actions.

CHAPTER 8

General Discussion

8.1 Introduction

CVDs are one of the most serious health problems and remain one of the leading causes of global mortality and morbidity. They continue to be a significant burden in terms of health and economics in current society since they are no longer restricted to developed countries due to the sustained increase in the global rates of risk factors such as obesity, diabetes and a sedentary lifestyle. The dominant cause of CVDs is atherosclerosis, a chronic low-grade inflammatory disorder that affects the arterial walls of medium and large arteries. The main feature of atherosclerosis is the formation of plaque that develops over the life-time and is finally subjected to rupture or erosion, leading to clinical complications, such as MI and cerebrovascular accident (stroke) (Libby et al. 2019; Libby 2021; Chan and Ramji 2022). The gold and first-line pharmaceutical therapy that is commonly prescribed is statins, a class of lipid-lowering agents that inhibit the rate-limiting step of endogenous cholesterol synthesis as well as having other pleiotropic effects such as anti-inflammatory action. Despite the significant impact of statins in reducing morbidity and mortality from atherosclerosis, several limitations and MACE are associated with their use. These include adverse side effects, such as myalgias and hepatic abnormalities and some of these side effects are severe although they are rare, such as rhabdomyolysis, resulting in patient non-compliance and ultimately uncontrolled levels of plasma cholesterol (Chan and Ramji 2022). Furthermore, the results from clinical trials are relatively disappointing since it has been reported that a substantial residual risk for CVDs remains post-statins therapy. Of interest, although the anti-inflammatory property of statins is widely accepted, numerous studies documented that increased secretion of IL-1β and IL-18 via activation of the NLRP3 inflammasome after statin administration, subsequently further aggravating the disease (Liberale et al. 2019; Koushki et al. 2021). Recently, the focus on anti-inflammatory strategies has increased especially since the anti-IL-1β monoclonal antibody (Canakinumab) effectively dampened levels of the residual pro-inflammatory cytokine in previous MI patients with high CRP levels (Ridker 2017). Moreover, broad-spectrum anti-inflammatory agent such as colchicine is another promising anti-inflammatory drug that has shown comparable success to canakinumab in lowering cardiovascular risk (Chan and Ramji 2022). Regardless of the effectiveness of the currently available therapies, their limitations and MACE associated with their use have encouraged substantial investigations into other alternatives. There is a significant amount of interest to

find alternatives with a safer, more effective and more affordable profile to combat the disease. Nutraceuticals are potentially promising alternatives as preventative/therapeutic agents against atherosclerosis or as a co-therapy with current pharmacological agents that are gaining attention due to their various anti-inflammatory and anti-oxidative protective roles as well as many previously mentioned advantages (Moss and Ramji 2016; Moss 2018). RSV is one of these natural compounds that has received a lot of scientific attention in the last few decades for its reported promising pharmacological potential (Magyar et al. 2012; Berman et al. 2017; Cheng et al. 2020a). According to the literature, RSV protects against chronic inflammation and lowers the risk of cardiovascular events such as atherosclerosis and thrombosis (Cheng et al. 2020a). Furthermore, it has been shown that administration of RSV improves human plasma lipid profile, reduces hypertension and exhibits anti-inflammatory actions (Table 1.6). Despite the fact that a number of investigations have been carried out on RSV in a variety of conditions, the actions and underlying mechanisms of RSV in the context of atherosclerosis *in vitro*, in animal models and in humans have not been fully investigated yet. Therefore, this project aimed to focus on delineating the anti-atherogenic, anti-inflammatory and antioxidant effects of RSV *in vitro* using a range of model systems. Furthermore, the potential therapeutic effect of RSV administration was investigated in the atherosclerotic $LDLR^{-/-}$ mouse model. An overview of the key aims, objectives and experimental strategy is illustrated in Figure 8.1.

8.2 Summary of key findings

8.2.1 *In vitro*

One of the aims of this project was to determine the anti-atherogenic effect of RSV *in vitro* using different cell lines and primary cell cultures, including THP-1 monocytes, macrophages, HASMCs and HAECs. Initially, a range of *in vitro* assays were utilised to identify the lowest effective concentration of RSV. This was achieved by carrying out preliminary investigations in a range of dose-response experiments with the aim of selecting a single optimal concentration that was then used in further experiments. Results from these initial investigations indicated that 50 µM is the lowest and most effective dose of RSV.

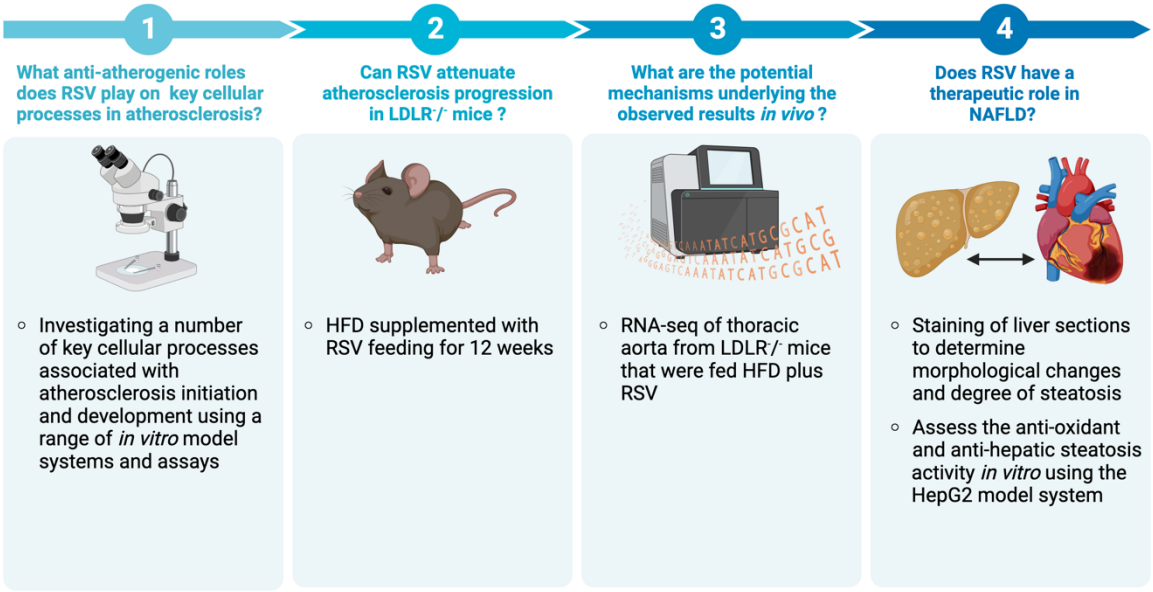

Figure 8.1 An overview of the key aims, objectives and experimental strategy

Abbreviations: LDLR, low-density lipoprotein receptor; HFD, high-fat diet; RNA-seq, RNA sequencing; NAFLD, non-alcoholic fatty liver disease. Image created with BioRender.com

Key findings from the data presented in chapter 3 include the attenuation of MCP-1-induced monocyte migration (Figure 3.7), HASMCs migration towards PDGF (Figure 3.20) and dramatically attenuated TBHP-induced ROS production in THP-1 monocytes (Figure 3.8A) and macrophages (Figure 3.8B), HMDMs (Figure 3.8C), HASMCs (Figure 3.21A) and HAECs (Figure 3.21B). Since substantial evidence supports a correlation between mitochondrial dysfunction and acceleration of atherosclerosis progression (Yu et al. 2013; Wang et al. 2017; Peng et al. 2019; Shemiakova et al. 2020), the assay that enables investigation of mitochondrial ROS production was utilised. The data showed that mitochondrial ROS production was significantly decreased by RSV (Figure 3.12). Taken together, these results demonstrate the anti-migratory and anti-oxidant properties of RSV.

Concurring the crucial role of lipid modulation in disease progression, investigations continued *in vitro* with more focus on lipid uptake, metabolism and efflux. RSV treatment was found to reduce ox-LDL uptake by macrophages (Figure 3.10) and HASMCs (Figure 3.24B). Along with the reduction in ox-LDL uptake, RSV also attenuates macropinocytosis in macrophages (Figure 3.9) and HASMs (Figure 3.23B). To confirm these findings, the assay was repeated using HMDMs. Both ox-LDL uptake and macropinocytosis were reduced in RSV-treated cells (Figure 3.24A and Figure 3.23A respectively). Intracellular cholesterol

metabolism was also investigated, and the results showed that RSV treatment can reduce the accumulation of TPL (Figure 3.25A), TG (Figure 3.25B) and CE (Figure 3.25C). Furthermore, RSV was found to induce cholesterol efflux from macrophages (not statistically significant) by around 29% (Figure 3.22). Together, these results strongly suggest that RSV can reduce/prevent the formation of macrophage and HASMC foam cells, a critical stage in atherosclerosis progression.

To understand the mechanisms underlying the reduction observed in ox-LDL uptake by macrophages, the expression of SRs was investigated at mRNA and protein levels. The mRNA levels of both SR-A and CD36 was significantly increased following RSV treatment (Figure 3.26A and B respectively). At the protein level, LDLR expression was also determined in addition to SR-A and CD36. The levels of SR-A were significantly decreased (Figure 3.27A) while CD36 and LDLR were increased after RSV incubation (Figure 3.27B and C respectively). However, as discussed in Chapter 3, there are other receptors implicated in cholesterol uptake by macrophages that need to be investigated.

The role of the NLRP3 inflammasome in promoting atherosclerosis and foam cell formation is well-known (Bobryshev et al. 2016). Therefore, it was of interest to assess inflammasome activation by measuring IL-1β concentration. In the current study, *in vitro* investigations revealed that treatment of cholesterol crystal-stimulated THP-1 macrophages with RSV resulted in a significant reduction in IL-1β secretion (Figure 3.13). Macrophage phagocytic activity plays a role in the accumulation of CE, and hence stimulates inflammasome activation (Bobryshev et al. 2016). Treatment of THP-1 macrophages with RSV in this study demonstrated a reduction in phagocytic activity (Figure 3.12). Further investigations of the anti-inflammatory effect of RSV were performed by investigating inflammation-associated gene expression. It was found that RSV was capable of reducing MCP-1 expression in IFN-γ-stimulated THP-1 macrophages and TNF-α-stimulated HAECs as shown in Figure 3.28A and Figure 3.28C respectively. On the other hand, the expression of ICAM-1 was significantly increased in IFN-γ-stimulated THP-1 macrophages and TNF-α-stimulated HAECs after RSV treatment (Figure 3.28B and Figure 3.28D respectively).

Considering the crucial role of SMCs in disease progression and plaque stability, the assessment of HASMCs proliferation post RSV treatment was investigated and found to be

enhanced on day 8 (Figure 3.17 and 3.18) suggesting that RSV may potentially have a beneficial effect on plaque stability. MMP activity is well-known to play a central role in plaque stability, and hence the effects of RSV on MMP activity in THP-1 macrophages were investigated at both 3 and 24 hours to determine both short- and long-term actions. It was found that the MMP activity was reduced by RSV after 3 hours (Figure 3.14A) but not after 24 hours (Figure 3.14B).

Taken together, findings from this study validated the anti-atherosclerotic potential of RSV across key cellular processes associated with atherosclerosis initiation and development.

8.2.2 *In vivo*

In the light of the anti-atherogenic effects of RSV that have been shown in all key cells implicated in atherosclerosis initiation and development *in vitro*, the study then continued to test the hypothesis that RSV could attenuate atherosclerosis development and progression *in vivo*. This was reinforced by promising results from previous studies using different animal models (Prasad 2012). Although these studies provide valuable insights into the atheroprotective effect of RSV *in vivo*, none of these studies reported the potential effect of RSV to prevent atherogenesis or disease development in detail, such as changes in plaque and cellular compositions, using the $LDLR^{-}/^{-}$ mouse model system. Therefore, a key aim of this project was to determine whether RSV supplementation of HFD could attenuate plaque formation and development and encourage plaque stabilisation along with beneficial changes in atherosclerosis-associated factors in $LDLR^{-}/^{-}$ mice, which is a more comparable model to diet-induced atherosclerosis in humans. In this study, $LDLR^{-}/^{-}$ mice that had received RSV at 20 mg/kg/day in HFD for 12 weeks demonstrated attenuation in plaque inflammation that was associated with a reduction in plaque composition of macrophages (Figure 5.3) and in $CD3^{+}$T cells (Figure 5.5). This was accompanied by attenuation in counts of WBCs (Figure 4.10) and the HSPCs population in the bone marrow (Figure 4.11, 4.12 and 4.13) and a trend towards reduction in T cells and B cells in the peripheral blood (Figure 4.14D, E and F). Despite this, there were no significant changes in plaque burden and lipid content (Figure 5.2) although there was a reduction in plasma LDL-C, TC and CE levels (Figure 4.8) as well as a trend towards reduction in LDL: HDL and TC: LDL ratios (Figure 4.9). These findings highlight

the fact that changes in plasma lipid profile are not always indicative of alterations in atherosclerotic plaque lipid content. Furthermore, markers of plaque stability was found to be enhanced by RSV intervention (Figure 5.8) as a consequence of increased presence of SMCs (Figure 5.6) and collagen content (Figure 5.7) combined with decreased macrophage content (Figure 5.3) in the plaque, implying suppression of development to an unstable phenotype. Moreover, although there was no change observed in the body, organs and fat pad weight, the liver weight was significantly decreased by RSV (Figure 4.6B), suggesting a reduction in hepatic steatosis. This finding encourages research to be continued that investigates the effect of RSV supplementation on NAFLD. A summary of the key changes modulated by RSV *in vitro* and *in vivo* are illustrated in Figure 8.2.

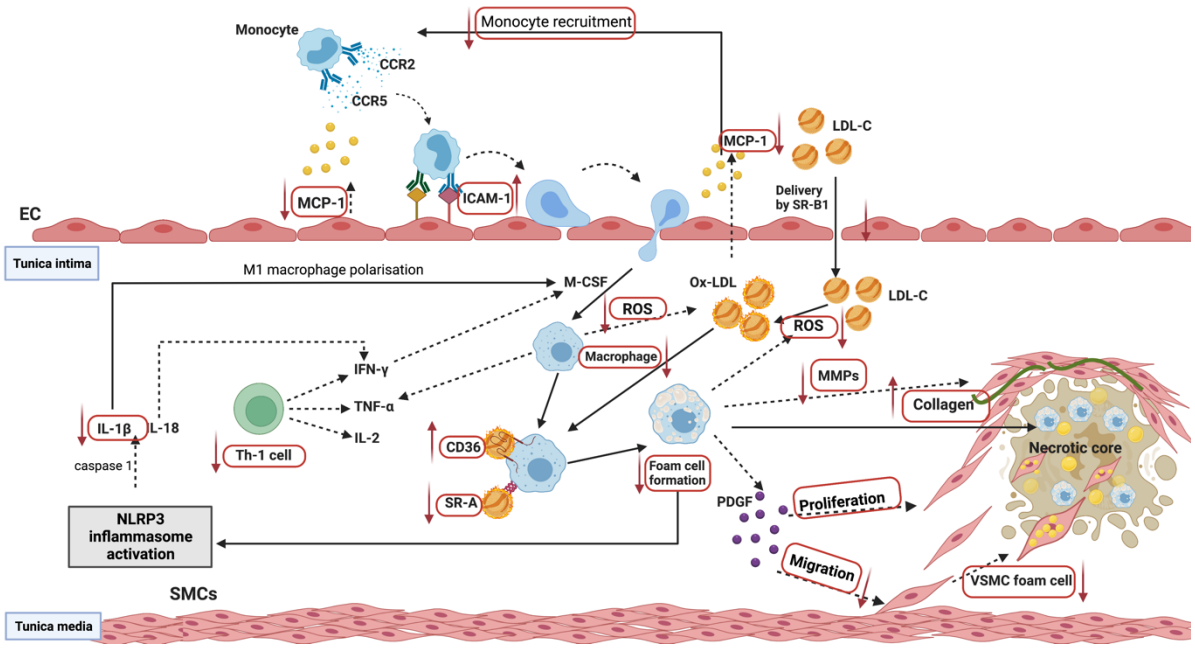

Figure 8.2 A summary of key *in vitro* and *in vivo* results

The red circles represent key processes that are significantly modulated by RSV while the corresponding changes are indicated with arrows. **Abbreviations:** LDL, low-density lipoprotein; ox-LDL, oxidised LDL; SR-B1, scavenger receptor-B1; MCP-1, monocyte chemotactic protein-1; ICAM-1, intercellular adhesion molecule-1; IL-1β, interleukin-1β; IL-18, interleukin-18; ROS, reactive oxygen species; M-CSF, macrophage-colony stimulating factor; SR, scavenger receptor; CD36, cluster of differentiation 36; IFN-γ, interferon-γ; TNF-α; tumour necrosis factor-α; IL-2, interleukin-2; Th1, T-helper 1 cell; NLRP3, nucleotide oligomerisation domain (NOD) leucine-rich repeat (LRR) and pyrin domain (PYD) containing protein 3; MMPs, matrix metalloproteinases; PDGF; platelet-derived growth factor; VSMC, vascular smooth muscle cell.

8.2.3 NAFLD

Given the strong association between NAFLD and atherosclerosis, it was hypothesised that RSV reduces liver weight owing to improved hepatic structure and function and improved lipid profile. Staining of neutral lipids in liver sections with ORO demonstrated a reduction in hepatic steatosis by RSV (Figure 7.3) along with improved hepatic cellularity showed by staining with H&E (Figure 7.2). This finding was verified by reduced lipid accumulation in HepG2 cells *in vitro* (Figure 7.5). Reducing ROS production is one of the possible mechanisms underlying the observed reduction in hepatic steatosis since the presence of ROS is essential for the "second hit" to progress the disease. Therefore, HepG2 cells were treated with RSV in the presence of TBHP- or OA/PA to induce ROS production. Results from these studies demonstrate the ability of RSV to reduce TBHP- and OA/PA-induced ROS production (Figure 7.7A and B respectively). The preliminary investigations in this study yield intriguing results that may be utilised as a basis for future research to acquire deeper mechanistic insights into the impact of RSV intervention on NAFLD development in the context of atherosclerosis.

8.3 Potential mechanisms of action

8.3.1 Atherosclerosis development and progression

As aforementioned, during inflammation, monocyte recruitment and infiltration of other leukocytes from the bloodstream into the arterial wall in response to endothelial dysfunction/activation is one of the initial events in atherogenesis. This is facilitated by arrays of cytokines (MCP-1, TNF-α, M-CSF) and adhesion molecules (ICAM-1, VCAM-1, E- and P-selectins, integrins) (Ramji and Davies 2015). Taken together, the results of the current study demonstrate attenuation of MCP-1-stimulated monocyte migration along with a reduction in MCP-1 expression induced by either TNF-α or IFN-γ. Furthermore, a reduction in ROS production by key cells implicated in disease progression as well as mitoROS production in PMA-differentiated THP-1 macrophages after RSV treatment was also observed *in vitro*. When combined with the reduction in $CD8^+$ T cell populations in the peripheral blood of RSV-supplemented $LDLR^{-/-}$ mice, these findings suggest a potential mechanism for the attenuation of macrophage contents in plaques. This proposition is constant with a previous study that revealed that the depletion of $CD8^+$ T cells in atherosclerotic $LDLR^{-/-}$ mice resulted in a

reduction in Ly6C^{high} counts in circulating blood and GMP in the spleen and bone marrow, along with a reduction in the accumulation of macrophage in plaques without a direct effect on monocyte recruitment (Cochain et al. 2015). Furthermore, a previous study indicated that suppression of mitoROS in hypercholesterolaemic LDLR$^{-/-}$ mice resulted in a marked reduction in macrophages and monocyte infiltration in plaques along with a reduction in MCP-1 expression and down-regulation of the NF-κB pathway (Wang et al. 2014b). Notably, in the current study, RNA-seq of the mouse aorta revealed a potential inhibition of the NF-κB pathway by RSV (Chapter 6) that may be because of a reduction in ROS. Importantly, the NF-κB pathway is activated via the degradation of its inhibitor via ROS (Moris et al. 2017). This transcription factor is a master regulator of inflammation and has been implicated in disease progression due to its ability to regulate several processes, including cell migration, adhesion and invasion, and T- cells differentiation (Kumar et al. 2004; Liu et al. 2017b). The reduction in the abundance of macrophages in the plaque may also be attributed to a reduction in T cells in plaques as a result of RSV intervention. Since there is an enhancement of ICAM-1 expression *in vitro*, it can be suggested that the reduction in T cells leads to reduced release of IFN-γ, hence reduced monocyte differentiation. However, investigating the expression of adhesion molecules *in vivo* would be more informative. The reduction in T cells in plaques was not surprising as their populations were decreased in the bone marrow and the peripheral blood, and also can be attributed to the inhibition of activation of T cell signalling seen from RNA-seq results. Interestingly, analysis of RNA-seq data showed inhibition of tryptophan degradation by RSV that may potentially participate in regulating macrophages and T cells within the aortic root since tryptophan emerges as an important regulator of inflammatory responses (discussed in detailed in Chapter 6).

The anti-inflammatory property of RSV in this study was not restricted to the aforementioned reduction in inflammatory markers but extended to the inhibition of activation of inflammasome *in vitro* (cholesterol crystals-stimulated THP-1 macrophages) and *in vivo* (thoracic aorta of RSV-treated mice; observed via down-regulation of NLRP3 inflammasome activation pathway) and thereby a reduction in the concentration of IL-1β. Although the reduction in plasma levels of CE, LDL-C and TC in this study *in vivo* did potentially not affect plaque lipid content, they may contribute to a reduction in inflammation along with a

decrease in the risk of disease initiation. This is supported by the modulation of cholesterol metabolism in macrophages *in vitro*. The improvement in plasma lipid profile of atherosclerotic LDLR^{-}/$^{-}$ mice receiving RSV could potentially be mediated by the reduction in the cholesterol biosynthesis pathway along with the activation of the Wnt/β-catenin signalling pathway. The prediction of the Wnt/β-catenin signalling activation by IPA was based on the inhibition of DKK1, which has been found to play a role in enhancing inflammation and plaque instability in hypercholesterolemic ApoE^{-}/$^{-}$ mice (Wang et al. 2013; Di et al. 2017).

Collectively, from the evidence discussed in this section, it can be concluded that RSV mediates its anti-atherogenic effects via its strong anti-inflammatory and anti-oxidative properties along with modulation of lipid metabolism rather than regulation of plaque morphology (i.e. plaque and vessel size, occlusion, lipid content). Furthermore, it could be suggested that RSV improves endothelial dysfunction by reducing ROS production and consequently inhibiting the activation of pro-inflammatory signalling (NF-κB pathway).

8.3.2 Plaque progression and stability

A further mechanism by which RSV may exert anti-atherogenic effects is by enhancing marker of plaque stability. In cultured HASMCs, RSV treatment significantly attenuated cellular ROS production, PDGF-stimulated cell invasion, and VSMCs foam cell formation, in addition to enhancing cell proliferation (Chapter 3). Moreover, macrophage MMP activity was attenuated after 3 hours (short-term) incubation with RSV (Chapter 3). *In vivo* study demonstrated that inclusion of RSV in HFD enhanced plaque stability by increasing the presence of α-SMA^{+} actin-expressing VSMCs and collagen content along with reduction in the abundance of macrophages within the aortic root plaques (Chapter 5). This is combined with a reduction of MDSC in the bone marrow (Chapter 4). Although the exact role of MDSC in atherosclerosis has not yet been fully elucidated, its ability to induce angiogenesis has been shown in a previous study (Camaré et al. 2017). Therefore, it can be suggested that the reduction in MDSC may contribute to plaque stability via reduced angiogenesis. Furthermore, the results of RNA-seq analyses of the thoracic aorta revealed that RSV significantly affected genes enriched in plaque stability and collagen synthesis (Chapter 6). Despite the *in vitro*

results, the MMPs expressions were not inhibited/down-regulated by RSV *in vivo*; however, the expression of TIMP was up-regulated by RSV.

The dual role of VSMCs as pro- and anti-atherogenic has been discussed early in this thesis (Chapters 1 and 3). This dual role refers to their heterogeneity and plasticity; for example, pathological conditions such as injury or inflammation trigger VSMCs phenotype switching in which they lose their expression of contractile proteins (αSMA), switching to a synthetic phenotype. This synthetic phenotype is characterised by migration, adverse proliferation and secretion of ECMs (Rohwedder et al. 2012; Petsophonsakul et al. 2019; Björkegren and Lusis 2022). Although the migration and proliferation of VSMCs are considered a pro-atherogenic process, enhanced proliferation may play a protective role via the formation of a fibrous cap that contributes to plaque stability (Petsophonsakul et al. 2019). On the other hand, exposure of VSMCs to PDGF enhances switching to VSMC-derived macrophage-like cells, contributing to lipid-laden foam cells (Gui et al. 2022). Apoptosis and senescence of VSMCs, as well as an increase in the presence of VSMC-derived macrophage-like cells, enhances plaque inflammation and development. Accordingly, VSMC proliferation is essential for fibrous plaque formation and maintaining plaque stability.

Taken together, the above results suggest that RSV might attenuate atherosclerotic plaque progression by attenuating PDGFR signalling-induced inflammation as evidenced by the attenuation of PDGF-stimulated invasion of VSMCs and reducing inflammation as shown by the reduction in ROS production and foam cell formation. In addition, RSV enhances the presence and proliferation of VSMCs and subsequently collagen synthesis, contributing to fibrous cap formation and hence plaque stability. Given the multifaceted function of VSMCs in disease progression, there is no doubt that research should be continued with an emphasis on understanding how VSMC-derived cells affect inflammation and plaque progression.

8.4 NAFLD and atherosclerosis

A growing body of evidence indicates that patients with NAFLD are more likely to develop atherosclerosis, and treatment of patients with NAFLD resulted in a reduction in their carotid intima-media thickness and CVD (Ghaffarifar et al. 2018; Wójcik-Cichy et al. 2018). Several studies demonstrated that oxidant stress and chronic inflammation that participates in the

production of pro-inflammatory cytokines, such as TNF-α, ILs and adipocytokines, are all involved in the pathogenesis of NAFLD (Wójcik-Cichy et al. 2018). The strong role of these factors in driving atherosclerosis has already been discussed in detail earlier in Chapter 1. Reduction in liver weight by RSV compared to HFD encouraged further research to investigate more the reasons behind this observation. The staining of neutral lipids in liver sections showed a significant reduction in lipid accumulation and an increase in liver cellularity following RSV intervention. This was confirmed *in vitro* using the HepG2 model system. Oxidative stress generated by ROS production was one of the possible mechanisms that was investigated. The attenuation of ROS by RSV is not surprising as the strong antioxidant activity of RSV is well-known and confirmed in this study using different cell lines and primary cultures (as shown in Chapter 3). An analysis of plasma lipid fractions in patients with NAFLD revealed atherogenic dyslipidemia pattern characterised by an elevation in TG and VLDL, and a reduction in HDL that may at least be partially responsible for NAFLD development in patients with atherosclerosis (Arguello et al. 2015; Wójcik-Cichy et al. 2018; Martin et al. 2022). This makes modulation of plasma lipid profile by RSV (results shown in Chapter 4) as another potential mechanism responsible for the alleviation of NAFLD in $LDLR^{-}/^{-}$ mice. Therefore, further investigations such as gene expression analyses via RNA-seq for the liver sample would be informative along with many other assays (e.g., TG content in the liver sample).

8.5 Strengths and limitations

8.5.1 *In vitro* assays

Although *in vitro* experiments are considered to be oversimplifications of *in vivo* processes and can provide mechanistic insights, they also have some limitations that should be considered. One of the substantial limitations of the experimental approach in this study, as with other *in vitro* studies, is lack of complexity since other external factors (e.g., cytokines) and other cell types (e.g., immune cells) that would be present *in vivo* are absent. For example, a major limitation of monocyte migration assay is that the assay was carried out under static flow condition which is not the case in human arteries. The constant flow of blood through the peripheral blood system in human arteries creates shear stress, which has a considerable effect on ECs function and, subsequently, cell migration. Furthermore, the

modified Boyden chamber does not accurately reflect the three-dimensional nature of the vascular environment *in vivo*. *In vivo*, cells migrate through a complex network of blood vessels, and they are exposed to a variety of physical and chemical signals that can influence their migration. Overall, while the modified Boyden chamber is a useful tool for studying cell migration, it is important to consider its limitations. To produce a further closer to *in vivo* state and confirm the findings, the assay could be carried out by replacing the porous membrane with a layer of ECs and subjecting the cells to different shear stress to mimic the arterial microenvironment. The shear stress could be induced via methods described by Meng *et a*l (Meng et al. 2022), which could provide new mechanistic insights. However, in the vast majority of cases such as atherosclerosis, it is difficult to precisely model its pathophysiology due to its complexity and multifactorial nature. Furthermore, the exact role of certain cytokines and immune cells implicated in driving the disease is still unknown. The *in vitro* assays allow for the investigation of certain cellular processes in isolation, providing a method for quantitatively examining the effects of diverse agents/drugs and characterising their activities. Consequently, this allows for direct comparisons between various drugs and gives insights into the potential underlying mechanisms that may be responsible for the effects observed *in vivo*, leading to future investigations. To date, as far as we are aware, this is the first study that investigates the actions of RSV *in vitro* and *in vivo* in such detail using a combination of different *in vitro* assays with an established mouse model of atherosclerosis ($LDLR^{-}/^{-}$ mice). This includes a range of key cellular processes carried out using multiple cell types implicated in the disease, and analysis of atherosclerotic plaque progression along with the disease-associated risk factors.

8.5.2 *In vivo*: using mouse models and HFD

Atherosclerosis is a complex disease with many contributing factors, including genetics, lifestyle, and environmental factors. It can also vary widely in its severity and progression among individuals. These factors make it difficult to study in humans, and animal models are often used to gain mechanistic insights and to understand the underlying pathophysiology of the disease. There are several different types of animal models that are used to study atherosclerosis, among them, mice are a predominant model system to study this disease due to arrays of advantages. These include ease of handling because of being small, ease os

controlling their environmental conditions and dietary intake, ease of breeding and rapid reproduction rates. They are also relatively inexpensive to maintain and breed, making them cost-effective for research. Additionally, mice can be genetically modified and atherosclerotic lesions can be induced in a reasonable time (Gisterå et al. 2022). Therefore, investigation of disease progression can be carried out in a comparatively short period of time. Furthermore, in comparison to other models using larger animals, the low cost of mice breeding, and maintenance allows for a high n number based on power calculations and adhering to 3Rs of animal research that subsequently has a stronger impact on statistical analysis. Nonetheless, despite their genetic resemblance to humans, mouse models have been criticised for failing to precisely mirror the characterisation of human disease. For example, unlike humans, mice lack CETP which affects their lipid metabolism as well as they differ in inflammation and lesion distribution (Gisterå et al. 2022). The atherosclerotic lesion distribution in mice differs from that of humans since the plaque often develops at the aortic root and brachiocephalic artery in mice whereas it occurs in peripheral and coronary arteries in humans. However, it is well established that there is a striking resemblance in the key features of the atherosclerotic process between humans and mice, particularly in ApoE^{-}/$^{-}$ and LDLR^{-}/$^{-}$ mice fed HFD (Von Scheidt et al. 2017).

Wild-type mice are relatively resistant to developing atherosclerosis as they have low levels of ApoB-containing lipoproteins; even after 12 months or more sustained administration of an atherogenic diet, only primitive lesion development in the form of fatty streaks is produced (Gisterå et al. 2022). Therefore, manipulation of genes involved in lipoprotein transport is necessary to make these mice susceptible to atherosclerosis in a short period of time. The two most commonly used mice in atherosclerosis studies are AopE^{-}/$^{-}$ and LDLR^{-}/$^{-}$. There are several differences between these two strains, as discussed previously in Chapters 1 and 4. Generally, the lack of ApoE and LDLR results in an increase in the sensitivity of mice to dietary lipids, and it can be seen by manifestation with an increase in plasma LDL of LDLR^{-}/$^{-}$ mice and an increase in plasma chylomicron remnants/VLDL in ApoE^{-}/$^{-}$ mice. Indeed, unlike LDLR^{-}/$^{-}$ mice, ApoE^{-}/$^{-}$ mice can develop the disease on a standard chow diet; however, feeding Western-type diet (i.e., atherogenic diet) can accelerate disease progression. Furthermore, ApoE^{-}/$^{-}$ mice have higher inflammation levels than LDLR^{-}/$^{-}$ mice, leading to an effect on several processes associated with disease progressions, such as RCT from macrophages and SMCs

proliferation and migration. Considering the fact that feeding Western-type diets is not necessary to instigate atherosclerotic plaques in the ApoE$^{-/-}$ strain, the plaque formed in this strain may differ from those that occur in humans as a result of Western-type diets (Gisterå et al. 2022). In the context of atherosclerosis, LDLR$^{-/-}$ mice exhibit less disturbed lipid metabolism and the immune system compared to ApoE$^{-/-}$ mice; however, interestingly it is well-documented that LDLR$^{-/-}$ mice exhibit increased sensitivity to hepatic inflammation and fibrosis in comparison to AopE$^{-/-}$ mice (Gisterå et al. 2022). Taken together, when all the aforementioned facts are combined, LDLR$^{-/-}$ mice have been the model of choice in such studies as well as in the host laboratory.

In this study, lard was the only source of fat in the HFD, which consisted of 21% (w/w) pork lard and 0.15 % (w/w) cholesterol. Although this is critical for encouraging the progression of atherosclerosis in these mice, the HFD has been deemed "extreme" due to its dubious resemblance to the "Westernised" diet actually consumed by individuals. However, the use of high concentrations of fat is necessary due to the relatively short period of feeding. Using HFD is a convenient and practical approach to triggering atherosclerosis in these mice as atherosclerosis in humans develops over decades, and considering that it is important to strike a balance between dietary alteration, feeding duration, and supplement dosage.

Both the type of HFD employed and the length of the feeding period were determined by prior optimisation studies performed in the host laboratory and the collective expertise of the researchers there and their colleagues. These studies revealed that 12 weeks of feeding HFD in 8-week-old LDLR$^{-/-}$ mice was enough to induce established atherosclerotic lesions. This was confirmed by the presence of atherosclerotic lesions and hypercholesterolaemia attributable to high levels of plasma LDL. As a result, this setup was used in this study since it has been proven to induce consistent and measurable intermediate atherosclerotic lesions. The down-stream images analysis methods for detailed plaque morphometric and histological changes utilised in this study, as well as all studies conducted in the host laboratory, were optimised in the host laboratory by researchers (Yee Chan and Reem Alotaibi) in order to establish a more systematic and consistent method. These methods were performed in a blinded manner where possible to eliminate any unconscious bias, which ultimately led to greater confidence in results. Using these kinds of methodologies will

undoubtedly minimise the subjectivity and heterogeneity of results generated from many studies employing the same mouse model, diet composition and feeding duration.

8.5.3 Dose of RSV: from bench to mouse to clinical trials

The final concentration of RSV used in *in vitro* experiments in this study was determined after initial pilot experiments that were performed in a dose-dependent manner with the aim of selecting a single optimal/effective concentration. Results from these experiments revealed that 50 μM was the lowest effective concentration of RSV that was then proceeded with in all subsequent experiments. However, the same dose was not applied to *in vivo* investigations. Therefore, the dose used for the *in vivo* study, 20mg/kg/day, was based on a previously published study using ApoE$^{-/-}$ mice (Chang et al. 2015a). Furthermore, RSV has extremely low solubility in water, which can make it difficult to administer to animals in a water-based solution. One way to overcome this issue is to dissolve RSV in DMSO, which is a polar solvent that can dissolve a wide range of compounds, including RSV. However, DMSO is toxic to cells at high concentrations and can have adverse effects on animals, hence, RSV was mixed with HFD as homogeneously as possible instead to avoid toxicity. The required amount of RSV to reach this dosage to administer to mice was calculated based on the estimated average of HFD consumption/day/mouse. This average of HFD consumption/day/mouse was based on previous experiments in the host laboratory monitoring daily consumption. However, the exact amount of diet consumed by individual mice could not be accurately quantified due to the presence of multiple mice per cage. Therefore, the precise amount of diet consumed by an individual mice may vary slightly, which may have an effect on the exact dose of RSV administered to each mouse. In spite of this, the consumption of diet either with or without RSD was measured for all cages throughout the whole duration of the study, and it was found that the two groups consumed a comparable amount of diet on average.

The only way to ensure delivering the exact dose of RSV to mice is through daily gavage. However, this method was impractical when working with a large number of mice, as in this study, along with the long duration of the study (12 weeks), which make it challenging to maintain the daily gavage regimen for the entire duration of the study. Moreover, the use of gavage for prolonged periods of time, on a regular basis, increases the potential for

complications in mice. Inadvertent tracheal administration, damage to the oesophagus or stomach, aspiration pneumonia, and injury to the digestive tract are all possible consequences of gavage that can increase morbidity and mortality (Hoggatt et al. 2010). Additionally, the insertion of a feeding tube can be stressful for the mice, which has been indicated previously by increased plasma corticosterone levels and increased blood pressure that, in combination with the aforementioned risk, could affect inflammation and hence affect the accuracy of study results (Kinder et al. 2014). Therefore, it may be more practical to administer the treatment by mixing well with HFD even though it may be difficult to accurately determine the actual dose consumed by each mouse.

Like any drug, the bioavailability of RSV can be a challenge when translating promising findings from cell culture and animal models into clinical use. Since the vast majority of human clinical trials have focused on the administration of RSV as single or multiple oral dosages (in the form of capsules and tablets). Detailed information on the concentrations of RSV and its metabolites in plasma from these studies can be found in Chapter 1, specifically in section 1.7. However, several strategies have been developed to increase bioavailability from oral delivery. This includes increasing the absorption rate of RSV into enterocytes and decreasing its intracellular metabolism; however, many of these strategies are in the early stages of development and reviewed by Smoliga and Blanchard (Smoliga and Blanchard 2014). A range of RSV concentrations have been used in clinical trials and has reported the safety of RSV at dosages up to 5 g/day with good tolerance (Patel et al. 2011; Zhang et al. 2021b). The 20 mg/kg dose of RSV used in this project would equate to approximately 1.62 mg/kg, based on human equivalent dose calculation based on body surface area described by Nair and Jacob (Nair and Jacob 2016), which is still in the safe range for humans. It is also important to note that the bioavailability of RSV can vary between individuals due to differences in absorption and metabolism. Some factors that may influence the bioavailability of RSV include age, sex, body weight and genetics. On the basis of this information, one important potential direction for the future would be to determine levels of RSV and its metabolites in plasma, urine/faeces and tissues such as the heart (as it was previously found that concentrations of RSV and its metabolites are high in the organ) (Böhmdorfer et al. 2017), discussed in Chapter 1) using gas chromatography-mass spectrometry to confirm the absorption and bioavailability.

8.6 Further directions and future perspectives

8.6.1 *In vitro*

Several *in vitro* studies have been conducted as part of this study; with a focus on macrophages since it is a major cell type implicated in disease initiation and progression and provides a significant overview into the function of RSV in several aspects correlated with the disease. However, there are a number of further experiments that would provide valuable insight into RSV activities as well as contribute to the development of knowledge of its mechanism of action in the context of atherosclerosis. For example, the anti-foam cell formation in macrophages and HASMCs should be expanded and confirmed by studying the mRNA and protein levels of scavenger receptors involved in the lipid uptake process. This should be carried out along with the expression of efflux genes to provide a complete understanding of the role of RSV as an anti-foam cell formation agent. Furthermore, the anti-inflammatory effect of RSV has been demonstrated in this study via its capacity to prevent inflammasome activation, hence reducing IL-1β concentration. To gain a further understanding of the anti-inflammatory activity, the research should be continued investigating other pro-atherogenic cytokines, such as IL-18, which could give further insights into the capabilities of RSV from a broader inflammasome-related perspectives. Given the integral roles of VSMCs and ECs in inflammation and in driving atherosclerosis, future studies should incorporate strategies to determine the effect of RSV on their role. For example, RNA-seq approaches could also be employed to determine how RSV alters VSMCs and ECs transcriptome at the cellular level. This could be combined with determining the effect of RSV on VSMCs dysfunction by investigating the effect of RSV on VSMC senescence and apoptosis. To achieve this, several potential experimental strategies can be used. These include use of annexin-V labelling to evaluate apoptosis and IHC staining for senescence markers (e.g., senescence-associated-β galactosidase)(Matthews et al. 2006). Considering the promising results from HepG2 cells, further investigations to determine the anti-inflammatory and anti-steatosis effects of RSV are crucial. Since the data from previous preclinical studies revealed the high concentration of RSV metabolites in certain tissues and suggested that RSV metabolites may be, at least in part, responsible for the observed effects; and no studies have been conducted before on them *in vitro* (as far as we are aware), it would be informative to

recapitulate the experiments on metabolites, such as RSV-sulfate, RSV-glucuronide, and RSV-sulfoglucuronide. A summary of possible future directions is illustrated in Figure 8.3.

8.6.2 *In vivo*

The results obtained from *in vivo* studies highlighted various beneficial effects of RSV supplementation on atherosclerosis progression and its associated risk factors. However, further experiments could be carried out using stored tissues, plasma, urine, and faeces obtained from the *in vivo* investigation of $LDLR^{-/-}$ mice supplemented with RSV at the end of the study. In addition to future studies aforementioned in Chapter 4, investigating the concentration of short chain fatty acids in the plasma and faeces, and analysis of RSV metabolites and their concentrations in tissues, plasma, urine, and faeces would be informative and would be an important future avenue. Furthermore, the current study provides evidence that RSV inclusion in HFD promotes plaque stability and protects against rupture. Although plaque rupture is a key event in the development of clinical complications in humans, it occurs very seldom in $ApoE^{-/-}$ and $LDLR^{-/-}$ mice and most other mouse models of atherosclerosis that has hence resulted in limited *in vivo* studies of plaque rupture. The plaque rupture in $ApoE^{-/-}$ and $LDLR^{-/-}$ mice is rare and unpredictable occurrence that may only occur over a lengthy period of time in some arterial beds, such as the brachiocephalic artery (Veseli et al. 2017). Therefore, considering the important role of RSV in promoting fibrous cap formation and protecting against plaque rupture, the ability of RSV on protecting against plaque rupture could be investigated using the $ApoE^{-/-}$ $Fbn1^{C1039+/-}$ mice. The mutation in the fibrillin 1 gene was found to accelerate plaque progression and instability (Veseli et al. 2017). Comparison between the effect of RSV in the attenuation of atherosclerosis progression between male and female $LDLR^{-/-}$ models should be carried out due to the influence of sex differences in disease development and severity. Moreover, the potential of RSV in the regression of established plaques in $LDLR^{-/-}$ should be investigated. This would involve feeding male $LDLR^{-/-}$ mice HFD for 12 weeks before switching to HFD or chow diet for 8 weeks containing RSV. Beyond this, since RSV is already commercially accessible in varying dosages, a logical next step is progression onto human clinical trials to investigate the ability of RSV to attenuate atherosclerosis progression and primary MACE. This could be done using

RSV as a co-thereby to statins, after determining the lowest effective dose and duration in humans. A summary of other possible future directions is summarised in Figure 8.3.

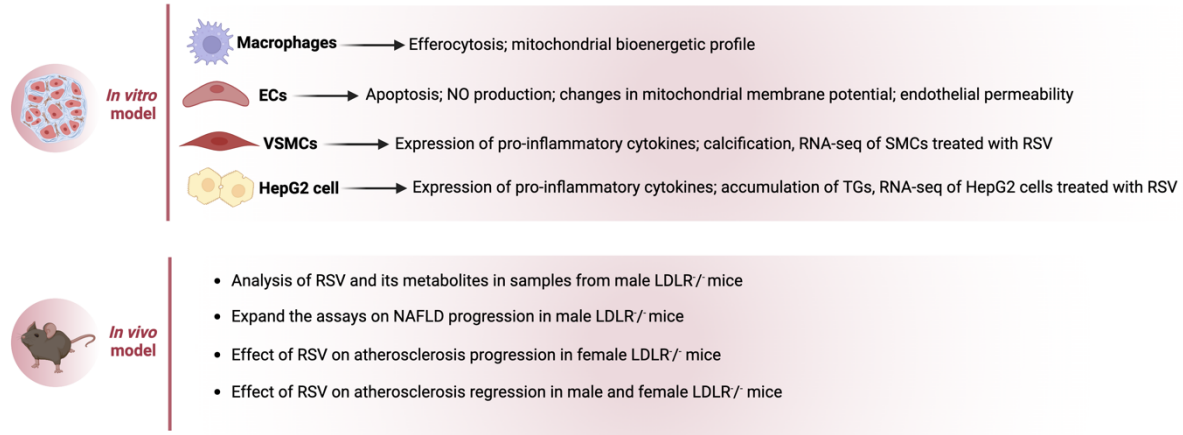

Figure 8.3 Overview of potential future directions *in vitro* and *in vivo*.

Abbreviations: VSMCs, vascular smooth muscle cells; ECs, endothelial cells; NO, nitric oxide; TG, triglyceride; LDLR, low-density lipoprotein receptor. NAFLD, non-alcoholic fatty liver. Image created with BioRender.com

8.7 Conclusions

The comprehensive investigation of the effects of RSV treatment *in vitro* demonstrated its anti-atherogenic effects that are associated with the attenuation of multiple key processes implicated in early atherosclerosis by RSV. This includes attenuation of monocyte migration and HASMCs invasion, inhibition of ROS and mitoROS production and inhibition of foam cell formation via reduction of lipid uptake by macrophages and HASMCs and enhancement in the efflux of cholesterol. Furthermore, RSV was capable of mitigating inflammasome-mediated IL-1β secretion and MCP-1 expression after cytokine-induced inflammatory responses. These atheroprotective effects were also observed *in vivo* using hypercholesterolaemic LDLR^{-}/$^{-}$ mice. Overall, the data obtained as a part of this study provides evidence supporting that supplementation of RSV attenuated atherosclerosis progression. This is associated with reduced macrophage and T cells-driven inflammation along with enhanced markers of plaque stability (mediated by increased collagen and SMCs presence in

the plaque). Clearly, these findings call for more research to be conducted in order to characterise how RSV affects VSMCs with regard to phenotypic switching, foam cell production, senescence, etc. Furthermore, the anti-inflammatory actions of RSV have been confirmed by reducing stem, progenitor, and mature cell populations within the bone marrow and by reducing the frequency of circulating T cells and B cells in the peripheral blood. Additionally, analysis of plasma lipids revealed a reduction in LDL-C, TC and CE with a corresponding increase in HDL-C (not statistically significant) in the plasma as well as reducing LDL: HDL and TC: HDL ratios, compared to the control, demonstrating lipid-modulating capability of RSV. These data are supported by the RNA-seq data from the thoracic aorta that provides valuable insights into the potential mechanisms responsible for these observations. With regards to NAFLD, the data obtained as part of this project support RSV as a potential promising nutraceutical capable of delaying the progression of NAFLD in $LDLR^{-/-}$ mice. Collectively, this study implicates RSV as a potential nutraceutical candidate that could be applied world-wide as a part of ongoing atherosclerotic CVD prevention and management strategies due to the lack of undesirable side effects and the comparatively low cost compared to standard pharmacological medications.

Chapter 9

Appendix

Appendix 1: Top 10 canonical pathways

	Control 45789 vs RSV 178	Control 45789 vs RSV 3456
1	Mitochondrial dysfunction	Mitochondrial dysfunction
2	Oxidative phosphorylation	Oxidative phosphorylation
3	Sirtuin signalling pathway	Sirtuin signalling pathway
4	Granzyme A Signalling	Valine degradation I
5	Fatty Acid -oxidation I	Fatty Acid -oxidation
6	AMPK signalling	Isoleucine degradation I
7	White adipose tissue browning pathway	SNARE signalling pathway
8	Estrogen receptor signalling	TCA cycle II
9	Valine degradation I	Granzyme A signalling
10	Dilated cardiomyopathy signalling pathway	Dilated cardiomyopathy signalling pathway

The shared canonical pathways between the 2 files are highlighted in yellow. However, the non-highlighted pathways are also shared between 2 files but in a different order.

Appendix 2: List of top 20 significant up-regulated DEGs

Control 45789 vs RSV 178	Control 45789 vs RSV 3456
Krt13	*Lmo7*
Rptn	*Cyp2f2*
Krt4	*Plekha6*
Sprr3	*Cacna1c*
Krt5	*Cilp2*
Crct1	*Scd4*
Cnfn	*Dnah5*
Myh8	*Dnah6*
Serpinb12	*Clic6*
Serpinb3a	*Wfdc2*
Lce3a	*Ifitm1*
Mt4	*Bpifb1*
Sec14l3	*Ktn1*
Defb4	*Tnfrsf19*
Lce3c	*Muc5b*
Lce3f	*Sec14l3*
Lce3b	*Ptpn3*
Pkp1	*Cdhr3*
Lce3e	*Aldh3a1*
Gm94	*Cbr2*

The shared DEGs between the 2 files are highlighted in yellow. However, the non-highlighted DEGs are also shared between 2 files but in a different order.

Appendix 3: List of top 20 significant down-regulated DEGs

Control 45789 vs RSV 178	**Control 45789 vs RSV 3456**
Hoxc9	*Gm9694*
Cntnap3	*Gm44005*
Gm5711	*Cntnap3*
Gm14239	*Adam4*
Gm13486	*Gm39929*
4930445N18Rik	*S100g*
Gm43582	*Ppp1r3g*
Gm7461	*Mfsd2a*
Gm14439	*Entpd4b*
Atg4a-ps	*Gm10790*
Scarna17	*Ctse*
Gm9694	*Gm43500*
Gm3442	*1700061I17Rik*
Grm3	*Gm42814*
Gm20369	*Sgk2*
Gm38118	*Gm45412*
Gm32281	*Rdh16*
Gm26833	*Gm32468*
Gm35552	*Themis*
Hoxa10	*Hoxc8*

The non-highlighted DEGs are shared between 2 files but in a different order.

Appendix 4: The most enriched GO terms bar chart

Control 45789 vs RSV 178

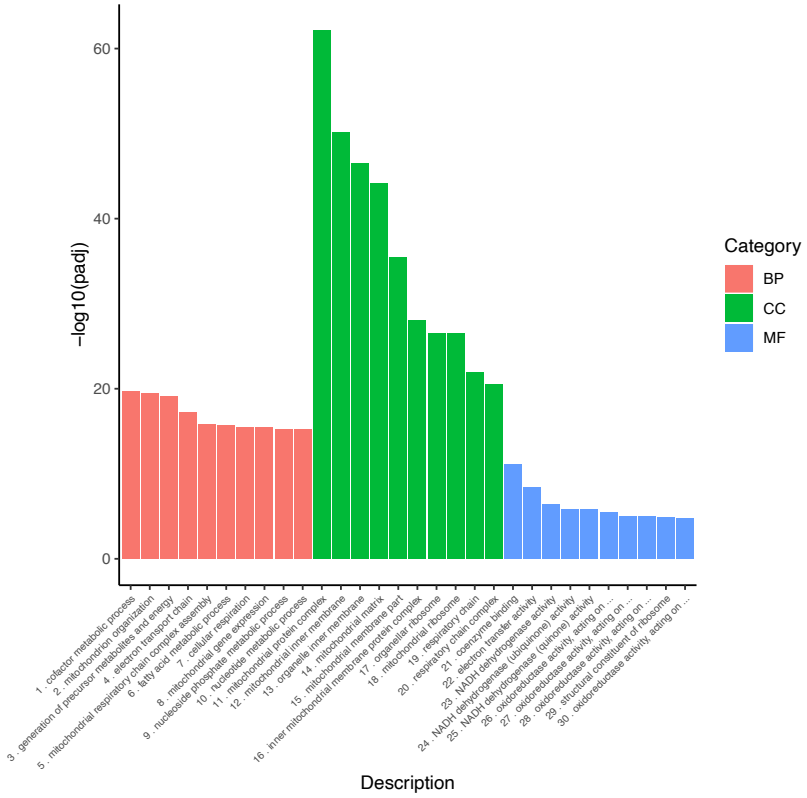

Control 45789 vs RSV 3456

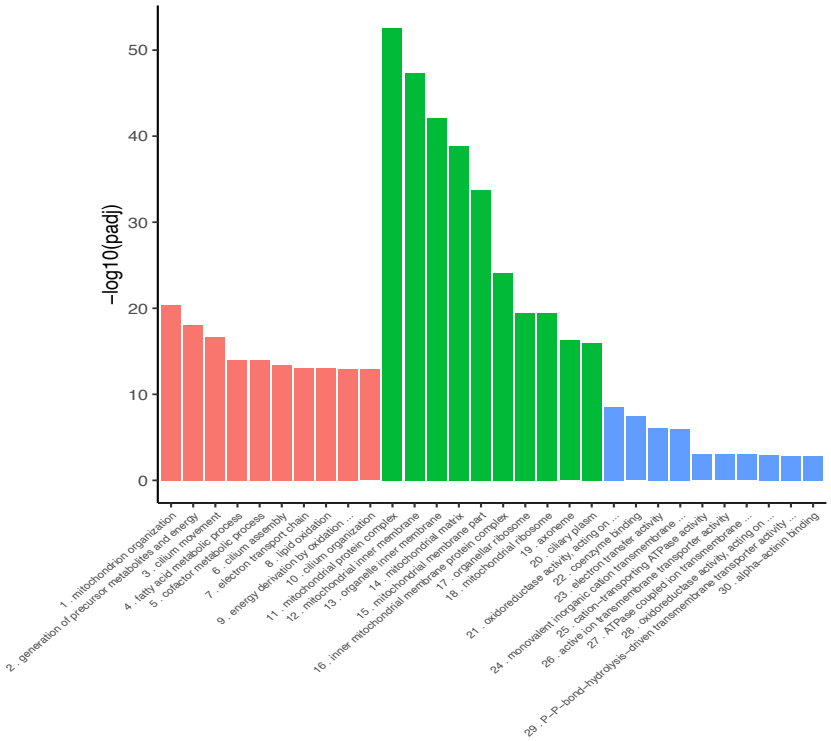

Appendix 5: The top upstream regulators affected by RSV

Control 45789 vs RSV 178	Control 45789 vs RSV 3456
Tle3	*Tead1*
Tead1	*Kdm5a*
Map4k4	*Map4k4*
Tp53	*Clpp*
Kdm5a	*Tp53*
Cpt1b	*Cpt1b*
Scd	*Slc27a2*
Clpp	*Insr*
Hba1/Hba2	*Esrra*
Dmd	*Ppargc1b*
Ppargc1b	*Hba1/hba2*
Esrra	*Klf15*
Smyd1	*Nr4a1*
Slc27a2	*Nrip1*
Rictor	*Dmd*
Cluh	*Eif6*
Eif6	*Nrf1*
Stk11	*Ppargc1a*
Pitx2	*Pitx2*
Trib1	*Por*
Flcn	*Rictor*
Med13	*Med13*
Nr4a1	*Ctnnb1*
Fgf21	*Nampt*
Insr	*Flcn*
Klf15	*Trib1*
Rb1	*Stk11*
Cidec	*Ppara*
Ucp1	*Ccnc*
2500002b13rik	*Cidec*
Ccnc	*Fgf21*
Nrip1	*Ucp1*
Prkcg	*Asxl1*
Tfam	*Nedd9*
Nrf1	*Txnrd1*
Asxl1	*Gsr*
Med30	*Pparg*
Por	*Irs1*
Pten	*Ehhadh*

The shared DEGs between the 2 files are highlighted in yellow. However, the non-highlighted DEGs are also shared between 2 files but in a different order.

Appendix 6: List of abbreviations for different genes

Gene	Full name
1700061i17rik	NA
Abat	4-aminobutyrate aminotransferase
Abca1	ATP binding cassette subfamily A member 1
Abcb	ATP binding cassette subfamily b
Abcc3	ATP binding cassette subfamily c member 3
Abhd5	Abhydrolase Domain Containing 5
Acaa	Acetyl-CoA acyltransferase
Acaca/B	Acetyl-CoA carboxylase alpha/beta
Acad	Acyl-CoA dehydrogenase family member
Acadl	Acyl-CoA dehydrogenase, long chain
Acadm	Acyl-CoA dehydrogenase medium chain
Acat1/2	Acetyl-CoA acetyltransferase 1/2
Aco1	Aconitase 1
Acsf2	Acyl-CoA synthetase family member 2
Acsl	Acyl-CoA synthetase long chain
Acsm1	Acyl-coenzyme A synthetase
Acss2	Acyl-coenzyme A synthetase short-chain family member 2
Actg2	Actin gamma 2, smooth muscle
Actn2	Alpha-actinin-2
Adam4	A disintegrin and metalloprotease domain 4
Adcy	Adenylate cyclase
Adipoq	Adiponectin
Adra	Adrenoceptor alpha
Adra1b	Adrenoceptor alpha 1B
Adrb3	Adrenoceptor beta 3
Agpat	Acylglycerol-3-phosphate acyltransferase
Agt	Angiotensinogen
Agtrap	Angiotensin II receptor associated protein
Ahi1	Abelson helper integration site 1
Aifm1	Apoptosis inducing factor mitochondria associated 1
Ak	Adenylate kinase

Akt2	V-akt murine thymoma viral oncogene homolog 2
Aldh3a1	Aldehyde dehydrogenase 3 family member A1
Aldh6a1	Aldehyde dehydrogenase 6 family member a1
Aldoa/C	Aldolase, Fructose-Bisphosphate A/C
Ank2	Ankyrin 2
Ankrd1	Ankyrin repeat domain 1
Anxa1	Annexin A1
App	Amyloid-beta precursor protein
Asb4	Ankyrin repeat and SOCS box containing 4
Aspg	Asparaginase
Atf2	Activating transcription factor 2
Atg	Autophagy-related protein
Atp2b	ATPase plasma membrane Ca^{2+} transporting
Atp5e	ATP synthase
Atp5f1a	ATP synthase F1 subunit alpha
Atp5f1b	ATP synthase F1 subunit beta
Atp5f1d	ATP synthase F1 subunit delta
Atp5mc1	ATP Synthase Membrane Subunit C Locus 1
Atp5mc3	ATP Synthase Membrane Subunit C Locus 3
Atp5mf	ATP synthase subunit F
Atp5mg	ATP synthase subunit G
Atp5pb	ATP synthase peripheral stalk-membrane subunit B
Atp5pf	ATP synthase peripheral stalk-membrane subunit F
Axl	Anexelekto
Bace2	Beta-secretase 2
Bag3	B cell lymphoma 2-associated athanogene 3
Bbs1	Bardet-biedl syndrome 1
Bcat2	Branched chain amino acid transaminase 2
Bckdha/B	Branched chain keto acid dehydrogenase E1 subunit alpha/beta
Bdh1/2	D-beta-hydroxybutyrate dehydrogenase 1/2, mitochondrial
Bpifb1	BPI fold containing family B, member 1
C1qtnf1	Complement C1q tumor necrosis factor-related protein 1
Cacna	Calcium voltage-gated channel subunit alpha

Cacnb	Calcium voltage-gated channel auxiliary subunit beta
Calcrl	Calcitonin receptor-like
Calm1	Calmodulin 1
Camk2a	Calcium/calmodulin dependent protein kinase
Capn	Calpain
Capns1	Calpain small subunit 1
Cartpt	Cocaine and amphetamine-regulated transcript prepropeptide
Casp3	Cysteine-aspartic acid protease
Cat	Chloramphenicol acetyltransferase
Cav3	Caveolin 3
Cbr2	Carbonyl reductase 2
Ccnd1	Cyclin D1
Cd36	Cluster of differentiation 36
Cdh1	Cadherin 1
Cdhr3	Cadherin related family member 3
Cdk	Cyclin-dependent kinase
Cenpa	Centromere protein A
Ces	Carboxylesterase
Cfl2	Cofilin 2
Chp1	Calcineurin like EF-hand protein 1
Chrm1	Cholinergic receptor muscarinic 1
Chrna	Cholinergic receptor nicotinic alpha
Chrnb4	Cholinergic receptor nicotinic beta
Chst11	Carbohydrate sulfotransferase 11
Cilp2	Cartilage intermediate layer protein 2
Ckm	Creatine kinase, muscle
Clic6	Chloride intracellular channel protein 6
Cntnap3	Contactin associated protein family member 3
Col11a1	Collagen type 11 alpha 1 chain
Colgalt2	Procollagen galactosyltransferase 2
Cox	Cytochrome c oxidase
Cox4i1	Cytochrome c oxidase subunit 4I1
Cox5a	Cytochrome C oxidase subunit 5A

Cox6a1	Cytochrome C oxidase subunit 6A1
Cox7a1	Cytochrome C oxidase subunit 7A1
Cpt1b	Carnitine palmitoyltransferase 1B
Cpt2	Carnitine palmitoyltransferase 2
Creb	Cyclic AMP-responsive element-binding protein
Creb	Cyclic AMP-responsive element-binding protein
Creb3l1	Cyclic AMP-responsive element-binding protein Like 1
Crls1	Cardiolipin synthase 1
Cs	Citrate synthase
Ctse	Cathepsin E
Cyb5b	Cytochrome b5 type B
Cyc1	Cytochrome C1
Cycs	Cytochrome C, Somatic
Cyp2f2	Cytochrome P450 2F1
Cyp2s1	Cytochrome P450 family 2 subfamily S member 1
Dapk1	Death-associated protein kinase 1
Daw1	Dynein assembly factor with WD repeats 1
Dbt	Dihydrolipoamide branched chain transacylase
Dbt	Dihydrolipoamide branched chain transacylase E2
Des	Desmin
Dgat1/2	Diacylglycerol acyltransferase-1/2
Dhcr7	7-dehydrocholesterol reductase
Dhodh	Dihydroorotate dehydrogenase
Dkk3	Dickkopf WNT signaling pathway inhibitor 3
Dld	Dihydrolipoamide dehydrogenase
Dlst	Dihydrolipoamide S-succinyltransferase
Dnah	Dynein axonemal heavy chain
Dnajc7	DnaJ heat shock protein family
Dot1l	Disruptor of telomeric silencing 1-like
Dsc2	Desmocollin 2
Dsg2	Desmoglein 2
Dsp	Desmoplakin
Dtna	Dystrobrevin alpha

Echdc3	Enoyl-CoA hydratase domain containing 3
Echs1	Enoyl-CoA hydratase, short chain 1
Eci1/2	Enoyl-CoA delta isomerase 1/2
Egf	Epidermal growth factor
Ehhadh	Enoyl-CoA hydratase and 3-hydroxyacyl CoA dehydrogenase
Eif	Eukaryotic initiation factors
Eif4ebp1	Eukaryotic translation initiation factor 4E-binding protein 1
Elovl6	Elongation of long-chain fatty acids family member 6
Enho	Energy homeostasis-associated
Eno	Enolase
Entpd4b	Ectonucleoside triphosphate diphosphohydrolase 4
Fabp4	Fatty acid-binding protein-4
Fasn	Fatty acid synthase
Fbp2	Fructose-bisphosphatase 2
Fbxo3	F-box protein 3
Fgfr3	Fibroblast growth factor receptor 3
Fh	Fumarate hydratase
Fhod3	Formin Homology 2 Domain Containing 3
Flnc	Filamin-C
Flt1/4	Fms related receptor tyrosine kinase 1/4
Fndc5	Fibronectin type III domain-containing protein 5
Foxa1	Forkhead box protein A1
Foxo	Forkhead box O
Fzd6	Frizzled class receptor 6
G6pd	Glucose-6-phosphate dehydrogenase
Gabarapl1	Gamma-aminobutyric acid receptor-associated protein-like 1
Gabpa	GA-binding protein alpha chain
Gadd45b	Growth arrest and DNA-damage-inducible, beta
Gal3st2	Galactose-3-O-Sulfotransferase 2
Gas6	Growth arrest – specific 6
Gata	GATA-binding factor 2
Gcdh	Glutaryl-CoA dehydrogenase
Git1	G-Protein-Coupled Receptor Kinase-Interacting Protein 1

Glrx2	Glutaredoxin 2
Gls	Glutaminase
Glud1	Glutamate dehydrogenase 1
Glul	Glutamate-ammonia ligase
Gm10790	NA
Gm32468	NA
Gm39929	NA
Gm42814	NA
Gm43500	NA
Gm44005	NA
Gm45412	NA
Gm9694	NA
Gna	Guanine nucleotide-binding protein subunit alpha
Gnai1	Guanine nucleotide binding protein, alpha inhibiting 1
Gnas	Guanine Nucleotide binding protein, Alpha Stimulating activity polypeptide
Gnb1	Guanine nucleotide-binding protein 1
Gng	Guanine nucleotide-binding protein subunit gamma
Got2	Glutamic-oxaloacetic transaminase 2
Gpam	Glycerol-3-phosphate acyltransferase, mitochondrial
Gpat4	Glycerol-3-phosphate acyltransferase 4
Gpd2	Glycerol-3-phosphate dehydrogenase
Gpi	Glucose phosphate isomerase
Gpx4	Glutathione peroxidase 4
Grb2	Growth-factor receptor-bound protein-2
Gsk3a	Glycogen synthase kinase-3 alpha
Gsta	Glutathione S-transferase A
Gstm	Glutathione S-transferase Mu
Gsto	Glutathione S-transferase omega
Gstt	Glutathione S-transferase theta
Gstt2/Gstt2b	Glutathione S-transferase theta 2B
Gstz1	Glutathione S-transferase Zeta 1
Gucy1a1	Guanylate cyclase 1 soluble subunit alpha 1
Gucy2d	Guanylate cyclase 2D

Gys	Glycogen synthase 1
Hacd2	3-Hydroxyacyl-CoA dehydratase 2
Hadha/B	Hydroxyacyl-CoA dehydrogenase trifunctional multienzyme complex subunit alpha/beta
Hand2	Heart- and neural crest derivatives-expressed protein 2
Hes1	Hairy and enhancer of split-1
Hibadh	3-hydroxyisobutyrate dehydrogenase
Hif1a	Hypoxia-inducible factor 1-alpha
Hltf	Helicase-like transcription factor
Hmgcl	3-hydroxy-3-methyl-glutaryl-coenzyme A lyase
Hmgcll1	3-Hydroxymethyl-3-Methylglutaryl-CoA Lyase Like 1
Hmgcs1	3-hydroxy-3-methylglutaryl-CoA synthase 1
Hopx	Homeodomain-only protein
Hoxc8	Homeobox protein Hox-C8
Hs6st2	Heparan sulfate 6-O-sulfotransferase 2
Hsd17b10	Hydroxysteroid 17-beta dehydrogenase 10
Hsd17b4	Hydroxysteroid 17-beta dehydrogenase 4
Hsd17b7	Hydroxysteroid 17-beta dehydrogenase 7
Hspb2	Heat shock protein family B
Hspb6	Heat shock protein beta-6
Hspd1	Heat Shock Protein Family D
Htra2	High-temperature requirement protein A2
Idh	Isocitrate dehydrogenase [NAD]
Idi1	Isopentenyl-diphosphate delta isomerase 1
Ifitm1	Interferon-induced transmembrane protein 1
Ifnar1	Interferon alpha and beta receptor subunit 1
Igf	Insulin-like growth factor
Irak4	Interleukin-1 receptor-associated kinase 4
Irs3	Insulin receptor substrate 3
Itgb	Integrin subunit beta
Itpr2	Inositol 1,4,5-trisphosphate receptor, type 2
Jak3	Janus kinase 3
Kcnt2	Potassium channel subfamily T, member 2

Klb	Klotho beta
Klf5	Krueppel-like factor 5
Kng1	Kininogen 1
Krt18	Keratin 18
Ktn1	Kinectin 1
L3hypdh	Trans-L-3-hydroxyproline dehydratase
Ldh	Lactate dehydrogenase
Lepr	Leptin receptor
Limk2	LIM domain kinase 2
Lipe	Lipase E
Lmo7	LIM domain only 7
Lmod2	Leiomodin 2
Lpcat2/3	Lysophosphatidylcholine acyltransferase 2/3
Lpin1	Lipin 1
Lpl	Lipoprotein lipase
Lrpprc	Leucine-rich PPR motif-containing protein
Lrrc10	Leucine-rich repeat containing protein 10
Lss	Lanosterol synthase
Map3k5	Mitogen-activated protein kinase kinase kinase 5
Mapk	Mitogen-activated protein kinase
Mb	Myoglobin
Mboat	Membrane bound O-ayltransferase domain containing
Mef2c	Myocyte enhancer factor 2C
Mfsd2a	Sodium-dependent lysophosphatidylcholine symporter 1
Mgst	Microsomal glutathione S-transferase
Mlxipl	MLX-interacting protein-like
Mlycd	Malonyl-CoA decarboxylase
Mmp	Matrix metalloproteinase
Mogat1	Monoacylglycerol O-acyltransferase 1
Mrap2	Melanocortin 2 receptor accessory protein 2
Mt-Atp6	Mitochondrially encoded ATP synthase membrane subunit 6
Mt-Nd	Mitochondrial encephalomyopathy
Mt-Nd	Mitochondrial encephalomyopathy

Mtor	Mammalian target of rapamycin
Muc5b	Mucin 5B
Mybpc3	Myosin Binding Protein C3
Myh	Myosin heavy chain
Myl	Myosin light chain
Myl	Myosin light chain
Mylk3	Myosin light chain kinase 3
Myo	Myosin X
Myocd	Myocardin
Myoz2	Myozenin 2
Nampt	Nicotinamide phosphoribosyltransferase
Nat8f3/4	N-acetyltransferase family 8 member 3/4
Nceh1	Neutral cholesterol ester hydrolase 1
Ncor2	Nuclear receptor co-repressor 2
Ndufa	NADH:ubiquinone oxidoreductase subunit A
Ndufb	NADH:ubiquinone oxidoreductase subunit B
Ndufs	NADH:ubiquinone oxidoreductase subunit S
Ndufv	NADH:ubiquinone Oxidoreductase Core Subunit V
Nexn	Nexilin F-actin binding protein
Ngfr	Nerve growth factor receptor
Nkx2.5	NK2 Homeobox 5
Notum	Notum, palmitoleoyl-protein carboxylesterase
Nppa/b	Natriuretic peptide A/B
Npr2	Natriuretic peptide receptor 2
Nqo1	NADPH quinone oxidoreductase
Nr0b2	Nuclear receptor subfamily 0, group B, member 2
Nr1h2	Nuclear receptor subfamily 1 group H member
Nr1i2	Nuclear receptor subfamily 1 group I member 2
Nrg1	Neuregulin 1
Nsdhl	NAD(P) dependent steroid dehydrogenase-like
Ogdh	Oxoglutarate dehydrogenase
Osgepl1	O-sialoglycoprotein endopeptidase like 1
Pak1	P21 (RAC1) activated kinase 1

Pam16	Presequence translocase associated motor 16
Parp1	Poly (ADP-ribose) polymerase 1
Parva	Parvin alpha
Parvb	Parvin beta
Pck1	Phosphoenolpyruvate carboxykinase 1
Pcsk1	Proprotein convertase subtilisin/kexin type 1
Pde1c	Phosphodiesterase 1c
Pde2a	phosphodiesterase 2A
Pde3b	Phosphodiesterase 3B
Pdha1	Pyruvate dehydrogenase E1 subunit alpha 1
Perm1	PPARGC1 and ESRR induced regulator, muscle 1
Pfkfb	6-Phosphofructo-2-Kinase/Fructose-2,6-Biphosphatase
Pfkl	Phosphofructokinase, liver type
Pfkm	Phosphofructokinase, Muscle
Pfkp	Phosphofructokinase, platelet
Pgam	Phosphoglycerate mutase
Pgam1	Phosphoglycerate mutase 1
Pgf	Placental growth factor
Pgk	phosphoglycerate kinase
Phospho	Phosphoethanolamine/Phosphocholine Phosphatase
Pik3c2b	Phosphatidylinositol-4-Phosphate 3-Kinase Catalytic Subunit Type 2 Beta
Pik3c2b	Phosphatidylinositol-4-phosphate 3-kinase C2 domain-containing beta polypeptide
Pik3r2/3	Phosphoinositide-3-kinase regulatory subunit 2/3
Pik3r2/3	Phosphoinositide-3-kinase regulatory subunit 2/3
Pkm	Pyruvate kinase M1/2
Pla2g5	Phospholipase A2 Group V
Plcb4	phospholipase C beta 4
Plch1/2	Phospholipase C eta 1/2
Plcl1	Inactive phospholipase C-like protein 1
Plekha6	Pleckstrin homology domain-containing family A member 6
Plin	Perilipin
Pln	Phospholamban

Plpp	Phospholipid phosphatase
Pmvk	Phosphomevalonate kinase
Pnpla2	Patatin like phospholipase domain containing 2
Polr1	RNA polymerase I
Pon2/3	Paraoxonase 2/3
Porcn	Porcupine O-acyltransferase
Ppara	Peroxisome proliferator-activated receptor alpha
Pparg	Peroxisome proliferator- activated receptor gamma
Ppat	Phosphoribosyl pyrophosphate amidotransferase
Ppif	Peptidylprolyl Isomerase F
Ppm1	Protein phosphatase 1
Ppp1ca	Protein phosphatase 1 catalytic subunit alpha
Ppp1r12b	Protein phosphatase 1 regulatory subunit 12B
Ppp1r14	Protein phosphatase 1 regulatory inhibitor subunit 14
Ppp1r3g	Protein phosphatase 1 regulatory subunit 3G
Ppp2r	Protein phosphatase 2 regulatory subunit
Prdx3	Peroxiredoxin3
Prka	Protein kinase AMP-activated catalytic subunit alpha
Prkca	Protein kinase C alpha
Prkcz	Protein kinase C, zeta
Prkd1	Protein kinase D1
Prkg1	Protein kinase CGMP-dependent 1
Prox1	Prospero-related homeobox 1
Ptgfr	Prostaglandin F receptor
Ptgs2	Prostaglandin-endoperoxide synthase 2
Ptpa	Protein phosphatase 2 phosphatase activator
Ptpn3	Protein tyrosine phosphatase non-receptor type 3
Pxn	Paxillin
Pygl	Glycogen phosphorylase L
Rab	Ras-related protein Rab-27A
Rac3	Ras-related C3 botulinum toxin substrate 3
Rala	RAS like proto-oncogene A
Rarg	Retinoic acid receptor gamma

Rb1	Retinoblastoma
Rbfox2	RNA binding motif protein 9
Rbl2	RB transcriptional corepressor like 2
Rdh16	Retinol dehydrogenase 16.
Reck	Reversion-inducing-cysteine-rich protein with kazal motifs
Rho	Rhodopsin
Rhobtb1/2	Rho-related BTB domain-containing protein 1/2
Rhot	Mitochondrial Rho GTPase
Rilp	Rab interacting lysosomal protein
Rock2	Rho associated coiled-coil containing protein kinase 2
Rps6kb1	Ribosomal protein S6 kinase beta-1
Runx1t1	Runt-related transcription factor 1
Rxrb	Retinoid X receptor beta
Ryr2	Ryanodine receptor 2
S100g	S100 Calcium Binding Protein G
Scd4	Stearoyl-coenzyme A desaturase 4
Scn5a	Sodium voltage-gated channel alpha subunit 5
Scnn1a	Sodium channel epithelial 1 subunit alpha
Scp2	Sterol carrier protein 2
Sdh	Succinate dehydrogenase complex flavoprotein
Sds	Serine dehydratase
Sec14l3	SEC14-like protein 3
Sgca	Sarcoglycan Alpha
Sgcg	Gamma-sarcoglycan
Sgk2	Serine/threonine-protein kinase
Sim2	Single-minded homolog 2
Sirt3	Sirtuin 3
Slc16a1	Solute carrier family 16 member 1
Slc18a3	Solute carrier family 18 member A3
Slc25	Solute carrier family 25
Slc27	Solute carrier family 27
Slc2a1	Solute carrier family 2 member 1
Slc7a1	Solute carrier family 7

Smad7	SMA- and MAD-related protein 7
Smarc	Matrix associated, actin dependent regulators of chromatin
Smarcc2	Matrix associated, actin dependent regulator of chromatin subfamily c member 2.
Smox	Spermine oxidase
Smyd1	Histone-lysine N-methyltransferase
Sod2	Superoxide dismutase 2
Speg	Striated muscle preferentially expressed protein kinase
Stc2	Stanniocalcin 2
Stim1	Stromal interaction molecule 1
Sucla2	Succinate-CoA ligase ADP-forming subunit beta
Suclg1	Succinate-CoA ligase GDP/ADP-forming subunit alpha
Sult1	Sulfotransferase family 1
Sult4a1	Sulfotransferase Family 4A
Surf1	Surfeit locus protein 1
Tbc1d1	Tre-2/USP6, BUB2, cdc16 domain family, member 1
Tbx5	T-box protein 5
Tcap	Titin-cap
Tesk1	Testis-specific protein kinase 1
Tfam	Transcription factor A, mitochondrial
Thbs2	Thrombospondin-2
Themis	thymocyte-expressed-molecule
Timm	Translocase of inner mitochondrial membrane
Tlr3	Toll like receptor 3
Tnfrsf	Tumor necrosis factor receptor superfamily
Tnnt2	Troponin T2, cardiac type
Tomm	Translocase of outer mitochondrial membrane
Tp53bp1	Tumor protein P53 binding protein 1
Trim63/54	Tripartite motif 63/54
Tspo	Translocator protein
Tuba	Tubulin alpha
Txn2	Thioredoxin 2
Txnrd2	Thioredoxin reductase 2

Tyro3	Tyrosine-protein kinase receptor
Ucp-2	Uncoupling protein 2
Ugt	UDP-glucuronosyltransferases
Uqcr	Ubiquinol-cytochrome C reductase
Vdac1	Voltage-dependent anion channels 1
Vdr	Vitamin D receptor
Vegfa	Vascular endothelial growth factor
Vgf	VGF nerve growth factor inducible
Wfdc2	whey acidic protein four-disulfide core domain protein 2
Wnt4	Wnt family member 4
Xirp1	Xin actin-binding repeat-containing protein 1
Xrcc	X-ray repair cross-complementing
Yap1	Yes-associated protein 1
Zdhhc7	Zinc finger DHHC-type palmitoyltransferase 7

Abbreviations: NA, not available/applicable.

References

Abdu, S. B. and Al-Bogami, F. M. 2019. Influence of resveratrol on liver fibrosis induced by dimethylnitrosamine in male rats. *Saudi Journal of Biological Sciences* 26(1), pp. 201-209.

Aday, A. and Ridker, P. 2019. targeting residual inflammatory risk: a shifting paradigm for atherosclerotic disease. Frontiers in cardiovascular medicine. 2019. 6: 16.

Adler, B. J., Green, D. E., Pagnotti, G. M., Chan, M. E. and Rubin, C. T. 2014. High fat diet rapidly suppresses B lymphopoiesis by disrupting the supportive capacity of the bone marrow niche. *PloS One* 9(3), p. e90639.

Agarwal, B. et al. 2013. Resveratrol for primary prevention of atherosclerosis: clinical trial evidence for improved gene expression in vascular endothelium. *International Journal of Cardiology* 166(1), pp. 246-248.

Aguilar, E. et al. 2014. Butyrate impairs atherogenesis by reducing plaque inflammation and vulnerability and decreasing NFκB activation. *Nutrition, Metabolism and Cardiovascular Diseases* 24(6), pp. 606-613.

Ahn, J., Cho, I., Kim, S., Kwon, D. and Ha, T. 2008. Dietary resveratrol alters lipid metabolism-related gene expression of mice on an atherogenic diet. *Journal of Hepatology* 49(6), pp. 1019-1028.

Ait-Oufella, H., Taleb, S., Mallat, Z. and Tedgui, A. 2011. Recent advances on the role of cytokines in atherosclerosis. *Arteriosclerosis, Thrombosis, and Vascular Biology* 31(5), pp. 969-979.

Akbari, M. et al. 2020. The effects of resveratrol on lipid profiles and liver enzymes in patients with metabolic syndrome and related disorders: a systematic review and meta-analysis of randomized controlled trials. *Lipids in Health and Disease* 19(1), pp. 1-12.

Akhtar, S. et al. 2015. Endothelial hypoxia-inducible factor-1α promotes atherosclerosis and monocyte recruitment by upregulating microRNA-19a. *Hypertension* 66(6), pp. 1220-1226.

Akil, L. and Ahmad, H. A. 2011. Relationships between obesity and cardiovascular diseases in four southern states and Colorado. *Journal of Health Care for The Poor and Underserved* 22(4 Suppl), p. 61.

Al-Mashhadi, R. H. et al. 2021. Local pressure drives low-density lipoprotein accumulation and coronary atherosclerosis in hypertensive minipigs. *Journal of the American College of Cardiology* 77(5), pp. 575-589.

Al-rashida, M. and Iqbal, J. 2014. Therapeutic potentials of ecto-nucleoside triphosphate diphosphohydrolase, ecto-nucleotide pyrophosphatase/phosphodiesterase, ecto-5'-nucleotidase, and alkaline phosphatase inhibitors. *Medicinal Research Reviews* 34(4), pp. 703-743.

Alberdi, G., Rodríguez, V. M., Macarulla, M. T., Miranda, J., Churruca, I. and Portillo, M. P. 2013. Hepatic lipid metabolic pathways modified by resveratrol in rats fed an obesogenic diet. *Nutrition* 29(3), pp. 562-567.

Alciaturi, J., Anesetti, G., Irigoin, F., Skowronek, F. and Sapiro, R. 2019. Distribution of sperm antigen 6 (SPAG6) and 16 (SPAG16) in mouse ciliated and non-ciliated tissues. *Journal of Molecular Histology* 50, pp. 189-202.

Allen, A. M. and Graham, A. 2012. Mitochondrial function is involved in regulation of cholesterol efflux to apolipoprotein (apo) AI from murine RAW 264.7 macrophages. *Lipids in Health and Disease* 11(1), pp. 1-8.

Allport, S. A., Kikah, N., Abu Saif, N., Ekokobe, F. and Atem, F. D. 2016. Parental age of onset of cardiovascular disease as a predictor for offspring age of onset of cardiovascular disease. *PloS One* 11(12), p. e0163334.

Altaany, Z., Moccia, F., Munaron, L., Mancardi, D. and Wang, R. 2014. Hydrogen sulfide and endothelial dysfunction: relationship with nitric oxide. *Current Medicinal Chemistry* 21(32), pp. 3646-3661.

Andrés-Manzano, M. J., Andrés, V. and Dorado, B. 2015. Oil red O and hematoxylin and eosin staining for quantification of atherosclerosis burden in mouse aorta and aortic root.*Methods in mouse atherosclerosis*. Springer, pp. 85-99.

Anzinger, J. J., Chang, J., Xu, Q., Barthwal, M. K., Bohnacker, T., Wymann, M. P. and Kruth, H. S. 2012. Murine bone marrow-derived macrophages differentiated with GM-CSF become foam cells by PI3Kγ-dependent fluid-phase pinocytosis of native LDL [S]. *Journal of Lipid Research* 53(1), pp. 34-42.

Anzinger, J. J. et al. 2010. Native low-density lipoprotein uptake by macrophage colony-stimulating factor–differentiated human macrophages is mediated by macropinocytosis and micropinocytosis. *Arteriosclerosis, Thrombosis, and Vascular Biology* 30(10), pp. 2022-2031.

Arguello, G., Balboa, E., Arrese, M. and Zanlungo, S. 2015. Recent insights on the role of cholesterol in non-alcoholic fatty liver disease. *Biochimica et Biophysica Acta (BBA)-Molecular Basis of Disease* 1852(9), pp. 1765-1778.

Armstrong, A. W., Voyles, S. V., Armstrong, E. J., Fuller, E. N. and Rutledge, J. C. 2011. Angiogenesis and oxidative stress: common mechanisms linking psoriasis with atherosclerosis. *Journal of Dermatological Science* 63(1), pp. 1-9.

Ates, A. H. et al. 2011. Total white blood cell count is associated with the presence, severity and extent of coronary atherosclerosis detected by dual-source multislice computed tomographic coronary angiography. *Cardiology Journal* 18(4), pp. 371-377.

Auwerx, J. 1991. The human leukemia cell line, THP-1: a multifacetted model for the study of monocyte-macrophage differentiation. *Experientia* 47(1), pp. 22-31.

Avellone, G., Di Garbo, V., Campisi, D., De Simone, R., Raneli, G., Scaglione, R. and Licata, G. 2006. Effects of moderate Sicilian red wine consumption on inflammatory biomarkers of atherosclerosis. *European Journal of Clinical Nutrition* 60(1), pp. 41-47.

Averill, L., Meagher, R. and Gerrity, R. 1989. Enhanced monocyte progenitor cell proliferation in bone marrow of hyperlipemic swine. *The American Journal of Pathology* 135(2), p. 369.

Averna, M. et al. 2017. Familial hypercholesterolemia: the Italian atherosclerosis society network (LIPIGEN). *Atherosclerosis Supplements* 29, pp. 11-16.

Babaev, V. R., Patel, M. B., Semenkovich, C. F., Fazio, S. and Linton, M. F. 2000. Macrophage lipoprotein lipase promotes foam cell formation and atherosclerosis in low density lipoprotein receptor-deficient mice. *Journal of Biological Chemistry* 275(34), pp. 26293-26299.

Bäck, M., Yurdagul, A., Tabas, I., Öörni, K. and Kovanen, P. T. 2019. Inflammation and its resolution in atherosclerosis: mediators and therapeutic opportunities. *Nature Reviews Cardiology* 16(7), pp. 389-406.

Badimon, L. and Vilahur, G. 2014. Thrombosis formation on atherosclerotic lesions and plaque rupture. *Journal of Internal Medicine* 276(6), pp. 618-632.

Bae, Y. S., Lee, J. H., Choi, S. H., Kim, S., Almazan, F., Witztum, J. L. and Miller, Y. I. 2009. Macrophages generate reactive oxygen species in response to minimally oxidized low-density lipoprotein: Toll-like receptor 4–and spleen tyrosine kinase–dependent activation of NADPH oxidase 2. *Circulation research* 104(2), pp. 210-218.

Bai, L. et al. 2017. Mediator 1 is atherosclerosis protective by regulating macrophage polarization. *Arteriosclerosis, Thrombosis, and Vascular Biology* 37(8), pp. 1470-1481.

Baidya, S. and Zeng, Q. 2005. Helper T cells and atherosclerosis: the cytokine web. *Postgraduate Medical Journal* 81(962), pp. 746-752.

Baigent, C. et al. 2005. Efficacy and safety of cholesterol-lowering treatment: prospective meta-analysis of data from 90,056 participants in 14 randomised trials of statins. *Lancet* 336, pp. 1267-1278.

Ballinger, S. W. et al. 2002. Mitochondrial integrity and function in atherogenesis. *Circulation* 106(5), pp. 544-549.

Balta, S. 2022. Atherosclerosis and Non-Alcoholic Fatty Liver Disease. *Angiology*, p. 00033197221091317.

Baron, C. S. et al. 2018. Single-cell transcriptomics reveal the dynamic of haematopoietic stem cell production in the aorta. *Nature Communications* 9(1), pp. 1-15.

Barthwal, M. K., Anzinger, J. J., Xu, Q., Bohnacker, T., Wymann, M. P. and Kruth, H. S. 2013. Fluid-phase pinocytosis of native low density lipoprotein promotes murine M-CSF differentiated macrophage foam cell formation. *PloS One* 8(3), p. e58054.

Bartlett, B., Ludewick, H. P., Misra, A., Lee, S. and Dwivedi, G. 2019. Macrophages and T cells in atherosclerosis: a translational perspective. *American Journal of Physiology-Heart and Circulatory Physiology* 317(2), pp. H375-H386.

Basatemur, G. L., Jørgensen, H. F., Clarke, M. C., Bennett, M. R. and Mallat, Z. 2019. Vascular smooth muscle cells in atherosclerosis. *Nature Reviews Cardiology* 16(12), pp. 727-744.

Bastin, J. and Djouadi, F. 2016. Resveratrol and myopathy. *Nutrients* 8(5), p. 254.

Baur, J. A. et al. 2006. Resveratrol improves health and survival of mice on a high-calorie diet. *Nature* 444(7117), pp. 337-342.

Bennett, M. R., Sinha, S. and Owens, G. K. 2016. Vascular smooth muscle cells in atherosclerosis. *Circulation research* 118(4), pp. 692-702.

Benowitz, N. L. and Burbank, A. D. 2016. Cardiovascular toxicity of nicotine: implications for electronic cigarette use. *Trends in Cardiovascular Medicine* 26(6), pp. 515-523.

Bentzon, J. F., Otsuka, F., Virmani, R. and Falk, E. 2014. Mechanisms of plaque formation and rupture. *Circulation research* 114(12), pp. 1852-1866.

Berbée, J. F. et al. 2013. Resveratrol protects against atherosclerosis, but does not add to the antiatherogenic effect of atorvastatin, in APOE* 3-Leiden. CETP mice. *The Journal of Nutritional Biochemistry* 24(8), pp. 1423-1430.

Bergheanu, S., Bodde, M. and Jukema, J. 2017. Pathophysiology and treatment of atherosclerosis. *Netherlands Heart Journal* 25(4), pp. 231-242.

Berman, A. Y., Motechin, R. A., Wiesenfeld, M. Y. and Holz, M. K. 2017. The therapeutic potential of resveratrol: a review of clinical trials. *NPJ Precision Oncology* 1(1), pp. 1-9.

Berrougui, H., Grenier, G., Loued, S., Drouin, G. and Khalil, A. 2009. A new insight into resveratrol as an atheroprotective compound: inhibition of lipid peroxidation and enhancement of cholesterol efflux. *Atherosclerosis* 207(2), pp. 420-427.

Bertelli, A. et al. 1999. Resveratrol, a natural stilbene in grapes and wine, enhances intraphagocytosis in human promonocytes: a co-factor in antiinflammatory and anticancer chemopreventive activity. *International Journal of Tissue Reactions* 21(4), pp. 93-104.

Bhatt, D. L. et al. 2019. Cardiovascular risk reduction with icosapent ethyl for hypertriglyceridemia. *New England Journal of Medicine* 380(1), pp. 11-22.

Bhattacharjee, J., Kirby, M., Softic, S., Miles, L., Salazar-Gonzalez, R. M., Shivakumar, P. and Kohli, R. 2017. Hepatic natural killer T-cell and CD8+ T-cell signatures in mice with nonalcoholic steatohepatitis. *Hepatology Communications* 1(4), pp. 299-310.

Bie, J. et al. 2013. Liver-specific cholesteryl ester hydrolase deficiency attenuates sterol elimination in the feces and increases atherosclerosis in ldlr−/− mice. *Arteriosclerosis, Thrombosis, and Vascular Biology* 33(8), pp. 1795-1802.

Biesinger, S., Michaels, H., Quadros, A., Qian, Y., Rabovsky, A., Badger, R. and Jalili, T. 2016. A combination of isolated phytochemicals and botanical extracts lowers diastolic blood pressure in a randomized controlled trial of hypertensive subjects. *European Journal of Clinical Nutrition* 70(1), pp. 10-16.

Binder, C. J., Papac-Milicevic, N. and Witztum, J. L. 2016. Innate sensing of oxidation-specific epitopes in health and disease. *Nature Reviews Immunology* 16(8), pp. 485-497.

Björkegren, J. L. and Lusis, A. J. 2022. Atherosclerosis: Recent developments. *Cell* 185(10), pp. 1630-1645.

Blanc, J. et al. 2003. Protective role of uncoupling protein 2 in atherosclerosis. *Circulation* 107(3), pp. 388-390.

Bobryshev, Y. V., Ivanova, E. A., Chistiakov, D. A., Nikiforov, N. G. and Orekhov, A. N. 2016. Macrophages and their role in atherosclerosis: pathophysiology and transcriptome analysis. *BioMed research international* 2016,

Böhmdorfer, M. et al. 2017. Involvement of UDP-glucuronosyltransferases and sulfotransferases in the excretion and tissue distribution of resveratrol in mice. *Nutrients* 9(12), p. 1347.

Bonomini, F., Favero, G. and Rezzani, R. 2015. NF-κB—A Key Factor in Atherogenesis and Atheroprogression.*Thrombosis, Atherosclerosis and Atherothrombosis-New Insights and Experimental Protocols*. IntechOpen.

Boocock, D. J. et al. 2007. Phase I dose escalation pharmacokinetic study in healthy volunteers of resveratrol, a potential cancer chemopreventive agent. *Cancer Epidemiology Biomarkers & Prevention* 16(6), pp. 1246-1252.

Boring, L., Gosling, J., Cleary, M. and Charo, I. F. 1998. Decreased lesion formation in CCR2−/− mice reveals a role for chemokines in the initiation of atherosclerosis. *Nature* 394(6696), pp. 894-897.

Boscolo, P. et al. 2003. Effects of resveratrol on lymphocyte proliferation and cytokine release. *Annals of Clinical & Laboratory Science* 33(2), pp. 226-231.

Bose, A., Teh, M.-T., Mackenzie, I. C. and Waseem, A. 2013. Keratin k15 as a biomarker of epidermal stem cells. *International Journal of Molecular Sciences* 14(10), pp. 19385-19398.

Boucher, P., Matz, R. L. and Terrand, J. 2020. atherosclerosis: gone with the Wnt? *Atherosclerosis* 301, pp. 15-22.

Bovi, A. P. D., Marciano, F., Mandato, C., Siano, M. A., Savoia, M. and Vajro, P. 2021. Oxidative stress in non-alcoholic fatty liver disease. An updated mini review. *Frontiers in Medicine* 8, p. 595371.

Brandts, J. and Ray, K. K. 2020. Bempedoic acid, an inhibitor of ATP citrate lyase for the treatment of hypercholesterolemia: early indications and potential. *Expert Opinion on Investigational Drugs* 29(8), pp. 763-770.

British Heart Foundation. 2022. *BHF Statistics Factsheet - UK* Available at: https://www.bhf.org.uk/what-we-do/our-research/heart-statistics [Accessed: April 2022].

Brown, A. et al. 2012. Genetic variants affecting the neural processing of human facial expressions: evidence using a genome-wide functional imaging approach. *Translational psychiatry* 2(7), pp. e143-e143.

Brown, K. S. et al. 2010. Effect of the bile acid sequestrant colesevelam on the pharmacokinetics of pioglitazone, repaglinide, estrogen estradiol, norethindrone, levothyroxine, and glyburide. *The Journal of Clinical Pharmacology* 50(5), pp. 554-565.

Bruder-Nascimento, T., Ekeledo, O. J., Anderson, R., Le, H. B. and Belin de Chantemèle, E. J. 2017. Long term high fat diet treatment: an appropriate approach to study the sex-specificity of the autonomic and cardiovascular responses to obesity in mice. *Frontiers in Physiology* 8, p. 32.

Buchanan, J. et al. 2005. Reduced cardiac efficiency and altered substrate metabolism precedes the onset of hyperglycemia and contractile dysfunction in two mouse models of insulin resistance and obesity. *Endocrinology* 146(12), pp. 5341-5349.

Buckley, M. L. and Ramji, D. P. 2015. The influence of dysfunctional signaling and lipid homeostasis in mediating the inflammatory responses during atherosclerosis. *Biochimica et Biophysica Acta (BBA)-Molecular Basis of Disease* 1852(7), pp. 1498-1510.

Budoff, M. J. et al. 2020. Effect of icosapent ethyl on progression of coronary atherosclerosis in patients with elevated triglycerides on statin therapy: final results of the EVAPORATE trial. *European Heart Journal* 41(40), pp. 3925-3932.

Buemann, B. and Uvnäs-Moberg, K. 2020. Oxytocin may have a therapeutical potential against cardiovascular disease. Possible pharmaceutical and behavioral approaches. *Medical Hypotheses* 138, p. 109597.

Buettner, R., Schölmerich, J. and Bollheimer, L. C. 2007. High-fat diets: modeling the metabolic disorders of human obesity in rodents. *Obesity* 15(4), pp. 798-808.

Bujanda, L. et al. 2008. Resveratrol inhibits nonalcoholic fatty liver disease in rats. *BMC Gastroenterology* 8(1), pp. 1-8.

Bullenkamp, J., Dinkla, S., Kaski, J. C. and Dumitriu, I. E. 2016. Targeting T cells to treat atherosclerosis: odyssey from bench to bedside. *European Heart Journal-Cardiovascular Pharmacotherapy* 2(3), pp. 194-199.

Buono, C., Come, C. E., Stavrakis, G., Maguire, G. F., Connelly, P. W. and Lichtman, A. H. 2003. Influence of interferon-γ on the extent and phenotype of diet-induced atherosclerosis in the LDLR-deficient mouse. *Arteriosclerosis, Thrombosis, and Vascular Biology* 23(3), pp. 454-460.

Burnett, M. S., Gaydos, C. A., Madico, G. E., Glad, S. M., Paigen, B., Quinn, T. C. and Epstein, S. E. 2001. Atherosclerosis in apoE knockout mice infected with multiple pathogens. *The Journal of Infectious Diseases* 183(2), pp. 226-231.

Burtenshaw, D., Kitching, M., Redmond, E. M., Megson, I. L. and Cahill, P. A. 2019. Reactive oxygen species (ROS), intimal thickening, and subclinical atherosclerotic disease. *Frontiers in Cardiovascular Medicine* 6, p. 89.

Buttari, B. et al. 2014. Resveratrol counteracts inflammation in human M1 and M2 macrophages upon challenge with 7-oxo-cholesterol: potential therapeutic implications in atherosclerosis. *Oxidative Medicine and Cellular Longevity* 2014,

Cachofeiro, V., Miana, M., Martín-Fernandez, B., Ballesteros, S., Balfagon, G. and Lahera, V. 2009. Inflammation: a link between hypertension and atherosclerosis. *Current Hypertension Reviews* 5(1), pp. 40-48.

Cai, T. et al. 2021. Associations between statins and adverse events in primary prevention of cardiovascular disease: systematic review with pairwise, network, and dose-response meta-analyses. *BMJ* 374,

Calvo, D., Gómez-Coronado, D., Suárez, Y., Lasunción, M. A. and Vega, M. A. 1998. Human CD36 is a high affinity receptor for the native lipoproteins HDL, LDL, and VLDL. *Journal of Lipid Research* 39(4), pp. 777-788.

Camaré, C., Pucelle, M., Nègre-Salvayre, A. and Salvayre, R. 2017. Angiogenesis in the atherosclerotic plaque. *Redox Biology* 12, pp. 18-34.

Cannon, C. P. et al. 2015. Ezetimibe added to statin therapy after acute coronary syndromes. *New England Journal of Medicine* 372(25), pp. 2387-2397.

Cao, X., Liao, W., Xia, H., Wang, S. and Sun, G. 2022. The Effect of Resveratrol on Blood Lipid Profile: A Dose-Response Meta-Analysis of Randomized Controlled Trials. *Nutrients* 14(18), p. 3755.

Cardilo-Reis, L. et al. 2012. Interleukin-13 protects from atherosclerosis and modulates plaque composition by skewing the macrophage phenotype. *EMBO Molecular Medicine* 4(10), pp. 1072-1086.

Carpino, G. et al. 2016. Macrophage activation in pediatric nonalcoholic fatty liver disease (NAFLD) correlates with hepatic progenitor cell response via Wnt3a pathway. *PloS One* 11(6), p. e0157246.

Catalán, Ú., de las Hazas, M.-C. L., Piñol, C., Rubió, L., Motilva, M.-J., Fernandez-Castillejo, S. and Solà, R. 2018. Hydroxytyrosol and its main plasma circulating metabolites attenuate the initial steps of atherosclerosis through inhibition of the MAPK pathway. *Journal of Functional Foods* 40, pp. 280-291.

Catalgol, B., Batirel, S., Taga, Y. and Ozer, N. K. 2012. Resveratrol: French paradox revisited. *Front Pharmacol* 3, p. 141. doi: 10.3389/fphar.2012.00141

Čejková, S., Králová-Lesná, I. and Poledne, R. 2016. Monocyte adhesion to the endothelium is an initial stage of atherosclerosis development. *Cor et Vasa* 58(4), pp. e419-e425.

Chan, J. K. 2014. The wonderful colors of the hematoxylin–eosin stain in diagnostic surgical pathology. *International Journal of Surgical Pathology* 22(1), pp. 12-32.

Chan, M. E., Adler, B. J., Green, D. E. and Rubin, C. T. 2012. Bone structure and B-cell populations, crippled by obesity, are partially rescued by brief daily exposure to low-magnitude mechanical signals. *The FASEB Journal* 26(12), pp. 4855-4863.

Chan, Y. 2021. *Anti-atherogenic actions of (+)-catechin.* Cardiff University.

Chan, Y.-H., Alahmadi, A., Alotibi, R. and Ramji, D. P. 2022a. Evaluation of Plaque Burden and Lipid Content in Atherosclerotic Plaques.*Atherosclerosis*. Springer, pp. 481-496.

Chan, Y.-H., Alotibi, R., Alahmadi, A. and Ramji, D. P. 2022b. Monitoring cellularity and expression of key markers in atherosclerotic plaques.*Atherosclerosis*. Springer, pp. 497-506.

Chan, Y.-H. and Ramji, D. P. 2022. Atherosclerosis: pathogenesis and key cellular processes, current and emerging therapies, key challenges, and future research directions.*Atherosclerosis*. Springer, pp. 3-19.

Chang, C.-C., Lin, K.-Y., Peng, K.-Y., Day, Y.-J. and Hung, L.-M. 2016. Resveratrol exerts anti-obesity effects in high-fat diet obese mice and displays differential dosage effects on cytotoxicity, differentiation, and lipolysis in 3T3-L1 cells. *Endocrine Journal*, pp. EJ15-0545.

Chang, C.-Y., Lee, T.-H. and Sheu, W. H. 2012. Anti-atherogenic effects of resveratrol via liver X receptor α-dependent upregulation of ATP-binding cassette transporters A1 and G1 in macrophages. *Journal of Functional Foods* 4(4), pp. 727-735.

Chang, G.-R., Chen, P.-L., Hou, P.-H. and Mao, F. C. 2015a. Resveratrol protects against diet-induced atherosclerosis by reducing low-density lipoprotein cholesterol and inhibiting inflammation in apolipoprotein E-deficient mice. *Iranian Journal of Basic Medical Sciences* 18(11), p. 1063.

Chang, Y. P. et al. 2015b. Resveratrol inhibits NLRP3 inflammasome activation by preserving mitochondrial integrity and augmenting autophagy. *Journal of Cellular Physiology* 230(7), pp. 1567-1579.

Chao, S.-C. et al. 2017. Induction of sirtuin-1 signaling by resveratrol induces human chondrosarcoma cell apoptosis and exhibits antitumor activity. *Scientific Reports* 7(1), pp. 1-11.

Chassot, L. N., Scolaro, B., Roschel, G. G., Cogliati, B., Cavalcanti, M. F., Abdalla, D. S. and Castro, I. A. 2018. Comparison between red wine and isolated trans-resveratrol on the prevention and regression of atherosclerosis in LDLr (−/−) mice. *The Journal of Nutritional Biochemistry* 61, pp. 48-55.

Checkouri, E., Blanchard, V. and Meilhac, O. 2021. Macrophages in atherosclerosis, first or second row players? *Biomedicines* 9(9), p. 1214.

Chellan, B., Reardon, C. A., Getz, G. S. and Hofmann Bowman, M. A. 2016. Enzymatically modified low-density lipoprotein promotes foam cell formation in smooth muscle cells via macropinocytosis and enhances receptor-mediated uptake of oxidized low-density lipoprotein. *Arteriosclerosis, Thrombosis, and Vascular Biology* 36(6), pp. 1101-1113.

Chen, H., Howatt, D. A., Franklin, M. K., Amioka, N., Sawada, H., Daugherty, A. and Lu, H. S. 2022. A mini-review on quantification of atherosclerosis in hypercholesterolemic mice. *Global Translational Medicine* 1(1),

Chen, J. et al. 2014. Berberine derivatives reduce atherosclerotic plaque size and vulnerability in apoE−/− mice. *Journal of Translational Medicine* 12(1), pp. 1-13.

Chen, Q., Wang, E., Ma, L. and Zhai, P. 2012. Dietary resveratrol increases the expression of hepatic 7α-hydroxylase and ameliorates hypercholesterolemia in high-fat fed C57BL/6J mice. *Lipids in Health and Disease* 11(1), pp. 1-8.

Chen, Q.-J. et al. 2016a. Appropriate LDL-C-to-HDL-C ratio cutoffs for categorization of cardiovascular disease risk factors among Uygur adults in Xinjiang, China. *International Journal of Environmental Research and Public Health* 13(2), p. 235.

Chen, S., Crother, T. R. and Arditi, M. 2010. Emerging role of IL-17 in atherosclerosis. *Journal of Innate Immunity* 2(4), pp. 325-333.

Chen, S. et al. 2020a. Sex-specific effects of the Nlrp3 inflammasome on atherogenesis in LDL receptor-deficient mice. *Basic to Translational Science* 5(6), pp. 582-598.

Chen, W. M. et al. 2016b. Hepatoprotective effect of resveratrol against ethanol-induced oxidative stress through induction of superoxide dismutase in vivo and in vitro. *Experimental and Therapeutic Medicine* 11(4), pp. 1231-1238.

Chen, Z., Tian, R., She, Z., Cai, J. and Li, H. 2020b. Role of oxidative stress in the pathogenesis of nonalcoholic fatty liver disease. *Free Radical Biology and Medicine* 152, pp. 116-141.

Cheng, C.-I., Tai, M.-H., Chang, H.-R., Chou, M.-H., Chen, G.-T., Chen, P.-H. and Kao, Y.-H. 2021. Oxidized low-density lipoprotein induced hepatoma-derived growth factor upregulation mediates foam cell formation of cultured rat aortic vascular smooth muscle cells. *European Journal of Cell Biology* 100(5-6), p. 151169.

Cheng, C. K., Luo, J. Y., Lau, C. W., Chen, Z. Y., Tian, X. Y. and Huang, Y. 2020a. Pharmacological basis and new insights of resveratrol action in the cardiovascular system. *British Journal of Pharmacology* 177(6), pp. 1258-1277.

Cheng, H., Zheng, Z. and Cheng, T. 2020b. New paradigms on hematopoietic stem cell differentiation. *Protein & Cell* 11(1), pp. 34-44.

Cheng, P. W. et al. 2014. Resveratrol decreases fructose-induced oxidative stress, mediated by NADPH oxidase via an AMPK-dependent mechanism. *British Journal of Pharmacology* 171(11), pp. 2739-2750.

Chien, C.-T. et al. 2004. Ascorbate supplement reduces oxidative stress in dyslipidemic patients undergoing apheresis. *Arteriosclerosis, Thrombosis, and Vascular Biology* 24(6), pp. 1111-1117.

Chimento, A. et al. 2019. Progress to improve oral bioavailability and beneficial effects of resveratrol. *International Journal of Molecular Sciences* 20(6), p. 1381.

Chinetti-Gbaguidi, G., Colin, S. and Staels, B. 2015. Macrophage subsets in atherosclerosis. *Nature Reviews Cardiology* 12(1), pp. 10-17.

Chistiakov, D. A., Bobryshev, Y. V. and Orekhov, A. N. 2016. Macrophage-mediated cholesterol handling in atherosclerosis. *Journal of Cellular and Molecular Medicine* 20(1), pp. 17-28.

Chistiakov, D. A., Melnichenko, A. A., Myasoedova, V. A., Grechko, A. V. and Orekhov, A. N. 2017. Mechanisms of foam cell formation in atherosclerosis. *Journal of Molecular Medicine* 95(11), pp. 1153-1165.

Cho, S.-J., Jung, U. J. and Choi, M.-S. 2012. Differential effects of low-dose resveratrol on adiposity and hepatic steatosis in diet-induced obese mice. *British Journal of Nutrition* 108(12), pp. 2166-2175.

Choe, S. S., Huh, J. Y., Hwang, I. J., Kim, J. I. and Kim, J. B. 2016. Adipose tissue remodeling: its role in energy metabolism and metabolic disorders. *Frontiers in Endocrinology* 7, p. 30.

Choi, K. H. et al. 2010. Phosphoinositide 3-kinase is a novel target of piceatannol for inhibiting PDGF-BB-induced proliferation and migration in human aortic smooth muscle cells. *Cardiovascular Research* 85(4), pp. 836-844.

Chupradit, S., Bokov, D., Zamanian, M. Y., Heidari, M. and Hakimizadeh, E. 2022. Hepatoprotective and therapeutic effects of resveratrol: A focus on anti-inflammatory and antioxidative activities. *Fundamental & Clinical Pharmacology* 36(3), pp. 468-485.

Citi, V., Martelli, A., Gorica, E., Brogi, S., Testai, L. and Calderone, V. 2021. Role of hydrogen sulfide in endothelial dysfunction: Pathophysiology and therapeutic approaches. *Journal of Advanced Research* 27, pp. 99-113.

Cochain, C., Koch, M., Chaudhari, S. M., Busch, M., Pelisek, J., Boon, L. and Zernecke, A. 2015. CD8+ T cells regulate monopoiesis and circulating Ly6Chigh monocyte levels in atherosclerosis in mice. *Circulation research* 117(3), pp. 244-253.

Combadière, C. et al. 2008. Combined inhibition of CCL2, CX3CR1, and CCR5 abrogates Ly6Chi and Ly6Clo monocytosis and almost abolishes atherosclerosis in hypercholesterolemic mice. *Circulation* 117(13), pp. 1649-1657.

Cotter, D. G., Schugar, R. C. and Crawford, P. A. 2013. Ketone body metabolism and cardiovascular disease. *American Journal of Physiology-Heart and Circulatory Physiology*,

Cui, Y., Blumenthal, R. S., Flaws, J. A., Whiteman, M. K., Langenberg, P., Bachorik, P. S. and Bush, T. L. 2001. Non–high-density lipoprotein cholesterol level as a predictor of cardiovascular disease mortality. *Archives of Internal Medicine* 161(11), pp. 1413-1419.

Cullen, J. P., Morrow, D., Jin, Y., von Offenberg Sweeney, N., Sitzmann, J. V., Cahill, P. A. and Redmond, E. M. 2007. Resveratrol inhibits expression and binding activity of the monocyte chemotactic protein-1 receptor, CCR2, on THP-1 monocytes. *Atherosclerosis* 195(1), pp. e125-e133.

Cuthbert, G. A., Shaik, F., Harrison, M. A., Ponnambalam, S. and Homer-Vanniasinkam, S. 2020. Scavenger Receptors as Biomarkers and Therapeutic Targets in Cardiovascular Disease. *Cells* 9(11), p. 2453.

D'Andrea, E., Hey, S. P., Ramirez, C. L. and Kesselheim, A. S. 2019. Assessment of the role of niacin in managing cardiovascular disease outcomes: a systematic review and meta-analysis. *JAMA Network Open* 2(4), pp. e192224-e192224.

Dai, H., Deng, H.-B., Wang, Y.-H. and Guo, J.-J. 2018. Resveratrol inhibits the growth of gastric cancer via the Wnt/β-catenin pathway. *Oncology Letters* 16(2), pp. 1579-1583.

Daugherty, A., Puré, E., Delfel-Butteiger, D., Chen, S., Leferovich, J., Roselaar, S. E. and Rader, D. J. 1997. The effects of total lymphocyte deficiency on the extent of atherosclerosis in apolipoprotein E-/-mice. *The Journal of Clinical Investigation* 100(6), pp. 1575-1580.

Davignon, J. 2005. Apolipoprotein E and atherosclerosis: beyond lipid effect. Am Heart Assoc.

Davignon, J. and Ganz, P. 2004. Role of endothelial dysfunction in atherosclerosis. *Circulation* 109(23_suppl_1), pp. III-27-III-32.

Davra, V. and Galluzzi, L. 2020. *International review of cell and molecular biology: TAM Receptors in Health and Disease*. First Edition ed. United Kingdom: Zoe Kruze.

Dayar, E. and Pechanova, O. 2022. Targeted Strategy in Lipid-Lowering Therapy. *Biomedicines* 10(5), p. 1090.

De Meyer, I., Martinet, W. and De Meyer, G. R. 2012. Therapeutic strategies to deplete macrophages in atherosclerotic plaques. *British Journal of Clinical Pharmacology* 74(2), pp. 246-263.

de Moura e Dias, M. et al. 2021. Diet-induced obesity in animal models: points to consider and influence on metabolic markers. *Diabetology & Metabolic Syndrome* 13(1), pp. 1-14.

Delmas, D., Jannin, B., Latruffe, N. and Latruffe, P. N. 2005. Resveratrol: natural properties against atherosclerosis, associated proinflammatory effects and aging. *Mol Nutr Food Res* 49, pp. 377-395.

Deng, Z. Y., Hu, M. M., Xin, Y. F. and Gang, C. 2015. Resveratrol alleviates vascular inflammatory injury by inhibiting inflammasome activation in rats with hypercholesterolemia and vitamin D2 treatment. *Inflammation Research* 64(5), pp. 321-332.

Devesa, A. et al. 2022. Bone marrow activation in response to metabolic syndrome and early atherosclerosis. *European Heart Journal* 43(19), pp. 1809-1828.

Dhingra, R. and Vasan, R. S. 2012. Age as a risk factor. *Medical Clinics* 96(1), pp. 87-91.

Di, M. et al. 2017. Dickkopf1 destabilizes atherosclerotic plaques and promotes plaque formation by inducing apoptosis of endothelial cells through activation of ER stress. *Cell Death & Disease* 8(7), pp. e2917-e2917.

Ding, L., Zhang, L., Kim, M., Byzova, T. and Podrez, E. 2017a. Akt3 kinase suppresses pinocytosis of low-density lipoprotein by macrophages via a novel WNK/SGK1/Cdc42 protein pathway. *Journal of Biological Chemistry* 292(22), pp. 9283-9293.

Ding, S., Jiang, H., Fang, J. and Liu, G. 2021. Regulatory Effect of Resveratrol on Inflammation Induced by Lipopolysaccharides via Reprograming Intestinal Microbes and Ameliorating Serum Metabolism Profiles. *Frontiers in Immunology*, p. 4568.

Ding, S., Jiang, J., Zhang, G., Bu, Y., Zhang, G. and Zhao, X. 2017b. Resveratrol and caloric restriction prevent hepatic steatosis by regulating SIRT1-autophagy pathway and alleviating endoplasmic reticulum stress in high-fat diet-fed rats. *PloS One* 12(8), p. e0183541.

Do, G.-M., Kwon, E.-Y., Kim, H.-J., Jeon, S.-M., Ha, T.-Y., Park, T. and Choi, M.-S. 2008. Long-term effects of resveratrol supplementation on suppression of atherogenic lesion formation and cholesterol synthesis in apo E-deficient mice. *Biochemical and Biophysical Research Communications* 374(1), pp. 55-59.

Dong, Q. et al. 2014a. Resveratrol ameliorates cardiac dysfunction induced by pressure overload in rats via structural protection and modulation of Ca2+ cycling proteins. *Journal of Translational Medicine* 12(1), pp. 1-12.

Dong, W. et al. 2014b. Inhibitory effects of resveratrol on foam cell formation are mediated through monocyte chemotactic protein-1 and lipid metabolism-related proteins. *International Journal of Molecular Medicine* 33(5), pp. 1161-1168.

Dorighello, G. G., Paim, B. A., Kiihl, S. F., Ferreira, M. S., Catharino, R. R., Vercesi, A. E. and Oliveira, H. C. 2016. Correlation between mitochondrial reactive oxygen and severity of atherosclerosis. *Oxidative Medicine and Cellular Longevity* 2016,

Döring, Y., Drechsler, M., Soehnlein, O. and Weber, C. 2015. Neutrophils in atherosclerosis: from mice to man. *Arteriosclerosis, Thrombosis, and Vascular Biology* 35(2), pp. 288-295.

Dove, D. E., Linton, M. F. and Fazio, S. 2005. ApoE-mediated cholesterol efflux from macrophages: separation of autocrine and paracrine effects. *American Journal of Physiology-Cell Physiology* 288(3), pp. C586-C592.

Dragoljevic, D., Westerterp, M., Veiga, C. B., Nagareddy, P. and Murphy, A. J. 2018. Disordered haematopoiesis and cardiovascular disease: a focus on myelopoiesis. *Clinical Science* 132(17), pp. 1889-1899.

Du, F. et al. 2021. Resveratrol improves liver steatosis and insulin resistance in non-alcoholic fatty liver disease in association with the gut microbiota. *Frontiers in Microbiology* 12, p. 611323.

Du, M. et al. 2016. Nkx2-5 Is Expressed in Atherosclerotic Plaques and Attenuates Development of Atherosclerosis in Apolipoprotein E–Deficient Mice. *Journal of the American Heart Association* 5(12), p. e004440.

Dubland, J. A. and Francis, G. A. 2016. So Much Cholesterol: the unrecognized importance of smooth muscle cells in atherosclerotic foam cell formation. *Current Opinion in Lipidology* 27(2), pp. 155-161.

Duell, P. B. et al. 2022. Nonalcoholic fatty liver disease and cardiovascular risk: a scientific statement from the American Heart Association. *Arteriosclerosis, Thrombosis, and Vascular Biology*, p. 10.1161/ATV. 0000000000000153.

Duester, G. 2000. Families of retinoid dehydrogenases regulating vitamin A function: production of visual pigment and retinoic acid. *European Journal of Biochemistry* 267(14), pp. 4315-4324.

Dull, A.-M., Moga, M. A., Dimienescu, O. G., Sechel, G., Burtea, V. and Anastasiu, C. V. 2019. Therapeutic approaches of resveratrol on endometriosis via anti-inflammatory and anti-angiogenic pathways. *Molecules* 24(4), p. 667.

Dyck, G. J., Raj, P., Zieroth, S., Dyck, J. R. and Ezekowitz, J. A. 2019. The effects of resveratrol in patients with cardiovascular disease and heart failure: a narrative review. *International Journal of Molecular Sciences* 20(4), p. 904.

Ekshyyan, V. P., Hebert, V. Y., Khandelwal, A. and Dugas, T. R. 2007. Resveratrol inhibits rat aortic vascular smooth muscle cell proliferation via estrogen receptor dependent nitric oxide production. *Journal of Cardiovascular Pharmacology* 50(1), pp. 83-93.

Emamat, H., Djafarian, K., Tangestani, H., Hekmatdoost, A. and Shab-Bidar, S. 2018. Resveratrol supplementation and flow-mediated dilation: a systematic review. *Nutrition & Food Science*,

Engelbertsen, D. et al. 2012. Increased inflammation in atherosclerotic lesions of diabetic akita-LDLr−/− mice compared to nondiabetic LDLr−/− mice. *Experimental Diabetes Research* 2012,

Eussen, S. J. et al. 2015. Kynurenines as predictors of acute coronary events in the Hordaland Health Study. *International Journal of Cardiology* 189, pp. 18-24.

Evans, M. A., Sano, S. and Walsh, K. 2020. Cardiovascular disease, aging, and clonal hematopoiesis. *Annual Review of Pathology: Mechanisms of Disease* 15, pp. 419-438.

Eyvazian, V. A. and Frishman, W. H. 2017. Evacetrapib: another CETP inhibitor for dyslipidemia with no clinical benefit. *Cardiology in Review* 25(2), pp. 43-52.

Faghihzadeh, F., Hekmatdoost, A. and Adibi, P. 2015. Resveratrol and liver: A systematic review. *Journal of Research in Medical Sciences: the Official Journal of Isfahan University of Medical Sciences* 20(8), p. 797.

Fain, J. N. et al. 2013. Exercise training does not increase muscle FNDC5 protein or mRNA expression in pigs. *Metabolism* 62(10), pp. 1503-1511.

Fan, B., Gu, J.-Q., Yan, R., Zhang, H., Feng, J. and Ikuyama, S. 2013. High glucose, insulin and free fatty acid concentrations synergistically enhance perilipin 3 expression and lipid accumulation in macrophages. *Metabolism* 62(8), pp. 1168-1179.

Fardoun, M. M., Maaliki, D., Halabi, N., Iratni, R., Bitto, A., Baydoun, E. and Eid, A. H. 2020. Flavonoids in adipose tissue inflammation and atherosclerosis: One arrow, two targets. *Clinical Science* 134(12), pp. 1403-1432.

Farrer, S. 2018. Beyond statins: emerging evidence for hdl-increasing therapies and diet in treating cardiovascular disease. *Advances in Preventive Medicine* 2018,

Farrokhi, E., Ghatreh-Samani, K., Salehi-Vanani, N. and Mahmoodi, A. 2018. The effect of resveratrol on expression of matrix metalloproteinase 9 and its tissue inhibitors in vascular smooth muscle cells. *ARYA Atherosclerosis* 14(4), p. 157.

Fatkhullina, A., Peshkova, I. and Koltsova, E. 2016. The role of cytokines in the development of atherosclerosis. *Biochemistry (Moscow)* 81(11), pp. 1358-1370.

Favari, E., Chroni, A., Tietge, U. J., Zanotti, I., Escolà-Gil, J. C. and Bernini, F. 2015. Cholesterol efflux and reverse cholesterol transport. *Handb Exp Pharmacol.*, pp. 181-206.

Fayad, Z. A. and Robson, P. M. 2021. Bringing Color to Atherosclerotic Plaque Calcification With 18F-Sodium Fluoride Positron Emission Tomography Imaging. Am Heart Assoc.

Fazio, S., Major, A. S., Swift, L. L., Gleaves, L. A., Accad, M., Linton, M. F. and Farese, R. V. 2001. Increased atherosclerosis in LDL receptor–null mice lacking ACAT1 in macrophages. *The Journal of Clinical Investigation* 107(2), pp. 163-171.

Feldman, D. L., Mogelesky, T. C., Liptak, B. F. and Gerrity, R. G. 1991. Leukocytosis in rabbits with diet-induced atherosclerosis. *Arteriosclerosis and Thrombosis: A Journal of Vascular Biology* 11(4), pp. 985-994.

Feng, Y. et al. 2012. Hematopoietic stem/progenitor cell proliferation and differentiation is differentially regulated by high-density and low-density lipoproteins in mice. *PloS One* 7(11), p. e47286.

Fernández-Quintela, A., González, M., Aguirre, L., Milton-Laskibar, I., Léniz, A. and Portillo, M. P. 2018. Resveratrol and Protection in Hepatic Steatosis: Antioxidant Effects.*The Liver*. Elsevier, pp. 199-209.

Filippatos, T. D., Kei, A. and Elisaf, M. S. 2017. Anacetrapib, a new CETP inhibitor: the new tool for the management of dyslipidemias? *Diseases* 5(4), p. 21.

Fischer, A. H., Jacobson, K. A., Rose, J. and Zeller, R. 2008. Hematoxylin and eosin staining of tissue and cell sections. *Cold Spring Harbor Protocols* 2008(5), p. pdb. prot4986.

Fishbein, M. C. 2010. The vulnerable and unstable atherosclerotic plaque. *Cardiovascular Pathology* 19(1), pp. 6-11.

Floreani, M., Napoli, E., Quintieri, L. and Palatini, P. 2003. Oral administration of trans-resveratrol to guinea pigs increases cardiac DT-diaphorase and catalase activities, and protects isolated atria from menadione toxicity. *Life Sciences* 72(24), pp. 2741-2750.

Foks, A. C. et al. 2016. CD11b+ Gr-1+ myeloid-derived suppressor cells reduce atherosclerotic lesion development in LDLr deficient mice. *Cardiovascular Research* 111(3), pp. 252-261.

Folbergrová, J., Ješina, P. and Otáhal, J. 2021. Treatment With Resveratrol Ameliorates Mitochondrial Dysfunction During the Acute Phase of Status Epilepticus in Immature Rats. *Frontiers in Neuroscience* 15, p. 199.

Folch, J., Lees, M. and Sloane Stanley, G. H. 1957. A simple method for the isolation and purification of total lipids from animal tissues. *J Biol Chem* 226(1), pp. 497-509.

Fontes-Cal, T. C. et al. 2021. Crosstalk between plasma cytokines, inflammation, and liver damage as a new strategy to monitoring NAFLD progression. *Frontiers in Immunology* 12,

Franco, J. G. et al. 2013. Resveratrol attenuates oxidative stress and prevents steatosis and hypertension in obese rats programmed by early weaning. *The Journal of Nutritional Biochemistry* 24(6), pp. 960-966.

Frankel, E. 1993. Inhibition of human LDL oxidation by resveratrol. *Lancet* 341, pp. 1103-1104.

Friedman, A. and Hao, W. 2015. A mathematical model of atherosclerosis with reverse cholesterol transport and associated risk factors. *Bulletin of Mathematical Biology* 77(5), pp. 758-781.

Fu, H. et al. 2014a. Interleukin-27 inhibits foam cell formation by promoting macrophage ABCA1 expression through JAK2/STAT3 pathway. *Biochemical and Biophysical Research Communications* 452(4), pp. 881-887.

Fu, Y. et al. 2014b. Resveratrol inhibits breast cancer stem-like cells and induces autophagy via suppressing Wnt/β-catenin signaling pathway. *PloS One* 9(7), p. e102535.

Fukao, H. et al. 2004. Effect of trans-resveratrol on the thrombogenicity and atherogenicity in apolipoprotein E-deficient and low-density lipoprotein receptor-deficient mice. *Blood Coagulation & Fibrinolysis* 15(6), pp. 441-446.

Furman, C. et al. 2004. Thioredoxin reductase 1 is upregulated in atherosclerotic plaques: specific induction of the promoter in human macrophages by oxidized low-density lipoproteins. *Free Radical Biology and Medicine* 37(1), pp. 71-85.

Gaikwad, A., Long, D. J., Stringer, J. L. and Jaiswal, A. K. 2001. In vivo role of NAD (P) H: quinone oxidoreductase 1 (NQO1) in the regulation of intracellular redox state and accumulation of abdominal adipose tissue. *Journal of Biological Chemistry* 276(25), pp. 22559-22564.

Gal, R. et al. 2020. Resveratrol improves heart function by moderating inflammatory processes in patients with systolic heart failure. *Antioxidants* 9(11), p. 1108.

Gal, R., Deres, L., Toth, K., Halmosi, R. and Habon, T. 2021. The effect of resveratrol on the cardiovascular system from molecular mechanisms to clinical results. *International Journal of Molecular Sciences* 22(18), p. 10152.

Galis, Z. S., Sukhova, G. K., Lark, M. W. and Libby, P. 1994. Increased expression of matrix metalloproteinases and matrix degrading activity in vulnerable regions of human atherosclerotic plaques. *The Journal of Clinical Investigation* 94(6), pp. 2493-2503.

Gallagher, H. 2016. *Anti-atherogenic actions of dihomo-gamma-linolenic acid in macrophages.* Cardiff University.

Gallagher, H. et al. 2019. Dihomo-γ-linolenic acid inhibits several key cellular processes associated with atherosclerosis. *Biochimica et Biophysica Acta (BBA)-Molecular Basis of Disease* 1865(9), pp. 2538-2550.

Gambini, J. et al. 2015. Properties of resveratrol: in vitro and in vivo studies about metabolism, bioavailability, and biological effects in animal models and humans. *Oxidative Medicine and Cellular Longevity* 2015,

Gao, M. et al. 2014. Regulation of high-density lipoprotein on hematopoietic stem/progenitor cells in atherosclerosis requires scavenger receptor type BI expression. *Arteriosclerosis, Thrombosis, and Vascular Biology* 34(9), pp. 1900-1909.

Gao, X., Xu, Y. X., Janakiraman, N., Chapman, R. A. and Gautam, S. C. 2001. Immunomodulatory activity of resveratrol: suppression of lymphocyte proliferation, development of cell-mediated cytotoxicity, and cytokine production. *Biochemical Pharmacology* 62(9), pp. 1299-1308.

Garcia-Calvo, M. et al. 2005. The target of ezetimibe is Niemann-Pick C1-Like 1 (NPC1L1). *Proceedings of the National Academy of Sciences* 102(23), pp. 8132-8137.

Georgakis, M. K., Bernhagen, J., Heitman, L. H., Weber, C. and Dichgans, M. 2022. Targeting the CCL2–CCR2 axis for atheroprotection. *European Heart Journal*,

Gerhardt, T. and Ley, K. 2015. Monocyte trafficking across the vessel wall. *Cardiovascular Research* 107(3), pp. 321-330.

Getz, G. S. and Reardon, C. A. 2018. Apoprotein E and reverse cholesterol transport. *International Journal of Molecular Sciences* 19(11), p. 3479.

Ghaffarifar, S., Khoshbaten, M., Dordaei, F., Nahandi, M. Z., Javad-Rashid, R. and Shahnazi, T. 2018. Is treatment of fatty liver effective on reducing carotid intima media thickness; a cohort study. *Gastroenterology and Hepatology from Bed to Bench* 11(1), p. 9.

Gholizadeh, Z., Yousefi, R. and Asadi, S. 2020. The Role of Mutations on Genes KRT5, POFUT1 & POGLUT1, in Dowling-Degos Syndrome. *International Journal of Innovative Research in Medical Science (IJIRMS)* 5(08),

Ghosh, S., Zhao, B., Bie, J. and Song, J. 2010. Macrophage cholesteryl ester mobilization and atherosclerosis. *Vascular Pharmacology* 52(1-2), pp. 1-10.

Giorgio, V., Prono, F., Graziano, F. and Nobili, V. 2013. Pediatric non alcoholic fatty liver disease: old and new concepts on development, progression, metabolic insight and potential treatment targets. *BMC Pediatrics* 13(1), pp. 1-10.

Gisterå, A., Ketelhuth, D. F., Malin, S. G. and Hansson, G. K. 2022. Animal models of atherosclerosis–supportive notes and tricks of the trade. *Circulation research* 130(12), pp. 1869-1887.

Gladine, C. et al. 2014. Lipid profiling following intake of the omega 3 fatty acid DHA identifies the peroxidized metabolites F4-neuroprostanes as the best predictors of atherosclerosis prevention. *PloS One* 9(2), p. e89393.

Gligorijević, N., Stanić-Vučinić, D., Radomirović, M., Stojadinović, M., Khulal, U., Nedić, O. and Ćirković Veličković, T. 2021. Role of resveratrol in prevention and control of cardiovascular disorders and cardiovascular complications related to COVID-19 disease: Mode of action and approaches explored to increase its bioavailability. *Molecules* 26(10), p. 2834.

Goldstein, J. L., Ho, Y., Basu, S. K. and Brown, M. S. 1979. Binding site on macrophages that mediates uptake and degradation of acetylated low density lipoprotein, producing massive cholesterol deposition. *Proceedings of the National Academy of Sciences* 76(1), pp. 333-337.

Gómez-Hernández, A. et al. 2014. Antagonistic effect of TNF-alpha and insulin on uncoupling protein 2 (UCP-2) expression and vascular damage. *Cardiovascular Diabetology* 13(1), pp. 1-10.

Gomez-Lechon, M. J., Donato, M. T., Martinez-Romero, A., Jiménez, N., Castell, J. V. and O'Connor, J.-E. 2007. A human hepatocellular in vitro model to investigate steatosis. *Chemico-Biological Interactions* 165(2), pp. 106-116.

Gómez-Zorita, S. et al. 2012. Resveratrol attenuates steatosis in obese Zucker rats by decreasing fatty acid availability and reducing oxidative stress. *British Journal of Nutrition* 107(2), pp. 202-210.

Gonzalez-Quesada, C. and Frangogiannis, N. G. 2009. Monocyte chemoattractant protein-1/CCL2 as a biomarker in acute coronary syndromes. *Current Atherosclerosis Reports* 11(2), pp. 131-138.

Gordon, D. J. et al. 1989. High-density lipoprotein cholesterol and cardiovascular disease. Four prospective American studies. *Circulation* 79(1), pp. 8-15.

Gosling, J. et al. 1999. MCP-1 deficiency reduces susceptibility to atherosclerosis in mice that overexpress human apolipoprotein B. *The Journal of Clinical Investigation* 103(6), pp. 773-778.

Grebe, A., Hoss, F. and Latz, E. 2018. NLRP3 inflammasome and the IL-1 pathway in atherosclerosis. *Circulation research* 122(12), pp. 1722-1740.

Greenow, K., Pearce, N. J. and Ramji, D. P. 2005. The key role of apolipoprotein E in atherosclerosis. *Journal of Molecular Medicine* 83(5), pp. 329-342.

Groh, L., Keating, S. T., Joosten, L. A., Netea, M. G. and Riksen, N. P. eds. 2018. *Monocyte and macrophage immunometabolism in atherosclerosis*. *Seminars in immunopathology.* Springer.

Grootaert, M. O. and Bennett, M. R. 2022. Sirtuins in atherosclerosis: guardians of healthspan and therapeutic targets. *Nature Reviews Cardiology*, pp. 1-16.

Grootaert, M. O., Moulis, M., Roth, L., Martinet, W., Vindis, C., Bennett, M. R. and De Meyer, G. R. 2018. Vascular smooth muscle cell death, autophagy and senescence in atherosclerosis. *Cardiovascular Research* 114(4), pp. 622-634.

Group, H. T. R. C. 2017. Effects of anacetrapib in patients with atherosclerotic vascular disease. *New England Journal of Medicine* 377(13), pp. 1217-1227.

Grujić-Milanović, J., Jaćević, V., Miloradović, Z., Jovović, D., Milosavljević, I., Milanović, S. D. and Mihailović-Stanojević, N. 2021. Resveratrol Protects Cardiac Tissue in Experimental Malignant Hypertension Due to Antioxidant, Anti-Inflammatory, and Anti-Apoptotic Properties. *International Journal of Molecular Sciences* 22(9), p. 5006.

Gu, L., Okada, Y., Clinton, S. K., Gerard, C., Sukhova, G. K., Libby, P. and Rollins, B. J. 1998. Absence of monocyte chemoattractant protein-1 reduces atherosclerosis in low density lipoprotein receptor–deficient mice. *Molecular Cell* 2(2), pp. 275-281.

Gu, L. et al. 2017. Lunasin functionally enhances LDL uptake via inhibiting PCSK9 and enhancing LDLR expression in vitro and in vivo. *Oncotarget* 8(46), p. 80826.

Gui, Y., Zheng, H. and Cao, R. Y. 2022. Foam Cells in Atherosclerosis: Novel Insights Into Its Origins, Consequences, and Molecular Mechanisms. *Frontiers in Cardiovascular Medicine*, p. 842.

Guo, R., Su, Y., Liu, B., Li, S., Zhou, S. and Xu, Y. 2014. Resveratrol suppresses oxidised low-density lipoprotein-induced macrophage apoptosis through inhibition of intracellular reactive oxygen species generation, LOX-1, and the p38 MAPK pathway. *Cellular Physiology and Biochemistry* 34(2), pp. 603-616.

Guo, W. et al. 2021. Dietary fruit and vegetable supplementation suppresses diet-induced atherosclerosis in LDL receptor knockout mice. *The Journal of Nutrition* 151(4), pp. 902-910.

Guo, Y., Wang, S., Wang, Y. and Zhu, T. 2016. Silymarin improved diet-induced liver damage and insulin resistance by decreasing inflammation in mice. *Pharmaceutical Biology* 54(12), pp. 2995-3000.

Gupta, S., Pablo, A. M., c Jiang, X., Wang, N., Tall, A. R. and Schindler, C. 1997. IFN-gamma potentiates atherosclerosis in ApoE knock-out mice. *The Journal of Clinical Investigation* 99(11), pp. 2752-2761.

Gürgöze, M. T., Muller-Hansma, A. H., Schreuder, M. M., Galema-Boers, A. M., Boersma, E. and Roeters van Lennep, J. E. 2019. Adverse Events Associated With PCSK 9 Inhibitors: A Real-World Experience. *Clinical Pharmacology & Therapeutics* 105(2), pp. 496-504.

Gutierrez-Pajares, J. L. et al. 2015. Caveolin-3 promotes a vascular smooth muscle contractile phenotype. *Frontiers in Cardiovascular Medicine* 2, p. 27.

Gweon, E. J. and Kim, S.-J. 2014. Resveratrol attenuates matrix metalloproteinase-9 and-2-regulated differentiation of HTB94 chondrosarcoma cells through the p38 kinase and JNK pathways. *Oncology Reports* 32(1), pp. 71-78.

Hai, O. Y., Voloshyna, I., Littlefield, M. J., Carsons, S. and Reiss, A. B. 2012. Resveratrol Enhances Cholesterol Efflux Through PPAR-γ--Dependent Signaling Pathways in Human Macrophages. Am Heart Assoc.

Halvorsen, B., Otterdal, K., Dahl, T. B., Skjelland, M., Gullestad, L., Øie, E. and Aukrust, P. 2008. Atherosclerotic plaque stability—what determines the fate of a plaque? *Progress in Cardiovascular Diseases* 51(3), pp. 183-194.

Han, Y.-M., Lee, Y.-J., Jang, Y.-N., Kim, H.-M., Seo, H. S., Jung, T. W. and Jeong, J. H. 2020. Aspirin improves nonalcoholic fatty liver disease and atherosclerosis through regulation of the PPARδ-AMPK-PGC-1α pathway in dyslipidemic conditions. *BioMed Research International* 2020,

Hanani, M. 2012. Lucifer yellow–an angel rather than the devil. *Journal of Cellular and Molecular Medicine* 16(1), pp. 22-31.

Hansen, S. E., Madsen, C. M., Varbo, A. and Nordestgaard, B. G. 2019. Low-grade inflammation in the association between mild-to-moderate hypertriglyceridemia and risk of acute pancreatitis: a study of more than 115000 individuals from the general population. *Clinical Chemistry* 65(2), pp. 321-332.

Hansson, G. K. and Hermansson, A. 2011. The immune system in atherosclerosis. *Nature Immunology* 12(3), pp. 204-212.

Hariri, N. and Thibault, L. 2010. High-fat diet-induced obesity in animal models. *Nutrition Research Reviews* 23(2), pp. 270-299.

Hasan, M. and Bae, H. 2017. An overview of stress-induced resveratrol synthesis in grapes: perspectives for resveratrol-enriched grape products. *Molecules* 22(2), p. 294.

Hasan, M. M. and Baek, K.-H. 2013. Induction of resveratrol biosynthesis in grape skins and leaves by ultrasonication treatment. *Horticultural Science & Technology* 31(4), pp. 496-502.

He, Y. et al. 2020. High fat diet significantly changed the global gene expression profile involved in hepatic drug metabolism and pharmacokinetic system in mice. *Nutrition & Metabolism* 17(1), pp. 1-15.

Heallen, T. R., Kadow, Z. A., Kim, J. H., Wang, J. and Martin, J. F. 2019. Stimulating cardiogenesis as a treatment for heart failure. *Circulation research* 124(11), pp. 1647-1657.

Helal, N. A., Eassa, H. A., Amer, A. M., Eltokhy, M. A., Edafiogho, I. and Nounou, M. I. 2019. Nutraceuticals' novel formulations: the good, the bad, the unknown and patents involved. *Recent Patents on Drug Delivery & Formulation* 13(2), pp. 105-156.

Hendgen-Cotta, U. B. et al. 2017. A novel physiological role for cardiac myoglobin in lipid metabolism. *Scientific Reports* 7(1), pp. 1-13.

Herijgers, N., Van Eck, M., Groot, P. H., Hoogerbrugge, P. M. and Van Berkel, T. J. 2000. Low density lipoprotein receptor of macrophages facilitates atherosclerotic lesion formation in C57Bl/6 mice. *Arteriosclerosis, Thrombosis, and Vascular Biology* 20(8), pp. 1961-1967.

Hermetet, F., Buffière, A., Aznague, A., Pais de Barros, J.-P., Bastie, J.-N., Delva, L. and Quéré, R. 2019. High-fat diet disturbs lipid raft/TGF-β signaling-mediated maintenance of hematopoietic stem cells in mouse bone marrow. *Nature Communications* 10(1), pp. 1-11.

Heyde, A. et al. 2021. Increased stem cell proliferation in atherosclerosis accelerates clonal hematopoiesis. *Cell* 184(5), pp. 1348-1361. e1322.

Hişmioğulları, Ş. E. et al. 2013. The protective effect of resveratrol in experimentally induced non-sterile clean wound inflammation in rats.

Hoggatt, A. F., Hoggatt, J., Honerlaw, M. and Pelus, L. M. 2010. A spoonful of sugar helps the medicine go down: a novel technique to improve oral gavage in mice. *Journal of the American Association for Laboratory Animal Science* 49(3), pp. 329-334.

Hoseini, A., Namazi, G., Farrokhian, A., Reiner, Ž., Aghadavod, E., Bahmani, F. and Asemi, Z. 2019. The effects of resveratrol on metabolic status in patients with type 2 diabetes mellitus and coronary heart disease. *Food & Function* 10(9), pp. 6042-6051.

Hoseini, Z., Sepahvand, F., Rashidi, B., Sahebkar, A., Masoudifar, A. and Mirzaei, H. 2017. NLRP3 inflammasome: Its regulation and involvement in atherosclerosis. *Journal of Cellular Physiology* 233(3), pp. 2116-2132.

Hu, D., Yin, C., Luo, S., Habenicht, A. J. and Mohanta, S. K. 2019. Vascular smooth muscle cells contribute to atherosclerosis immunity. *Frontiers in Immunology* 10, p. 1101.

Hu, X. et al. 2020. Ubiquitin-Fold Modifier-1 Participates in the Diabetic Inflammatory Response by Regulating NF-κB p65 Nuclear Translocation and the Ubiquitination and Degradation of IκBα. *Drug Design, Development and Therapy* 14, p. 795.

Hu, X., Zhang, Y., Xue, Y., Zhang, Z. and Wang, J. 2018. Berberine is a potential therapeutic agent for metabolic syndrome via brown adipose tissue activation and metabolism regulation. *American Journal of Translational Research* 10(11), p. 3322.

Hu, Y. et al. 2021. Resveratrol inhibits necroptosis by mediating the TNF-α/RIP1/RIP3/MLKL pathway in myocardial hypoxia/reoxygenation injury. *Acta Biochimica et Biophysica Sinica* 53(4), pp. 430-437.

Huang, L. et al. 2019. SR-B1 drives endothelial cell LDL transcytosis via DOCK4 to promote atherosclerosis. *Nature* 569(7757), pp. 565-569.

Huang, X. et al. 2022. Osteopontin-Targeted and PPARδ-Agonist-Loaded Nanoparticles Efficiently Reduce Atherosclerosis in Apolipoprotein E–/–Mice. *ACS Omega* 7(33), pp. 28767-28778.

Huang, Y. et al. 2020. Resveratrol protects against nonalcoholic fatty liver disease by improving lipid metabolism and redox homeostasis via the PPARα pathway. *Applied Physiology, Nutrition, and Metabolism* 45(3), pp. 227-239.

Hurtado-Bagès, S., Knobloch, G., Ladurner, A. G. and Buschbeck, M. 2020. The taming of PARP1 and its impact on NAD+ metabolism. *Molecular Metabolism* 38, p. 100950.

Hurwitz, S. N., Jung, S. K. and Kurre, P. 2020. Hematopoietic stem and progenitor cell signaling in the niche. *Leukemia* 34(12), pp. 3136-3148.

Ilhan, F. and Kalkanli, S. T. 2015. Atherosclerosis and the role of immune cells. *World Journal of Clinical Cases: WJCC* 3(4), p. 345.

Im, K., Mareninov, S., Diaz, M. and Yong, W. H. 2019. An introduction to performing immunofluorescence staining. *Biobanking*, pp. 299-311.

Imazio, M. and Nidorf, M. 2021. Colchicine and the heart. *European Heart Journal* 42(28), pp. 2745-2760.

Inoue, S. et al. 2002. Anti-monocyte chemoattractant protein-1 gene therapy limits progression and destabilization of established atherosclerosis in apolipoprotein E–knockout mice. *Circulation* 106(21), pp. 2700-2706.

Ishii, H. et al. 2014. Epithelial splicing regulatory proteins 1 (ESRP1) and 2 (ESRP2) suppress cancer cell motility via different mechanisms. *Journal of Biological Chemistry* 289(40), pp. 27386-27399.

Iyori, M. et al. 2008. Resveratrol modulates phagocytosis of bacteria through an NF-κB-dependent gene program. *Antimicrobial Agents and Chemotherapy* 52(1), pp. 121-127.

Izdebska, M. et al. 2017. The beneficial effects of resveratrol on steatosis and mitochondrial oxidative stress in HepG2 cells. *Canadian Journal of Physiology and Pharmacology* 95(12), pp. 1442-1453.

Izzo, C. et al. 2021. The role of resveratrol in liver disease: A comprehensive review from in vitro to clinical trials. *Nutrients* 13(3), p. 933.

Jack, B. U., Malherbe, C. J., Mamushi, M., Muller, C. J., Joubert, E., Louw, J. and Pheiffer, C. 2019. Adipose tissue as a possible therapeutic target for polyphenols: A case for Cyclopia extracts as anti-obesity nutraceuticals. *Biomedicine & Pharmacotherapy* 120, p. 109439.

Jaiswal, S. et al. 2014. Age-related clonal hematopoiesis associated with adverse outcomes. *New England Journal of Medicine* 371(26), pp. 2488-2498.

Jaiswal, S. et al. 2017. Clonal hematopoiesis and risk of atherosclerotic cardiovascular disease. *New England Journal of Medicine* 377(2), pp. 111-121.

Jaminon, A., Reesink, K., Kroon, A. and Schurgers, L. 2019. The role of vascular smooth muscle cells in arterial remodeling: focus on calcification-related processes. *International Journal of Molecular Sciences* 20(22), p. 5694.

Javadifar, A., Rastgoo, S., Banach, M., Jamialahmadi, T., Johnston, T. P. and Sahebkar, A. 2021. Foam cells as therapeutic targets in atherosclerosis with a focus on the regulatory roles of non-coding RNAs. *International Journal of Molecular Sciences* 22(5), p. 2529.

Jayakumar, T. et al. 2014. Brazilin ameliorates high glucose-induced vascular inflammation via inhibiting ROS and CAMs production in human umbilical vein endothelial cells. *BioMed Research International* 2014,

Jensen-Urstad, A. P. and Semenkovich, C. F. 2012. Fatty acid synthase and liver triglyceride metabolism: housekeeper or messenger? *Biochimica et Biophysica Acta (BBA)-Molecular and Cell Biology of Lipids* 1821(5), pp. 747-753.

Jeon, B. T. et al. 2012. Resveratrol attenuates obesity-associated peripheral and central inflammation and improves memory deficit in mice fed a high-fat diet. *Diabetes* 61(6), pp. 1444-1454.

Jeon, S.-M., Lee, S.-A. and Choi, M.-S. 2014. Antiobesity and vasoprotective effects of resveratrol in apoE-deficient mice. *Journal of Medicinal Food* 17(3), pp. 310-316.

Ji, Q. et al. 2013. Resveratrol inhibits invasion and metastasis of colorectal cancer cells via MALAT1 mediated Wnt/β-catenin signal pathway. *PloS One* 8(11), p. e78700.

Ji, W., Sun, J., Hu, Z. and Sun, B. 2022. Resveratrol protects against atherosclerosis by downregulating the PI3K/AKT/mTOR signaling pathway in atherosclerosis model mice. *Experimental and Therapeutic Medicine* 23(6), pp. 1-9.

Jia, Z., Zhu, H., Misra, B. R., Mahaney, J. E., Li, Y. and Misra, H. P. 2008. EPR studies on the superoxide-scavenging capacity of the nutraceutical resveratrol. *Molecular and Cellular Biochemistry* 313(1), pp. 187-194.

Jiang, Y.-H., Jiang, L.-Y., Wang, Y.-C., Ma, D.-F. and Li, X. 2020. Quercetin attenuates atherosclerosis via modulating oxidized LDL-induced endothelial cellular senescence. *Frontiers in Pharmacology* 11, p. 512.

Jiao, W. et al. 2021. Therapeutic effects of an inhibitor of thioredoxin reductase on liver fibrosis by inhibiting the transforming growth factor-β1/smads pathway. *Frontiers in Molecular Biosciences* 8,

Jin, P. et al. 2018. Homocysteine accelerates atherosclerosis via inhibiting LXRα–mediated ABCA1/ABCG1–dependent cholesterol efflux from macrophages. *Life Sciences* 214, pp. 41-50.

Jin, Y. and Fu, J. 2019. Novel insights into the NLRP 3 inflammasome in atherosclerosis. *Journal of the American Heart Association* 8(12), p. e012219.

Jones, R. D., Taylor, A. M., Tong, E. Y. and Repa, J. J. 2013. Carboxylesterases are uniquely expressed among tissues and regulated by nuclear hormone receptors in the mouse. *Drug Metabolism and Disposition* 41(1), pp. 40-49.

Jung, M.-J. et al. 2016. Chronic repression of mTOR complex 2 induces changes in the gut microbiota of diet-induced obese mice. *Scientific Reports* 6(1), pp. 1-10.

Junjvlieke, Z. et al. 2020. Effect of ELOVL6 on the lipid metabolism of bovine adipocytes. *Genomics* 112(3), pp. 2282-2290.

Kanagalingam, T., Lazarte, J., Wong, D. K. and Hegele, R. A. 2021. Liver injury associated with ezetimibe monotherapy. *CJC Open* 3(2), pp. 195-197.

Kang, D.-G., Lee, H. J., Lee, C. J. and Park, J. S. 2018. Inhibition of the expression of matrix metalloproteinases in articular chondrocytes by resveratrol through affecting nuclear factor-kappa B signaling pathway. *Biomolecules & Therapeutics* 26(6), p. 560.

Kang, H. et al. 2021. The Entry and Egress of Monocytes in Atherosclerosis: A Biochemical and Biomechanical Driven Process. *Cardiovascular Therapeutics* 2021,

Kang, H., Lu, J., Yang, J., Fan, Y. and Deng, X. 2019. Interaction of arterial proteoglycans with low density lipoproteins (LDLs): From theory to promising therapeutic approaches. *Medicine in Novel Technology and Devices* 3, p. 100016.

Kang, W. et al. 2012. Resveratrol improves insulin signaling in a tissue-specific manner under insulin-resistant conditions only: in vitro and in vivo experiments in rodents. *Metabolism* 61(3), pp. 424-433.

Kansu, B. and Lang, D. 2017. Genetic polymorphisms as predictive markers for statin therapy: a route to improved cardiovascular patient outcomes? *Bioscience Horizons: The International Journal of Student Research* 10,

Karunakaran, D. et al. 2016. Targeting macrophage necroptosis for therapeutic and diagnostic interventions in atherosclerosis. *Science Advances* 2(7), p. e1600224.

Kasdallah-Grissa, A., Mornagui, B., Aouani, E., Hammami, M., Gharbi, N., Kamoun, A. and El-Fazaa, S. 2006. Protective effect of resveratrol on ethanol-induced lipid peroxidation in rats. *Alcohol and Alcoholism* 41(3), pp. 236-239.

Kasper, P., Martin, A., Lang, S., Kütting, F., Goeser, T., Demir, M. and Steffen, H.-M. 2021. NAFLD and cardiovascular diseases: a clinical review. *Clinical Research in Cardiology* 110(7), pp. 921-937.

Kavurma, M. M., Rayner, K. J. and Karunakaran, D. 2017. The walking dead: macrophage inflammation and death in atherosclerosis. *Current Opinion in Lipidology* 28(2), p. 91.

Ke, Y., Wang, C., Zhang, J., Zhong, X., Wang, R., Zeng, X. and Ba, X. 2019. The role of PARPs in inflammation—and metabolic—related diseases: molecular mechanisms and beyond. *Cells* 8(9), p. 1047.

Kelley, N., Jeltema, D., Duan, Y. and He, Y. 2019. The NLRP3 inflammasome: an overview of mechanisms of activation and regulation. *International Journal of Molecular Sciences* 20(13), p. 3328.

Kepp, O., Galluzzi, L. and Kroemer, G. 2011. Mitochondrial control of the NLRP3 inflammasome. *Nature Immunology* 12(3), pp. 199-200.

Khaleel, E. F., Abdel-Aleem, G. A. and Mostafa, D. G. 2018. Resveratrol improves high-fat diet induced fatty liver and insulin resistance by concomitantly inhibiting proteolytic cleavage of sterol regulatory element-binding proteins, free fatty acid oxidation, and

intestinal triglyceride absorption. *Canadian Journal of Physiology and Pharmacology* 96(2), pp. 145-157.

Khera, A. V. and Rader, D. J. 2010. Future therapeutic directions in reverse cholesterol transport. *Current Atherosclerosis Reports* 12(1), pp. 73-81.

Kim, J. H., Lim, S., Park, K. S., Jang, H. C. and Choi, S. H. 2017. Total and differential WBC counts are related with coronary artery atherosclerosis and increase the risk for cardiovascular disease in Koreans. *PloS One* 12(7), p. e0180332.

Kim, S., Jin, Y., Choi, Y. and Park, T. 2011. Resveratrol exerts anti-obesity effects via mechanisms involving down-regulation of adipogenic and inflammatory processes in mice. *Biochemical Pharmacology* 81(11), pp. 1343-1351.

Kim, S.-W. et al. 2019a. Statins and inflammation: new therapeutic opportunities in psychiatry. *Frontiers in Psychiatry* 10, p. 103.

Kim, T. H., Park, J. H. and Woo, J. S. 2019b. Resveratrol induces cell death through ROS-dependent downregulation of Notch1/PTEN/Akt signaling in ovarian cancer cells. *Molecular Medicine Reports* 19(4), pp. 3353-3360.

Kinder, J. M., Then, J. E., Hansel, P. M., Molinero, L. L. and Bruns, H. A. 2014. Long-term repeated daily use of intragastric gavage hinders induction of oral tolerance to ovalbumin in mice. *Comparative Medicine* 64(5), pp. 369-376.

Koenen, R. R. and Weber, C. 2010. Therapeutic targeting of chemokine interactions in atherosclerosis. *Nature Reviews Drug Discovery* 9(2), pp. 141-153.

Koga, M. et al. 2007. Inhibition of progression and stabilization of plaques by postnatal interferon-γ function blocking in ApoE-knockout mice. *Circulation research* 101(4), pp. 348-356.

Kologrivova, I., Suslova, T., Koshelskaya, O., Trubacheva, O., Haritonova, O. and Vinnitskaya, I. 2020. Frequency of monocyte subsets is linked to the severity of atherosclerosis in patients with ischemic heart disease: A case-control study. *BioMedicine* 10(2), p. 36.

Kondo, M. 2010. Lymphoid and myeloid lineage commitment in multipotent hematopoietic progenitors. *Immunological Reviews* 238(1), pp. 37-46.

Kong, L., Smith, W. and Hao, D. 2019. Overview of RAW264. 7 for osteoclastogensis study: Phenotype and stimuli. *Journal of Cellular and Molecular Medicine* 23(5), pp. 3077-3087.

Kong, P., Cui, Z.-Y., Huang, X.-F., Zhang, D.-D., Guo, R.-J. and Han, M. 2022. Inflammation and atherosclerosis: signaling pathways and therapeutic intervention. *Signal Transduction and Targeted Therapy* 7(1), pp. 1-24.

Konje, V. C. et al. 2021. Tryptophan levels associate with incident cardiovascular disease in chronic kidney disease. *Clinical Kidney Journal* 14(4), pp. 1097-1105.

Kopeć, A., Piątkowska, E., Leszczyńska, T. and Koronowicz, A. 2013. Effect of long term administration of resveratrol on lipid concentration in selected organs and liver's histology in rats fed high fructose diet. *Journal of Functional Foods* 5(1), pp. 299-305.

Kosmas, C. E. et al. 2018. High-density lipoprotein (HDL) functionality and its relevance to atherosclerotic cardiovascular disease. *Drugs in Context* 7,

Koushki, K. et al. 2021. Anti-inflammatory action of statins in cardiovascular disease: the role of inflammasome and toll-like receptor pathways. *Clinical Reviews in Allergy & Immunology* 60(2), pp. 175-199.

Koushki, M., Dashatan, N. A. and Meshkani, R. 2018. Effect of resveratrol supplementation on inflammatory markers: a systematic review and meta-analysis of randomized controlled trials. *Clinical Therapeutics* 40(7), pp. 1180-1192. e1185.

Koushki, M., Zare, M., Shabani, M., Teimouri, M., Hosseini, H., Khorzoughi, R. B. and Meshkani, R. 2020. Resveratrol Reduces Lipid Accumulation through Upregulating the Expression of MicroRNAs Regulating Fatty Acid Bet Oxidation in Liver Cells: Evidence from In-vivo and In-vitro Studies. *Iranian Journal of Pharmaceutical Research: IJPR* 19(2), p. 333.

Kratofil, R. M., Kubes, P. and Deniset, J. F. 2017. Monocyte conversion during inflammation and injury. *Arteriosclerosis, Thrombosis, and Vascular Biology* 37(1), pp. 35-42.

Kruth, H. S., Huang, W., Ishii, I. and Zhang, W.-Y. 2002. Macrophage foam cell formation with native low density lipoprotein. *Journal of Biological Chemistry* 277(37), pp. 34573-34580.

Kruth, H. S. et al. 2005. Macropinocytosis is the endocytic pathway that mediates macrophage foam cell formation with native low density lipoprotein. *Journal of Biological Chemistry* 280(3), pp. 2352-2360.

Kumar, A., Takada, Y., Boriek, A. M. and Aggarwal, B. B. 2004. Nuclear factor-κB: its role in health and disease. *Journal of Molecular Medicine* 82(7), pp. 434-448.

Kunjathoor, V. V. et al. 2002. Scavenger receptors class AI/II and CD36 are the principal receptors responsible for the uptake of modified low density lipoprotein leading to lipid loading in macrophages. *Journal of Biological Chemistry* 277(51), pp. 49982-49988.

Kunutsor, S. K., Zaccardi, F., Karppi, J., Kurl, S. and Laukkanen, J. A. 2016. Is high serum LDL/HDL cholesterol ratio an emerging risk factor for sudden cardiac death? Findings from the KIHD study. *Journal of Atherosclerosis and Thrombosis*, p. 37184.

Kurotani, R., Tomita, T., Yang, Q., Carlson, B. A., Chen, C. and Kimura, S. 2008. Role of secretoglobin 3A2 in lung development. *American Journal of Respiratory and Critical Care Medicine* 178(4), pp. 389-398.

Kusunoki, J., Hansoty, D. K., Aragane, K., Fallon, J. T., Badimon, J. J. and Fisher, E. A. 2001. Acyl-CoA: cholesterol acyltransferase inhibition reduces atherosclerosis in apolipoprotein E–deficient mice. *Circulation* 103(21), pp. 2604-2609.

Kwok, K. H., Lam, K. S. and Xu, A. 2016. Heterogeneity of white adipose tissue: molecular basis and clinical implications. *Experimental & Molecular Medicine* 48(3), pp. e215-e215.

Kyaw, T. et al. 2013. Cytotoxic and proinflammatory CD8+ T lymphocytes promote development of vulnerable atherosclerotic plaques in apoE-deficient mice. *Circulation* 127(9), pp. 1028-1039.

Kzhyshkowska, J., Neyen, C. and Gordon, S. 2012. Role of macrophage scavenger receptors in atherosclerosis. *Immunobiology* 217(5), pp. 492-502.

Lachowicz-Scroggins, M. E., Yuan, S., Kerr, S. C., Dunican, E. M., Yu, M., Carrington, S. D. and Fahy, J. V. 2016. Abnormalities in MUC5AC and MUC5B protein in airway mucus in asthma. *American Journal of Respiratory and Critical Care Medicine* 194(10), pp. 1296-1299.

Laguna-Fernandez, A. et al. 2018. ERV1/ChemR23 signaling protects against atherosclerosis by modifying oxidized low-density lipoprotein uptake and phagocytosis in macrophages. *Circulation* 138(16), pp. 1693-1705.

Landecho, M. F., Tuero, C., Valentí, V., Bilbao, I., de la Higuera, M. and Frühbeck, G. 2019. Relevance of leptin and other adipokines in obesity-associated cardiovascular risk. *Nutrients* 11(11), p. 2664.

Lang, J. K. and Cimato, T. R. 2014. Cholesterol and hematopoietic stem cells: inflammatory mediators of atherosclerosis. *Stem Cells Translational Medicine* 3(5), pp. 549-552.

Lassila, M., Allen, T. J., Cao, Z., Thallas, V., Jandeleit-Dahm, K. A., Candido, R. and Cooper, M. E. 2004. Imatinib attenuates diabetes-associated atherosclerosis. *Arteriosclerosis, Thrombosis, and Vascular Biology* 24(5), pp. 935-942.

Laxton, R. C. et al. 2009. A role of matrix metalloproteinase-8 in atherosclerosis. *Circulation research* 105(9), pp. 921-929.

Lee, B. and Moon, S.-K. 2005. Resveratrol Inhibits TNF-α–Induced Proliferation and Matrix Metalloproteinase Expression in Human Vascular Smooth Muscle Cells. *The Journal of Nutrition* 135(12), pp. 2767-2773.

Lee, J. J. et al. 2021. Cholesterol Efflux Capacity and Its Association With Adverse Cardiovascular Events: A Systematic Review and Meta-Analysis. *Frontiers in Cardiovascular Medicine* 8,

Lee, S.-G. et al. 2018. Macrophage polarization and acceleration of atherosclerotic plaques in a swine model. *PloS One* 13(3), p. e0193005.

Leibundgut, G., Witztum, J. L. and Tsimikas, S. 2013. Oxidation-specific epitopes and immunological responses: Translational biotheranostic implications for atherosclerosis. *Current Opinion in Pharmacology* 13(2), pp. 168-179.

Lelis, F. J. et al. 2017. Myeloid-derived suppressor cells modulate B-cell responses. *Immunology Letters* 188, pp. 108-115.

Lent-Schochet, D. and Jialal, I. 2019. Antilipemic agent bile acid sequestrants.

Leopoldini, M., Marino, T., Russo, N. and Toscano, M. 2004. Antioxidant properties of phenolic compounds: H-atom versus electron transfer mechanism. *The Journal of Physical Chemistry A* 108(22), pp. 4916-4922.

Lesourne, R. et al. 2009. Themis, a T cell–specific protein important for late thymocyte development. *Nature Immunology* 10(8), pp. 840-847.

Leth-Larsen, R. et al. 2005. A common polymorphism in the SFTPD gene influences assembly, function, and concentration of surfactant protein D. *The Journal of Immunology* 174(3), pp. 1532-1538.

Li, A. C. and Glass, C. K. 2002. The macrophage foam cell as a target for therapeutic intervention. *Nature Medicine* 8(11), pp. 1235-1242.

Li, H., Xia, N., Hasselwander, S. and Daiber, A. 2019a. Resveratrol and vascular function. *International Journal of Molecular Sciences* 20(9), p. 2155.

Li, J., Xu, P., Wang, L., Feng, M., Chen, D., Yu, X. and Lu, Y. 2020a. Molecular biology of BPIFB1 and its advances in disease. *Annals of Translational Medicine* 8(10),

Li, J., Zhong, Z., Yuan, J., Chen, X., Huang, Z. and Wu, Z. 2019b. Resveratrol improves endothelial dysfunction and attenuates atherogenesis in apolipoprotein E-deficient mice. *The Journal of Nutritional Biochemistry* 67, pp. 63-71.

Li, L., Wang, M., Ma, Q., Ye, J. and Sun, G. 2022a. Role of glycolysis in the development of atherosclerosis. *American Journal of Physiology-Cell Physiology* 323(2), pp. C617-C629.

Li, M., Li, P., Tang, R. and Lu, H. 2022b. Resveratrol and its derivates improve inflammatory bowel disease by targeting gut microbiota and inflammatory signaling pathways. *Food Science and Human Wellness* 11(1), pp. 22-31.

Li, W. et al. 2022c. NF-κB and its crosstalk with endoplasmic reticulum stress in atherosclerosis. *Frontiers in Cardiovascular Medicine* 9,

Li, Y., Cao, Z. and Zhu, H. 2006. Upregulation of endogenous antioxidants and phase 2 enzymes by the red wine polyphenol, resveratrol in cultured aortic smooth muscle cells leads to cytoprotection against oxidative and electrophilic stress. *Pharmacological Research* 53(1), pp. 6-15.

Li, Z. et al. 2020b. Resveratrol promotes white adipocytes browning and improves metabolic disorders in Sirt1-dependent manner in mice. *The FASEB Journal* 34(3), pp. 4527-4539.

Liang, Y., Chen, Y., Li, L., Zhang, S., Xiao, J. and Wei, D. 2022. Krebs Cycle Rewired: Driver of Atherosclerosis Progression? *Current Medicinal Chemistry* 29(13), pp. 2322-2333.

Liao, W. et al. 2018. Resveratrol-induced white adipose tissue browning in obese mice by remodeling fecal microbiota. *Molecules* 23(12), p. 3356.

Libby, P. 2021. The changing landscape of atherosclerosis. *Nature* 592(7855), pp. 524-533.

Libby, P. et al. 2019. Atherosclerosis. *Nature Reviews Disease Primers* 5(1), p. 56. doi: 10.1038/s41572-019-0106-z

Libby, P. and Everett, B. M. 2019. Novel antiatherosclerotic therapies. *Arteriosclerosis, Thrombosis, and Vascular Biology* 39(4), pp. 538-545.

Libby, P. and Hansson, G. K. 2019. From focal lipid storage to systemic inflammation: JACC review topic of the week. *Journal of the American College of Cardiology* 74(12), pp. 1594-1607.

Liberale, L., Carbone, F., Camici, G. G. and Montecucco, F. 2019. IL-1β and statin treatment in patients with myocardial infarction and diabetic cardiomyopathy. *Journal of Clinical Medicine* 8(11), p. 1764.

Liberale, L., Montecucco, F., G Camici, G., Dallegri, F., Vecchie, A., Carbone, F. and Bonaventura, A. 2017. Treatment with proprotein convertase subtilisin/kexin type 9 (PCSK9) inhibitors to reduce cardiovascular inflammation and outcomes. *Current Medicinal Chemistry* 24(14), pp. 1403-1416.

Lim, J. P. and Gleeson, P. A. 2011. Macropinocytosis: an endocytic pathway for internalising large gulps. *Immunology and Cell Biology* 89(8), pp. 836-843.

Lin, P., Ji, H.-H., Li, Y.-J. and Guo, S.-D. 2021. Macrophage plasticity and atherosclerosis therapy. *Frontiers in Molecular Biosciences* 8, p. 679797.

Lin, X.-L. et al. 2017. Allicin induces the upregulation of ABCA1 expression via PPARγ/LXRα signaling in THP-1 macrophage-derived foam cells. *International Journal of Molecular Medicine* 39(6), pp. 1452-1460.

Lin, X. P., Mintern, J. D. and Gleeson, P. A. 2020. Macropinocytosis in different cell types: Similarities and differences. *Membranes* 10(8), p. 177.

Lin, Y. et al. 2015. Practical assessment of the quantification of atherosclerotic lesions in apoE-/-mice. *Molecular Medicine Reports* 12(4), pp. 5298-5306.

Linton, M. F. et al. 2019. The role of lipids and lipoproteins in atherosclerosis. *Endotext [Internet]*,

Liu, C.-W. et al. 2017a. Resveratrol attenuates ICAM-1 expression and monocyte adhesiveness to TNF-α-treated endothelial cells: evidence for an anti-inflammatory cascade mediated by the miR-221/222/AMPK/p38/NF-κB pathway. *Scientific Reports* 7(1), pp. 1-14.

Liu, F.-C., Tsai, Y.-F., Tsai, H.-I. and Yu, H.-P. 2015a. Anti-inflammatory and organ-protective effects of resveratrol in trauma-hemorrhagic injury. *Mediators of Inflammation* 2015,

Liu, H., Li, X., Yan, G. and Lun, R. 2019a. Knockdown of USP14 inhibits PDGF-BB-induced vascular smooth muscle cell dedifferentiation via inhibiting mTOR/P70S6K signaling pathway. *RSC Advances* 9(63), pp. 36649-36657.

Liu, T. et al. 2015b. Resveratrol attenuates oxidative stress and extends life span in the annual fish Nothobranchius guentheri. *Rejuvenation Research* 18(3), pp. 225-233.

Liu, T., Zhang, L., Joo, D. and Sun, S.-C. 2017b. NF-κB signaling in inflammation. *Signal Transduction and Targeted Therapy* 2(1), pp. 1-9.

Liu, X. et al. 2019b. Gpihbp1 deficiency accelerates atherosclerosis and plaque instability in diabetic Ldlr-/-mice. *Atherosclerosis* 282, pp. 100-109.

Liu, X., Wu, J., Tian, R., Su, S., Deng, S. and Meng, X. 2020. Targeting foam cell formation and macrophage polarization in atherosclerosis: The Therapeutic potential of rhubarb. *Biomedicine & Pharmacotherapy* 129, p. 110433.

Liu, Y. et al. 2019c. SGK2 promotes renal cancer progression via enhancing ERK 1/2 and AKT phosphorylation. *Eur Rev Med Pharmacol Sci* 23(7), pp. 2756-2767.

Liu, Y., Chen, X. and Li, J. 2017c. Resveratrol protects against oxidized low-density lipoprotein-induced human umbilical vein endothelial cell apoptosis via inhibition of mitochondrial-derived oxidative stress. *Molecular Medicine Reports* 15(5), pp. 2457-2464.

Liu, Y.-C., Zou, X.-B., Chai, Y.-F. and Yao, Y.-M. 2014. Macrophage polarization in inflammatory diseases. *International Journal of Biological Sciences* 10(5), p. 520.

Liu, Z.-B. and Shen, X. 2009. Thioredoxin reductase 1 upregulates MCP-1 release in human endothelial cells. *Biochemical and Biophysical Research Communications* 386(4), pp. 703-708.

Liu, Z.-H. et al. 2019d. SIRT1 activation attenuates cardiac fibrosis by endothelial-to-mesenchymal transition. *Biomedicine & Pharmacotherapy* 118, p. 109227.

Lo Sasso, G., Schlage, W. K., Boué, S., Veljkovic, E., Peitsch, M. C. and Hoeng, J. 2016. The Apoe−/− mouse model: a suitable model to study cardiovascular and respiratory diseases in the context of cigarette smoke exposure and harm reduction. *Journal of Translational Medicine* 14(1), pp. 1-16.

Lonardo, A. et al. 2019. Sex differences in nonalcoholic fatty liver disease: state of the art and identification of research gaps. *Hepatology* 70(4), pp. 1457-1469.

Lonardo, A. and Suzuki, A. 2020. Sexual dimorphism of NAFLD in adults. Focus on clinical aspects and implications for practice and translational research. *Journal of Clinical Medicine* 9(5), p. 1278.

Lou, Z., Li, X., Zhao, X., Du, K., Li, X. and Wang, B. 2018. Resveratrol attenuates hydrogen peroxide-induced apoptosis, reactive oxygen species generation, and PSGL-1 and VWF activation in human umbilical vein endothelial cells, potentially via MAPK signalling pathways. *Molecular Medicine Reports* 17(2), pp. 2479-2487.

Louis, S. F. and Zahradka, P. 2010. Vascular smooth muscle cell motility: From migration to invasion. *Experimental & Clinical Cardiology* 15(4), p. e75.

Lu, M. and Gursky, O. 2013. Aggregation and fusion of low-density lipoproteins in vivo and in vitro. *Biomolecular Concepts* 4(5), pp. 501-518.

Lu, Y.-E. and Chen, Y.-J. 2021. Resveratrol inhibits matrix metalloproteinase-1 and-3 expression by suppressing of p300/NFκB acetylation in TNF-α-treated human dermal fibroblasts. *Chemico-Biological Interactions* 337, p. 109395.

Lu, Z., Li, Y., Syn, W.-K., Wang, Z., Lopes-Virella, M. F., Lyons, T. J. and Huang, Y. 2020. Amitriptyline inhibits nonalcoholic steatohepatitis and atherosclerosis induced by high-fat diet and LPS through modulation of sphingolipid metabolism. *American Journal of Physiology-Endocrinology and Metabolism* 318(2), pp. E131-E144.

Lucas, E., Vila-Bedmar, R., Arcones, A. C., Cruces-Sande, M., Cachofeiro, V., Mayor, F. and Murga, C. 2016. Obesity-induced cardiac lipid accumulation in adult mice is modulated by G protein-coupled receptor kinase 2 levels. *Cardiovascular Diabetology* 15(1), pp. 1-13.

Luo, X. et al. 2021. Plaque erosion: a distinctive pathological mechanism of acute coronary syndrome. *Frontiers in Cardiovascular Medicine*, p. 1176.

Lust, S. T., Shanahan, C. M., Shipley, R. J., Lamata, P. and Gentleman, E. 2021. Design considerations for engineering 3D models to study vascular pathologies in vitro. *Acta Biomaterialia* 132, pp. 114-128.

Ma, S. et al. 2018. Melatonin ameliorates the progression of atherosclerosis via mitophagy activation and NLRP3 inflammasome inhibition. *Oxidative Medicine and Cellular Longevity* 2018,

Ma, S. D., Mussbacher, M. and Galkina, E. V. 2021a. Functional role of B cells in atherosclerosis. *Cells* 10(2), p. 270.

Ma, X. and Feng, Y. 2016. Hypercholesterolemia tunes hematopoietic stem/progenitor cells for inflammation and atherosclerosis. *International Journal of Molecular Sciences* 17(7), p. 1162.

Ma, Y. et al. 2021b. Resveratrol on the Metabolic Reprogramming in Liver: Implications for Advanced Atherosclerosis. *Frontiers in Pharmacology*, p. 2428.

Maayah, Z. H. et al. 2021. Resveratrol reduces cardiac NLRP3-inflammasome activation and systemic inflammation to lessen doxorubicin-induced cardiotoxicity in juvenile mice. *FEBS Letters* 595(12), pp. 1681-1695.

Machado, R. M. et al. 2012. Omega-6 polyunsaturated fatty acids prevent atherosclerosis development in LDLr-KO mice, in spite of displaying a pro-inflammatory profile similar to trans fatty acids. *Atherosclerosis* 224(1), pp. 66-74.

Madjid, M., Awan, I., Willerson, J. T. and Casscells, S. W. 2004. Leukocyte count and coronary heart disease: implications for risk assessment. *Journal of the American College of Cardiology* 44(10), pp. 1945-1956.

Madjid, M. and Fatemi, O. 2013. Components of the complete blood count as risk predictors for coronary heart disease: in-depth review and update. *Texas Heart Institute Journal* 40(1), p. 17.

Maeda, K. et al. 2003. Green tea catechins inhibit the cultured smooth muscle cell invasion through the basement barrier. *Atherosclerosis* 166(1), pp. 23-30.

Magyar, K. et al. 2012. Cardioprotection by resveratrol: A human clinical trial in patients with stable coronary artery disease. *Clinical Hemorheology and Microcirculation* 50(3), pp. 179-187.

Mai, W. and Liao, Y. 2020. Targeting IL-1β in the Treatment of Atherosclerosis. *Frontiers in Immunology*, p. 3141.

Majeed, M. L., Ghafil, F. A., Fatima, G., Hadi, N. R. and Mahdi, H. F. 2021. Anti-Atherosclerotic and Anti-Inflammatory Effects of Curcumin on Hypercholesterolemic Male Rabbits. *Indian Journal of Clinical Biochemistry* 36(1), pp. 74-80.

Major, A. S., Fazio, S. and Linton, M. F. 2002. B-lymphocyte deficiency increases atherosclerosis in LDL receptor–null mice. *Arteriosclerosis, Thrombosis, and Vascular Biology* 22(11), pp. 1892-1898.

Mäkinen, P. I. et al. 2010. Silencing of either SR-A or CD36 reduces atherosclerosis in hyperlipidaemic mice and reveals reciprocal upregulation of these receptors. *Cardiovascular Research* 88(3), pp. 530-538.

Malaguarnera, L. 2019. Influence of resveratrol on the immune response. *Nutrients* 11(5), p. 946.

Mallat, Z., Taleb, S., Ait-Oufella, H. and Tedgui, A. 2009. The role of adaptive T cell immunity in atherosclerosis. *Journal of Lipid Research* 50, pp. S364-S369.

Mallavia, B. et al. 2013. Peptide inhibitor of NF-κB translocation ameliorates experimental atherosclerosis. *The American Journal of Pathology* 182(5), pp. 1910-1921.

Man, J. J., Beckman, J. A. and Jaffe, I. Z. 2020. Sex as a biological variable in atherosclerosis. *Circulation research* 126(9), pp. 1297-1319.

Mangels, D. R. and Mohler III, E. R. 2017. Catechins as potential mediators of cardiovascular health. *Arteriosclerosis, Thrombosis, and Vascular Biology* 37(5), pp. 757-763.

Mangge, H., Stelzer, I., Reininghaus, E., Weghuber, D., Postolache, T. and Fuchs, D. 2014. Disturbed tryptophan metabolism in cardiovascular disease. *Current Medicinal Chemistry* 21(17), pp. 1931-1937.

Mantovani, A., Garlanda, C. and Locati, M. 2009. Macrophage diversity and polarization in atherosclerosis: a question of balance. *Arteriosclerosis, Thrombosis, and Vascular Biology* 29(10), pp. 1419-1423.

Marín-Aguilar, F., Pavillard, L. E., Giampieri, F., Bullón, P. and Cordero, M. D. 2017. Adenosine monophosphate (AMP)-activated protein kinase: a new target for nutraceutical compounds. *International Journal of Molecular Sciences* 18(2), p. 288.

Marques, B., Trindade, M., Aquino, J., Cunha, A., Gismondi, R., Neves, M. and Oigman, W. 2018a. Beneficial effects of acute trans-resveratrol supplementation in treated hypertensive patients with endothelial dysfunction. *Clinical and Experimental Hypertension* 40(3), pp. 218-223.

Marques, L. R., Diniz, T. A., Antunes, B. M., Rossi, F. E., Caperuto, E. C., Lira, F. S. and Gonçalves, D. C. 2018b. Reverse cholesterol transport: molecular mechanisms and the non-medical approach to enhance HDL cholesterol. *Frontiers in Physiology* 9, p. 526.

Martin, A., Lang, S., Goeser, T., Demir, M., Steffen, H.-M. and Kasper, P. 2022. Management of Dyslipidemia in Patients with Non-Alcoholic Fatty Liver Disease. *Current Atherosclerosis Reports*, pp. 1-14.

Martin, J. F., Perin, E. C. and Willerson, J. T. 2017. Direct stimulation of cardiogenesis: a new paradigm for treating heart disease. *Circulation research* 121(1), pp. 13-15.

Matsuda, K. 1994. ACAT inhibitors as antiatherosclerotic agents: compounds and mechanisms. *Medicinal Research Reviews* 14(3), pp. 271-305.

Matsumoto, T. et al. 2016. Overexpression of cytotoxic T-lymphocyte–associated antigen-4 prevents atherosclerosis in mice. *Arteriosclerosis, Thrombosis, and Vascular Biology* 36(6), pp. 1141-1151.

Matsumura, N. et al. 2018. Resveratrol improves cardiac function and exercise performance in MI-induced heart failure through the inhibition of cardiotoxic HETE metabolites. *Journal of Molecular and Cellular Cardiology* 125, pp. 162-173.

Matsuo, M., Ito, F., Konto, A., Aketa, M., Tomoi, M. and Shimomura, K. 1995. Effect of FR145237, a novel ACAT inhibitor, on atherogenesis in cholesterol-fed and WHHL rabbits. Evidence for a direct effect on the arterial wall. *Biochimica et Biophysica Acta (BBA)-Lipids and Lipid Metabolism* 1259(3), pp. 254-260.

Matthews, C. et al. 2006. Vascular smooth muscle cells undergo telomere-based senescence in human atherosclerosis: effects of telomerase and oxidative stress. *Circulation research* 99(2), pp. 156-164.

Mazidi, M., Rezaie, P., Karimi, E. and Kengne, A. P. 2017. The effects of bile acid sequestrants on lipid profile and blood glucose concentrations: a systematic review and meta-analysis of randomized controlled trials. *International Journal of Cardiology* 227, pp. 850-857.

McCarthy, M. 2014. Niacin fails to reduce vascular events in large randomised trial. *BMJ* 349,

McLaren, J. E., Michael, D. R., Ashlin, T. G. and Ramji, D. P. 2011. Cytokines, macrophage lipid metabolism and foam cells: implications for cardiovascular disease therapy. *Progress in lipid research* 50(4), pp. 331-347.

McLaren, J. E. et al. 2010. IL-33 reduces macrophage foam cell formation. *The Journal of Immunology* 185(2), pp. 1222-1229.

Mehlem, A., Hagberg, C. E., Muhl, L., Eriksson, U. and Falkevall, A. 2013. Imaging of neutral lipids by oil red O for analyzing the metabolic status in health and disease. *Nature Protocols* 8(6), pp. 1149-1154.

Mehu, M., Narasimhulu, C. A. and Singla, D. K. 2022. Inflammatory Cells in Atherosclerosis. *Antioxidants* 11(2), p. 233.

Melhem, N. J. and Taleb, S. 2021. Tryptophan: from diet to cardiovascular diseases. *International Journal of Molecular Sciences* 22(18), p. 9904.

Meng, F., Cheng, H., Qian, J., Dai, X., Huang, Y. and Fan, Y. 2022. In vitro fluidic systems: Applying shear stress on endothelial cells. *Medicine in Novel Technology and Devices*, p. 100143.

Meng, N., Li, Y., Zhang, H. and Sun, X.-F. 2008. RECK, a novel matrix metalloproteinase regulator. *Histology and Histopathology*,

Meng, T., Xiao, D., Muhammed, A., Deng, J., Chen, L. and He, J. 2021. Anti-inflammatory action and mechanisms of resveratrol. *Molecules* 26(1), p. 229.

Menu, P., Pellegrin, M., Aubert, J., Bouzourene, K., Tardivel, A., Mazzolai, L. and Tschopp, J. 2011. Atherosclerosis in ApoE-deficient mice progresses independently of the NLRP3 inflammasome. *Cell Death & Disease* 2(3), pp. e137-e137.

Meyer, J. M., Ji, A., Cai, L. and van der Westhuyzen, D. R. 2012. High-capacity selective uptake of cholesteryl ester from native LDL during macrophage foam cell formation. *Journal of Lipid Research* 53(10), pp. 2081-2091.

Miao, X. et al. 2019. A comparative meta-analysis of the efficacy of statin–ezetimibe co-therapy versus statin monotherapy in reducing cardiovascular and cerebrovascular adverse events in patients with type 2 diabetes mellitus. *Eur Rev Med Pharmacol Sci* 23(5), pp. 2302-2310.

Michael, D. R., Ashlin, T. G., Buckley, M. L. and Ramji, D. P. 2012. Macrophages, lipid metabolism and gene expression in atherogenesis: a therapeutic target of the future? *Clinical Lipidology* 7(1), pp. 37-48.

Michael, D. R., Ashlin, T. G., Davies, C. S., Gallagher, H., Stoneman, T. W., Buckley, M. L. and Ramji, D. P. 2013. Differential regulation of macropinocytosis in macrophages by cytokines: implications for foam cell formation and atherosclerosis. *Cytokine* 64(1), pp. 357-361.

Mietus-Snyder, M., Gowri, M. S. and Pitas, R. E. 2000. Class A Scavenger Receptor Up-regulation in Smooth Muscle Cells by Oxidized Low Density Lipoprotein*: ENHANCEMENT BY CALCIUM FLUX AND CONCURRENT CYCLOOXYGENASE-2 UP-REGULATION. *Journal of Biological Chemistry* 275(23), pp. 17661-17670.

Milasan, A., Smaani, A. and Martel, C. 2019. Early rescue of lymphatic function limits atherosclerosis progression in Ldlr−/− mice. *Atherosclerosis* 283, pp. 106-119.

Millán, J. et al. 2009. Lipoprotein ratios: physiological significance and clinical usefulness in cardiovascular prevention. *Vascular Health and Risk Management* 5, p. 757.

Min, K., Kour, A., Sano, S. and Walsh, K. 2020. The role of clonal haematopoiesis in cardiovascular diseases: epidemiology and experimental studies. *Journal of Internal Medicine* 288(5), pp. 507-517.

Mirzaei, H., Ferns, G. A., Avan, A. and Mobarhan, M. G. 2017. Cytokines and microRNA in coronary artery disease. *Advances in Clinical Chemistry* 82, pp. 47-70.

Miura, K., Yang, L., van Rooijen, N., Ohnishi, H. and Seki, E. 2012. Hepatic recruitment of macrophages promotes nonalcoholic steatohepatitis through CCR2. *American Journal of Physiology-Gastrointestinal and Liver Physiology* 302(11), pp. G1310-G1321.

Miyazaki, A. et al. 1998. Expression of ACAT-1 protein in human atherosclerotic lesions and cultured human monocytes-macrophages. *Arteriosclerosis, Thrombosis, and Vascular Biology* 18(10), pp. 1568-1574.

Moore, K. J. et al. 2005. Loss of receptor-mediated lipid uptake via scavenger receptor A or CD36 pathways does not ameliorate atherosclerosis in hyperlipidemic mice. *The Journal of Clinical Investigation* 115(8), pp. 2192-2201.

Moore, K. J., Sheedy, F. J. and Fisher, E. A. 2013. Macrophages in atherosclerosis: a dynamic balance. *Nature Reviews Immunology* 13(10), pp. 709-721.

Moore, K. J. and Tabas, I. 2011a. The cellular biology of macrophages in atherosclerosis. *Cell* 145(3), p. 341.

Moore, K. J. and Tabas, I. 2011b. Macrophages in the pathogenesis of atherosclerosis. *Cell* 145(3), pp. 341-355.

Mootz, M., Jakwerth, C. A., Schmidt-Weber, C. B. and Zissler, U. M. 2022. Secretoglobins in the big picture of immunoregulation in airway diseases. *Allergy* 77(3), pp. 767-777.

Moraes, D. S., Moreira, D. C., Andrade, J. M. O. and Santos, S. H. S. 2020. Sirtuins, brain and cognition: A review of resveratrol effects. *IBRO Reports* 9, pp. 46-51.

Moris, D. et al. 2017. The role of reactive oxygen species in myocardial redox signaling and regulation. *Annals of Translational Medicine* 5(16),

Moss, J. 2018. *Anti-inflammatory actions of nutraceuticals: Novel emerging therapies for atherosclerosis?* Cardiff University.

Moss, J. W. and Ramji, D. P. 2015. Interferon-γ: Promising therapeutic target in atherosclerosis. *World Journal of Experimental Medicine* 5(3), p. 154.

Moss, J. W. and Ramji, D. P. 2016. Nutraceutical therapies for atherosclerosis. *Nature Reviews Cardiology* 13(9), pp. 513-532.

Moss, J. W., Williams, J. O. and Ramji, D. P. 2018. Nutraceuticals as therapeutic agents for atherosclerosis. *Biochimica et Biophysica Acta (BBA)-Molecular Basis of Disease* 1864(5), pp. 1562-1572.

Moya, M. et al. 2012. Foxa1 reduces lipid accumulation in human hepatocytes and is down-regulated in nonalcoholic fatty liver. *PloS One* 7(1), p. e30014.

Mozos, I., Malainer, C., Horbańczuk, J., Gug, C., Stoian, D., Luca, C. T. and Atanasov, A. G. 2017. Inflammatory markers for arterial stiffness in cardiovascular diseases. *Frontiers in Immunology* 8, p. 1058.

Mukherjee, S., Dudley, J. and Das, D. 2010. Dose-dependency of resveratrol in providing health benefits. *Dose Response* 8(4), pp. 478-500.

Mullard, A. 2018. Anti-inflammatory cardiovascular therapies take another hit. *Nature Reviews Drug Discovery* 17(12), pp. 853-854.

Murphy, A. J. et al. 2011. ApoE regulates hematopoietic stem cell proliferation, monocytosis, and monocyte accumulation in atherosclerotic lesions in mice. *The Journal of Clinical Investigation* 121(10), pp. 4138-4149.

Murphy, A. J. and Tall, A. R. 2016. Disordered haematopoiesis and athero-thrombosis. *European Heart Journal* 37(14), pp. 1113-1121.

Murphy, M. P. 2009. How mitochondria produce reactive oxygen species. *Biochemical Journal* 417(1), pp. 1-13.

Nadkarni, S. K., Bouma, B. E., de Boer, J. and Tearney, G. J. 2009. Evaluation of collagen in atherosclerotic plaques: the use of two coherent laser-based imaging methods. *Lasers in Medical Science* 24(3), pp. 439-445.

Nair, A. B. and Jacob, S. 2016. A simple practice guide for dose conversion between animals and human. *Journal of Basic and Clinical Pharmacy* 7(2), p. 27.

Nallasamy, P., Kang, Z. Y., Sun, X., Anandh Babu, P. V., Liu, D. and Jia, Z. 2021. Natural Compound Resveratrol Attenuates TNF-Alpha-Induced Vascular Dysfunction in Mice and Human Endothelial Cells: The Involvement of the NF-κB Signaling Pathway. *International Journal of Molecular Sciences* 22(22), p. 12486.

Nanizawa, E. et al. 2020. Short-term high-fat diet intake leads to exacerbation of concanavalin A-induced liver injury through the induction of procoagulation state. *Biochemistry and Biophysics Reports* 22, p. 100736.

Nasr, S. H. and Huang, X. 2021. Nanotechnology for targeted therapy of atherosclerosis. *Frontiers in Pharmacology* 12,

Nathan, N., Taytard, J., Duquesnoy, P., Thouvenin, G., Corvol, H., Amselem, S. and Clement, A. 2016. Surfactant protein A: A key player in lung homeostasis. *The International Journal of Biochemistry & Cell Biology* 81, pp. 151-155.

Navarro-Orcajada, S., Conesa, I., Vidal-Sánchez, F. J., Matencio, A., Albaladejo-Maricó, L., García-Carmona, F. and López-Nicolás, J. M. 2022. Stilbenes: Characterization, bioactivity, encapsulation and structural modifications. A review of their current limitations and promising approaches. *Critical Reviews in Food Science and Nutrition*, pp. 1-19.

Negi, S. I. et al. 2013. A novel mutation in the ABCA1 gene causing an atypical phenotype of Tangier disease. *Journal of Clinical Lipidology* 7(1), pp. 82-87.

Negre-Salvayre, A., Guerby, P., Gayral, S., Laffargue, M. and Salvayre, R. 2020. Role of reactive oxygen species in atherosclerosis: Lessons from murine genetic models. *Free Radical Biology and Medicine* 149, pp. 8-22.

Nevado, R. M., Hamczyk, M. R. and Andrés, V. 2022. Isolation of Mouse Aortic RNA for Transcriptomics.*Atherosclerosis*. Springer, pp. 611-627.

Newby, A. C. 2008. Metalloproteinase expression in monocytes and macrophages and its relationship to atherosclerotic plaque instability. *Arteriosclerosis, Thrombosis, and Vascular Biology* 28(12), pp. 2108-2114.

Newby, A. C. 2016. Metalloproteinase production from macrophages–a perfect storm leading to atherosclerotic plaque rupture and myocardial infarction. *Experimental Physiology* 101(11), pp. 1327-1337.

Nicolosi, R. J., Wilson, T. A. and Krause, B. R. 1998. The ACAT inhibitor, CI-1011 is effective in the prevention and regression of aortic fatty streak area in hamsters. *Atherosclerosis* 137(1), pp. 77-85.

Nidorf, S. M. et al. 2020. Colchicine in patients with chronic coronary disease. *New England Journal of Medicine* 383(19), pp. 1838-1847.

Nie, J., Zhang, L., Zhao, G. and Du, X. 2019. Quercetin reduces atherosclerotic lesions by altering the gut microbiota and reducing atherogenic lipid metabolites. *Journal of Applied Microbiology* 127(6), pp. 1824-1834.

Niemann, B., Rohrbach, S., Miller, M., Newby, D., Fuster, V. and Kovacic, J. 2017. Oxidative stress and obesity, diabetes, smoking, and pollution: Part 3 of a 3-Part Series. *J Am Coll Cardiol* 70(2), pp. 230-251.

Nishizawa, T. and Bornfeldt, K. E. 2012. Diabetic vascular disease and the potential role of macrophage glucose metabolism. *Annals of Medicine* 44(6), pp. 555-563.

Nofer, J.-R. 2012. Estrogens and atherosclerosis: insights from animal models and cell systems. *Journal of Molecular Endocrinology* 48(2), pp. R13-R29.

Norata, G. D., Marchesi, P., Passamonti, S., Pirillo, A., Violi, F. and Catapano, A. L. 2007. Anti-inflammatory and anti-atherogenic effects of cathechin, caffeic acid and trans-resveratrol in apolipoprotein E deficient mice. *Atherosclerosis* 191(2), pp. 265-271.

Nowak, W. N., Deng, J., Ruan, X. Z. and Xu, Q. 2017. Reactive oxygen species generation and atherosclerosis. *Arteriosclerosis, Thrombosis, and Vascular Biology* 37(5), pp. e41-e52.

O'Morain, V. 2019. *The beneficial effects of the Lab4 probiotic consortium in atherosclerosis.* Cardiff University.

Ogura, M., Hori, M. and Harada-Shiba, M. 2016. Association between cholesterol efflux capacity and atherosclerotic cardiovascular disease in patients with familial hypercholesterolemia. *Arteriosclerosis, Thrombosis, and Vascular Biology* 36(1), pp. 181-188.

Okuda, M. et al. 2001. Expression of glutaredoxin in human coronary arteries: its potential role in antioxidant protection against atherosclerosis. *Arteriosclerosis, Thrombosis, and Vascular Biology* 21(9), pp. 1483-1487.

Olejarz, W., Łacheta, D. and Kubiak-Tomaszewska, G. 2020. Matrix metalloproteinases as biomarkers of atherosclerotic plaque instability. *International Journal of Molecular Sciences* 21(11), p. 3946.

Olivares-Marin, I. K., González-Hernández, J. C. and Madrigal-Perez, L. A. 2019. Resveratrol cytotoxicity is energy-dependent. *Journal of Food Biochemistry* 43(9), p. e13008.

Oliveira, C. H. et al. 2005. Oxidative stress in atherosclerosis-prone mouse is due to low antioxidant capacity of mitochondria. *The FASEB Journal* 19(2), pp. 1-14.

Olson, E. R., Naugle, J. E., Zhang, X., Bomser, J. A. and Meszaros, J. G. 2005. Inhibition of cardiac fibroblast proliferation and myofibroblast differentiation by resveratrol. *American Journal of Physiology-Heart and Circulatory Physiology* 288(3), pp. H1131-H1138.

Olszanecki, R. et al. 2005. Effect of curcumin on atherosclerosis in apoE/LDLR-double knockout mice. *Journal of Physiology and Pharmacology: an Official Journal of the Polish Physiological Society* 56(4), pp. 627-635.

Ong, E.-T., Hwang, T.-L., Huang, Y.-L., Lin, C.-F. and Wu, W.-B. 2011. Vitisin B, a resveratrol tetramer, inhibits migration through inhibition of PDGF signaling and enhancement of cell adhesiveness in cultured vascular smooth muscle cells. *Toxicology and Applied Pharmacology* 256(2), pp. 198-208.

Oppi, S., Lüscher, T. F. and Stein, S. 2019. Mouse models for atherosclerosis research—which is my line? *Frontiers in Cardiovascular Medicine*, p. 46.

Orekhov, A. N. et al. 2020. Role of phagocytosis in the pro-inflammatory response in LDL-induced foam cell formation; a transcriptome analysis. *International Journal of Molecular Sciences* 21(3), p. 817.

Orekhov, A. N. et al. 2019. Monocyte differentiation and macrophage polarization. *Vessel Plus* 3, p. 10.

Otsuka, F. et al. 2015. Natural progression of atherosclerosis from pathologic intimal thickening to late fibroatheroma in human coronary arteries: a pathology study. *Atherosclerosis* 241(2), pp. 772-782.

Ouimet, M. and Marcel, Y. L. 2012. Regulation of lipid droplet cholesterol efflux from macrophage foam cells. *Arteriosclerosis, Thrombosis, and Vascular Biology* 32(3), pp. 575-581.

Pahwa, S., Sharma, R. and Singh, B. 2017. Role of glutathione S-transferase in coronary artery disease patients with and without type 2 diabetes mellitus. *Journal of Clinical and Diagnostic Research: JCDR* 11(1), p. BC05.

Paik, D. T., Cho, S., Tian, L., Chang, H. Y. and Wu, J. C. 2020. Single-cell RNA sequencing in cardiovascular development, disease and medicine. *Nature Reviews Cardiology* 17(8), pp. 457-473.

Pal, P., Gandhi, H., Giridhar, R. and Yadav, M. R. 2013. ACAT inhibitors: the search for novel cholesterol lowering agents. *Mini Reviews in Medicinal Chemistry* 13(8), pp. 1195-1219.

Palacz-Wrobel, M., Borkowska, P., Paul-Samojedny, M., Kowalczyk, M., Fila-Danilow, A., Suchanek-Raif, R. and Kowalski, J. 2017. Effect of apigenin, kaempferol and resveratrol on the gene expression and protein secretion of tumor necrosis factor alpha (TNF-α) and interleukin-10 (IL-10) in RAW-264.7 macrophages. *Biomedicine & Pharmacotherapy* 93, pp. 1205-1212.

Palano, M. T. et al. 2022. When a Friend Becomes Your Enemy: Natural Killer Cells in Atherosclerosis and Atherosclerosis-Associated Risk Factors. *Frontiers in Immunology*, p. 5718.

Pallauf, K. et al. 2019. Resveratrol, lunularin and dihydroresveratrol do not act as caloric restriction mimetics when administered intraperitoneally in mice. *Scientific Reports* 9(1), pp. 1-12.

Pan, W., Yu, H., Huang, S. and Zhu, P. 2016. Resveratrol protects against TNF-α-induced injury in human umbilical endothelial cells through promoting sirtuin-1-induced repression of NF-KB and p38 MAPK. *PloS One* 11(1), p. e0147034.

Pan, Y., Zhang, H., Zheng, Y., Zhou, J., Yuan, J., Yu, Y. and Wang, J. 2017. Resveratrol exerts antioxidant effects by activating SIRT2 to deacetylate Prx1. *Biochemistry* 56(48), pp. 6325-6328.

Pandey, A. K., Bhattacharya, P., Shukla, S. C., Paul, S. and Patnaik, R. 2015. Resveratrol inhibits matrix metalloproteinases to attenuate neuronal damage in cerebral ischemia: a

molecular docking study exploring possible neuroprotection. *Neural Regeneration Research* 10(4), p. 568.

Pannu, N. and Bhatnagar, A. 2019. Resveratrol: From enhanced biosynthesis and bioavailability to multitargeting chronic diseases. *Biomedicine & Pharmacotherapy* 109, pp. 2237-2251.

Park, C.-S., Lee, Y.-C., Kim, J.-D., Kim, H.-M. and Kim, C.-H. 2004. Inhibitory effects of Polygonum cuspidatum water extract (PCWE) and its component rasveratrol on acyl-coenzyme A–cholesterol acyltransferase activity for cholesteryl ester synthesis in HepG2 cells. *Vascular Pharmacology* 40(6), pp. 279-284.

Park, D.-W., Baek, K., Kim, J.-R., Lee, J.-J., Ryu, S.-H., Chin, B.-R. and Baek, S.-H. 2009a. Resveratrol inhibits foam cell formation via NADPH oxidase 1-mediated reactive oxygen species and monocyte chemotactic protein-1. *Experimental & Molecular Medicine* 41(3), pp. 171-179.

Park, J. S., Kim, K. M., Kim, M. H., Chang, H. J., Baek, M. K., Kim, S. M. and Do Jung, Y. 2009b. Resveratrol inhibits tumor cell adhesion to endothelial cells by blocking ICAM-1 expression. *Anticancer Research* 29(1), pp. 355-362.

Park, J. Y., Lim, J.-H., Ahn, J.-H. and Kim, B.-G. 2021. Biosynthesis of resveratrol using metabolically engineered Escherichia coli. *Applied Biological Chemistry* 64(1), pp. 1-13.

Park, Y. M. 2014. CD36, a scavenger receptor implicated in atherosclerosis. *Experimental & Molecular Medicine* 46(6), pp. e99-e99.

Partida, R. A., Libby, P., Crea, F. and Jang, I.-K. 2018. Plaque erosion: a new in vivo diagnosis and a potential major shift in the management of patients with acute coronary syndromes. *European Heart Journal* 39(22), pp. 2070-2076.

Pashirzad, M., Johnston, T. P. and Sahebkar, A. 2021. Therapeutic effects of polyphenols on the treatment of colorectal cancer by regulating wnt β-catenin signaling pathway. *Journal of Oncology* 2021,

Patel, K. R. et al. 2013. Sulfate metabolites provide an intracellular pool for resveratrol generation and induce autophagy with senescence. *Science translational medicine* 5(205), pp. 205ra133-205ra133.

Patel, K. R., Scott, E., Brown, V. A., Gescher, A. J., Steward, W. P. and Brown, K. 2011. Clinical trials of resveratrol. *Annals of the New York Academy of Sciences* 1215(1), pp. 161-169.

Patterson, E., Wall, R., Fitzgerald, G., Ross, R. and Stanton, C. 2012. Health implications of high dietary omega-6 polyunsaturated fatty acids. *Journal of Nutrition and Metabolism* 2012,

Pello Lázaro, A. M., Blanco-Colio, L. M., Franco Peláez, J. A. and Tuñón, J. 2021. Anti-Inflammatory Drugs in Patients with Ischemic Heart Disease. *Journal of Clinical Medicine* 10(13), p. 2835.

Peng, W. et al. 2019. Mitochondrial dysfunction in atherosclerosis. *DNA and Cell Biology* 38(7), pp. 597-606.

Penumathsa, S. V. et al. 2007. Statin and resveratrol in combination induces cardioprotection against myocardial infarction in hypercholesterolemic rat. *Journal of Molecular and Cellular Cardiology* 42(3), pp. 508-516.

Perrotta, P. et al. 2020. Partial inhibition of glycolysis reduces atherogenesis independent of intraplaque neovascularization in mice. *Arteriosclerosis, Thrombosis, and Vascular Biology* 40(5), pp. 1168-1181.

Petryshen, T. et al. 2005. Genetic investigation of chromosome 5q GABAA receptor subunit genes in schizophrenia. *Molecular psychiatry* 10(12), pp. 1074-1088.

Petsophonsakul, P. et al. 2019. Role of vascular smooth muscle cell phenotypic switching and calcification in aortic aneurysm formation: Involvement of vitamin K-dependent processes. *Arteriosclerosis, Thrombosis, and Vascular Biology* 39(7), pp. 1351-1368.

Phillips, M. C. 2014. Molecular mechanisms of cellular cholesterol efflux. *Journal of Biological Chemistry* 289(35), pp. 24020-24029.

Piao, L., Choi, J., Kwon, G. and Ha, H. 2017. Endogenous catalase delays high-fat diet-induced liver injury in mice. *The Korean Journal of Physiology & Pharmacology* 21(3), pp. 317-325.

Pilling, D., Karhadkar, T. R. and Gomer, R. H. 2021. High-fat diet–induced adipose tissue and liver inflammation and steatosis in mice are reduced by inhibiting sialidases. *The American Journal of Pathology* 191(1), pp. 131-143.

Pinal-Fernandez, I., Casal-Dominguez, M. and Mammen, A. L. 2018. Statins: pros and cons. *Medicina Clínica (English Edition)* 150(10), pp. 398-402.

Poels, K. et al. 2020. Inhibition of PFKFB3 hampers the progression of atherosclerosis and promotes plaque stability. *Frontiers in Cell and Developmental Biology* 8, p. 581641.

Polyzos, K. and Ketelhuth, D. 2015. The role of the kynurenine pathway of tryptophan metabolism in cardiovascular disease. *Hämostaseologie* 35(02), pp. 128-136.

Poussier, B., Cordova, A. C., Becquemin, J.-P. and Sumpio, B. E. 2005. Resveratrol inhibits vascular smooth muscle cell proliferation and induces apoptosis. *Journal of Vascular Surgery* 42(6), pp. 1190-1190. e1114.

Powell-Wiley, T. M. et al. 2021. Obesity and cardiovascular disease: a scientific statement from the American Heart Association. *Circulation* 143(21), pp. e984-e1010.

Poznyak, A. V., Nikiforov, N. G., Markin, A. M., Kashirskikh, D. A., Myasoedova, V. A., Gerasimova, E. V. and Orekhov, A. N. 2021. Overview of OxLDL and its impact on cardiovascular health: focus on atherosclerosis. *Frontiers in Pharmacology*, p. 2248.

Pradhan, A., Bhandari, M. and Sethi, R. 2020. Ezetimibe and improving cardiovascular outcomes: current evidence and perspectives. *Cardiology Research and Practice* 2020,

Prasad, K. 2012. Resveratrol, wine, and atherosclerosis. *International Journal of Angiology* 21(01), pp. 007-018.

Przybyszewski, E. M., Targher, G., Roden, M. and Corey, K. E. 2021. Nonalcoholic fatty liver disease and cardiovascular disease. *Clinical Liver Disease* 17(1), pp. 19-22.

Pshenichnyuk, S. A. and Komolov, A. S. 2015. Dissociative electron attachment to resveratrol as a likely pathway for generation of the H2 antioxidant species inside mitochondria. *The Journal of Physical Chemistry Letters* 6(7), pp. 1104-1110.

Puri, R. et al. 2013. C-reactive protein, but not low-density lipoprotein cholesterol levels, associate with coronary atheroma regression and cardiovascular events after maximally intensive statin therapy. *Circulation* 128(22), pp. 2395-2403.

Qiao, Y., Sun, J., Xia, S., Tang, X., Shi, Y. and Le, G. 2014. Effects of resveratrol on gut microbiota and fat storage in a mouse model with high-fat-induced obesity. *Food & Function* 5(6), pp. 1241-1249.

Qin, Z. 2012. The use of THP-1 cells as a model for mimicking the function and regulation of monocytes and macrophages in the vasculature. *Atherosclerosis* 221(1), pp. 2-11.

Rafieian-Kopaei, M., Setorki, M., Doudi, M., Baradaran, A. and Nasri, H. 2014. Atherosclerosis: process, indicators, risk factors and new hopes. *International journal of preventive medicine* 5(8), p. 927.

Rajamani, K. and Fisher, M. 2017. An overview of atherosclerosis. *Primer on Cerebrovascular Diseases*, pp. 105-108.

Ramji, D. P. and Davies, T. S. 2015. Cytokines in atherosclerosis: Key players in all stages of disease and promising therapeutic targets. *Cytokine & growth factor reviews* 26(6), pp. 673-685.

Ramkumar, S., Raghunath, A. and Raghunath, S. 2016. Statin therapy: review of safety and potential side effects. *Acta Cardiologica Sinica* 32(6), p. 631.

Raniolo, S., Vindigni, G. and Biocca, S. 2016. Cholesterol level regulates lectin-like oxidized low-density lipoprotein receptor-1 function. *Biomedical Spectroscopy and Imaging* 5(s1), pp. S87-S99.

Rask-Madsen, C. and King, G. L. 2013. Vascular complications of diabetes: mechanisms of injury and protective factors. *Cell Metabolism* 17(1), pp. 20-33.

Rattazzi, M. et al. 2005. Calcification of advanced atherosclerotic lesions in the innominate arteries of ApoE-deficient mice: potential role of chondrocyte-like cells. *Arteriosclerosis, Thrombosis, and Vascular Biology* 25(7), pp. 1420-1425.

Reardon, C. A. et al. 2001. Effect of immune deficiency on lipoproteins and atherosclerosis in male apolipoprotein E–deficient mice. *Arteriosclerosis, Thrombosis, and Vascular Biology* 21(6), pp. 1011-1016.

Relucenti, M., Heyn, R., Petruzziello, L., Pugliese, G., Taurino, M. and Familiari, G. 2010. Detecting microcalcifications in atherosclerotic plaques by a simple trichromic staining method for epoxy embedded carotid endarterectomies. *European Journal of Histochemistry: EJH* 54(3),

Remmerie, A. and Scott, C. L. 2018. Macrophages and lipid metabolism. *Cellular Immunology* 330, pp. 27-42.

Riazi, K. et al. 2022. The prevalence and incidence of NAFLD worldwide: a systematic review and meta-analysis. *The Lancet Gastroenterology & Hepatology*,

Riba, A., Deres, L., Sumegi, B., Toth, K., Szabados, E. and Halmosi, R. 2017. Cardioprotective effect of resveratrol in a postinfarction heart failure model. *Oxidative Medicine and Cellular Longevity* 2017,

Richards, L. B., Li, M., van Esch, B. C., Garssen, J. and Folkerts, G. 2016. The effects of short-chain fatty acids on the cardiovascular system. *PharmaNutrition* 4(2), pp. 68-111.

Ridker, P. M. 2017. How common is residual inflammatory risk? *Circulation research* 120(4), pp. 617-619.

Ridker, P. M. et al. 2019. Low-dose methotrexate for the prevention of atherosclerotic events. *New England Journal of Medicine* 380(8), pp. 752-762.

Ridker, P. M. et al. 2017. Antiinflammatory therapy with canakinumab for atherosclerotic disease. *New England Journal of Medicine* 377(12), pp. 1119-1131.

Ridker, P. M. et al. 2018. Modulation of the interleukin-6 signalling pathway and incidence rates of atherosclerotic events and all-cause mortality: analyses from the Canakinumab Anti-Inflammatory Thrombosis Outcomes Study (CANTOS). *European Heart Journal* 39(38), pp. 3499-3507.

Riggs, K. A. and Rohatgi, A. 2019. High-Density Lipoprotein and High-Density Lipoprotein Cholesterol.*Biomarkers in Cardiovascular Disease*. Elsevier, pp. 61-69.

Rimmelé, P., Lofek-Czubek, S. and Ghaffari, S. 2014. Resveratrol increases the bone marrow hematopoietic stem and progenitor cell capacity. *American Journal of Hematology* 89(12), pp. E235-E238.

Rivera, J. et al. 2013. Accumulation of serum lipids by vascular smooth muscle cells involves a macropinocytosis-like uptake pathway and is associated with the downregulation of the ATP-binding cassette transporter A1. *Naunyn-Schmiedeberg's archives of pharmacology* 386(12), pp. 1081-1093.

Rivera, L., Morón, R., Zarzuelo, A. and Galisteo, M. 2009. Long-term resveratrol administration reduces metabolic disturbances and lowers blood pressure in obese Zucker rats. *Biochemical Pharmacology* 77(6), pp. 1053-1063.

Robbins, C. S. et al. 2012. Extramedullary hematopoiesis generates Ly-6Chigh monocytes that infiltrate atherosclerotic lesions. *Circulation* 125(2), pp. 364-374.

Robichaud, S. et al. 2021. Identification of novel lipid droplet factors that regulate lipophagy and cholesterol efflux in macrophage foam cells. *Autophagy* 17(11), pp. 3671-3689.

Rocha, K., Souza, G., Ebaid, G. X., Seiva, F., Cataneo, A. and Novelli, E. 2009. Resveratrol toxicity: effects on risk factors for atherosclerosis and hepatic oxidative stress in standard and high-fat diets. *Food and Chemical Toxicology* 47(6), pp. 1362-1367.

Rodgers, J. L. et al. 2019. Cardiovascular risks associated with gender and aging. *Journal of Cardiovascular Development and Disease* 6(2), p. 19.

Roh, J. S. and Sohn, D. H. 2018. Damage-associated molecular patterns in inflammatory diseases. *Immune Network* 18(4),

Rohwedder, I. et al. 2012. Plasma fibronectin deficiency impedes atherosclerosis progression and fibrous cap formation. *EMBO Molecular Medicine* 4(7), pp. 564-576.

Roth, C. L., Molica, F. and Kwak, B. R. 2021. Browning of white adipose tissue as a therapeutic tool in the fight against atherosclerosis. *Metabolites* 11(5), p. 319.

Ru, Y.-X., Shang, H.-C., Dong, S.-X., Zhao, S.-X., Liang, H.-Y. and Zhu, C.-J. 2020. Foam cell origination from degenerated vascular smooth muscle cells in atherosclerosis: An ultrastructural study on hyperlipidemic rabbits. *Ultrastructural Pathology* 44(1), pp. 103-115.

Rubiolo, J. A., Mithieux, G. and Vega, F. V. 2008. Resveratrol protects primary rat hepatocytes against oxidative stress damage:: Activation of the Nrf2 transcription factor and augmented activities of antioxidant enzymes. *European Journal of Pharmacology* 591(1-3), pp. 66-72.

Ruchi, S., Amanjot, K., Sourav, T., Keerti, B. and Sujit, B. 2017. Role of nutraceuticals in health care: A review. *Int. J. Green Pharm* 11(03),

Rudijanto, A. 2007. The role of vascular smooth muscle cells on the pathogenesis of atherosclerosis. *Acta Med Indones* 39(2), pp. 86-93.

Russo, M. W. and Jacobson, I. M. 2004. How to use statins in patients with chronic liver disease. *Cleveland Clinic Journal of Medicine* 71(1), pp. 58-62.

Saferali, A., Tang, A. C., Strug, L. J., Quon, B. S., Zlosnik, J., Sandford, A. J. and Turvey, S. E. 2020. Immunomodulatory function of the cystic fibrosis modifier gene BPIFA1. *PloS One* 15(1), p. e0227067.

Saha, A. and Garg, A. 2021. Severe Liver Injury Associated With High-Dose Atorvastatin Therapy. *Journal of Investigative Medicine High Impact Case Reports* 9, p. 23247096211014050.

Saito, R. et al. 2011. Macrophage Elovl6 deficiency ameliorates foam cell formation and reduces atherosclerosis in low-density lipoprotein receptor-deficient mice. *Arteriosclerosis, Thrombosis, and Vascular Biology* 31(9), pp. 1973-1979.

Saleh, H. A., Ramdan, E., Elmazar, M. M., Azzazy, H. M. and Abdelnaser, A. 2021. Comparing the protective effects of resveratrol, curcumin and sulforaphane against LPS/IFN-γ-mediated inflammation in doxorubicin-treated macrophages. *Scientific Reports* 11(1), pp. 1-16.

Salehi, B. et al. 2018. Resveratrol: A double-edged sword in health benefits. *Biomedicines* 6(3), p. 91.

San Cheang, W. et al. 2019. Resveratrol ameliorates endothelial dysfunction in diabetic and obese mice through sirtuin 1 and peroxisome proliferator-activated receptor δ. *Pharmacological Research* 139, pp. 384-394.

Sanda, G. M., Stancu, C. S., Deleanu, M., Toma, L., Niculescu, L. S. and Sima, A. V. 2021. Aggregated LDL turn human macrophages into foam cells and induce mitochondrial dysfunction without triggering oxidative or endoplasmic reticulum stress. *PloS One* 16(1), p. e0245797.

Sangle, G. V. and Shen, G. X. 2010. Signaling mechanisms for oxidized LDL-induced oxidative stress and the upregulation of plasminogen activator inhibitor-I in vascular cells. *Clinical Lipidology* 5(2), pp. 221-232.

Sankaralingam, S. et al. 2015. Lowering body weight in obese mice with diastolic heart failure improves cardiac insulin sensitivity and function: implications for the obesity paradox. *Diabetes* 64(5), pp. 1643-1657.

Sarrazy, V. et al. 2016. Disruption of Glut1 in hematopoietic stem cells prevents myelopoiesis and enhanced glucose flux in atheromatous plaques of ApoE−/− mice. *Circulation research* 118(7), pp. 1062-1077.

Sattar, N., Forrest, E. and Preiss, D. 2014. Non-alcoholic fatty liver disease. *BMJ* 349,

Schäfer, S. and Zernecke, A. 2020. CD8+ T cells in atherosclerosis. *Cells* 10(1), p. 37.

Schiller, N. K., Boisvert, W. A. and Curtiss, L. K. 2002. Inflammation in Atherosclerosis: Lesion Formation in LDL Receptor–Deficient Mice With Perforin and Lyst beige Mutations. *Arteriosclerosis, Thrombosis, and Vascular Biology* 22(8), pp. 1341-1346.

Schlieper, G. et al. 2010. Ultrastructural analysis of vascular calcifications in uremia. *Journal of the American Society of Nephrology* 21(4), pp. 689-696.

Schmidt, A. F. et al. 2021. Cholesteryl ester transfer protein (CETP) as a drug target for cardiovascular disease. *Nature Communications* 12(1), pp. 1-10.

Schmitt, M. M. et al. 2014. Endothelial junctional adhesion molecule-a guides monocytes into flow-dependent predilection sites of atherosclerosis. *Circulation* 129(1), pp. 66-76.

Schnoor, M., Alcaide, P., Voisin, M.-B. and van Buul, J. D. 2015. Crossing the vascular wall: common and unique mechanisms exploited by different leukocyte subsets during extravasation. *Mediators of Inflammation* 2015,

Schrauwen, P. and Westerterp, K. R. 2000. The role of high-fat diets and physical activity in the regulation of body weight. *British Journal of Nutrition* 84(4), pp. 417-427.

Schrijvers, D. M., De Meyer, G. R., Herman, A. G. and Martinet, W. 2007. Phagocytosis in atherosclerosis: Molecular mechanisms and implications for plaque progression and stability. *Cardiovascular Research* 73(3), pp. 470-480.

Schrottmaier, W. C., Mussbacher, M., Salzmann, M. and Assinger, A. 2020. Platelet-leukocyte interplay during vascular disease. *Atherosclerosis* 307, pp. 109-120.

Seita, J. and Weissman, I. L. 2010. Hematopoietic stem cell: self-renewal versus differentiation. *Wiley Interdisciplinary Reviews: Systems Biology and Medicine* 2(6), pp. 640-653.

Selathurai, A., Deswaerte, V., Kanellakis, P., Tipping, P., Toh, B.-H., Bobik, A. and Kyaw, T. 2014. Natural killer (NK) cells augment atherosclerosis by cytotoxic-dependent mechanisms. *Cardiovascular Research* 102(1), pp. 128-137.

Sena, C. M., Leandro, A., Azul, L., Seica, R. and Perry, G. 2018. Vascular oxidative stress: impact and therapeutic approaches. *Frontiers in Physiology*, p. 1668.

Seo, Y. et al. 2019. Antiatherogenic effect of resveratrol attributed to decreased expression of ICAM-1 (Intercellular adhesion Molecule-1) mechanistic link from focal adhesion to monocyte adhesion. *Arteriosclerosis, Thrombosis, and Vascular Biology* 39(4), pp. 675-684.

Sevov, M., Elfineh, L. and Cavelier, L. B. 2006. Resveratrol regulates the expression of LXR-α in human macrophages. *Biochemical and Biophysical Research Communications* 348(3), pp. 1047-1054.

Shabani, M., Sadeghi, A., Hosseini, H., Teimouri, M., Babaei Khorzoughi, R., Pasalar, P. and Meshkani, R. 2020. Resveratrol alleviates obesity-induced skeletal muscle inflammation via decreasing M1 macrophage polarization and increasing the regulatory T cell population. *Scientific Reports* 10(1), pp. 1-13.

Shah, P. K. 2019. Inflammation, infection and atherosclerosis. *Trends in Cardiovascular Medicine* 29(8), pp. 468-472.

Shang, J., Chen, L.-l., Xiao, F.-x., Sun, H., Ding, H.-c. and Xiao, H. 2008. Resveratrol improves non-alcoholic fatty liver disease by activating AMP-activated protein kinase. *Acta Pharmacologica Sinica* 29(6), pp. 698-706.

Shemiakova, T., Ivanova, E., Grechko, A. V., Gerasimova, E. V., Sobenin, I. A. and Orekhov, A. N. 2020. Mitochondrial dysfunction and DNA damage in the context of pathogenesis of atherosclerosis. *Biomedicines* 8(6), p. 166.

Shen, X., Zhang, S., Guo, Z., Xing, D. and Chen, W. 2020. The crosstalk of ABCA1 and ANXA1: A potential mechanism for protection against atherosclerosis. *Molecular Medicine* 26(1), p. 84.

Shi, G., Hua, M., Xu, Q. and Ren, T. 2017. Resveratrol improves treatment outcome and laboratory parameters in patients with Takayasu arteritis: A randomized double-blind and placebo-controlled trial. *Immunobiology* 222(2), pp. 164-168.

Shirai, T., Hilhorst, M., Harrison, D. G., Goronzy, J. J. and Weyand, C. M. 2015. Macrophages in vascular inflammation–from atherosclerosis to vasculitis. *Autoimmunity* 48(3), pp. 139-151.

Shu, M. et al. 2022. Single-cell RNA sequencing reveals Nestin+ active neural stem cells outside the central canal after spinal cord injury. *Science China Life Sciences* 65(2), pp. 295-308.

Sikder, K., Shukla, S. K., Patel, N., Singh, H. and Rafiq, K. 2018. High fat diet upregulates fatty acid oxidation and ketogenesis via intervention of PPAR-γ. *Cellular Physiology and Biochemistry* 48(3), pp. 1317-1331.

Simental-Mendía, L. E. and Guerrero-Romero, F. 2019. Effect of resveratrol supplementation on lipid profile in subjects with dyslipidemia: A randomized double-blind, placebo-controlled trial. *Nutrition* 58, pp. 7-10.

Simon, T. G. et al. 2018. Circulating Interleukin-6 is a biomarker for coronary atherosclerosis in nonalcoholic fatty liver disease: Results from the Multi-Ethnic Study of Atherosclerosis. *International Journal of Cardiology* 259, pp. 198-204.

Singer, K. et al. 2014. Diet-induced obesity promotes myelopoiesis in hematopoietic stem cells. *Molecular Metabolism* 3(6), pp. 664-675.

Sirol, M. 2005. Atherosclerosis plaque imaging and characterization using magnetic resonance imaging. *US Cardiology* 2, pp. 129-132.

Smoliga, J. M. and Blanchard, O. 2014. Enhancing the delivery of resveratrol in humans: if low bioavailability is the problem, what is the solution? *Molecules* 19(11), pp. 17154-17172.

Snarski, P. et al. 2022. Macrophage-Specific IGF-1 Overexpression Reduces CXCL12 Chemokine Levels and Suppresses Atherosclerotic Burden in Apoe-Deficient Mice. *Arteriosclerosis, Thrombosis, and Vascular Biology* 42(2), pp. 113-126.

Sobenin, I. A., Andrianova, I. V., Lakunin, K. Y., Karagodin, V. P., Bobryshev, Y. V. and Orekhov, A. N. 2016. Anti-atherosclerotic effects of garlic preparation in freeze injury model of atherosclerosis in cholesterol-fed rabbits. *Phytomedicine* 23(11), pp. 1235-1239.

Solanki, S., Dube, P. R., Birnbaumer, L. and Vazquez, G. 2017. Reduced necrosis and content of apoptotic M1 macrophages in advanced atherosclerotic plaques of mice with macrophage-specific loss of Trpc3. *Scientific Reports* 7(1), pp. 1-11.

Song, L., Leung, C. and Schindler, C. 2001. Lymphocytes are important in early atherosclerosis. *The Journal of Clinical Investigation* 108(2), pp. 251-259.

Song, R. et al. 2013. Resveratrol reduces inflammatory cytokines via inhibiting nuclear factor-κB and mitogen-activated protein kinase signal pathway in a rabbit atherosclerosis model. *Zhonghua Xin Xue Guan Bing Za Zhi* 41(10), pp. 866-869.

Sorokin, V., Vickneson, K., Kofidis, T., Woo, C. C., Lin, X. Y., Foo, R. and Shanahan, C. M. 2020. Role of vascular smooth muscle cell plasticity and interactions in vessel wall inflammation. *Frontiers in Immunology* 11, p. 599415.

Springer, M. and Moco, S. 2019. Resveratrol and its human metabolites—Effects on metabolic health and obesity. *Nutrients* 11(1), p. 143.

Srivastava, D. 2006. Genetic regulation of cardiogenesis and congenital heart disease. *Annual Review of Patholog* 1, p. 199.

Srivastava, S. 2016. Emerging therapeutic roles for NAD+ metabolism in mitochondrial and age-related disorders. *Clinical and Translational Medicine* 5(1), pp. 1-11.

Stacchiotti, A., Favero, G. and Rezzani, R. 2018. Resveratrol and SIRT1 activators for the treatment of aging and age-related diseases. *IntechOpen*,

Stephen, S. L. et al. 2010. Scavenger receptors and their potential as therapeutic targets in the treatment of cardiovascular disease. *International Journal of Hypertension* 2010,

Stewart, C. R. et al. 2010. CD36 ligands promote sterile inflammation through assembly of a Toll-like receptor 4 and 6 heterodimer. *Nature Immunology* 11(2), pp. 155-161.

Stoekenbroek, R. M., Kallend, D., Wijngaard, P. L. and Kastelein, J. J. 2018. Inclisiran for the treatment of cardiovascular disease: the ORION clinical development program. *Future Cardiology* 14(6), pp. 433-442.

Stokes, K. Y., Clanton, E. C., Clements, K. P. and Granger, D. N. 2003. Role of interferon-γ in hypercholesterolemia-induced leukocyte–endothelial cell adhesion. *Circulation* 107(16), pp. 2140-2145.

Subramanian, S. et al. 2011. Dietary cholesterol exacerbates hepatic steatosis and inflammation in obese LDL receptor-deficient mice. *Journal of Lipid Research* 52(9), pp. 1626-1635.

Sukhorukov, V. N., Khotina, V. A., Chegodaev, Y. S., Ivanova, E., Sobenin, I. A. and Orekhov, A. N. 2020. Lipid metabolism in macrophages: focus on atherosclerosis. *Biomedicines* 8(8), p. 262.

Sukhovershin, R. A., Furman, N. E. T., Tasciotti, E. and Trachtenberg, B. H. 2016. Local inhibition of macrophage and smooth muscle cell proliferation to suppress plaque progression. *Methodist DeBakey cardiovascular journal* 12(3), p. 141.

Sun, C. y., Hu, Y., Guo, T., WANG, H. f., ZHANG, X. p., HE, W. j. and Tan, H. 2006. Resveratrol as a novel agent for treatment of multiple myeloma with matrix metalloproteinase inhibitory activity. *Acta Pharmacologica Sinica* 27(11), pp. 1447-1452.

Sun, H.-J. et al. 2016. Salusin-β induces foam cell formation and monocyte adhesion in human vascular smooth muscle cells via miR155/NOX2/NFκB pathway. *Scientific Reports* 6(1), pp. 1-12.

Sun, K., Eriksson, S. E., Tan, Y., Zhang, L., Arnér, E. S. and Zhang, J. 2014. Serum thioredoxin reductase levels increase in response to chemically induced acute liver injury. *Biochimica et Biophysica Acta (BBA)-General Subjects* 1840(7), pp. 2105-2111.

Sun, K.-j., Liu, L.-l., Hu, J.-h., Chen, Y.-y. and Xu, D.-y. 2021. Methotrexate can prevent cardiovascular events in patients with rheumatoid arthritis: An updated meta-analysis. *Medicine* 100(7),

Sun, S. et al. 2017. Resveratrol suppresses lipoprotein-associated phospholipase A2 expression by reducing oxidative stress in macrophages and animal models. *Molecular Nutrition & Food Research* 61(10), p. 1601112.

Sung, M. M. et al. 2015. Resveratrol treatment of mice with pressure-overload–induced heart failure improves diastolic function and cardiac energy metabolism. *Circulation: Heart Failure* 8(1), pp. 128-137.

Sung, M. M. and Dyck, J. R. 2015. Therapeutic potential of resveratrol in heart failure. *Annals of the New York Academy of Sciences* 1348(1), pp. 32-45.

Susanti, E., Ratnawati, R. and Aulanni'am Aulanni'am, A. R. 2019. Catechins green tea upregulates the expression of ABCA1, ABCG1, and SRB1 in rats induced atherogenic diet. *Journal of Applied Pharmaceutical Science* 9(03), pp. 091-097.

Susser, L. I. and Rayner, K. J. 2022. Through the layers: how macrophages drive atherosclerosis across the vessel wall. *Journal of Clinical Investigation* 132(9), p. e157011.

Sutriyo, D. A. P. 2019. The Chemical Stability, Anticancer Activity, Metabolism, And Delivery Systems of Resveratrol: A Review, 2019. *International Journal of Current Research in Life Sciences* 8(04), pp. 3056-3061.

Swanson, J. and Silverstein, S. C. 1988. Pinocytic flow through macrophages. *Processing and Presentation of Antigens*, pp. 15-27.

Swirski, F. K., Libby, P., Aikawa, E., Alcaide, P., Luscinskas, F. W., Weissleder, R. and Pittet, M. J. 2007. Ly-6C hi monocytes dominate hypercholesterolemia-associated monocytosis and give rise to macrophages in atheromata. *The Journal of Clinical Investigation* 117(1), pp. 195-205.

Szeto, F. L. et al. 2012. Vitamin D receptor signaling inhibits atherosclerosis in mice. *Molecular Endocrinology* 26(7), pp. 1091-1101.

Tacke, F. et al. 2007. Monocyte subsets differentially employ CCR2, CCR5, and CX3CR1 to accumulate within atherosclerotic plaques. *The Journal of Clinical Investigation* 117(1), pp. 185-194.

Tahir, S. and Steffens, S. 2021. Nonclassical monocytes in cardiovascular physiology and disease. *American Journal of Physiology-Cell Physiology* 320(5), pp. C761-C770.

Tajbakhsh, A., Kovanen, P. T., Rezaee, M., Banach, M., Moallem, S. A. and Sahebkar, A. 2020. Regulation of efferocytosis by caspase-dependent apoptotic cell death in atherosclerosis. *The International Journal of Biochemistry & Cell Biology* 120, p. 105684.

Takashima, A. et al. 2016. Combination of n-3 polyunsaturated fatty acids reduces atherogenesis in apolipoprotein E-deficient mice by inhibiting macrophage activation. *Atherosclerosis* 254, pp. 142-150.

Takeuchi, O. and Akira, S. 2010. Pattern recognition receptors and inflammation. *Cell* 140(6), pp. 805-820.

Tall, A. R. and Rader, D. J. 2018. Trials and tribulations of CETP inhibitors. *Circulation research* 122(1), pp. 106-112.

Tall, A. R. and Yvan-Charvet, L. 2015. Cholesterol, inflammation and innate immunity. *Nature Reviews Immunology* 15(2), pp. 104-116.

Tang, K., Wang, F., Zeng, Y., Chen, X. and Xu, X. 2018. Salusin-α attenuates hepatic steatosis and atherosclerosis in high fat diet-fed low density lipoprotein receptor deficient mice. *European Journal of Pharmacology* 830, pp. 76-86.

Tang, L. Y., Chen, Y., Rui, B. B. and Hu, C. M. 2016. Resveratrol ameliorates lipid accumulation in HepG2 cells, associated with down-regulation of lipin1 expression. *Canadian Journal of Physiology and Pharmacology* 94(2), pp. 185-189.

Tang, X. et al. 2022. Clinical outcome of non-alcoholic fatty liver disease: an 11-year follow-up study. *BMJ Open* 12(6), p. e054891.

Tanizawa, S., Ueda, M., van der Loos, C. M., van der Wal, A. C. and Becker, A. E. 1996. Expression of platelet derived growth factor B chain and beta receptor in human coronary arteries after percutaneous transluminal coronary angioplasty: an immunohistochemical study. *Heart* 75(6), pp. 549-556.

Tao, R., Xiong, X., DePinho, R. A., Deng, C.-X. and Dong, X. C. 2013. FoxO3 transcription factor and Sirt6 deacetylase regulate low density lipoprotein (LDL)-cholesterol homeostasis via control of the proprotein convertase subtilisin/kexin type 9 (Pcsk9) gene expression. *Journal of Biological Chemistry* 288(41), pp. 29252-29259.

Targher, G., Byrne, C. D. and Tilg, H. 2020. NAFLD and increased risk of cardiovascular disease: clinical associations, pathophysiological mechanisms and pharmacological implications. *Gut* 69(9), pp. 1691-1705.

Taylor, P. 2017. *CETP inhibitor class finally dies as Merck abandons anacetrapib*. The PMLiVE website. Available at: https://www.pmlive.com/pharma_news/cetp_inhibitor_class_finally_dies_as_merck_abandons_anacetrapib_1208239 [Accessed: March 2022].

Tedgui, A. and Mallat, Z. 2006. Cytokines in atherosclerosis: pathogenic and regulatory pathways. *Physiological reviews* 86(2), pp. 515-581.

Teimouri, M., Homayouni-Tabrizi, M., Rajabian, A., Amiri, H. and Hosseini, H. 2022. Anti-inflammatory effects of resveratrol in patients with cardiovascular disease: A systematic review and meta-analysis of randomized controlled trials. *Complementary Therapies in Medicine*, p. 102863.

Thapa, S. B., Pandey, R. P., Park, Y. I. and Sohng, J. K. 2019. Biotechnological advances in resveratrol production and its chemical diversity. *Molecules* 24(14), p. 2571.

Theodotou, M., Fokianos, K., Mouzouridou, A., Konstantinou, C., Aristotelous, A., Prodromou, D. and Chrysikou, A. 2017. The effect of resveratrol on hypertension: A clinical trial. *Experimental and Therapeutic Medicine* 13(1), pp. 295-301.

Thomas, C., Leleu, D. and Masson, D. 2022. Cholesterol and HIF-1α: dangerous liaisons in atherosclerosis. *Frontiers in Immunology*, p. 1183.

Thongtang, N., Diffenderfer, M. R., Ooi, E. M., Asztalos, B. F., Dolnikowski, G. G., Lamon-Fava, S. and Schaefer, E. J. 2013. Effects of atorvastatin on human C-reactive protein metabolism. *Atherosclerosis* 226(2), pp. 466-470.

Tian, K., Xu, Y., Sahebkar, A. and Xu, S. 2020. CD36 in atherosclerosis: pathophysiological mechanisms and therapeutic implications. *Current Atherosclerosis Reports* 22(10), pp. 1-10.

Tian, X. Y., Ma, S., Tse, G., Wong, W. T. and Huang, Y. 2018. Uncoupling protein 2 in cardiovascular health and disease. *Frontiers in Physiology* 9, p. 1060.

Tian, Y., Ma, J., Wang, W., Zhang, L., Xu, J., Wang, K. and Li, D. 2016. Resveratrol supplement inhibited the NF-κB inflammation pathway through activating AMPKα-SIRT1 pathway in mice with fatty liver. *Molecular and Cellular Biochemistry* 422(1), pp. 75-84.

Timmers, S. et al. 2011. Calorie restriction-like effects of 30 days of resveratrol supplementation on energy metabolism and metabolic profile in obese humans. *Cell Metabolism* 14(5), pp. 612-622.

Tirichen, H., Yaigoub, H., Xu, W., Wu, C., Li, R. and Li, Y. 2021. Mitochondrial reactive oxygen species and their contribution in chronic kidney disease progression through oxidative stress. *Frontiers in Physiology*, p. 398.

Tomé-Carneiro, J. et al. 2013. One-year supplementation with a grape extract containing resveratrol modulates inflammatory-related microRNAs and cytokines expression in peripheral blood mononuclear cells of type 2 diabetes and hypertensive patients with coronary artery disease. *Pharmacological Research* 72, pp. 69-82.

Tong, D.-l. et al. 2019. The critical role of ASD-related gene CNTNAP3 in regulating synaptic development and social behavior in mice. *Neurobiology of Disease* 130, p. 104486.

Tousoulis, D., Oikonomou, E., Economou, E. K., Crea, F. and Kaski, J. C. 2016. Inflammatory cytokines in atherosclerosis: current therapeutic approaches. *European Heart Journal* 37(22), pp. 1723-1732.

Townsend, K. L., Lorenzi, M. M. and Widmaier, E. P. 2008. High-fat diet-induced changes in body mass and hypothalamic gene expression in wild-type and leptin-deficient mice. *Endocrine* 33(2), pp. 176-188.

Trigatti, B., Rigotti, A. and Krieger, M. 2000a. The role of the high-density lipoprotein receptor SR-BI in cholesterol metabolism. *Current Opinion in Lipidology* 11(2), pp. 123-131.

Trigatti, B. L., Rigotti, A. and Braun, A. 2000b. Cellular and physiological roles of SR-BI, a lipoprotein receptor which mediates selective lipid uptake. *Biochimica et Biophysica Acta (BBA)-Molecular and Cell Biology of Lipids* 1529(1-3), pp. 276-286.

Truong, V. L., Jun, M. and Jeong, W. S. 2018. Role of resveratrol in regulation of cellular defense systems against oxidative stress. *Biofactors* 44(1), pp. 36-49.

Tse, K., Tse, H., Sidney, J., Sette, A. and Ley, K. 2013. T cells in atherosclerosis. *International Immunology* 25(11), pp. 615-622.

Tsuru, H., Osaka, M., Hiraoka, Y. and Yoshida, M. 2020. HFD-induced hepatic lipid accumulation and inflammation are decreased in Factor D deficient mouse. *Scientific Reports* 10(1), pp. 1-10.

Tufekci, K. U., Eltutan, B. I., Isci, K. B. and Genc, S. 2021. Resveratrol Inhibits NLRP3 Inflammasome-Induced Pyroptosis and miR-155 Expression in Microglia Through Sirt1/AMPK Pathway. *Neurotoxicity Research* 39(6), pp. 1812-1829.

Urpí-Sardà, M., Jáuregui, O., Lamuela-Raventós, R. M., Jaeger, W., Miksits, M., Covas, M.-I. and Andres-Lacueva, C. 2005. Uptake of diet resveratrol into the human low-density lipoprotein. Identification and quantification of resveratrol metabolites by liquid chromatography coupled with tandem mass spectrometry. *Analytical Chemistry* 77(10), pp. 3149-3155.

Van der Heijden, T. et al. 2017. NLRP3 inflammasome inhibition by MCC950 reduces atherosclerotic lesion development in apolipoprotein E–deficient mice—brief report. *Arteriosclerosis, Thrombosis, and Vascular Biology* 37(8), pp. 1457-1461.

Van der Valk, F. M. et al. 2017. Increased haematopoietic activity in patients with atherosclerosis. *European Heart Journal* 38(6), pp. 425-432.

Van der Vorst, E. P., Keijbeck, A. A., de Winther, M. P. and Donners, M. M. 2012. A disintegrin and metalloproteases: molecular scissors in angiogenesis, inflammation and atherosclerosis. *Atherosclerosis* 224(2), pp. 302-308.

Van Gaal, L. F., Mertens, I. L. and De Block, C. E. 2006. Mechanisms linking obesity with cardiovascular disease. *Nature* 444(7121), pp. 875-880.

Van Vré, E. A., Ait-Oufella, H., Tedgui, A. and Mallat, Z. 2012. Apoptotic cell death and efferocytosis in atherosclerosis. *Arteriosclerosis, Thrombosis, and Vascular Biology* 32(4), pp. 887-893.

Vanhie, J. J., Ngu, M. and De Lisio, M. 2020. Recent advances in understanding the role of high fat diets and their components on hematopoiesis and the hematopoietic stem cell niche. *Current Opinion in Food Science* 34, pp. 30-37.

Vasamsetti, S. B., Karnewar, S., Gopoju, R., Gollavilli, P. N., Narra, S. R., Kumar, J. M. and Kotamraju, S. 2016. Resveratrol attenuates monocyte-to-macrophage differentiation and associated inflammation via modulation of intracellular GSH homeostasis: Relevance in atherosclerosis. *Free Radical Biology and Medicine* 96, pp. 392-405.

Venkatesan, B. et al. 2008. Resveratrol inhibits PDGF receptor mitogenic signaling in mesangial cells: role of PTP1B. *The FASEB Journal* 22(10), pp. 3469-3482.

Veseli, B. E., Perrotta, P., De Meyer, G. R., Roth, L., Van der Donckt, C., Martinet, W. and De Meyer, G. R. 2017. Animal models of atherosclerosis. *European Journal of Pharmacology* 816, pp. 3-13.

Viola, A., Munari, F., Sánchez-Rodríguez, R., Scolaro, T. and Castegna, A. 2019. The metabolic signature of macrophage responses. *Frontiers in Immunology* 10, p. 1462.

Volobueva, A., Zhang, D., Grechko, A. V. and Orekhov, A. N. 2018. Foam cell formation and cholesterol trafficking and metabolism disturbances in atherosclerosis. *Cor et Vasa*,

Voloshyna, I., Hai, O., Littlefield, M. J., Carsons, S. and Reiss, A. B. 2013. Resveratrol mediates anti-atherogenic effects on cholesterol flux in human macrophages and endothelium via PPARγ and adenosine. *European Journal of Pharmacology* 698(1-3), pp. 299-309.

Von Scheidt, M. et al. 2017. Applications and limitations of mouse models for understanding human atherosclerosis. *Cell Metabolism* 25(2), pp. 248-261.

Wakabayashi, I. and Takeda, Y. 2013. Inhibitory effects of resveratrol on MCP-1, IL-6, and IL-8 production in human coronary artery smooth muscle cells. *Naunyn-Schmiedeberg's archives of pharmacology* 386(9), pp. 835-839.

Walle, T. 2011. Bioavailability of resveratrol. *Annals of the New York Academy of Sciences* 1215(1), pp. 9-15.

Walle, T., Hsieh, F., DeLegge, M. H., Oatis, J. E. and Walle, U. K. 2004. High absorption but very low bioavailability of oral resveratrol in humans. *Drug Metabolism and Disposition* 32(12), pp. 1377-1382.

Wallerath, T., Deckert, G., Ternes, T., Anderson, H., Li, H., Witte, K. and Förstermann, U. 2002. Resveratrol, a polyphenolic phytoalexin present in red wine, enhances expression and activity of endothelial nitric oxide synthase. *Circulation* 106(13), pp. 1652-1658.

Wan, Q., Yang, M., Liu, Z. and Wu, J. 2021. Atmospheric fine particulate matter exposure exacerbates atherosclerosis in apolipoprotein E knockout mice by inhibiting autophagy in macrophages via the PI3K/Akt/mTOR signaling pathway. *Ecotoxicology and Environmental Safety* 208, p. 111440.

Wang, B. et al. 2020a. Resveratrol attenuates TLR-4 mediated inflammation and elicits therapeutic potential in models of sepsis. *Scientific Reports* 10(1), pp. 1-17.

Wang, D. et al. 2019a. Targeting foam cell formation in atherosclerosis: therapeutic potential of natural products. *Pharmacological reviews* 71(4), pp. 596-670.

Wang, K. et al. 2020b. Resveratrol attenuates aortic dissection by increasing endothelial barrier function through the SIRT1 pathway. *Journal of Cardiovascular Pharmacology* 76(1), p. 86.

Wang, L. et al. 2013. Dickkopf-1 as a novel predictor is associated with risk stratification by GRACE risk scores for predictive value in patients with acute coronary syndrome: a retrospective research. *PloS One* 8(1), p. e54731.

Wang, L. et al. 2019b. FoxO3 regulates hepatic triglyceride metabolism via modulation of the expression of sterol regulatory-element binding protein 1c. *Lipids in Health and Disease* 18(1), pp. 1-12.

Wang, N., Liang, H. and Zen, K. 2014a. Molecular mechanisms that influence the macrophage M1–M2 polarization balance. *Frontiers in Immunology* 5, p. 614.

Wang, P. et al. 2020c. Resveratrol reduces obesity in high-fat diet-fed mice via modulating the composition and metabolic function of the gut microbiota. *Free Radical Biology and Medicine* 156, pp. 83-98.

Wang, P. et al. 2019c. Therapeutic potential of oxytocin in atherosclerotic cardiovascular disease: mechanisms and signaling pathways. *Frontiers in Neuroscience* 13, p. 454.

Wang, R., Wang, Y., Wu, J., Guo, Y., Xiao, H., Zhang, Y. and Ma, K. 2022. Resveratrol Targets AKT1 to Inhibit Inflammasome Activation in Cardiomyocytes Under Acute Sympathetic Stress. *Frontiers in Pharmacology* 13,

Wang, T. and Butany, J. 2017. Pathogenesis of atherosclerosis. *Diagnostic Histopathology* 23(11), pp. 473-478.

Wang, W. et al. 2021. CFAP65 is required in the acrosome biogenesis and mitochondrial sheath assembly during spermiogenesis. *Human Molecular Genetics* 30(23), pp. 2240-2254.

Wang, X. et al. 2018. Roles of nitric oxide signaling pathway in atherosclerosis. *Atheroscler Open Access* 3(1), p. 120.

Wang, Y. et al. 2019d. Smooth muscle cells contribute the majority of foam cells in ApoE (Apolipoprotein E)-deficient mouse atherosclerosis. *Arteriosclerosis, Thrombosis, and Vascular Biology* 39(5), pp. 876-887.

Wang, Y., Wang, G. Z., Rabinovitch, P. S. and Tabas, I. 2014b. Macrophage mitochondrial oxidative stress promotes atherosclerosis and nuclear factor-κB–mediated inflammation in macrophages. *Circulation research* 114(3), pp. 421-433.

Wang, Y., Wang, W., Wang, N., Tall, A. R. and Tabas, I. 2017. Mitochondrial oxidative stress promotes atherosclerosis and neutrophil extracellular traps in aged mice. *Arteriosclerosis, Thrombosis, and Vascular Biology* 37(8), pp. e99-e107.

Wang, Y.-g. et al. 2015. Expansion of myeloid-derived suppressor cells in patients with acute coronary syndrome. *Cellular Physiology and Biochemistry* 35(1), pp. 292-304.

Wang, Z., Huang, Y., Zou, J., Cao, K., Xu, Y. and Wu, J. M. 2002. Effects of red wine and wine polyphenol resveratrol on platelet aggregation in vivo and in vitro. *International Journal of Molecular Medicine* 9(1), pp. 77-79.

Wang, Z. et al. 2020d. Wnt signaling activates MFSD2A to suppress vascular endothelial transcytosis and maintain blood-retinal barrier. *Science Advances* 6(35), p. eaba7457.

Wang, Z., Zou, J., Cao, K., Hsieh, T.-C., Huang, Y. and Wu, J. M. 2005. Dealcoholized red wine containing known amounts of resveratrol suppresses atherosclerosis in hypercholesterolemic rabbits without affecting plasma lipid levels. *International Journal of Molecular Medicine* 16(4), pp. 533-540.

Warboys, C. M., Amini, N., de Luca, A. and Evans, P. C. 2011. The role of blood flow in determining the sites of atherosclerotic plaques. *F1000 Medicine Reports* 3,

Weber, C. and Noels, H. 2011. Atherosclerosis: current pathogenesis and therapeutic options. *Nature Medicine* 17(11), pp. 1410-1422.

Westerterp, M. and Tall, A. R. 2020. A new pathway of macrophage cholesterol efflux. *Proceedings of the National Academy of Sciences* 117(22), pp. 11853-11855.

Whitman, S. C. 2004. A practical approach to using mice in atherosclerosis research. *The Clinical Biochemist Reviews* 25(1), p. 81.

Whitman, S. C., Ravisankar, P. and Daugherty, A. 2002. IFN-γ deficiency exerts gender-specific effects on atherogenesis in apolipoprotein E-/-mice. *Journal of Interferon & Cytokine Research* 22(6), pp. 661-670.

Whitman, S. C., Ravisankar, P., Elam, H. and Daugherty, A. 2000. Exogenous interferon-γ enhances atherosclerosis in apolipoprotein E−/− mice. *The American Journal of Pathology* 157(6), pp. 1819-1824.

Willemsen, L. and de Winther, M. P. 2020. Macrophage subsets in atherosclerosis as defined by single-cell technologies. *The Journal of Pathology* 250(5), pp. 705-714.

Winkels, H. and Wolf, D. 2021. Heterogeneity of T cells in atherosclerosis defined by single-cell RNA-sequencing and cytometry by time of flight. *Arteriosclerosis, Thrombosis, and Vascular Biology* 41(2), pp. 549-563.

Winneberger, J. et al. 2021. Platelet endothelial cell adhesion molecule-1 is a gatekeeper of neutrophil transendothelial migration in ischemic stroke. *Brain, Behavior, and Immunity* 93, pp. 277-287.

Winnik, S., Auwerx, J., Sinclair, D. A. and Matter, C. M. 2015. Protective effects of sirtuins in cardiovascular diseases: from bench to bedside. *European Heart Journal* 36(48), pp. 3404-3412.

Wirleitner, B. et al. 2003. Immune activation and degradation of tryptophan in coronary heart disease. *European Journal of Clinical Investigation* 33(7), pp. 550-554.

Wójcik-Cichy, K., Koślińska-Berkan, E. and Piekarska, A. 2018. The influence of NAFLD on the risk of atherosclerosis and cardiovascular diseases. *Clinical and Experimental Hepatology* 4(1), pp. 1-6.

Wolf, A. A., Yáñez, A., Barman, P. K. and Goodridge, H. S. 2019. The ontogeny of monocyte subsets. *Frontiers in Immunology* 10, p. 1642.

Wong, E. T. and Tergaonkar, V. 2009. Roles of NF-κB in health and disease: mechanisms and therapeutic potential. *Clinical Science* 116(6), pp. 451-465.

Wong, N. D. et al. 2017. Residual atherosclerotic cardiovascular disease risk in statin-treated adults: the multi-ethnic study of atherosclerosis. *Journal of Clinical Lipidology* 11(5), pp. 1223-1233.

Wong, R., Howe, P., Buckley, J., Coates, A., Kunz, I. and Berry, N. 2011. Acute resveratrol supplementation improves flow-mediated dilatation in overweight/obese individuals with mildly elevated blood pressure. *Nutrition, Metabolism and Cardiovascular Diseases* 21(11), pp. 851-856.

Wong, R. H., Coates, A. M., Buckley, J. D. and Howe, P. R. 2013. Evidence for circulatory benefits of resveratrol in humans. *Annals of the New York Academy of Sciences* 1290(1), pp. 52-58.

Wu, C.-M., Zheng, L., Wang, Q. and Hu, Y.-W. 2021a. The emerging role of cell senescence in atherosclerosis. *Clinical Chemistry and Laboratory Medicine (CCLM)* 59(1), pp. 27-38.

Wu, M.-Y., Li, C.-J., Hou, M.-F. and Chu, P.-Y. 2017. New insights into the role of inflammation in the pathogenesis of atherosclerosis. *International Journal of Molecular Sciences* 18(10), p. 2034.

Wu, Q. et al. 2021b. Acetylcholine reduces palmitate-induced cardiomyocyte apoptosis by promoting lipid droplet lipolysis and perilipin 5-mediated lipid droplet-mitochondria interaction. *Cell Cycle* 20(18), pp. 1890-1906.

Wu, X., Wang, Q., Lu, Y., Zhang, J., Yin, H. and Yi, Y. 2021c. Clinical application of thioredoxin reductase as a novel biomarker in liver cancer. *Scientific Reports* 11(1), pp. 1-12.

Wueest, S. and Konrad, D. 2020. The controversial role of IL-6 in adipose tissue on obesity-induced dysregulation of glucose metabolism. *American Journal of Physiology-Endocrinology and Metabolism* 319(3), pp. E607-E613.

Wung, B., Hsu, M., Wu, C. and Hsieh, C. 2005. Resveratrol suppresses IL-6-induced ICAM-1 gene expression in endothelial cells: effects on the inhibition of STAT3 phosphorylation. *Life Sciences* 78(4), pp. 389-397.

Xi, D., Zhao, J., Zhao, M., Fu, W., Guo, Z. and Chen, H. 2017. Identification of gene expression changes in the aorta of ApoE null mice fed a high-fat diet. *Genes* 8(10), p. 289.

Xia, F. et al. 2013. IRGM1 regulates oxidized LDL uptake by macrophage via actin-dependent receptor internalization during atherosclerosis. *Scientific Reports* 3(1), pp. 1-6.

Xia, N. et al. 2010. Resveratrol reverses endothelial nitric-oxide synthase uncoupling in apolipoprotein E knockout mice. *Journal of Pharmacology and Experimental Therapeutics* 335(1), pp. 149-154.

Xiao, X. et al. 2020. S100 proteins in atherosclerosis. *Clinica Chimica Acta* 502, pp. 293-304.

Xie, H., Han, H.-P., Chen, Z. and He, J.-P. 2014. A study on the effect of resveratrol on lipid metabolism in hyperlipidemic mice. *African Journal of Traditional, Complementary and Alternative Medicines* 11(1), pp. 209-212.

Xie, Y. et al. 2019. Resveratrol blocks atherosclerosis development by inhibiting IL-1β in macrophages induced by cholesterol. *Archives of Biological Sciences* 71(3), pp. 551-559.

Xin, P. et al. 2013. Alleviative effects of resveratrol on nonalcoholic fatty liver disease are associated with up regulation of hepatic low density lipoprotein receptor and scavenger receptor class B type I gene expressions in rats. *Food and Chemical Toxicology* 52, pp. 12-18.

Xu, B.-F. et al. 2020a. Identification of key genes in ruptured atherosclerotic plaques by weighted gene correlation network analysis. *Scientific Reports* 10(1), pp. 1-10.

Xu, H., Jiang, J., Chen, W., Li, W. and Chen, Z. 2019. Vascular macrophages in atherosclerosis. *Journal of Immunology Research* 2019,

Xu, H., Wang, Z., Sun, Z., Ni, Y. and Zheng, L. 2018. GATA4 protects against hyperglycemia-induced endothelial dysfunction by regulating NOX4 transcription. *Molecular Medicine Reports* 17(1), pp. 1485-1492.

Xu, M., Yang, W., Wang, X. and Nayak, D. K. 2020b. Lung secretoglobin Scgb1a1 influences alveolar macrophage-mediated inflammation and immunity. *Frontiers in Immunology* 11, p. 584310.

Xu, S. et al. 2021. Endothelial dysfunction in atherosclerotic cardiovascular diseases and beyond: from mechanism to pharmacotherapies. *Pharmacological Reviews* 73(3), pp. 924-967.

Xu, X., Lu, L., Dong, Q., Li, X., Zhang, N., Xin, Y. and Xuan, S. 2015. Research advances in the relationship between nonalcoholic fatty liver disease and atherosclerosis. *Lipids in Health and Disease* 14(1), pp. 1-8.

Xuzhu, G., Komai-Koma, M., Leung, B. P., Howe, H. S., McSharry, C., McInnes, I. B. and Xu, D. 2012. Resveratrol modulates murine collagen-induced arthritis by inhibiting Th17 and B-cell function. *Annals of the Rheumatic Diseases* 71(1), pp. 129-135.

Yamada, S. et al. 2018. Inhibition of local macrophage growth ameliorates focal inflammation and suppresses atherosclerosis. *Arteriosclerosis, Thrombosis, and Vascular Biology* 38(5), pp. 994-1006.

Yang, S. et al. 2020. Macrophage polarization in atherosclerosis. *Clinica Chimica Acta* 501, pp. 142-146.

Yang, S. J. and Lim, Y. 2014. Resveratrol ameliorates hepatic metaflammation and inhibits NLRP3 inflammasome activation. *Metabolism* 63(5), pp. 693-701.

Yao, W., Li, K. and Liao, K. 2009. Macropinocytosis contributes to the macrophage foam cell formation in RAW264. 7 cells. *Acta Biochim Biophys Sin* 41(9), pp. 773-780.

Yao, Y., Xu, X.-H. and Jin, L. 2019. Macrophage polarization in physiological and pathological pregnancy. *Frontiers in Immunology* 10, p. 792.

Ye, G. et al. 2019. Resveratrol inhibits lipid accumulation in the intestine of atherosclerotic mice and macrophages. *Journal of Cellular and Molecular Medicine* 23(6), pp. 4313-4325.

Ye, Z., Wang, S., Zhang, C. and Zhao, Y. 2020. Coordinated modulation of energy metabolism and inflammation by branched-chain amino acids and fatty acids. *Frontiers in Endocrinology* 11, p. 617.

Yen, G.-C., Duh, P.-D. and Lin, C.-W. 2003. Effects of resveratrol and 4-hexylresorcinol on hydrogen peroxide-induced oxidative DNA damage in human lymphocytes. *Free radical research* 37(5), pp. 509-514.

Yi, H. et al. 2009. Pattern recognition scavenger receptor SRA/CD204 down-regulates Toll-like receptor 4 signaling–dependent CD8 T-cell activation. *Blood, The Journal of the American Society of Hematology* 113(23), pp. 5819-5828.

Yokota, T., Nomura, K., Nagashima, M. and Kamimura, N. 2016. Fucoidan alleviates high-fat diet-induced dyslipidemia and atherosclerosis in ApoEshl mice deficient in apolipoprotein E expression. *The Journal of Nutritional Biochemistry* 32, pp. 46-54.

Yu, D., Tang, Z., Li, B., Yu, J., Li, W., Liu, Z. and Tian, C. 2021a. Resveratrol against Cardiac Fibrosis: Research Progress in Experimental Animal Models. *Molecules* 26(22), p. 6860.

Yu, E. et al. 2013. Mitochondrial DNA damage can promote atherosclerosis independently of reactive oxygen species through effects on smooth muscle cells and monocytes and correlates with higher-risk plaques in humans. *Circulation* 128(7), pp. 702-712.

Yu, E. et al. 2017. Increases in plasma tryptophan are inversely associated with incident cardiovascular disease in the Prevencion con Dieta Mediterranea (PREDIMED) Study. *The Journal of Nutrition* 147(3), pp. 314-322.

Yu, J.-H., Ustach, C. and ChoiKim, H.-R. 2003. Platelet-derived growth factor signaling and human cancer. *Bmb Reports* 36(1), pp. 49-59.

Yu, M.-H. et al. 2021b. Neochlorogenic Acid Attenuates Hepatic Lipid Accumulation and Inflammation via Regulating miR-34a In Vitro. *International Journal of Molecular Sciences* 22(23), p. 13163.

Yuan, W., Zhang, M., Wang, C., Li, B., Li, L., Ye, F. and Xu, C. 2022. Resveratrol Attenuates High-Fat Diet–Induced Hepatic Lipotoxicity by Upregulating Bmi-1 Expression. *Journal of Pharmacology and Experimental Therapeutics* 381(2), pp. 96-105.

Yurdagul Jr, A. 2022. Crosstalk Between Macrophages and Vascular Smooth Muscle Cells in Atherosclerotic Plaque Stability. *Arteriosclerosis, Thrombosis, and Vascular Biology*, p. ATVBAHA. 121.316233.

Yvan-Charvet, L. and Ivanov, S. 2020. Metabolic reprogramming of macrophages in atherosclerosis: is it all about cholesterol? *Journal of Lipid and Atherosclerosis* 9(2), p. 231.

Zamora-Ros, R. et al. 2012. High urinary levels of resveratrol metabolites are associated with a reduction in the prevalence of cardiovascular risk factors in high-risk patients. *Pharmacological Research* 65(6), pp. 615-620.

Zang, N. et al. 2011. Resveratrol-mediated gamma interferon reduction prevents airway inflammation and airway hyperresponsiveness in respiratory syncytial virus-infected immunocompromised mice. *Journal of Virology* 85(24), pp. 13061-13068.

Zeng, W. et al. 2021. The selective NLRP3 inhibitor MCC950 hinders atherosclerosis development by attenuating inflammation and pyroptosis in macrophages. *Scientific Reports* 11(1), pp. 1-12.

Zernecke, A. and Weber, C. 2014. Chemokines in atherosclerosis: proceedings resumed. *Arteriosclerosis, Thrombosis, and Vascular Biology* 34(4), pp. 742-750.

Zeya, B., Arjuman, A. and Chandra, N. C. 2016. Lectin-like oxidized low-density lipoprotein (LDL) receptor (LOX-1): a chameleon receptor for oxidized LDL. *Biochemistry* 55(32), pp. 4437-4444.

Zhang, D., He, S., Wang, Q., Pu, S., Zhou, Z. and Wu, Q. 2020a. Impact of aging on the characterization of brown and white adipose tissue-derived stem cells in mice. *Cells Tissues Organs* 209(1), pp. 26-36.

Zhang, F.-s., He, Q.-z., Qin, C. H., Little, P. J., Weng, J.-p. and Xu, S.-w. 2022a. Therapeutic potential of colchicine in cardiovascular medicine: a pharmacological review. *Acta Pharmacologica Sinica*, pp. 1-18.

Zhang, G., Li, C., Zhu, N., Chen, Y., Yu, Q., Liu, E. and Wang, R. 2018. Sex differences in the formation of atherosclerosis lesion in apoE-/-mice and the effect of 17β-estrodiol on protein S-nitrosylation. *Biomedicine & Pharmacotherapy* 99, pp. 1014-1021.

Zhang, L., Chen, J., Yan, L., He, Q., Xie, H. and Chen, M. 2021a. Resveratrol ameliorates cardiac remodeling in a murine model of heart failure with preserved ejection fraction. *Frontiers in Pharmacology* 12, p. 1356.

Zhang, L., Ovchinnikova, O., Jönsson, A., Lundberg, A. M., Berg, M., Hansson, G. K. and Ketelhuth, D. F. 2012. The tryptophan metabolite 3-hydroxyanthranilic acid lowers plasma lipids and decreases atherosclerosis in hypercholesterolaemic mice. *European Heart Journal* 33(16), pp. 2025-2034.

Zhang, L., Ussher, J. R., Oka, T., Cadete, V. J., Wagg, C. and Lopaschuk, G. D. 2011a. Cardiac diacylglycerol accumulation in high fat-fed mice is associated with impaired insulin-stimulated glucose oxidation. *Cardiovascular Research* 89(1), pp. 148-156.

Zhang, L.-X. et al. 2021b. Resveratrol (RV): A pharmacological review and call for further research. *Biomedicine & Pharmacotherapy* 143, p. 112164.

Zhang, M. et al. 2019. Resveratrol inhibits MMP3 and MMP9 expression and secretion by suppressing TLR4/NF-κB/STAT3 activation in Ox-LDL-treated HUVECs. *Oxidative Medicine and Cellular Longevity* 2019,

Zhang, S.-S., Liu, M., Liu, D.-N., Shang, Y.-F., Wang, Y.-H. and Du, G.-H. 2022b. ST2825, a Small Molecule Inhibitor of MyD88, Suppresses NF-κB Activation and the ROS/NLRP3/Cleaved Caspase-1 Signaling Pathway to Attenuate Lipopolysaccharide-Stimulated Neuroinflammation. *Molecules* 27(9), p. 2990.

Zhang, X., Liu, X., Shang, H., Xu, Y. and Qian, M. 2011b. Monocyte chemoattractant protein-1 induces endothelial cell apoptosis in vitro through a p53-dependent mitochondrial pathway. *Acta Biochim Biophys Sin* 43(10), pp. 787-795.

Zhang, X., Meng, Q., Kong, F., Wang, K. and Du, L. 2020b. SLC5A8 regulates the biological behaviors of cervical cancer cells through mediating the Wnt signaling pathway. *Eur. Rev. Med. Pharmacol. Sci* 24, pp. 4679-4686.

Zhang, X. et al. 2020c. Hydroxytyrosol Plays Antiatherosclerotic Effects through Regulating Lipid Metabolism via Inhibiting the p38 Signal Pathway. *BioMed Research International* 2020,

Zhang, Y. et al. 2015. Resveratrol improves hepatic steatosis by inducing autophagy through the cAMP signaling pathway. *Molecular Nutrition & Food Research* 59(8), pp. 1443-1457.

Zhang, Y. et al. 2021c. Resveratrol affects the migration and apoptosis of monocytes by blocking HMGB1/NF-κB pathway. *Translational Cancer Research* 10(8), p. 3647.

Zhang, Y., Liu, H., Tang, W., Qiu, Q. and Peng, J. 2020d. Resveratrol prevents TNF-α-induced VCAM-1 and ICAM-1 upregulation in endothelial progenitor cells via reduction of NF-κ B activation. *Journal of International Medical Research* 48(9), p. 0300060520945131.

Zhang, Y., Ma, K. L., Ruan, X. Z. and Liu, B. C. 2016. Dysregulation of the low-density lipoprotein receptor pathway is involved in lipid disorder-mediated organ injury. *International Journal of Biological Sciences* 12(5), p. 569.

Zhang, Y. et al. 2014. Regulation of glucose homeostasis and lipid metabolism by PPP1R3G-mediated hepatic glycogenesis. *Molecular Endocrinology* 28(1), pp. 116-126.

Zhao, C. F. and Herrington, D. M. 2016. The function of cathepsins B, D, and X in atherosclerosis. *American Journal of Cardiovascular Disease* 6(4), p. 163.

Zhao, D. et al. 2020. TL1A inhibits atherosclerosis in apoE-deficient mice by regulating the phenotype of vascular smooth muscle cells. *Journal of Biological Chemistry* 295(48), pp. 16314-16327.

Zhao, G. et al. 2021. Single-cell RNA sequencing reveals the cellular heterogeneity of aneurysmal infrarenal abdominal aorta. *Cardiovascular Research* 117(5), pp. 1402-1416.

Zhe-Wei, S., Li-Sha, G. and Yue-Chun, L. 2018. The role of necroptosis in cardiovascular disease. *Frontiers in Pharmacology* 9, p. 721.

Zheng, F., Xing, S., Gong, Z., Mu, W. and Xing, Q. 2014. Silence of NLRP3 suppresses atherosclerosis and stabilizes plaques in apolipoprotein E-deficient mice. *Mediators of Inflammation* 2014,

Zheng, F., Xing, S., Gong, Z. and Xing, Q. 2013. NLRP3 inflammasomes show high expression in aorta of patients with atherosclerosis. *Heart, Lung and Circulation* 22(9), pp. 746-750.

Zhou, L., Long, J., Sun, Y., Chen, W., Qiu, R. and Yuan, D. 2020. Resveratrol ameliorates atherosclerosis induced by high-fat diet and LPS in ApoE−/− mice and inhibits the activation of CD4+ T cells. *Nutrition & Metabolism* 17(1), pp. 1-12.

Zhou, L. et al. 2018a. Cardioprotective role of myeloid-derived suppressor cells in heart failure. *Circulation* 138(2), pp. 181-197.

Zhou, L., Xiao, X., Zhang, Q., Zheng, J. and Deng, M. 2019a. Deciphering the anti-obesity benefits of resveratrol: the "gut microbiota-adipose tissue" axis. *Frontiers in Endocrinology*, p. 413.

Zhou, X., Chen, M., Zeng, X., Yang, J., Deng, H., Yi, L. and Mi, M. 2014. Resveratrol regulates mitochondrial reactive oxygen species homeostasis through Sirt3 signaling pathway in human vascular endothelial cells. *Cell Death & Disease* 5(12), pp. e1576-e1576.

Zhou, X. et al. 2011. A novel defensive mechanism against acetaminophen toxicity in the mouse lateral nasal gland: role of CYP2A5-mediated regulation of testosterone homeostasis and salivary androgen-binding protein expression. *Molecular Pharmacology* 79(4), pp. 710-723.

Zhou, X. et al. 2019b. Resveratrol attenuates endothelial oxidative injury by inducing autophagy via the activation of transcription factor EB. *Nutrition & Metabolism* 16(1), pp. 1-12.

Zhou, Y. Y. et al. 2018b. Nonalcoholic fatty liver disease contributes to subclinical atherosclerosis: a systematic review and meta-analysis. *Hepatology Communications* 2(4), pp. 376-392.

Zhu, C., Xie, P., Zhao, F., Zhang, L., An, W. and Zhan, Y. 2014. Mechanism of the promotion of steatotic HepG2 cell apoptosis by cholesterol. *International Journal of Clinical and Experimental Pathology* 7(10), p. 6807.

Zhu, J. et al. 2008. Anti-inflammatory effect of resveratrol on TNF-α-induced MCP-1 expression in adipocytes. *Biochemical and Biophysical Research Communications* 369(2), pp. 471-477.

Zhu, Q. et al. 2022. SEC14L3 plays a tumor-suppressive role in breast cancer through a Wnt/β-catenin-related way. *Experimental Cell Research* 417(1), p. 113161.

Zou, P., Liu, X., Li, G. and Wang, Y. 2018. Resveratrol pretreatment attenuates traumatic brain injury in rats by suppressing NLRP3 inflammasome activation via SIRT1. *Molecular Medicine Reports* 17(2), pp. 3212-3217.

Zu, Y. et al. 2021. Browning white adipose tissue using adipose stromal cell-targeted resveratrol-loaded nanoparticles for combating obesity. *Journal of Controlled Release* 333, pp. 339-351.

Zunino, S. J., Hwang, D. H., Huang, S. and Storms, D. H. 2018. Resveratrol increases phagocytosis and lipopolysaccharide-induced interleukin-1β production, but decreases surface expression of Toll-like receptor 2 in THP-1 monocytes. *Cytokine* 102, pp. 141-144.